Advances in Photosynthesis and Respiration 42
Including Bioenergy and Related Processes

Kouki Hikosaka
Ülo Niinemets
Niels P.R. Anten *Editors*

Canopy Photosynthesis: From Basics to Applications

Springer

Canopy Photosynthesis: From Basics to Applications

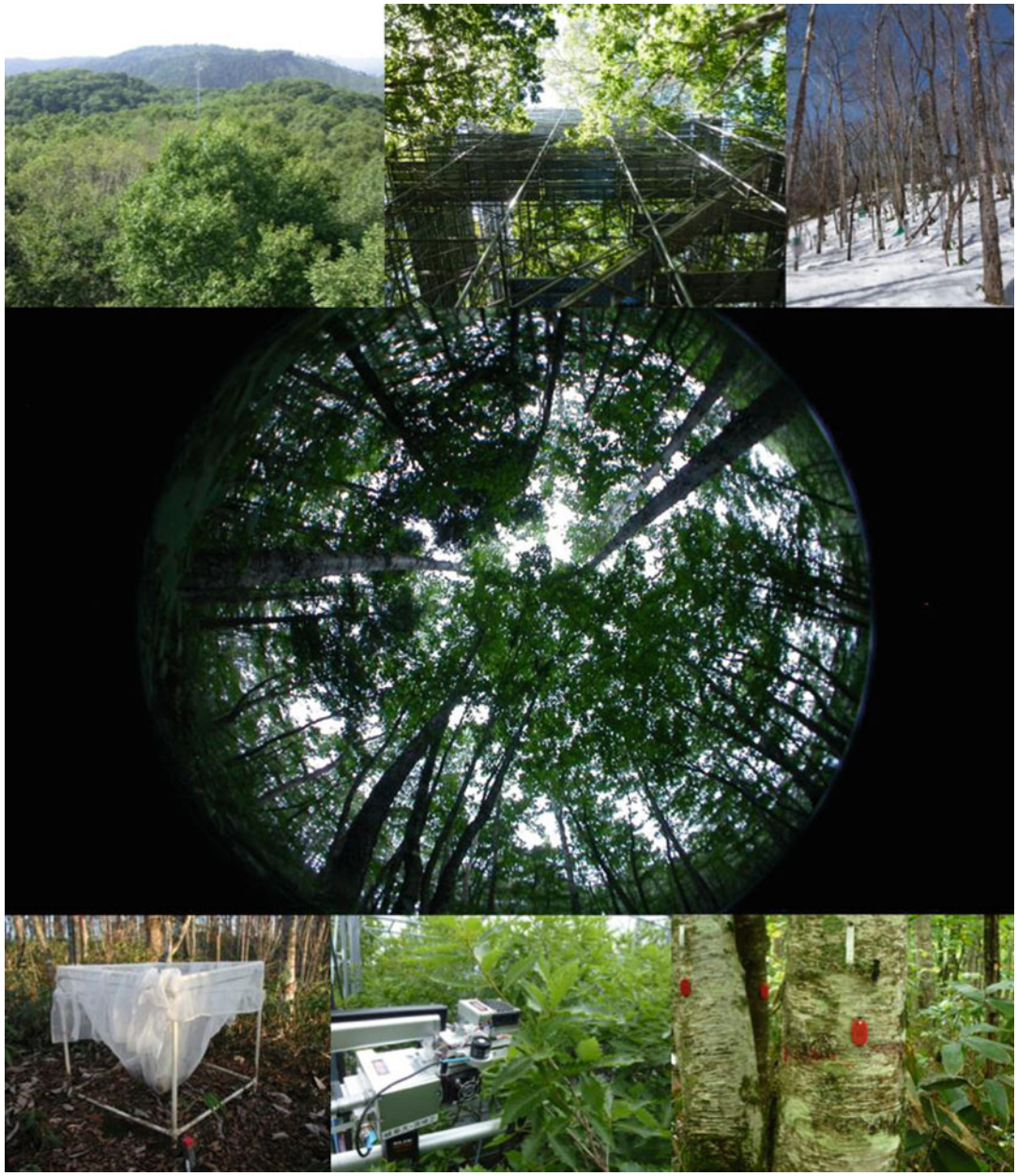

Measurements of carbon cycle in the Takayama Experimental Forest, Japan. Meteorological CO_2 flux observation tower (*left-top*; National Institute of Advanced Science and Technology), canopy tower (*center-top*), forest in winter time (*right-top*), canopy hemispherical photograph from the understory (*center*), litter trap (*left-bottom*), leaf gas exchange measurements on canopy tower (*center-bottom*), and tree biomass survey (*right-bottom*). Photographs were taken by Hiroyuki Muraoka. See Chap. 12

Advances in Photosynthesis and Respiration
Including Bioenergy and Related Processes

VOLUME 42

This book series ADVANCES IN PHOTOSYNTHESIS AND RESPIRATION: *Including Bioenergy and Related Processes* provides a comprehensive and state-of-the-art account of research in photosynthesis, respiration and related processes. Virtually all life on our planet Earth ultimately depends on photosynthetic energy capture and conversion to energy-rich organic molecules. These are used for food, fuel, and fiber. Photosynthesis is the source of almost all bioenergy on Earth. The fuel and energy uses of photosynthesized products and processes have become an important area of study, and competition between food and fuel has led to resurgence in photosynthesis research. This series of books spans topics from physics to agronomy and medicine; from femtosecond processes through season-long production to evolutionary changes over the course of the history of the Earth; from the photophysics of light absorption, excitation energy transfer in the antenna to the reaction centers, where the highly-efficient primary conversion of light energy to charge separation occurs, through the electrochemistry of intermediate electron transfer, to the physiology of whole organisms and ecosystems; and from X-ray crystallography of proteins to the morphology of organelles and intact organisms. In addition to photosynthesis in natural systems, genetic engineering of photosynthesis and artificial photosynthesis is included in this series. The goal of the series is to offer beginning researchers, advanced undergraduate students, graduate students, and even research specialists, a comprehensive, up-to-date picture of the remarkable advances across the full scope of research on photosynthesis and related energy processes. The purpose of this series is to improve understanding of photosynthesis and respiration at many levels both to improve basic understanding of these important processes and to enhance our ability to use photosynthesis for the improvement of the human condition.

For other titles published in this series, go to http://www.springer.com/series/5599

Canopy Photosynthesis: From Basics to Applications

Edited by

Kouki Hikosaka
Graduate School of Life Sciences
Tohoku University
Sendai
Japan

Ülo Niinemets
Environmental Sciences
Estonian University of Life Sciences
Tartu
Estonia

and

Niels P.R. Anten
Crop and Weed Ecology
Centre for Crop Systems Analysis
Wageningen University
Wageningen
The Netherlands

Springer

Editors
Kouki Hikosaka
Graduate School of Life Sciences
Tohoku University
Sendai, Japan

Ülo Niinemets
Environmental Sciences
Estonian University of Life Sciences
Tartu, Estonia

Niels P.R. Anten
Crop and Weed Ecology
Centre for Crop Systems Analysis
Wageningen University
Wageningen, The Netherlands

ISSN 1572-0233 ISSN 2215-0102 (electronic)
Advances in Photosynthesis and Respiration
ISBN 978-94-017-7290-7 ISBN 978-94-017-7291-4 (eBook)
DOI 10.1007/978-94-017-7291-4

Library of Congress Control Number: 2015957424

Springer Dordrecht Heidelberg New York London

Printed on acid-free paper

Springer Science+Business Media B.V. Dordrecht is part of Springer Science+Business Media (www.springer.com)

From the Series Editors

Advances in Photosynthesis and Respiration Including Bioenergy and Related Processes

Volume 42: Canopy Photosynthesis: From Basics to Applications

We are delighted to announce the publication of Volume 42 in this series. We believe these books provide a forum for discussion of important developments in the field in a more in-depth and complete way than can be achieved in individual papers or even in extended reviews. The publisher has taken steps to ensure that these books and individual chapters are easily found. A large number of university libraries buy electronic access. Downloaded PDFs are of high quality. Data can be downloaded for easy import into reference management programs. Because most distribution is now digital, there are no longer significant constraints on the use of color or placement of figures within the text. In view of the interdisciplinary character of research in photosynthesis and respiration, it is our earnest hope that this series of books will be used in educating students and researchers not only in plant sciences, molecular and cell biology, integrative biology, biotechnology, agricultural sciences, microbiology, biochemistry, chemical biology, biological physics, and biophysics, but also in bioengineering, chemistry, and physics.

This Book: Volume 42

Canopy Photosynthesis: From Basics to Applications addresses how the display of photosynthetic structures affects photosynthesis. Photosynthesis provides the energy and basic substrates for life on earth. Knowledge of photosynthetic functioning at the physiological and molecular level is advancing rapidly, but its relevance for food production, ecosystem carbon cycling, and climate feedback acts at the level of vegetation stands such as forests, grasslands, or agricultural crops. The canopies of these vegetation types are highly complex and varied, presenting a wide range of plant architectures and leaf displays. Understanding the complex relationships between leaf display and photosynthesis requires a quantitative approach to understanding light distribution, leaf heating, and optimal distribution of resources such as nitrogen among the leaves experiencing different environmental conditions through their life. These quantitative approaches are often thought of in terms of forest canopies but these concepts are important when studying any canopy, including a canopy of the standard lab plant *Arabidopsis*. Simulating canopy processes involves the application of rigorous physical concepts such as energy balance equations that can predict leaf temperature from its radiation environment and evaporation rate. In some cases, energy balance estimates are more representative of leaf temperature than direct measurement because of the difficulties of measuring leaf temperature without changing it. Another area of study important in canopy photosynthesis is called micrometeorology. Wind field structure, including 3D frictional velocity distribution, turbulence characteristics, and water content of the air are some of the fundamental issues that must be understood in sufficient detail to study canopy photosynthesis.

We, the series editors, are indeed delighted that three scientists who have made major contributions to the understanding of canopy photosynthesis agreed to edit this volume. Kouki Hikosaka (from Japan), Ülo Niinemets (from Estonia), and Niels P. R. Anten (from the Netherlands) have conceived a book in five parts with three to four chapters per section. The sections progress from leaf-specific issues like temperature and light distribution among leaves in Part 1 through successively larger scales to ecological and evolutionary processes in Part 5. Twenty-five authors (see list of contributors) from seven countries (UK, USA, Canada, Estonia, Japan, Netherlands, and Switzerland) have contributed to this volume.

With the knowledge gained from reading this book it will be easier to understand two interesting "counter-intuitive" observations: (*1*) Under humid conditions, increasing wind speed can reduce evaporation, and (*2*) sometimes when volcanoes inject dust into the atmosphere, reducing the intensity of sunlight by increased light scattering, global photosynthesis increases. In the first case energy balance equations show that the cooling by increased wind speed of sun-warmed leaves reduces the potential for evaporation more than it increases conductance for water loss. The second case happens if scattered light penetrates deeper into the canopy, striking more leaves than what the direct beam of the sun can reach.

Many of our readers will want to have a good reference for the equations and their applications, and they will be found in this book. Further, for those who study photosynthesis in leaves, chapters in this volume will help them understand the steps involved in measuring how leaves gather light and how we obtain leaf temperature.

Our Books: Now 42 Volumes

We list below information on the 41 volumes that have been published thus far (see http://www.springer.com/series/5599 for the series web site). Electronic access to individual chapters depends on subscription (ask your librarian) but Springer provides free downloadable front matter as well as indexes for nearly all volumes. The available web sites of the books in the Series are listed below.

- **Volume 41 (2015) Cytochrome Complexes: Evolution, Structures, Energy Transduction, and Signaling**, Edited by William A. Cramer and Tovio Kallas from the USA. Thirty five chapters – In press
- **Volume 40 (2015) Non-Photochemical Quenching and Energy Dissipation in Plants, Algae and Cyanobacteria**, edited by Barbara Demmig-Adams, Győző Garab, William W. Adams III, and Govindjee from USA and Hungary. Twenty eight chapters, 649 pp, Hardcover ISBN 978-94-017-9031-4, eBook ISBN 978-94-017-9032-1 [http://www.springer.com/life+sciences/plant+sciences/book/978-94-017-9031-4]
- **Volume 39 (2014) The Structural Basis of Biological Energy Generation**, edited by Martin F. Hohmann-Marriott from Norway. Twenty four chapters, 483 pp, Hardcover ISBN 978-94-017-8741-3, eBook ISBN 978-94-017-8742-0 [http://www.springer.com/life+sciences/book/978-94-017-8741-3]
- **Volume 38 (2014) Microbial BioEnergy: Hydrogen Production**, edited by Davide Zannoni and Roberto De Phillipis, from Italy. Eighteen chapters, 366 pp, Hardcover ISBN 978-94-017-8553-2, eBook ISBN 978-94- 017-8554-9 [http://www.springer.com/life+sciences/plant+sciences/book/978-94-017-8553-2]
- **Volume 37 (2014) Photosynthesis in Bryophytes and Early Land Plants**, edited by David T. Hanson and Steven K. Rice, from USA. Eighteen chapters, approx. 342 pp, Hardcover ISBN 978-94-007-6987-8, eBook ISBN 978-94-007-6988-5 [http://www.springer.com/life+sciences/plant+sciences/book/978-94-007-6987-8]
- **Volume 36 (2013) Plastid Development in Leaves during Growth and Senescence**, edited by Basanti Biswal, Karin Krupinska

and Udaya Biswal, from India and Germany. Twenty-eight chapters, 837 pp, Hardcover ISBN 978-94-007-5723-33, eBook ISBN 978-94-007-5724-0 [http://www.springer.com/life+sciences/plant+sciences/book/978-94-007-5723-3]

- **Volume 35 (2012) Genomics of Chloroplasts and Mitochondria**, edited by Ralph Bock and Volker Knoop, from Germany. Nineteen chapters, 475 pp, Hardcover ISBN 978-94-007-2919-3 eBook ISBN 978-94-007-2920-9 [http://www.springer.com/life+sciences/plant+sciences/book/978-94-007-2919-3]
- **Volume 34 (2012) Photosynthesis – Plastid Biology, Energy Conversion and Carbon Assimilation**, edited by Julian Eaton-Rye, Baishnab C. Tripathy, and Thomas D. Sharkey, from New Zealand, India, and USA. Thirty-three chapters, 854 pp, Hardcover, ISBN 978-94-007-1578-3, eBook ISBN 978-94-007-1579-0 [http://www.springer.com/life+sciences/plant+sciences/book/978-94-007-1578-3]
- **Volume 33 (2012): Functional Genomics and Evolution of Photosynthetic Systems**, edited by Robert L. Burnap and Willem F. J. Vermaas, from USA. Fifteen chapters, 428 pp, Hardcover ISBN 978-94-007-1532-5, Softcover ISBN 978-94-007-3832-4, eBook ISBN 978-94-007-1533-2 [http://www.springer.com/life+sciences/book/978-94-007-1532-5]
- **Volume 32 (2011): C_4 Photosynthesis and Related CO_2 Concentrating Mechanisms,** edited by Agepati S. Raghavendra and Rowan Sage, from India and Canada. Nineteen chapters, 425 pp, Hardcover ISBN 978-90-481-9406-3, Softcover ISBN 978-94-007-3381-7, eBook ISBN 978-90-481-9407-0 [http://www.springer.com/life+sciences/plant+sciences/book/978-90-481-9406-3]
- **Volume 31 (2010): The Chloroplast: Basics and Applications,** edited by Constantin Rebeiz (USA), Christoph Benning (USA), Hans J. Bohnert (USA), Henry Daniell (USA), J. Kenneth Hoober (USA), Hartmut K. Lichtenthaler (Germany), Archie R. Portis (USA), and Baishnab C. Tripathy (India). Twenty-five chapters, 451 pp, Hardcover ISBN 978-90-481-8530-6, Softcover ISBN 978-94-007-3287-2, eBook ISBN 978-90-481-8531-3 [http://www.springer.com/life+sciences/plant+sciences/book/978-90-481-8530-6]
- **Volume 30 (2009): Lipids in Photosynthesis: Essential and Regulatory Functions,** edited by Hajime Wada and Norio Murata, both from Japan. Twenty chapters, 506 pp, Hardcover ISBN 978-90-481-2862-4, Softcover ISBN 978-94-007-3073-1 eBook ISBN 978-90-481-2863-1 [http://www.springer.com/life+sciences/plant+sciences/book/978-90-481-2862-4]
- **Volume 29 (2009): Photosynthesis in Silico: Understanding Complexity from Molecules,** edited by Agu Laisk, Ladislav Nedbal, and Govindjee, from Estonia, The Czech Republic, and USA. Twenty chapters, 525 pp, Hardcover ISBN 978-1-4020-9236-7, Softcover ISBN 978-94-007-1533-2, eBook ISBN 978-1-4020-9237-4 [http://www.springer.com/life+sciences/plant+sciences/book/978-1-4020-9236-7]
- **Volume 28 (2009): The Purple Phototrophic Bacteria,** edited by C. Neil Hunter, Fevzi Daldal, Marion C. Thurnauer and J. Thomas Beatty, from UK, USA and Canada. Forty-eight chapters, 1053 pp, Hardcover ISBN 978-1-4020-8814-8, eBook ISBN 978-1-4020-8815-5 [http://www.springer.com/life+sciences/plant+sciences/book/978-1-4020-8814-8]
- **Volume 27 (2008): Sulfur Metabolism in Phototrophic Organisms**, edited by Christiane Dahl, Rüdiger Hell, David Knaff and Thomas Leustek, from Germany and USA. Twenty-four chapters, 551 pp, Hardcover ISBN 978-4020-6862-1, Softcover ISBN 978-90-481-7742-4, eBook ISBN 978-1-4020-6863-8 [http://www.springer.com/life+sciences/plant+sciences/book/978-1-4020-6862-1]
- **Volume 26 (2008): Biophysical Techniques Photosynthesis**, Volume II, edited by Thijs

Aartsma and Jörg Matysik, both from The Netherlands. Twenty-four chapters, 548 pp, Hardcover, ISBN 978-1-4020-8249-8, Softcover ISBN 978-90-481-7820-9, eBook ISBN 978-1-4020-8250-4 [http://www.springer.com/life+sciences/plant+sciences/book/978-1-4020-8249-8]

- **Volume 25 (2006): Chlorophylls and Bacteriochlorophylls: Biochemistry, Biophysics, Functions and Applications,** edited by Bernhard Grimm, Robert J. Porra, Wolfhart Rüdiger, and Hugo Scheer, from Germany and Australia. Thirty-seven chapters, 603 pp, Hardcover, ISBN 978-1-40204515-8, Softcover ISBN 978-90-481-7140-8, eBook ISBN 978-1-4020-4516-5 [http://www.springer.com/life+sciences/plant+sciences/book/978-1-4020-4515-8]
- **Volume 24 (2006): Photosystem I: The Light-Driven Plastocyanin: Ferredoxin Oxidoreductase,** edited by John H. Golbeck, from USA. Forty chapters, 716 pp, Hardcover ISBN 978-1-40204255-3, Softcover ISBN 978-90-481-7088-3, eBook ISBN 978-1-4020-4256-0 [http://www.springer.com/life+sciences/plant+sciences/book/978-1-4020-4255-3]
- **Volume 23 (2006): The Structure and Function of Plastids**, edited by Robert R. Wise and J. Kenneth Hoober, from USA. Twenty-seven chapters, 575 pp, Softcover, ISBN: 978-1-4020-6570–6; Hardcover ISBN 978-1-4020-4060-3, Softcover ISBN 978-1-4020-6570-5, eBook ISBN 978-1-4020-4061-0 [http://www.springer.com/life+sciences/plant+sciences/book/978-1-4020-4060-3]
- **Volume 22 (2005): Photosystem II: The Light-Driven Water: Plastoquinone Oxidoreductase**, edited by Thomas J. Wydrzynski and Kimiyuki Satoh, from Australia and Japan. Thirty-four chapters, 786 pp, Hardcover ISBN 978-1-4020-4249-2, eBook ISBN 978-1-4020-4254-6 [http://www.springer.com/life+sciences/plant+sciences/book/978-1-4020-4249-2]
- **Volume 21 (2005): Photoprotection, Photoinhibition, Gene Regulation, and Environment,** edited by Barbara Demmig-Adams, William W. Adams III and Autar K. Mattoo, from USA. Twenty-one chapters, 380 pp, Hardcover ISBN 978-14020-3564-7, Softcover ISBN 978-1-4020-9281-7, eBook ISBN 978-1-4020-3579-1 [http://www.springer.com/life+sciences/plant+sciences/book/978-1-4020-3564-7]
- **Volume 20 (2006): Discoveries in Photosynthesis**, edited by Govindjee, J. Thomas Beatty, Howard Gest and John F. Allen, from USA, Canada and UK. One hundred and eleven chapters, 1304 pp, Hardcover ISBN 978-1-4020-3323-0, eBook ISBN 978-1-4020-3324-7 [http://www.springer.com/life+sciences/plant+sciences/book/978-1-4020-3323-0]
- **Volume 19 (2004): Chlorophyll *a* Fluorescence: A Signature of Photosynthesis**, edited by George C. Papageorgiou and Govindjee, from Greece and USA. Thirty-one chapters, 820 pp, Hardcover, ISBN 978-1-4020-3217-2, Softcover ISBN 978-90-481-3882-1, eBook ISBN 978-1-4020-3218-9 [http://www.springer.com/life+sciences/biochemistry+%26+biophysics/book/978-1-4020-3217-2]
- **Volume 18 (2005): Plant Respiration: From Cell to Ecosystem,** edited by Hans Lambers and Miquel Ribas-Carbo, from Australia and Spain. Thirteen chapters, 250 pp, Hardcover ISBN 978-14020-3588-3, Softcover ISBN 978-90-481-6903-0, eBook ISBN 978-1-4020-3589-0 [http://www.springer.com/life+sciences/plant+sciences/book/978-1-4020-3588-3]
- **Volume 17 (2004): Plant Mitochondria: From Genome to Function**, edited by David Day, A. Harvey Millar and James Whelan, from Australia. Fourteen chapters, 325 pp, Hardcover, ISBN: 978-1-4020-2399-6, Softcover ISBN 978-90-481-6651-0, eBook ISBN 978-1-4020-2400-9 [http://www.springer.com/life+sciences/cell+biology/book/978-1-4020-2399-6]
- **Volume 16 (2004): Respiration in Archaea and Bacteria: Diversity of Prokaryotic Respiratory Systems,** edited by Davide

Zannoni, from Italy. Thirteen chapters, 310 pp, Hardcover ISBN 978-14020-2002-5, Softcover ISBN 978-90-481-6571-1, eBook ISBN 978-1-4020-3163-2 [http://www.springer.com/life+sciences/plant+sciences/book/978-1-4020-2002-5]

- **Volume 15 (2004): Respiration in Archaea and Bacteria: Diversity of Prokaryotic Electron Transport Carriers**, edited by Davide Zannoni, from Italy. Thirteen chapters, 350 pp, Hardcover ISBN 978-1-4020-2001-8, Softcover ISBN 978-90-481-6570-4 (no eBook at this time) [http://www.springer.com/life+sciences/biochemistry+%26+biophysics/book/978-1-4020-2001-8]
- **Volume 14 (2004): Photosynthesis in Algae**, edited by Anthony W. Larkum, Susan Douglas and John A. Raven, from Australia, Canada and UK. Nineteen chapters, 500 pp, Hardcover ISBN 978-0-7923-6333-0, Softcover ISBN 978-94-010-3772-3, eBook ISBN 978-94-007-1038-2 [http://www.springer.com/life+sciences/plant+sciences/book/978-0-7923-6333-0]
- **Volume 13 (2003): Light-Harvesting Antennas in Photosynthesis**, edited by Beverley R. Green and William W. Parson, from Canada and USA. Seventeen chapters, 544 pp, Hardcover ISBN 978-07923-6335-4, Softcover ISBN 978-90-481-5468-5, eBook ISBN 978-94-017-2087-8 [http://www.springer.com/life+sciences/plant+sciences/book/978-0-7923-6335-4]
- **Volume 12 (2003): Photosynthetic Nitrogen Assimilation and Associated Carbon and Respiratory Metabolism,** edited by Christine H. Foyer and Graham Noctor, from UK and France. Sixteen chapters, 304 pp, Hardcover ISBN 978-07923-6336-1, Softcover ISBN 978-90-481-5469-2, eBook ISBN 978-0-306-48138-3 [http://www.springer.com/life+sciences/plant+sciences/book/978-0-7923-6336-1]
- **Volume 11 (2001): Regulation of Photosynthesis,** edited by Eva-Mari Aro and Bertil Andersson, from Finland and Sweden. Thirty-two chapters, 640 pp, Hardcover ISBN 978-0-7923-6332-3, Softcover ISBN 978-94-017-4146-0, eBook ISBN 978-0-306-48148-2 [http://www.springer.com/life+sciences/plant+sciences/book/978-0-7923-6332-3]
- **Volume 10 (2001): Photosynthesis: Photobiochemistry and Photobiophysics,** authored by Bacon Ke, from USA. Thirty-six chapters, 792 pp, Hardcover ISBN 978-0-7923-6334-7, Softcover ISBN 978-0-7923-6791-8, eBook ISBN 978-0-306-48136-9 [http://www.springer.com/life+sciences/plant+sciences/book/978-0-7923-6334-7]
- **Volume 9 (2000): Photosynthesis: Physiology and Metabolism,** edited by Richard C. Leegood, Thomas D. Sharkey and Susanne von Caemmerer, from UK, USA and Australia. Twenty-four chapters, 644 pp, Hardcover ISBN 978-07923-6143-5, Softcover ISBN 978-90-481-5386-2, eBook ISBN 978-0-306-48137-6 [http://www.springer.com/life+sciences/plant+sciences/book/978-0-7923-6143-5]
- **Volume 8 (1999): The Photochemistry of Carotenoids,** edited by Harry A. Frank, Andrew J. Young, George Britton and Richard J. Cogdell, from USA and UK. Twenty chapters, 420 pp, Hardcover ISBN 978-0-7923-5942-5, Softcover ISBN 978-90-481-5310-7, eBook ISBN 978-0-306-48209-0 [http://www.springer.com/life+sciences/plant+sciences/book/978-0-7923-5942-5]
- **Volume 7 (1998): The Molecular Biology of Chloroplasts and Mitochondria in *Chlamydomonas*,** edited by Jean David Rochaix, Michel Goldschmidt-Clermont and Sabeeha Merchant, from Switzerland and USA. Thirty-six chapters, 760 pp, Hardcover ISBN 978-0-7923-5174-0, Softcover ISBN 978-94-017-4187-3, eBook ISBN 978-0-306-48204-5 [http://www.springer.com/life+sciences/plant+sciences/book/978-0-7923-5174-0]
- **Volume 6 (1998): Lipids in Photosynthesis: Structure, Function and Genetics**, edited by

Paul-André Siegenthaler and Norio Murata, from Switzerland and Japan. Fifteen chapters, 332 pp. Hardcover ISBN 978-0-7923-5173-3, Softcover ISBN 978-90-481-5068-7, eBook ISBN 978-0-306-48087-4 [http://www.springer.com/life+sciences/plant+sciences/book/978-0-7923-5173-3]

- **Volume 5 (1997): Photosynthesis and the Environment,** edited by Neil R. Baker, from UK. Twenty chapters, 508 pp, Hardcover ISBN 978-07923-4316-5, Softcover ISBN 978-90-481-4768-7, eBook ISBN 978-0-306-48135-2 [http://www.springer.com/life+sciences/plant+sciences/book/978-0-7923-4316-5]
- **Volume 4 (1996): Oxygenic Photosynthesis: The Light Reactions**, edited by Donald R. Ort and Charles F. Yocum, from USA. Thirty-four chapters, 696 pp, Hardcover ISBN 978-0-7923-3683-9, Softcover ISBN 978-0-7923- 3684–6, eBook ISBN 978-0-306-48127-7 [http://www.springer.com/life+sciences/plant+sciences/book/978-0-7923-3683-9]
- **Volume 3 (1996): Biophysical Techniques in Photosynthesis**, edited by Jan Amesz and Arnold J. Hoff, from The Netherlands. Twenty-four chapters, 426 pp, Hardcover ISBN 978-0-7923-3642-6, Softcover ISBN 978-90-481-4596-6, eBook ISBN 978-0-306-47960-1 [http://www.springer.com/life+sciences/plant+sciences/book/978-0-7923-3642-6]
- **Volume 2 (1995): Anoxygenic Photosynthetic Bacteria**, edited by Robert E. Blankenship, Michael T. Madigan and Carl E. Bauer, from USA. Sixty-two chapters, 1331 pp, Hardcover ISBN 978-0-7923-3682-8, Softcover ISBN 978-0-7923-3682-2, eBook ISBN 978-0-306-47954-0 [http://www.springer.com/life+sciences/plant+sciences/book/978-0-7923-3681-5]
- **Volume 1 (1994): The Molecular Biology of Cyanobacteria**, edited by Donald R. Bryant, from USA. Twenty-eight chapters, 916 pp, Hardcover, ISBN 978-0-7923-3222-0, Softcover ISBN 978-0-7923-3273-2, eBook ISBN 978-94-011-0227-8 [http://www.springer.com/life+sciences/plant+sciences/book/978-0-7923-3222-0]

Further information on these books and ordering instructions are available at http://www.springer.com/series/5599. Front matter of volumes 1–25 can also be found at <http://www.life.uiuc.edu/govindjee/photosynSeries/ttocs.html>.

Special 25 % discounts are available to members of the International Society of Photosynthesis Research, ISPR http://www.photosynthesisresearch.org/. See http://www.springer.com/ispr.

Future Advances in Photosynthesis and Respiration and Other Related Books

The readers of the current series are encouraged to watch for the publication of forthcoming books (not necessarily arranged in the order of future appearance).

- *Photosynthesis and Climate Change* (working title) (Editor Joy K. Ward)
- *Cyanobacteria* (Editor Donald Bryant)
- *Leaf Photosynthesis* (Editors William W. Adams III, Ichiro Terashima)
- *Photosynthesis in Algae* (Editors Anthony Larkum and Arthur Grossman)
- *Global Photosynthesis* (Editors Lianhong Gu et al.)
- *Plant Respiration: Metabolic Fluxes and Carbon Balance* (Editors Guillaume Tcherkez, Jaleh Ghashghaie)

In addition to the above-contracted books, the following topics are under consideration:

Algae, Cyanobacteria: Biofuel and Bioenergy
Artificial Photosynthesis
ATP Synthase: Structure and Function
Bacterial Respiration II
Carotenoids II
Evolution of Photosynthesis
Green Bacteria and Heliobacteria
Interactions between Photosynthesis and other Metabolic Processes
Limits of Photosynthesis: Where do we go from here?

Photosynthesis, Biomass and Bioenergy
Photosynthesis under Abiotic and Biotic Stress
Plant Respiration II

If you have any interest in editing/coediting any of the above-listed books, or being an author, please send an e-mail to Tom Sharkey (tsharkey@msu.edu) and/or to Govindjee at gov@illinois.edu. Suggestions for additional topics are also welcome.

We take this opportunity to thank and congratulate Kouki Hikosaka and his coeditors Ülo Niinemets and Niels Anten for their outstanding editorial work; they have done a fantastic job, not only in editing but also in organizing this book for all of us and for their highly professional dealing with the reviewing process. We thank all 25 authors of this book (see the contributor list); without their authoritative chapters, there would be no such volume. We give special thanks to Manjusha Nalamolu and S. Bhuvanalakshmi of SPi Global, India, for directing the typesetting of this book; their expertise have been crucial in bringing this book to completion. We owe thanks to Jacco Flipsen, Andre Tournois, Corina VanderGiessen and Ineke Ravesloot (of Springer) for their friendly working relation with us that led to the production of this book.

January 1, 2016

Thomas D. Sharkey
Department of Biochemistry
and Molecular Biology
Michigan State University
East Lansing, MI 48824, USA
tsharkey@msu.edu

Govindjee
Department of Plant Biology
Department of Biochemistry and Center
of Biophysics & Quantitative Biology
University of Illinois at Urbana-Champaign
Urbana, IL 61801, USA
gov@illinois.edu

Series Editors

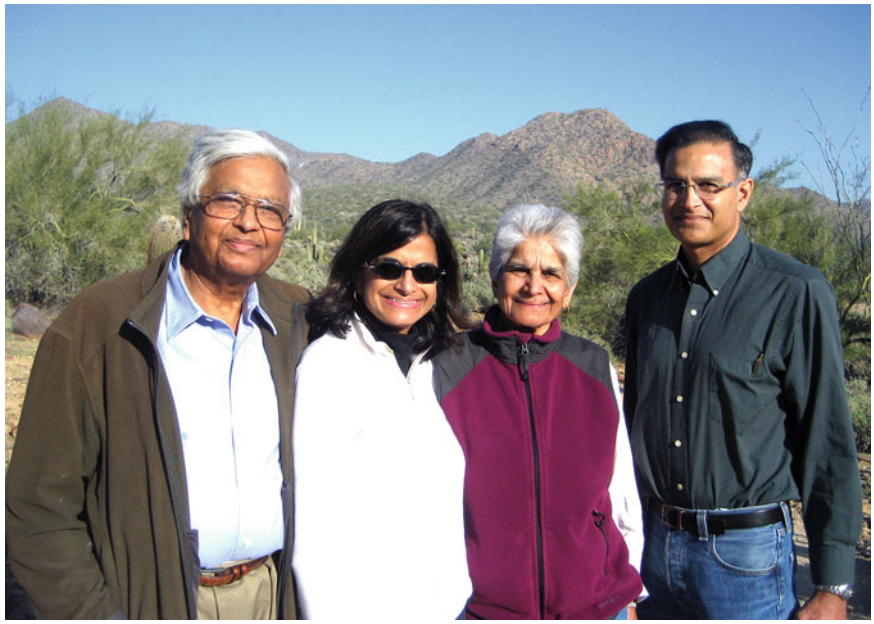

Left to right: Govindjee, Anita, Rajni, and Sanjay. Photo was taken in December 2014 in Arizona

Govindjee, who uses one name only, was born on October 24, 1932, in Allahabad, India. Since 1999, he has been professor emeritus of biochemistry, biophysics, and plant biology at the University of Illinois at Urbana-Champaign (UIUC), Urbana, IL, USA. He obtained his B.Sc. (chemistry, botany and zoology) and M.Sc. (botany, plant physiology) in 1952 and 1954, from the University of Allahabad. He studied "Photosynthesis" at the UIUC, under two giants in the field, Robert Emerson and Eugene Rabinowitch, obtaining his Ph.D. in 1960, in biophysics. He is best known for his research on excitation energy transfer, light emission (prompt and delayed fluorescence and thermoluminescence), primary photochemistry, and electron transfer in "photosystem II" (PS II, water-plastoquinone oxidoreductase). His research, with many collaborators, has included the discovery of a short-wavelength form of chlorophyll (Chl) *a* functioning in PS II; of the two-light effect in Chl *a* fluorescence; and, with his wife Rajni Govindjee, of the two-light effect (Emerson Enhancement) in NADP reduction in chloroplasts. His major achievements, together with several other researchers, include an understanding of the basic relationship between Chl *a* fluorescence and photosynthetic reactions; a unique role of bicarbonate/carbonate on the electron acceptor side of PS II, particularly in the protonation events involving the Q_B binding region; the theory of thermoluminescence in plants; the first picosecond measurements on the primary photochemistry of PS II; and the use of fluorescence lifetime imaging microscopy (FLIM) of Chl *a* fluorescence in understanding *photoprotection* by plants

against excess light. His current focus is on the "history of photosynthesis research", and in "photosynthesis education." He has served on the faculty of the UIUC for ~40 years.

Govindjee's honors include fellow of the American Association of Advancement of Science (AAAS); distinguished lecturer of the School of Life Sciences, UIUC; fellow and lifetime member of the National Academy of Sciences (India); president of the American Society for Photobiology (1980–1981); Fulbright scholar (1956), Fulbright senior lecturer (1997), and Fulbright specialist (2012); honorary president of the 2004 International Photosynthesis Congress (Montréal, Canada); the first recipient of the Lifetime Achievement Award of the Rebeiz Foundation for Basic Biology, 2006; and recipient of the Communication Award of the International Society of Photosynthesis Research, 2007; and of the Liberal Arts and Sciences Lifetime Achievement Award of the UIUC, (2008). Further, Govindjee has been honored **(1)** in 2007, through 2 special volumes of *Photosynthesis Research*, celebrating his 75th birthday and for his 50-year dedicated research in *Photosynthesis* (guest editor: Julian Eaton-Rye); **(2)** in 2008, through a special International Symposium on "Photosynthesis in a Global Perspective,", held in November 2008, at the University of Indore, India; **(3)** in 2012, through Volume 34 of this series *Photosynthesis - Plastid Biology, Energy Conversion and Carbon Assimilation*, edited by Julian Eaton-Rye, Baishnab C. Tripathy, and one of us (TDS); it was dedicated to him, celebrating his academic career; and (**4**) in 2013, through special issues of *Photosynthesis Research* (volumes 117 and 118) edited by Suleyman Allakhverdiev, Gerald Edwards and Jian-Ren Shen celebrating his 80th (or rather 81st) birthday. An additional honor was the celebration of his birthday in Třeboň, the Czech Republic (O. Prasil [2014] Govindjee, an institution, at his 80th [or rather 81st] birthday in Třeboň in October, 2013: A pictorial essay. Photosynth Res **122**: 113–119). His unique teaching of the Z-scheme of photosynthesis, where students act as different intermediates, was recently published (P.K. Mohapatra and N.R. Singh [2015] Teaching the Z-Scheme of electron transport in photosynthesis: a perspective. Photosynth Res **123**:105–114).

Govindjee is coauthor of a classic and popular book *Photosynthesis* (John Wiley, 1969; available free on his web site); he is editor (or coeditor) of many books, published by several publishers including Academic Press and Kluwer Academic Publishers (now Springer).

Since 2007, each year a Govindjee and Rajni Govindjee Award is being given to graduate students, by the Department of Plant Biology (odd years) and by the Department of Biochemistry (even years), at the UIUC, to recognize excellence in biological sciences. For further information on Govindjee, see his website at http://www.life.illinois.edu/govindjee.

Tom Sharkey, October 2012 in Taiwan

Thomas D. (Tom) Sharkey obtained his Bachelor's degree in biology in 1974 from Lyman Briggs College, a residential science college at Michigan State University, East Lansing, Michigan, USA. After 2 years as a research technician, Tom entered a Ph.D. program in the Department of Energy Plant Research Laboratory at Michigan State University under the mentorship of Klaus Raschke and finished in 1979. His postdoctoral research was carried out with Graham Farquhar at the Australian National University, in Canberra, where he coauthored a landmark review on photosynthesis and stomatal conductance. For 5 years he worked at the Desert Research Institute, Reno, Nevada. After Reno, Tom spent 20 years as professor of botany at the University of Wisconsin in Madison. In 2008, Tom became professor and chair of the Department of Biochemistry and Molecular Biology at Michigan State University. Tom's research interests center on the exchange of gases between plants and the atmosphere and carbon metabolism of photosynthesis. The biochemistry and biophysics underlying carbon dioxide uptake and isoprene emission from plants form the two major research topics in his laboratory. Among his contributions are measurement of the carbon dioxide concentration inside leaves, an exhaustive study of short-term feedback effects in carbon metabolism, and a significant contribution to elucidation of the pathway by which leaf starch breaks down at night. In the isoprene research field, Tom is recognized as the leading advocate for thermotolerance of photosynthesis as the explanation for why plants emit isoprene. In addition, his laboratory has cloned many of the genes that underlie isoprene synthesis and published many important papers on the biochemical regulation of isoprene synthesis. Tom has coedited three books, the first on trace gas emissions from plants in 1991 (with Elizabeth Holland and Hal Mooney) and then Volume 9 of this series (with Richard Leegood and Susanne von Caemmerer) on the physiology of carbon metabolism of photosynthesis in 2000 and Volume 34 (with Julian Eaton-Rye and Baishnab C. Tripathy) entitled *Photosynthesis*: *Plastid Biology*, *Energy Conversion and Carbon Assimilation*. Tom has been co-series editor of this series since Volume 31.

Contents

Part II: Physiological Processes from Leaves to Canopies

Part III: Whole-plant Processes in Leaf Canopies

Part IV: Assessments of Vegetation Functioning

Part V: Application to Ecological and Evolutionary Processes

Preface

A plant canopy, a collection of leaves, is an ecosystem-level unit of photosynthesis that assimilates carbon dioxide and exchanges other gases and energy with the atmosphere in a manner highly sensitive to ambient conditions including atmospheric carbon dioxide and water vapor concentrations, light and temperature, and soil resource availability. In addition to providing carbon skeletons and chemical energy for most of the living organisms, these key canopy functions affect global climate through modification of atmospheric carbon dioxide concentration and through altering surface albedo. This interaction, the climate-carbon cycle feedback, is one of the most uncertain processes for projection of future global climate.

Rapid increase in human population in combination with global change poses major challenges for human life on Earth. The population increase drives the need for enhanced food and (renewable) energy supply, while global change potentially entails negative impacts on plant productivity. Carbon dioxide assimilation by plant canopies is one of the most important determinants of food and energy crop yields. Thus, understanding canopy functioning is indispensable for establishing sustainable agricultural practices and for breeding of crops that would have higher productivity under future climate.

Canopy photosynthesis is an integration of various physical, chemical, and biological processes extending from molecular, cellular, and organ-level processes to turbulent transport. About a hundred years ago, Peter Boysen Jensen first determined canopy photosynthesis of a plant stand – though it was a tiny stand established in a small pot and demonstrated that the canopy photosynthetic rate is not simply a product of the leaf photosynthetic rate and the number of the leaves. He correctly argued that canopy photosynthesis is influenced not only by conditions above the canopy but also by canopy structure and by heterogeneity of the microclimate and of leaf traits within the canopy. Masami Monsi, Toshiro Saeki, Cornelis T. de Wit, John L. Monteith, William G. Duncan, and other early researchers have succeeded in integrating these complex processes into mathematical models capable of simulating canopy photosynthetic rate under changing environmental conditions. Advances in photosynthesis physiology and modeling studies improved our understanding and prediction of environmental responses of leaf-level gas exchange rates. In particular, modeling of Rubisco and electron transport processes (Graham D. Farquhar, Susanne von Caemmerer, and Joseph A. Berry) and linking photosynthesis and stomatal processes (J. Timothy Ball, Ian E. Woodrow, and Joseph A. Berry) were the key milestones that made it possible to simulate carbon dioxide responses of photosynthesis. These models are now essential parts of larger models for prediction and simulation of crop production, climate change, and regional and global carbon dynamics.

Advances in molecular techniques have helped clarify molecular mechanisms of morphogenesis and regulation in leaf canopies, though there still remain many uncertainties. On the other hand, meteorological studies have permitted estimates of gas and energy exchange in vegetation at a landscape scale. Remote sensing techniques have enabled us to evaluate vegetative functions at a global scale. One of the main challenges lies in quantitatively scaling between these levels of organization. Systems biology is evolving to address this but tends to regard the cellular level as the upper limit. There is a need to further develop this well beyond the current levels.

The development of leaf canopy studies has contributed to deeper understanding of other ecological phenomena. Photosynthesis provides both the energy and the carbon for growth, reproduction and other plant functions, while regulation of transpiration plays an important role in the water and temperature balance of plants. Plant gas exchange traits and their response to different growth conditions therefore have important adaptive values. Modeling of canopy gas exchange, thus, plays an increasingly important role in evolutionary ecological research. A particular issue of interest here has been competition for light between individuals as well as between species as this is one of the most important constraints influencing population density, stand biomass, species composition, and, in turn, biodiversity in plant communities. Canopy photosynthesis models have been a good tool to analyze light interception by individuals or by species in plant communities.

This book describes our current knowledge of canopy photosynthesis that has accumulated over the last hundred years since the pioneering study of P. Boysen Jensen. The book provides a comprehensive analysis of plant canopy physiology, ecology, and physics with emphasis on predictive modeling techniques. The book is divided into five parts covering the hierarchy of canopy processes in time and space. Two chapters in Part I discuss the basic physical processes on light attenuation and energy transfer in plant canopies, while three chapters in Part II deal with the principle mechanisms of leaf gas-exchange regulation and the patterns and mechanisms of variations in leaf traits. Three chapters in Part III focus on whole-plant processes in plant canopies. Part IV (in four chapters) describes how vegetation functions are assessed by modeling, eddy-covariance techniques, and remote sensing and forest inventory. Finally, three chapters in Part V discuss the relationships between canopy photosynthesis and other vegetation processes in plant stands.

The book is designed primarily for graduate students and beginning scientists interested in measuring and modeling vegetation performance, and we hope that it will help in raising a new generation of scientists who are fascinated by the challenge of understanding the varied functions of the canopy of plants. Thus, each chapter of the book describes the basic background of the specific topic and provides equations that are indispensable for its quantitative understanding. In fact, we believe that readers would even be able to construct their own canopy model based on the equations provided in this book. On the other hand, we hope that this synthesis is also beneficial to the mentors of these students and ecologists, foresters, crop physiologists, and agronomists broadly interested in improving crop productivity and simulating vegetation-climate feedbacks. We are of the opinion that being involved in canopy research is a highly stimulating, perspective-widening, and often an exciting experience.

All the chapters were peer reviewed by the editors, authors and/or ad hoc reviewers. We, the editors, especially thank all the reviewers and acknowledge by name the reviewers: Kohei Koyama, Martijn Slot, Kaoru Kitajima, Hisae Nagashima, and Yusuke Onoda. We also thank Govindjee and Tom Sharkey, series editors of *Advances in Photosynthesis and Respiration*, for their continuous advice and support through the preparation of this book.

We hope that this book will be useful not only to beginning scientists, in the field of canopy photosynthesis, but to teachers and researchers alike who are interested in solving the problem of plant productivity in the world for the benefit of all.

Kouki Hikosaka
Sendai, Japan

Ülo Niinemets
Tartu, Estonia

Niels P.R. Anten
Wageningen, The Netherlands

The Editors

Kouki Hikosaka (*center*) with his wife Hisae Nagashima (*left*), who is a plant ecologist and a reviewer, and their daughter Romi (*right*)

Kouki Hikosaka was born on January 25, 1968, in Odate, Akita, Japan. He was a high jumper when he was a student and the best record was 2m13cm in 1989. He received his bachelor of science degree in 1990 for nitrogen allocation between leaves in a plant canopy under the guidance of Professor Tadaki Hirose in the Department of Biology, Faculty of Science, Tohoku University, Japan. Subsequently, he studied nitrogen allocation not only between but also within leaves as a Ph.D. student under the guidance of Dr. Ichiro Terashima (a contributor to this volume) and Professor Sakae Katoh in the Department of Botany, Graduate School of Science, the University of Tokyo, Japan. He used a vine grown horizontally and manipulated the light environment of each leaf to assess effects of leaf age and light environment on leaf nitrogen content and photosynthetic characteristics separately. He constructed a mathematical model of optimal nitrogen partitioning in the photosynthetic apparatus and tested the optimality in actual plants. In addition, he studied photosynthetic nitrogen use efficiency, which is a key physiological trait for leaf economics spectrum, in species belonging to different functional groups and found that nitrogen allocation to Rubisco and Rubisco use efficiency vary among species. After receiving his Ph.D. in 1995, he returned to Tohoku University as an assistant professor in the laboratory of Professor Tadaki Hirose. Currently he is professor in the Graduate School of Life Sciences, Tohoku University.

His interests are diverse in scales from molecules to the globe, but always related

to ecological significance of plant functions. For biochemical levels, he has investigated how parameters of photosynthesis models respond to environmental change and how such changes are related to the improvement of resource use efficiency in biomass production under changing environment. For example, he has found that leaves alter the balance between carboxylation and regeneration of RuBP depending on growth temperature, which contributes to optimization of nitrogen use. He has also found that leaves, including canopy leaves in a deciduous forest, change temperature dependence of RuBP carboxylation rate depending on growth temperature, which causes a shift of optimal temperature of photosynthesis. For canopy levels, he has extended the optimal nitrogen allocation theory to leaf dynamics and has studied leaf dynamics in actual plants. He has also incorporated the game theory to canopy photosynthesis model to understand the role of light competition with neighbors in canopy productivity. Recently these two theories were combined in collaboration with Professor Niels Anten (coeditor of this volume). For population and community levels, he has analyzed photosynthetic production of an individual or species as the product of resource acquisition efficiency and resource use efficiency and is attempting to understand the roles of plant functional traits in competition and coexistence in a plant community. For global issues, he is attempting to improve the accuracy of the canopy photosynthesis scheme in global carbon flux simulations. He studies environmental response (including elevated CO_2 concentrations) and interspecific variation in parameters in canopy photosynthesis models with Dr. Akihiko Ito (a contributor in this volume) and other collaborators.

Ülo Niinemets after giving the inaugural lecture (Oratie) on the occasion of his appointment to F. C. Donders Chair at the Utrecht University in Autumn 2007

Ülo Niinemets was born on March 19, 1970, in Tartu, Estonia. In 1996, he was awarded a Ph.D. in plant ecophysiology from the University of Tartu, Estonia (adviser: Prof. Olevi Kull). At the time of his Ph.D., in the newly independent Estonia, the availability of research equipment was extremely limited, and his Ph.D. was focused on structural factors on shade tolerance of forest trees, a work that did not require much equipment. One of the main conclusions from this work was that foliage structure was a key controlling factor in determining species shade tolerance. As a broader message from this work, guiding his future studies was that structural factors are often as significant in affecting leaf photosynthetic capacity as photosynthetic potential of single cells. With all the new sophisticated equipment becoming available, researchers increasingly tend to forget structure, although it is central in understanding plant performance under stressful environment in the field.

As the research environment improved in independent Estonia, his research focus gradually shifted to more physiologically oriented work, especially on tree acclimation to within-canopy gradients. He initiated the Estonian forest tree acclimation project in 1994. Within this project, tall scaffoldings of 27 m were erected in a mixed deciduous forest in south-eastern Estonia, and acclimation of tree foliage photosynthetic characteristics, morphology, anatomy and chemistry to within-canopy light gradients were extensively investigated by him and his coworkers over several years. This work has resulted in detailed understanding of the overall extent of photosynthetic acclimation, structural, chemical, and physiological controls of acclimation and acclimation time constants. He is currently chair of the Department of Plant Physiology at the Estonian University of Life Sciences where his team focuses on quantification and predictive modeling of plant carbon gain and trace gas exchange from genes to leaves and from leaves to ecosystem, landscape, and biome scales under globally changing climates.

Apart from the work in Estonia, he has been very active internationally. He has conducted postdoctoral work at the University of Bayreuth, Germany, where he initiated the development of process-based isoprenoid emission models; at the University of Antwerp, Belgium, where he studied physiological controls of species invasions; and at the Centro di Ecologia Alpina, Trento, Italy, where he investigated structural controls of mesophyll diffusion conductance. His international faculty appointments include: Erskine Fellow (2002, Canterbury

University, New Zealand), annual G. P. Wilder Chair (2006–2007, University of Hawaii, U.S.A.), and F. C. Donders Chair (Utrecht University, the Netherlands). He has collaborated with more than 550 scientists from 44 countries and has (co-)authored more than 250 international articles and book chapters. He currently serves the community as an editor or as editorial board member of international plant science journals such as *Tree Physiology, Oecologia, Frontiers in Plant Science, AoB Plants, Journal of Plant Research,* and *Plant, Cell and Environment and* Springer *Tree Physiology* book series as well as a board member of several international research programs and science policy committees such as the Scientific Committee for Life, Environmental and Geo Sciences (LEGS) of Science Europe.

Niels Anten enjoying a cold autumn morning in Limburg in the south of The Netherlands

Niels P.R. Anten was born on May 14, 1966, in Bukumbi, Tanzania. He spent a large part of his childhood in Tanzania and Nepal and enjoyed the spectacular nature of those countries, but also became acquainted with their challenges in sustainably producing food. Probably not surprisingly he then spent a career zigzagging between crop science and ecology of natural plant systems. Niels completed his masters, in 1990, in Tropical Crop Science at Wageningen University, the Netherlands, where among other things he had the privilege to do his thesis on modeling cocoa growth with Prof. Jan Goudriaan (author of Chap. 1) and Prof. Marius Wessel. He then went on to do a Ph.D. in plant ecology at Utrecht University under the guidance of Prof. Marinus J.A. Werger and Prof. Ernesto Medina (IVIC, Venezuela) studying nitrogen use at the canopy level of C_3 and C_4 plants in Venezuela. In 1995, he obtained his Ph.D. with honors. He then went on to do a postdoc with Prof. Tadaki Hirose at Tohoku University in Japan, studying competition and species coexistence in Japanese grasslands. Here he also started a close collaboration with Prof. Kouki Hikosaka (coeditor of this book). After Japan, Prof. David Ackerly invited Niels to do a postdoc with him at Stanford University, USA, studying the sustainable harvesting of non-timber forest products in Mexico. After another stay at Tohoku University, in 2002, he obtained a tenured position at Utrecht University, where he stayed until 2012, when he took his current position as professor in Crop and Weed Ecology at the Centre of Crop Systems Analysis, Wageningen University.

Niels' main research line is the analysis of how emerging properties at the level of natural or agricultural plant communities, e.g., vegetation structure, productivity and species diversity, arise from basic physiological processes and plant functional traits. He pursues this scaling question through a combination of computer modeling, experiments and field observations and builds this work from basic optimization and game theories, as well as from disciplines of engineering. He uses this approach not only to understand the ecological interaction that drives the functioning of natural plant communities but increasingly also to see how this, in turn, can be applied to (semi-)agricultural systems. Based on game theory, he has worked with the idea that natural selection tends to lead to plant communities that are non-optimal in the sense of maximum per unit land area production, a so-called tragedy of the commons. This in turn, he hopes, would provide ideas for crop breeding or crop management. Similarly, newer concepts about diversity effects on plant community functioning in natural systems may provide ideas for highly productive diverse cropping

systems. His analyses increasingly incorporate vegetation-climate feedbacks and how these in turn are mediated by plant competition. New directions of his work involve plant-insect and plant-pathogen interactions as well as the links between below and aboveground plant-plant interactions.

Contributors

Niels P.R. Anten
Crop and Weed Ecology, Centre for Crop Systems Analysis, Wageningen University, Wageningen, The Netherlands
niels.anten@wur.nl

Lammert Bastiaans
Crop and Weed Ecology, Centre for Crop Systems Analysis, Wageningen University, P.O. Box 430, 6700 AK Wageningen, The Netherlands
lammert.bastiaans@wur.nl

Mieke de Wit
Centre for integrative genomics, Faculty of biology and medicine, University of Lausanne, CH-1015 Lausanne, Switzerland
mieke.dewit@unil.ch

Mathias Disney
Department of Geography, University College London, Gower Street, London WC1E 6BT, UK

NERC National Centre for Earth Observation,
ylo.niinemets@emu.ee

Jochem B. Evers
Centre for Crop Systems Analysis, Wageningen UR, Droevendaalsesteeg 1, Wageningen 6708 PB, The Netherlands
jochem.evers@wur.nl

Jan Goudriaan
Department of Plant Science, Plant Production Systems Group, Wageningen University, P.O. Box 430, 6700 AK Wageningen, The Netherlands
jangouds@xs4all.nl

Vincent P. Gutschick
Global Change Consulting Consortium, Inc., Las Cruces, NM 88011, USA
vinceg@gcconsortium.com

Kouki Hikosaka
Graduate School of Life Sciences, Tohoku University, Aoba, Sendai 980-8578, Japan

CREST, JST, Tokyo, Japan
hikosaka@m.tohoku.ac.jp

Yasuo Iimura
School of Environmental Science, The University of Shiga Prefecture, Hikone, Shiga 522-8533, Japan
iimura.y@ses.usp.ac.jp

Akihiko Ito
National Institute for Environmental Studies, Tsukuba, Ibaraki 305-8506, Japan
itoh@nies.go.jp

Kihachiro Kikuzawa
Ishikawa Prefectural University, Nonoichi, Japan, Onoecho 14-16, Zushioku, Yamashina, Kyoto 607-8453, Japan
kkikuzawa@kyoto.zaq.jp

Hiroshi Koizumi
Faculty of Education and Integrated Arts and Sciences, Waseda University, Shinjuku, Tokyo 162-8480, Japan
hkoizumi@waseda.jp

Tomo'omi Kumagai
Institute for Space-Earth Environmental, Nagoya University, Chikusa-ku, Nagoya 464-8601, Japan
tomoomikumagai@gmail.com

Martin J. Lechowicz
Department of Biology, McGill University, 1205 Avenue Dr. Penfield, Montréal, QC H3A 1B1, Canada
martin.lechowicz@mcgill.ca

Katherine A. McCulloh
Department of Botany, University of Wisconsin-Madison, Madison, WI 53705, USA
kmcculloh@wisc.edu

Frederick C. Meinzer
USDA Forest Service, Forestry Sciences Laboratory, Corvallis, OR 97331, USA
rick.meinzer@oregonstate.edu

Hiroyuki Muraoka
River Basin Research Center, Gifu University, Gifu, Gifu 501-1193, Japan
muraoka@green.gifu-u.ac.jp

Ülo Niinemets
Estonian University of Life Sciences, Kreutzwaldi 1, 51014 Tartu, Estonia

Estonian Academy of Sciences, Kohtu 6, 10130 Tallinn, Estonia
ylo.niinemets@emu.ee

Ko Noguchi
School of Life Sciences, Tokyo University of Pharmacy and Life Sciences, 1432-1, Horinouchi, Hachioji, Tokyo 192-0392, Japan
knoguchi@toyaku.ac.jp

Toshiyuki Ohtsuka
River Basin Research Center, Gifu University, Gifu, Gifu 501-1193, Japan
toshi@green.gifu-u.ac.jp

Ronald Pierik
Plant Ecophysiology, Institute of Environmental Biology, Utrecht University, Padualaan 8, Utrecht 3584 CH, The Netherlands
r.pierik@uu.nl

Thijs L. Pons
Department Plant Ecophysiology, Institute of Environmental Biology, Utrecht University, Padualaan 8, Utrecht 3508 CH, Netherlands
T.L.Pons@uu.nl

Nobuko Saigusa
Center of Global Environmental Research, National Institute for Environmental Study, Tsukuba, Ibaraki 305-8506, Japan
n.saigusa@nies.go.jp

Ichiro Terashima
School of Science, The University of Tokyo, Hongo, Bunkyo-ku, Tokyo 113-0033, Japan
itera@bs.s.u-tokyo.ac.jp

David R. Woodruff
USDA Forest Service, Forestry Sciences Laboratory, Corvallis, OR 97331, USA
dwoodruff@fs.fed.us

Author Index

Part I

Physical Processes in Leaf Canopies

Chapter 1

Light Distribution

Jan Goudriaan*
Department of Plant Science, Plant Production Systems Group, Wageningen University, Wageningen, The Netherlands

Summary

This chapter describes (1) how light distributes within a leaf canopy and (2) light interception by leaves. Basic equations are shown so that readers can make light distribution models by themselves.

Keywords Leaf angle • Solar angle • Scattering • Direct and diffuse light • Leaf spatial distribution (regular, random, and cluster)

*Author for correspondence, e-mail: jangouds@xs4all.nl

K. Hikosaka, Ü. Niinemets, and N.P.R. Anten (eds.), *Canopy Photosynthesis: From Basics to Applications*, DOI 10.1007/978-94-017-7291-4_1

I. Incoming Radiation

A. Its Total Value

The total flux of natural daylight at ground level is called Global Radiation. Outside the atmosphere the energy flux from the sun through one square meter, measured in a perpendicular position towards the solar rays, is about 1370 W m^{-2} (Monteith and Unsworth 1990). This number is called the solar 'constant' although it is not really a constant. Most of its variation is due to the eccentricity of the earth's orbit around the sun which causes a regular annual variation of the flux of 3.3 % above and below its average value. The solar output itself has a much smaller variation, mainly due to sunspots.

The flux that reaches the earth surface is, of course, dominated by the day-night regime, but also it is strongly affected by absorption in the atmosphere. Absorption of ultraviolet radiation by ozone in the stratosphere weakens the flux by about 25 %. As a result, Global Radiation at ground level has a maximum of about 1000 W m^{-2} which should still be multiplied by the sine of solar height (or to the cosine of zenithal distance) to get the intensity at a horizontal ground surface. Cloudy conditions will further reduce the Global Radiation.

In contrast to the solar constant and the sine of solar height, atmospheric transmission cannot be accurately predicted. Generally it varies between about 0.2 and 0.7, but it may occasionally wander outside this range. Atmospheric transmission is really a climatic variable and it must therefore be continuously measured if we want to know its value at all times, and this is also the case in Global Radiation.

B. Spectral Energy Distribution

The spectral properties of leaves permit us to work with only three major wavebands (McCree 1981; Gausman and Allen 1973; Gates 1980): Ultraviolet Radiation (UV) (about 4 %) between 350 and 400 nm, Photosynthetically Active Radiation (PAR) (about 50–60 %) between 400 and 700 nm and Near Infrared Radiation (NIR) (about 40 to 45 %) between 700 and 2000 nm (Fig. 1.1). Outside the atmosphere the fraction of PAR is equal to 0.368, which means a solar constant for PAR at 504 W m^{-2}. At ground level, the maximum level of PAR is reduced but not to the same extent as that of NIR and particularly of UV, resulting in a higher fraction of PAR at ground level than outside the atmosphere. Leaves absorb UV almost completely, but NIR is strongly scattered. The chlorophyll pigment, which is the most important pigment in leaves, is translucent to NIR. These facts enable a strong simplification in modelling radiation absorption in green crops. It is normally not needed to distinguish dozens of different waveband regions, but it is sufficient to just lump all PAR and lump all NIR radiation, so that we end up with only two major radiation

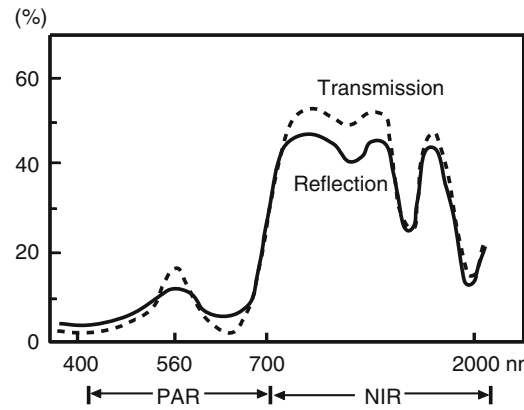

Fig. 1.1. Typical spectral distribution of reflection and transmission of a green leaf

Abbreviations: F – Fraction; h – Height; I_c – Absorbed flux per leaf area; I_d – Downward flux; I_u – Upward flux; k – Light extinction coefficient; k' – Light extinction coefficient for "black" leaves; L – Cumulative amount of leaf area per unit soil area; L_t – Total amount of leaf area per unit soil area; LAI – Leaf area index; N – Sky radiance; n – Layer; NIR – Near infrared radiation; p – Path width; PAR – Photosynthetically active radiation; r – Radius; S – Soil surface; T – Temperature in Kelvin; UOC – Uniform overcast sky; UV – Ultraviolet radiation; w – Width; α – Azimuth; β – Solarelevation; ζ – Angle between leaf normal and solar ray; ρ – Reflection coefficient; λ – Leaf angle; σ – Scattering coefficient; τ – Transmission coefficient

bands in the solar spectrum. Light is the term that is usually reserved for visible radiation and it is practically identical to PAR. The most common leaf color is green, which means that leaves scatter more green light than blue and red light (Fig. 1.1). Radiation outside these boundaries is not visible nor does it have any photosynthetic effects but it still carries energy. As noted, NIR represents an energy flux of similar magnitude to that of visible radiation.

Remarkably, in non-succulent plants leaf reflection and transmission are of similar magnitude, both in the PAR and in the NIR region, although leaf color is stronger in transmission than in reflection. Unlike transmission, leaf reflection contains a colorless component of about 4 % of direct reflection on the cuticular surface. After passage through the cuticula the radiation is partly absorbed and scattered into all directions, both as transmitted and as reflected radiation.

Values for leaf reflection and leaf transmission are about 0.1 and 0.4 for PAR and NIR respectively. This means that leaf scattering is about 0.2 and 0.8 in PAR and NIR respectively for non-senescent leaves, though the former value may differ somewhat between and within species depending on e.g. leaf thickness, anatomy and cholorophyll content (Lambers et al. 1998).

C. Directional Distribution

If light has a direction, what then is its direction? It is obvious for solar beams. The position of the sun at the sky can be precisely calculated, both in terms of solar elevation and azimuthal position (compass position), which is expressed as the angular distance with respect to the south, measured in clockwise direction. Therefore, in the northern hemisphere, north of the Tropics, the azimuth will be negative in the morning, pass through zero around noon and be positive at sunset. For the calculation of the solar azimuth and solar elevation, see Box 1.1. The algorithm, given in this Box, is also valid for the southern hemisphere and for the tropical regions (Goudriaan and Van Laar 1994).

Box 1.1: Solar Coordinates

Maximum solar declination is equal to the latitude of the tropics:

$$\delta_{\max} = 23.44\pi/180 \qquad \text{(B1.1.1)}$$

Sine and cosine of solar declination δ depend on day number t_{day} counted from 1 January onwards:

$$\sin\delta = -\sin\delta_{\max}\cos\left[\frac{2\pi\left(t_{\text{day}}+10\right)}{365.24}\right] \qquad \text{(B1.1.2a)}$$

$$\cos\delta = \sqrt{1-\sin^2\delta} \qquad \text{(B1.1.2b)}$$

Intermediate variables a and b dependent on local latitude λ and solar declination δ

$$a = \sin\lambda\sin\delta \qquad \text{(B1.1.3a)}$$

$$b = \cos\lambda\cos\delta \qquad \text{(B1.1.3b)}$$

Daylength D_L expressed in hours:

$$D_L = 12\left[1+\frac{2\arcsin\frac{a}{b}}{\pi}\right] \qquad \text{(B1.1.4)}$$

Sine and cosine of solar elevation β, dependent on solar time t_h (hr):

$$\sin\beta = a + b\cos\frac{2\pi(t_h-12)}{24} \qquad \text{(B1.1.5a)}$$

$$\cos\beta = \sqrt{1-\sin^2\beta} \qquad \text{(B1.1.5b)}$$

Cosine of solar azimuth α_s:

$$\cos\alpha_s = \frac{\sin\beta\sin\lambda-\sin\delta}{\cos\beta\cos\lambda} \qquad \text{(B1.1.6a)}$$

$$\alpha_s = -\arccos(\cos\alpha_s) \quad \text{if } t_{\text{h}} < 12 \qquad \text{(B1.1.6b)}$$

$$\alpha_s = \arccos(\cos\alpha_s) \quad \text{if } t_{\text{h}} > = 12 \qquad \text{(B1.1.6c)}$$

The apparent size of the solar disc is very small, about half a degree in diameter, so that the solar rays are practically all parallel and we may consider the solar disc as a point source of light. Objects will then cast shadows with well-defined outlines. Diffuse light coming from other parts of the sky will enter the shaded areas and is additional to the light coming directly from the solar disc. Very small or narrow leaves, such as conifer needles, do not cast full shade on lower leaves if they are far enough apart. They are then too small to mask the solar disc completely. A rigid treatment of this partial shade (penumbra) is outside the scope of this study. A practical approximation is to consider part of the direct sunlight as diffuse radiation, in other words to increase the fraction of diffuse radiation.

Observed values of the fraction diffuse versus direct radiation are often not available, and one should then use statistical approximations, for instance on the basis of daily radiation sums (Spitters et al. 1986). The diffuse sky radiation can be measured by carefully shielding the sun using a small disc mounted on a thin bar. Ideally there should be no other shading objects that stand out above the horizon in order to make sure that the radiometer receives all radiation from the hemisphere of the sky except direct solar radiation. However, in this way we can only measure the total diffuse radiation, not how the radiance is distributed over the sky dome. As a first guess the radiance is often assumed to be uniform, the Uniform Overcast Sky (UOC) (Monteith and Unsworth 1990). In this situation azimuth does not matter. The contribution of a sky portion is proportional to the sine of its elevation (or cosine of its zenith angle) and to its size which is expressed in solid angles. In plane geometry the unit for an angle of a portion of a circle is a radian, defined as the ratio between the arc and its radius. Similarly, for an area on a sphere the unit for its size (its "solid angle" expressed in steradians, sr) is given by the ratio between the area on the sphere and the radius squared of this sphere. In this way the value of the solid angle is dimensionless and does not depend on the size of the sphere itself.

D. Radiance and Irradiance

Irradiance is an energy flux that enters a surface and it is expressed in J s^{-1} m^{-2} or in W m^{-2}. Global Radiation, mentioned above, is an example. If it is confined to a spectral region, for instance UV, it is still an Irradiance, but with the specification UV Irradiance. Radiance refers to the brightness of the radiating surface and indicates the energy flux that is emitted per unit surface area per unit solid angle. For an isotropically radiating surface, the radiance is independent of the angle of view. The solid angle of a hemisphere is equal to 2π sr. If the sky has a radiance with a value N W m^{-2} sr^{-1}, what will then be the corresponding irradiance on the ground surface? If we consider a small portion of the sky located at elevation β and azimuth α, and with a very small height $d\beta$ and width $d\alpha$, its solid angle will be $\cos\beta\, d\alpha\, d\beta$. Its contribution to the irradiance at the ground will be equal to N times $\sin\beta\, \cos\beta\, d\alpha\, d\beta$. The cosine factor arises from the fact that the sky portions will get narrower towards the zenith and the sine factor arises from the angle of incidence effect. Now, let us extend the small portion all over the azimuth from 0 to 2π, because azimuth does not matter anyway. We then have an annular sky zone at elevation α and with a solid angle $2\pi\, \cos\beta\, d\beta$ and consequently contributing $N2\pi\, \sin\beta\, \cos\beta\, d\beta$ to the ground irradiance. In order to find the total irradiance from a homogeneous dome with radiance N we have to integrate this value over a range for β from 0 to $\pi/2$. Elementary calculus shows that the result is equal to πN. This somewhat strange result reminds us to the fact that the unit of irradiance is W m^{-2} whereas the unit of radiance is W m^{-2} sr^{-1}. To give an example, if the global radiation under a UOC is equal to 100 W m^{-2}, the radiance of the UOC is equal to 31.83 W m^{-2} sr^{-1}. It is interesting to compare this value to that of the solar disc. The solar disc has a diameter of half a

degree. Its solid angle is therefore equal to $0.0598\ 10^{-3}$ sr (you can check this). Outside the atmosphere the solar irradiance is equal to 1370 W m^{-2} and therefore the radiance of the solar surface is equal $22.9\ 10^{6}$ W m^{-2} sr^{-1}. Imagine the whole sky to be as bright as the naked sun, the irradiance would then be equal to 72 MW m^{-2} ! This value is also equal to the outgoing radiation flux at the solar surface. Using the equation for thermal blackbody radiation ($\sigma\ T^4$, where T is temperature in Kelvin) we can calculate a thermal radiative temperature of 5970 K, not too far from the observed value of the temperature of the solar surface of 5778 K (p. 84 in Phillips 1992).

II. Modelling Radiation in Leaf Canopies

We are going to develop a mathematical model for the absorption and scattering of radiation in leaf canopies. We will find expressions for the reflection and transmission by a leaf canopy as a whole, and also for the distribution of irradiation of individual leaves. Leaves differ in place and orientation and therefore their irradiation and absorption should be a function of their position in the leaf canopy and of their orientation towards the sun. These expressions for radiation absorption per leaf area are needed for the calculation of photosynthesis and transpiration, first for individual leaves, and by integration of the leaf rates also for the whole canopy. The expressions for leaf absorption will be continuous functions of canopy depth where the latter is usually defined as the cumulative amount of of leaf area per unit soil area (Leaf Area Index, LAI) above a given point (Monsi and Saeki 1953). Because of the distinct character of direct light, the functions will be different for sunlit and shaded leaves.

We will now gradually derive such expressions, starting with a simple model situation of black horizontal leaves

A. Black Horizontal Leaves

A thin layer of non-overlapping horizontal leaves with an area of ΔL m^2 leaf per m^2 of ground area will intercept a same fraction ΔL of the incoming radiation so that the fraction transmitted will be equal to $1 - \Delta L$. If there are many layers of leaves, the positioning of leaves in each subsequent layer is supposed to be independent of that in other layers so that each subsequent layer will reduce the transmission by the same fraction $1 - \Delta L$ (Fig. 1.2). If there are n such layers, one below the other, with leaf positioning at random, the downward flux just under layer n will be given by:

$$I_{d,n} = I_{d,0}(1 - \Delta L)^n \tag{1.1}$$

where $I_{d,n}$ is the downward flux after n layers, and $I_{d,0}$ is the downward flux above the crop.

Of course, the area of all leaf layers together is equal to $n\Delta L$. So far, we have considered leaves to be spaced in discrete layers but it is more realistic to assume that the leaves are homogeneously distributed. We can represent this situation by increasing the number of layers while proportionally reducing the area per layer, so that the total leaf area L is kept the same. We can write the number of layers n as the ratio $L/\Delta L$:

$$I_d = I_{d,0}(1 - \Delta L)^{\frac{L}{\Delta L}} \tag{1.2}$$

When ΔL approaches zero (and the number of layers (n) becomes very large), this expression becomes:

$$I_d = I_{d,0}\exp(-L) \tag{1.3}$$

Here, the depth (L) in the canopy represents the leaf area above the level considered, varying between zero and the total LAI. The radiation flux that reaches the soil surface can be found by substituting the value of the LAI.

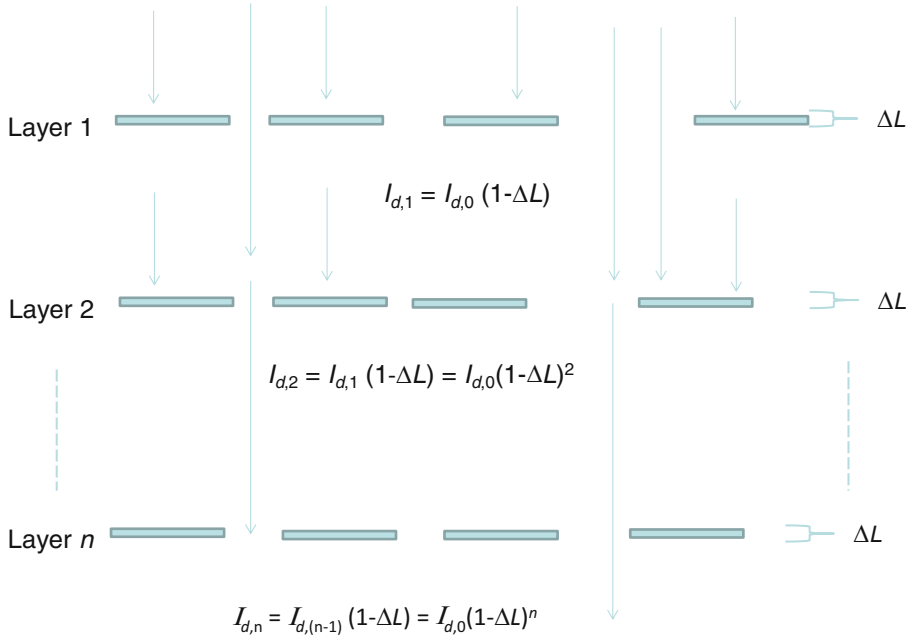

Fig. 1.2. Scheme of leaf layers and fluxes of downward and upward radiation in a model canopy with a horizontal leaf angle distribution

B. Non-horizontal Leaves

It is an exception that all leaves are horizontal. The size of the shade cast on an underlying horizontal surface is normally not identical to the area of the shading leaf but it will differ by a factor k. For a direct beam and a single leaf orientation, the value of k will be equal to $\cos(\zeta)/\sin(\beta)$ (Fig. 1.3), in which ζ stands for the angle between the leaf normal and the solar rays and β stands for the angle between the horizon and the solar rays ("solar elevation"). By the same procedure as given earlier for horizontal leaves the equation for exponential extinction now becomes

$$I_d = I_{d,0}\exp(-kL) \qquad (1.4)$$

Because of its function as a multiplier in the expression for extinction, k is generally called *extinction coefficient*. The theoretical extinction coefficient for a leaf canopy with leaves with different leaf orientations can be found by weighted addition of the values of $\cos(\zeta)$ for the different leaves weighted for their presence in the leaf angle distribution.

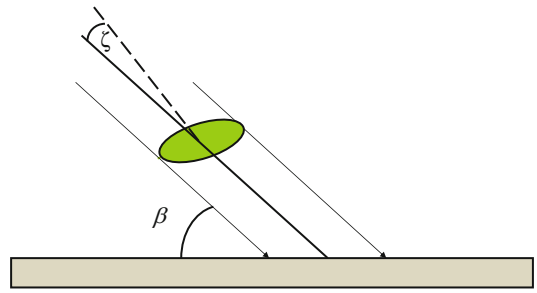

Fig. 1.3. A flat leaf, inclined with angle ζ with respect to the solar rays. The sun has an elevation angle β. The size of the shade on the ground is equal to the size of the leaf multiplied by $\cos\zeta/\sin\beta$

The exponential extinction equation is a powerful approximation of real-world radiation profiles in plant canopies. However, the conditions for which it was derived are never satisfied in practice. Therefore, empirical values of k, which can be obtained by fitting this equation to observed values of I_d versus L, may vary considerably in a range between 0.5 and 1. The physical meaning of k is the

average absorbed radiation per leaf area as a fraction of the downward radiation flux at the same canopy depth. For low solar elevation, the irradiation of the leaves may largely exceed the irradiation of a horizontal surface, so that the value of k may then be larger than unity, especially when the leaves have a dominant upright position. The description of leaf angle distribution and its effect follows next.

C. Leaf Angle Distribution

The orientation of a single leaf can be specified by its normal, the vector perpendicular to the leaf surface, for which we need its inclination above the horizon and also its azimuth. For a horizontal leaf the normal points towards the zenith and no azimuth is needed, but in general we need the compass direction (azimuth) of the leaf normal as well, for instance West. Figure 1.3 is drawn such that the azimuthal direction of the leaf normal is precisely towards the sun, but this is in general not the case. Any orientation is possible and a full description of the leaf angle distribution consists of its statistical distribution over inclination and azimuth. We now make the important simplifying assumption that the leaves do not have an azimuthal preference, in other words they are not preferentially oriented towards a certain compass direction, even though they may have a fixed inclination with respect to the horizon. The second simplifying assumption is that their distribution of inclination is the same as that of the surface elements of a sphere. This distribution is known by different names that all mean the same thing: the spherical –, the isotropic – and the random leaf angle distribution respectively (de Wit 1965; Ross 1981). In crop science it is customary to refer to the leaf angle by the inclination of its surface, not to that of its normal. Therefore the leaf angle λ of a vertically standing leaf is set at 90° ($\pi/2$ radians), although its normal is in fact horizontal. Using this convention, the density distribution of a spherical leaf angle distribution is given by $\cos(\lambda)$, in accordance to the fact that the density of the surface elements of a sphere per inclination angle decreases towards the top of the sphere.

When illuminated by a direct beam, a sphere intercepts an area that is identical to its largest cross-section, which is a quarter of the external sphere surface area. The total area intercepted by leaves with a spherical leaf angle distribution, however, is not a quarter but half of the leaf area because the leaves are initially considered not to shade each other. We could think of them as of the fragments of a shattered sphere that keep their original orientation wherever they may be. Now the ratio between the total leaf area and the corresponding shade area is identical to that of a hemisphere that is oriented towards the sun. At a solar elevation β, the shade that a hemisphere, precisely oriented towards the sun, casts on a horizontal ground surface, is equal to $0.5/\sin(\beta)$ times its own area (Fig. 1.4). This ratio $0.5/\sin(\beta)$ gives also the value of the extinction coefficient for black leaves with a spherical leaf angle distribution. It varies between 0.5 when the sun is in zenith, passing through 1 when the sun is at 30° elevation and getting infinitely large when the sun reaches the horizon. The canopies of several plant species have leaf angle distributions that are indeed approximately spherical (e.g. maize and sorghum), but other plant species (e.g. many grasses and Eucalyptus) tend to have more vertically inclined leaves whereas other species have more horizontal ones. The above concept of a sphere can be extended to an ellipsoid whose height to width ratio reflects the extent to which leaves are vertically inclined.

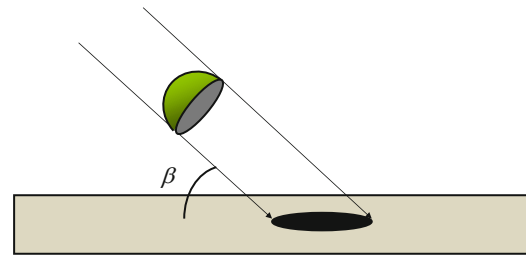

Fig. 1.4. For a spherical leaf angle distribution the relative size of the shade is equal to $1/(2\sin\beta)$

A description of that model can be found in Campbell (1990).

For purposes of calculation of canopy photosynthesis, a resolution of leaf angle distribution into just three equally spaced classes of leaf angle between 0 and 90° is sufficient (Goudriaan 1988).

D. Leaf Scattering and Canopy Reflection

Leaves are not black, which means that they reflect and transmit some of the radiation that they receive. The fraction that they reflect is called leaf reflection coefficient and the fraction that they transmit is called leaf transmission coefficient. Reflection and transmission together is called scattering. Conservation of energy requires that the sum of reflection, transmission and absorption is equal to incident radiation. When radiation is scattered by leaves it may be reabsorbed by other leaves but it may also disappear towards the sky or to the soil surface. Normally the radiation level decreases downward in a crop canopy. The soil will also receive some radiation and reflect some of it. The theory of the relation between leaf scattering and the resulting radiation profile in the canopy, and between the leaf scattering and the reflection coefficient of the canopy as a whole is based on the work of Kubelka and Munk (1931), who have written an analysis of radiation absorption and scattering in homogeneous substances such as paint. Their analysis can be applied to leaf canopies. In the most concise version of their analysis there is only one layer of leaves above a soil surface that has a reflection coefficient ρ_{soil}. The leaves are horizontal and non-overlapping, similar to the situation presented above for black leaves. They are all at precisely the same height so that they do not shade each other. Their total area is ΔL m^2 leaf per m^2 of ground area. Reflection by leaves and soil and also transmission by leaves is assumed to be independent of the direction of the incident radiation. With these assumptions there are just two directions of radiation

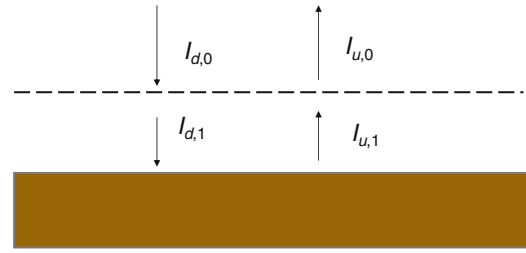

Fig. 1.5. A very sparse leaf canopy with only one layer above a soil surface. The incoming flux $I_{d,0}$ is the starting point for the calculation of the transmitted and reflected fluxes

flux, one downward and one upward (the "two-stream simplification") as shown in Fig. 1.5.

Out of the incoming downward radiation $I_{d,0}$,the leaves intercept a fraction $k'\Delta L$. The apostrophe is used to indicate the k value for non-scattering, thus for interception only. Subsequently a fraction τ_{leaf} will be scattered downward and a fraction ρ_{leaf} will be scattered upward. Transmitted and scattered fluxes together constitute a downward flux $I_{d,1}$ under the leaf layer, of which the underlying soil surface reflects a fraction ρ_{soil}. The upward flux $I_{u,1}$ between the soil surface and the leaf layer is therefore given by ρ_{soil} times $I_{d,1}$. A fraction $1 - k'\Delta L$ of this intermediate upward flux will pass the leaf layer immediately but a fraction ρ_{leaf} out of the complementary fraction $k'\Delta L$ will be reflected back to the soil surface and likewise a fraction τ_{leaf} will be transmitted towards the sky. The two downward and the two upward fluxes are related by equations that are now known as the Kubelka-Munk equations. Using our symbols we have for the intermediate fluxes $I_{d,1}$ and $I_{u,1}$:

$$I_{d,1} = \left[1 - k'\Delta L(1 - \tau_{\text{leaf}})\right] I_{d,0} + k'\Delta L \rho_{\text{leaf}} I_{u,1} \tag{1.5a}$$

$$I_{u,1} = \rho_{\text{soil}} I_{d,1} \tag{1.5b}$$

These two linear equations with the two unknowns $I_{d,1}$ and $I_{u,1}$ can be solved by

algebraic elimination of the unknowns, which gives:

$$I_{d,1} = \frac{\left[1 - k^{'}\Delta L(1-\tau_{\text{leaf}})\right] I_{d,0}}{1 - k^{'}\Delta L \rho_{\text{leaf}} \rho_{\text{soil}}} \tag{1.6a}$$

$$I_{u,1} = \rho_{\text{soil}} \frac{\left[1 - k^{'}\Delta L(1-\tau_{\text{leaf}})\right] I_{d,0}}{1 - k^{'}\Delta L \rho_{\text{leaf}} \rho_{\text{soil}}} \tag{1.6b}$$

The upward flux $I_{u,0}$ above the leaves is related to the intermediate upward flux and the incoming downward flux as:

$$I_{u,0} = \left[1 - k^{'}\Delta L(1-\tau_{\text{leaf}})\right] I_{u,1} + k^{'}\Delta L \rho_{\text{leaf}} I_{d,0} \tag{1.7}$$

It can now be immediately expressed in the incoming downward flux alone by substitution of Eq. 1.6b:

$$I_{u,0} = \left\{ \frac{\rho_{\text{leaf}} \left[1 - k^{'}\Delta L(1-\tau_{\text{leaf}})\right]^2}{1 - k^{'}\Delta L \rho_{\text{leaf}} \rho_{\text{soil}}} + k^{'}\Delta L \rho_{\text{leaf}} \right\} I_{d,0} \tag{1.8}$$

The ratio $I_{u,0}/I_{d,0}$ is the same as the reflection coefficient of the leaf-soil system, which we denote by ρ_{system}. We have now found the expression for the reflection coefficient of the leaf soil-system as a function of leaf and soil properties for the case of one single leaf layer above a bare soil surface:

$$\rho_{\text{system}} = \rho_{\text{soil}} \frac{\left\{1 - k^{'}\Delta L(1-\tau_{\text{leaf}})\right\}^2}{1 - k^{'}\Delta L \rho_{\text{leaf}} \rho_{\text{soil}}} + k^{'}\Delta L \rho_{\text{leaf}} \tag{1.9}$$

What about a canopy with a large LAI? In principle it is possible to add more layers, thus increasing the number of linear equations and solve them by matrix inversion, but this is cumbersome and it does not result in a neat expression. There is a better method.

1. The Reflection Coefficient of a Leaf Canopy with a Large Leaf Area Index

If we have a leaf canopy with a very large leaf area index, the soil underneath does not have any effect on the reflection coefficient of the canopy. We may apply the expressions that we have just derived, to the top leaf layer of the large leaf canopy. This time however, the entire leaf-canopy has the same role as the soil surface in the earlier calculation, so that we can replace both ρ_{soil} and ρ_{system} by ρ_c:

$$\rho_{\text{canopy}} = \rho_c \frac{\left[1 - k^{'}\Delta L(1-\tau_{\text{leaf}})\right]^2}{1 - k^{'}\Delta L \rho_{\text{leaf}} \rho_c} + k^{'}\Delta L \rho_{\text{leaf}} \tag{1.10}$$

This expression results in a second order equation in ρ_c, which can of course be solved (see Eq. 1.21), but before doing so it is useful to realize that this equation is valid locally at any depth in the canopy as long as the effect of the soil surface can be neglected. In other words, well above the soil surface the ratio between upward and downward radiation fluxes is constant. This constancy of ratio will now be used.

2. Extinction of Radiation Within the Leaf Canopy

There must also be constancy of ratio between the fluxes going down or going up at either side of any layer with same size ΔL, because there is no other difference in properties and environment of the layers than the magnitude of the fluxes. A constant ratio per leaf area index ΔL is equivalent to exponential decrease of radiation at a constant value of extinction coefficient k. It should be remembered that this is only true under the condition that there is no variation in leaf optical properties. Exponential extinction was derived before for the case of black horizontal leaves (zero scattering). If the leaves do not absorb all radiation, the extinction coefficient k will be smaller than the value of k' for black leaves (and which is equal to unity for black horizontal leaves). What is the value now in terms of leaf reflection and absorption coefficient?

The expression can be found by solving the differential equations for upward and downward fluxes, but it is also possible to

use the expression for the net radiation flux, which is the difference between the downward and the upward flux. The absorption per leaf area is identical to the rate of decrease of the net flux per leaf area index at leaf level L. For the exponential function $\exp(-kL)$ this rate of decrease is equal to its first derivative $k\exp(-kL)$ times the net flux above the canopy, so that net absorbed radiation per leaf area is given by:

$$I_c = (I_d - I_u)k\exp(-kL) \tag{1.11}$$

As I_u is equal to I_d times ρ_c, this expression is identical to

$$I_c = I_d(1-\rho_c)k\exp(-kL) \tag{1.12}$$

On the other hand, the absorption per leaf area must be equal to the sum of the radiation absorbed from above and the radiation absorbed from below. A fraction k' $(1-\tau_{\text{leaf}}-\rho_{\text{leaf}})$ will be absorbed out of each of these two fluxes. This leads to a second expression for the absorbed radiation per leaf area, which must of course be equal to the one above:

$$I_c = (1+\rho_c)k'(1-\tau_{\text{leaf}}-\rho_{\text{leaf}})exp(-kL)I_d \tag{1.13}$$

Combining the two expressions for the absorbed radiation per leaf area gives:

$$(1-\rho_c)k = (1+\rho_c)k'(1-\tau_{\text{leaf}}-\rho_{\text{leaf}}) \tag{1.14}$$

A second relation between k and ρ_c can be found by using the upward scattering per leaf area at depth L, keeping in mind that the total reflected radiation consists of the contributions of upward scattering of all leaf layers together. This upward scattering per leaf layer at depth L is equal to $k'(\tau_{\text{leaf}} I_{u,L} + \rho_{\text{leaf}} I_{d,L})$ or to $k'I_{d,0}$ $(\tau_{\text{leaf}}\rho_c + \rho_{\text{leaf}})\exp(-kL)$. Not all of the radiation that is scattered upward at depth L will reach the top of the crop canopy because of partial masking by leaves overhead. This interception proceeds in the same way as the extinction of radiation by black leaves, because only the direct lines of visibility count. Therefore only a fraction $\exp(-k'L)$ and not $\exp(-kL)$ will escape to the top of the canopy. This means that the total reflected radiation must be equal to the integral of the product of upward scattering and this escape fraction, so that the crop canopy reflection coefficient is given by

$$\rho_c = \int_0^{\infty} (\tau_{\text{leaf}}\rho_c + \rho_{\text{leaf}})k'\exp(-kL)exp(-k'L)dL \tag{1.15}$$

or

$$\rho_c = \frac{\tau_{\text{leaf}}\rho_c + \rho_{\text{leaf}}}{k'+k}k' \tag{1.16}$$

The two Eqs. 1.14 and 1.16 relate k and ρ_c to the canopy property k' and the leaf properties τ_{leaf} and ρ_{leaf}. Algebraic manipulation leads to the explicit expressions:

$$k = k'\sqrt{(1-\tau_{\text{leaf}})^2 - \rho_{\text{leaf}}{}^2} \tag{1.17}$$

$$\rho_c = \frac{\rho_{\text{leaf}}}{k/k' + 1 - \tau_{\text{leaf}}} \tag{1.18}$$

and also to

$$k = k'(1-\tau_{\text{leaf}})\frac{1-\rho_c{}^2}{1+\rho_c{}^2} \tag{1.19}$$

In Sect. I.B, we have seen that leaf reflection and leaf transmission do not differ much, each being practically equal to half the scattering coefficient σ_{leaf}. The equations for k and ρ_c can then be further simplified to (Cowan 1968):

$$k = k'\sqrt{1-\sigma_{\text{leaf}}} \tag{1.20}$$

$$\rho_c = \frac{1-\sqrt{1-\sigma_{\text{leaf}}}}{1+\sqrt{1-\sigma_{\text{leaf}}}} \tag{1.21}$$

The latter two equations occur frequently as building blocks in simulation models for

plant growth. This equation for ρ_c approaches $\sigma_{leaf}/4$ (or $\rho_{leaf}/2$) when the leaves have a small reflection and transmission coefficient. This is usually the case in the PAR region of the spectrum where reflection and transmission coefficient are about equal to 0.1. Therefore the reflection coefficient of a closed canopy in the PAR region is typically about 5 %. Note that this calculation does not consider the effect of solar elevation on ρ_c that occurs for non-horizontal leaf angle distributions. In Sect. IV under Eq. 1.34, I will show that ρ_c will then be larger than 5 % under low solar elevation and smaller under high solar elevation.

III. Absorption of Radiation in Row Crops

A. Directional Distribution of Incoming Radiation

So far I have treated canopies as being horizontally homogenous. This may apply to uniformly sown crop stands or natural mono-species stands. Most vegetation however is horizontally heterogenous, there being different species or plants of the same species forming discontinuous canopies. Further in the book some of these cases will be treated e.g. mixed species vegetation (Chap. 14 Anten and Bastiaans 2016) and 3D architecture of plants (Chap. 8, Evers 2016). Here I discuss a specific but very common example of a discontinuous stand, the row crop.

The irradiance on a horizontal surface coming from a well-defined sky portion, for instance, a window, can be calculated by a double integration of sky radiance $N(\alpha,\beta)$ over azimuth α and elevation β , using the formula:

$$I = \frac{1}{\pi}\int N(\alpha,\beta)\sin\beta\cos\beta d\beta d\alpha \qquad (1.22)$$

If the radiance N is the same for all directions (Uniform Overcast Sky), N can be used as a constant multiplier in the integration. In the case that the boundaries of azimuth and elevation are independent, the integration is straightforward. To give an example, a horizontal circular window in a zenithal position at height h and with radius r is bounded at $\arctan(h/r)$ for all azimuthal values, resulting in a relative irradiance of $r^2/(h^2 + r^2)$.

B. Row Crops

A row crop has heterogeneity, it has the leaves clustered into the rows. Due to clustering, row crops absorb less radiation as compared to a fully homogeneous crop. Radiation absorption is the primary factory that determines crop photosynthesis and therefore it is to be expected that a row crop has a smaller rate of photosynthesis than a homogeneous crop at the same LAI. It is our goal to quantify this reduction. We know that row crops are common practice in agriculture and it would therefore be strange if the reduction of photosynthesis is large. We investigate the reduction by considering model situations with increasing complexity.

1. Infinite LAI, Black Leaves

At the soil surface on a path between rows, the sky is only partly visible (Fig. 1.6). The outline of a row is simplified to a rectangular hedge, at height h, width w, separated by path widths p. For simplicity, the crop field is considered infinitely large and so row length does not matter. It is illustrative to use orthographic projection to find the relative irradiance (Monteith and Unsworth 1990). In the orthographic projection the sky portion that is visible is first projected onto the imaginary dome of the upper hemisphere which is subsequently projected vertically downward onto its horizontal circular base. The relative size of the projected sky portion on the area of the base is equal to its relative contribution to the irradiance. The correction for the sine of incidence is automatically taken into account by the inclination of a piece on the sky dome when it is vertically projected. Some types of fish-eye lenses do indeed produce an orthographic projection, but this

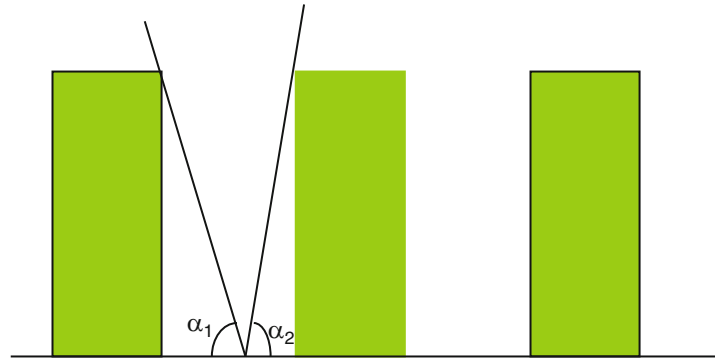

Fig. 1.6. Cross-section through a simplified row crop. The angles α_1 and α_2 delimit the part of the sky that is visible from the given point at the soil surface

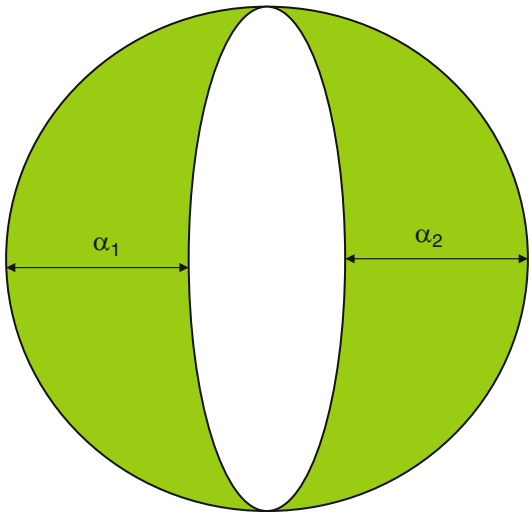

Fig. 1.7. The rows and the gap of the path as seen in a fish eye projection from the same point as in Fig. 1.6

type of projection does not retain the solid angle because vertical angular distances near the horizon will get compressed. In Fig. 1.7 the orthographic projection of the visible sky is drawn for a point halfway the path between the two adjacent rows.

The relative irradiance at such a point is given by the projected area as a fraction of the whole circle area. This fraction is identical to half the sum of the two cosine values of α_1 and α_2 in Fig. 1.6, which can be calculated from row height and lateral distance of the point. The fraction value will slightly vary from a maximum in the middle of the path to the minimum value at each side of the row. Its average value over the path is found by analytical integration (Goudriaan 1977) and is equal to

$$I_{\text{path}} = \frac{\sqrt{h^2 + p^2} - h}{p} \qquad (1.23)$$

In an extremely dense row crop with black leaves, this is all radiation that is transmitted. The complementary fraction is absorbed by the crop.

This model situation is unrealistic: the row structure is so dense that no radiation can penetrate to the soil surface under a row itself because it has infinite LAI and it is completely black. Yet, it is a useful starting point for the situation in which radiation does penetrate the rows.

2. Non-infinite LAI, Black Leaves

A precise geometric calculation is possible (Gijzen and Goudriaan 1989; Röhrig et al. 1999; Colaizzi et al. 2012) but it is rather complicated. It involves the distinction of the zones delimited by the row edges of many subsequent adjacent rows. Here, we will aim at a much faster approximation that is sufficiently accurate in practice and that also gives more insight.

To do so, we distinguish two configurations at the same averaged LAI between which the row crop is situated. The first one is the completely homogeneous crop that we have considered already. The

radiation level at the soil surface under this crop is given by:

$$S_{\text{homogeneous}} = \exp(-kL_t) \tag{1.24}$$

where L_t is the total LAI. In the other one all rows are pushed together so that we get a new homogeneous, but denser, crop at part of the total land area being equal to the sum of all row area. The local leaf area index, $L_{t\text{comp}}$, of this compressed crop is equal to the original LAI multiplied by the ratio $(w + p)/w$. The radiation level at the soil surface under this compressed crop is equal to:

$$S_{\text{comp}} = \exp\left(-kL_{t\text{comp}}\right) \tag{1.25}$$

In the actual row crop we have two types of soil surface, one right under row itself and one right under the path.

The radiation level at the soil surface of the path contains of course the unobstructed component I_{path} (Eq. 1.23) but in addition there is radiation penetrating through the rows adjacent to the path. The view factor for this radiation is complementary to I_{path}. As an approximation we assume that for laterally penetrating light the row crop is identical to a homogeneous crop, so that the fraction laterally penetrating is identical to $S_{\text{homogeneous}}$ (as it turns out, this assumption causes a small systematic error to which I will come back right below Eq. 1.29).

The sum of the two components is now given by

$$S_{\text{path}} = I_{\text{path}} + \left(1 - I_{\text{path}}\right)S_{\text{homogeneous}} \tag{1.26}$$

For the radiation level at the soil surface right under the row we follow a similar approach: it is also separated in two parts, one transmitted through the top of the row and one transmitted through the sides of the row. For the first component we need the view factor of the row I_{row}, in the same way as was done for the path (Fig. 1.6), but this time multiplied by extinction in the row. The extinction is calculated with the LAI value within the row, which is the same as that of the compressed crop. For the radiation that enters laterally we use the LAI value of the homogeneous crop (averaged L_t) multiplied by the view factor that is complementary to I_{row}. Combining the two components we find for the S_{row}:

$$S_{\text{row}} = I_{\text{row}}S_{\text{comp}} + (1 - I_{\text{row}})S_{\text{homogeneous}} \tag{1.27}$$

For the entire soil surface we use the weighted average of the two components for path and row:

$$S_{\text{soil}} = \frac{wS_{\text{row}} + pS_{\text{path}}}{w + p} \tag{1.28}$$

The fraction of radiation absorbed by the crop is the complement of the fraction of radiation absorbed by the soil surface:

$$F_{\text{crop}} = 1 - S_{\text{soil}} \tag{1.29}$$

However, one correction to the equation for S_{path} is still needed, because in the present form the radiation absorbed by the crop for near zero values of leaf area index deviates from kL. We know that the first derivative of absorbed radiation with respect to L at $L = 0$ should be equal to k because there is no mutual shading in the limit transition to zero LAI. Algebraic analysis shows that this requirement is met if S_{path} is corrected by a small term in the lateral view factor:

$$S_{\text{path}} = I_{\text{path}} + \left[1 - I_{\text{path}} - \left(1 - S_{\text{homogeneous}}\right)\left(I_{\text{path}} - I_{\text{row}}\right)\right]S_{\text{homogeneous}} \tag{1.30}$$

Apparently the lateral penetration of radiation in a row canopy to the bottom of the path is slightly different from that in a homogeneous canopy, which was assumed in the simpler equation. Usually the correction is small, but in a sparse row crop with narrow rows and wide paths it cannot be ignored. This correction is a price that must be paid for the brevity of the approximative equation.

3. Loss of Radiation due to Plant Arrangement in Rows

The equation for the radiation that is lost on the path (Eq. 1.23) is an upper limit to the relative loss. It shows that the losses will rarely exceed 30 % and usually be in the order of 10–20 %. In a homogeneous crop there is also transmission to the soil surface and in fact we should compare the result of Eq. 1.28 (S_{soil}) with that of Eq. 1.24 ($S_{\text{homogeneous}}$). The difference between these two values gets smaller as LAI gets smaller. For LAI = 0.5 the relative loss will only be about 5–10 %.

A general conclusion is that there only a moderate loss of intercepted radiation due to row cultivation as compared to that in a homogeneous crop.

The same conclusion proably applies to even more complicated plant arrangements, such as in tree nurseries (Pronk et al. 2003) in which small trees are regularly positioned between intersecting rows. A more sophisticated approach of a similar plant arrangement can be found in Röhrig et al. (1999).

IV. Direct and Diffuse Light in Photosynthesis Modeling

Leaf photosynthesis is a curvi-linear function of radiation absorption that gets saturated (i.e., it levels off) at high light intensities. If we simply multiplied the average radiation absorption and quantum efficiency, we would end up with a gross overestimation of canopy photosynthesis. There are two major causes of variation of radiation absorption in a leaf canopy: first the exponential extinction with increasing canopy depth, and second the unevenness among sunlit and shaded leaves, even at the same height within the canopy. Thus we need to consider the distinction between direct beam radiation and diffuse radiation (both diffuse sky radiation and scattered light in the canopy) that is intercepted by all leaves. This section therefore deals with the modeling of diffuse and direct radiation in relation to canopy photosynthesis.

With a completely overcast sky there is no direct radiation, and the radiation extinction in this situation is treated by assuming a single value for the extinction coefficient k for diffuse light, called k_{dif}, and likewise for canopy reflection, ρ_{dif}, usually with nominal values of 0.7 and 0.05 respectively. These values can be refined if needed. If we consider a leaf canopy with an LAI value that is small, (less than 1), we make a small error if we assume that all leaves have the same level of radiation absorption. A good estimate for this radiation absorption can be obtained by using Eq. 1.12, which gave the radiation absorption at canopy depth L. We should however be careful about the value for L that we are going to use. Clearly LAI itself is not correct: we then get the radiation absorption at the bottom of the canopy which is an underestimate for the average value. A better estimate is the one in the middle at one half of LAI, let us call it L_{middle}. The expression that we thus get for radiation absorption per leaf area is:

$$I_{c,\text{dif}} = I_{\text{dif}}(1-\rho_{\text{dif}})k_{\text{dif}}\exp(-k_{\text{dif}}L_{\text{middle}}) \tag{1.31}$$

Energy conservation requires that total LAI (L_t) times this quantity be identical to the difference in net radiation above and below the canopy. The expression for net radiation at any level L in the canopy is $I_{\text{dif}}\,(1-\rho_{\text{dif}})\exp(-k_{\text{dif}}\,L)$, and so the total absorption is equal to $I_{\text{dif}}\,(1-\rho_{\text{dif}})(1-\exp(-k_{\text{dif}}\,L_t))$. The result of Equation 1.31 times LAI is not identical to this total absorption, but it is a very good approximation, getting better as LAI gets smaller. In mathematical terms, the first derivative of a function of x is approximated by its difference over dx divided by dx, as dx approaches zero. Check for yourself at, for instance, $L_t = 0.4$ and see if you also get 0.23201 and 0.23125 times I_{dif}, using the nominal values of k and ρ at 0.7 and 0.05 respectively.

The reason to work with the leaf absorption level in the middle, rather than with the difference of net radiation above and below the layer divided by its layer size, is anticipation upon the numerical procedure of Gaussian integration that we will use later in a more general model for canopy photosynthesis.

The Gaussian integration procedure solves the problem that the above approximation begins to fall short as LAI gets larger. For instance, at $L_t = 5$, the balance method gives 0.921 of I_{dif}, whereas the midpoint method of Eq. 1.31 gives 0.578 of I_{dif} which is far too small. As the balance method gives the right result for the total radiation absorption, you may wonder why not just using this method of balancing above and below the leaf canopy. However, the problem we then get is that we overestimate canopy photosynthesis due to the mentioned saturation of leaf photosynthesis at high radiation levels. The best way out of this problem is to calculate leaf photosynthesis at a number of carefully chosen levels in the leaf canopy, using the radiation absorption in situ (see Box 1.2). Having chosen these points, the radiation absorption per leaf area is calculated at each point, subsequently the leaf photosynthesis that goes with it, and finally leaf photosynthesis over the whole canopy is found by integration. For reasons of balance checking it is sensible to do the integration for absorbed radiation as well, and compare it with the result of the balance method for net radiation.

Box 1.2: Example of Calculation of Photosynthesis When There Is only Diffuse Radiation

```
C   Input data, normally available through
subroutine arguments:
C       LAI = 3., REFH = 0.05, KDF = 0.7,
PARDF = 100., EFF = 0.011, AMAX = 1.
C   Units mg(of CO2), m, s, J (of PAR),
C       Gaussian numbers
        DIMENSION WGAUSS(3), XGAUSS(3)
        DATA IGAUSS/3/
        DATA XGAUSS/0.112702,0.5,0.887298/
        DATA WGAUSS/
        0.277778,0.444444,0.277778/
C   Canopy photosynthesis and absorbed
radiation are initialized at zero:
        PHOT = 0.
        RADABS = 0.
        DO I = 1,IGAUSS
C   Calculate the three Gaussian depths
          LAIC = XGAUSS(I)*LAI
C   Calculate absorbed radiation at that depth
          VISDF = PARDF*(1. –REFH)
          *KDF*EXP(–KDF*LAIC)
C   Calculate the resulting rate of
photosynthesis
          PHOTL = AMAX*(1. – EXP
          (–EFF*VISDF/AMAX))
C   Weighted addition
          PHOT = PHOT + WGAUSS(I) *
          PHOTL
          RADABS = RADABS + WGAUSS
          (I)*VISDF
        ENDDO
C   Calculate totals from the mean values:
        PHOTT = PHOT*LAI
        RADBST = RADABS*LAI
```

Up to this point we have dealt with canopy photosynthesis under an overcast sky with just diffuse radiation.

If the sun shines there is also a large unevenness in the distribution over sunlit and shaded leaves. You can appreciate this in a forest understorey where sun flecks are considerably brighter than the rest of the understory. First the diffuse component in incoming radiation must be singled out (Spitters et al. 1986). The incoming diffuse radiation can be dealt with in the same way as above, but in addition all leaves will receive radiation originating from the direct component. As mentioned before, the sunlit leaves receive the direct radiation, but also all leaves, including the sunlit ones, will receive a small amount from scattering by directly illuminated leaves. This additionally scattered radiation is intercepted on its turn and it is decreasing both, as goes down and as it goes up into the canopy. This secondary illumination seems to burden us with a complicated iterative problem, but it is possible to implicitly take care of this iteration, in the same way as it was handled in Eq. 1.12 for absorbed radiation at the leaf level. The

coefficients for leaf scattering were already incorporated into canopy reflection and extinction by using Eqs. 1.20 and 1.21.

By setting apart the incoming diffuse component, the direct radiation component can be treated as if the rest of the sky is black. Direct radiation is intercepted and partly scattered, but no matter how large this scattering, it is lost from the direct beam. This means that the direct beam will follow an exponential extinction curve with a k-value that was derived earlier for black leaves ($k = 0.5/\sin(\beta)$ for a spherical leaf angle distribution), which we will denote by k_{dir}. The fraction of sunlit leaves at canopy depth L is now given by $\exp(-k_{\text{dir}}L)$ and it is identical to the frequency of sunflecks at that same level. Conversely, the fraction of shaded leaves is equal to its complement. The incidence angle of the direct beam is usually not perpendicular to a leaf (Fig. 1.3), which must be taken into account in the calculation of the radiation absorbed on a leaf area basis. As explained earlier and implied in the value of k_{dir}, for a spherical leaf angle distribution the average sine of incidence (or cosine to the leaf's normal) has a value of 0.5, irrespective of solar height, whereas the actual value of the sine of incidence for an individual leaf may vary between 0 and 1. In the procedure for calculating canopy photosynthesis this variation is taken into account by integration over the sine of incidence while allowing for its frequency distribution. Here again Gaussian integration will be used. The frequency distribution of leaf area with the sine of incidence is simple for a spherical leaf angle distribution: it is uniform between the values 0 and 1.

The effect of scattering needs special attention as it implies a redistribution of radiation from sunlit leaves to shaded leaves. The sunlit leaves absorb a fraction $(1 - \sigma)$ of what is incident upon them, and then they scatter the fraction σ into all directions, which in turn is intercepted by both other sunlit leaves and by shaded leaves. We assume that there is no difference between sunlit and shaded leaves at the same canopy height as far as the absorption of the scattered radiation is concerned.

The mean total absorption rate at depth L, averaged over both sunlit and shaded leaves is given by:

$$I_{\text{mean, dir}} = I_{\text{dir}}(1 - \rho_c)k\exp(-kL) \qquad (1.32)$$

where k is the overall extinction coefficient given by $k'\sqrt{1-\sigma}$. This average total absorption is the sum of absorption of direct radiation in sunlit leaves only and of scattered, diffused radiation in both sunlit and shaded leaves. The first term, the absorption rate of the direct radiation in the sunlit leaves only, must be equal to:

$$I_{c,\text{dir}} = I_{\text{dir}}(1 - \sigma)k'_{\text{dir}}\exp\left(-k'_{\text{dir}}L\right) \qquad (1.33)$$

which is smaller than $I_{\text{mean,direct}}$. The difference between Eqs. 1.32 and 1.33, defined by $I_{c,\text{sca}} = I_{\text{mean,direct}} - I_{\text{sunlit,direct}}$, represents absorption of scattered radiation (secondary, but also tertiary, etc), which is the same for all leaves at that same height in the canopy, whether sunlit or shaded.

For PAR the scattering coefficient is about 0.2 which means that tertiary and higher order scattering can be ignored. A mathematical series development shows that the first order approximation of the difference $I_{\text{mean,direct}} - I_{\text{sunlit,direct}}$ for a spherical leaf angle distribution is given by

$$I_{\text{sca}} = \sigma\left[\frac{1}{2(1+2\sin\beta)} + \frac{L}{8\sin^2\beta}\right]\exp\left(-\frac{2L}{\sin\beta}\right) \qquad (1.34)$$

The integral of this expression over the whole canopy from 0 to infinity is equal to σ $(1 + 4\sin\beta)/(2 + 4\sin\beta)$, which varies between $\sigma/2$ for very small solar heights passing 3 $\sigma/4$ at 30° solar height to 5 $\sigma/6$ for a zenithal position of the sun. Because the primary scattering is equal to σ itself, the remainder must have escaped as radiation reflected by the canopy (at infinite LAI there is no absorption by the soil surface).

This means that the reflection coefficient of the canopy is equal to $\sigma/(2 + 4 \sin\beta)$ which is a decreasing function of solar height. At 30° solar height this is equal to $\sigma/4$, the same as for a horizontal leaf angle distribution. Thus, for a lower sun most canopies will reflect a slightly larger fraction and for a higher sun they will reflect a slightly smaller fraction.

This "second-hand" absorbed radiation enhances total crop photosynthesis particularly because the shaded leaves will use it much more efficiently than the sunlit leaves. Finally the absorption from the diffuse sky radiation (see Eq. 1.31) (that we had temporarily set apart) must be added to get the total absorption rate of diffuse radiation, $I_{c,\mathrm{sh}}$, which is common to sunlit and shaded leaves:

$$I_{c,\mathrm{sh}} = I_{c,\mathrm{dif}} + I_{c,\mathrm{sca}} \tag{1.35}$$

The rate of photosynthesis of the shaded leaves at the canopy depth L can now be calculated. Their contribution to crop photosynthesis on a ground area basis still requires multiplication by the fraction shaded which is equal to $1 - \exp(-k_{\mathrm{dir}}L)$.

To get the photosynthesis of the sunlit leaves the absorption rate of direct light should be added to the absorption rate for the shaded leaves that we have just obtained. On a ground area basis this absorption rate of direct light is given by Eq. 1.33. On a leaf area basis it is equal to (see also Fig. 1.3):

$$I_{c,\mathrm{su}} = I_{\mathrm{dir}}(1-\sigma)\frac{\cos}{\zeta \sin\beta} \tag{1.36}$$

with $I_{c,\mathrm{sh}}$ the total absorption rate of diffuse radiation, ζ the angle between the leaf normal and the solar beam and β the solar inclination angle. For horizontal leaves, $\cos(\zeta)$ is equal to $\sin(\beta)$ so that the photosynthesis rate of the sunlit leaves can be immediately calculated, but for any other leaf angle distribution $\cos(\zeta)$ varies and we need another integration over $\cos(\zeta)$ that is nested within the integration over canopy depth. For a spherical leaf angle distribution (see also Fig. 1.4) $\cos(\zeta)$ varies uniformly between 0 and 1.irrespective of solar height.

We can now choose a photosynthesis-light response curve in order to calculate the contribution of the sunlit leaves at the considered canopy depth L. For the often-used negative exponential function $A_{\max}(1 - \exp(-\varepsilon I/A_{\max}))$ an analytical solution exists for this case, and with I given by $I_{\mathrm{dir}} \cos(\zeta)$ it is equal to

$$A_{max}(1 + A_{max}/(\varepsilon I_{dir})\ (1\ \exp(-\varepsilon I_{dir}/A_{max})\ )\ ) \tag{1.37}$$

with $A_{\max}$ the photosynthetic at saturating light and ε the initial slope of the light response curve (i.e., the apparent quantum yield). Other equations can be used such as the non-rectangular hyperbola which also includes a curvature factor (Marshal and Biscoe 1980; see Chap. 9 Hikosaka et al. 2016). This expression could be used in a numerical model but there are two reasons not to do so: first there is a zero division for $I_{\mathrm{dir}} = 0$, and second it excludes the use of another light response curve. It does, however, give a chance to check the numerical performance of the Gaussian integration procedure. For $\varepsilon\ I_{\mathrm{dir}}/A_{\max} = 1$ the analytical solution gives 0.3678794 $A_{\max}$ whereas the numerical three-point approximation gives 0.3678797 $A_{\max}$, so that in this situation the Gaussian integration is extremely accurate.

A modelling example of the nested Do – loop is given in Box 1.3.

Box 1.3: Example of Calculation of Canopy Photosynthesis When There Is also Direct Radiation

```
C   Input data, normally available through
subroutine arguments:
C       LAI = 3., KDF = 0.7,
PARDF = 100., PARDR = 200., EFF = 0.011
C       AMAX = 1.,SIGMA = 0.2,
SINB = 0.7
C   Units mg(of CO2), m, s, J (of PAR),
      REFH = (1.-SQRT(1.-SIGMA))/
      (1. + SQRT(1.-SIGMA))
      REFS = REFH*2./(1. + 2.*SINB)
      KBL = 0.5/SINB
      KDRT = KBL*SQRT(1.-SIGMA)
C   Gaussian numbers
      DIMENSION WGAUSS(3), XGAUSS(3)
      DATA IGAUSS/3/
      DATA XGAUSS/0.112702,0.5,0.887298/
      DATA WGAUSS/
      0.277778,0.444444,0.277778/
C   Canopy photosynthesis and absorbed
radiation are initialized at zero:
      PHOT = 0.
      VISABS = 0.
      DO I = 1,IGAUSS
C   Calculate the three Gaussian depths
        LAIC = XGAUSS(I)*LAI
C   Calculate absorbed radiation at that depth
        VISDF = PARDF*(1. –REFH)
        *KDF*EXP(−KDF*LAIC)
        VIST = PARDR*(1.-REFS)
        *KDRT*EXP(−KDRT*LAIC)
        VISD = PARDR*KBL*EXP
        (−KBL*LAIC)
        VISSHD = VISDF + VIST-VISD
C   Calculate the resulting rate of
photosynthesis
        PHOSHD = AMAX*(1. – EXP(−
                 EFF*VISSHD/
                 AMAX))
        VISPP = PARDR*(1.-SCP)/SINB
        PHOSUN = 0.
        VISLL = 0.
        DO I2 = 1,IGAUSS
        VISSUN = VISSHD +
                 VISPP*XGAUSS(I2)
        PHOS = AMAX*(1.-EXP
               (−EFF*VISSUN/AMAX))
        PHOSUN = PHOSUN +
                 PHOS*WGAUSS(I2)
        VISLL = VISLL +
                VISSUN*WGAUSS(I2)
        ENDDO
        FSSLA = EXP(−KBL*LAIC)
        PHOTL = FSSLA*PHOSUN+
                (1.-FSSLA)*PHOSHD
        VISL = FSSLA*VISLL+(1.-
               FSSLA)*VISSHD
C   Weighted addition
        PHOT = PHOT + WGAUSS(I) *
               PHOTL
        VISABS = VISABS + WGAUSS(I)
                 *VISL
      ENDDO
C   Calculate totals from the mean values:
      PHOTT = PHOT*LAI
      VISABST = VISABS*LAI
```

Even the three-point Gaussian integration is not accurate enough for a leaf area index larger than 3. Therefore, it is advisable to use a 5-point method for larger leaf area indices.

The following table gives the Gaussian distances and weights for the 5-point method (see Lanczos 1957; Scheid 1968):

```
DATA IGAUSS/5/
DATA  XGAUSS/0.0469101,0.2307534,0.5,
   0.7692465,0.9530899/
DATA WGAUSS/0.1184635,0.2393144,
   0.2844444,0.2393144,0.1184635/
```

V. Conclusions and Prospects

Real plant canopies exhibit fuzzy features that are superimposed on the regular and smooth model skeleton which was used for the description of the canopies in this chapter. The idealizing model approach may be criticized for this reason, arguing that real canopies are very different. However, it will not be an easy task to show and prove to what extent the irregularities in real crops modify the outcomes provided by the approach given here. It will be an enormous effort to collect the statistical attributes of 3-D plant forms that are needed, let alone to properly include them in a model (see Chap. 8 Evers 2016).

Another criticism to the modelling approaches as presented in this chapter is that they tend to be unbalanced: too much emphasis on the mathematical analysis,

thereby suggesting an unjustified accuracy, and shying away from the harder to grasp biological and agricultural variability. For instance, how can we include and describe the spatial and temporal variations in photosynthetic leaf properties? This topic is treated in the Chap. 4 (Niinemets 2016) and 5 (Pons 2016) of this book.

Such criticisms tell us as modellers to be cautious. Our results are vulnerable, depending as they are on the underlying assumptions. This may be a weakness of the modelling approach, but at the same time this weakness turns into a strength when it gives us also the power to analyze the sensitivity of the model outputs to these same assumptions.

References

Anten NPR, Bastiaans L (2016) The use of canopy models to analyze light competition among plants. In: Hikosaka K, Niinemets Ü, Anten N (eds) Canopy Photosynthesis: From Basics to Applications. Springer, Berlin, pp 379–395

Campbell G (1990) Derivation of an angle density function for canopies with ellipsoidal leaf angle distributions. Agri For Meteorol 49:173–176

Colaizzi PD, Evett SR, Howell TA, Li F, Kustas WP, Anderson MC (2012) Radiation model for row crops: I. Geometric view factors and parameter optimization. Agron J 104:225–240

Cowan IR (1968) The interception and absorption of radiation in plant stands. J Appl Ecol 5:367–379

de Wit CT (1965) Photosynthesis of Leaf Canopies. Centre for Agricultural Publications and Documentation, Wageningen

Evers JB (2016) Simulating crop growth and development using functional-structural plant modeling. In: Hikosaka K, Niinemets Ü, Anten N (eds) Canopy Photosynthesis: From Basics to Applications. Springer, Berlin, pp 219–236

Gates DM (1980) Biophysical Ecology. Springer, New York

Gausman HW, Allen WA (1973) Optical parameters of leaves of 30 plant species. Plant Physiol 52:57–62

Gijzen H, Goudriaan J (1989) A flexible and explanatory model of light distribution and photosynthesis in row crops. Agri For Meteorol 48:1–20

Goudriaan J (1977) Crop Micrometeorology: A Simulation Study, Simulation monographs. Pudoc, Wageningen

Goudriaan J (1988) The bare bones of leaf angle distribution in radiation models for canopy photosynthesis and energy exchange. Agri For Meteorol 38:251–255

Goudriaan J, Van Laar HH (1994) Modelling Potential Crop Growth Processes. Kluwer Academic Publishers, Dordrecht

Hikosaka K, Kumagai T, Ito A (2016) Modeling canopy photosynthesis. In: Hikosaka K, Niinemets Ü, Anten N (eds) Canopy Photosynthesis: From Basics to Applications. Springer, Berlin, pp 239–268

Kubelka P, Munk F (1931) Ein Beitrag zur Optik der Farbanstriche. Z Tech Phys 12:593–601

Lambers H, Chapin FS III, Pons TL (1998) Plant Physiological Ecology. Springer, Berlin

Lanczos C (1957) Applied Analysis. Pitman and Sons, London

Marshal B, Biscoe PV (1980) A model for C_3 leaves describing the dependence of net photosynthesis on irradiance. J Exp Bot 31:29–39

McCree KJ (1981) Photosynthetically active radiation. In: Encyclopedia of Plant Physiology, vol 12A. Springer, Berlin, pp 41–55

Monsi M, Saeki T (1953) Über den Lichtfaktor in den Pflanzengesellschaften und seine Bedeutung für die Stoffproduktion. Jpn J Bot 14:22–52. *Translated as*: Monsi M, Saeki T (2005) On the factor light in plant communities and its importance for matter production. Ann Bot 95:549–567

Monteith JL, Unsworth MH (1990) Principles of Environmental Physics. Edward Arnold, London

Niinemets Ü (2016) Within-canopy variations in functional leaf traits: structural, chemical and ecological controls and diversity of responses. In: Hikosaka K, Niinemets Ü, Anten N (eds) Canopy Photosynthesis: From Basics to Applications. Springer, Berlin, pp 101–141

Phillips KJH (1992) Guide to the Sun. Cambridge University Press, Cambridge

Pons TL (2016) Regulation of leaf traits in canopy gradients. In: Hikosaka K, Niinemets Ü, Anten N (eds) Canopy Photosynthesis: From Basics to Applications. Springer, Berlin, pp 143–168

Pronk AA, Goudriaan J, Stilma E, Challa H (2003) A simple method to estimate radiation interception by nursery stock conifers: a case study of eastern white cedar. Neth J Agric Sci 51:279–295

Röhrig M, Stützel H, Alt C (1999) A three-dimensional approach to modeling light interception in heterogeneous canopies. Agron J 91:1024–1032

Ross J (1981) The Radiation Regime and Architecture of Plant Stands. Dr W Junk Publishers, The Hague

Scheid F (1968) Numerical Analysis, Schaum's outline series. McGraw-Hill Book Company, New York

Spitters CJT, Toussaint HAJM, Goudriaan J (1986) Separating the diffuse and direct component of global radiation and its implications for modeling canopy photosynthesis. Part I. Components of incoming radiation. Agri For Meteorol 38:217–229

Chapter 2

Leaf Energy Balance: Basics, and Modeling from Leaves to Canopies

Vincent P. Gutschick*
Global Change Consulting Consortium, Inc., Las Cruces, NM 88011, USA

*Author for correspondence, e-mail: vinceg@gcconsortium.com
http://gcconsortium.com

K. Hikosaka, Ü. Niinemets, and N.P.R. Anten (eds.), *Canopy Photosynthesis: From Basics to Applications*, DOI 10.1007/978-94-017-7291-4_2

Summary

An initial review of diverse studies from leaf to globe clarifies the importance of accurate modeling of leaf temperature. The body of the discussion here then shows that the tools for modeling exist at diverse levels of process detail. Modelers are able to assemble a workable toolkit from the whole set of such tools. I present explicit equations for leaves in isolation and in canopies. Toward enabling comprehensive process-based modeling, I discuss energy-balance modeling in the forward direction for prediction of photosynthesis, transpiration, and other measures, including collateral effects such as leaf damage from excess temperatures. Included here are several useful mathematical solution methods for highly-coupled processes, such as energy balance, photosynthesis, stomatal control, and scalar transport. I review inverse modeling to estimate evapotranspiration and plant water stress from measured leaf temperatures. Quantitative arguments indicate the range and limits of validity of various approximations, such as ignoring lateral heat

Symbols: A – Leaf photosynthetic rate per area [μmol m^{-2} s^{-1}]; A_{LL} – Light-limited A [μmol m^{-2} s^{-1}]; A_{sat} – Light-saturated A [μmol m^{-2} s^{-1}]; a_{NIR} – Absorptance of leaves in the NIR [-]; a_{PAR} – Absorptance of leaves in the PAR [-]; b_{BB} – Residual stomatal conductance in Ball-Berry equation [mol m^{-2} s^{-1}]; b_c, b_E, b_{TIR} – Derivative of energy-balance terms with respect to temperature [W m^{-2} K^{-1}]; B – Sum of the derivatives of the energy-balance terms [W m^{-2} K^{-1}]; C_a, C_c, C_i, C_s – Partial pressure of CO_2 in ambient air, at the chloroplast, in the leaf interior (substomatal cavities), at the leaf surface beneath the boundary layer [Pa]; $C_{P,m}$ – (Molar) heat capacity of air [J mol^{-1} K^{-1}]; $C_{P,a}$ – Leaf heat capacity per unit area [J m^{-2} K^{-1}]; d – Zero-plane displacement height in a canopy [m]; d_{leaf} – Characteristic linear dimension of a leaf for heat transfer (m); E_{leaf} – Leaf transpiration rate [mol m^{-2} s^{-1}]; e_a, e_i, e_s – Partial pressure of water vapor in ambient air, in the leaf interior (substomatal chamber), at the leaf surface beneath the boundary layer [Pa]; e_{sat} – Saturated water vapor pressure [Pa]; E_{NIR}, E_{PAR}, E_{TIR} – Energy flux density in the NIR, PAR, TIR [W m^{-2}]; ET – Evapotranspiration rate [various units, including mm d^{-1}]; G – Soil heat flux density [W m^{-2}]; g_{aH} – Canopy aerodynamic conductance for heat [preferred as mol m^{-2} s^{-1}]; g_b, g_b' – Leaf boundary-layer conductance for water vapor, CO_2 [mol m^{-2} s^{-1}]; g_{bh} – Boundary-layer conductance for heat [preferred as mol m^{-2} s^{-1}]; g_{bs}, g_{bs}' – Combined boundary-layer and stomatal conductance of leaves for water vapor, CO_2 [mol m^{-2} s^{-1}]; g_s, g_s' – Stomatal conductance for water vapor, CO_2 [mol m^{-2} s^{-1}]; h – Canopy height [m]; h_s – Relative humidity at the leaf surface, beneath the boundary layer [-]; H – Sensible heat flux density (leaf or canopy) [W m^{-2}]; k – von Karman's constant [-]; K_{CO} – Effective Michaelis constant for CO_2 binding to Rubisco [Pa]; K_H, K_w, K_{CO_2} – Eddy diffusivity for heat, water vapor CO_2 [m^2 s^{-1}]; LE – Latent heat flux density [W m^{-2}]; m_{BB} – Slope in the Ball-Berry equation for stomatal conductance [-]; P_a – Total air pressure [Pa]; NIR – Near-infrared radiation (700–2500 nm); PAR – Photosynthetically active radiation (400–700 nm); $PPFD$ – Photosynthetic photon flux density [mol m^{-2} s^{-1}]; Q – Generic heat flux density [W m^{-2}]; Q_c^-, Q_E^- – Flux density of heat loss from convection, transpiration [W m^{-2}]; Q_{SW}^+, Q_{TIR}^+ – Flux density of energy gain from shortwave, TIR absorption [W m^{-2}]; Q_{TIR}^- – Flux density of energy loss from TIR emission [W m^{-2}]; R_d – Dark respiration rate per leaf area [μmol m^{-2} s^{-1}]; R_n – Net radiation flux density [W m^{-2}]; T – Temperature [°C or K, as appropriate]; T_{air} – Air temperature [°C or K, as appropriate]; T_{leaf} – Leaf temperature [°C]; T_{mean} – Mean temperature to which dark respiration acclimates [°C]; TIR – Thermal infared radiation (2.5–15 μm, long-wave radiation); u – Wind speed [m s^{-1}]; u_* – Friction velocity [m s^{-1}]; $V_{c,\max}$ – Maximal carboxylation capacity per leaf area [μmol m^{-2} s^{-1}]; z – Height above the soil [m]; z_H, z_m – Roughness lengths for heat transport, momentum [m]; ΔT – Shift in leaf temperature as transient [°C or K]; δ – Small nominal change in incoming shortwave solar energy flux density [W m^{-2}]; Γ^* – Compensation partial pressure of CO_2 in photosynthesis without dark respiration [Pa]; ε, $\varepsilon_{sky,eff}$ – Thermal emissivity of leaf, sky [-]; ς – Atmospheric stability measure [-]; θ – Transition parameter between light-limited and light-saturated photosynthetic rates [-]; λ – Latent heat of vaporization of water [preferred as J mol^{-1}]; ρ – Molar density of air [mol m^{-3}]; σ – Stefan-Boltzmann constant [W m^{-2} K^{-4}]; φ – Initial quantum yield of photosynthesis [mol CO_2 (mol photons)$^{-1}$]; ψ_{leaf} – Leaf water potential [MPa]; ψ_H, ψ_m – Atmospheric stability corrections for heat, momentum transfer [-]

conduction in the leaf lamina or, on certain time-scales, transients in leaf temperature. Overall, the review emphasizes the importance of including the energy balance in models and provides suggestions for making practical error estimates of process-model inaccuracies and process incompleteness. The current limitations compel the development of improved models.

Keywords Temperature • Energy balance • Leaves • Modeling • Radiation • Convection • Stomatal conductance • Transpiration • Canopies • Transients • Turbulent transport • Inverse modeling

I. Introduction: Why Leaf Energy Balance is Important to Model

Leaves cover approximately half of the land surface of the Earth at any one time (Myneni et al. 2002). They are correspondingly critical surfaces on land for the exchange of radiation and momentum and for scalar fluxes of heat, water vapor, CO_2, and other atmospheric constituents. Transpiration from leaves accounts for approximately half of total water emission from land surfaces (Lawrence et al. 2006), with simple evaporation (or sublimation of ice, snow) from soil accounting for the remainder. Leaves are key determinants of the carbon and water cycles and of climatic processes. Additionally, their trace gas emissions of terpenes and other volatile "secondary" metabolic compounds are important in atmospheric chemistry (e.g., Räisänen et al. 2009) and in contributing condensation nuclei for the formation of clouds (Kavouras et al. 1998; Hartz et al. 2005). The emission of both isoprene and terpenes is heavily dependent upon leaf temperature (Peñuelas and Llusià 2003; Monson et al. 2012; Grote et al. 2013).

Leaf energy balance (total or gross energy balance) determines leaf temperature. In turn, leaf temperature conditions affect numerous physiological processes as well as climatic processes. Physiologically, leaf temperature sets the activation of biochemical processes, particularly photosynthesis and respiration (Chap. 3, Hikosaka et al. 2016a), as one sees incorporated in all current models of leaf photosynthesis, largely based on the seminal model of Farquhar et al. (1980). By extension, leaf temperature can also generate deactivation, directly via enzyme deactivation, commonly at high temperatures but also at low temperatures, particularly for C_4 plants, whose PEP carboxylase enzyme deactivates or even falls apart reversibly at low temperatures (Kleczkowski and Edwards 1991; Sage and Kubien 2007). Temperature extremes also may generate photoinhibition of photosynthetic quantum yields or capacity over short to long duration (Ball et al. 2002; Demmig-Adams and Adams 2006), when high fluxes of absorbed photosynthetic photon flux density, or PPFD, cannot be driven productively into photosynthetic photochemistry nor dumped by radiationless relaxation of the xanthophyll pigments. Leaf temperature also acts with genetic programs in determining plant development; the empirical degree-day model has been verified at scales ranging from molecular to whole plant (Granier et al. 2000). At the level of the plant, leaf temperature is also an important factor in the propagation of plant diseases, particularly fungal diseases (Schuepp 1993; Harvell et al. 2002).

Leaf energy balance includes the exchanges of sensible and latent heat with the air as well as radiative processes. Exchanges of sensible and latent heat with the atmosphere by leaves and soil (or other non-leafy surfaces) are the principal energy inputs to the atmosphere over land, balanced in the long term by thermal infra-red (TIR) emissions to space (Hartmann 1994). On diverse spatial scales, these exchanges generate convective air flows – free convection on single leaves (see Campbell and Norman 1998), up to mesoscale flows that may lead to cloud formation (Anthes 1984; Segal et al. 1988), and on to larger scales, ultimately global. Physiology re-enters the formulation of heat exchanges at leaves: photosynthesis, itself temperature-dependent, is tightly

coupled to leaf stomatal conductance, g_s, as expressed in many empirical models of g_s (Ball et al. 1987; Dewar 2002; Leuning 1995). In turn, conductance is a factor in leaf transpiration (latent heat exchange) thereby affecting leaf temperature which ultimately couples back to photosynthesis. The need for coupled models of leaf energy balance, stomatal conductance, photosynthesis, and physical transport of heat and gases is apparent, as will be covered below. It may be surprising that, until 1986 (Verstraete and Dickinson 1986), climate models (general circulation models, or GCMs) did not consider leafed area on the globe as physiologically dynamic, rather they set a simple, uniform physical boundary condition for vegetated area. Now, the attention to the physiology of vegetated surfaces in GCMs is intense, and the role of vegetation in controlling temperature is well-recognized (e.g., Sellers et al. 1997).

An accurate knowledge of leaf temperature, whether by measurement or modeling or both, is necessary for comprehension and prediction of climate, including climate change. From a paleoclimatic perspective, understanding the relation of leaf temperature to climate is necessary to infer paleoclimate from tree rings. This is particularly true in attempting to use the stable isotopic composition (^{13}C, ^{2}H, ^{18}O) to infer climatic conditions – e.g., estimating past water stress via the relations among the $^{13}C/^{12}C$ ratio, the leaf's ratio of internal to external CO_2 partial pressures, water-use efficiency, and water stress (Barbour 2007).

The radiative portion of leaf energy balance merits attention on its own, for its effects on neighboring leaves and non-foliar surfaces that intercept scattered radiation from leaves and for total radiative interception on land (Chap. 1, Goudriaan 2016). Variably according to optical properties and orientation, leaves absorb and reflect at all major radiation wavebands: photosynthetically active (PAR, 400–700 nm), near infrared (NIR, 700–200 nm) and thermal infrared (TIR, 2.5–15 μm) radiations. Leaves also strongly absorb ultraviolet (UV) radiation, but it is a minor energy component. They also emit much TIR, as do all bodies. The transfers of radiation to and from leaves generate much of the complexity in models of leaf energy balance within canopies, given the vectorial rather than scalar nature of the propagation of radiation. Regarding the large-scale radiative balances, the deficit in absorption, or albedo, sets the overall availability of solar energy in the climate system. Recently the effect of leaf presence on regional albedo has received considerable attention in the discussion of climate (Hales et al. 2004) and of global warming (for a review see Bonan 2008). Afforestation at high latitudes is estimated to have a net warming effect, due to reduced surface albedo despite the ability of forests to take up CO_2 as a greenhouse gas (Bonan 2008).

All the process studies and modeling are an intellectual challenge in their own right and they also have much practical application. Understanding the components of leaf energy balance is needed in modeling crop productivity, whether for on-farm management or predictions of market conditions or famine warnings; in ecological studies of net primary production; in estimating water balance of landscapes, whether for irrigation management or predicting surface water balance for human use or ecosystem status; and, of course, in the climate modeling. Furthermore, inverse modeling of leaf temperature is also an important exercise (Box 2.1).

This review of the processes of energy balance and their consequences has diverse goals. It may impart to researchers with theoretical backgrounds but who are nonspecialists in biophysical modeling an appreciation of the various levels of phenomena. For researchers dealing with the biophysical phenomena but more focused on experimental approaches than a body of theory, it may aid in developing quantitative studies with the full power and accuracy of biophysical theory. For specialists attuned to biophysical theory, it may offer a more comprehensive view, such as by bringing attention to less-appreciated but important links of phenomena. One example is the importance of sky thermal infrared interception as a distinct energy input. Another example is providing justification for neglecting photosynthetic and thermal energy storage on most scales of space and time. Finally, for advanced students of botany, physiology,

physics, and other disciplines who are in their early careers, this review is offered to give context to reading of the extensive literature related to leaf energy balance, and, one hopes, to generate fruitful research ideas.

Box 2.1 Inferring Water Stress and Water Use from Leaf Temperature

Measured leaf temperature can be used to infer water stress on plants, as in the classic crop water stress index of Idso et al. (1981) and in the numerous rectifications (Jackson et al. 1988) and extensions (Fuchs 1990), including in remote sensing (Kogan 1997). In related fashion, measured surface (leaf, soil) temperature can be used in estimating evapotranspiration (ET), a mass flux of water, a critical indicator of both plant productivity and surface water balance. One of the simpler effective models for this is the Surface Energy Balance Land (SEBAL) model, used in remote sensing (Bastiaanssen et al. 1998). The net radiative energy input, R_n, to the surface as an energy flux density is estimated from measured reflected fluxes and additional information (the solar constant, estimated atmospheric absorption, angle of solar illumination). The temperature difference from leaves to air is estimated from surface radiative temperature, invoking a calibration using hot ($ET = 0$) and cold (ET as maximal, sensible heat flux $H = 0$) extreme parts of the scene. Along with estimates of surface roughness, hence, of conductance for sensible heat, this allows for the estimation of H. Finally, one estimates latent heat energy flux density, λE, as a residual, $\lambda E = R_n - G - H$. Here, E is the evapotranspiration rate written as a single-letter symbol, G is the flux into the soil, estimated empirically. More sophisticated process modeling is incorporated into allied inverse models that resolve leaf and soil temperatures (Li et al. 2009; Timmermans et al. 2007).

II. Calculations of Leaf Energy Balance: Basic Processes in the Steady State

A. Energy Balance Equation in the Steady State

1. Chief Components of Leaf Energy Balance

A useful place to begin is the calculation of the steady state, under constant radiation and atmospheric conditions and leaf orientation. I may write the energy-balance equation on a per-area basis (W m^{-2}) as the sum of radiative inputs minus outputs and of transfers of latent and sensible heat to the air:

$$0 = Q_{SW}^{+} + Q_{TIR}^{+} - Q_{TIR}^{-} - Q_{E}^{-} - Q_c - Q_s \tag{2.1}$$

Here, Q_{SW}^{+} is the energy flux density in leaf-absorbed shortwave radiation, arriving directly from the sun or scattered from other leaves, soil, etc.; Q_{TIR}^{+} is the energy flux density in absorbed thermal infrared radiation, which is contributed almost exclusively by atmospheric or "sky" radiation by water molecules combined with thermal emissions from leaves, soil, etc. – direct flux from the sun is negligible; Q_{TIR}- is the energy flux density in the TIR emitted by the leaves, acting nearly as classic blackbodies; Q_E-$= \lambda E$ is the flux density of latent heat, formulated as the flux density of water vapor from the leaf, E, multiplied by the latent heat of evaporation, λ; Q_c is the convective loss of heat to the air through the leaf boundary layer, and this may be positive or negative; and Q_S is the storage term, composed of thermal storage during transient heating (or, with a negative sign, cooling) plus chemical energy storage in photosynthesis (less respiration). Figure 2.1 presents a simple geometric sketch of the fluxes.

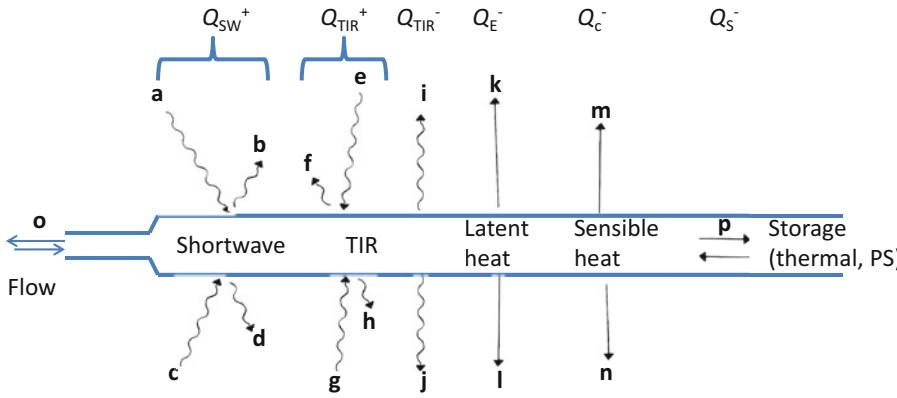

Fig. 2.1. Elements of energy balance of a flat-bladed leaf (not a needle or cladode), viewed edge-on. By convention, the top is the adaxial surface, though wind may invert a leaf. All the elements occur at each unit of surface area. Elements of net shortwave energy gain $\left(Q_{SW}^{+}\right)$: (*a*) shortwave radiation incident on nominal top or adaxial surface (UV, PAR, NIR); the illumination geometry must be known to compute this; it may include radiation reflected from other vegetative or soil surfaces (the leaf can twist in the wind to face the soil in part); (*b*) reflected shortwave radiation incident on the adaxial surface, computed from the sum of reflectivities in each band multiplied by the flux density in the band, plus transmitted shortwave radiation incident from abaxial surface; (*c*) shortwave radiation incident on the nominal bottom or abaxial surface; generally this is only radiation reflected from other surfaces; (*d*) reflected shortwave radiation from abaxial surface, plus transmitted shortwave radiation incident from the adaxial surface. Elements of net gain of thermal infrared (TIR) energy $\left(Q_{TIR}^{+}\right)$: (*e*) TIR incident on adaxial surface; a combination of sky emission and emission from terrestrial surfaces, weighted by associated fractional hemispherical views; (*f*) TIR radiation reflected from adaxial surface; typically only about 4 % of incident flux density; note that transmission of TIR radiation is negligible; (*g*), (*h*) corresponding fluxes from the abaxial surface. Elements of TIR loss $\left(Q_{TIR}^{+}\right)$ (*i*), (*j*) emission of TIR radiation by the adaxial and abxial surfaces, respectively, at the blackbody rate multiplied by the thermal emissivity; magnitudes of (*i*) and (*j*) are essentially equal because thermal gradients in leaves tend to be very small except on thick cladodes. Elements of sensible heat loss $\left(Q_{E}\text{-}\right)$: (*k*) loss from adaxial surface; (*l*) loss from abaxial surface, which may differ in magnitude from adaxial rate because the boundary-layer conductances differ between sides. Elements of latent heat loss $\left(Q_{c}\text{-}\right)$: (*m*) loss from adaxial surface; (*n*) loss from abaxial surface; again, magnitudes generally differ because of differences in boundary-layer conductances. Transport loss (not cited in text): (*o*) transport in xylem flow; typically very small; conduction along petiole is even smaller. Storage $\left(Q_{s}\text{-}\right)$: (*p*) thermal as heat gain, photosynthetic as chemical enthalpy gain

2. Role of Energy Flows in Transient Heating, Photosynthesis, and Respiration

The last term in the energy balance considered is energy storage, which is given with a negative sign because it subtracts from the energy at the leaf surface. Thermal storage occurs during transients. A sudden sunfleck heats the leaf mass, or a sudden shading cools the leaf mass. Thermal transients are discussed in Sect. IV.B. Photosynthetic carbon fixation (and nitrate reduction) represents chemical energy storage. This is typically small and often neglected in energy balance calculations. Consider the highest rates of photosynthesis observed, approximately 40 μmol CO_2 m^{-2} s^{-1}, which are about twice the highest rates of most crops and about 4 to 8 times the rates of common non-crop trees. The rate expressed as moles of glucose production is 1/6 that of CO_2 fixation, or about 6.7 μmol glu m^{-2} s^{-1}. The heat (enthalpy) of formation of glucose under standard conditions is about 2805 kJ mol^{-1}, to be moderately adjusted for the nonstandard conditions in the leaf (e.g., the partial pressures of CO_2 and O_2 are not 1 atm). Then, the rate of enthalpy storage is the rate of glucose formation, multiplied by the enthalpy stored per mole of glucose. The rate is then approximately 6.7×10^{-6} mol glu m^{-2} s^{-1} *

2.8×10^6 J mol^{-1} glu, or 17 W m^{-2}. This magnitude is to be contrasted with other energy flux densities, which in photosynthetic conditions are each typically several hundred watts per square meter. We may make similar arguments about the leaf respiration rate, which is typically a small fraction of the photosynthetic rate, often 8–10 % at most temperatures after leaves acclimate (Atkin et al. 2005; Wythers et al. 2005), with the bulk of respiration occurring in heterotrophic tissues of the plant or in soil organisms.

B. Defining the Individual Terms of the Energy Balance Equation

To use the original steady-state equation, we must resolve the individual terms, using driving variables such as solar radiation, leaf (essentially fixed) parameters such as shortwave absorptivities, boundary conditions such as atmospheric conditions, and temperature as a state variable. We can use the formula for the average T of a whole leaf or solve the equation segment-wise using the finite element method (Chelle 2005).

1. Shortwave Energy Input

Shortwave energy absorption is given as:

$$Q_{SW}^{+} = a_{PAR}E_{PAR} + a_{NIR}E_{NIR} \tag{2.2}$$

Here, the a's are absorptivities in the two wavebands (and we can consider resolving wavebands more finely) and the E's are energy flux densities in those wavebands, projected onto the leaf lamina normally. The absorptivities need to be measured, as they depend upon nutritional state (the difference between pale and dark leaves in a_{PAR} may be between 0.7 and 0.85 or higher), leaf hairiness and waxiness, and, to some extent, the angle of illumination. The lower side of the leaf typically has a lower PAR absorptivity. Absorptivity in the NIR is low, near 0.35, as indicated in numerous studies. More generally, absorption for radiation at any wavelength varies with the angle of incidence on the leaf. For diffuse radiation such as skylight that comes from many directions, a more comprehensive treatment is needed both in theory and in field measurement for accurate estimation of the absorbed fraction of radiation. One uses the concept of the bidirectional reflectance distribution function (BRDF; Schaepman-Strub et al. 2006; Chelle 2006; Chap. 11, Disney 2016). The BRDF describes the partitioning of radiation incident from one direction into reflected (and transmitted) radiation in all directions. Integration of the BRDF over all outgoing directions yields a fraction less than unity. This deficit is the absorbed fraction. This level of detail is not often demanded in simple calculations.

The values of E_{PAR} and E_{NIR} are composed of the direct solar energy flux densities and the scattered energy flux densities. Considerable complexity attends the calculation of the scattered radiation, as will be discussed in the section on leaves in canopies, but some useful simplifications are available. In some modeling efforts, the values of the solar energy fluxes will be given directly in energy units, as W m^{-2}. In other efforts, we may have available the quantum flux densities, in mol m^{-2} for the PAR, with the conversion that 1 mol of photons has roughly 220 kJ of energy. However, for precise conversion, one needs the spectrum of solar energy (Ross and Sulev 2000). It is unusual to have NIR energy flux density quoted in moles, and often it is not given; one must use the relation that the PAR and NIR energy flux densities in sunlight are nearly identical, with some finer approximations being available, particularly to correct for shifts caused by cloudiness, aerosols, etc. (Escobedo et al. 2009).

2. Thermal Infrared Input

Continuing, we may formulate the TIR input in terms of the energy flux density in the TIR band as

$$Q_{TIR}^{+} = \varepsilon E_{TIR} \tag{2.3}$$

Here, ε is the thermal absorptivity of the leaf, which equals its emissivity, by the

physical principle of microscopic reversibility. The absorptivity is commonly very closely to 0.96, because it is dominated by the water content. Very waxy leaves may have modestly lower values. The incident TIR energy flux density, E_{TIR}, has, as noted, contributions from the sky and from terrestrial sources. Sky TIR, as we may call it, can be measured directly, with multiband radiometers. However, these are expensive and not used in most situations calling for modeling of leaf performance. Consequently, we usually need to use approximate equations that estimate E_{TIR} from ground-level weather variables, the air temperature and humidity. The TIR flux is continuously absorbed and emitted at all levels of the atmosphere. Accurate prediction requires a radiative transport model, and a knowledge of the distribution of the content of water (the by-far dominant TIR-active molecule) at all levels. For a standard atmospheric profile of temperature and water vapor content (not always the case!), the TIR emission of water molecules at all levels is prescribed, as is the transport of this TIR radiation with transmission, absorption, and reemission occurring at all levels. The transport equation can be solved, as it often is for satellite meteorology (Zhang et al. 2004) but more commonly a plant modeler will use an empirical relation, such as that of Brutsaert (1984):

$$E_{TIR} = \varepsilon_{sky,eff}\sigma T_{abs,sky}^4 \tag{2.4}$$

with σ as the Stefan-Boltzmann constant, $T_{abs,sky}$ (K) as the temperature of the air at screen height, and the effective emissivity of the sky as

$$\varepsilon_{sky,eff} = 1.72\left(\frac{e_{air}}{T_{air,obs}}\right)^{0.143} \tag{2.5}$$

where e_{air} (kPa) is the partial pressure of water vapor in the air at screen height. For air masses of low relative humidity, the effective sky temperature (representing the sky as a black body at this effective temperature),

$$T_{eff,sky} = \left(\frac{E_{TIR}}{\sigma}\right)^{\frac{1}{4}} \tag{2.6}$$

can be many tens of degrees below air temperature, and the "deficit" in E_{TIR} relative to the value it would take at an effective emissivity of unity can exceed 150 W m^{-2}. The coldness of the sky in such conditions must be taken into account in accurate models of leaf energy balance. Note that clouds have high emissivities, near 1.00 (Hartmann 1994; Houghton 1977) and emit effectively at the temperature of their bases, which is T at screen height minus the lapse, which is likely to be simply the dry adiabatic lapse rate (ca. 10 K km^{-1}) multiplied by the cloud base height above ground level. For partly cloudy skies one must use both the clear sky and cloud values of E_{TIR} with weighting by fraction of sky coverage.

The contribution of terrestrial radiation sources to the TIR flux is complicated in plant canopies, as it is for shortwave radiation. The emissivity (equal to TIR absorptivity) of leaves is high, approximately 0.96, and most soils are similarly high, about 0.95, although low-iron sands may have emissivities of 0.90. The reflectivity $1 - \varepsilon$, is then low. There is very little reflected TIR inside canopies. As a result, one may estimate TIR fluxes from surrounding leaves, branches, soil, etc. as being their black body radiant flux densities at their body or kinetic temperatures. One then weights the contribution from all these surfaces in the proportion of solid angle each source subtends at the leaf in question. In a simple case, a layered canopy, one may with decent accuracy weight the flux density from each layer by the penetration probability of hemispherically uniform radiation from each layer to the layer of the leaf under consideration.

3. Thermal Infra-Red Losses

The TIR energy loss from the leaf surface, Q_{TIR}-, is rather simply formulated as

$$Q_{TIR}^{-} = 2\varepsilon\sigma T_{abs,leaf}^{4} \tag{2.7}$$

where T_{leaf} (K) is the leaf temperature. The factor of two originates from the leaf having two sides that are effectively at the same temperature, at least in the case of thin leaves. Very thick leaves, and the thick phyllodes of succulent plants, merit a formulation that accounts for their geometry and the T gradients around their periphery.

4. Latent Heat Loss

The latent heat loss by transpiration, λE_{leaf}, is readily expressed for leaves in the common condition of not having surface water, snow, or ice. In this case, water loss occurs from the leaf interior (water vapor partial pressure e_i) through the stomata and the leaf boundary layer to ambient air outside the boundary layer (water vapor partial pressure e_a). Using modern molar units for conductances (Ball 1987), we may write

$$E_{leaf} = g_{bs}\frac{(e_i - e_a)}{P_a} \tag{2.8}$$

or, more accurately to account for mass flow as well as diffusion (Farquhar and Sharkey 1982),

$$E_{leaf} = g_{bs}\frac{e_i - e_a}{Pa - \frac{e_i+e_a}{2}} \tag{2.9}$$

where water vapor partial pressures and air pressure are in Pa and g_{bs} is the total conductance of stomata and the boundary-layer acting as series resistances:

$$\begin{aligned} g_{bs} &= 1/(1/g_s + 1/g_b) \\ &= g_s g_b/(g_s + g_b) \end{aligned} \tag{2.10}$$

Here, g_b and g_s are the conductances of the boundary layer and of stomata for water vapor (moderately different from their conductances for heat or for CO_2; Ball 1987).

The values of e_a and P_a are typically obtained from weather data. The value of e_i is commonly taken equal the saturated water vapor partial pressure at leaf T, $e_{sat}(T)$, and is thus, a function of leaf T only. There are many useful analytical approximations for $e_{sat}(T)$ such as that from Murray (1967), here giving the result in units of Pascals:

$$e_{sat}(T) = 610.8exp\left(\frac{17.269T}{237.2+T}\right) \tag{2.11}$$

For internal consistency, I note that there is generally a small correction for leaf water potential (ψ_{leaf}). This corrections given as $e_{sat}(T)\exp(\psi_{leaf}\ V_w/(RT))$, with V_w as the molar volume of water ($18 \times 10^{-6}\,m^3\,mol^{-1}$). For moderately low water potential of -1 MPa, this factor is about 1 – 1.8/2500, which is essentially negligible.

In conditions of modest wind speed, the leaf boundary layer is commonly laminar, and we can use a formula for leaves of uncomplicated shape (e.g., Campbell and Norman 1998):

$$g_b = a\sqrt{u/d_{leaf}} \tag{2.12}$$

where $a \approx 0.147$ mol m^{-2} $s^{-1/2}$ for a single side of a leaf and u (m s^{-1}) is wind speed at the leaf location, and d_{leaf} is a characteristic leaf dimension, transverse to the wind direction. For highly indented or irregular leaves the reader is referred to Gurevitch and Schuepp (1990). For leaves having stomata on both leaf sides, and with unequal distribution of stomatal conductance (g_s) for leaf lower and upper side (LI-COR Biosciences 2004) (Parkinson 1985):

$$g_b = \frac{(1+K)^2}{K^2+1}g_{b,1} \tag{2.13}$$

with K being the ratio of g_s on the two sides of the leaf, and $g_{b,1}$ being the one-sided

boundary-layer conductance. I note that this equation refers to calculation of water vapor and CO_2 transfer conductance from ambient air to leaf intercellular air space (Eqs. 2.8 and 2.9) not for calculation of transfer conductance for heat exchange.

For high wind speeds, the boundary layer can become mixed laminar-turbulent, and the leaf dimensions can change from leaf rolling (Alben et al. 2002; Jarvis and McNaughton 1986 – see p. 42). Leaf fluttering can alter g_b and can occur at low wind speeds, as in the iconic quaking aspen, *Populus tremuloides* (Roden and Pearcy 1993). At very low wind speeds, convection undergoes a transition from forced convection by external wind toward free convection driven by thermal gradients in the air. At the free-convection limit, we have

$$g_b = \alpha\left(\frac{T_{leaf} - T_{air}}{d}\right)^{\frac{1}{4}} \qquad (2.14)$$

with $\alpha = 0.05$ mol $m^{-\frac{7}{4}}$ $s^{-1}K^{-\frac{1}{4}}$ There are formulas for intermediate cases (Kreith 1965; Schuepp 1993). While anything approaching free convection is rare under weather conditions in which photosynthesis occurs at a significant rate, the time intervals in which free convection occurs can be important for photosynthesis at other times of day. Ball et al. (2002) give a classic example from snow gum (*Eucalyptus pauciflora*) seedlings in an Australian forest clearing in wintertime. Pre-dawn and immediately post-dawn, u is near zero, giving a very low value of g_b and thus of convective heat transfer rate, Q_c-. Radiative energy balance becomes critical; leaf T drops about 2–4 °C below air T. Leaves freeze, but the damage to photosynthetic capacity arises almost exclusively from photoinhibition, in turn caused by very low T and high solar irradiance on leaves.

To continue, we must also know the value of stomatal conductance, g_s, in order to compute latent heat flux density from the leaf. A simple solution of the energy balance equation is possible if this is a known, fixed value.

5. Convective Heat Exchange

Finally, I the basic formula for the convective heat-loss rate is:

$$Q_C^- = g_{b,h}C_{P,air}\left(T_{leaf} - T_{air}\right) \qquad (2.15)$$

where $g_{b,h}$ is the boundary-layer conductance for heat (about 0.92 that for water vapor; Campbell and Norman 1998) in usual molar units and $C_{P,m}$ is the molar heat capacity for air. Of course, the flux density can be negative under advective conditions when the air is hotter than the leaves.

6. Solving the Leaf Energy Balance Equation

Once we have all the terms in the energy-balance equation, we have a form in which all quantities are fixed other than leaf T, and one may apply any of the iterative schemes to find the steady-state temperature. No precise analytic solution is possible because the equation is transcendental in T: the TIR emission from the leaf, Q_{TIR}-, is quartic in T, the convective loss, Q_c, is linear in T, and the latent heat loss is approximately exponential in T. An iterative solution is almost always affordable (Box 2.2). In addition, various approximate solutions have been proposed that in general provide a good approximation of leaf temperature (Paw 1987; Greek et al. 1989), and under certain assumptions leaf energy balance can be calculated using a quadratic analytical solution (Baldocchi 1994).

Box 2.2 Iterative Solution of the Leaf Energy Balance Equation

One can guess the value of T and then use the Newton-Raphson method of root-finding. Expressing the energy-balance equation as $f(T) = 0$, we assume that, at any T, $f(T)$ is nearly linear in T in some small neighborhood, or $f(T + dT) \approx f(T) + f'(T)\,dT$. If $f(T)$ at the estimated T is nonzero, we can posit that there is a dT that

(continued)

Box 2.2 (continued)

makes $f(T + dT) = 0$, or $dT = -f(T)/f'(T)$. This will give an improved value, which we may then improve in the next iteration until $f(T)$ is sufficiently small, say 1 W m^{-2} or less. The values of $f(T)$ and $f'(T)$ can easily be computed numerically using the very accurate analytic formulas for the partial pressure of water vapor, which generates a corresponding analytic formula for the derivative with respect to T. For example, if we use Eq. (2.12) above, the derivative of $e_{sat}(T)$ is e_{sat} itself, multiplied by the factor $(17.269*237.2)/(237.2 + T)^2$. At 25°, this factor is 0.060; that is, saturated water vapor pressure rises 6 % per degree Celsius. In the iterations for T using the Newton-Raphson method, it may be necessary to hobble the increments, dT, to perhaps 3–5 °C to avoid overshoots and oscillations.

An inherently stable alternative method of solving the transcendental equation for T is a binary search (Burden and Faires 1985), one of several such numerical root-finding methods (McCalla 1967). For a monotonic function such as energy balance with only one real root, the process is straightforward. A binary search for the root of an equation $f(T) = 0$ begins with the evaluation of $f(T)$ at two endpoints that are estimated to contain a root. Consider a notional case in which at the lower limit, T_0, $f(T)$ is positive, and at the upper limit, T_1, it is negative. One then knows that the root lies between these points. One then evaluates $f(T)$ at the midpoint, which we may call T_2. Suppose that $f(T_2)$ shows up as a negative value, indicating that the root lies between T_0 and T_2. One then makes T_2 the new upper limit in the search. The search continues, with evaluation at T_3, which, with $f(T_3) < 0$, clearly becomes the new lower limit, and so on. Binary searches are rapid, halving the uncertainty each iteration or by $1/2^n$ in n iterations. An initial search interval of 10 °C drops to <0.1 °C in 8 iterations. The modest disadvantage of a binary search is that it requires significantly more lines of code that a simple Newton-Raphson iteration, especially when one includes adaptive expansion of the search limits if the initial endpoints do not encompass a root (e.g., $f(T)$ is positive at both points, or negative at both points).

C. Leaves in Artificial Environments: Growth Chambers, Greenhouses, and Warming Experiments

Similarly to sunlight, the terms in the energy balance equations are the same for leaves in any other situation, and they may be measured by the same or equivalent means, e.g., PAR meters, anemometers, etc. There is one change that is often overlooked when artificial illumination is used, the change in TIR input to the leaves. The sun emits negligible TIR in comparison to its shortwave (SW) radiation in the PAR and NIR. In contrast, growth lamps emit even more TIR than SW radiation – about 3-fold more for fluorescent lamps, and 20-fold more for incandescent lamps, which no modern system uses, except when perhaps supplementing gas-discharge or fluorescent lamps by far-red light. One must account for the increased TIR in modeling plant growth in a growth chamber or artificially illuminated greenhouse, unless the TIR has been filtered out. This filtering can be achieved with a water-filled plenum between the lamps and the plants (Gutschick et al. 1988). In addition, as the energy decreases with the square of distance from the light sources, energy gradients within vegetation are much greater in artificial growth conditions than in outside where the energy source distance effect is negligible, at least for PAR and NIR (Chelle et al. 2007; Delepoulle et al. 2009; Niinemets and Keenan 2012). Furthermore, even outdoors, modelling plant energy balance in artificial environments such as cities is complicated due to shading effects and

different optical and heat capacitance characteristics of buildings.

The copious emission of TIR by lamps is used to effect in outdoor warming experiments (e.g., Kimball 2005). The effect, however, is not equivalent to the warming of air under climate change. Put most simply, the topmost leaves warm the most and lower leaves less so, because the interception of TIR by leaves above a location depletes the TIR flux density and the energy density is also reduced by distance from TIR source (depending in the geometry of used TIR source). To put it another way, the flux of TIR is vectorial, not equivalent to a uniform change in scalar air temperature. The degree of unrealism is not readily assessed. While upper leaves contribute most to photosynthesis, respiration, and transpiration, there is an extra gradient in leaf temperature through the depth of canopy, over and above the one that develops naturally from differential interception of SW radiation and other effects. This may affect development and fruiting.

D. Detection of Leaf Temperature and of Energy-Balance Components

Although difficult, validation of modeled leaf energy balance and leaf temperature is a necessary pursuit. Models predict the kinetic temperatures of leaves. These temperatures can be measured by contact methods such as thermocouples. Sampling many leaves, at various canopy locations and leaf angular orientations, can easily become impractical. I may relate an amusing anecdote from Marilyn Ball of the Australian National University. Decades ago, the renowned modeler Ian Cowan decided to do a field experiment, in which he added a very large number of sensors, including thermocouples, to a plant. The results were confusing, until it was realized that Cowan had accidentally kicked the plant at its base and severed its stem; only the sensor wires alone were holding the plant up. Even in experiments unconfounded by damage, the presence of a large number of sensors and their stiff or weighty wiring can add artifacts to the results.

The common alternative to contact measurement is measuring the TIR emission by the leaves. The most affordable instruments, simple infrared "guns" or infrared thermocouples, do not image the area being viewed; rather, they average a finite solid angle. Their view into a canopy depends upon the orientation of the sensor, the canopy structure (esp. as row crops), and the position of the sun. Kimes et al. (1981) and many others (e.g., Lagouarde et al. 1995; Smith et al. 1997; Kustas et al. 2007) have analyzed this challenge, without a simple answer, because the question is not simple: does one want the average leaf T or that of a specific canopy stratum? Does one want the average leaf T weighted by area, or by transpiration rate, or by photosynthetic rate? A step toward resolving the problem is using imaging TIR cameras that provide a spatial distribution of leaf temperatures. However, they are quite costly, typically US$ 10 K or more. Some informative results have come forth, including use of thermal imagery to infer the spatial distribution of stomatal conductance (Fig. 2.2; Jones et al. 2002; Leinonen et al. 2006).

For large-scale sensing, such as from satellites, imaging of leaves is impossible. This results in significant problems and inaccuracies in the interpretation of surface (canopy) T for inference of stand transpiration rates, by methods that are discussed in Sect. VI. Many satellite sensors such as MODIS cover wide areas at semi-oblique angles. The spread in view angles incurs the problem of radiative T varying with view angle, noted at the beginning of this paragraph. Satellite remote sensing faces an additional problem, that of distortion of the TIR signal by absorption and emission of TIR in the atmosphere between the satellite and the plant. A great deal of work has gone into deriving accurate models that extract the TIR signal at the surface. The claim for MODIS TIR data is that the inferred surface temperatures are accurate within a standard deviation on the order of 1 °C (Wan et al. 2004).

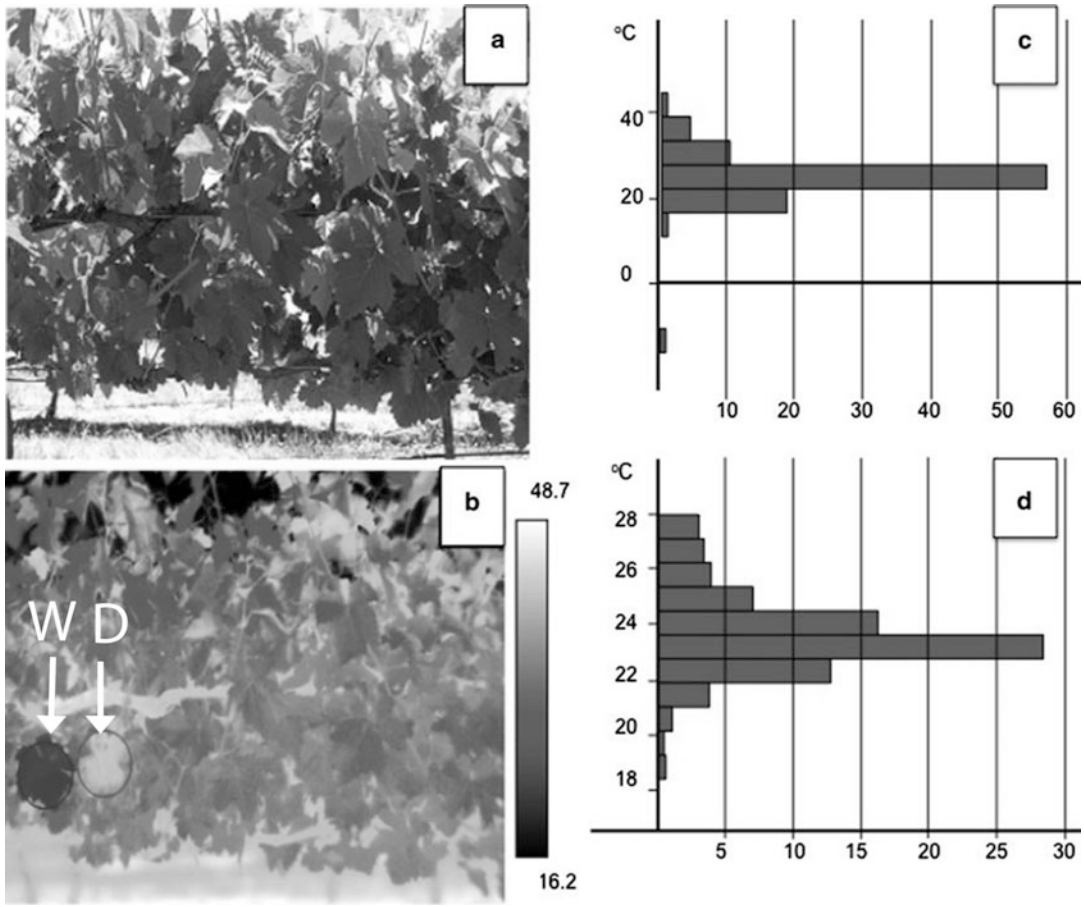

Fig. 2.2. Optical (**a**) and thermal imagery (**b**) of a grapevine canopy in midday, showing a wide range of leaf temperatures arising primarily from varied interception of solar shortwave radiation at varied leaf angular orientations. *Arrows* point to reference leaves that are wet and cool (W) and dry and hot (D). Histograms of temperature derived from thermal imagery are presented for the complete scene (**c**) and for leaves only (**d**), i.e., excluding hot soil and "cold" sky. Minimally modified from Fig. 2.1 of Fuentes et al. (2005) – converted to grayscale, with addition of more obvious arrows for reference leaves in panel (**b**); lower end of temperature scale for panel (**b**) corrected to +16.2 °C from −16.2 °C; used with permission

E. Meeting the Challenges of Measurement and Theory

Using the concepts of energy balance is clearly fraught with a number of challenges. Some arise from limitations of data. One challenge that is rife, especially for studies over large areas or multispecies assemblages is, Can one measure enough parameters such as optical absorptivities, stomatal control parameters, or photosynthetic capacities to predict energy balance and the processes linked to it? One lead here is that there are often rather robust approximations suitable for initial studies. For example, in stomatal control modeled with the Ball-Berry formula (Ball et al. 1987), the slope parameter is close to 10 for most species that have the C_3 photosynthetic pathway (Gutschick and Simmoneau 2002).

Other challenges arise from conceptual complexity and attendant mathematical complexity. Conceptual complexity is not, however, conceptual uncertainty;

biophysical and physiological theory is well developed. Admittedly, one often needs to develop simplifications to reduce complexity. One may simplify the description of radiative transport within a plant canopy, perhaps using two-stream models of upward- and downward-propagating radiation (Liang and Strahler 1993; extensions by Gutschick and Wiegel 1984; Dai and Sun 2006). One must be aware that the approximation must be tested and that its accuracy is likely to vary with canopy structure, such as leaf angle distribution. Mathematical complexity succumbs to mathematical abilities, which might be effectively "contracted out" to collaborators or else dug out of the literature. Even the coupled nonlinear processes of energy balance, photosynthesis, stomatal control, and scalar transport in leaves became tractable long ago, as in the work of Collatz et al. (1991; see also Sect. III.C here). Computational complexity, that is, generating a computer program to handle the math and to run at an affordable rate, is often only weakly related to mathematical complexity. A very large number of equations that are inherently linear or well approximated by linearization can be handled readily by linear algebra, even with very many variables. On the other hand, problems that are simply formulated mathematically, such as the classic traveling salesman problem or the box-packing problem (engaging popular account by Graham 1978) have no algorithms short of trying every possible choice. Powerful approximation methods do exist for these, including simulated annealing (Kirkpatrick et al. 1983; Gershenfeld 1999) and genetic algorithms (Gershenfeld 1999). Raw computing power has ceased to be the limiting factor for most problems in the field of biology, certainly not being problematic for energy balance.

Experimental measurement and the design of experiments pose some persistent problems. Estimating transpiration from fields or landscapes (or its reduction, as a measure of stress) by remote sensing relies on measuring thermal radiation from the surfaces, primarily. Radiation moves as a vector, in straight lines, but actual kinetic temperature that conditions the transpiration rates of leaves is a scalar. Its spatial distribution is sampled with different weightings as the view angles of the radiation sensor change, as noted above. One gain on the problem is recognition that one must be clear about which spatially integrated temperature one wants. Is it weighted by canopy scalar transport capacity, for calculating sensible heat flux? Is it weighted by, primarily, stomatal conductance for calculating canopy transpiration? One might develop empirical relations between radiative temperature (perhaps over several view angles) and the fluxes one wishes to measure. One must be aware that these measures will be fairly specific to the canopy physical structure, for one. One might also add in models of photosynthesis and stomatal conductance to get a more general method. Good problems for future research await being addressed.

III. Physiological Feedbacks Affecting Leaf Energy Balance

In a free-running model of a plant canopy, which predicts all fluxes from plant parameters and driving variables, one must model the stomatal conductance of any given leaf from biochemical and physical processes, which depend upon leaf temperature. In effect, we must solve simultaneously the equations for energy balance, photosynthetic rate, stomatal conductance, and CO_2 transport, all but one (transport) being nonlinear.

A. Dependence of Stomatal Conductance on Environmental Drivers

Stomatal conductance to water vapor, g_s is tightly linked to very temperature-dependent photosynthetic rate itself, as expressed in various useful empirical formulas. I use here the seminal formula of Ball et al. (1987), which has been modified (see esp. Leuning 1995 and Dewar 2002), but often found as accurate as the modified

versions (e.g., Gutschick and Simmoneau 2002; Chap. 3 Hikosaka et al. 2016a):

$$g_s = m_{BB}\frac{Ah_s}{C_s} + b_{BB} \tag{2.16}$$

Here, m and b are empirical constants, with surprisingly low variation among well-watered plants (Ball et al. 1987; Collatz et al. 1991; Gutschick 2007), A is the net photosynthetic rate, and h_s is the relative humidity and C_s the CO_2 mixing ratio, both at the leaf surface, beneath the boundary layer. The values of m_{BB} and b_{BB} are sensitive to water stress (Gutschick and Simmoneau 2002). The formula for h_s is simply e_s/e_i, with e_s defined as the saturated water vapor pressure at the leaf surface. We can solve for e_s considering that in the steady-state the leaf transpiration rate,

$$\begin{aligned} E &= g_b\frac{(e_s - e_a)}{P_a} = g_s\frac{(e_i - e_s)}{P_a} \\ \rightarrow h_s &= \frac{e_s}{e_i} = \frac{\left(\frac{e_a}{e_i} + \frac{g_s}{g_b}\right)}{\left(1 + \frac{g_s}{g_b}\right)} \end{aligned} \tag{2.17}$$

We need to determine A as a function of temperature in a way that is consistent with transport through the combined conductance of CO_2, $g_{bs}^{'}$, which uses the expressions relating conductances for CO_2 to conductances for water vapor,

$$g_b^{'} = 0.72g_b, \quad g_s^{'} = 0.62g_s \tag{2.18}$$

B. Biochemical Limitations of Photosynthesis

Photosynthesis has both light-limited regimes ($A = A_{LL}$) and light-saturated regimes ($A = A_{sat}$), with a good approximation for any light level being (Johnson and Thornley 1984; Farquhar et al. 1980)

$$\vartheta A^2 - (A_{LL} + A_{sat})A + A_{LL}A_{sat} = 0 \tag{2.19}$$

Here, A is the *gross* rate of CO_2 fixation, excluding respiratory losses, θ is a transition parameter; at $\theta = 1$, A shows a completely sharp transition between regimes; typical values seen in studies to date cluster around 0.8 (variation discussed by Jones et al. 2014). The net rate of CO_2 fixation is the gross rate debited for "dark" respiration, R_d. More or less complex models of dark respiration exist. A simple one is that it acclimates as a fairly constant fraction of net photosynthesis at the mean temperature of the photoperiod in the preceding week or two (T_{mean}; see Sect. II above; Wythers et al. 2005), varying with the diurnal temperature cycle as a simple exponential activation such as exp[0.07 $(T - T_{mean})$].

The biochemical expressions for A_{LL} and A_{sat} have been elegantly simplified in the work of Farquhar et al. (1980, with later elaborations). For C_3 plants, we have commonly

$$A_{sat} = V_{c,\max}\frac{(C_i - \Gamma^*)}{(C_i - K_{CO})} \tag{2.20}$$

where $V_{c,\max}$ is the maximal ribulose 1,5-bisphosphate carboxylation capacity, Γ* is a hypothetical compensation partial pressure without dark respiration, but accounting for photochemical carbon oxidation or "photorespiration", and K_{CO} is an effective Michaelis constant for enzymatic binding of CO_2 to the rate-limiting Rubisco enzyme, and C_i is the CO_2 partial pressure inside the leaf; accuracy is gained by using C_c, the partial pressure at the carboxylating enzyme, Rubisco, in the chloroplasts (Niinemets et al. 2009). C_c is lower than C_i due to a significant CO_2 diffusion resistance in the gas, liquid and lipid phases from substomatal cavities to chloroplasts. $V_{c,\max}$, Γ* and K_{CO} are functions of temperature, and Γ*and K_{CO} are functions of the partial pressure of oxygen. This form applies when CO_2 fixation by Rubisco enzyme is the limiting factor. In some conditions, electron transport or triose-phosphate transport may be limiting (Farquhar et al. 1980; Wullschleger 1993).

Similarly, we have the light-limited rate as an "initial quantum yield," ϕ, multiplied by the photosynthetic quantum flux density, I_L,

which may be expressed either as incident or absorbed light:

$$A_{LL} = \phi I_L = \phi_0 \frac{(C_i - \Gamma)}{(C_i + 2\Gamma)} \tag{2.21}$$

Here, ϕ_0 is the quantum yield at saturating CO_2 levels. As an example, we may consider the completely light-saturated case. We equate the biochemical and transport formulations for net photosynthesis, A, to obtain

$$A = V_{c,\max} \frac{(C_i - \Gamma^*)}{(C_i - K_{CO})} - R_d = g'_{bs} \frac{(C_a + C_i)}{Pa} \tag{2.22}$$

Here, C_a is the partial pressure of CO_2 in ambient air. We can multiply both sides by $(C_i + K_{CO})$ to obtain a quadratic equation in C_i, which can be solved explicitly. One can then insert the value of C_i into either equation to obtain the value of A. Note that a more accurate form for the transport relation requires consideration of mass flow (Farquhar and Sharkey 1982),

$$A = \frac{g'_{bs}(C_a - C_i)}{P_a} - \frac{C_i + C_a}{2P_a} E_{leaf} \tag{2.23}$$

which creates a modest complication in the solution. The correction to A due to mass flow is on the order of 5 % for a mesophytic C_3 plant with relatively high transpiration rate.

In the more general case, one can use the Johnson-Thornley expression for A, expressing both A_{LL} and A_{sat} in terms of C_i (→ just algebra; needs no reference). One gets a quartic equation in C_i, which can be solved by a binary or golden-ratio search (http://en.wikipedia.org/wiki/Bisection_method).

C. Solving a Combined Stomata-Photosynthesis Model

With these methods to estimate A, we are ready to get a consistent solution for photosynthetic rate, stomatal conductance, energy balance, and CO_2 transport. An analytic solution is available that however requires definition of a few additional constraints (Baldocchi 1994). In my own work, I find an effective algorithm to be:

- Set up a range of g_s over which to do a binary search
- At any given estimate of g_s, leaf energy balance is set, and so is T
- The value of T sets the values of the biochemical parameters $V_{c,\max}$, Γ^*, and K_{CO}
- The value of C_i can be solved, as just noted, and thus we can obtain the value of A. We also obtain the value of $C_s = C_a - AP_a/g'_b$
- The function whose root is to be sought uses the Ball-Berry equation, or similar equation of one's choice. One composes $f(g_s) = g_s - (m_{BB}Ah_s/C_s + b_{BB})$, and seeks for the root $f(g_s) = 0$.

The binary search is relatively rapid computationally and stable. One needs reasonable estimates of the search interval in g_s, and programming that allows expansion of the range if no root is evident in the initial range. This whole method has been programmed and is available from the author as a standalone program in Fortran 90 source code or as a Windows executable. I have also used inverse modeling in a larger model of climate change impacts in which the above model is at the core. The exercise may be of interest to modelers (Gutschick 2007). The inverse model inferred plant physiological parameters from final performance measures, such as photosynthesis, transpiration, and nitrogen-use efficiency. I then projected (variable) changes in the physiology to do forward modeling of new values of final plant performance measures. A whole-plant model of these coupled processes, including water transport and water potential, has been constructed (Tuzet et al. 2003). Fig. 2.4 presents a flowchart of the calculations presented to this point. Gutschick and Sheng (2013) present more

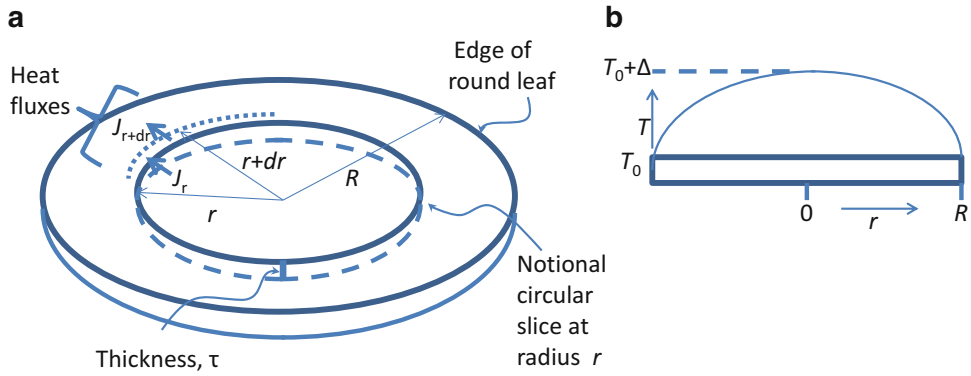

Fig 2.3. Geometry of radial heat flux in a round leaf. (**a**) Slant view of leaf. Azimuthal symmetry of temperature and heat flux is assumed. Flux J_r crosses the area given by the perimeter at radius r multiplied by depth (thickness) τ. Flux J_{r+dr} crosses the area at radius $r + dr$. (**b**) Notional temperature gradient treated in the text is a parabolic function of radius r, peaking at the center at temperature $T = T_0 + \Delta$ in the center and falling to $T = T_0$ at the edge

complete computational details from their study using a model that also treats leaves within the environment set by a complete canopy (see Sect. IV, below).

The strong coupling of the various processes is evident in simulations using varied values of environmental driving variables such as air temperature and of plant parameters such as photosynthetic capacity, $V_{c,\max}$. Evolutionary selection pressure is also implied in the form of the stomatal control program. The Ball-Berry form tends to preserve water-use efficiency by coupling changes in the various processes (Gutschick 2007).

Schemes for predicting the coupled behavior of energy balance, photosynthesis, and transport, such as the one just described, certainly are complex. One might hope for an equation that expresses any flux such as A directly in terms of the driving variables (PAR and NIR flux densities; wind speed; air temperature, relative humidity, and CO_2 partial pressure) and plant parameters (optical properties, photosynthetic parameters, stomatal control parameters, and leaf dimension). This equation would have to be derived by a high-dimensional fitting of data, such as by nonlinear least squares. Although such an equation could be potentially derived, it seems wholly impractical.

D. Advanced Problems

There are several extensions of the technique outlined in Sect. III.C. Foremost, the enzyme-kinetic form for C_4 plants differs from that for C_3 plants used here in the example. The C_4 formulas have been developed, including variants that account for CO_2 leakage out of the bundle-sheath cells (Jenkins 1997; von Caemmerer and Furbank 2003). Collatz et al. (1991) used these in providing a solution of the combined equations of photosynthesis, stomatal conductance (with the Ball-Berry model), energy balance, and CO_2 transport. Note also that the value of C_i is affected by mass transport of water vapor that opposes the inflow of CO_2; corrected expressions are given by Farquhar and Sharkey (1982).

Greater complications arise from the presence of liquid water, ice, or snow on the leaf surface. The least complicated case may be that of dewfall on a leaf with essentially closed stomata. In this case, water vapor flows from air to the leaf surface, releasing the heat of condensation, of magnitude λ times the rate of water condensation on surface. Dewfall will not occur during times when leaves have even modest sunlight interception, but the load of dew

must be evaporated during the latter times. Energy balance is clearly affected by this extra source of water vapor flux away from the leaf. Photosynthesis is also affected by water droplets or films blocking stomata on the upper leaf surface (Hanba et al. 2004). The formulation of dewfall rate as a function of atmospheric conditions, TIR radiative balance, and leaf orientation is beyond the scope of this chapter. Similarly, I leave the discussion of the melting, dripping, and sublimation of ice and snow from leaves to more specialized publications (e.g., Gelfan et al. 2004; Ni-Meister and Gao 2011). This is not to imply that snow and ice dynamics on leaves are relatively unimportant. The vast regions of boreal forest, tundra, and other ice-prone areas are important in climate and the carbon and water cycles on spatial scales from region to globe.

IV. Transients in Energy Balance and in Processes Dependent on Temperature

A. Independence of Different Leaf Regions

We may omit conduction of heat through the petiole or even between different regions of the leaf lamina. The argument is based on a consideration of numerical magnitudes. Consider a leaf of the type that may develop a large gradient in temperature laterally, such as a wide leaf in strong sunlight at low airflow (low boundary-layer conductance, g_b). A sunflower leaf is a good example (Guilioni et al. 2000). For simplicity, consider the T gradient to be (admittedly crudely) radial on a circular leaf, which has a thickness τ (Fig. 2.3). An annulus lying between r and $r + dr$ has a cross sectional area across the thickness of $A = 2\pi r\tau$. The net flow of heat, J, between heat moving in at radius r and heat moving out at radius $r + dr$ is

$$J = A(r)k_{th}\frac{\partial T}{\partial r}|_r + A(r+dr)k_{th}\frac{\partial T}{\partial r}|_{r+dr} \rightarrow Ak_{th}\frac{\partial^2 T}{\partial r^2} \quad (2.24)$$

This is the heat input into the annulus (a ring) having a surface area $2\pi r\ dr$, such that the heat flux density, Q, per unit area of the annulus is the expression above divided by this area, or, using $A = 2\pi r\tau$ again,

$$Q = \tau k_{th}\frac{\partial^2 T}{\partial r^2} \quad (2.25)$$

For a leaf thickness of 200 μm with a quadratic gradient in T covering, say, 8 °C over a final radius R, the second partial derivative is $-16\ K/R^2$. Using the thermal conductivity as that of water, about 0.6 W m^{-1} K^{-1}, we estimate Q as 0.53 W m^{-2}. This is wholly negligible compared to all other terms in the energy balance. A conclusion we may draw is that energy balance may be considered independently for various segments of a leaf that have developed different boundary layer thicknesses (from differences in distance from the leaf leading edge in the wind) or are displayed at different angles to sunlight. The differences can be important for the temperature-dependent processes of leaf or floral initiation (ibid.).

B. Dynamics in Leaf Temperature After Changes in Energy Balance Components

1. Time-Dependent Changes in Temperature After Modifications in Radiation Input

Leaves flutter in the wind, sunflecks come and go. Consequently, the terms in the energy-balance equation shift, as does leaf temperature and the T-dependent processes in the leaf such as photosynthesis. In many cases, it is appropriate to average the leaf performance among the varying conditions, weighting performance contributions by the

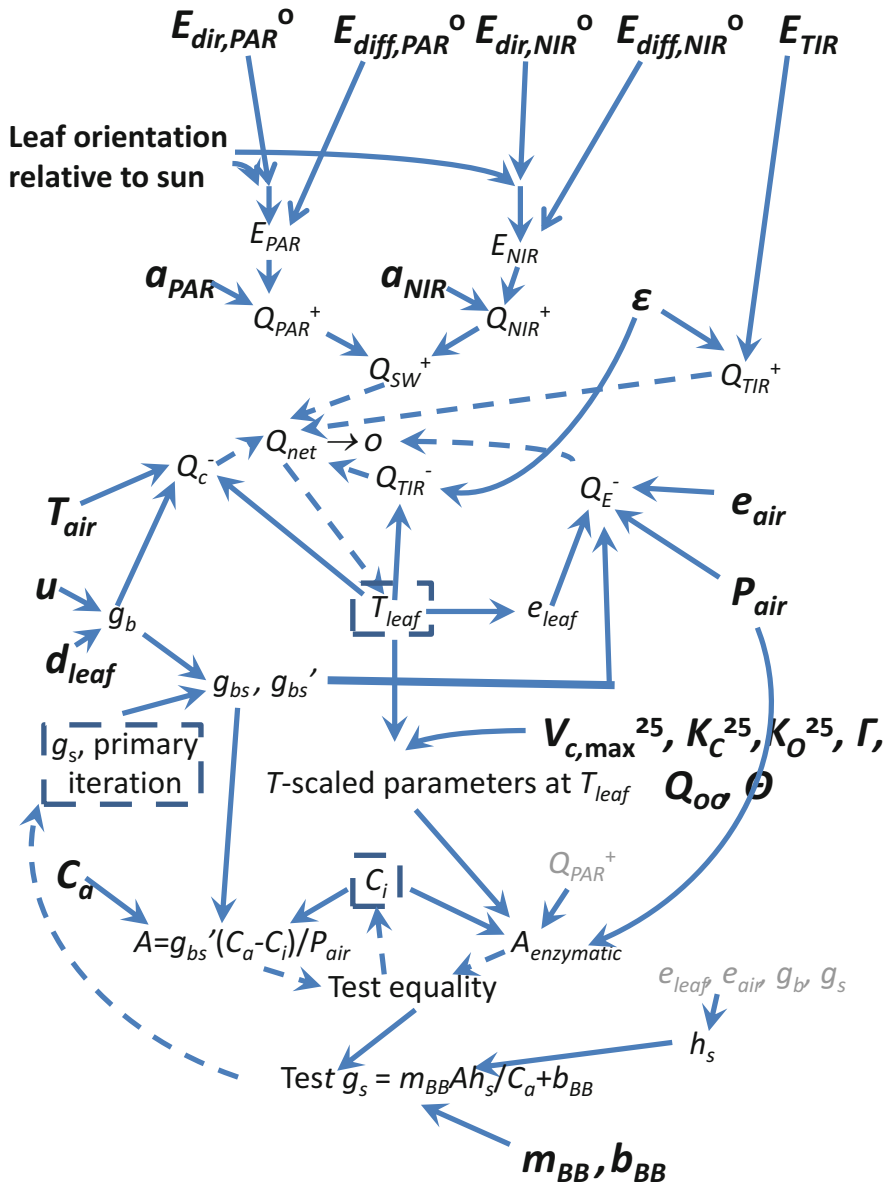

Fig. 2.4. Flowchart for fully mechanistic calculation of energy balance and accompanying fluxes, for an isolated leaf in fully specified environmental conditions. Entries in *large boldface* text are fixed environmental conditions in assumed steady state, as well as fixed physiological, optical, and structural properties of a leaf blade. All other quantities are results of calculations. Shaded quantities are repeated from other locations in the diagram rather than using long arrows from other locations that add complexity. Notation generally follows that in the text, with some added detail, such as expanded subscripts to distinguish contributions of direct and diffuse energy flux densities in the PAR and NIR wavebands (compare simpler notation in Eq. 2.2 in the text). *Solid arrows* indicate forward calculations using equations given in the text or related publications. *Dashed arrows* indicate feedback of results for iterative correction of quantities at the arrow heads with new input values. With all environmental conditions and parameters being set, the origin of iterations is setting the stomatal conductance, g_s, leading to estimation of evaporative heat loss, Q_E-. This allows, in turn, estimation of leaf temperature (T_{leaf} here, for clarity; denoted T_l in text). After leaf temperature estimates have converged, the photosynthetic rate is computed iteratively by adjusting leaf internal CO_2 partial pressure, C_i, so that the rate computed from transport through stomatal and boundary-layer resistances (A in equation on *right* near *bottom*) equals the rate computed from enzyme kinetics ($A_{enzymatic}$, as in Eqs. 2.20, 2.21, 2.22, and 2.23 in text). The value of g_s is then compared to the value required for consistency with the stomatal control model, here given as the Ball-Berry form (Ball et al. 1987; Eq. 2.16 in text). A difference greater than a chosen tolerance incurs iteration with a new value of g_s, chosen effectively with a binary search method

Table 2.1. Representative flux densities, W m^{-2}. Q_S- from photosynthesis, except (*th*) = thermal

Condition	Q^+_{SW}	Q^+_{TIR}	Q_{TIR}-	Q_E-	Q_c-	Q_S-
Crop, full sun; warm, dry	550	800	900	400	50	5–18
Crop, night; warm, dry	0	700	800	≈0	−100	−0.5 to −2
Needle leaf; lower sun, cool	200	650	700	100	50	0–2
Desert evergreen; low sun, winter	150	650	700	50	50	0–3
Crop, sunfleck; warm, dry	550	800	850 → 900	100 → 400	0 → 50	400 (*th*) → 0

fraction of time spent in each condition. There are, however, cases in which transient behavior is very important. Both measurements and models have been made on understory plants that see infrequent sunflecks of short duration (Chazdon and Pearcy 1991; Pearcy et al. 1997). The plant must accomplish its photosynthetic carbon gain in these sunflecks with rapid adjustments of stomatal conductance and of the activation state of Rubisco. The latter phenomena merit discussion in other venues and in other chapters in this book. Here, we may consider the transient behavior in leaf energy balance and temperature. The energy-balance equation modified for time-dependent behavior must account for the net rate of heat gain, *J*,

$$Q^+_{SW} + Q^+_{TIR} - Q^-_{TIR} - Q^-_E - Q_c = C_{P,a}(dT/dt) \tag{2.26}$$

Here, $C_{P,a}$ is the heat capacity of the leaf per unit area, which is simply the heat capacity per unit leaf fresh mass multiplied by the fresh mass per unit leaf area. If the leaf is 20 % dry matter, its heat capacity per mass is 0.8 times the heat capacity of water, about 4200 J kg^{-1} K^{-1}, plus 0.2 times the heat capacity of dry matter, 1000 J kg^{-1} K^{-1}. This yields a heat capacity per mass of 3560 J kg^{-1} K^{-1}. Per area, the heat capacity is the value per mass multiplied by the mass per area. In Table 2.1, to be explained shortly, one example is a thin leaf, 0.2 mm thick, with 0.2 kg of fresh mass per square meter. The heat capacity per area, $C_{P,a}$, is then 712 J kg^{-1} m^{-2}. Now consider a leaf in which the terms in Eq. 2.1 shift from an initial steady state. A very common case is a change in a direct energy input, as a change in shortwave energy input (change in sunlight amount). Let the change in Q^+_{SW} be by an amount δ. Let the original values of the energy terms be denoted with an additional subscript "0" (e.g., $Q^+_{\mathrm{SW},0}$) and their derivatives with respect to temperature be denoted by appropriately subscripted quantities b_i. For example, $(d/dT)Q_E$-$= b_E$, which we can evaluate from Eq. 2.8 as $\lambda g_{bs}(de_{sat}/dT)/P_a$. Let ΔT be the change in temperature from the original steady value, T-T_0. Eq. 2.26 above becomes

$$\begin{aligned} C_{P,a}\frac{dT}{dt} &= Q^+_{SW,0} + \delta + Q^+_{TIR,0} - Q^-_{TIR,0} \\ &\quad - b_{TIR}\Delta T - Q^+_{E,0} - b_E\Delta T \\ &\quad - Q^-_{c,0} - b_c\Delta T \end{aligned} \tag{2.27}$$

$$\begin{aligned} &= \left(Q^+_{SW,0} + Q^+_{TIR,0} - Q^-_{TIR,0} - Q^-_{E,0} - Q^-_{c,0}\right) \\ &\quad + \delta - (b_{TIR} + b_E + b_c)\Delta T \\ &= \delta - B\Delta T \end{aligned} \tag{2.28}$$

Here, B_{net} is the sum of the derivatives, $b_{TIR} + b_E + b_c$. I ignore here the higher-order terms in $\Delta T$with the second derivatives of the terms with respect to temperature; this is acceptable for a first estimate. The sum of the terms in the first parentheses is clearly zero, representing the initial steady state. We can rewrite this once more, using $(d/dt)\Delta T = (d/dt)T$, so that, dividing by $C_{P,a}$, it has the form

$$\frac{d\Delta T}{dt} = a' - B'\Delta T \tag{2.29}$$

with $a' = \delta/C_{P,a}$ and $B' = B_{net}/C_{P,a}$. This is a simple relaxation equation with the readily-verified solution

$$\Delta T = \frac{a'}{B'}\left(1 - e^{-B't}\right) \tag{2.30}$$

That is, the asymptotic shift in temperature is a'/B', with a characteristic relaxation time $\tau_r = 1/B'$, as the time for the response to reach half its final value. We may make a quick estimate of this time. Table 2.1 presents examples for a thin leaf, 200 μm thick, with a fresh mass per area of 0.2 kg m^{-2}, and a thick cactus phyllode, 20 mm thick. Let the sudden change in absorbed shortwave loading, δ, be 200 W m^{-2}. The estimation of B and then of B' is lengthy; Table 2.1 presents the numerical values of all the terms in the equations, for the environmental conditions specified in the header. The relaxation time is $1/B' = 18.4$ s, quite short for the thin leaves that have very little thermal inertia. The transients in thick phyllodes are correspondingly slower, over 0.7 h. The calculation for phyllodes involves more significant approximations. Their curved surfaces present different angles to incident radiation at different locations. The transport of heat laterally is also more effective than in thin leaves. Accurate calculation of their energy balance requires explicit accounting of space and time, using a partial differential equation. With complex geometry, one must use finite elements.

2. Changes in Temperature After Modifications in Convective Heat Exchange

We can do a similar exercise to estimate the transient response to a change in wind speed. This does not change an energy input directly; rather, it changes the value of g_b, a parameter, not a driving variable such as Q^+_{SW}. All the temperature derivatives of energy terms appear, as in the case presented in the preceding section. The driving term, δ, has a new form, which we see when we formulate the equation for relaxation with a bit more algebra. Letting $g_b \rightarrow g_b' = g_{b,0} + \Delta g_b$, and noting that the leaf temperature changes by an amount ΔT, we may write

$$\begin{aligned}\frac{Q^-_{cc,0}}{C_P} &\rightarrow \left(g_{b,0} + \Delta g_b\right)\left(T_0 + \Delta T - T_{air}\right)\\ &= g_{b,0}(T_0 - T_{air}) + g_{b,0}\Delta T\\ &\quad + \Delta g_b(T_0 - T_{air}) + \Delta g_b \Delta T\\ &= g_{b,0}(T_0 - T_{air})\\ &\quad + \Delta g_b(T_0 - T_{air}) + g_{b,0}\Delta T\end{aligned} \tag{2.31}$$

The first term when grouped with the initial values of the radiative and latent heat terms, makes a sum of zero, because these values are from the initial steady state. The new driving term is $\Delta g_b(T_0\text{-}T_{air})$, which we may denote as δ, as in the previous case. There is a new temperature derivative of the Q_c- term, which is $b_c = C_P g_b$; it includes the contribution of Δg_b. Let us consider the same initial steady state, with the perturbation being a doubling of g_b as the wind increases, changing $C_P g_b$ from 16.7 to 33.4 W m^{-2}. The new δ term is then -16.7 W m^{-2} K^{-1} × 3 K = -50 W m^{-2} (negative; the leaf is cooled). The new B_{net} term is the same as the value calculated for the case of a change in solar irradiance, except that the contribution of b_c is twice as large. The new value of B_{net} is then 62.9 W m^{-2} K^{-1}. The asymptotic change in leaf T is $\Delta T = \delta/B_{net} = -50/62.9$ K $= -0.8$ K. The relaxation time is somewhat shorter, since B_{net} has increased in magnitude by a factor 62.9/46.1 = 1.36; now this time is 18.4 s/1.36 = 13.5 s.

3. Importance of Temperature Transients for Photosynthesis

The change in temperature with a change in energy-balance terms occurs on a time scale that is short relative to response times of (most) stomata, which are on the order of (sometimes many) minutes (Grantz and Zeiger 1986; Way and Pearcy 2012). On the other hand, it is long with respect to some photosynthetic biochemical responses such as changes in ribulose-1,5-bisphosphate pool size (Pearcy et al. 1997). Although such changes are somewhat buffered by existing metabolite pool sizes, they can still

alter photosynthesis in fluctuating environments such as during lightflecks intervened by significant periods in darkness (Pearcy 1988). However, such changes are not included in the steady-state Farquhar et al. (1980) photosynthesis model considered here (Eqs. 2.21 and 2.22). A model that accounts for transients have been advanced by Pearcy et al. (1997).

Changes in the activation of Rubisco enzyme by Rubisco activase are also generally relatively slow (Pearcy et al. 1997 for representative kinetic constants). Perhaps most plants that experience significant excursions in leaf temperature have two different Rubisco activases, one for low *T* and one for high *T*, such as has been found in maize (*Zea mays*) (Salvucci and Crafts-Brandner 2004). These change slowly in dominance in the cell, via changes in gene expression over time scales closer to tens of minutes or an hour. This means that a modeler must use the short-term responses of photosynthesis to T, not the long-term responses that include changes in activase expression.

V. Leaves in Canopies

A. General Principles

The principal changes from isolated leaves to leaves in canopies are in radiation interception (shortwave and TIR, both), wind speed, and air temperature and water vapor content. These variations are directly related to the 3-D architecture of leaf (and stem) placement within the canopy (Chap. 8, Evers 2016). There are also correlated changes in leaf properties, such as gradients in leaf photosynthetic capacity with mean light level that varies throughout a canopy (Chap. 4, Niinemets 2016) The net effect of the microenvironmental and physiological variations throughout the canopy is an added level of complexity in computing whole-canopy photosynthesis (Chap. 9, Hikosaka et al. 2016b). The measurement of whole-canopy photosynthesis, such as by eddy covariance (Chap. 10, Kumagai 2016) tests the accuracy of modeling of whole-canopy fluxes of CO_2, water vapor, and sensible heat.

The changes in radiation interception are discussed in the preceding chapter (Chap. 1, Goudriaan 2016). I note that the changes in TIR flux densities are important to model correctly (topmost leaves see as downwelling TIR the relatively "cold" sky-radiated TIR, while leaves deeper in the canopy see more of the "warm" TIR from other leaves, stems, and soil). The changes in wind speed, *u*, can be modeled with a variety of models, some of them simple (Baldocchi et al. 1983; Goudriaan 1977), commonly as negative exponentials, for the attenuation of *u* with depth in the canopy expressed as leaf area index (useful only in horizontally uniform layered canopies):

$$u(z) = u(h)e^{a(z/h-1)} \qquad (2.32)$$

where *h* is the top of the canopy, z is the height and the coefficient *a* can be related to canopy leaf area index, height, and mean leaf spacing (Goudriaan 1977; formulas reported in Campbell and Norman 1998; see also Cescatti and Marcolla 2004).

Atmospheric conditions – air temperature and partial pressures of water vapor and of CO_2 – vary by position within the canopy. In a simple layered canopy, one may average out some variations and regard these scalar variables as functions of a single dimension, depth (Chelle 2005). Basically, the transport of these scalar quantities between layers (and, of course, right to the top of the canopy) is against eddy-diffusive resistances throughout the canopy. There is also an effective resistance of a whole-canopy boundary layer above the canopy, to the height at which one is interested in modeling or measuring fluxes. As a result, the canopy humidifies and heats (or cools) its air under common conditions. This changes the leaf microenvironments (local air *T*, etc.), at all levels, in turn, changing the leaf fluxes in a feedback loop. Models of the effects have no analytical solutions, so that iterative solutions are needed.

B. Modelling Turbulent Transport and Canopy Profiles of Environmental Drivers

The formulation of the transport resistances for heat and water vapor (and momentum) within and above a plant canopy can be complex. Consider first the transport within the canopy. For laterally uniform canopies that can effectively be regarded as layered, one can resolve layers of finite thickness (finite elements). One attributes to each layer a set of microenvironmental conditions of air temperature, humidity, and CO_2 partial pressure. Each layer then represents a source of the scalar quantities – heat, water vapor, and CO_2 (negative for leaves doing net photosynthesis). Between layers there are resistances, formulated as the reciprocals of eddy diffusivities (Denmead 1964; Denmead and Bradley 1987). Eddy diffusivities are the analog of molecular diffusivities, and they arise from bulk air movement in eddies moving in the air (see Campbell and Norman 1998 for an extensive discussion). There are some simple approximations, such as that the eddy diffusivities of the scalars are all equal to each other, $K_H = K_{wv} = K_{CO_2} = K(z)$, with z = height above the soil, and that $K(z) =$ constant $x\ u(z)$. Wind speed at the top of the canopy, $z = h$, is impractical to measure, so that one uses wind speed at a reference height above the canopy and then extrapolates it to the top of the canopy, using the standard wind profile

$$u(z) = u_* ln\left(\frac{z-d}{z_m}\right) \tag{2.33}$$

Here, u_* is a friction velocity (effectively a fitting constant), $d \approx 0.65\ h$ is the so-called zero plane displacement (an effective depth within the canopy of a drag sink, at which $u \rightarrow 0$), and $z_m \approx 0.1\ h$ is the canopy roughness length. These quantities actually vary with wind speed, because wind distorts the canopies, but the effect is generally considered rather too complex to factor in.

To use this so-called K-theory of transport (Wilson et al. 2003), one relates the concentration of each scalar at a given canopy layer to the concentration of that scalar in the layer below, plus the source strength of the layer below multiplied by the transport resistance between the two layers. The boundary conditions (the magnitudes of the scalars) are only given at the top of the canopy, from measurements at, perhaps, a weather station. One ends up with a series of simultaneous quasi-linear equations. I use the qualifier "quasi" because the sources at one layer affect the microenvironment at the next layer and change its source strength in a nonlinear fashion – that is, transpiration by leaves in any environment is not a linear function of temperature, nor of humidity or CO_2 partial pressure. Iterative solutions are merited.

One can also consider the canopy microenvironment and the canopy resistances as bulked – the microenvironment is uniform inside the canopy, and the canopy resistances to scalar transport are calculated by integrating the eddy diffusivity from the zero-plane displacement height to any chosen reference height, z. The development of the equations is somewhat lengthy, so that I refer to reader to Campbell and Norman (1998). Part of the complexity is that turbulent transport is enhanced if the canopy is liberating sensible heat ($H > 0$) and it is suppressed if the canopy is absorbing sensible heat ($H < 0$). The stability corrections to transport have been formulated using similarity theory, with the following result for the canopy aerodynamic conductance for sensible heat at height z above the canopy $(z > h)$:

$$g_{aH} = \frac{k^2 \rho u(z)}{\left[\ln\left(\frac{z-d}{z_m}\right) + \psi_m\right]\left[\ln\left(\frac{z-d}{z_H}\right) + \psi_H\right]} \tag{2.34}$$

Here, $k = 0.41$ is unitless von Karman's constant, ρ is the molar density of air (mol m^{-3}, when we want g_{aH} in molar units), $z_H = 0.2 z_m$ is the roughness length

for heat transport, and the ψ values correct for transport under stable or unstable conditions. Air is stable when it does not spontaneously rise (and by turbulence carry sensible heat upward, $H > 0$); the rate of temperature decrease with height must be less than the rate that would occur by free expansion of air without heat exchange to neighboring air, the adiabatic lapse rate, about 0.098 K per meter (Chapter 4 in Campbell and Norman 1998). The stability correction factors depend upon whether the surface is undergoing net heating or cooling. With net heating ($H > 0$) , air parcels near the ground become less dense, making them rise by turbulent transport. The atmosphere is then unstable. With net cooling ($H < 0$), the atmosphere becomes increasingly stratified, or stable. The factors ψ_m and ψ_H have been calculated, partly by theory and partly empirically, as follows:

$$\psi_m = \psi_H = 6\ln(1+\xi) \quad \text{in stable conditions } (H<0) \tag{2.35}$$

$$\psi_H = -2\ln\left[\frac{1+(1+16\xi)}{2}\right]^{\frac{1}{2}},$$
$$\psi_m = 0.6\ \psi_H \quad \text{in unstable conditions } (H>0) \tag{2.36}$$

Here, the stability parameter is

$$\zeta = \frac{z}{L} = -\frac{kgzH}{\rho C_{P,m} T_{air} u_*^3} \tag{2.37}$$

and $C_{P,m}$ is the molar heat capacity of air, g (m s^{-2}) is the acceleration due to gravity, and T_{air}(K) is the air temperature. Because H is involved in the calculation of the resistance (or conductance) for its own generation by the canopy, the solution is iterative, although convergence is not generally problematic. A simpler approximation to the full method above is to use $g_{aH} = Cu$, where the constant C is a function of leaf area index and its vertical distribution (Sellers et al. 1996).

The calculation here applies to reasonably dense, homogeneous canopies. In sparse or non-homogeneous canopies, the theory is only partially developed and partially satisfactory (e.g., Kustas et al. 1994). Even for laterally homogeneous canopies, the theory above applies where the profiles of the scalars are well equilibrated with the surface. If a parcel of air crosses to an area with different vegetation, equilibration to the "new" fluxes from vegetation occurs at a distance ("fetch") that is about 100 times the height above the canopy at which one is measuring the scalar values in the air. At the leading edge of such a change in canopy type, the phenomenon of advection occurs (Klaassen 1992; Raupach 1991; Lee et al. 2004). For example, at the edge of a crop canopy in an arid environment, the incoming air at the leading edge is hot and dry, driving sensible heat influx into the canopy and commonly, higher transpiration than occurs further into the crop along the fetch distance. This is a topic whose quantitative treatment is beyond the scope of this chapter.

This relatively simple K-theory (Wilson et al. 2003) works well in the forward modeling of heat, water vapor, and CO_2 as they diffuse out of the canopy. More sophisticated Lagrangian theories (Raupach 1989; McNaughton and van den Hurk 1995) give very similar results in the forward direction of modeling from leaf or stratum to fluxes, although they give very different results when used in inverse modeling to infer source strengths of heat, water vapor, and CO_2 at different canopy layers (Raupach 1987; Warland and Thurtell 2000).

Other canopy phenomena affect the leaf microenvironments, including cold-air drainage along topographic gradients (Goulden et al. 2006) and sub-canopy blow-through of air beneath the leaf area masses in forests, near the ground where bare trunks are found (Staebler and Fitzjarrald 2004; Vicker et al. 2012). Finally, I note that soil emits fluxes of the scalars, also altering leaf microenvironments. The incorporation of these diverse phenomena into canopy models is an extensive enterprise that is not yet well-covered in the literature. The final pattern of leaf temperature by canopy location and leaf orientation contributes to

patterns of leaf and floral development, posing a further important topic for modelers.

In canopies, rain and snow (and dust) get deposited and then redistributed in fairly complex patterns (e.g., Crockford and Richardson 2000), affecting leaf and whole-canopy energy balance as well as photosynthesis and other physiological processes. Modeling the pattern of leaf wetness or snow cover involves a suite of process submodels, for the mechanics of hydrometeor impacts, leaf mechanical responses, and surface flows, including redistribution driven by wind events. The topic is important for boreal forests and rainforests, and I refer interested readers to Gusev and Nasonova (2003) and Niu and Yang (2004).

Figure 2.5 outlines the calculation of energy balance for leaves within a canopy, incorporating the considerations given above, as well as inclusion of the effects of water balance and attendant water stress. Notation for the additional factors involving water is explained in the figure caption. Gutschick and Sheng (2013) present full details for computing radiation penetration statistics from structural information on a canopy composed of a set of trees described by crown positions, sizes, orientations, and foliage density. Other methods are effective for canopies of different structure, such as grasses. Gutschick and Sheng (2013) used simple and possibly novel descriptions of radiation scattered from other leaves and soil to leaves of interest. More accurate radiative-transfer calculations use scattering amplitudes between volume elements (e.g., Sinoquet et al. 2001) or even the individual leaf area elements (e.g., Chelle and Andrieu 1998). The level of computational effort that is merited depends upon the phenomena one wishes to characterize. Simpler methods may suffice for estimation of whole-canopy fluxes for, say, landscape water balance. More detailed methods enable the resolution of microclimates on individual leaves ("phylloclimate"), for studies such as fungal development on leaves (Chelle 2005).

VI. Outlook: Estimation of Large-Scale Fluxes using Leaf Temperature

Leaf temperature enters in a big way in understanding current climate, as well as in predicting future climate. Satellites measure surface temperatures and other variables that can be used to estimate heat fluxes. Atmospheric circulation is driven by the patterns of sensible heat flux, H, and, via conversion of embodied energy to sensible heat as clouds condense, by the latent heat flux, LE. Consequently, estimates of H and LE from satellite measurements inform weather prediction. They also test regional and global climate models, which need verification for their reliability in predicting future climate. Two recent reviews of wide scope on these topics are by Shuttleworth (2007) and by Wang and Dickinson (2012).

Over the land, as opposed to oceans and other bodies of water, leaves cover half the surface area (Myneni et al. 2002), so that knowing leaf temperature is critical. The leaf-to-air temperature difference can be used to compute the sensible heat flux density, H (or, for single leaves, Q_c-), when combined with a knowledge of the boundary-layer conductance. This is readily seen in Eq. 2.16. We may combine the calculation (estimation) of H with estimation of the radiative part of the energy balance in order to estimate latent heat flux, thus, transpiration. Using the more common notation of energy flux densities (W m^{-2}) over scales larger than single leaves, $\lambda E = Q_E$- and $H = Q_c$-, we have $\lambda E =$ (sum of the radiative terms, or net radiation) $- H$. We then obtain an estimate of λE as a residual in the energy-balance equation. When applying this to a canopy viewed as a single layer, such as viewed by satellite, we must resolve as well the term for conduction of heat into the underlying soil, G. We may write $\lambda E = R_n$

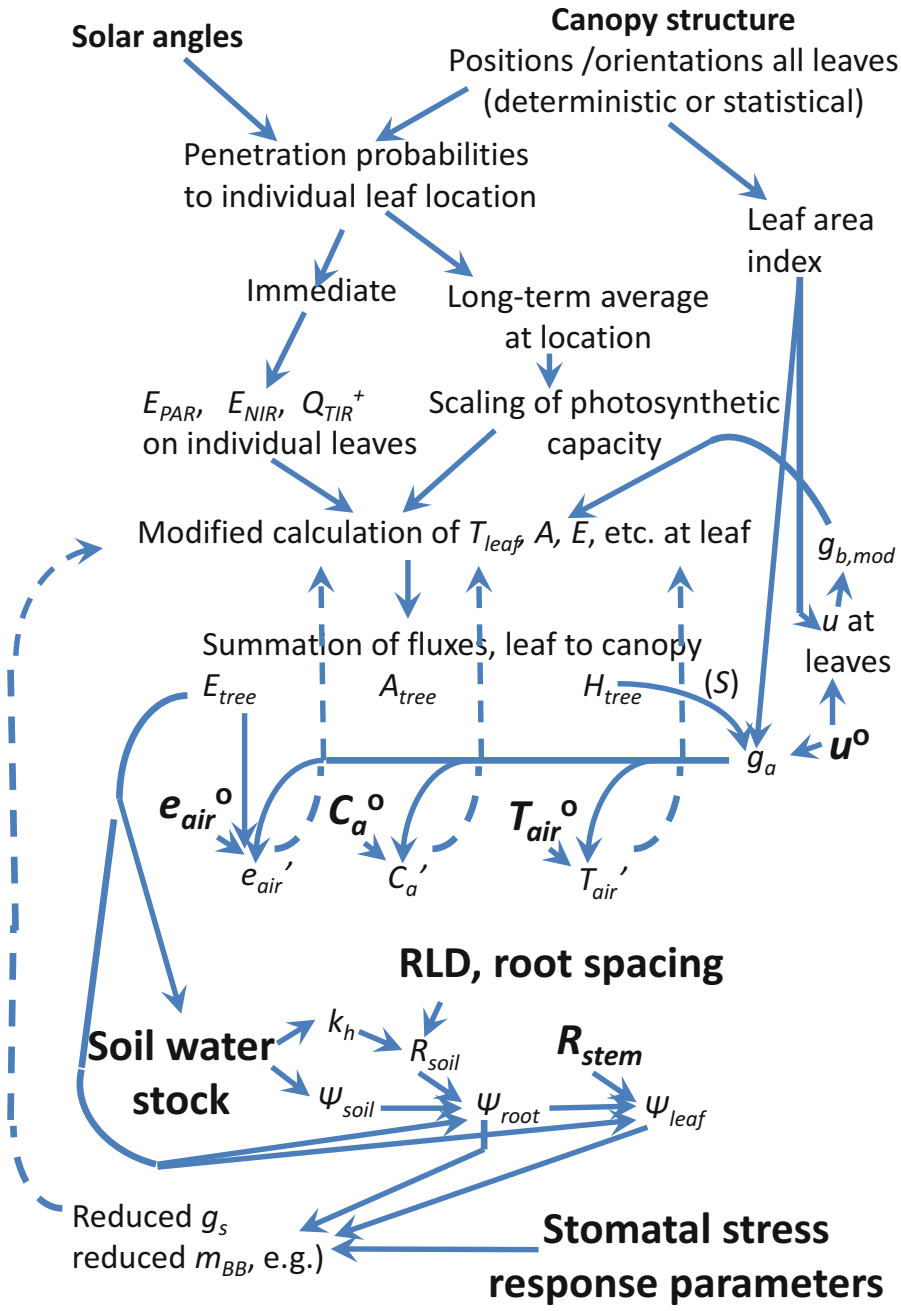

Fig. 2.5. Flowchart for a representative calculation of energy balance and accompanying fluxes of leaves in a canopy. Commonly, the task is calculation of energy balance and fluxes from a representative sample of all leaves on a tree (or other canopy components) in order to compose whole-canopy flux estimates. For a given leaf in the representative sample, the presence of other leaves, stems, and soil affects the propagation of PAR, NIR, and TIR radiation to this leaf. Canopy structure can be described in full for use of a complete radiative transport model, or else statistically using a common turbid medium model (e.g., Gutschick and Sheng 2013). Leaf physiological parameters vary with canopy position; scaling of photosynthetic capacity ($V_{c,\max}^{25}$) often scales with longer-term average PAR irradiance on a leaf (Niinemets 2007), which is computable from radiative transport models run with weather data over a prior time interval. Whole-canopy fluxes (perhaps scaled from individual tree fluxes

$-H-G$. All the terms, R_n, *H, and G* may be modeled or may be measured.

The estimation of the radiant fluxes is considered (perhaps with an excess of optimism) as generally accurate. Shortwave energy flux densities are estimated as downwelling SW (using the solar constant 1367 W m^{-2}, with slight variations depending on solar activity) minus the reflected radiation sensed at the satellite. The reflected radiation, of course, arises not only from the surface (canopy and soil) but also from aerosols in the atmosphere. To correct the surface-intercepted radiation for scattering and absorption by aerosols, their content in the atmosphere aerosols must be measured. This is done at very few locations, so that empirical relations are used elsewhere, involving multiple SW wavebands. See, for example, Bastiaanssen et al. (1998). The accounting for varied angles of illumination angles on tilted surfaces is also complex, but possible (Mariotto et al. 2011).

The calculation of H requires that we know the quantity T_{leaf}-T_{air}. Much effort has gone into getting independent, accurate measurements of both temperatures. The air temperature may be taken from ground measurements, or, where these are unavailable, from profiles of air temperature derived by inverse modeling of the TIR fluxes from different atmospheric layers (Strow et al. 2003; King et al. 2003; mathematical background in Twomey 1977; Glasko 1988). Sensing of several different TIR wavebands must be used, each being differentially sensitive to the different temperatures in the layers of the atmosphere. The calculations rely upon small differences in radiative properties of air (really, its water vapor content) at different temperatures, so that the extraction of T_{air} as a function of height in the atmosphere is very sensitive to small errors. It is termed as ill-conditioned in mathematics. Nonetheless, accurate radiative transfer physical theory and mathematical methods such as constrained linear inversion (Twomey 1977) now appear to provide T_{air} near the surface with a root-mean square error cited as slightly below 1 °C (Coll et al. 2009). Before one gets overly optimistic, it is worth noting that an error of 1 °C can lead to notable errors in calculation of H over surfaces with high aerodynamic conductances, g_{aH}, such as tall forests. With $g_{aH} = 3$ mol m^{-2} s^{-1} in modest wind, the error is g_{aH} multiplied by the heat capacity of air, 29 J mol^{-1} K^{-1} and by the temperature error, or 87 W m^{-2}. This is of the order of H itself in many conditions.

The sensing of leaf temperature itself involves the methods and challenges discussed in the previous Sects. II.D and II.E. A satellite with a wide field of view, say, nearly a radian as with the polar orbiting satellites, will image different parts of the scene at significantly different view angles. This yields different offsets between

Fig. 2.5. (continued) and tree density) alter the in-canopy environment from that of free air conditions measured above the canopy (water vapor and CO_2 contents ${e_{air}}^0$ and ${C_a}^0$ and air temperature ${T_{air}}^0$). Calculation of the in-canopy values (e_{air}, C_a, T_{air}) is iterative. A simple average environment can be calculated from the above-canopy values and the summed canopy fluxes (here, E_{tree} as latent heat flux density, A_{tree} as photosynthetic CO_2 flux density, and H_{tree} as sensible heat flux density) convolved with the aerodynamic conductance of the canopy, g_a (cf. Eq. 2.34 in text). The *arrow* labeled (S) notes application of the stability corrections (Eqs. 2.33, 2.34, 2.35, and 2.36 in text). Dashed arrows indicate propagation of the new computed values for iterative improvement. At bottom is the calculation of soil water fluxes. Mass balance allows calculation of soil water content, hence, hydraulic conductivity k_h and water potential ψ_{soil}. In turn, k_h combined with knowledge of root-length density (*RLD*) and root radius enables calculation of soil-to-root hydraulic conductance, R_{soil}. Then, the product $E_{tree}R_{soil}$ allows calculation of root water potential, ψ_{root}. Whole-tree flux E_{tree} multiplied by stem hydraulic resistance, R_{stem}, allows calculation of leaf water potential, ψ_{leaf}. In several usable models of stomatal responses to water stress, both ψ_{root} and ψ_{leaf} are used along with fixed parameters to calculate a multiplicative factor (<1) applied to conductance, g_s. This factor (*dashed* arrow from *bottom right*) is applied in a new iteration of calculating values of g_s and all leaf fluxes

radiative and kinetic temperatures in different parts of the scene. Variations in view angle also lead to varying corrections for aerosol interference, which can be accounted with some care. A larger problem is that both soil and vegetation are visible at many locations on Earth. Satellites cannot resolve single plants, so that the radiative temperature recorded in a scene element, a pixel, is essentially an algebraic average of the radiative temperatures of the soil and the vegetation (Box 2.3). Problematically, the sensible heat flux is not related simply to any average temperature nor to any average aerodynamic resistance through which soil and vegetation generate sensible heat flux (Box 2.4). It is imperative, then, to find a remedy for this mixing of temperatures. One straightforward method (French et al. 2003) of modest accuracy is to set vegetation temperature equal to air temperature. Then, one solves for soil temperature from the equation relating average radiative temperature to soil and air temperatures and the fractions of soil and vegetation in view (Box 2.3). This approximation does not allow for accurate flux determination when the vegetation is stressed, having reduced transpiration and (unknown) higher temperature.

Box 2.3 Radiative Temperatures Add in a Nonlinear Fashion

The soil and vegetation radiative temperatures combine almost but not quite linearly as an average radiative temperature. The satellite sensor records an energy flux density that it interprets as originating from a blackbody at a uniform radiative temperature, T_{eff}, at a rate per unit area equal to σT_{eff}^4, where σ is the Stefan-Boltzmann constant. Ignoring the complication of TIR emissivities differing slightly from unity, we may formulate the energy flux density as coming from two sources, one at a temperature T_{veg} that occupies a fraction f_{veg} of the view and another at a temperature T_{soil} occupying a fraction $f_{soil} = 1 - f_{veg}$. Factoring out σ in all the terms, we write

$$T_{eff}^4 = f_{veg} T_{veg}^4 + f_{soil} T_{soil}^4$$

Here, we must use the absolute or Kelvin temperature. We may write $T_{soil} = T_{veg} + \Delta T$. Expanding ${T_{soil}}^4$, we have $T_{veg}^4 = 4T_{veg}^3 \Delta T +$ higher order terms (*h.o.t.*). Taking the fourth root of both sides and using the power series representation that $(a+b)^n = a^n(1 + n[a/b] + n(n\text{-}1)\,[a/b]^2/2 + \ldots)$, we have, by a series of algebraic steps,

$$\begin{aligned}
T_{eff} &= \left[f_{veg}T_{veg}^4 + \left(1-f_{veg}\right)\left(T_{veg}^4 + 4T_{veg}^3\Delta T + h.o.t\right)\right]^{(1/4)} \\
&= \left[T_{veg}^4 + \left(1-f_{veg}\right)\left(4T_{veg}^3\Delta T + h.o.t.\right)\right]^{(1/4)} \\
&= \left(T_{veg}^4\right)^{(1/4)}\left[1 + \frac{1}{4}\left(1-f_{veg}\right)\frac{4T_{veg}^3\Delta T + h.o.t.}{T_{veg}^4} + \ldots\right] \\
&= T_{veg}\left[1 + \left(1-f_{veg}\right)\frac{\left(T_{soil}-T_{veg}\right)}{T_{veg}} + \ldots\right] \\
&= T_{veg}\left[1 + f_{soil}\frac{T_{soil}}{T_{veg}} - \left(1-f_{veg}\right)\frac{T_{veg}}{T_{veg}} + \ldots\right] \\
&= T_{veg}\left[f_{veg} + f_{soil}\frac{T_{soil}}{T_{veg}} + \ldots\right] \\
&= f_{veg}T_{veg} + f_{soil}T_{soil} + \ldots
\end{aligned}$$

The omitted correction terms are tedious to display but have some significance. As a numerical example, consider a the vegetation fraction is 0.3, T_{veg} is 35 °C = 298.2 K, and T_{soil} is 30 °C hotter, as in a hot desert at midday. The linear approximation yields T_{eff} = 0.3*35 + 0.7*65 = 56 °C. The accurate formula yields T_{eff} = 330.0 K = 56.8 °C. The error is of a similar magnitude to the error in air temperature and adds to that error as a statistically independent source. As a more reassuring numerical example, appropriate to temperate farmland with nearly complete canopy closure, take f_{veg} = 0.8, T_{veg} = 28°, and T_{soil} = 37 °C. The linear approximation yields 29.8 °C, while the accurate formula yields a very similar 29.9 °C.

Box 2.4 Difficulties in Separating Fluxes from Soil and from Vegetation

Vegetation and soil contribute essentially independent fluxes of sensible heat, but through quite different aerodynamic conductances. Again using f_{veg} and f_{soil} as fractional coverages of the land, we may write

$$H = f_{veg}H_{veg} + f_{soil}H_{soil}$$

Here, H_{veg} is the sensible heat flux density (W m^{-2}) over pure vegetation-covered areas, and H_{soil} is that for soil. Each of the two components of H can be written in terms of the molar heat capacity of air, $C_{P,m}$, the aerodynamic conductance above that surface (g_{ver} or g_{soil}), and the temperatures as

$$H = C_{P,m}\left[f_{veg}g_{veg}\left(T_{veg} - T_{air}\right) + f_{soil}g_{soil}(T_{soil} - T_{air})\right]$$

We would like to get an expression that uses average temperature, $T_{eff} = f_{veg}T_{veg} + f_{soil}T_{soil}$. This would require that there is a single value of g, but we can't set g_{soil} equal to g_{veg}, as it is often an order of magnitude smaller. We might attempt to define a mean conductance, g_{eff}, evaluating the error terms this introduces:

$$\begin{aligned} H = {} & C_{P,m}g_{eff}\left[f_{veg}\left(T_{veg} - T_{air}\right)\right. \\ & + f_{soil}(T_{soil} - T_{air}) \\ & + C_{P,m}\left[f_{veg}\left(g_{veg} - g_{eff}\right)\times\right. \\ & \left.\left(T_{veg} - T_{air}\right) + f_{soil}\left(g_{soil} - g_{eff}\right)\times\right. \\ & \left.\left.(T_{soil} - T_{air})\right]\right] \end{aligned}$$

The first line above takes a desirable form, as $C_{P,m}g_{eff}[T_{eff} - T_{air}]$. The second line introduces the separate temperatures of soil and vegetation, which we could not estimate from one measurement. The two-source approximation introduced as in the work of French et al. (2003) sets T_{veg} equal to T_{air}. This allows a solution but makes the contribution from vegetation inaccurate.

One longstanding approach is to eliminate surface temperature in the estimation of λE. One can combine Eq. 2.1 for energy balance with Eqs. 2.2, 2.3, 2.7 and 2.15, with extra assumptions about the stomatal and aerodynamic resistances. One obtains the Penman-Monteith equation (Penman 1948; Monteith 1964). To avoid presenting a slew of alternative notation that is more familiar to meteorologists, I offer a summary. One rearranges Eq. 2.1 and coalesces some terms, as done four paragraphs above, writing $\lambda E = R_n - H - G$. All the components of R_n are measurable. The aerodynamic resistance and G are also measurable, though one must know the height of the vegetation to estimate g_{aH}. One also needs the windspeed, commonly by interpolating values from the nearest ground weather stations. The whole land surface is treated as uniform, as a "big leaf." One writes λE as a linear function of temperature, making a linear approximation for the dependence of water vapor partial pressure upon temperature. Critically, the stomatal conductance (used as its inverse, resistance) is set at a fixed, estimated value, acting as a conductance for the whole canopy of vegetation. The result is a linear equation for surface temperature. This temperature is plugged back into the equation for λE, which can then expressed in terms of net radiation R_n, the canopy and aerodynamic resistances, air temperature (for the vapor pressure deficit), and the initial value of water vapor partial pressure at air temperature and its derivative with respect to temperature. The Penman-Monteith equation is used widely in satellite remote sensing, but it has serious limitations. First, soil and vegetation are treated as having the same properties. Applying the equation over sparse vegetation requires elaborate and rather inaccurate corrections. The

literature on corrections is quite extensive. Second, it assumes that we have an accurate estimate of stomatal conductance per leaf area. One also needs measurements of leaf area index to scale this up to a whole-canopy conductance, roughly multiplying by sunlit leaf area that varies with solar angle, leaf area index, and leaf angle distribution. However, plant species vary dramatically in stomatal conductance, even under uniform sunlit conditions. Crop species average about threefold higher conductance than wild species (Kelliher et al. 1995). Empirical formulas can be developed for different types of vegetation, as a first correction. Conductance for any given species or genotype is not constant. It varies with photosynthetic rate, thus, with temperature, humidity, light level, etc., as discussed in Sect. III.A. Tellingly, conductance varies with stress, either water stress or nutrient stress. Detection of stress is one major goal of remote sensing, but the Penman-Monteith approach cannot be used for this.

An alternative method has been devised (Bastiaanssen et al. 1998), in which the leaf-to-air temperature difference, $T_{leaf} - T_{air}$ is directly estimated from a calibration scheme. One finds the hottest and coldest pixels in a remotely-sensed scene and identifies these, respectively, as surfaces with $\lambda E = 0$ and $\lambda E = \lambda E_{\max}$, the latter having $H = 0$. The assumption is made, with good justification, that T_L-T_a is linearly related to the radiative temperature alone. Several problems remain. We need an estimate of g_b at the canopy scale, often formulated (Sect. V.B) in terms of surface roughness height, which is a somewhat uncertain small fraction of the height of the vegetation (Rowntree 1988). Vegetation height and leaf area index are the dominant determinants of roughness or of g_b. It is of some help that leaf area index can be estimated with some accuracy from various spectral indices such as the normalized difference vegetation index (Baret and Guyot 1991; Huete et al. 2002; see also Huang et al. 2007). There are numerous improvements on it, as well. However, the only reliable way to estimate vegetation height in a satellite scene is from a knowledge of the plant species in each pixel and their degree of development. There are no useful species identifiers derivable from measurements of surface reflectivity at different wavelengths, despite early optimism (http://ntrs.nasa.gov/archive/nasa/casi.ntrs.nasa.gov/NTRS-PDF/19810020973_1981020973.pdf). This problem is nearly insuperable in many areas of the globe. The estimates are possible in smaller regions with intensive surveys abetted by ground-based studies; a fine example is provided by the Carnegie Airborne Observatory (Asner et al. 2007). A problem shared with Penman-Monteith is that soil and vegetation contributions to fluxes are mixed. Additional problems arise from variation in the angle of illumination over portions of the surface with different slope. Some effective modifications have been offered (Mariotto et al. 2011).

One more problem is intriguing. Over smaller areas of tens to hundreds of meters (sometimes resolved with high-resolution imagery), is that the fluxes H and LE are spatially non-uniform, even for surfaces uniformly covered with vegetation and uniformly lit by the sun. The phenomenon of symmetry breaking is the origin: heated air must rise, just at water heated from below in a pot must rise, but neither fluid can rise as an intact layers. Plumes form at regular or irregular locations, with air sinking in other areas. This structure of Bénard cells (Rayleigh-Bénard convection, see http://en.wikipedia.org/wiki/Rayleigh-Bénard_convection) is readily observed in cooking pots and has been observed on vegetated areas (Cooper et al. 2000; see also Albertson et al. 2001). This means that the differences among pixels at any one time, as in a satellite "snapshot" do not necessarily indicate differences in fluxes on time scales longer than fractions of an hour, after which plume sites shift.

Finally, the interest in estimating λE is heavily in daily-total λE, not instantaneous λE at the time of satellite overpass. Various schemes are used to interpolate LE to all

other times of day, often assuming that the evaporative fraction, $\lambda E/(\lambda E + H)$, is constant over the daylight hours (Rowntree 1988). This is moderately crude, as evidenced in ground-base measurements using eddy covariance (Nichols and Cuenca 1993). Modeling of the canopy fluxes could be very helpful in this effort.

VII. Encouragement

Leaf temperature, both in measurement and in theory, involves a wealth of phenomena. It is also a useful variable in many areas of research, extending from photosynthetic physiology to climate change. The problems cited in this chapter are certainly rather numerous but must be viewed as opportunities for research. Collaborations among researchers in plant physiology, biophysics, remote sensing, agronomy, and other fields can surely advance the solutions. Individual researchers can also increase the prospects for progress by mastering fields divergent from their original career experience. It may be little known that Graham Farquhar, who has opened wide areas of research in stable isotopic methods, photosynthetic biochemistry, and more began his career as a nuclear physicist. Some of my own contributions derive some novelty from having begun as a chemical physicist, moving into – perhaps intruding on – fields of plant physiology, ecology, radiative transfer, ecology, and the like. At sufficient intervals, boldness and much work are rewarding.

References

Agristars (1981) http://ntrs.nasa.gov/archive/nasa/casi.ntrs.nasa.gov/NTRS-PDF/19810020973_1981020973.pdf

Alben S, Shelley M, Zhang J (2002) Drag reduction through self-similar bending of a flexible body. Nature 420:479–481

Albertson JD, Katul GG, Wiberg P (2001) Relative importance of local and regional controls on coupled water, carbon, and energy fluxes. Adv Water Resour 24:1103–1118

Anthes RA (1984) Enhancement of convective precipitation by mesoscale variations in vegetative covering in semiarid regions. J Clim Appl Meteorol 23:541–554

Asner GP, Knapp DE, Kennedy-Bowdoin T, Jones MO, Martin RE, Boardman J, Field CB (2007) Carnegie Airborne Observatory: in-flight fusion of hyperspectral imaging and waveform light detection and ranging (wLiDAR) for three-dimensional studies of ecosystems. J Appl Remote Sens 1, 013536. doi:10.1117/1.2794018

Atkin OK, Bruhn D, Hurry VM, Tjoelker MG (2005) The hot and the cold: unraveling the variable response of plant respiration to temperature. Funct Plant Biol 32:87–105

Baldocchi D (1994) An analytical solution for coupled leaf photosynthesis and stomatal conductance models. Tree Physiol 14:1069–1079

Baldocchi DD, Verma SB, Rosenberg NJ (1983) Characteristics of air-flow above and within soybean canopies. Bound Layer Meteorol 25:43–54

Ball JT (1987) Calculations related to gas exchange. In: Zeiger E, Farquhar GD, Cowan IR (eds) Stomatal Function. Stanford University Press, Stanford, pp 445–476

Ball JT, Woodrow IE, Berry JA (1987) A model predicting stomatal conductance and its contribution to the control of photosynthesis under different environmental conditions. In: Biggins JM (ed) Progress in Photosynthesis Research, vol 4. Nijhoff Publishers, Dordrecht, pp 221–224

Ball MC, Egerton JJG, Lutze JL, Gutschick VP, Cunningham RB (2002) Mechanisms of competition: thermal inhibition of tree seedling growth by grass. Oecologia 133:120–130

Barbour MM (2007) Stable oxygen isotope composition of plant tissue: a review. Funct Plant Biol 34:83–94

Baret F, Guyot G (1991) Potentials and limits of vegetation indexes for LAI and APAR assessment. Remote Sens Environ 35:161–173

Bastiaanssen WGM, Menenti M, Feddes RA, Holtslag AAM (1998) A remote sensing surface energy balance algorithm for land (SEBAL) – 1. Formulation. J Hydrol 212:198–212

Bonan GB (2008) Forests and climate change: forcings, feedbacks, and the climate benefits of forests. Science 320:1444–1449

Brutsaert W (1984) Evaporation into the Atmosphere: Theory, History, and Applications. Reidel, Boston

Burden RL, Faires JD (1985) Numerical Analysis, 3rd edn. PWS Publishers, Boston

Campbell GS, Norman JM (1998) An Introduction to Environmental Biophysics, 2nd edn. Springer, New York

Cescatti A, Marcolla B (2004) Drag coefficient and turbulence intensity in conifer canopies. Agric For Meteorol 121:197–206

Chazdon RL, Pearcy RW (1991) The importance of sunflecks for forest understory plants – photosynthetic machinery appears adapted to brief, unpredictable periods of radiation. Bioscience 41:760–766

Chelle M (2005) Phylloclimate or the climate perceived by individual plant organs: what is it? How to model it? What for? New Phytol 166:781–790

Chelle M (2006) Could plant leaves be treated as Lambertian surfaces in dense crop canopies to estimate light absorption? Ecol Model 198:219–228

Chelle M, Andrieu B (1998) The nested radiosity model for the distribution of light within plant canopies. Ecol Model 111:75–91

Chelle M, Renaud C, Delepoulle S, Combes D (2007) Modeling light phylloclimate within growth chambers. In: Prusinkiewicz P (ed) Proceedings of the 5th International Workshop on Functional Structural Plant Models. Napier, New Zealand Print Solutions Hawke's Bay Limited, Napier, pp 571–574

Coll C, Wan ZM, Galve JM (2009) Temperature-based and radiance-based validation of the V5 MODIS land surface temperature product. J Geophys Res Atmos 114, D20102. doi:10.1029/2009JD012038

Collatz GJ, Ball JT, Grivet C, Berry JA (1991) Physiological and environmental regulation of stomatal conductance, photosynthesis and transpiration: a model that includes a laminar boundary layer. Agric For Meteorol 54:107–136

Cooper DI, Eichinger WE, Kao J, Hipps L, Reisner J, Smith S, Schaeffer SM, Williams DG (2000) Spatial and temporal properties of water vapor and latent energy flux over a riparian canopy. Agric For Meteorol 105:161–183

Crockford RH, Richardson DP (2000) Partitioning of rainfall into throughfall, stemflow and interception: effect of forest type, ground cover and climate. Hydrol Proced 14:2903–2920

Dai QD, Sun SF (2006) A generalized layered radiative transfer model in the vegetation canopy. Adv Atmos Sci 23:243–257

Delepoulle S, Renaud C, Chelle M (2009) Genetic algorithms for light sources positioning. In: Plemenos D, Miaoulis G (eds) Proceedings of the 11th 3IA: International Conference on Computer Graphics and Artificial Intelligence. Universite de Limoges, Limoges, p 11

Demmig-Adams B, Adams WW III (2006) Photoprotection in an ecological context: the remarkable complexity of thermal energy dissipation: Tansley review. New Phytol 172:11–21

Denmead OT (1964) Evaporation sources and apparent diffusivities in a forest canopy. J Appl Meteorol 3:383–389

Denmead OT, Bradley EF (1987) On scalar transport in plant canopies. Irrig Sci 8:131–149

Dewar RC (2002) The Ball-Berry-Leuning and Tardieu-Davies stomatal models: synthesis and extension within a spatially aggregated picture of guard cell function. Plant Cell Environ 25:1383–1398

Disney M (2016) Remote sensing of vegetation: potentials, limitations, developments and applications. In: Hikosaka K, Niinemets Ü, Anten N (eds) Canopy Photosynthesis: From Basics to Applications. Springer, Berlin, pp 289–331

Escobedo JF, Gomes EN, Oliveira AP, Soares J (2009) Modeling hourly and daily fractions of UV, PAR and NIR to global solar radiation under various sky conditions at Botucatu, Brazil. Appl Energy 86:299–309

Evers JB (2016) Simulating Crop Growth and Development using Functional-Structural Plant Modeling. In: Hikosaka K, Niinemets Ü, Anten N (eds) Canopy Photosynthesis: From Basics to Applications. Springer, Berlin, pp 219–236

Farquhar GD, Sharkey TD (1982) Stomatal conductance and photosynthesis. Annu Rev Plant Physiol 33:317–345

Farquhar GD, von Caemmerer S, Berry JA (1980) A biochemical model of photosynthetic CO_2 assimilation in leaves of C_3 plants. Planta 149:78–90

French AN, Schmugge TJ, Kustas WP, Brubaker KL, Prueger J (2003) Surface energy fluxes over El Reno, Oklahoma, using high-resolution remotely sensed data. Water Resour Res 39, 1164. doi:10.1029/2002WR001734

Fuentes S, De Bei R, Pech J, Tyerman S (2005) Computational water stress indices obtained from thermal image analysis of grapevine canopies. Irrig Sci 30:523–536

Fuchs M (1990) Infrared measurement of canopy temperature and detection of plant water-stress. Theor Appl Climatol 42:253–261

Gelfan AN, Pomeroy JW, Kuchment LS (2004) Modeling forest cover influences on snow accumulation, sublimation, and melt. J Hydrometeorol 5:785–803

Gershenfeld N (1999) The Nature of Mathematical Modeling. Cambridge University Press, Cambridge, pp 162–166

Glasko VB (1988) Inverse Problems of Mathematical Physics. American Institute of Physics, New York, Transl. of Russian original (1984) by Bincer A

Goudriaan J (1977) Crop Micrometeorology: A Simulation Study. Centre for Agricultural Publishing and Documentation, Wageningen

Goudriaan J (2016) Light Distribution. In: Hikosaka K, Niinemets Ü, Anten N (eds) Canopy Photosynthesis: From Basics to Applications. Springer, Berlin, pp 3–22

Goulden ML, Miller SD, da Rocha HR (2006) Nocturnal cold air drainage and pooling in a tropical forest. J Geophys Res Atmos 111, D08S04. doi:10.1029/2005JD006037

Graham RL (1978) Combinatorial scheduling theory. In: Steen LA (ed) Mathematics Today. Vintage Books, New York, pp 183–211

Granier C, Inze D, Tardieu F (2000) Spatial distribution of cell division rate can be deduced from that of p34(cdc2) kinase activity in maize leaves grown at contrasting temperatures and soil water conditions. Plant Physiol 124:1393–1402

Grantz DA, Zeiger E (1986) Stomatal responses to light and leaf-air water vapor pressure difference show similar kinetics in sugarcane and soybean. Plant Physiol 81:865–868

Greek TJ, Paw U KT, Weathers WW (1989) A comparison of operative temperature estimated by taxidermic mounts and meteorological data. J Therm Biol 14:19–26

Grote R, Monson RK, Niinemets Ü (2013) Leaf-level models of constitutive and stress-driven volatile organic compound emissions. In: Niinemets Ü, Monson RK (eds) Biology, Controls and Models of Tree Volatile Organic Compound Emissions. Springer, Berlin, pp 315–355

Guilioni L, Cellier P, Ruget F, Nicoullaud B, Bonhomme R (2000) A model to estimate the temperature of a maize apex from meteorological data. Agric For Meteorol 100:213–230

Gurevitch J, Schuepp PH (1990) Boundary-layer properties of highly dissected leaves – an investigation using an electrochemical fluid tunnel. Plant Cell Environ 13:783–792

Gusev YM, Nasonova ON (2003) The simulation of heat and water exchange in the boreal spruce forest by the land-surface model SWAP. J Hydrol 280:162–191

Gutschick VP (2007) Plant acclimation to elevated CO_2 – from simple regularities to biogeographic chaos. Ecol Model 200:433–451

Gutschick VP, Pushnik JC, Swanton BA (1988) Use of plant growth chambers at high irradiance levels. Bioscience 38:44–47

Gutschick VP, Sheng Z (2013) Control of atmospheric fluxes from a pecan orchard by physiology, meteorology, and canopy structure: modeling and measurement. Agric Water Manag 129:200–211

Gutschick VP, Simmoneau T (2002) Modelling stomatal conductance of field-grown sunflower under varying soil water status and leaf environment: comparison of three models of response to leaf environment and coupling with an ABA-based model of response to soil drying. Plant Cell Environ 25:1423–1434

Gutschick VP, Wiegel FW (1984) Radiative transfer in plant canopies and other layered media: rapidly solvable exact integral equation not requiring Fourier resolution. J Quant Spectrosc Radiat Transf 31:71–82

Hales K, Neelin JD, Zeng N (2004) Sensitivity of tropical land climate to leaf area index: role of surface conductance versus albedo. J Climate 17:1459–1473

Hanba YT, Moriya A, Kimura K (2004) Effect of leaf surface wetness and wettability on photosynthesis in bean and pea. Plant Cell Environ 27:413–421

Hartmann DL (1994) Global Physical Climatology. Academic, San Diego

Hartz KEH, Rosenørn T, Ferchak SR, Raymond TM, Bilde M, Donahue NM, Pandi SN (2005) Cloud condensation nuclei activation of monoterpene and sesquiterpene secondary organic aerosol. J Geophys Res 110, D14208. doi:10.1029/2004JD005754

Harvell CD, Mitchell CE, Ward JR, Altizer S, Dobson AP, Ostfeld RS, Samuel MD (2002) Ecology – Climate warming and disease risks for terrestrial and marine biota. Science 296:2158–2162

Hikosaka K, Noguchi K, Terashima I (2016a) Modeling leaf gas exchange. In: Hikosaka K, Niinemets Ü, Anten N (eds) Canopy Photosynthesis: From Basics to Applications. Springer, Berlin, pp 61–100

Hikosaka K, Kumagai T, Ito A (2016b) Modeling canopy photosynthesis. In: Hikosaka K, Niinemets Ü, Anten N (eds) Canopy Photosynthesis: From Basics to Applications. Springer, Berlin, pp 239–268

Houghton JT (1977) The Physics of Atmospheres. Cambridge University Press, Cambridge

Huang D, Knyazikhin Y, Dickinson RE, Rautiainen M, Stenberg P, Disney M, Lewis P, …, Myneni RB (2007) Canopy spectral invariants for remote sensing and model applications. Remote Sens Environ 106:106–122

Huete A, Didan K, Miura T, Rodriguez EP, Gao X, Ferreira LG (2002) Overview of the radiometric and biophysical performance of the MODIS vegetation indices. Remote Sens Environ 83:195–213

Idso SB, Reginato RJ, Reicosky DC, Hatfield JL (1981) Determining soil-induced plant water potential depressions in alfalfa by means of infrared thermometry. Agron J 73:826–830

Jackson RD, Kustas WP, Choudhury BJ (1988) A reexamination of the crop water-stress index. Irrig Sci 9:309–317

Jarvis PG, McNaughton KG (1986) Stomatal control of transpiration: scaling up from leaf to region. Adv Ecol Res 15:1–49

Jenkins CLD (1997) The CO_2 concentrating mechanism of C_4 photosynthesis: bundle sheath cell CO_2 concentration and leakage. Aus J Plant Physiol 24:543–547

Johnson IR, Thornley JHM (1984) A model of instantaneous and daily canopy photosynthesis. J Theor Biol 107:531–545

Jones HG, Stoll M, Santos T, de Sousa C, Chaves MM, Grant OM (2002) Use of infrared thermography for monitoring stomatal closure in the field: application to grapevine. J Exp Bot 53:2249–2260

Jones CT, Craig SE, Barnett AB, MacIntyre HL, Cullen JJ (2014) Curvature in models of the photosynthesis-irradiance response. J Phycol 50:341–355

Kavouras IG, Mihalopoulos N, Stephanou EG (1998) Formation of atmospheric particles from organic acids produced by forests. Nature 395:683–686

Kelliher FM, Leuning R, Raupach MR, Schulze E-D (1995) Maximum conductances for evaporation from global vegetation types. Agric For Meteorol 73:1–16

Kimball BA (2005) Theory and performance of an infrared heater for ecosystem warming. Glob Chang Biol 11:2041–2056

Kimes DS, Smith JA, Link LE (1981) Thermal IR exitance model of a plant canopy. Appl Optics 20:623–632

King MD, Menzel WP, Kaufman YJ, Tanre D, Gao BC, Platnick S, Ackerman SA, . . ., Hubanks PA (2003) Cloud and aerosol properties, precipitable water, and profiles of temperature and water vapor from MODIS. IEEE Trans Geosci Remote Sens 41:442–458

Kirkpatrick S, Gelatt CD Jr, Vecchi MP (1983) Optimization by simulated annealing. Science 220:671–680

Klaassen W (1992) Average fluxes from heterogeneous vegetated regions. Bound Layer Meteorol 58:329–354

Kleczkowski LA, Edwards GE (1991) A low temperature-induced reversible transition between different kinetic forms of maize leaf phosphoenolpyruvate carboxylase. Plant Physiol Biochem 29:9–17

Kogan FN (1997) Global drought watch from space. Bull Am Meteorol Soc 78:621–636

Kreith F (1965) Principles of Heat Transfer. International Textbook Company, Scranton

Kumagai T (2016) Observation and modeling of net ecosystem carbon exchange over canopy. In: Hikosaka K, Niinemets Ü, Anten N (eds) Canopy Photosynthesis: From Basics to Applications. Springer, Berlin, pp 269–287

Kustas WP, Anderson MC, Norman JM (2007) Utility of radiometric-aerodynamic temperature relations for heat flux estimation. Bound Layer Meteorol 122:167–187

Kustas WP, Blanford JH, Stannard DI, Daughtry CST, Nichols WD, Weltz MA (1994) Local energy flux estimates for unstable conditions using variance data in semiarid rangelands. Water Resour Res 30:1351–1361

Lagouarde JP, Kerr YH, Brunet Y (1995) An experimental-study of angular effects on surface-temperature for various plant canopies and bare soils. Agric For Meteorol 77:167–190

Lawrence DM, Thornton PE, Oleson KW, Bonan GB (2006) The partitioning of evapotranspiration into transpiration, soil evaporation, and canopy evaporation in a GCM: impacts on land–atmosphere interaction. J Hydrometeorol 8:862–880

Lee X, Yu Q, Sun X, Liu J, Min Q, Liu Y, Zhang X (2004) Micrometeorological fluxes under the influence of regional and local advection: a revisit. Agric For Meteorol 122:111–124

Leinonen I, Grant OM, Tagliavia CPP, Chaves MM, Jones HG (2006) Estimating stomatal conductance with thermal imagery. Plant Cell Environ 29:1508–1518

Leuning R (1995) A critical appraisal of a combined stomatal-photosynthesis model for C3 plants. Plant Cell Environ 18:339–355

LI-COR Biosciences (2004) Using the LI-6400-XT/ Portable Photosynthesis System. LI-COR Biosciences, Lincoln, NE, USA

Li Z-L, Tang R, Wan Z, Bi Y, Zhou C, Tang B, Yan G, Zhang X (2009) A review of current methodologies for regional evapotranspiration estimation from remotely sensed data. Sensors 9:3801–3853

Liang SL, Strahler AH (1993) An analytical BRDF model of canopy radiative transfer and its inversion. IEEE Trans Geosci Remote Sens 31:1081–1092

Mariotto I, Gutschick VP, Clason DL (2011) Mapping evapotranspiration from ASTER Data through GIS spatial integration of vegetation and terrain features. Photogramm Eng Remote Sens 77:483–493

McCalla TR (1967) Introduction to Numerical Methods and FORTRAN Programming. Wiley, New York

McNaughton KG, Van den Hurk BJJM (1995) A Lagrangian revision of the resistors in the 2-layer model for calculating the energy budget of a plant canopy. Bound Layer Meteorol 74:261–288

Monson RK, Grote R, Niinemets Ü, Schnitzler J-P (2012) Tansley review. Modeling the isoprene emission rate from leaves. New Phytol 195:541–559

Monteith JL (1964) Evaporation and environment. In: The State and Movement of Water in Living Organisms. 19th Symp Soc Exp Biol. Academic, New York, pp 205–234

Murray FW (1967) On the computation of saturation vapor pressure. J Appl Meteorol 6:203–204

Myneni RB, Hoffman S, Knyazikhin Y, Privette JL, Glassy J, Tian Y, Wang Y, . . ., Running SW (2002) Global products of vegetation leaf area and fraction absorbed PAR from year one of MODIS data. Remote Sens Environ 83:214–231

Nichols WE, Cuenca RH (1993) Evaluation of the evaporative fraction for parameterization of the surface energy-balance. Water Resour Res 29:3681–3690

Niinemets Ü (2007) Photosynthesis and resource distribution through plant canopies. Plant Cell Environ 30:1052–1071

Niinemets Ü (2016) Within-canopy variations in functional leaf traits: structural, chemical and ecological controls and diversity of responses. In: Hikosaka K, Niinemets Ü, Anten N (eds) Canopy Photosynthesis: From Basics to Applications. Springer, Berlin, pp 101–141

Niinemets Ü, Diaz-Espejo A, Flexas J, Galmes J, Warren CR (2009) Importance of mesophyll diffusion conductance in estimation of plant photosynthesis in the field. J Exp Bot 60:2271–2282

Niinemets Ü, Keenan TF (2012) Measures of light in studies on light-driven plant plasticity in artificial environments. Front Plant Sci 3:156

Ni-Meister W, Gao HL (2011) Assessing the impacts of vegetation heterogeneity on energy fluxes and snowmelt in boreal forests. J Plant Ecol 4:37–47

Niu G-Y, Yang Z-L (2004) Effects of vegetation canopy processes on snow surface energy and mass balances. J Geophy Res 109, D23111. doi:10.1029/2004JD004884

Parkinson KJ (1985) Porometry. In: Marshall B, Woodward FI (eds) Instrumentation for Environmental Physiology. Cambridge University Press, Cambridge/New York/New Rochelle/Melbourne/Sydney, pp 171–191

Paw U KT (1987) Mathematical analysis of the operative temperature and energy budget. J Therm Biol 12:227–233

Pearcy RW (1988) Photosynthetic utilization of lightflecks by understory plants. Aust J Plant Physiol 15:223–238

Pearcy RW, Gross LJ, He D (1997) An improved dynamic model of photosynthesis for estimation of carbon gain in sunfleck light regimes. Plant Cell Environ 20:411–424

Penman HL (1948) Natural evapotranspiration from open water, bare soil, and grass. Proc R Soc London Ser A 193:120–145

Peñuelas J, Llusià J (2003) BVOCs: plant defense against climate warming? Trends Plant Sci 8:105–109

Räisänen T, Ryyppö A, Kellomäki S (2009) Monoterpene emission of a boreal Scots pine (*Pinus sylvestris* L.) forest. Agric For Meteorol 149:808–819

Raupach MR (1987) A Lagrangian analysis of scalar transfer in vegetation canopies. Q J R Meteorol Soc 113:107–120

Raupach MR (1989) Applying Lagrangian fluid mechanics to infer scalar source distributions from concentration profiles in plant canopies. Agric For Meteorol 47:85–108

Raupach MR (1991) Vegetation-atmosphere interaction in homogeneous and heterogeneous terrain – some implications of mixed-layer dynamics. Vegetatio 91:105–120

Roden JS, Pearcy RW (1993) Effect of leaf flutter on the light environment of poplars. Oecologia 93:201–207

Ross J, Sulev M (2000) Sources of errors in measurements of PAR. Agric For Meteorol 100:103–125

Rowntree PR (1988) Atmospheric parametrization schemes for evaporation over land: basic concepts and climate modeling aspects. In: Schmugge TJ, André J-C (eds) Land Surface Evaporation: Measurement and Parametrization. Springer, New York, pp 5–29

Sage RF, Kubien DS (2007) The temperature response of C_3 and C_4 photosynthesis. Plant Cell Environ 30:1086–1106

Salvucci ME, Crafts-Brandner SJ (2004) Inhibition of photosynthesis by heat stress: the activation state of Rubisco as a limiting factor in photosynthesis. Physiol Plant 120:179–186

Schaepman-Strub G, Schaepman ME, Painter TH, Dangel S, Martonchik JV (2006) Reflectance quantities in optical remote sensing-definitions and case studies. Remote Sens Environ 103:27–42

Schuepp PH (1993) Tansley review No. 59: leaf boundary layers. New Phytol 125:477–507

Segal M, Avissar R, McCumber MC, Pielke RA (1988) Evaluation of vegetation effects on the generation

and modification of mesoscale circulations. J Atmos Sci 45:2268–2292

Sellers PJ, Dickinson RE, Randall DA, Betts AK, Hall FG, Berry JA, Collatz GJ, . . ., Henderson-Sellers A (1997) Modeling the exchanges of energy, water, and carbon between continents and the atmosphere. Science 275:502–509

Sellers PJ, Randall DA, Collatz GJ, Field CB, Dazlich DA, Zhang C, Collelo GD, Bounoua L (1996) A revised land surface parametrization (SiB2) for atmospheric GCMs. Part I: model formulation. J Climate 9:676–705

Shuttleworth WJ (2007) Putting the 'vap' into evaporation. Hydrol Earth Syst Sci 11:210–244

Sinoquet H, Le Roux X, Adam B, Ameglio T, Daudet FA (2001) RATP, a model for simulating the spatial distribution of radiation absorption, transpiration and photosynthesis within canopies: application to an isolated tree crown. Plant Cell Environ 24:395–406

Smith JA, Ballard JR, Pedelty JA (1997) Effect of three-dimensional canopy architecture on thermal infrared exitance. Opt Eng 36:3093–3100

Staebler RM, Fitzjarrald DR (2004) Observing subcanopy CO2 advection. Agric For Meteorol 122:139–156

Strow LL, Hannon SE, De Souza-Machado S, Motteler HE, Tobin D (2003) An overview of the AIRS radiative transfer model. IEEE Trans Geosci Remote Sens 41:303–313

Timmermans WJ, Kustas WP, Anderson MC, French AN (2007) An intercomparison of the surface energy balance algorithm for land (SEBAL) and the two-source energy balance (TSEB) modeling schemes. Remote Sens Environ 108:369–384

Tuzet A, Perrier A, Leuning R (2003) A coupled model of stomatal conductance, photosynthesis and transpiration. Plant Cell Environ 26:1097–1116

Twomey S (1977) Introduction to the Mathematics of Inversion in Remote Sensing and Indirect Measurements. Elsevier, Amsterdam, Reprinted by Dover Publications, Mineola, NY, USA

Verstraete MM, Dickinson RE (1986) Modeling surface processes in atmospheric general-circulation models. Ann Geophys Ser B Terres Planet Phys 4:357–364

Vicker D, Irvine J, Martin JG, Law BE (2012) Nocturnal subcanopy flow regimes and missing carbon dioxide. Agric For Meteorol 152:101–108

von Caemmerer S, Furbank RT (2003) The C_4 pathway: an efficient CO_2 pump. Photosynth Res 77:191–207

Wan Z, Zhang Y, Zhang Q, Li ZL (2004) Quality assessment and validation of the MODIS global land surface temperature. Int J Remote Sens 25:261–274

Wang KC, Dickinson RE (2012) A review of global terrestrial evapotranspiration observation, modeling, climatology, and climatic variability. Rev Geophys 10, RG2005. doi:10.1029/2011RG000373

Warland JS, Thurtell GW (2000) A Lagrangian solution to the relationship between a distributed source and concentration profile. Bound Layer Meteorol 96:453–471

Way DA, Pearcy RW (2012) Sunflecks in trees and forests: from photosynthetic physiology to global change biology. Tree Physiol 32:1066–1081

Wilson TB, Norman JM, Bland WL, Kucharik CJ (2003) Evaluation of the importance of Lagrangian canopy turbulence formulations in a soil-plant-atmosphere model. Agric For Meteorol 115:51–69

Wullschleger SD (1993) Biochemical limitations to carbon assimilation in C_3 plants – a retrospective analysis of the A/C_i curves from 109 species. J Exp Bot 44:907–920

Wythers KR, Reich PB, Tjoelker MG, Bolstad PB (2005) Foliar respiration acclimation to temperature and temperature variable Q(10) alter ecosystem carbon balance. Glob Change Biol 11:435–449

Zhang YC, Rossow WB, Lacis AA, Oinas V, Mishchenko MI (2004) Calculation of radiative fluxes from the surface to top of atmosphere based on ISCCP and other global data sets: refinements of the radiative transfer model and the input data. J Geophys Res Atmos 109, D19105. doi:10.1029/2003JD004457

Part II

Physiological Processes from Leaves to Canopies

Chapter 3

Modeling Leaf Gas Exchange

Kouki Hikosaka*
Graduate School of Life Sciences, Tohoku University, Sendai 980-8578, Japan

CREST, JST, Tokyo, Japan

Ko Noguchi
School of Life Sciences, Tokyo University of Pharmacy and Life Sciences, 1432-1, Horinouchi, Hachioji, Tokyo 192-0392, Japan

and

Ichiro Terashima
School of Science, The University of Tokyo, Hongo, Bunkyo-ku, Tokyo 113-0033, Japan

*Author for correspondence, e-mail: hikosaka@m.tohoku.ac.jp

e-mail: knoguchi@toyaku.ac.jp

e-mail: itera@bs.s.u-tokyo.ac.jp

K. Hikosaka, Ü. Niinemets, and N.P.R. Anten (eds.), *Canopy Photosynthesis: From Basics to Applications*, DOI 10.1007/978-94-017-7291-4_3

Summary

Leaves are photosynthetic organs that absorb light and convert the photon energy of light to chemical energy for use in CO_2 assimilation. Here we review how CO_2 assimilation rates vary, depending on environmental factors and among leaves. Net CO_2 assimilation is a balance between the carboxylation of ribulose 1,5-bisphosphate (RuBP) catalyzed by ribulose-1,5-bisphosphate carboxylase/oxygenase (Rubisco) and the release of CO_2 by photorespiration and mitochondrial respiration. The steady-state biochemical model of CO_2 assimilation considers photosynthetic metabolism as a composite of two processes, namely, RuBP carboxylation and regeneration. The former, modeled based on the Rubisco kinetics, is limited mainly by CO_2 supply, whereas the latter is assumed to be limited by the rate of photon absorption at low light and by its use in electron transport at high light. CO_2 concentration at the assimilation sites in chloroplasts depends on the stomatal and mesophyll conductances for CO_2 diffusion. Both these conductances are sensitive to environmental variables, but no mechanistic models of environmental responses for these conductances are available. Various empirical models have been developed and combined with the biochemical photosynthesis model allowing for expression of CO_2 assimilation rates as a function of environmental variables.

Abbreviations: A – Net CO_2 assimilation rate; A_c – RuBP-saturated A; A_j – RuBP-limited A; A_{max} – Maximum A (photosynthetic capacity); A_t – A limited by TP use; ABA – Abscisic acid; AOX – Cyanide-resistant alternative oxidase; B_n – Net anabolic NADH supply; C_a C_c, C_f and C_i – CO_2 partial pressures at air, chloroplast, leaf surface and intercellular space respectively; c_p – Heat capacity of air; CP – Cytochrome pathway; D – Leaf-to-air vapor pressure deficit; D_0 – Fitted parameter for D in Eq. 3.29; d_{min} – Minimum ion diffusion rate in modeling stomatal conductance in Eq. 3.36; E – Evapotranspiration rate; E_a – Activation energy; E_o – Activation energy of the respiratory pathway; E_{oref} – Activation energy at the reference temperature; f_i and f_{ref} – Value of f at T = ∞ and the reference temperature; f_m – Fraction of photorespiratory NADH that remains in mitochondria; F_v/F_m – Maximum dark-adapted quantum yield for photosystem II; $f_{\Psi v}$ – Sensitivity of stomata to leaf water potential; $FADH_2$ – Flavin adenine dinucleotide; g – Total diffusion conductance for CO_2 from air to chloroplasts; g_0 and g_1 – Fitted parameters for stomatal conductance; g_b g_m, and g_s – Conductances for CO_2 diffusion across boundary layer, mesophyll and stomata; g_{bh} – Leaf boundary layer for heat conductance; g_c – Leaf CO_2 conductance including stomatal and boundary layer conductances; g_{wc} – Leaf water vapor conductance including stomatal and boundary layer conductances; H – Sensible heat flux; H_d – Energy of deactivation; h_r – Relative humidity at the leaf surface; HT – High temperature; I – Photosynthetically active photon flux density (irradiance); J – Electron transport rate; J_{max} – Maximum J; K_c and K_o – Michaelis–Menten constants for carboxylation and oxygenation; k_{cat} – Rubisco turnover rate (rate of CO_2 fixation per Rubisco active site); K_{tot} – Hydraulic conductance for the whole plant; LMA – Leaf mass per area; LT – Low temperature; m – Empirical constant in Eq. 3.32; M – Plant dry mass; MDH – Malate dehydrogenase; $NADH_m$ – Fraction of photorespiratory NADH that remains in mitochondria; NDs – Type II NAD(P)H dehydrogenases; O – O_2 partial pressure in chloroplasts; OAA – Oxaloacetic acid; OPPP – Oxidative pentose phosphate pathway; P_g and P_e – Pressure potentials of the guard cells and the bulk epidermal cells; P_p – Export rate of triose phosphate; PDH – Pyruvate dehydrogenase complex; PEPCase – Phospho*enol*pyruvate carboxylase; PGA – 3-phosphoglycerate; PQ – Plastoquinone; PSII – Photosystem II; Q_{10} – Ratio of the process rate at a reference temperature + 10 K to the rate at the reference temperature; r – Total resistance to CO_2 diffusion from air to chloroplasts; r_b, r_m, and r_s – Resistances to CO_2 diffusion at boundary layer, mesophyll, and stomata; r_{wb} and r_{ws} – Resistances to water vapor at boundary

Keywords CO_2 assimilation • CO_2 response • Dark respiration • Day respiration • Interspecific variation • Light response • Mesophyll conductance • Rubisco • Stomatal conductance • Temperature dependence

I. Introduction

Leaf gas exchange rates vary depending upon environmental conditions such as light, temperature, CO_2 concentration and humidity. These rates also vary among leaves even within an individual plant depending upon the leaf ontogeny and growth environments. Farquhar et al. (1980) developed a steady-state biochemical model for C_3 photosynthesis based on a simple mechanism of potential limitation of photosynthesis, using reliable kinetic properties of ribulose-1,5-bisphosphate carboxylase/oxygenase (Rubisco). After incorporating a semi-empirical model of stomatal conductance (e.g. Ball et al. 1987), the rates of CO_2 assimilation and transpiration could be described as a function of environmental variables (Harley and Tenhunen 1991; Harley and Baldocchi 1995). Variants of this combined photosynthesis/stomata model are widely used as a tool for the prediction of plant growth and primary production under changing environment in agriculture, ecology, and Earth system science (Farquhar et al. 2001).

In this chapter, we review the models describing environmental dependencies of leaf gas exchange with emphasis on C_3 photosynthesis. Furthermore, we describe the biochemical model of C_3 photosynthesis and empirical models for environmental response for respiration and CO_2 diffusion conductance. Based on these models, we discuss typical environmental response of gas exchange and interspecific variations in the model parameters.

layer and stomata; $\boldsymbol{R}$ – Universal gas constant; R_C – Rate of non-photorespiratory CO_2 release; R_d – Respiration rate in the light; R_g – Growth respiration coefficient; R_m – Maintenance respiration rate; R_n – Respiration rate in the dark; R_N – Net radiation; R_O – Rate of non-photorespiratory O_2 consumption; R_{PR} – Photorespiratory rate; R_{ref} – Respiration rate at the reference temperature; R_{min} – Minimum R_{d}; RGR – Relative growth rate; Rubisco – Ribulose-1,5-bisphosphate carboxylase/oxygenase; RuBP – Ribulose 1,5-bisphosphate; S_{c} – Chloroplast surface area; $S_{\mathrm{c/o}}$ – Relative specificity of Rubisco (specificity factor); S_V – Sensitivity parameter in Eq. 3.38; SA and SD – Starch-accumulating and deficient species; TP – Triose-phosphate; T_l and T_a – Leaf and air temperatures; T_k – Temperature in Kelvin; T_{opt} – Optimal temperature; T_{ref} – Reference temperature; T_{sky} – Temperature of the sky; UCP – Uncoupling protein; UQ – Ubiquinone; V_{by} – Rate of carbon flow to CO_2 as a by-product of flows into anabolic products; V_c – Rate of carboxylation; V_{cat} – Rate of CO_2 release due to catabolic substrate oxidation; V_{cmax} – Maximum V_{c}; V_o – Rate of oxygenation; V_{opc} – CO_2 release rate from substrate oxidation via cytosolic OPPP; V_{omax} – Maximum V_{o}; V_{opp} – CO_2 release rate from substrate oxidation via chloroplastic OPPP; V_{px} – Photo-reductant export rate; VPD – Vapor pressure deficit; W_a and W_i – Water vapor pressures in air and intercellular air space; α – Leaf absorptance; α_S and α_{IR} – Shortwave and infrared absorptances; β_a – Empirical constant in Eq. 3.34; γ and ξ – Empirical constants in Eq. 3.36; δ – Coefficient to describe dynamic response of E_{o} to temperature; δ_{w} – Thickness of mesophyll cell wall; ΔS – Entropy term; ε – Leaf long-wave emissivity; φ – Ratio of RuBP oxygenation to carboxylation rates; ϕ_{x} – Initial slopes of the light response curve; Γ – CO_2 compensation point of CO_2 assimilation; Γ^* – CO_2 compensation point of CO_2 assimilation in the absence of R_{d}; λ – Heat of vaporization; λ_s – Marginal water cost of carbon gain; π_a – Osmotic potential of apoplastic water near the stomatal guard cells; π_e – Osmotic potential of epidermis cells; π_g – Osmotic potential in the guard cells; θ_{x} – Curvature factors in Eqs. 3.11, 3.12 and 3.16; ρ – Shortwave reflectance of the surroundings; σ – Stefan–Boltzmann constant; τ – Scale R_{o} to a daily rate; τ_{a} – ATP concentration in the guard cells; υ – Slope of light response of R_{d}; χ – Hydraulic conductance between the bulk epidermis and stomatal guard cells; ψ_e – Water potential of epidermis cell; ψ_g – Water potential of guard cell; ψ_{ref} – Reference potential; ψ_s – Soil water potential; ψ_V – Bulk leaf water potential

II. Biochemical Model of C_3 Photosynthesis

In C_3 photosynthesis, the first step of CO_2 assimilation is the carboxylation of ribulose 1,5-bisphosphate (RuBP), which is catalyzed by Rubisco. Triose phosphate (TP) is synthesized from the product, 3-phosphoglycerate (PGA), with the consumption of ATP and NADPH. One sixth of the TP can be exported to the cytosol for sucrose synthesis or used for synthesis of chloroplastic starch, and the remaining part is utilized for the regeneration of RuBP. ATP and NADPH are synthesized in the thylakoid membranes using light energy. A substantial amount of the regenerated RuBP is consumed by oxygenation, which is also catalyzed by Rubisco. One of the products, 2-phosphoglycolate, is recycled to form PGA with the consumption of ATP and reducing power accompanied by the release of CO_2 (photorespiration).

Here we describe the equations of the Farquhar et al. (1980) model with brief explanations. Refer to Farquhar and von Caemmerer (1982) and von Caemmerer (2000) for a detailed biochemical background. A steady-state biochemical model of C_4 photosynthesis is described in Box 3.1.

In the model, net CO_2 assimilation rate (A) is given as follows:

$$A = V_c - 0.5V_o - R_d \tag{3.1}$$

where V_c and V_o are the rates of carboxylation and that of oxygenation, respectively, and R_d is the respiration rate in the light (day respiration rate), which is the mitochondrial CO_2 release from processes other than photorespiration. Based on Rubisco kinetics, when the concentration of RuBP is saturated, V_c and V_o are described as follows:

$$V_c = \frac{V_{c\max} C_c}{C_c + K_c(1 + O/K_o)} \tag{3.2}$$

$$V_o = \frac{V_{o\max} O}{O + K_o(1 + C_c/K_c)} \tag{3.3}$$

where $V_{c\max}$ and $V_{o\max}$ are the maximum rates of carboxylation and oxygenation, respectively, K_c and K_o are the Michaelis–Menten constants for carboxylation and oxygenation, respectively, and C_c and O are the levels of CO_2 and O_2 at the Rubisco active sites in the chloroplast stroma, respectively. Although Rubisco is located in the liquid phase, C_c and O are generally expressed as the air molar fractions (mol mol^{-1}) or the partial pressures (Pa). We can calculate their concentrations in the liquid phase (mol m^{-3}) using equilibration solubility coefficients that depend on temperature. Partial pressure is favored, because the mole fraction is not proportional to the liquid-phase concentration when the air pressure changes, which is particularly relevant when one compares measurements conducted at different elevations (Terashima et al. 1995). Due to a very high concentration, O is generally assumed to be the same as O_2 partial pressure in the ambient air. Substituting Eqs. 3.2 and 3.3 into Eq. 3.1 gives the following equation:

$$A_c = \frac{V_{c\max}(C_c - \Gamma^*)}{C_c + K_c(1 + O/K_o)} - R_d \tag{3.4}$$

where A_c is the RuBP-saturated rate of CO_2 assimilation and Γ^* is the CO_2 compensation point of CO_2 assimilation in the absence of R_d (Laisk 1977), given by

$$\Gamma^* = \frac{0.5O}{S_{c/o}} \tag{3.5}$$

where $S_{c/o}$ is the relative specificity of Rubisco given as:

$$S_{c/o} = \frac{V_{c\max} K_o}{V_{o\max} K_c} \tag{3.6}$$

$S_{c/o}$, O and C_c determine the ratio of rates of oxygenation to carboxylation, φ, i.e., the ratio of oxygenation rate to carboxylation rate:

$$\varphi = \frac{2\Gamma^*}{C_c} \tag{3.7}$$

NADPH and ATP are required for the regeneration of RuBP in the Calvin-Benson

cycle; therefore, the rate of Rubisco reaction may be limited by RuBP regeneration. Here we assume that RuBP regeneration is limited by the NADPH supply. Per each carboxylation, two molecules of NADPH (four electrons) are consumed in the Calvin-Benson cycle. Similarly, four electrons per oxygenation are needed in photorespiration. Thus, the RuBP-limited rate of CO_2 assimilation, A_j, is given by

$$A_j = \frac{J\left(C_c - \Gamma^*\right)}{4C_c + 8\Gamma^*} - R_d \qquad (3.8)$$

where J is the rate of electron transport.

When CO_2 partial pressure is high, and/or O_2 partial pressure is low and temperature is low, the CO_2 assimilation rate is often limited by the rate of triose phosphate (TP) utilization for sucrose synthesis (Sharkey 1985; Sage 1990). The TP-utilization limited rate of CO_2 assimilation (A_t) is given by

$$A_t = 3P_p - R_d \qquad (3.9)$$

where P_p is the TP export rate from the chloroplast, which is equal to the rate of inorganic phosphate supply to the chloroplast.

The realized net rate of CO_2 assimilation is given as the minimum of the potential assimilation rates A_c, A_j and A_t.

$$A = \min\left(A_c, A_j, A_t\right) \qquad (3.10)$$

Note that Eq. 3.10 is only valid when $C_c \geq \Gamma^*$. Figure 3.1a shows a typical CO_2-response curve of CO_2 assimilation, and Fig. 3.1b demonstrates changes in the CO_2-response curve depending on leaf biochemical capacities. RuBP limitation generally occurs at higher CO_2 partial pressures, whereas the RuBP pool size is saturated at lower CO_2 partial pressures.

If we ignore A_t, Eq. 3.10 can be approximated by

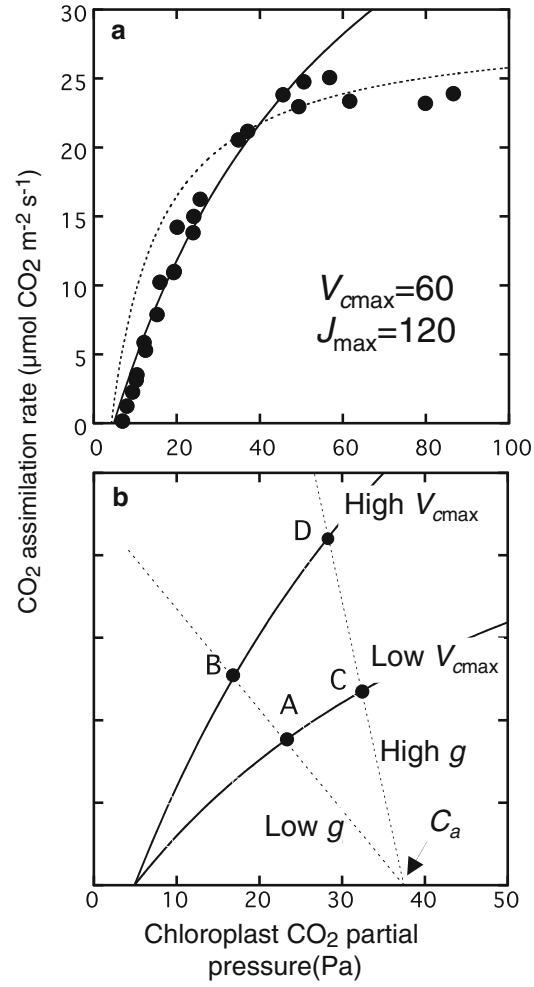

Fig. 3.1. Net CO_2 assimilation rate (A) as a function of chloroplastic CO_2 concentration (C_c). An example of A-C_c response in grapevine leaves (**a**) and effects of Ribulose-1,5-bisphosphate (RuBP) carboxylation capacity (V_{cmax}) and total conductance (g; this includes both stomatal and mesophyll conductances) on A (**b**). In (**a**), the data of Flexas et al. (2006a) are fitted by Eqs. 3.4 (*continuous line*) and 3.8 (*dotted line*). In (**b**), the "demand function" (Eq. 3.4) is shown by a solid line and the "supply function" (Eq. 3.23) by a *dotted line*. As compared with a leaf with low V_{cmax} and low g (**A**), plants can increase assimilation rates by increasing V_{cmax} (**B**), g (**C**) or both (**D**)

$$\theta_{cj}A^2 - A\left(A_c + A_j\right) + A_cA_j = 0 \qquad (3.11)$$

where θ_{cj} is a curvature in the transition from one to the other limitation ($0 < \theta_{cj} < 1$;

Collatz et al. 1991). Although θ_{cj} does not have a clear mechanistic explanation, this equation overcomes the problem of a too "sudden" switch from one limitation to the other at the transition point in Eq. 3.10.

The rate of electron transport, J, depends on light intensity. Various functions have been used to describe the light responses of J, but the non-rectangular hyperbola is recommended because of its high flexibility (see Boote and Loomis 1991).

$$J = \frac{\phi_j I + J_{\max} - \sqrt{\left(\phi_j I + J_{\max}\right)^2 - 4\phi_j I J_{\max}\theta_j}}{2\theta_j} \tag{3.12}$$

where I is photosynthetically active photon flux density (PFD) intercepted by the leaf, $J_{\max}$ is the light-saturated rate of electron transport, θ_j is the convexity of the curve and ϕ_j is the initial slope.

ϕ_j represents the apparent quantum yield of electron transport at low light and is one of the key determinants of the CO_2 assimilation rate. For linear transport of one electron, absorption of one photon by each of the two photosystems is necessary. Therefore, the potential maximum of ϕ_j is 0.5. However, real values of ϕ_j are generally lower than 0.5 due to several reasons. One of the reasons is that the absorptance of leaves (absorbed light per incident light) is lower than 1 due to light reflection and transmission. ϕ_j is thus given by

$$\phi_j = \alpha\phi_q \tag{3.13}$$

where α is the absorptance of the leaf and ϕ_q is the quantum yield of electron transport on an absorbed quantum basis. The value of ϕ_q is affected by efficiency in photochemistry. Part of the absorbed energy is dissipated as heat or fluorescence. At least 17 % of energy absorbed by photosystem II (PSII) is dissipated as heat under low light conditions even in healthy leaves, and in photoinhibited leaves this proportion is much bigger leading to significantly lower values of ϕ_q (see Sect. VI.D). Photon absorption by other pigments and inefficient partitioning of light absorption between the two photosystems may reduce ϕ_q. In healthy C_3 leaves, ϕ_q is commonly similar between species when determined with the same method: 0.356–0.384 (determined with CO_2 exchange; Long et al. 1993) and 0.408–0.448 (determined with O_2 exchange; Björkman and Demmig 1987).

Most of the biochemical model parameters exhibit strong temperature dependence. The temperature dependence of some of the kinetic constants (or rates), f, can be described by an Arrhenius function:

$$\begin{aligned} f &= f_i \exp\left(-\frac{E_a}{\boldsymbol{R}T_k}\right) \\ &= f_{\text{ref}} \exp\left[\frac{E_a(T_k - T_{\text{ref}})}{\boldsymbol{R}T_k T_{\text{ref}}}\right] \end{aligned} \tag{3.14}$$

where T_k and T_{ref} are leaf temperature and reference temperature in Kelvin, respectively, f_i and f_{ref} correspond to the value of f at $Tk = 0$ and the reference temperature, respectively, E_a is the activation energy of f, and $\boldsymbol{R}$ is the universal gas constant (8.314 J mol^{-1} K^{-1}). The temperature dependence of K_c, K_o, and Γ* are generally expressed by the Arrhenius function (Fig. 3.2). A peak model is often applied if deactivation at high temperatures is substantial.

$$f = \frac{f_{\text{ref}} \exp\left[\frac{E_a(T_k - T_{\text{ref}})}{\boldsymbol{R}T_k T_{\text{ref}}}\right]\left[1 + \exp\left(\frac{T_{\text{ref}}\Delta S - H_d}{\boldsymbol{R}T_{\text{ref}}}\right)\right]}{1 + \exp\left(\frac{T_k \Delta S - H_d}{\boldsymbol{R}T_k}\right)} \tag{3.15}$$

where H_d is the energy of deactivation and ΔS is an entropy term (Johnson et al. 1942; von Caemmerer 2000; Medlyn et al. 2002).

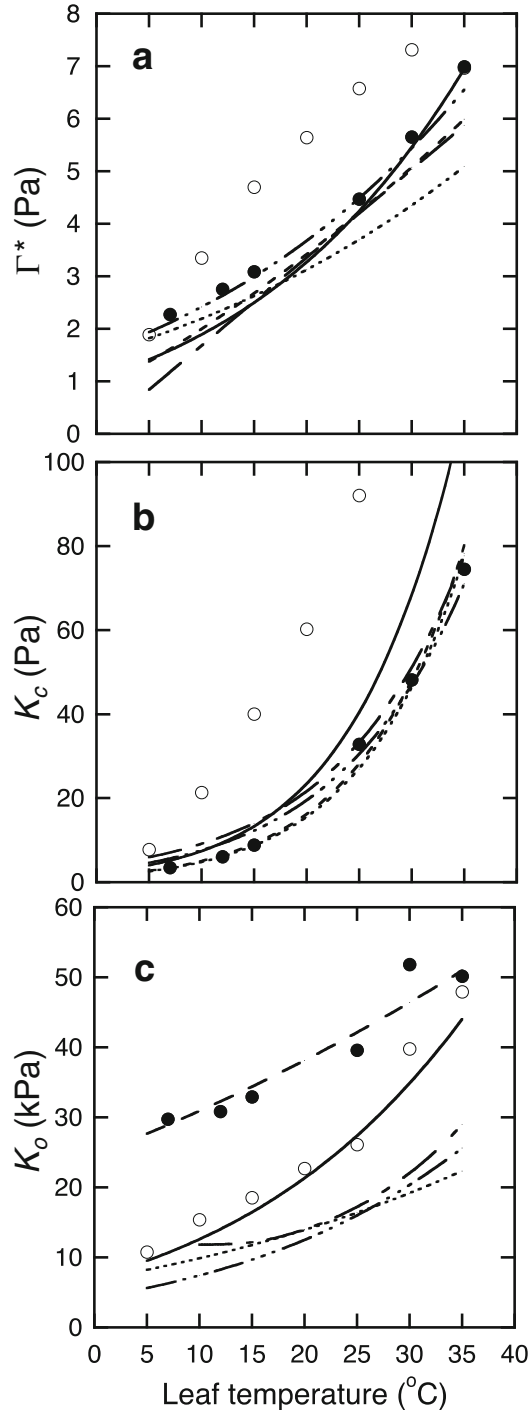

Fig. 3.2. Temperature dependence of Ribulose-1,5-bisphosphate carboxylase/oxygenase (Rubisco) kinetic parameters, the CO_2 compensation point in the absence of mitochondrial respiration, Γ* (**a**); the Michaelis–Menten constant for CO_2, K_c (**b**); and the Michaelis–Menten constant for O_2, K_o (**c**). *Filled symbols* correspond to *in vitro* data for *Spinacea oleracea* reported by Jordan and Ögren (1984) and *open symbols* to *in vitro* data for *Atriplex glabriuscula* from Badger and Collatz (1977). *Continuous, dotted*, *3-dot dash*, and *broken lines* are the regression presented by Bernacchi et al. (2001) for *Nicotiana tabacum* (C_i-based), Bernacchi et al. (2002) for *Nicotiana tabacum* (C_c-based), Harley and Tenhunen (1991) (C_i-based), and Brooks and Farquhar (1985) for *Phaseolus vulgaris* (C_i-based), respectively. The *dot-dashed line* is the regression presented by Farquhar (1988) for Γ* (C_i-based) and by McMurtrie and Wang (1993) for K_c and K_o (C_i-based)

Box 3.1: Biochemical Model of C_4 Photosynthesis

In C_4 photosynthesis, C_4 acids are generated by fixation of bicarbonate by PEP (phospho*enol*pyruvate) carboxylase in the cytosol of mesophyll cells, then diffuse to the bundle-sheath cells where they are decarboxylated (Fig. B3.1). Released CO_2 is re-fixed by the C_3 photosynthetic pathway in the chloroplasts of the bundle-sheath cells. PEP carboxylase has a much higher affinity for CO_2 (in ionized bicarbonate equivalents) and does not react with O_2. Because bundle-sheath cells are bounded by gas-tight cell walls, CO_2 is concentrated in bundle-sheath cells and thus, photorespiration is suppressed. Steady-state models of C_4 photosynthesis have been developed by Berry and Farquhar (1978) and Peisker (1979). Because the complete model is very complicated, here we present a simplified model. See von Caemmerer (2000) for a detailed steady-state model and Laisk and Edwards (2002) for a detailed dynamic model.

CO_2 assimilation rate of C_4 photosynthesis is potentially limited either by PEP carboxylation, RuBP carboxylation, NADPH production or ATP synthesis. In general, PEP carboxylation limits photosynthesis at very low CO_2 partial pressures ($C_i < 10$ Pa) under high light. The rate of PEP carboxylation V_p is given by

$$V_p = \frac{C_m V_{p\max}}{C_m + K_p} \qquad \text{(B3.1.1)}$$

where C_m is the CO_2 partial pressure in the cytosol of mesophyll cells, $V_{p\max}$ is the maximum rate of PEP carboxylation and K_p is the Michaelis–Menten constant for CO_2 in equilibrium with bicarbonate. The CO_2 assimilation rate limited by PEP carboxylation (A_p) is given by

$$A_p = V_p + g_{bs} C_m - R_{mes} \qquad \text{(B3.1.2)}$$

where g_{bs} is the CO_2 diffusion conductance from mesophyll to bundle-sheath cells and R_{mes} is the respiration rate of the mesophyll cells. $g_{bs}C_m$ is the rate of CO_2 diffusion from mesophyll to bundle-sheath cells and can be ignored because the CO_2 flux is only

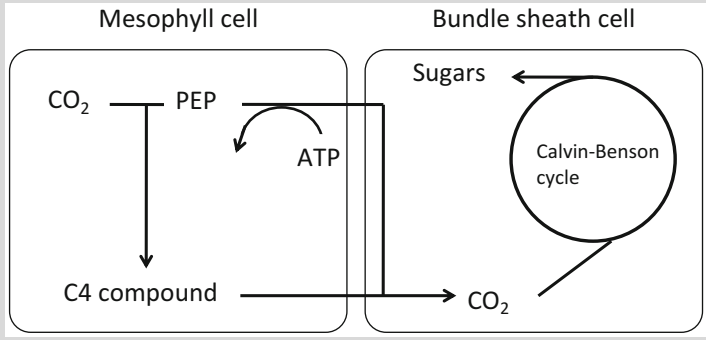

Fig. B3.1. A simple scheme of C_4 photosynthesis. In C_4 photosynthesis, C_4 acids are generated by fixation of bicarbonate by PEP (phospho*enol*pyruvate) carboxylase in the cytosol of mesophyll cells, then diffuse to the bundle-sheath cells where they are decarboxylated. Released CO_2 is re-fixed by the C_3 photosynthetic pathway in the chloroplasts of the bundle-sheath cells

(continued)

Box 3.1 (continued)

0.3 μmol m^{-2} s^{-1} at C_m of 10 Pa (von Caemmerer 2000). CO_2 release from respiration at the bundle-sheath cells does not affect the CO_2 assimilation rate when PEP carboxylation limits photosynthesis because it is re-assimilated in C_3 photosynthesis in the cells.

The CO_2 assimilation rate limited by RuBP carboxylation is affected by CO_2 and O_2 partial pressures in the bundle-sheath cell as described in Eqs. 3.2 and 3.3. However, when the PEP carboxylation rate is high enough, CO_2 is concentrated in the bundle-sheath cells and oxygenation and photorespiration can thus be ignored. The RuBP-saturated rate of CO_2 assimilation A_c can be approximated by

$$A_c = V_{c\max} - R_d \qquad \text{(B3.1.3)}$$

At low light, electron transport rate can limit photosynthesis. For 1 mol of CO_2 assimilation in C_4 photosynthesis, 2 and 3 mol ATP are required for the C_4 and C_3 pathways, respectively. Photorespiration also requires energy but is negligibly small. In most cases, ATP supply in the bundle-sheath cells is a limiting step of photosynthesis. If we assume that 3 mol ATP is synthesized per proton, the electron transport-limited rate of CO_2 assimilation A_j is approximated as

$$A_j = \frac{(1-x)J}{3} - R_d \qquad \text{(B3.1.4)}$$

where x is the fraction of photons absorbed in mesophyll cells ($0 < x < 1$). J is the electron transport rate obtained as in Eq. 3.12.

CO_2 assimilation rate is thus given by

$$A = \min\left(A_p, A_c, A_j\right) \qquad \text{(B3.1.5)}$$

III. Respiration

In the plant respiratory system, carbohydrates are decomposed into pyruvate via glycolysis and the oxidative pentose phosphate pathway (OPPP) in the cytosol and plastids. The end product, pyruvate, is imported into the mitochondria and catabolized by the pyruvate dehydrogenase complex (PDH) and the TCA cycle, in which the reducing equivalents (NADH and $FADH_2$) are produced and CO_2 is released. When organic acids in the TCA cycle are used as the carbon skeleton for anabolic processes or the nitrogen assimilation process, oxaloacetic acid (OAA) is complemented by phospho*enol*pyruvate carboxylase (PEPCase) and malate dehydrogenase (MDH) in the cytosol and consumed in the TCA cycle (the anaplerotic pathway). The reducing equivalents produced via glycolysis, OPPP, and the TCA cycle, are oxidized by the respiratory electron transport chain and the electrons are passed to O_2. The respiratory electron transport chain in plants consists of not only the phosphorylating pathway, containing complexes I (NADH-quinone oxidoreductase), III (cytochrome *c* reductase), and IV (cytochrome *c* oxidase) of the oxidative electron transport chain, but also several non-phosphorylating pathways, such as those including type II NAD(P)H dehydrogenases (NDs) and the cyanide-resistant alternative oxidase (AOX) (Finnegan et al. 2004). The uncoupling protein (UCP) facilitates the re-entry of H^+ into the mitochondrial matrix, bypassing ATP synthesis (Hourton-Cabassa et al. 2004). In the respiratory system, 36 molecules of ATP are produced from one molecule of glucose. Because the transport of respiratory substrates and phosphates consumes ATP, 29 molecules of ATP are produced from one molecule of glucose in the most efficient state (Amthor 1994). When NDs, AOX or UCP are used, the efficiency of ATP production decreases. In this section, we discuss the respiratory pathway from the perspective of CO_2 release and O_2 consumption.

A. Dark and Day Respiration

The respiration rate is influenced by various environmental factors. Presence of light is known to reduce respiration rates (Brooks and Farquhar 1985; Villar et al. 1994), although its detailed mechanism still remains unclear (Atkin et al. 2000a; Tcherkez et al. 2012). Determination of the true day respiration rate (R_d; respiration in the light) is somewhat difficult, as simultaneous photosynthetic gas exchange due to CO_2 assimilation and photorespiration needs to be eliminated. Several methods have been developed so far to estimate R_d (see Box 3.2). Table 3.1 shows an example of the correspondence between R_d and the respiration rate in the dark (R_n) for starch-accumulating (SA) and starch-deficient (SD) species. The difference in the R_d/R_n ratio between SA and SD species may be related to the possibility that starch is not involved in supplying substrates for respiration in SA species (Pärnik and Keerberg 2007). The R_d/R_n ratio generally decreases with increasing measurement irradiance (Brooks and Farquhar 1985; Atkin et al. 1998, 2000b). This decrease occurs at very low light, typically lower than the light-compensation point of photosynthesis. Consequently, a change in the initial slope of the light response curve is often observed, known as the Kok effect (Kok 1948; Fig. 3.3a). Thus, we may formulate light dependence of R_d as follows:

$$\theta_R R_d^2 - (R_n - \upsilon I + R_{\min})R_d + (R_n - \upsilon I)R_{\min} = 0 \quad (3.16)$$

Table 3.1. Rates of photorespiration (R_{PR}), respiration in the light (R_d), respiration in the dark (R_n), mitochondrial NADH production in the light ($NADH_d$) and mitochondrial NADH production rate in the dark ($NADH_n$) estimated from the data reported by Pärnik and Keerberg (2007)

	SA species	SD species
	Rates (μmol m^{-2} s^{-1})	
R_{PR}	2.49	2.47
R_d	0.36	0.42
R_n	1.37	0.82
$NADH_d$	2.21	2.32
$NADH_n$	2.74	1.64
	Ratios of rates	
R_d/R_n	0.26	0.51
$NADH_d/NADH_n$	0.81	1.42

SA refers to starch-accumulating species and SD to starch-deficient species (mean values for four species in both cases) In the calculations, we assumed that: (1) 40 % of NADH released by photorespiratory glycine dehydrogenase complex (GDC) is exported to the cytosol for the reduction of hydroxypyruvate and the remaining part is reduced by the mitochondrial respiratory chain, (2) six molecules of NADH and $FADH_2$ are produced from glycolysis and the TCA cycle when three molecules of CO_2 are released, and (3) one molecule of NADH is produced in the photorespiratory pathway when one molecule of CO_2 is released.

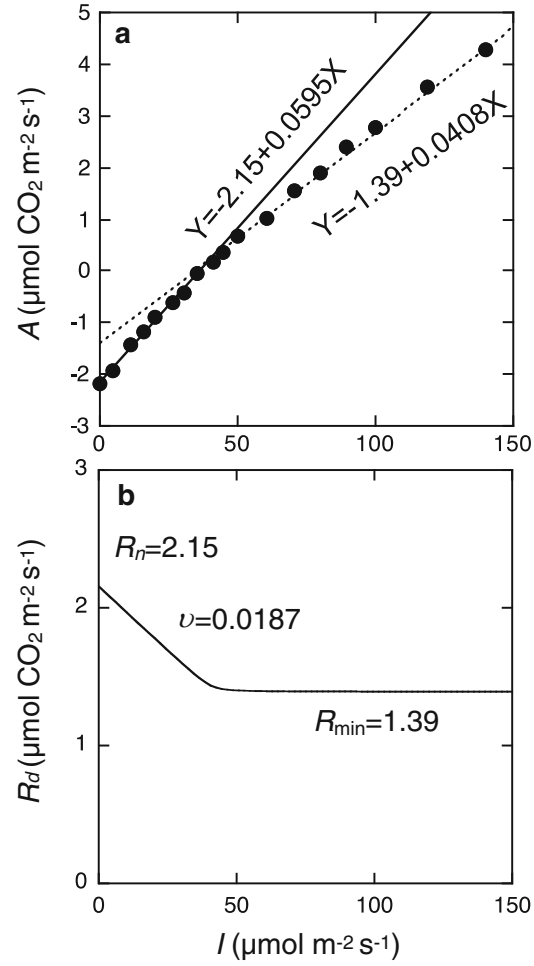

Fig. 3.3. Net CO_2 assimilation rate (A) (**a**) and day respiration rate (R_d) (**b**) as a function of the photon flux density (PFD) in a mature leaf of *Glycine max* (K. Noguchi, unpublished data). *Continuous* and *dotted lines* in (**a**) are linear regression for PFD below and above the light compensation point, respectively. PFD dependence of R_d is calculated according to Eq. 3.16

where R_{min} is the minimum R_d that is found at higher irradiance, θ_R is the curvature factor, and υ is the slope of light response of R_d, which is calculated as the difference between the light dependence of A above and below the light compensation point. Figure 3.3b shows an example of fitting the data by Eq. 3.16.

Although R_d (R_{min}) values are correlated with R_n values in many cases, the R_d/R_n ratio often changes depending on short-term or long-term environmental changes. R_d also decreases with increasing CO_2 concentration in the measurement system (Tcherkez et al. 2008). The measurement temperature also influences the value of R_d/R_n (Atkin et al. 2000a, 2006; Zaragoza-Castells et al. 2007). For the long-term changes, the R_d/R_n ratio changes with nitrogen availability (Shapiro et al. 2004), drought treatment (Ayub et al. 2011), growth temperature (Atkin et al. 2006; Zaragoza-Castells et al. 2007; Ayub et al. 2011), light environment (Zaragoza-Castells et al. 2007) and CO_2 condition (Wang et al. 2001; Shapiro et al. 2004). In some cases, the R_d/R_n ratio has been reported to be more than one (e.g., Atkin et al. 2000b), but its underlying mechanism remains unclear.

As mentioned above, R_d of C_3 plants has often been inhibited as compared with R_n, but this inhibition in the light does not necessarily hold true for the mitochondrial O_2 consumption. Using mass spectrometric analysis of O_2 exchange, it was demonstrated that the rate of mitochondrial O_2 consumption increased with increasing light intensity in the green alga, *Chlamydomonas reinhardtii* (Xue et al. 1996). Their data suggested that the rate of mitochondrial O_2 consumption increased with increases in the export of photogenerated reducing equivalents from the chloroplasts.

To further evaluate the possible modifications of O_2 uptake by changes in the light level, we calculated the rates of mitochondrial NADH production and O_2 consumption in illuminated leaves. In this calculation, we used the average values of photorespiration rate (R_{PR}), R_d and R_n reported by Pärnik and Keerberg (2007) (Table 3.1). The rates of mitochondrial NADH production in the light amounted to 0.81- and 1.42-fold the rates of mitochondrial NADH production in the dark in starch-accumulating and starch-deficient species, respectively (Table 3.1). Because the rate of mitochondrial O_2 consumption is proportional to the rate of mitochondrial NADH production, and considering that the R_d values as the CO_2 efflux rate are 26–51 % of the R_n values, we conclude that the mitochondrial O_2 consumption is not always inhibited in the light.

At high irradiance, excessive reducing equivalents are exported from the chloroplasts via a malate/OAA shuttle and consumed by the mitochondrial respiratory chain (Yoshida et al. 2007). This mechanism should lead to the enhancement of the mitochondrial O_2 consumption in the light. The enhancement of the mitochondrial NADH production in the light is supported by the data on the changes in the redox state of ubiquinone (UQ). After the transfer of the leaves from the dark to high irradiance, the redox state of UQ as well as that of plastoquinone (PQ) shifts to the reduced state (Yoshida et al. 2011). The AOX and the cytochrome pathway (CP) of the mitochondrial respiratory chain consume O_2 depending on the redox state of UQ; therefore, the rate of mitochondrial O_2 consumption in the light should be enhanced at high irradiance. At high irradiance, the non-phosphorylating pathways, AOX and NDs, may efficiently dissipate excess reducing equivalents to maintain moderate states of UQ and PQ. The capacity of AOX in *Arabidopsis thaliana* leaves increases under high growth irradiance (Florez-Sarasa et al. 2011).

Box 3.2: Measurement of Dark and Day Respiration Rates in Leaves

The dark respiration rate (R_n) is usually measured as CO_2 efflux rate or O_2 consumption rate in the dark when ATP and the reducing equivalents are produced mainly by the mitochondrial respiratory system. However, in illuminated leaves of C_3 plants, CO_2 is fixed by Rubisco and PEPCase, whereas CO_2 is released by glycine dehydrogenase complex (GDC) of the photorespiratory pathway, the pyruvate dehydrogenase complex (PDH), the TCA cycle, and the oxidative pentose phosphate pathway (OPPP). Thus, determination of the mitochondrial CO_2 release (R_d) is complicated in the light (Atkin et al. 2000a; Hurry et al. 2005). In the light, the mitochondrial O_2 consumption is also difficult to measure because O_2 is released by PSII and O_2 is consumed by the water-water cycle, Rubisco oxygenation, and the mitochondrial O_2 consumption. Determination of R_d is important for estimation of gross photosynthetic rate, Rubisco kinetic parameters, and for simulation of net assimilation rate using the Farquhar et al. (1980) biochemical photosynthesis model. Thus, several methods for the determination of R_d have been proposed and these are summarized here. In leaf ecophysiological studies, R_d has often been estimated by two indirect methods based on leaf gas exchange: the Laisk method and the Kok method. Other methods based on the gas exchange have also been proposed (Laisk and Loreto 1996; Peisker and Apel 2001).

A. The Laisk Method

This method has been widely used for R_d determination (Laisk 1977; Brooks and Farquhar 1985; Villar et al. 1994). The net CO_2 assimilation rate (A) is given by Eq. 3.1. When the partial pressure of CO_2 in the intercellular space in the leaf, C_i, decreases, the amount of CO_2 fixed by Rubisco and that released by photorespiration become equal, i.e., $V_c = 0.5V_o$. The partial pressure of CO_2 in the carboxylation site, C_c, corresponding to this condition is noted as Γ^*, the CO_2 compensation point in the absence of R_d. As the mitochondrial respiration continues, the CO_2 efflux rate at Γ^* is the measure of R_d. To determinate R_d, regressions of A versus C_i at different irradiances are constructed and the value of R_d is identified as the y-coordinate of the common intersection point of A versus C_i (Fig. B3.2a). Γ^* can be calculated from the x-coordinate of the common intersection point of A versus C_i and the equation, $C_c = C_i - A/g_m$, where g_m is the mesophyll conductance. The Laisk method assumes that R_d does not vary with irradiance within the irradiance ranges used, and that respiratory substrates are not limiting during prolonged exposure to low CO_2 concentrations (Atkin et al. 2000a). To avoid the limitation of R_d by the availability of respiratory substrates, fast-response gas exchange systems have been used to estimate R_d (Atkin et al. 1998).

Another potential problem with this method is if one uses clamp-on leaf chambers (e.g., LI-6400). With such chambers using foam gaskets, determination of R_d and Γ^* at low CO_2 concentration is problematic because of inward diffusion of CO_2 from the surrounding atmosphere into the chamber, leading to the overestimates of R_d (Hurry et al. 2005). Such diffusion leaks can be minimized by a custom-made skirt

(continued)

Box 3.2 (continued)

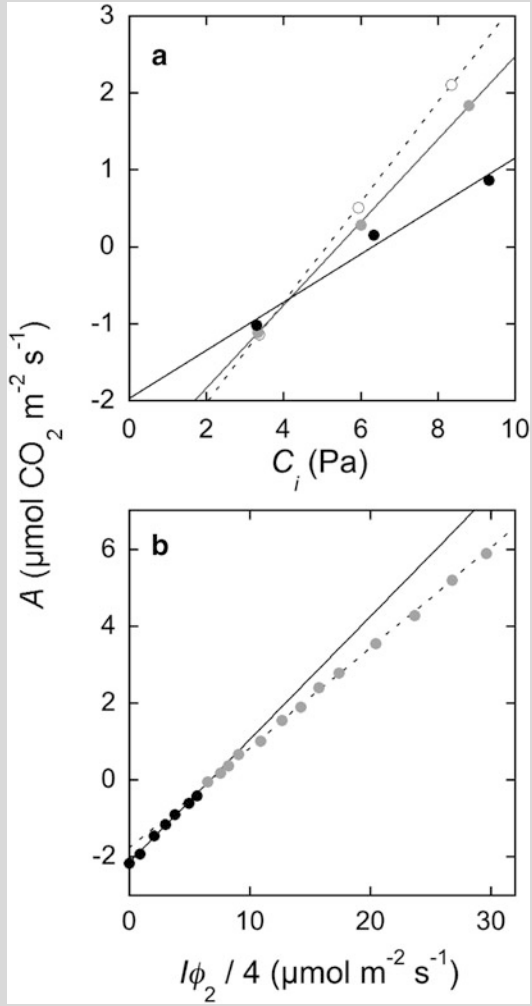

Fig. B3.2. Net CO_2 assimilation rate as a function of intercellular CO_2 concentration (C_i) (**a**) in mature leaves of *Nicotiana tabacum* (**a**, Okajima et al., unpublished data), and net CO_2 assimilation rate as a function of the variable ($I\phi_2$)/4 (I is the irradiance and ϕ_2 is the quantum efficiency of PSII electron transport, Eq. B3.2.2) in a mature leaf of *Glycine max* (**b**, K. Noguchi, unpublished data). In (**a**), the data correspond to incident irradiances of 347 (*open*), 174 (*gray*) and 87 (*black symbols*) μmol photons m^{-2} s^{-1} at O_2 concentration of 20 %. *Regression lines* were fitted to the data and the absolute value of the y-coordinate as R_d (0.721 μmol CO_2 m^{-2} s^{-1}) was taken. In **b**, *solid* and *dashed lines* represent linear regressions fitted to the data below the break-point (*black symbols*) and to the data above the break-point (*gray symbols*), respectively. Extrapolations of the *solid* and *dashed* regression lines to the zero irradiance give estimates of $-R_n$ (2.16 μmol m^{-2} s^{-1}), respiratory rate in the dark, and $-R_d$ (1.77 μmol m^{-2} s^{-1}), respiratory rate in the light, respectively. In this experiment, concomitant measurements of net CO_2 assimilation rate and chlorophyll fluorescence were conducted according to Araya et al. (2008). Concentrations of CO_2 in the leaf chamber were kept at 400 μmol mol^{-1}

(continued)

Box 3.2 (continued)

with which the chamber exhaust air is used to control the CO_2 concentration at the outer surface of the foam gaskets (Miyazawa and Terashima 2001; Rodeghiero et al. 2007). In addition to the diffusion leak from the ambient air, inward diffusion of respiratory CO_2 from darkened leaf material under the gasket into the chamber will be also likely, again leading to overestimates of R_d (Hurry et al. 2005; Pons and Welschen 2002). The correction for the CO_2 diffusion effects results in the increase in the apparent inhibition of mitochondrial CO_2 release in the light (Fig. 5 in Hurry et al. 2005), and also abolishes direct CO_2 dependence on R_d (Pons and Welschen 2002).

B. The Kok Method

R_d has often been determined using the Kok effect (Sect. III.A). According to this method, R_d is estimated by the extrapolation of the linear region above the net assimilation vs. irradiance break-point to zero irradiance (Fig. 3.3a). One problem in the Kok method is that the decrease in irradiance can result in a gradual increase of C_i and a concomitant relative increase in the rate of net assimilation in the linear region, leading to underestimation of R_d (Villar et al. 1994). The R_d value can be corrected following the method of Kirschbaum and Farquhar (1987). In all cases, the apparent rate of photosynthetic electron transport (J) needed to assimilate CO_2 with a rate A is given by Brooks and Farquhar (1985),

$$J = \frac{4(A + R_d)\left(C_i + 2\Gamma^*\right)}{C_i - \Gamma^*} \qquad \text{(B3.2.1)}$$

Provided R_d is independent of C_i and irradiance under the measurement conditions, R_d is adjusted to ensure that the intercept of plots of J against absorbed irradiance is minimized. The Kok method often results in lower estimates than the Laisk method, even after this correction (Villar et al. 1994).

In the correction procedure of Kirschbaum and Farquhar (1987), g_m is assumed to be infinite and therefore, the value of J obtained is an apparent electron transport rate. However, g_m values are finite and they are comparable with the values of stomatal conductance (g_s) (Evans et al. 2009; Flexas et al. 2012). In Ayub et al. (2011), g_m was assumed to be proportional to light-saturated photosynthetic rate and C_c was calculated. The calculated C_c was used for the correction procedure instead of C_i in Eq. B3.2.1.

C. A Modified Kok Method

Recently, Yin et al. (2011) proposed a new method for the estimation of R_d using the concomitant measurements of gas exchange and chlorophyll fluorescence. At low irradiance, A is limited by RuBP regeneration rate, and the A value can be given by,

$$A = \rho_2 \alpha I \phi_2 \left(1 - \frac{f_{pseudo}}{1 - f_{cyc}}\right)\left(\frac{C_c - \Gamma^*}{C_c + 2\Gamma^*}\right) /(4 - R_d) \qquad \text{(B3.2.2)}$$

where ρ_2 is the fraction of absorbed irradiance partitioned to PSII, α is the absorptance by leaf photosynthetic pigments, I is the irradiance, ϕ_2 is the electron transport efficiency of PSII, and f_{cyc} and f_{pseudo} represent fractions of the total electron flux passing PSI through cyclic and pseudocyclic (water-water) pathways, respectively. The observed A against $(I\phi_2)/4$ are plotted, and the intercept of the

(continued)

Box 3.2 (continued)

regression yields an estimate of R_d (Fig. B3.2b). Thus, this method is similar to the Kok method. In the Kok method, the slope of the *A*-*I* relationship gradually declines due to the decrease of quantum yield with increasing irradiance (Fig. 3.3a), but in the new method, the slope of the *A* versus $(I\phi_2)/4$ relationship is constant over a wide range of irradiances (Fig. B3.2b). The values of R_d estimated by this method have been reported to be consistently higher than those by the Kok method and comparable to those by the Laisk method (Yin et al. 2011).

D. The ^{14}C-labelling Method

A portion of CO_2 released from PDH and the TCA cycle can be re-assimilated by Rubisco inside the leaf. This re-assimilated flux (R_{dr}) cannot be estimated by the outlined indirect methods for R_d estimation. Thus, these methods measure the apparent R_d that is the difference between the true R_d and R_{dr}. In the radiogasometric pulse-chase method (Pärnik and Keerberg 2007), the re-assimilated flux (R_{dr}) can be separately estimated and the true value of R_d is derived. According to this method, the leaves are illuminated under $^{14}CO_2$ to saturate the pools of primary photosynthates with ^{14}C, and then the release of $^{14}CO_2$ is measured under non-radioactive atmosphere with different concentrations of O_2 and $^{12}CO_2$. Rates of photorespiration (R_{PR}) and respiration (R_d) can be distinguished on the basis of data obtained from the measurement of $^{14}CO_2$ release under normal (21 %) and low (1.5 %) concentrations of oxygen, assuming that photorespiration is linearly dependent on oxygen concentration up to 21 %, while respiration becomes saturated with oxygen at about 1.5 %. The re-assimilated flux (R_{dr}) is determined in the high CO_2 condition (3 % CO_2). This is based on the assumption that probability of $^{14}CO_2$ re-assimilation by Rubisco is close to zero because the $^{14}C/^{12}C$ ratio of C_i is too low. This method is also based on the assumption that different concentrations of O_2 and CO_2 do not influence the R_d value. Using this technique, R_d has been reported to be lower than R_n (Table 3.1; Pärnik and Keerberg 1995, 2007).

E. The Methods Using the Stable Isotopes

Haupt-Herting et al. (2001) proposed the method to determine R_d using $^{13}CO_2$ and isotope-ratio mass spectrometry. Loreto et al. (2001) also demonstrated the method using $^{13}CO_2$ and an infrared gas analyzer with very low sensitivity to $^{13}CO_2$. These methods also assumed that photorespiration is inhibited, but the CO_2 release from PDH and the TCA cycle are not inhibited by the high CO_2 condition. Tcherkez et al. (2008) proposed a method in that the CO_2 released from PDH and the TCA cycle can be estimated in illuminated leaves, to which ^{13}C-labeled respiratory substrates are fed through their petioles.

B. Temperature Dependence

R_n initially increases exponentially with increasing temperature until it reaches a maximum value and decreases thereafter (Hüve et al. 2011, 2012). The initial exponential part of the temperature dependence of R_n dynamically responds to short- and

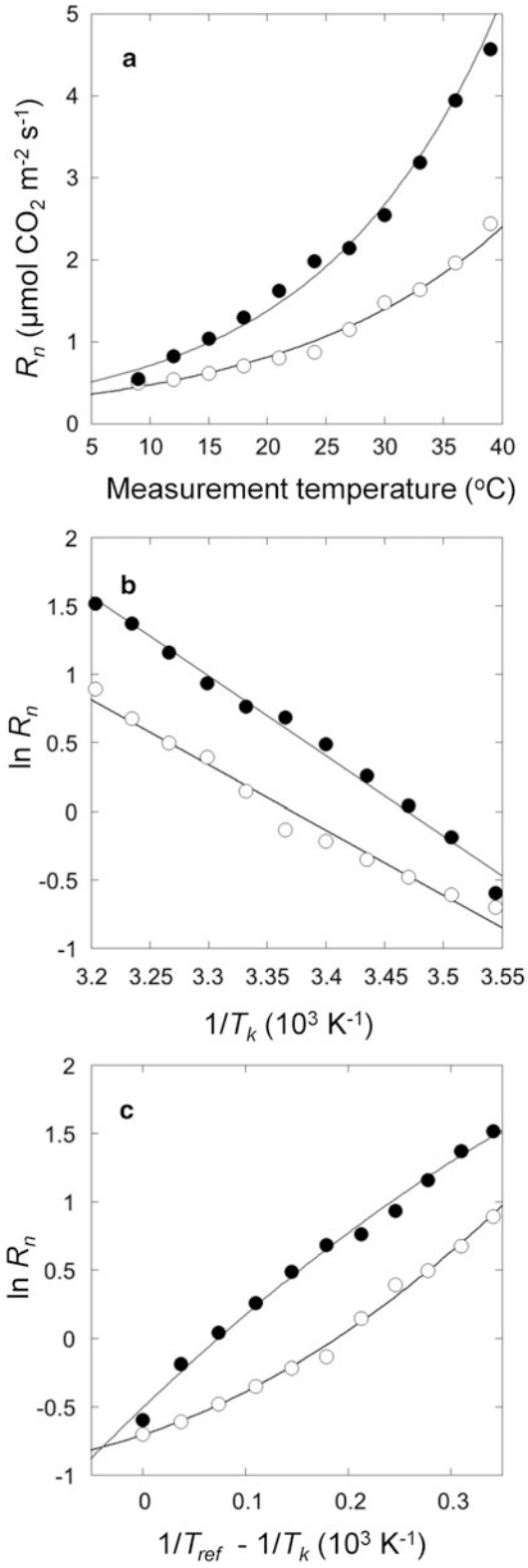

Fig. 3.4. Illustration of fitting of the temperature dependencies of the dark respiration rate of mature leaves of *Spinacea oleracea* grown at the low day/night temperature of 15/10 °C (LT, *filled symbols*) and high temperature of 30/25 °C (HT, *open symbols*; from Yamori et al. 2005). (**a**) Fitting of non-transformed values of the dark respiration rate versus the measurement temperature by the Q_{10} model (Eq. 3.17). (**b**) Fitting of ln-transformed respiration rate versus the reciprocal of the measurement temperature by Eq. 3.14. (**c**) Fitting of ln-transformed respiration rate versus the variable $1/T_{\mathrm{ref}} - 1/T$ by Eq. 3.18. In the latter fit, T_{ref} was taken as 9 °C. Estimated parameters of each model and the degrees of explained variance (r^2) are shown in Table 3.2

long-term changes in the temperature (Atkin and Tjoelker 2003; Atkin et al. 2005), and the heat-stability or R_n is also driven by environmental characteristics (Hüve et al. 2012). Often, the Q_{10} value, the ratio of process rates at temperature $T_{\mathrm{ref}} + 10$ K to the rates at reference temperature T_{ref}, is used to characterize the initial temperature response of respiration rate:

$$R_n = R_{\mathrm{ref}} Q_{10}^{\frac{T_k - T_{\mathrm{ref}}}{10}} \tag{3.17}$$

The Q_{10} relationship has been widely used, describing the proportional change of respiration in response to a temperature increase of 10 °C. Figure 3.4 shows an example of the temperature dependence of respiration rates of spinach leaves grown at low day/night temperature of 15/10 °C (LT) and high temperature of 30/25 °C (HT; Yamori et al. 2005). From the exponential curve fitted to the data points, Q_{10} of LT- and HT-leaves can be calculated (Table 3.2). The Arrhenius function has also been used to characterize the initial response (Eq. 3.14; Lloyd and Taylor 1994; Turnbull et al. 2003, 2005; Shapiro et al. 2004). In Fig. 3.4b, values of ln R_n of spinach leaves are plotted against the reciprocal of the measurement temperature. From the slope of the regression line, the activation energy of the respiratory pathway (E_o) of LT- and HT-leaves can be calculated (Table 3.2).

The regression lines of the plot of ln R_n against the reciprocal of the temperature often have different slopes between the plants grown at different temperatures, indicating modification of the temperature

Table 3.2. Parameters of three different models simulating the temperature dependence of respiratory rate

	Q_{10} model (Eq. 3.17)	Arrhenius model (Eq. 3.14)	Modified Arrhenius model (Kruse model, Eq. 3.18)		
	Q_{10}	E_o kJ mol^{-1}	R_{ref} μmol m^{-2} s^{-1}	$E_{o\text{ref}}$ kJ mol^{-1}	δ
LT	1.94	48.5	0.60	59.8	−4.0
HT	1.72	39.5	0.49	20.7	6.6

Data are taken from mature leaves of *Spinacea oleracea* grown at low day/night temperatures of 15/10 °C (LT) and high temperature of 30/25 °C (HT) reported by Yamori et al. (2005)
Each value is calculated from the regressions in Fig. 3.4
Determination coefficients are 0.984 for both LT and HT in the Q_{10} model, 0.988 and 0.978 for LT and HT, respectively, in the Arrhenius model, and 0.993 and 0.994 for LT and HT, respectively, in the modified Arrhenius model.

response by growth temperature (Fig. 3.4b). These changes can reflect modifications of the activation energy or the onset of the heat-damage processes (Hüve et al. 2012).

Kruse and Adams (2008) suggested that the initial part of the respiration vs. temperature response is better fitted by a second-order polynomial (Fig. 3.4c) and the factor δ describes the dynamic response of E_o to temperature. Thus, the Arrhenius model is further modified as follows:

$$\ln R_n = \ln R_{\text{ref}} + \frac{E_{o\text{ref}}}{\boldsymbol{R}}\left(\frac{1}{T_{\text{ref}}} - \frac{1}{T_k}\right) + \delta\left(\frac{1}{T_{\text{ref}}} - \frac{1}{T_k}\right)^2 \quad (3.18)$$

where $E_{o\text{ref}}$ is the activation energy at this reference temperature. In Fig. 3.4c, the ln R_n of spinach leaves is plotted against ($1/T_{\text{ref}}$-$1/T$) and a second polynomial equation is fitted. From the fitted curve, R_{ref}, $E_{o\text{ref}}$, and δ can be calculated. The values of parameters in each model are listed in Table 3.2. The activation energy at any temperature other than the low reference temperature can be calculated from the first derivative of Eq. 3.18. The δ value is negatively correlated with $E_{o\text{ref}}$ and becomes zero when $E_{o\text{ref}}$ is ca. 45 kJ mol^{-1} (Kruse and Adams 2008; Kruse et al. 2011, 2012). This means that the activation energy does not change with measurement temperature when the δ value is zero.

C. Construction and Maintenance Respiration

At the whole-plant level, respiration rate is affected by the growth rate of the plant itself. Faster growth requires more energy for tissue construction, leading to a higher respiration rate. Previous models have divided respiration into growth and maintenance respirations (McCree 1970; Thornley 1970; Hesketh et al. 1971; Kimura et al. 1978):

$$\frac{R_n}{M} = R_g \times RGR + R_m \quad (3.19)$$

where R_n/M is the whole plant respiration rate per unit plant dry mass, R_g is the growth respiration coefficient (amount of CO_2 released due to growth), RGR is the relative growth rate (growth rate per plant mass), and R_m is the maintenance respiration rate per plant dry mass (rate of CO_2 release due to maintenance of existing biomass). The two coefficients, R_g and R_m, can be estimated from the slope and intercept of the regression line that is fitted to a plot of R_n/M against RGR. On the basis of this model, growth and maintenance respiration rates have been estimated in many studies using the growth analysis and gas exchange measurements (Amthor 1989). In roots, respiratory ATP is consumed by the uptake of nutrient ions and this fraction is occasionally large (Lambers et al. 2008). In the modified model of Eq. 3.19, the respiration rate of roots has

been separated into three parts, namely, growth, maintenance and ion transport (Johnson 1983). Maintenance respiration rate has been measured as the respiratory rate of tissues exposed to a prolonged dark period or estimated as the respiration rate of non-growing mature tissues. This is used for the measurements of stem or branch respiration because *RGR* of these materials is difficult to estimate (Wullschleger et al. 1995).

The two-component model has some flaws. For example, (1) there is no evidence that the maintenance respiration coefficient is constant or that the growth respiration is proportional to the growth, irrespective of environmental changes; (2) in illuminated tissues, photosynthetic intermediates are used for the growth and maintenance processes, but this model assumes that growth and maintenance are supported only by the respiratory energy, and; (3) the respiration rate cannot be related to growth when the non-phosphorylating pathways are utilized. These flaws are attributed to the problem that the coefficients, R_g and R_m, cannot be related to the metabolic processes in plants, but represent hypothetical understanding of how respiration rate is associated with growth rate.

D. The Flux Balance Model

Buckley and Adams (2011) constructed an analytical model for non-photorespiratory CO_2 release and O_2 consumption based on the flux balance approach of Penning de Vries et al. (1974) and Penning de Vries (1975). Their steady-state model is derived from the stoichiometric constraints of the ATP, reducing equivalent, CO_2, and O_2 fluxes that arise from biosynthesis, maintenance, and photosynthesis. In their model, leaf composition in terms of basic compound classes and the turnover rate of each broad chemical compound class were determined from the literature data, and required amounts of ATP and the reducing equivalents were estimated using *RGR* and nitrogen assimilation rates. Using estimated rates of the required ATP and reducing equivalents, carbon flows to anabolic processes or non-photorespiratory CO_2 release were calculated. The rate of non-photorespiratory CO_2 release (R_C) and that of O_2 consumption (R_O) are given by

$$R_C = V_{opp} + V_{opc} + V_{cat} + V_{by} \tag{3.20}$$

where V_{opp} is the CO_2 release rate from substrate oxidation via chloroplastic OPPP, V_{opc} is the CO_2 release rate from substrate oxidation via cytosolic OPPP, V_{cat} is the CO_2 release rate due to catabolic substrate oxidation, and V_{by} is the carbon flow rate to CO_2 as a by-product of the flows into anabolic products.

$$R_O = V_{cat} + \frac{1}{2}\left(B_n + V_{px} + \frac{1}{2}NADH_m \varphi V_c\right) \tag{3.21}$$

where B_n is the net anabolic NADH supply, V_{px} is the photo-reductant export rate, $NADH_m$ is the fraction of photorespiratory NADH that remains in mitochondria, V_c is the RuBP carboxylation rate, and φ is the ratio of RuBP oxygenation rate to V_c.

Because their model includes the flux of excess reducing equivalents from the chloroplasts to the mitochondria and the oxidation of photorespiratory reducing equivalents by the mitochondrial respiratory chain in illuminated leaves, R_d can be compared with R_n. Their model can predict the Kok effect at low irradiance and the changes in the R_d/R_n ratio depending on the leaf age. Their model can only be applied to leaves, but if the basic parameters for other organs and for different plant species accumulate, their model can also be incorporated in large-scale models.

IV. Diffusion of CO_2 and H_2O

A. Conductance and Assimilation Rate

In C_3 photosynthesis, CO_2 is transferred from air to chloroplasts due to diffusion.

According to Fick's first law, CO_2 diffusion at a steady-state can be given by

$$A = g(C_a - C_c) = \frac{C_a - C_c}{r} \tag{3.22}$$

or

$$C_c = C_a - \frac{A}{g} \tag{3.23}$$

where C_a is partial pressure of CO_2 in the air and g and r are conductance and resistance of CO_2 diffusion from the ambient air to the carboxylation sites in chloroplasts, respectively (conductance is the reciprocal of resistance).

CO_2 assimilation rate, A, is given as a solution of Eqs. 3.10 and 3.22 (Farquhar and Sharkey 1982). Converting Eq. 3.22 as $A = gC_a - gC_c$, these two equations can be expressed on an A-C_c plot (Fig. 3.1b). Equation 3.10 gives CO_2 dependence of A (demand function). Equation 3.22 is a linear line from an X-intercept where $C_a = C_c$ with the slope of $-g$ (supply function). Thus, plants can increase A by increasing $V_{c\max}$ (or $J_{\max}$), g, or both (Fig. 3.1b).

There are three important steps that limit CO_2 diffusion: boundary layer, stomata, and mesophyll. Thus,

$$\begin{aligned} A &= \frac{C_a - C_c}{r_b + r_s + r_m} = g_b(C_a - C_f) \\ &= g_s(C_f - C_i) = g_m(C_i - C_c) \end{aligned} \tag{3.24}$$

where subscript b, f, s, i, and m denote boundary layer, leaf surface, stomata, intercellular space (or substomatal cavity), and mesophyll, respectively. Under normal conditions, even with slight wind, boundary layer conductance is much greater than stomatal conductance (g_b is up to 10 mol m^{-2} s^{-1} at wind speeds of up to 5 m s^{-1} whereas g_s is up to 1 mol m^{-2} s^{-1} when stomata fully open), so that boundary layer conductance is often ignored or combined with stomatal conductance as leaf conductance g_c ($1/g_c = r_b + r_s$) (Lambers et al. 2008).

Water is evaporated at the mesophyll cell surface and transferred to air. Evapotranspiration rate (E) is given by

$$E = \frac{W_i - W_a}{r_{wb} + r_{ws}} \tag{3.25}$$

where W_i and W_a are water vapor pressure at intercellular space and air, respectively, and r_{wb} and r_{ws} are resistances to water vapor diffusion in the boundary layer and through stomata, respectively. Resistance to CO_2 diffusion is related to that for water vapor diffusion (Ball 1987; Lambers et al. 2008):

$$r_b = 1.37 r_{wb} \tag{3.26}$$

$$r_s = 1.6 r_{ws} \tag{3.27}$$

The values of A, C_a, E and W_a can be obtained from measurement of CO_2 and water vapor flux of a leaf inside a chamber. r_{ws} can be determined from the evaporation rate of water-saturated paper inside the chamber, and W_i from saturated vapor pressure vs. temperature relationship, assuming that water vapor pressure is saturated in intercellular space at a given leaf temperature. Using these dependencies, g_b, g_s, and C_i can be estimated.

B. Stomatal Conductance

Stomatal conductance changes in response to changes in environmental conditions. In general, stomatal conductance is higher at higher light intensity, humidity, soil water content, and lower CO_2 concentrations (Cowan 1977). Here we review several wide-spread stomatal conductance models. For a more extended overview of modeling stomatal conductance, refer to Damour et al. (2010), where 35 stomatal models were critically reviewed. Besides, Buckley (2005) and Buckley and Mott (2013) are insightful reviews.

Although recent advances in molecular biology have revealed various mechanisms involved in stomatal response, our understanding required for construction of fully

mechanistic models of environmental responses of stomatal conductance remains limited. Instead, several empirical and semi-mechanistic models have been proposed. Based on a series of leaf gas exchange experiments, Ball et al. (1987) derived the following empirical expression:

$$g_s = g_0 + g_1 \frac{Ah_r}{C_f} \tag{3.28}$$

where g_0 and g_1 are fitted parameters, h_r is relative humidity at the leaf surface, and C_f is CO_2 concentration at the leaf surface. This model has been criticized because g_s responds to transpiration rate rather than to the relative humidity (Aphalo and Jarvis 1991; Mott and Parkhurst 1991). Leuning (1995) modified the equation:

$$g_s = g_0 + g_1 \frac{A}{(C_f - \Gamma)(1 + D/D_0)} \tag{3.29}$$

where Γ is the CO_2 compensation point of net CO_2 assimilation in the presence of dark respiration, D is the leaf-to-air vapor pressure deficit (VPD) and D_0 is a fitted parameter.

As an alternative approach, stomatal conductance has been modeled on the premise of relative cost of water use. An increase in stomatal conductance is costly in terms of water loss whereas it is indispensable for CO_2 assimilation. Evolutionary selection might have favored plants that regulate stomatal conductance to maximize carbon gain with a minimum water loss. Cowan and Farquhar (1977) developed a model for optimal stomatal conductance. They defined optimal stomatal conductance that maximizes carbon gain in photosynthesis minus carbon cost related to supply of water flow. The optimal solution is then obtained as follows:

$$\lambda_s = \frac{\partial E}{\partial A} \tag{3.30}$$

where λ_s is a marginal water cost of carbon gain, which represents the cost of water loss relative to the carbon gain.

Katul et al. (2010) succeeded in incorporating both the models defined by Eq. 3.29 and Eq. 3.30 into one model. Medlyn et al. (2011) showed that the optimal model could be used to derive a new model that is closely analogous to the empirical models:

$$g_s^* \approx g_0 + \left(1 + \frac{g_1}{\sqrt{D}}\right)\frac{A}{C_a} \tag{3.31}$$

Their model provided good predictions of the responses of stomatal conductance to environmental variables. All the tested models predict diurnal variation of stomatal conductance relatively well with only minor differences in the degree of explained variance (Fig. 3.5).

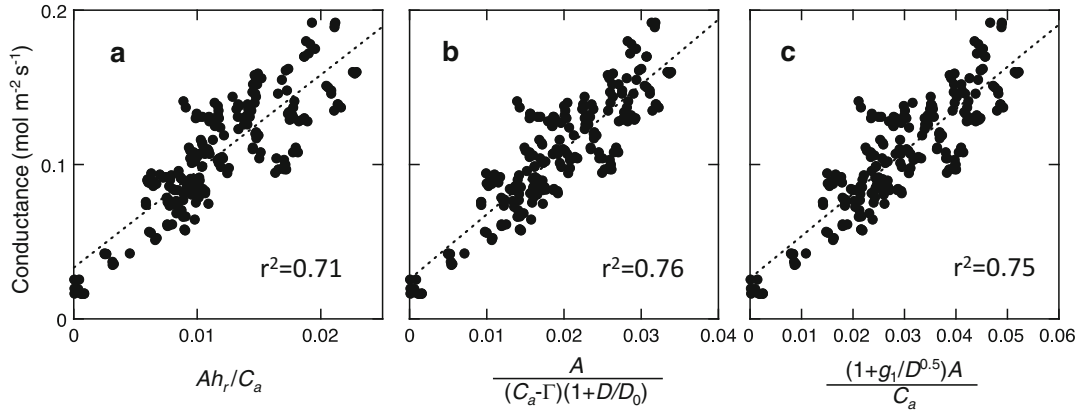

Fig. 3.5. Measured values of stomatal conductance to water vapor plotted against predicted values by three different models: Eqs. 3.28 (**a**), 3.29 (**b**), and 3.31 (**c**). Data were obtained from diurnal changes in gas exchange characteristics in canopy leaves of *Quercus crispula* (K. Hikosaka, unpublished data)

Besides the models linking stomatal conductance directly to environmental drivers, there have been some attempts to incorporate the mechanisms of stomatal opening in the conductance models. Buckley et al. (2003) expressed stomatal conductance as a function of the turgor difference between the stomatal guard cells and bulk epidermal cells, and also considered hydraulic conductance of the whole plant (K_{tot}). The set of equations needed to solve for g_s is as follows:

$$g_s = \chi\left(P_g - mP_e\right) = \chi\left(\psi_g + \pi_g - mP_e\right) \tag{3.32}$$

$$g_s = \frac{K_{tot}\left(\psi_s - \psi_g\right)}{D} \tag{3.33}$$

$$\Delta\pi_g = \pi_g - \pi_a = \beta_a \tau_a P_e \tag{3.34}$$

where χ is the hydraulic conductance between the bulk epidermis and stomatal guard cells, ψ_g and ψ_s are the guard cell and soil water potentials, respectively, D is the water vapor pressure deficit, π_g is the guard cell osmotic pressure, m is a coefficient for adjustment often termed as the mechanical advantage of the epidermis, $\Delta\pi_g$ denotes the difference in the osmotic pressure between the guard cell and that of the apoplast near the stomatal complex (π_a), β_a is an empirical constant, and τ_a is the ATP concentration in the guard cells obtained by a model similar to the photosynthesis model of Farquhar et al. (1980). P_g and P_e are the pressure potentials of the guard cells and the bulk epidermal cells. Effects of environmental variables can then be expressed as affecting τ_a, which is related to the photosynthetic rate, and P_e, which depends on plant water status. In principle, this model can predict the transient stomatal behavior on abrupt changes in the environmental variables.

Most of the models of stomatal conductance, including the models considered here (Eqs. 3.28, 3.29, 3.30, 3.31, 3.32, 3.33, and 3.34), however, do not satisfactorily incorporate the effects of water stress. Although D in Eq. 3.29 or h_r in Eq. 3.28 express air dryness, effects of soil dryness or plant water stress is indirectly expressed by A that is in turn controlled by g_s leading to a certain circularity. Thus, early attempts to incorporate water stress in stomatal models altered g_1 parameter in Eq. 3.28, for example linking it to the predawn leaf water potential (Tenhunen et al. 1990; Harley and Tenhunen 1991; Sala and Tenhunen 1996). The marginal water cost, λ_s in Eq. 3.30 has also been associated with soil water status (Manzoni et al. 2011).

In the case of semi-mechanistic models, plant water status is expressed more directly by the terms of water potential in Eqs. 3.32 and 3.33. Dewer (2002) expressed g_s in a way similar to Eq. 3.32, but without m. They also used abscisic acid (ABA) concentration ([ABA]) in xylem sap as an indicator of plant water status:

$$g_s = \chi\left(P_g - P_e\right) = \chi\left[\left(\psi_g + \pi_g\right) - \left(\psi_e + \pi_e\right)\right] \tag{3.35}$$

$$\pi_g - \pi_e = \frac{A + R_n}{C_i d_{\min} \exp\left\{[\mathrm{ABA}]\gamma \exp\left(\xi\psi_g\right)\right\}} \tag{3.36}$$

where ψ_e is water potential of epidermal cells, π_e is osmotic pressure in epidermal cells, $d_{\min}$ is the minimum diffusion rate for ions from the guard cell to the apoplast, and γ and ξ are the empirical constants.

Tuzet et al. (2003) modified the model by Leuning (1995), incorporating stomatal response to leaf water potential:

$$g_s = g_0 + g_1 \frac{A f_{\psi_V}}{C_i - \Gamma} \tag{3.37}$$

where $f_{\Psi v}$ expresses sensitivity of stomata to leaf water potential. $f_{\Psi v}$ is expressed as follows:

$$f_{\psi_V} = \frac{1 + \exp(s_V \psi_{\mathrm{ref}})}{1 + \exp[s_V(\psi_{\mathrm{ref}} - \psi_V)]} \tag{3.38}$$

where ψ_{ref} is a reference potential, s_V is a sensitivity parameter and ψ_V is the bulk leaf

water potential. When ψ_{ref} approaches zero, the stomatal conductance becomes insensitive to ψ_{ref}. With the decrease in ψ_{ref}, stomatal conductance decreases. The sensitivity function can be combined with other models including the hydraulic conductance models for the leaf or plant and water absorption models by roots. Equation 3.37 uses C_i instead C_f. Because we cannot measure C_f, the modification also improves the testability of the model.

Although all the models can be parameterized relatively well to current ambient CO_2 concentrations, we note that one should be cautious in applying these models for the prediction of photosynthesis and transpiration in the future high CO_2 world. Most tests of these models were made using the data obtained by instantaneous measurements of photosynthesis and transpiration by changing CO_2 concentrations, and thus, simple extrapolation of the models to high growth CO_2 concentrations, which involves acclimation processes, could be risky. Acclimation to high CO_2 might change the relationships and constants considerably, as has already demonstrated by Katul et al. (2010).

C. Mesophyll Conductance

CO_2 diffuses in the gas phase from the sub-stomatal cavities through the intercellular air space to the cell wall surface of mesophyll cells. CO_2 is further dissolved in water and transferred through the cell walls, cell membrane, cytosol, and chloroplast membrane to the stroma, and then to the site of carboxylation. Laisk et al. (1970) and Kariya and Tsunoda (1972) pointed out the importance of total chloroplast surface area facing the intercellular spaces in photosynthesis. This area corresponds to the area for CO_2 dissolution in the intercellular space. Linear relationships between the mesophyll conductance expressed on the leaf area basis and the cumulative chloroplast surface area on the leaf area basis (S_c) have been reported for many species (Terashima et al. 2005, 2011), including tobacco (*Nicotiana tabacum*) mutants having less Rubisco and thereby a small S_c (Evans et al. 1994). Another important determinant of g_m is cell wall properties. Because CO_2 diffuses in the apoplastic solution in the cell wall, thickness, porosity, and tortuosity of the cell wall, and pH of the apoplastic solution that is normally acidic, are particularly important (Terashima et al. 2011; Tomás et al. 2013). Using the data of well-watered plants ranging from annual herbs to evergreen trees, g_m at 25 °C in mol m^{-2} s^{-1} may be roughly expressed as follows:

$$g_m = \frac{S_c}{28 + 3.4 \times 10^8 \times \delta_w} \tag{3.39}$$

where δ_w is the thickness of the mesophyll cell wall in meters (Terashima et al. 2011). In this model, the porosity/tortuosity value giving the best fit, 0.052, was used (compare, for example 0.3 in Nobel 2009). However, the porosity can vary among species (Tomás et al. 2013), and thus Eq. 3.39 should be regarded as a crude simplification. For more detailed mechanistic models that take account of the intracellular fluxes of CO_2 between chloroplasts and mitochondria, see Tholen and Zhu (2011) and Tholen et al. (2012).

It has been shown that the importance of g_m in constraining the photosynthetic rate is on the same order as that of g_s, i.e., the difference in the CO_2 partial pressure between the intercellular space and stroma is similar to that between air and intercellular space (Fig. 3.6; Niinemets et al. 2009b; Flexas et al. 2012). However, the relative control of stomata vs. mesophyll can differ among different plant functional types as predicted by Eq. 3.39 with sclerophyllous species having lower S_c and greater δ_w being more strongly limited by g_m (Niinemets et al. 2009b, 2011; Flexas et al. 2013).

Many studies have shown that mesophyll conductance changes in response to environmental conditions. For example, water stress other than temporally high VPD decreases g_m and g_s (Flexas et al. 2013). At high VPD, only g_s decreased, at least initially (Warren

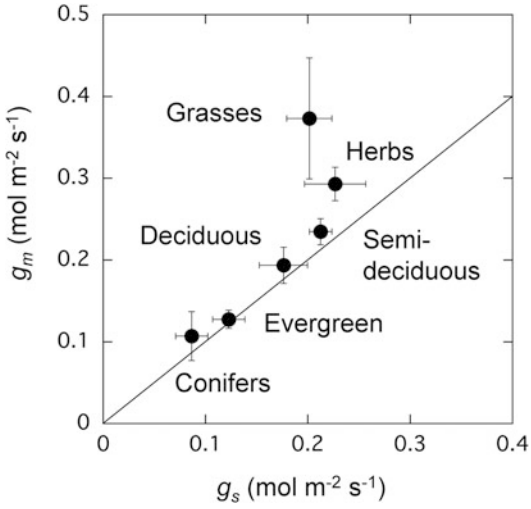

Fig. 3.6. Average values of stomatal and mesophyll conductances to CO_2 in various plant functional types (Drawn using data shown by Flexas et al. 2012)

2008). CO_2 elevation could also decrease g_m (Tazoe et al. 2011). However, mechanisms of the rapid environmental responses of g_m are largely unknown. For the simultaneous decreases in g_s and g_m under water-stressed conditions, involvement of ABA has been postulated (Flexas et al. 2006b). At a mechanistic level, such rapid changes in g_m in response to changes in environmental variables have been attributed to the changes in abundance and activities of CO_2-permeating aquaporins (cooporins) or carbonic anhydrases (Terashima et al. 2006, 2011; Evans et al. 2009). The changes in the apoplastic pH may be also responsible. Tholen et al. (2012) theoretically showed that at least part of the apparent decrease in g_m in the air containing high O_2 such as 21 % is due to the decrease in g_s.

There are several ways to consider mesophyll conductance in photosynthesis models. Interspecific variability in mesophyll conductance can be considered using anatomical models such as Eq. 3.39 (see also Tomás et al. 2013). To consider environmental effects, a simple approach is to assume that mesophyll conductance changes together with stomatal conductance. This may be valid if water stress is considered, but not necessarily correct to consider effects of modifications in environmental conditions. For example, CO_2 response of mesophyll conductance is much smaller than that of stomatal conductance (Tazoe et al. 2011). Alternatively, many modelers have considered mesophyll conductance as infinite, completely ignoring mesophyll conductance. In the case of non-stressed leaves with high stomatal conductance, it is possible to obtain almost correct environmental responses of CO_2 assimilation rates if appropriate values of Rubisco kinetics are used. In tobacco leaves, for example, Eq. 3.4 provides a good fit to the CO_2 response of Rubisco-limited rate of CO_2 assimilation for cases in which mesophyll conductance is incorporated and ignored: values of K_c, K_o and Γ^* were 25.9 Pa, 17.9 kPa and 3.86 Pa, respectively, when the actual value of g_m was used and 40.4 Pa, 24.8 kPa and 3.69 Pa, respectively when g_m was assumed to be infinite (von Caemmerer et al. 1994). It should be noted that values of Rubisco kinetics are apparent values when g_m is assumed to be infinite. In particular, variations in V_{cmax} (termed as "apparent V_{cmax}") do involve changes in g_m. However, we note that, under water stress, lack of g_m in simulations of diurnal time courses of net assimilation rate results in strongly biased estimates of net assimilation due to too strong CO_2 gradients (Niinemets et al. 2009a; Niinemets and Keenan 2014). It has been argued that ignoring g_m can bias global models of photosynthesis (Sun et al. 2014).

V. Leaf Heat Exchange

Because many models have temperature terms, and because the leaf temperature, T_l, can differ considerably from the air temperature, T_a, it is of crucial importance to appropriately treat T_l. For a leaf, the heat balance

equation terms including the net radiation (R_N), the latent heat transfer (λE), and the sensible heat flux (H) can be written as:

$$R_N = H + \lambda E \tag{3.40}$$

$$R_N = \alpha_S(1+\rho)\mathrm{S} + \alpha_{IR}\sigma\left(T_{sky}^4 + T_a^4\right) - 2\varepsilon\sigma T_l^4 \tag{3.41}$$

$$H = 2g_{bh}c_p(T_l - T_a) \tag{3.42}$$

$$L = \lambda E = \lambda g_{wc} D \tag{3.43}$$

where α_S and α_{IR} are the leaf shortwave and infrared absorptance, respectively, ρ is the shortwave reflectance of the surroundings, S is shortwave radiation, σ is the Stefan–Boltzmann constant, ε is leaf long-wave emissivity, T_{sky} is the temperature of the sky when the sky is treated as an ideal black body, g_{bh} is the leaf boundary layer conductance for heat, c_p is the heat capacity of air, λ is the heat of vaporization, and g_{wc} is the total water vapor conductance including stomatal and boundary layer conductance. Chapter 2 (Gutschick 2016) in this book provides further details of simulating leaf energy balance.

If stomatal and boundary layer conductances are fixed, T_l can be calculated from the measured values of environmental variables. The Penman–Monteith equation can be used to express T_l as a linear function of T_a (Jones 1992). Alternatively, T_l can be solved numerically. However, as in many g_s models, g_s is actually affected by D and A, both of which are strongly affected by T_l. Thus, the equations for g_s, A, and the heat balance should be solved simultaneously (see for example Okajima et al. 2012).

Although effects of the boundary layer tend to be neglected in many studies, proper treatment of the boundary layer is preferable. In Fig. 3.7, effects of wind speed and leaf

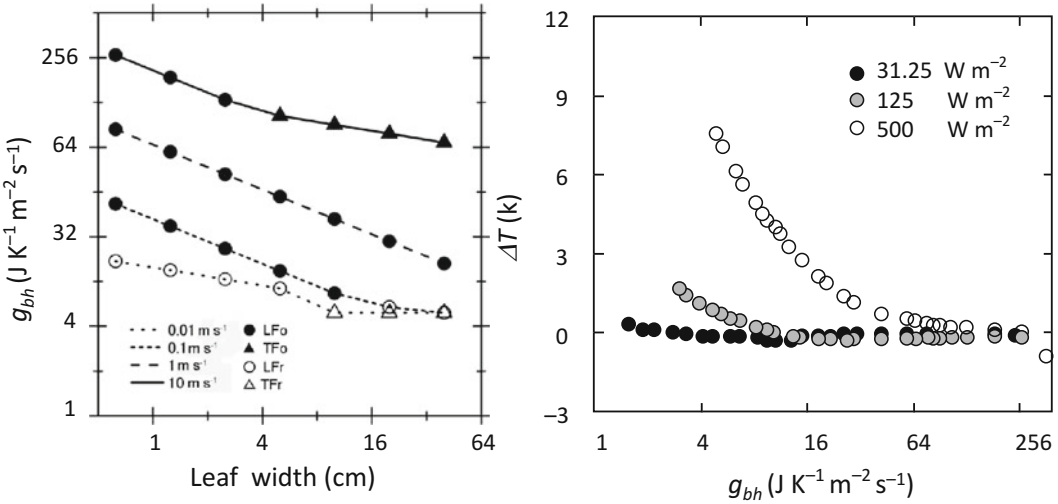

Fig. 3.7. Simulated effects of leaf size on the boundary layer conductance for heat exchange (g_{bh}) at four wind speeds (0.01, 0.1, 1, and 10 m s^{-1}; *left* panel), and the effects of g_{bh} on the temperature difference between the leaf and air ($\Delta T = T_l - T_a$) for three intensities of short-wave radiation (31.25, 125, and 500 W m^{-2}) fitted by Eq. 3.40 (*right* panel). In the *left panel*, *filled circles* denote the boundary layer for forced convection with laminar flow (LF_o); *open circles*, boundary layer for free convection with laminar flow (LF_r); *filled triangles*, boundary layer for forced convection with turbulent flow (TF_o); *open triangles*, boundary layer of free convection with turbulent flow. In the *right panel*, circles denote calculated values taking account of temperature acclimation of photosynthesis (For details, see Okajima et al. 2012). Redrawn from Okajima et al. (2012)

width on g_b are demonstrated together with the mode of the boundary layer. For the leaves of plants on the dense forest floor or in the densely-leafed canopies, g_{bh} can be very small, and strong light intensities during sunflecks can cause very high T_l, particularly in large leaves. As shown in Fig. 3.7, it may be relevant to assume that the boundary layer, in most cases, is in the mode of laminar air flow with forced convection for the boundary layer (Okajima et al. 2012).

VI. Environmental Responses of Net CO_2 Assimilation Rate

A. CO_2 Response

CO_2 assimilation is limited by A_c at low CO_2 concentration and by A_j at high CO_2 concentration (Fig. 1a). In most leaves, A_c and A_j co-limit CO_2 assimilation at 35–50 Pa C_a (345–493 μmol mol^{-1} at normal air pressure) (Wullschleger 1993).

B. Light Response

Light dependence of CO_2 assimilation is characterized by a saturating response (Fig. 3.8) and can be approximated by a non-rectangular hyperbola analogous to that used to fit the light dependence of the photosynthetic electron transport rate (Eq. 3.12).

$$A = \frac{\phi I + A_{\max} - \sqrt{(\phi I + A_{\max})^2 - 4\phi I A_{\max}\theta}}{2\theta} \tag{3.44}$$

where $A_{\max}$ is the light-saturated rate of net assimilation rate, θ is the convexity of the curve ($0 < \theta < 1$), and ϕ is the initial slope.

The value of θ is commonly in the range of 0.7–0.9 in most leaves. However, θ can vary within a leaf depending on the direction of illumination. For example, θ can be high when light is illuminated from both adaxial and abaxial sides, whereas it is significantly lower when the illumination is from the abaxial (lower) side (Terashima and Saeki 1985). This is because θ reflects not only the biochemical aspect of chloroplastic light use, but also the arrangement and acclimation of the chloroplasts within a leaf.

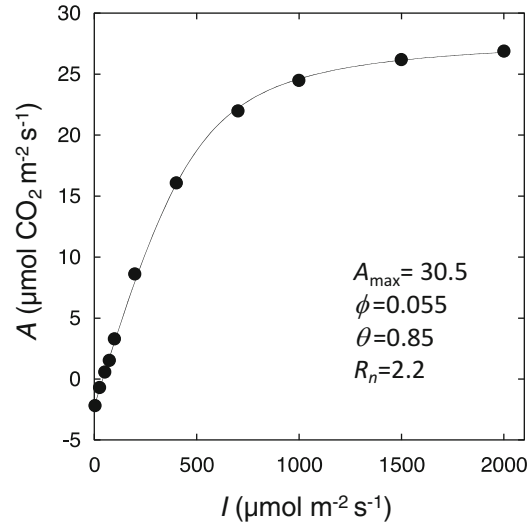

Fig. 3.8. CO_2 exchange rate (A) as a function of photon flux density (PFD) in *Chenopodium album* (Hikosaka et al. 2004) fitted by Eq. 3.44

C. Temperature Response

In most plants, the light-saturated rates of photosynthesis are low at extremely low and high temperatures and have an optimum at intermediate temperatures (Berry and Björkman 1980; Hikosaka et al. 2006; Sage and Kubien 2007). This involves temperature dependence of many parameters of the model. *In vitro* Rubisco activity at saturating CO_2 concentrations exponentially increases with temperature (Jordan and Ögren 1984). Similarly, in many species, the apparent V_{cmax} exponentially increases (Hikosaka et al. 2007; Ishikawa et al. 2007), but the deactivation is often substantial at very high temperature (Harley and Tenhunen 1991; Leuning 2002; Medlyn et al. 2002; Han et al. 2004). Figure 3.9 shows temperature dependence of V_{cmax} and A_c in *Plantago asiatica* grown at contrasting temperatures. In *Plantago asiatica*, deactivation was not obvious until 40 °C, so the Arrhenius model was fitted to the data (Fig. 3.9).

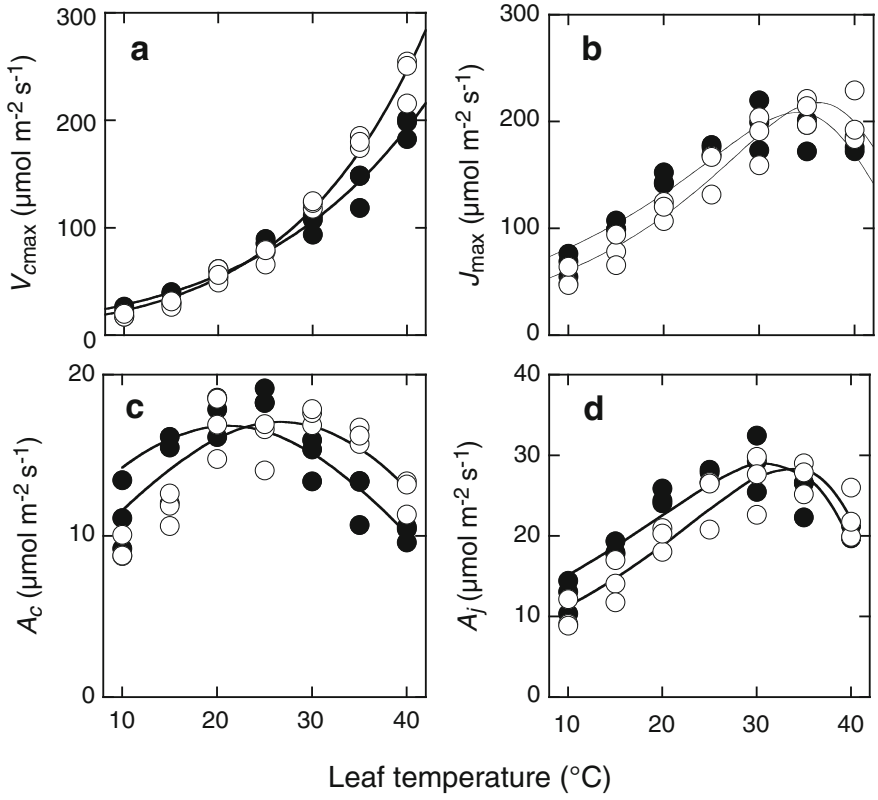

Fig. 3.9. Temperature dependence of apparent V_{cmax} (**a**), apparent J_{max} (**b**), RuBP-saturated potential rate of CO_2 assimilation (A_c; c), and RuBP-limited potential rate of CO_2 assimilation (A_j; d) in *Plantago asiatica* leaves grown at a low temperature of 15 °C (*filled symbols*) and a high temperature 30 °C (*open symbols*). *Fitted curves* are Eqs. 3.14 and 3.15 for V_{cmax} and J_{max}, respectively. Lines for A_c and A_j are calculated from the *fitting curve* for V_{cmax} and J_{max} using Eqs. 3.4 and 3.8, respectively (Redrawn from Hikosaka et al. (2006)). V_{cmax} and J_{max} are termed here as apparent estimates here because they are obtained by fitting net assimilation (A) versus intercellular CO_2 response curves rather than by fitting A vs. chloroplastic CO_2 responses

However, more often the peak model (Eq. 3.15) is used to fit the data, particularly when deactivation is obvious at high temperatures.

J_{max} at a leaf level can be assessed using several methods: gas exchange (Farquhar et al. 1980), O_2 evolution at saturating CO_2 (Yamasaki et al. 2002), and chlorophyll fluorescence analysis (Niinemets et al. 1999). As with V_{cmax}, deactivation of J_{max} occurs at high temperatures, typically at temperatures higher than 40 °C (Fig. 3.9; Harley and Tenhunen 1991; Leuning 2002; Medlyn et al. 2002; Niinemets et al. 1999). The reduction of J_{max} at high temperatures affects the temperature dependence of A_j (Fig. 3.9).

Temperature dependence of CO_2 assimilation rate changes depending on light intensity and CO_2 concentration. The initial slope of the light-response curve (ϕ) decreases with increasing temperature (Berry and Björkman 1980) due to an increase in Γ* (Fig. 3.2). At high light levels, the optimal temperature (T_{opt}) for A increases with increasing CO_2 concentration (Berry and Björkman 1980; Hikosaka et al. 2006). Two factors are involved in this shift of T_{opt} (Kirschbaum and Farquhar 1984). First, the shift among the biochemical steps limiting A affects T_{opt}. In many species, the T_{opt} for A_j is higher than that for A_c (Kirschbaum and Farquhar 1984; Hikosaka et al. 1999, 2006) and RuBP regeneration generally limits

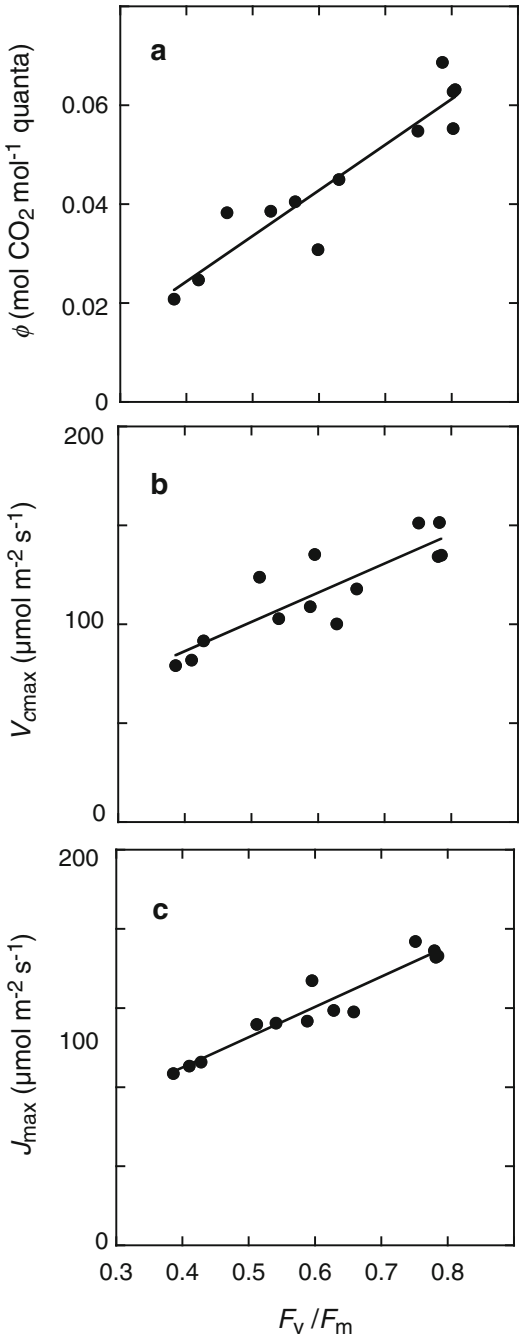

Fig. 3.10. Correlations of the initial slope of the light response curve of assimilation (ϕ, **a**), apparent V_{cmax} (**b**), and apparent J_{max} (**c**) with the dark-adapted quantum yield of photosystem II (PSII) (F_v/F_m). F_v/F_m characterizes the maximum quantum yield of PSII that in healthy leaves with fully open PSII and without non-photochemical quenching is >0.8. Reductions in F_v/F_m reflect sustained non-photochemical quenching and damage of PSII, and thus characterize photoinhibition. Data were fitted by linear regressions (Modified from Hikosaka et al. 2004)

photosynthesis at higher CO_2 concentrations. Second, kinetics of Rubisco have a large effect on A_c. At low CO_2 concentrations, the carboxylation rate is less sensitive to temperature because an increase in K_c partly cancels the increase in V_{cmax}. Furthermore, the photorespiration rate increases with temperature because Γ* increases (Fig. 3.2). These effects are smaller at higher CO_2 concentrations, leading to an increase in the T_{opt} of A_c. The T_{opt} of A_c increases by ca. 0.05 °C per 0.1 Pa CO_2 (Hikosaka et al. 2006).

D. Photoinhibition

Both the photosystems, particularly photosystems II (PSII), are often inactivated due to stress (Aro et al. 1993; Terashima et al. 1994; Oguchi et al. 2011). Inactivation of PSII occurs due to photoinhibitory damage (chronic photoinhibition) or due to increases in heat dissipation through regulated mechanisms (dynamic photoinhibition; Osmond 1994). The fraction of functional PSII can be evaluated with chlorophyll fluorescence (Schreiber et al. 1994). Because CO_2 assimilation is limited by photochemical reactions at low light, ϕ and ϕ_j are almost proportional to the fraction of functional PSII (Hikosaka et al. 2004). Even though PSII is not considered as a limiting step at high light, A_{max}, V_{max} and J_{max} also can decrease with decreasing functional PSII under conditions of chronic photoinhibition (Hikosaka et al. 2004; Fig. 3.10). Consequently, photoinactivation leads to a decrease in CO_2 assimilation at both high and low light intensities (Hikosaka et al. 2004).

E. Modeling Diurnal Change in Gas Exchange Rates of a Leaf

Harley and coworkers combined the biochemical model of photosynthesis (Eq. 3.11) with a semi-empirical model of stomatal conductance (Eq. 3.28) (Harley et al. 1986; Tenhunen et al. 1990; Harley and Tenhunen 1991). Baldocchi (1994) developed an analytical solution of the two models. They successfully simulated diurnal changes in leaf gas exchange rates (Harley and Tenhunen 1991; Harley and Baldocchi 1995), and scaled the models up to a canopy level (Baldocchi and Harley 1995; Falge et al. 1996; Ryel et al. 2001). Figure 3.11 shows examples of measured and predicted rates of CO_2 assimilation and transpiration in leaves of the tree seedlings at gap and understory of a temperate forest (Oguchi et al. 2008).

VII. Variations in Parameters of the Biochemical Leaf Photosynthesis Model among Leaves and among Species

A. Rubisco Kinetics

Interspecific variation in Rubisco kinetic parameters, K_c, K_o and Γ*, demonstrated so far is not very large and thus, in most modeling studies, idealized constant Rubisco kinetic parameters based on tobacco and spinach data have been widely used. However, values are slightly but significantly different among studies (see Fig. 3.2). It has been pointed out that there is a trade-off between the Michaelis–Menten constant for CO_2 (K_c) and the catalytic efficiency of Rubisco (k_{cat}; the maximum catalytic rate per unit active site) for carboxylation. Although there are large variations in K_c or

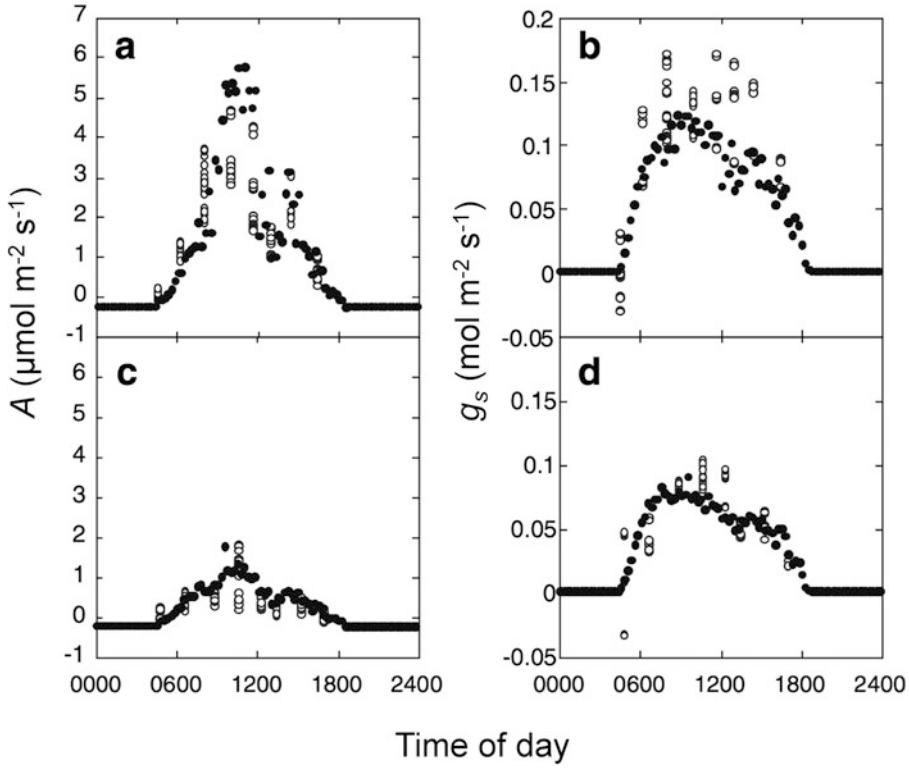

Fig. 3.11. Diurnal changes in net CO_2 assimilation rate, A, (**a**, **c**), and stomatal conductance, g_s (**b**, **d**), of *Kalopanax pictus* seedlings at the gap site (**a**, **b**) and the control site (**c**, **d**) in a cool-temperate forest. *Open* and *closed circles* denote the measured and modeled values, respectively (Redrawn from Oguchi et al. 2008)

k_{cat}, even for the same species depending on the methods, laboratories, and varieties, the trade-off trends have often been seen when the data particularly from the same laboratory, have been analyzed, and especially when C_3 and C_4 species are analyzed together (Sage 2002; Tcherkez et al. 2006; Ishikawa et al. 2009). This trade-off implies that there are combinations of high k_{cat} with high K_c and low k_{cat} with low K_c, whereas there is no Rubisco with high k_{cat} and low K_c. It is also worth pointing out that both k_{cat} and K_c are negatively and strongly related to the Rubisco specificity factor (Tcherkez et al. 2006; Savir et al. 2010).

C_4 species have Rubisco with higher k_{cat} and higher K_c than C_3 species because C_4 species concentrate CO_2 in their bundle sheath cells (Sage 2002; Ishikawa et al. 2009). Among C_3 plants, the plants from cold habitats tend to have Rubisco with high k_{cat} and high K_c (Ishikawa et al. 2009). Rubisco with High k_{cat} and high K_c would be favored at low temperatures, probably because CO_2 concentration in the liquid phase is higher at low temperatures partly due to higher solubility, whereas k_{cat} tends to be suppressed by low temperatures. At high temperatures, low K_c would be more important, at least when one considers the past 10,000 years until the start of the rapid rise of CO_2 concentration due to the industrial revolution in the 19th century. Galmés et al. (2005) argued that Rubisco with low k_{cat} and low K_c are favored in dry habitats. In addition, they argued that evergreen tree species with low g_m would have Rubisco with low k_{cat} and low K_c.

B. V_{cmax} and J_{max}

V_{cmax}, generally expressed on a leaf area basis, considerably varies among the leaves and species. Even within a species, V_{cmax} often varies by an order of magnitude, leading to large variations in photosynthetic capacity among leaves (Chap. 4, Niinemets 2016). V_{cmax} is mainly determined by the activity of Rubisco and there is a strong correlation between V_{cmax} and the in vitro

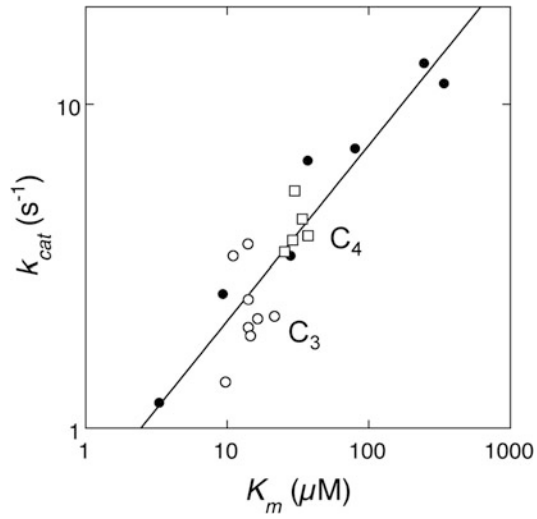

Fig. 3.12. Correlation between the Rubisco turnover rate (k_{cat}) and the Michaelis-Menten constant for CO_2 across various photosynthetic organisms. k_{cat} is defined as the substrate-saturated rate of carboxylation per unit catalytic site (one molecule of Rubisco has eight catalytic sites). *Open circles* denote Rubiscos from C_3 plants and *open squares* from C_4 plants. Data are taken from the reviews of Tcherkez et al. (2006) and Ishikawa et al. (2009)

Rubisco activity (von Caemmerer and Farquhar 1981). In fact, transgenic plants with a reduced expression of Rubisco gene have reduced V_{cmax} (von Caemmerer et al. 1994; Makino et al. 1997). Rubisco activity per unit leaf area is influenced by the Rubisco content and the activation state of Rubisco. In most cases Rubisco is nearly fully activated at high light, and thus the variation in V_{cmax} is mainly explained by the Rubisco content (Fig. 3.13). This evidence collectively supports the assumption that the RuBP-saturated rate of photosynthesis can be simulated on the basis of the Rubisco amount and kinetics (Farquhar et al. 1980).

The RuBP regeneration process involves many steps, and in general, J_{max} is strongly correlated with contents and activities of related components. For example, J_{max} is almost proportional to in vitro electron transport rate (von Caemmerer and Farquhar 1981), PSII content, cytochrome b_6/f content (Terashima and Evans 1988; Makino

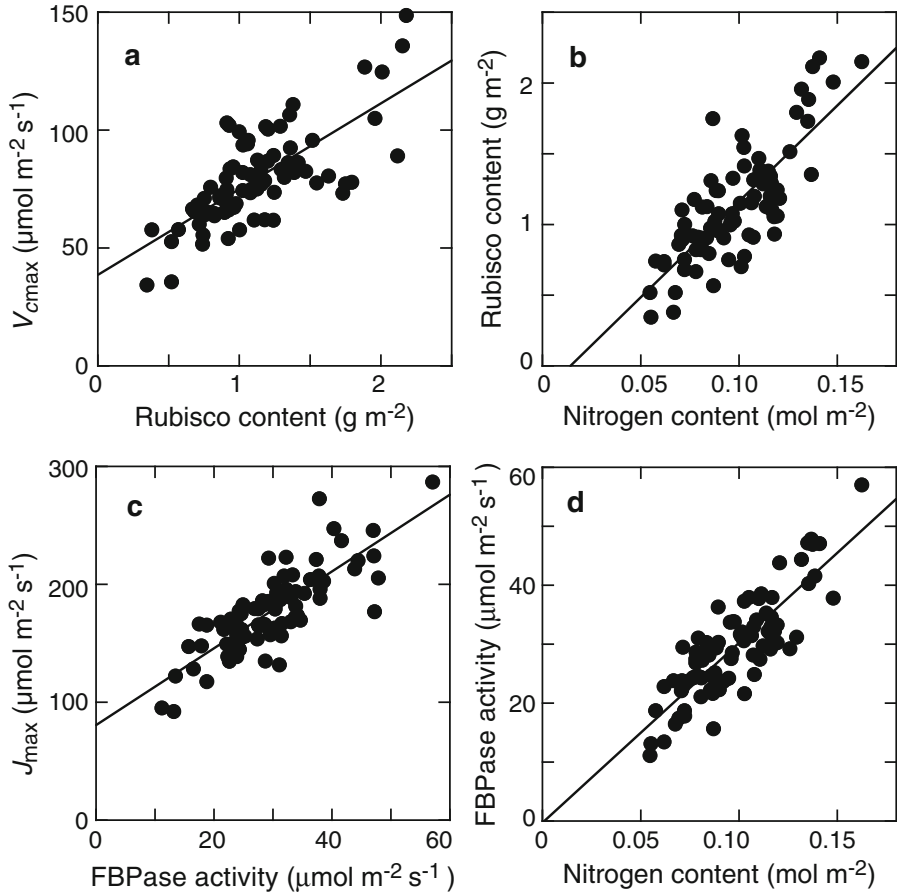

Fig. 3.13. Relationships between the apparent V_{cmax} and Rubisco content (**a**), apparent J_{max} and stromal fructose bisphosphatase (FBPase) activity (**b**), Rubisco content (**c**) and FPB activity (**d**) and leaf nitrogen content in *Polygonum sachalinense*. Modified from Akita et al. (2012)

et al. 1994; Hikosaka and Terashima 1996), ATPase content (Makino et al. 1994), and FBPase activity (Akita et al. 2012; Fig. 3.13). These results suggest that the RuBP regeneration rate is almost co-limited by related processes. Recently, Rosenthal et al. (2011) showed that overexpression of sedoheptulose-1, 7-bisphosphatase increased J_{max} in tobacco and improved biomass production at an elevated CO_2 concentration.

C. Initial Slope of the Light-Response Curve

As mentioned in Sect. II, ϕ is determined by quantum yield of electron transport, chloroplastic CO_2 and oxygen concentrations, and leaf absorptance. Because the quantum yield on an absorbed quantum basis (ϕ_q) is similar among C_3 plants (Sect. II), variation in ϕ among leaves is mainly caused by absorptance. In general ϕ and absorptance are saturating functions of the leaf chlorophyll content (Gabrielsen 1948). However, some species such as sclerophylls have lower absorptance due to higher reflection from waxy or hairy epidermal surfaces (e.g. Syvertsen et al. 1995).

D. Temperature Dependence of Kinetic Parameters

The temperature response curve of A varies among species and changes within species depending on growth temperature (Berry

and Björkman 1980; Hikosaka et al. 2006; Yamori et al. 2014). In general, plants grown at higher temperatures have a higher optimal temperature for A (T_{opt}) than those grown at lower temperatures (Berry and Björkman 1980; Hikosaka et al. 2006; Yamori et al. 2014). Various biochemical mechanisms are responsible for these differences. E_a of V_{cmax} has been reported to increase with growth temperature when the Arrhenius model is used (Hikosaka et al. 2006). When the peak model (Eq. 3.15) is used to fit, ΔS may explain the variation in temperature dependence of V_{cmax} rather than E_a (Kattge and Knorr 2007). Shifts of the optimal temperature for apparent J_{max} with growth temperatures was observed in some species (Fig. 3.9; Badger et al. 1982; Niinemets et al. 1999; Yamasaki et al. 2002), and was absent in others (Armond et al. 1978; Mitchell and Barber 1986; Sage et al. 1995). The slope of the curve below the optimal temperature increases with growth temperature in many studies (Armond et al. 1978; Badger et al. 1982; Mitchell and Barber 1986; Sage et al. 1995; Hikosaka et al. 1999; Yamasaki et al. 2002). In *Plantago asiatica*, E_a of apparent J_{max} in the peak model significantly increased with growth temperature (Fig. 3.9). In fact, temperature response of J_{max} can even vary during the day (Hüve et al. 2006).

Because temperature dependencies of A_c and A_j are different from each other (Fig. 3.9), the balance between carboxylation and regeneration of RuBP, indicated as the J_{max}/V_{cmax} ratio, is also an influential factor modifying the temperature dependence of A (Hikosaka 1997). Growth temperature has been reported to modify the J_{max}/V_{cmax} ratio in some species but not in others (Hikosaka et al. 1999, 2006; Yamori et al. 2005, 2010).

E. Leaf Nitrogen Content as a Driver of Photosynthetic Capacity

Because almost half of the leaf nitrogen is invested in the photosynthetic apparatus, various photosynthetic parameters and amounts of photosynthetic components are correlated with the leaf nitrogen content (Evans 1989; Hikosaka and Terashima 1995). In particular, the light-saturated rate of photosynthesis (A_{max}) shows strong correlation with the leaf nitrogen content (Evans 1989). The A_{max}-nitrogen relationship is generally linear or curved with a positive x-intercept. Similarly, V_{cmax} and J_{max} have been related to leaf nitrogen content in numerous studies (e.g. Akita et al. 2012; Fig. 3.13).

Some of the other photosynthetic parameters are also related with leaf nitrogen content. In many studies, respiration rate has been positively correlated with leaf nitrogen content (Hirose and Werger 1987; Terashima and Evans 1988), probably because more maintenance cost is necessary in leaves with higher protein content. The initial slope of the light-response curve of photosynthesis (ϕ) exhibited weakly positive correlation with leaf nitrogen content in some studies (Hirose and Werger 1987) because ϕ increases with chlorophyll content (see Sect. VII.C), which is greater in leaves with higher nitrogen content if growth irradiance is constant (Terashima and Evans 1988). The convexity of the light-response curve of photosynthesis (θ) often exhibits negative correlation with leaf nitrogen content (Hirose and Werger 1987; Matsumoto et al. 2008), probably because of greater mutual shading within the leaf with higher nitrogen content.

Hirose and Werger (1987) applied a non-rectangular hyperbola model to fit the light response curves of photosynthesis (Eq. 3.44) and derived ϕ, R_n, θ and A_{max} values, and further related these parameters with leaf nitrogen content. This enabled them to express the daily carbon gain as a function of the leaf nitrogen content. Although A_{max} is linearly correlated with leaf nitrogen content, the relationship between daily carbon gain and leaf nitrogen content is a saturating curve because photosynthetic rate is less dependent on leaf nitrogen content when it is light-limited (Hirose and Werger 1987; see also Fig. 13.1 in Chap. 13, Anten 2016).

F. Interspecific Variation in Leaf Traits

Photosynthetic capacity is known to vary among species even when grown under the same condition. Wright et al. (2004) conducted a global survey involving 1 % of Earth's vascular plant species and revealed that photosynthetic capacity varied by 120- and 40-fold when expressed on a dry mass and a leaf area basis, respectively. There is a convergence in the variation in leaf traits on a dry mass basis; at one end of the axis, species have higher photosynthetic capacity, a higher nitrogen concentration, a smaller leaf mass per area (LMA), and a shorter leaf life-span, and the opposite is true at the other end (Reich et al. 1997; Wright et al. 2004, 2005). Such a large variation is related with the strategy or niche of a species. For example, higher photosynthetic capacities are found more often in herbs than in woody species, in early-successional than in later-successional species and in fast- than in slow-growing species (Wright et al. 2005; Hikosaka 2010).

The variation in the leaf nitrogen content explains the intraspecific variation in A_{max}, whereas the interspecific variation in A_{max} is not necessarily explained by nitrogen content because species with low A_{max} tend to have similar or higher leaf nitrogen content per leaf area than species with high A_{max} (Wright et al. 2005). Therefore, the relationship between A_{max} and the leaf nitrogen content is different among species (Evans 1989). When compared at a given leaf nitrogen content, A_{max} is lower in leaves with a longer leaf life-span or with a greater LMA (Hikosaka 2004). Photosynthetic nitrogen use efficiency (PNUE; A_{max} per leaf nitrogen) is used to characterize interspecific variations in photosynthetic nitrogen use (Pons et al. 1994; Hikosaka 2004, 2010). Multiple factors are responsible for interspecific variation in PNUE. Species with low PNUE tend to have a low CO_2 concentration in chloroplasts due to low stomatal and mesophyll conductances, and have a smaller allocation of leaf nitrogen into the photosynthetic apparatus (Hikosaka et al. 1998; Hikosaka and Shigeno 2009; Poorter and Evans 1998; Takashima et al. 2004). Such inefficiency in photosynthesis may be a result of a trade-off between photosynthetic production and persistence of the leaves. Low PNUE species invest biomass and nitrogen in cell walls, which may contribute to the leaf toughness and longer leaf life-span, with a resulting trade-off of inefficient CO_2 diffusion and reduced nitrogen allocation to the components of the photosynthetic machinery (Hikosaka 2004).

VIII. Future Perspective

Models shown in this chapter have successfully described environmental dependence of leaf photosynthesis. These models were incorporated in models of canopy photosynthesis and carbon cycling in terrestrial ecosystems and predicted carbon exchange rates were highly correlated to those directly observed using the eddy covariance method (see Chap. 9, Hikosaka et al. 2016). However, the models still ignore some important environmental responses in gas exchange. One of these is variations in the mesophyll conductance. Although a number of papers have been published on mesophyll conductance, most of these were determined in laboratory; therefore its behavior under field conditions is poorly understood. In most models, mesophyll conductance is ignored or assumed to be constant, though recent studies have shown that it changes depending on environmental conditions such as CO_2 concentration (Sect. IV). Second, previous models assumed that photosynthesis is always in the steady-state. However, temporal changes in environmental variables often occur so rapidly that gas exchange rates cannot follow immediately. This is particularly the case for sudden changes in irradiance, which is very frequent within the understory in the dense canopy. Because activation of some enzymes and stomatal opening require time, gas exchange rates gradually increase after a sudden increase in irradiance (Pearcy 1990).

Although several models of non-steady-state photosynthesis have been proposed (e.g. Gross et al. 1991), they are not incorporated in models at larger scales. Third, variations in respiration rates between leaves are not fully understood. Incorporating such uncertainties may improve correctness for predicting gas exchange rates under changing environment.

Acknowledgements

We thank Ülo Niinemets for the valuable comments. This work was supported by Grants-in-Aid for Scientific Research on Innovative Areas (Nos. 21114001, 21114007, 21114009), by KAKENHI (Nos. 20677001, 25291095 and 25660113) and by CREST, JST, Japan.

References

Akita R, Kamiyama C, Hikosaka K (2012) *Polygonum sachalinense* alters the balance between capacities of regeneration and carboxylation of ribulose-1,5-bisphosphate in response to growth CO_2 increment but not the nitrogen allocation within the photosynthetic apparatus. Physiol Plant 146:404–412

Amthor JS (1989) Respiration and Crop Productivity. Springer, New York

Amthor JS (1994) Respiration and carbon assimilate use. In: Boote KJ, Bennett JM, Sinclair TR, Paulsen GM (eds) Physiology and Determination of Crop Yield. American Society of Agronomy, Madison, pp 221–250

Anten NPR (2016) Optimization and game theory in canopy models. In: Hikosaka K, Niinemets Ü, Anten N (eds) Canopy Photosynthesis: From Basics to Applications. Springer, Berlin, pp 355–377

Anten NPR, Schieving F, Werger MJA (1995) Patterns of light and nitrogen distribution in relation to whole canopy carbon gain in C_3 and C_4 mono- and dicotyledonous species. Oecologia 101:504–513

Aphalo PJ, Jarvis PG (1991) Do stomata respond to relative humidity? Plant Cell Environ 14:127–132

Araya T, Noguchi K, Terashima I (2008) Manipulation of light and CO_2 environments of the primary leaves of bean (*Phaseolus vulgaris* L.) affects photosynthesis in both the primary and the first trifoliate leaves: involvement of systemic regulation. Plant Cell Environ 31:50–61

Armond PA, Schreiber U, Björkman O (1978) Photosynthetic acclimation to temperature in the desert shrub, *Larrea divaricata*. II. Light-harvesting efficiency and electron transport. Plant Physiol 61:411–415

Aro EM, Virgin I, Andersson B (1993) Photoinhibition of photosystem II – inactivation, protein damage and turnover. Biochim Biophys Acta 1143:113–134

Atkin OK, Tjoelker MG (2003) Thermal acclimation and the dynamic response of plant respiration to temperature. Trends Plant Sci 8:343–351

Atkin OK, Evans JR, Siebke K (1998) Relationship between the inhibition of leaf respiration by light and enhancement of leaf dark respiration following light treatment. Aust J Plant Physiol 25:437–443

Atkin OK, Millar AH, Gardeström P, Day DA (2000a) Photosynthesis, carbohydrate metabolism and respiration in leaves of higher plants. In: Leegood RC, Sharkey TD, von Caemmerer S (eds) Photosynthesis: Physiology and Metabolism. Kluwer Academic Publishers, Dordrecht, pp 153–175

Atkin OK, Evans JR, Ball MC, Lambers H, Pons TL (2000b) Leaf respiration of snow gum in the light and dark. Interactions between temperature and irradiance. Plant Physiol 122:915–923

Atkin OK, Bruhn D, Hurry VM, Tjoelker MG (2005) The hot and the cold: unravelling the variable response of plant respiration to temperature. Funct Plant Biol 32:87–105

Atkin OK, Scheurwater I, Pons TL (2006) High thermal acclimation potential of both photosynthesis and respiration in two lowland *Plantago* species in contrast to an alpine congeneric. Global Chang Biol 12:500–515

Ayub G, Smith RA, Tissue DT, Atkin OK (2011) Impacts of drought on leaf respiration in darkness and light in *Eucalyptus saligna* exposed to industrial-age atmospheric CO_2 and growth temperature. New Phytol 190:1003–1018

Badger MR, Björkman O, Armond PA (1982) An analysis of photosynthetic response and adaptation to temperature in higher plants: temperature acclimation in the desert evergreen *Nerium oleander* L. Plant Cell Environ 5:85–99

Badger MR, Collatz GJ (1977) Studies on the kinetic mechanism of ribulose-1, 5-bisphosphate carboxylase and oxygenase reactions, with particular reference to the effect of temperature on kinetic parameters. Carnegie Institute Year Book 76:355–361

Baldocchi D (1994) An analytical solution for coupled leaf photosynthesis and stomatal conductance models. Tree Physiol 14:1069–1079

Baldocchi DD, Harley PC (1995) Scaling carbon dioxide and water vapour exchange from leaf to canopy in a deciduous forest. II. Model testing and application. Plant Cell Environ 18:1157–1173

Ball JT (1987) Calculations related to gas exchange. In: Zeiger E, Farquhar GD, Cowan IR (eds) Stomatal Function. Stanford University Press, Stanford, pp 445–476

Ball JT, Woodrow IE, Berry JA (1987) A model predicting stomatal conductance and its contribution to the control of photosynthesis under different environmental conditions. In: Biggins I (ed) Progress in Photosynthesis Research. Martinus Nijhoff, La Hague, pp 221–224

Bernacchi CJ, Singsaas EL, Pimentel C, Portis AR Jr, Long SP (2001) Improved temperature response functions for models of Rubisco-limited photosynthesis. Plant Cell Environ 24:253–259

Bernacchi CJ, Portis AR, Nakano H, Von Caemmerer S, Long SP (2002) Temperature response of mesophyll conductance. Implications for the determination of Rubisco enzyme kinetics and for limitations to photosynthesis *in vivo*. Plant Physiol 130:1992–1998

Berry JA, Björkman O (1980) Photosynthetic response and adaptation to temperature in higher plants. Annu Rev Plant Physiol 31:491–543

Berry JA, Farquhar GD (1978) The CO_2 concentration function of C_4 photosynthesis: a biochemical model. In: Hall D, Coombs J, Goodwin T (eds) Proceedings of the 4th International Congress on Photosynthesis. Biochemical Society, London, pp 119–131

Björkman O, Demmig B (1987) Photon yield of O_2 evolution and chlorophyll fluorescence characteristics at 77K among vascular plants of diverse origins. Planta 170:489–504

Boote KJ, Loomis RS (1991) The prediction of canopy assimilation. In: Boote KJ, Loomis RS (eds) Modelling Crop Photosynthesis – From Biochemistry to Canopy. CSSA, Madison, pp 109–140

Brooks A, Farquhar GD (1985) Effect of temperature on the CO_2/O_2 specificity of ribulose-1,5-bisphosphate carboxylase/oxygenase and the rate of respiration in the light. Planta 165:397–406

Buckley TN (2005) The control of stomata by water balance. New Phytol 168:275–292

Buckley TN, Adams MA (2011) An analytical model of non-photorespiratory CO_2 release in the light and dark in leaves of C_3 species based on stoichiometric flux balance. Plant Cell Environ 34:89–112

Buckley TN, Mott KA (2013) Modeling stomatal conductance in response to environmental Factor. Plant Cell Environ 36:1691–1699

Buckley TN, Mott KA, Farquhar GD (2003) A hydromechanical and biochemical model of stomatal conductance. Plant Cell Environ 26:1767–1785

Collatz GJ, Ball JT, Grivet C, Berry JA (1991) Physiological and environmental regulation of stomatal conductance, photosynthesis and transpiration: a model that includes a laminar boundary layer. Agr Forest Meteorol 54:107–136

Cowan IR (1977) Stomatal behaviour and environment. Adv Bot Res 4:117–228

Cowan IR, Farquhar GD (1977) Stomata1 function in relation to leaf metabolism and environment. In: Jennings DH (ed) Integration of Activity in the Higher Plant. Cambridge University Press, Cambridge, pp 471–505

Damour G, Simonneau T, Cochard H, Urban L (2010) An overview of models of stomatal conductance at the leaf level. Plant Cell Environ 33:1419–1438

Dewer RC (2002) The Ball-Berry-Leuning and Tardieu-Daview stomatal models: synthesis and extension within a spatially aggregated picture of guard cell function. Plant Cell Environ 25:1383–1398

Evans JR (1989) Photosynthesis and nitrogen relationships in leaves of C_3 plants. Oecologia 78:9–19

Evans JR, Kaldenhoff R, Genty B, Terashima I (2009) Resistance along the CO_2 diffusion pathway inside leaves. J Exp Bot 60:2235–2248

Evans JR, von Caemmerer S, Setchell BA, Hudson GS (1994) The relationship between CO_2 transfer conductance and leaf anatomy in transgenic tobacco with a reduced content of Rubisco. Aust J Plant Physiol 21:475–495

Falge E, Graber W, Siegwolf R, Tenhunen JD (1996) A model of the gas exchange response of Picea abies to habitat conditions. Trees 10:277–287

Farquhar GD (1988) Models relating subcellular effects of temperature to whole plant responses. Symp Soc Exp Biol 42:395

Farquhar GD, von Caemmerer S (1982) Modelling of photosynthetic response to environment. In: Lange OL, Nobel PS, Osmond CB, Ziegler H (eds) Encyclopedia of Plant Physiology, vol 12B, New Series. Springer, Berlin, pp 549–587

Farquhar GD, Sharkey TD (1982) Stomatal conductance and photosynthesis. Annu Rev Plant Physiol 33:317–345

Farquhar GD, von Caemmerer S, Berry JA (1980) A biochemical model of photosynthetic CO_2 assimilation in leaves of C_3 plants. Planta 149:78–90

Farquhar GD, von Caemmerer S, Berry JA (2001) Models of photosynthesis. Plant Physiol 125:42–45

Finnegan PM, Soole KL, Umbach AL (2004) Alternative mitochondrial electron transport proteins in higher plants. In: Day DA, Millar AH, Whelan J (eds) Plant Mitochondria: From Genome to Function. Kluwer Academic Publishers, Dordrecht, pp 163–230

Flexas J, Bota J, Galmés J, Medrano H, Ribas-Carbó M (2006a) Keeping a positive carbon balance under adverse conditions: responses of photosynthesis and respiration to water stress. Physiol Plant 127:343–352

Flexas J, Ribas-Carbó M, Bota J, Galmés J, Henkle M, Marínez-Cañellas MH (2006b) Decreased Rubisco activity during water stress is not induced by decreased relative water content but related to conditions of low stomatal conductance and chloroplast CO_2 concentration. New Phytol 172:73–82

Flexas J, Barbour MM, Brendel O, Cabrera HM, Carriquí M, Díaz-Espejo A, Douthe C, . . ., Warren CR (2012) Mesophyll diffusion conductance to CO_2: an unappreciated central player in photosynthesis. Plant Sci 193–194:70–84

Flexas J, Niinemets Ü, Gallé A, Barbour MM, Centritto M, Diaz-Espejo A, Douthe C, . . ., Medrano H (2013) Diffusional conductances to CO_2 as a target for increasing photosynthesis and photosynthetic water-use efficiency. Photosynthesis Research 117:45–59

Florez-Sarasa I, Flexas J, Rasmusson AG, Umbach AL, Siedow JN, Ribas-Carbo M (2011) In vivo cytochrome and alternative pathway respiration in leaves of *Arabidopsis thaliana* plants with altered alternative oxidase under different light conditions. Plant Cell Environ 34:1373–1383

Gabrielsen EK (1948) Effects of different chlorophyll concentrations on photosynthesis in foliage leaves. Physiol Plant 1:5–37

Galmés J, Flexas J, Keys AJ, Cifre J, Mitchell RAC, Madgwick PJ, Haslam RP, . . ., Parry MAJ (2005) Rubisco specificity factor tends to be larger in plant species from drier habitats and in species with persistent leaves. Plant Cell Environ 28:571–579

Gross LJ, Kirschbaum MUF, Pearcy RW (1991) A dynamic model of photosynthesis in varying light taking account of stomatal conductance, C_3-cycle intermediates, photorespiration and RuBisCO activation. Plant Cell Environ 14:881–893

Gutschick VP (2016) Leaf energy balance: basics, and modeling from leaves to Canopies. In: Hikosaka K, Niinemets Ü, Anten N (eds) Canopy Photosynthesis: From Basics to Applications. Springer, Berlin, pp 23–58

Han Q, Kawasaki T, Nakano T, Chiba Y (2004) Spatial and seasonal variability of temperature responses of biochemical photosynthesis parameters and leaf nitrogen content within a *Pinus densiflora* crown. Tree Physiol 24:737–744

Harley PC, Baldocchi DD (1995) Scaling carbon dioxide and water vapour exchange from leaf to canopy in a deciduous forest. I. Leaf model parameterization. Plant Cell Environ 18:1146–1156

Harley PC, Tenhunen JD (1991) Modelling the photosynthetic response of C_3 leaves to environmental factors. In: Boote KJ, Loomis RS (eds) Modelling Crop Photosynthesis – From Biochemistry to Canopy. CSSA, Madison, pp 17–39

Harley PC, Tenhunen JD, Lange OL (1986) Use of an analytical model to study limitations on net photosynthesis in Arbutus unedo under field conditions. Oecologia 70:393–401

Haupt-Herting S, Klug K, Fock HP (2001) A new approach to measure gross CO_2 fluxes in leaves. Gross CO_2 assimilation, photorespiration, and mitochondrial respiration in the light in tomato under drought stress. Plant Physiol 126:389–396

Hesketh JD, Baker DN, Duncan WG (1971) Simulation of growth and yield in cotton: respiration and the carbon balance. Crop Sci 11:394–399

Hikosaka K (1997) Modelling optimal temperature acclimation of the photosynthetic apparatus in C_3 plants with respect to nitrogen use. Ann Bot 80:721–730

Hikosaka K (2004) Interspecific difference in the photosynthesis–nitrogen relationship: patterns, physiological causes, and ecological importance. J Plant Res 117:481–494

Hikosaka K (2010) Mechanisms underlying interspecific variation in photosynthetic capacity across wild plant species. Plant Biotech 27:223–229

Hikosaka K, Shigeno A (2009) The role of Rubisco and cell walls for the interspecific variation in photosynthetic capacity. Oecologia 160:443–451

Hikosaka K, Terashima I (1995) A model of the acclimation of photosynthesis in the leaves of C_3 plants to sun and shade with respect to nitrogen use. Plant Cell Environ 18:605–618

Hikosaka K, Terashima I (1996) Nitrogen partitioning among photosynthetic components and its consequence in sun and shade plants. Funct Ecol 10:335–343

Hikosaka K, Hanba YT, Hirose T, Terashima I (1998) Photosynthetic nitrogen-use efficiency in woody and herbaceous plants. Funct Ecol 12:896–905

Hikosaka K, Murakami A, Hirose T (1999) Balancing carboxylation and regeneration of ribulose bisphosphate in leaf photosynthesis: temperature acclimation in an evergreen tree, *Quercus myrsinaefolia*. Plant Cell Environ 22:841–849

Hikosaka K, Kato MC, Hirose T (2004) Photosynthetic rates and partitioning of absorbed light energy in photoinhibited leaves. Physiol Plant 121:699–708

Hikosaka K, Ishikawa K, Borjigidai A, Muller O, Onoda Y (2006) Temperature acclimation of photosynthesis: mechanisms involved in the changes in temperature dependence of photosynthetic rate. J Exp Bot 57:291–302

Hikosaka K, Nabeshima E, Hiura T (2007) Seasonal changes in temperature response of photosynthesis in canopy leaves of *Quercus crispula* in a cool-temperate forest. Tree Physiol 27:1035–1041

Hikosaka K, Kumagai T, Ito A (2016) Modeling canopy photosynthesis. In: Hikosaka K, Niinemets Ü, Anten N (eds) Canopy Photosynthesis: From Basics to Applications. Springer, Berlin, pp 239–268

Hirose T, Werger MJA (1987) Nitrogen use efficiency in instantaneous and daily photosynthesis of leaves in the canopy of *Solidago altissima* stand. Physiol Plant 70:215–222

Hourton-Cabassa C, Matos AR, Zachowski A, Moreau F (2004) The plant uncoupling protein homologues: a new family of energy dissipating proteins in plant mitochondria. Plant Physiol Biochem 42:283–290

Hurry V, Igamberdiev AU, Keerberg O, Pärnik T, Atkin OK, Zaragoza-Castells J, Gardeström P (2005) Respiration in photosynthetic cells: gas exchange components, interactions with photorespiration and the operation of mitochondria in the light. In: Lambers H, Ribas-Carbo M (eds) Plant Respiration: From Cell to Ecosystem. Springer, Berlin, pp 43–61

Hüve K, Bichele I, Tobias M, Niinemets Ü (2006) Heat sensitivity of photosynthetic electron transport varies during the day due to changes in sugars and osmotic potential. Plant Cell Environ 29:212–228

Hüve K, Bichele I, Rasulov B, Niinemets Ü (2011) When it is too hot for photosynthesis: heat-induced instability of photosynthesis in relation to respiratory burst, cell permeability changes and H_2O_2 formation. Plant Cell Environ 34:113–126

Hüve K, Bichele I, Ivanova H, Keerberg O, Pärnik T, Rasulov B, Tobias M, Niinemets Ü (2012) Temperature responses of dark respiration in relation to leaf sugar concentration. Physiol Plant 144:320–334

Ishikawa C, Hatanaka T, Misoo S, Fukayama H (2009) Screening of high k_{cat} Rubisco among Poaceae for improvement of photosynthetic CO_2 assimilation in rice. Plant Prot Sci 12:345–350

Ishikawa K, Onoda Y, Hikosaka K (2007) Intraspecific variation in temperature dependence of gas exchange characteristics of *Plantago asiatica* ecotypes from different temperature regimes. New Phytol 176:356–364

Johnson F, Erying H, Williams R (1942) The nature of enzyme inhibitions in bacterial luminescence: sulphanilamide, urethane, temperature, pressure. J Cell Comp Physiol 20:247–268

Johnson IR (1983) Nitrate uptake and respiration in roots and shoots: a model. Physiol Plant 58:145–147

Jones HG (1992) Plants and Microclimate, 2nd edn. Cambridge University Press, Cambridge

Jordan DB, Ögren WL (1984) The CO_2/O_2 specificity of ribulose 1,5-bisphosphate carboxylase/oxygenase. Dependence on ribulose bisphosphate concentration, pH and temperature. Planta 161:308–313

Kariya K, Tsunoda S (1972) Relationship of chlorophyll content, chloroplast area index and leaf photosynthesis rate in *Brassica*. Tohoku J Agr Res 23:1–14

Kattge J, Knorr W (2007) Temperature acclimation in a biochemical model of photosynthesis: a reanalysis of data from 36 species. Plant Cell Environ 30:1176–1190

Katul G, Manzoni S, Palmroth S, Oren R (2010) A stomatal optimization theory to describe the effects of atmospheric CO_2 on leaf photosynthesis and transpiration. Ann Bot 105:431–442

Kimura M, Yokoi Y, Hogetsu K (1978) Quantitative relationships between growth and respiration. II. Evaluation of constructive and maintenance respiration in growing *Helianthus tuberosus* leaves. Bot Mag Tokyo 91:43–56

Kirschbaum MUF, Farquhar GD (1984) Temperature dependence of whole-leaf photosynthesis in *Eucalyptus pauciflora* Sieb. ex Spreng. Aust J Plant Physiol 11:519–538

Kirschbaum MUF, Farquhar GD (1987) Investigation of the CO_2 dependence of quantum yield and respiration in *Eucalyptus pauciflora*. Plant Physiol 83:1032–1036

Kok B (1948) A critical consideration of the quantum yield of *Chlorella*-photosynthesis. Enzymology 13:1–56

Kruse J, Adams MA (2008) Three parameters comprehensively describe the temperature response of respiratory oxygen reduction. Plant Cell Environ 31:954–967

Kruse J, Rennenberg H, Adams MA (2011) Steps towards a mechanistic understanding of respiratory temperature responses. New Phytol 189:659–677

Kruse J, Turnbull TL, Adams MA (2012) Disentangling respiratory acclimation and adaptation to growth temperature by *Eucalyptus*. New Phytol 195:149–163

Laisk AH (1977) Kinetics of Photosynthesis and Photorespiration of C_3-Plants. Nauka, Moscow

Laisk A, Edwards GE (2002) A mathematical model of C_4 photosynthesis: The mechanism of concentrating CO_2 in NADP-malic enzyme type species. Photosynth Res 66:199–224

Laisk A, Loreto F (1996) Determining photosynthetic parameters from leaf CO_2 exchange and chlorophyll fluorescence. Ribulose-1,5-bisphosphate carboxylase/oxygenase specificity factor, dark respiration in the light, excitation distribution between photosystems, alternative electron transport rate, and mesophyll diffusion resistance. Plant Physiol 110:903–912

Laisk A, Oja V, Rahi M (1970) Diffusion resistance of leaves in connection with their anatomy. Soviet Plant Physiol 17:31–38 (translated from Fiziologiya Rastenii 17: 40–48)

Lambers H, Chapin FS, Pons TL (2008) Plant Physiological Ecology, 2nd edn. Springer, New York

Leuning R (1995) A critical appraisal of a combined stomatal-photosynthesis model for C_3 plants. Plant Cell Environ 18:339–355

Leuning R (2002) Temperature dependence of two parameters in a photosynthesis model. Plant Cell Environ 25:1205–1210

Lloyd J, Taylor JA (1994) On the temperature dependence of soil respiration. Funct Ecol 8:315–323

Long SP, Postl WF, Bolhár-Nordenkampf HR (1993) Quantum yields for uptake of carbon dioxide in C_3 vascular plants of contrasting habitats and taxonomic groupings. Planta 189:226–234

Loreto F, Celikova V, Di Marco G (2001) Respiration in the light measured by $^{12}CO_2$ emission in $^{13}CO_2$ atmosphere in maze leaves. Aust J Plant Physiol 28:1103–1108

Makino A, Nakano H, Mae T (1994) Responses of ribulose-1,5-bisphosphate carboxylase, cytochrome f, and sucrose synthesis enzymes in rice leaves to leaf nitrogen and their relationships to photosynthesis. Plant Physiol 105:173–179

Makino A, Shimada T, Takumi S, Kaneko K, Matsuoka M, Shimamoto K, Nakano H, …, Yamamoto N (1997) Does decrease in ribulose-1,5-bisphosphate carboxylase by antisense rbcS lead to a higher N-use efficiency of photosynthesis under conditions of saturating CO_2 and light in rice plants? Plant Physiol 114:483–491

Manzoni S, Vico G, Katul G, Fay PA, Polley W, Palmroth S, Porporato A (2011) Optimizing stomatal conductance for maximum carbon gain under water stress: a meta-analysis across plant functional types and climates. Funct Ecol 5:456–467

Matsumoto Y, Oikawa S, Yasumura Y, Hirose T, Hikosaka K (2008) Reproductive yield of individuals competing for light in a dense stand of *Xanthium canadense*. Oecologia 157:185–195

McCree KJ (1970) An equation for the rate of respiration of white clover plants grown under controlled conditions. In: Setlik I (ed) Prediction and Measurement of Photosynthetic Productivity. Pudoc, Wageningen, pp 221–229

McMurtrie RE, Wang YP (1993) Mathematical models of the photosynthetic response of tree stands to rising CO_2 concentrations and temperatures. Plant Cell Environ 16:1–13

Medlyn BR, Dreyer E, Ellsworth D, Forstreuter M, Harley PC, Kirschbaum MUF, Le Roux X, …, Loustau D (2002) Temperature response of parameters of a biochemically based model of photosynthesis. II. A review of experimental data. Plant Cell Environ 25:1167–1179

Medlyn BE, Duursma RA, Eamus D, Ellsworth DS, Prentice IC, Barton CVM, Crous KY, …, Wingate L (2011) Reconciling the optimal and empirical approaches to modelling stomatal conductance. Global Chang Biol 17:2134–2144

Mitchell RAC, Barber J (1986) Adaptation of photosynthetic electron-transport rate to growth temperature in pea. Planta 169:429–436

Miyazawa S-I, Terashima I (2001) Slow development of leaf photosynthesis in an evergreen broad-leaved tree, *Castanopsis sieboldii*: relationships between leaf anatomical characteristics and photosynthetic rate. Plant Cell Environ 24:279–291

Mott KA, Parkhurst DF (1991) Stomatal responses to humidity in air and helox. Plant Cell Environ 14:509–515

Niinemets Ü (2016) Within-canopy variations in functional leaf traits: structural, chemical and ecological controls and diversity of responses. In: Hikosaka K, Niinemets Ü, Anten N (eds) Canopy Photosynthesis: From Basics to Applications. Springer, Berlin, pp 101–141

Niinemets Ü, Keenan TF (2014) Photosynthetic responses to stress in Mediterranean evergreens: mechanisms and models. Environ Exp Bot 103:24–41

Niinemets Ü, Díaz-Espejo A, Flexas J, Galmés J, Warren CR (2009a) Importance of mesophyll diffusion conductance in estimation of plant photosynthesis in the field. J Exp Bot 60:2271–2282

Niinemets Ü, Díaz-Espejo A, Flexas J, Galmés J, Warren CR (2009b) Role of mesophyll diffusion conductance in constraining potential photosynthetic productivity in the field. J Exp Bot 60:2249–2270

Niinemets Ü, Flexas J, Peñuelas J (2011) Evergreens favored by higher responsiveness to increased CO_2. Trend Ecol Evol 26:136–142

Niinemets Ü, Oja V, Kull O (1999) Shape of leaf photosynthetic electron transport versus temperature response curve is not constant along canopy light gradients in temperate deciduous trees. Plant Cell Environ 22:1497–1513

Nobel PS (2009) Physicochemical and Environmental Plant Physiology, 4th edn. CA Academic Press/ Elsevier, San Diego

Oguchi R, Hikosaka K, Hiura T, Hirose T (2008) Costs and benefits of photosynthetic light acclimation of tree seedlings in response to gap formation. Oecologia 155:665–675

Oguchi R, Terashima I, Kou J, Chow WS (2011) Operation of dual mechanisms that both lead to photoinactivation of photosystem II in leaves by visible light. Physiol Plant 142:47–55

Okajima Y, Taneda H, Noguchi K, Terashima I (2012) Optimum leaf size predicted by the leaf energy balance model incorporating dependencies of photosynthesis to light and temperature. Ecol Res 27:333–346

Osmond CB (1994) What is photoinhibition? Some insights from comparisons of shade and sun plants. In: Baker NR, Bowyer JR (eds) Photoinhibition of Photosynthesis: From Molecular Mechanisms to the Field. BIOS Scientific Publishing Ltd, Oxford, pp 1–24

Pärnik T, Keerberg O (1995) Decarboxylation of primary and end products of photosynthesis at different oxygen concentrations. J Exp Bot 46:1439–1447

Pärnik T, Keerberg O (2007) Advanced radiogasometric method for the determination of the rates of photorespiratory and respiratory decarboxylations of primary and stored photosynthates under steady-state photosynthesis. Physiol Plant 129:34–44

Pearcy RW (1990) Sunflecks and photosynthesis in plant canopies. Annu Rev Plant Physiol Plant Mol Biol 41:421–453

Peisker M (1979) Conditions for low, and oxygen-independent CO_2 compensation concentrations in C_4 plants as derived from a simple model. Photosynthetica 13:198–207

Peisker M, Apel H (2001) Inhibition by light of CO_2 evolution from dark respiration: Comparison of two gas exchange methods. Photosynth Res 70:291–298

Penning de Vries FWT (1975) The cost of maintenance processes in plant cells. Ann Bot 39:77–92

Penning de Vries FWT, Brunsting AHM, Van Laar HH (1974) Products, requirements and efficiency of biosynthesis: a quantitative approach. J Theor Biol 45:339–377

Pons TL, van der Werf A, Lambers H (1994) Photosynthetic nitrogen use efficiency of inherently low- and fast-growing species: possible explanations for observed differences. In: Roy J, Garnier E (eds) A Whole Plant Perspective on Carbon–Nitrogen Interactions. SPB, The Hague, pp 61–77

Pons TL, Welschen RAM (2002) Overestimation of respiration rates in commercially available clamp-on leaf chambers. Complications with measurement of net photosynthesis. Plant Cell Environ 25:1367–1372

Poorter H, Evans JR (1998) Photosynthetic nitrogen-use efficiency of species that differ inherently in specific area. Oecologia 116:26–37

Reich PB, Walters MB, Ellsworth DS (1997) From tropics to tundra: global convergence in plant functioning. Pro Natl Acad Sci USA 94:13730–13734

Rosenthal DM, Locke AM, Khozaei M, Raines CA, Long SP, Ort DR (2011) Over-expressing the C_3 photosynthesis cycle enzyme sedoheptulose-1-7 bisphosphatase improves photosynthetic carbon gain and yield under fully open air CO_2 fumigation (FACE). BMC Plant Biol 11:123

Ryel RJ, Falge E, Joss U, Geyer R, Tenhunen JD (2001) Penumbral and foliage distribution effects on Pinus sylvestris canopy gas exchange. Theor Appl Climatol 68:109–124

Sage RF (1990) A model describing the regulation of ribulose-1,5-bisphosphate carboxylase, electron transport, and triose phosphate use in response to light intensity and CO_2 in C_3 plants. Plant Physiol 94:1728–1734

Sage RF (2002) Variation in the k_{cat} of Rubisco in C_3 and C_4 plants and some implications for photosynthetic performance at high and low temperature. J Exp Bot 53:609–620

Sage RF, Kubien DS (2007) The temperature response of C_3 and C_4 photosynthesis. Plant Cell Environ 30:1086–1106

Sage RF, Santrucek J, Grise DJ (1995) Temperature effects on the photosynthetic response of C_3 plants to long-term CO_2 enrichment. Vegetatio 121:67–77

Sala A, Tenhunen JD (1996) Simulations of canopy net photosynthesis and transpiration in *Quercus ilex* L. under the influence of seasonal drought. Agric For Meteorol 78:203–222

Savir Y, Noor E, Milo R, Tlusty T (2010) Cross-species analysis traces adaptation of Rubisco toward optimality in a low-dimensional landscape. Proc Natl Acad Sci U S A 107:3475–3480

Schreiber U, Bilger W, Neubauer C (1994) Chlorophyll fluorescence as a nonintrusive indicator for rapid assessment of in vivo photosynthesis. In: Schulze ED, Caldwell MM (eds) Ecophysiology of Photosynthesis. Springer, Berlin, pp 49–70

Shapiro JB, Griffin KL, Lewis JD, Tissue DT (2004) Response of *Xanthium strumarium* leaf respiration

in the light to elevated CO_2 concentration, nitrogen availability and temperature. New Phytol 162:377–386

Sharkey TD (1985) Photosynthesis in intact leaves of C_3 plants: physics, physiology, and rate limitations. Bot Rev 51:53–105

Sun Y, Gu L, Dickinson RE, Norby RJ, Pallardy SG, Hoffman FM (2014) Impact of mesophyll diffusion on estimated global land CO_2 fertilization. Proc Natl Acad Sci U S A 111:15774–15779

Syvertsen JP, Lloyd J, McConchie C, Kriedemann PE, Farquhar GD (1995) On the relationship between leaf anatomy and CO_2 diffusion through the mesophyll of hypostomatous leaves. Plant Cell Environ 18:149–157

Takashima T, Hikosaka K, Hirose T (2004) Photosynthesis or persistence: nitrogen allocation in leaves of evergreen and deciduous *Quercus* species. Plant Cell Environ 27:1047–1054

Tazoe Y, von Caemmerer S, Estavillo GM, Evans JR (2011) Using tunable diode laser spectroscopy to measure carbon isotope discrimination and mesophyll conductance of CO_2 diffusion dynamically at different CO_2 concentrations. Plant Cell Environ 34:580–591

Tcherkez G, Bligny R, Gout E, Mahé A, Hodges M, Cornic G (2008) Respiratory metabolism of illuminated leaves depends on CO_2 and O_2 conditions. Proc Natl Acad Sci U S A 105:797–802

Tcherkez G, Boex-Fontvieille E, Mahé A, Hodges M (2012) Respiratory carbon flux in leaves. Curr Opin Plant Biol 15:301–314

Tcherkez GG, Farquhar GD, Andrews TJ (2006) Despite slow catalysis and confused substrate specificity, all ribulose bisphosphate carboxylases may be nearly perfectly optimized. Proc Natl Acad Sci U S A 103:7246–7251

Tenhunen JD, Sala SA, Harley PC, Dougherty RL, Reynolds JF (1990) Factors influencing carbon fixation and water use by Mediterranean sclerophyll shrubs during summer drought. Oecologia 82:381–393

Terashima I, Evans JR (1988) Effects of light and nitrogen nutrition on the organization of the photosynthetic apparatus in spinach. Plant Cell Physiol 29:143–155

Terashima I, Saeki T (1985) A new model for leaf photosynthesis incorporating the gradients of light environment and of photosynthetic properties of chloroplasts within a leaf. Ann Bot 56:489–499

Terashima I, Araya T, Miyazawa S-I, Sone K, Yano S (2005) Construction and maintenance of the optimal photosynthetic systems of the leaf, herbaceous plant and tree: an eco-developmental treatise. Ann Bot 95:507–519

Terashima I, Funayama S, Sonoike K (1994) The site of photoinhibition in leaves of *Cucumis sativus* L. at low temperatures is photosystem I, not photosystem II. Planta 193:300–306

Terashima I, Hanba YT, Tazoe Y, Vyas P, Yano S (2006) Irradiance and phenotype: comparative eco-development of sun and shade leaves in relation to photosynthetic CO_2 diffusion. J Exp Bot 57:343–354

Terashima I, Hanba YT, Tholen D, Niinemets U (2011) Leaf functional anatomy in relation to photosynthesis. Plant Physiol 155:108–116

Terashima I, Masuzawa T, Ohba H, Yokoi Y (1995) Does low atmospheric pressure in the alpine environment suppress photosynthesis? Ecology 76:2663–2668

Tholen D, Zhu XG (2011) The mechanistic basis of internal conductance: a theoretical analysis of mesophyll cell photosynthesis and CO_2 diffusion. Plant Physiol 156:90–105

Tholen D, Ethier G, Genty B, Pepipn S, Zhu XG (2012) Variable mesophyll conductance revisited: theoretical background and experimental implications. Plant Cell Environ 35:2087–2103

Thornley JHM (1970) Respiration, growth and maintenance in plants. Nature 227:304–305

Tomás M, Flexas J, Copolovici L, Galmés J, Hallik L, Medrano H, Tosens T, …, Niinemets Ü (2013) Importance of leaf anatomy in determining mesophyll diffusion conductance to CO_2 across species: quantitative limitations and scaling up by models. J Exp Bot 64:2269–2281

Turnbull MH, Tissue DT, Griffin KL, Richardson SJ, Peltzer DA, Whitehead D (2005) Respiration characteristics in temperature rainforest tree species differ along a long-term soil development chronosequence. Oecologia 143:271–279

Turnbull MH, Whitehead D, Tissue DT, Schuster WSF, Brown KJ, Griffin KL (2003) Scaling foliar respiration in two contrasting forest canopies. Funct Ecol 17:101–114

Tuzet A, Perrier A, Leuning R (2003) A coupled model of stomatal conductance, photosynthesis and transpiration. Plant Cell Environ 26:1097–1116

Villar R, Held AA, Merino J (1994) Comparison of methods to estimate dark respiration in the light in leaves of two woody species. Plant Physiol 105:167–172

von Caemmerer S (2000) Biochemical Models of Leaf Photosynthesis. CSIRO Publishing, Canberra

von Caemmerer S, Farquhar GD (1981) Some relationships between the biochemistry of

photosynthesis and the gas exchange of leaves. Planta 153:376–387

von Caemmerer S, Evans JR, Hudson GS, Andrews TJ (1994) The kinetics of ribulose-1,5-bisphosphate carboxylase/oxygenase in vivo inferred from measurements of photosynthesis in leaves of transgenic tobacco. Planta 195:88–97

Wang X, Lewis JD, Tissue DT, Seemann JR, Griffin KL (2001) Effects of elevated atmospheric CO_2 concentration on leaf dark respiration of *Xanthium strumarium* in light and darkness. Proc Natl Acad Sci U S A 98:2479–2484

Warren CR (2008) Soil water deficit decrease the internal conductance to CO_2 transfer but atmospheric water deficits do not. J Exp Bot 59:327–334

Wright IJ, Reich PB, Cornelissen JHC, Falster DS, Garnier E, Hikosaka K, Lamont BB, . . ., Westoby M (2005) Assessing the generality of global leaf trait relationships. New Phytol 166:485–496

Wright IJ, Reich PB, Westoby B, Ackerly DD, Baruch Z, Bongers F, Cavendar-Bares J, . . ., Villar R (2004) The worldwide leaf economics spectrum. Nature 428:821–827

Wullschleger SD (1993) Biochemical limitations to carbon assimilation in C_3 plants – a retrospective analysis of the A/C_i curves from 109 species. J Exp Bot 44:907–920

Wullschleger SD, Norby RJ, Hanson PJ (1995) Growth and maintenance respiration in stems of *Quercus alba* after four years of CO_2 enrichment. Physiol Plant 93:47–54

Xue X, Gauthier DA, Turpin DH, Weger HG (1996) Interaction between photosynthesis and respiration in the green alga *Chlamydomonas reinhardtii*. Plant Physiol 112:1005–1014

Yamasaki T, Yamakawa T, Yamane Y, Koike H, Satoh K, Katoh S (2002) Temperature acclimation of photosynthesis and related changes in photosystem II electron transport in winter wheat. Plant Physiol 128:1087–1097

Yamori W, Noguchi K, Terashima I (2005) Temperature acclimation of photosynthesis in spinach leaves: analysis of photosynthetic components and temperature dependencies of photosynthetic partial reactions. Plant Cell Environ 28:536–547

Yamori W, Noguchi K, Hikosaka K, Terashima I (2010) Phenotypic plasticity in photosynthetic temperature acclimation among crop species with different cold tolerance. Plant Physiol 152:388–399

Yamori W, Hikosaka K, Way D (2014) Temperature response of photosynthesis in C_3, C_4 and CAM plants: temperature acclimation and temperature adaptation. Photosynth Res 119:101–117

Yin X, Sun Z, Struik PC, Gu J (2011) Evaluating a new method to estimate the rate of leaf respiration in the light by analysis of combined gas exchange and chlorophyll fluorescence measurements. J Exp Bot 62:3489–3499

Yoshida K, Terashima I, Noguchi K (2007) Up-regulation of mitochondrial alternative oxidase concomitant with chloroplast over-reduction by excess light. Plant Cell Physiol 48:606–614

Yoshida K, Watanabe CK, Hachiya T, Tholen D, Shibata M, Terashima I, Noguchi K (2011) Distinct responses of the mitochondrial respiratory chain to long- and short-term high light environments in *Arabidopsis thaliana*. Plant Cell Environ 34:618–628

Zaragoza-Castells J, Sánchez-Gómez D, Valladares F, Hurry V, Atkin OK (2007) Does growth irradiance affect temperature dependence and thermal acclimation of leaf respiration? Insights from a Mediterranean tree with long-lived leaves. Plant Cell Environ 30:820–833

Chapter 4

Within-Canopy Variations in Functional Leaf Traits: Structural, Chemical and Ecological Controls and Diversity of Responses

Ülo Niinemets*
Environmental Sciences, Estonian University of Life Sciences, Tartu, Estonia

*Author for correspondence, e-mail: ylo.niinemets@emu.ee

K. Hikosaka, Ü. Niinemets, and N.P.R. Anten (eds.), *Canopy Photosynthesis: From Basics to Applications*, DOI 10.1007/978-94-017-7291-4_4

Summary

Plant canopies are characterized by extensive gradients in light availability that importantly alter the photosynthetic productivity of leaves in different canopy layers and result in acclimatory changes in leaf structural, chemical and physiological traits. These within-canopy variations are further importantly driven by species functional type and ecological characteristics such as shade tolerance (ecological controls). This chapter explores the within-canopy variations in key functional traits among different plant functional types and in species with different ecological potentials using a simple methodology to separate the importance of different leaf-level traits in foliage photosynthetic acclimation. As a major acclimatory change, foliage photosynthetic capacity per leaf area (A_{max}^{A}) increases with increasing long-term average integrated quantum flux density (Q_{int}) in the canopy. Within-canopy variation in A_{max}^{A} results in a greater whole canopy carbon gain than having A_{max}^{A} constant through the canopy. The increase in A_{max}^{A} with Q_{int} can potentially result from increases in leaf dry mass per unit area (M_A), nitrogen content per unit dry mass (N_M) and nitrogen allocation to rate-limiting photosynthetic proteins. This analysis indicates that the importance of these three key factors varies among plant functional types. In species with relatively low rates of canopy expansion and leaf turnover such as woody evergreens and woody deciduous species, within-canopy variation in A_{max}^{A} is primarily determined by M_A, while in herbaceous species with high rates of canopy growth and leaf turnover, the variation is mainly driven by changes in N_M and nitrogen allocation to rate-limiting proteins of photosynthetic machinery. Furthermore, there are large within-canopy modifications in structural traits such as leaf angles and spatial aggregation modulating light harvesting and light avoidance, and in chemical traits such as xanthophyll cycle carotenoid content and isoprene emission contributing to abiotic stress resistance. As the result of light-dependent alterations in these

Abbreviations: A – Net assimilation rate; $A_{c,con}$ – Canopy photosynthesis for constant leaf biochemical potentials; $A_{c,var}$ – Canopy photosynthesis for variable leaf biochemical potentials; A_{max} – Photosynthetic capacity; A_{max}^{A} – Photosynthetic capacity per unit area; A_{max}^{M} – Photosynthetic capacity per unit dry mass; B_C – Chlorophyll binding (amount of chlorophyll per unit nitrogen invested in light harvesting Eq. 4.4); Chl – Chlorophyll; C_a – Ambient CO_2 concentration; C_c – Chloroplastic CO_2 concentration; C_i – CO_2 concentration in the intercellular air space; E_N – Photosynthetic nitrogen use efficiency; F_B – Fraction of leaf nitrogen in rate-limiting proteins of photosynthetic electron transport; F_L – Fraction of leaf nitrogen in light harvesting; F_R – Fraction of leaf nitrogen in Rubisco; g_m – Mesophyll diffusion conductance; g_s – Stomatal conductance; J_{max} – Capacity for photosynthetic electron transport; J_{max}^{A} – Capacity for photosynthetic electron transport per unit area; J_{mc} – Capacity for photosynthetic electron transport per unit cytochrome f; k – Light extinction coefficient; L – Leaf area index; LHC II – Light harvesting complex II; M_A – Leaf dry mass per unit area; N_A – Nitrogen content per unit area; N_M – Leaf nitrogen content per unit dry mass; PS I – Photosystem I; PS II – Photosystem II; Q – Photosynthetic quantum flux density; Q_0 – Above-canopy Q; Q_{int} – Incident integrated Q during leaf growth and development; R_c – Light-dependent change of a given trait (Eq. 4.5); SC – Shade tolerance score; S_T/S_P – Total to projected leaf area ratio; VAZ – Xanthophyll cycle carotenoids (violaxanthin antheraxanthin and zeaxanthin); V_{cmax} – Maximum carboxylase activity of Rubisco; $V_{cmax,b}$ – V_{cmax} at the bottom of the canopy; $V_{cmax,t}$ – V_{cmax} at the top of the canopy; V_{cmax}^{A} – Maximum carboxylase activity of Rubisco per unit area; V_{cr} – Specific activity of Rubisco (maximum rate of ribulose-1,5-bisphosphate carboxylation per unit Rubisco protein); V_i – Trait value at a seasonal average quantum flux density of i ($Q_{int,i}$); α – Initial quantum yield for photosynthetic electron transport; $\alpha_{p,a}$ – Initial quantum yield of photosynthesis for an absorbed light; $\alpha_{p,i}$ – Initial quantum yield of photosynthesis for an incident light; θ – Lamina cross-sectional angle; ξ – Leaf absorptance; χ_A – Chlorophyll content per unit area; χ_M – Chlorophyll content per unit dry mass; φ_F – Leaf lamina inclination angle at leaf fall-line; $|\phi_L|$ – Absolute lamina inclination angle (average angle between the normal to the leaf plane and the vertical direction); φ_P – Petiole inclination angle; Ω – Leaf clumping index

traits, lower canopy leaves have a greater light harvesting efficiency, while upper canopy leaves a greater capacity for excess radiation dissipation and resistance to abiotic stress. Plasticity for foliar modifications varies among woody species of different ecological potentials with shade-intolerant species tending to have a greater photosynthetic plasticity, while shade-tolerant species greater leaf areas and higher canopy light interception. This review emphasizes the overall large within-canopy variation in key foliage functional traits and underscores the important differences among plant functional types and in species with different ecological potentials in their acclimation to within-canopy environment.

Keywords Acclimation • Chlorophyll content • Carotenoids • Dry mass per unit area • Isoprene emission • Leaf age • Leaf life span • Leaf morphology • Nitrogen content • Nitrogen partitioning • Optimization • Photosynthetic capacity • Shade tolerance

I. Introduction

Variation in light availability is one of the most conspicuous features of plant canopies. Daily integrated average light flux varies often more than 50-fold between canopy top and bottom in dense plant canopies (Fig. 4.1, Hirose et al. 1988; Koike et al. 2001; Valladares 2003; Niinemets and Anten 2009; Chap. 9, Hikosaka et al. 2016b), but unexpectedly, the gradient is still 10–20-fold in relatively open canopies (Hirose et al. 1988; Werger and Hirose 1988; Rambal 2001; Joffre et al. 2007). Even in free-standing plants, foliage is importantly aggregated within the canopy envelope, and leaves at the top shade the leaves positioned lower in the canopy, resulting in major light gradients (e.g., Le Roux et al. 1999; Chap. 11, Disney 2016).

Foliage photosynthetic capacities acclimate to these extensive long-term light gradients through plant canopies such that whole canopy photosynthetic response cannot be predicted from "an average leaf response", but is the integrated response of leaves in different canopy positions with different physiological potentials tuned to their specific light environment (Hirose and Werger 1987b; Ellsworth and Reich 1993; Anten 1997; Pons and Anten 2004; Niinemets and Anten 2009; Chap. 5, Pons 2016). In fact, multiple leaf structural and chemical traits vary between canopy top and bottom, including leaf dry mass per unit area, leaf nitrogen content and nitrogen partitioning among proteins of photosynthetic machinery (Hirose and Werger 1987b; Ellsworth and Reich 1993; Anten 1997; Pons and Anten 2004; Niinemets and Anten 2009; Chap. 5, Pons 2016). Variations in these key functional traits ultimately drive within-canopy photosynthetic acclimation. Various structural and chemical traits have inherently different plasticities to within-canopy light conditions in different plant life forms and in species with different ecological potentials, leading to a spectrum of within-canopy photosynthetic acclimation responses across species (Niinemets and Anten 2009 for a review).

In addition to long-term variations in light availability, the environmental setting in plant canopies is much more complex. Light is a highly dynamic environmental factor that varies strongly during the day and among the days and seasons. Despite photosynthetic acclimation, leaves at the top of the canopy can be exposed to excess irradiance on clear days, resulting in photoinhibition and oxidative stress (Osmond et al. 1999; Werner et al. 2001b; Demmig-Adams and Adams 2006). Photoinhibition can become particularly pronounced when photosynthesis rates are reduced due to other abiotic stress factors such as soil drought (Ramalho et al. 2000; Werner et al. 2002; Valladares et al. 2005; Niinemets and Keenan 2014). There are major within-canopy gradients in the leaf capacity to adjust to dynamically changing light conditions (Niinemets et al. 2003; García-Plazaola et al. 2004), indicating that

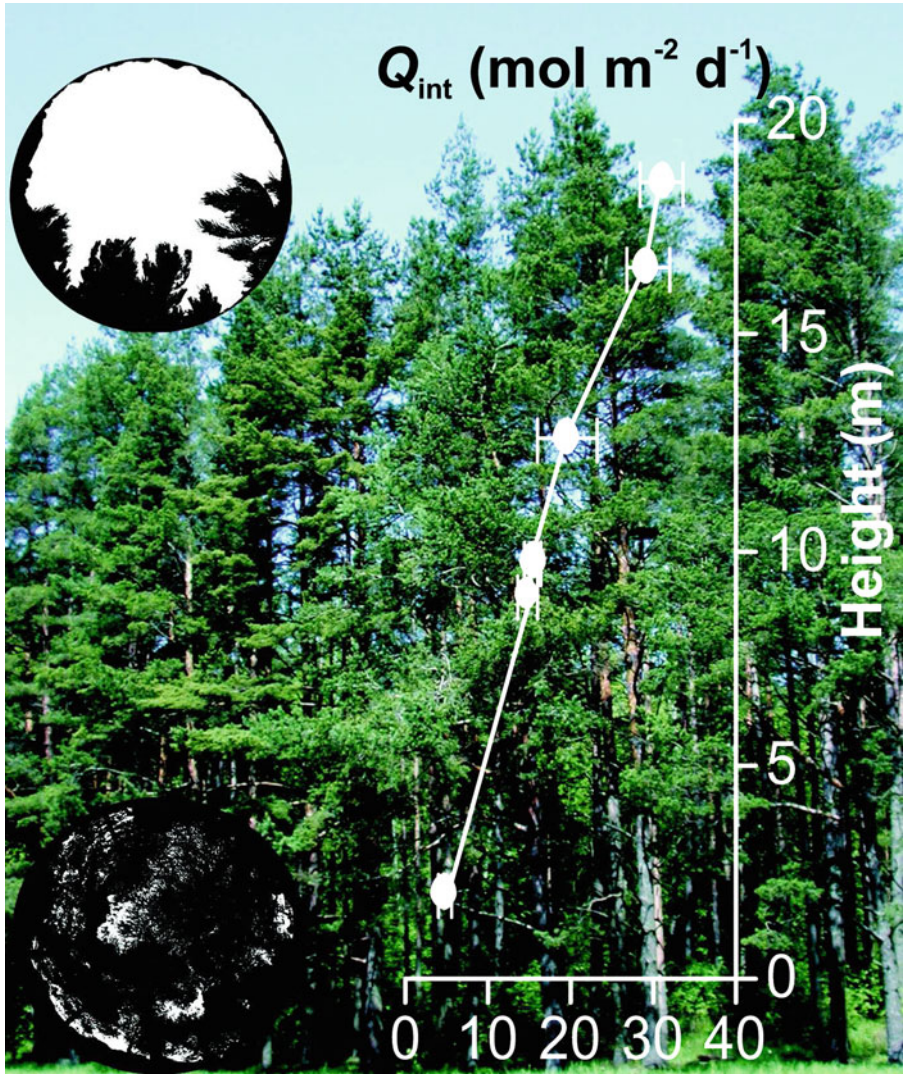

Fig. 4.1. Illustration of within-canopy variation in incident seasonal average integrated quantum flux density (Q_{int}) in a temperate evergreen conifer *Pinus sylvestris* canopy in Ahunapalu (58°19′ N, 27°17′ E, elevation ca. 60 m). Niinemets et al. (2001) provides further details of the stand. Hemispherical photographs taken from the upper part of the canopy (height of 18 m, $Q_{int} = 31.2$ mol m^{-2} d^{-1}) and lower part of the canopy within the shrub layer (height of 1.5 m, $Q_{int} = 3.85$ mol m^{-2} d^{-1}) are also demonstrated. Error bars show ± SD of average Q_{int} at each height level. Q_{int} is defined as the average daily integrated quantum flux density during foliage growth and development. Hemispherical photo analysis is a classic method for obtaining the relative potential penetrating quantum flux density in different locations of the canopy (e.g., Anderson 1964). The obtained relative potential values of incident diffuse and direct light availability need to be calibrated by long-term quantum flux density measurements to estimate Q_{int} for each canopy location (e.g., Niinemets et al. 1998a). Note that for illustrative purposes, the *y*-axis crosses with the *x*-axis at the highest Q_{int} value

coping with excess light can be importantly determined by past leaf light regime.

In addition to light, air temperatures increase from canopy bottom that receives less radiation toward canopy top that is exposed to greater radiation (Niinemets et al. 1999b; Zhang et al. 2010; Krédl et al. 2012; Pinheiro Prado et al. 2013; Zhang et al. 2013). These gradients in temperature are also associated with gradients in relative air humidity (Chiariello 1984; Krédl et al. 2012; Zhang et al. 2013). Lower humidity coupled with greater temperature and radiation input leads to greater

evaporative demands and potentially greater water stress in the upper canopy (Niinemets et al. 1999c; Hubbard et al. 2002; Aasamaa et al. 2004; Niinemets et al. 2004d; Sellin and Kupper 2004). In fact, the hydraulic conductivity of stem and branches can limit water transport to upper canopy in clear days with high radiation input (Joyce and Steiner 1995; Brodribb et al. 2005; Renninger et al. 2006; Ewers et al. 2007; Peltoniemi et al. 2012; Chap. 7, Woodruff et al. 2016). Thus, upper canopy leaves may become water-stressed even in situations with ample soil water supply (Joyce and Steiner 1995; Lemoine et al. 2002; Ewers et al. 2007). Stronger water stress in turn can lead to more severe photoinhibition and oxidative stress in leaves in the upper canopy.

This evidence suggests that, apart from changes in photosynthetic capacity, acclimation to within-canopy light gradients also involves structural and chemical adjustments to avoid excess light interception and increase the resistance to photoinhibition and oxidative stress in the upper canopy leaves (Rasmuson et al. 1994; Hikosaka and Hirose 1997; During 1999; Ishida et al. 1999a; James and Bell 2000; Werner et al. 2001b; Niinemets et al. 2003; García-Plazaola et al. 2004). It has been even suggested that interactions among environmental drivers and co-occurrence of multiple stresses can constrain the photosynthetic acclimation to within-canopy light environment, and as the result, "full acclimation" to within-canopy light is principally not possible (Niinemets and Valladares 2004; Niinemets 2012; Peltoniemi et al. 2012).

This chapter describes within-canopy variations in leaf photosynthetic rates and analyzes underlying sources of variation due to modifications in leaf structural, chemical and physiological characteristics. First, a methodology to separate structural, chemical and allocational controls on the variations in foliage photosynthetic rates within plant canopies is introduced. Then a short meta-analyses in broad-leaved evergreen species *Quercus ilex* is carried out to highlight the many facets of within-canopy foliage structural, chemical and physiological acclimation. The compiled dataset of *Q. ilex* foliar characteristics is unique in that it covers variations in all key leaf functional traits including diffusion conductances from ambient air to chloroplasts. The comprehensive analysis of the variation patterns in *Q. ilex* with high leaf longevity is used as a baseline to compare within-canopy acclimation responses in other plant functional types with higher leaf turnover.

This review also analyses the overall significance of variations in photosynthetic capacity in altering the whole canopy carbon gain and considers the possible structural and chemical constraints on the acclimation of photosynthetic capacity. This chapter further focuses on structural traits determining efficient light harvesting in the lower canopy and avoidance of excess radiation interception in the upper canopy, and on chemical traits responsible for safe dissipation of excess light and increasing resistance to enhanced oxidative stress in the upper canopy. The review emphasizes that there is an important within-canopy variation in how the stress resistance traits respond to dynamic alterations in light availability. Finally, this chapter analyses the variations in plasticity in whole-canopy acclimation among species with different shade tolerance that characteristically colonize habitats with varying light availability. This review emphasizes the strong within-canopy acclimation in key leaf traits and outlines the richness of responses in different plant functional types and in species with different shade tolerance.

II. Evaluation of the Role of Different Leaf Functional Traits Involved in Variation of Photosynthesis Through Plant Canopies

Variation in environmental drivers through plant canopies, in particular, variation in average daily incident integrated quantum

flux density during foliage growth and development (Q_{int}) alters a plethora of foliage structural, chemical and photosynthetic traits (Terashima and Hikosaka 1995; Anten et al. 1996, 1998; Koike et al. 2001; Lemoine et al. 2002; Meir et al. 2002; Wright et al. 2006; Niinemets 2007). As a key change, foliage photosynthetic capacity (A_{max}) typically increases with increasing Q_{int} from canopy bottom to top (Terashima and Hikosaka 1995; Anten et al. 1998; Koike et al. 2001; Lemoine et al. 2002; Meir et al. 2002; Wright et al. 2006; Niinemets 2007). Apart from A_{max} that determines foliage assimilation rate at high light, foliage light harvesting efficiency importantly drives photosynthesis at lower light intensities. The initial quantum yield of photosynthesis also often varies, although the within-canopy variation in quantum yield is less than in A_{max}, at least under non-stressed conditions (Cartechini and Palliotti 1995; Sands 1996; Niinemets and Kull 2001; Werner et al. 2001b).

To gain mechanistic insight into sources of within-canopy variation in A_{max} and the initial quantum yield of photosynthesis, the steady-state photosynthesis model of Farquhar et al. (1980) is typically used (Chap. 3, Hikosaka et al. 2016a). According to Farquhar et al. (1980) photosynthesis model, A_{max} is determined by the biochemical potentials of photosynthesis, the maximum carboxylase activity of Rubisco (V_{cmax}) and the capacity for photosynthetic electron transport (J_{max}), and by the stomatal (g_s) and mesophyll diffusion (g_m) conductances for photosynthesis, while the initial quantum yield of photosynthesis is mainly determined by the initial quantum yield for photosynthetic electron transport (α).

Within-canopy acclimation of J_{max}, V_{cmax} and α results from changes in multiple underlying traits. In the following, I define the modeling framework to evaluate the role of different leaf traits responsible for variations in J_{max}, V_{cmax} and α. The modeling framework will be used further through the chapter to gain insight into the importance of within-canopy variations in leaf structure and chemistry.

A. Determinants of Foliage Biochemical Potentials

Changes in biochemical photosynthesis potentials are determined by modifications in leaf structural and chemical traits, and the key question is to what extent different traits control variations in V_{cmax} and J_{max}. To separate among the effects of various structural and chemical traits on foliage biochemical potentials, V_{cmax} and J_{max} can be expressed as composites of several independent characteristics. For V_{cmax}:

$$V_{cmax} = 6.25 V_{cr} M_A F_R N_M, \qquad (4.1)$$

where V_{cr} is the specific activity of Rubisco, i.e., the maximum rate of ribulose-1,5-bisphosphate carboxylation per unit Rubisco protein (μmol g^{-1} s^{-1}), M_A is the leaf dry mass per unit area (g m^{-2}), F_R is the fraction of leaf nitrogen in Rubisco, N_M is the leaf nitrogen content per unit dry mass (g g^{-1}) and 6.25 (g g^{-1}) is the nitrogen content of Rubisco protein (Niinemets and Tenhunen 1997). Analogously, J_{max} is given as:

$$J_{max} = 8.06 J_{mc} M_A F_B N_M, \qquad (4.2)$$

where J_{mc} is the capacity for photosynthetic electron transport per unit cytochrome *f*, F_B is the fraction of nitrogen in rate-limiting proteins of photosynthetic electron transport, and the factor 8.06 considers the nitrogen content of proteins and molar stoichiometry relative to cytochrome *f* (Niinemets and Tenhunen 1997). Implicit in this expression is that the capacity for linear electron transport rate is determined by electron carriers between photosystems I and II (Niinemets and Tenhunen 1997 for a discussion).

Estimates of J_{max} and V_{cmax} are typically obtained from net assimilation vs. CO_2 response curves, ideally from net assimilation (A) vs. chloroplastic CO_2 concentration (C_c) response curves. In the past, C_c was not routinely estimated due to difficulties with estimation of mesophyll diffusion conductance ($C_c = C_i - A/g_m$, where C_i is the CO_2 concentration in the intercellular air space).

Thus, in the majority of past studies, V_{cmax} and J_{max} estimates were derived from A vs. C_i response curves assuming that g_m is infinite. However, recent work has demonstrated that g_m is finite, and that it varies among species and can limit photosynthesis as significantly as stomatal conductance (Flexas et al. 2012 for a review). Thus, estimates of foliage biochemical potentials from A vs. C_i response curves provide apparent, underestimated, values of V_{cmax} and J_{max}, and accordingly F_R and F_B according to equations 4.1 and 4.2 are also apparent fractions of N in rate-limiting proteins.

Apart from CO_2 response curves, inverse modeling techniques can be used to estimate J_{max} and V_{cmax} from light response curves of photosynthesis (e.g., Niinemets and Tenhunen 1997; Niinemets et al. 1999d; Patrick et al. 2009) and estimate V_{cmax} from the light-saturated net assimilation rate (e.g., Niinemets 1999). However, for inverse modeling, one needs an estimate of CO_2 concentration in the chloroplasts or at least an estimate of C_i. Alternatively, many studies have calculated the photosynthetic nitrogen use efficiency (E_N), the ratio of A_{max} to foliage N content (Hirose and Werger 1987a, 1994; Hikosaka et al. 1998; Hirose and Bazzaz 1998; Yasumura et al. 2002; Escudero and Mediavilla 2003; Pons and Westbeek 2004). Photosynthetic nitrogen use efficiency provides another estimate of the allocation of N to rate-limiting components of photosynthesis, but differently from F_R that is standardized for variations in g_s and g_m (C_c-based estimate of F_R) or g_s (C_i-based apparent F_R), within-canopy and species differences in E_N can be affected by differences in diffusion conductances.

B. Traits Affecting Light Harvesting and Initial Quantum Yield

Classic studies have demonstrated that the initial quantum yield of photosynthesis for an absorbed light measured at a given chloroplastic CO_2 and oxygen concentration and temperature ($\alpha_{p,a}$) is remarkably constant among C_3 plants (Ehleringer and Björkman 1977; Leverenz 1987, 1988, 1994). However, quantum yields for an incident light ($\alpha_{p,i}$) importantly vary due to differences in leaf absorptance (ξ) that modifies the amount of light intercepted at a given incident light intensity, thereby altering the quantum yield ($\alpha_{p,i} = \xi\alpha_{p,a}$) (Leverenz 1987, 1988, 1994; Long et al. 1993; Oberhuber et al. 1993).

Leaf absorptance is primarily a function of leaf chlorophyll content per unit area (χ_A, mmol m^{-2}) (Evans 1993a; Evans and Poorter 2001), except for hairy or waxy leaves that often have enhanced reflectance (Ehleringer and Björkman 1978; Evans and Poorter 2001; Cescatti and Niinemets 2004). For leaves without such highly reflective epidermal characteristics, Evans (1993a) developed an empirical relationship between ξ and χ_A that describes well variations in ξ for a broad range of species with differing foliage architectures (Evans and Poorter 2001):

$$\xi = \frac{\chi_A}{\chi_A + 0.076}, \tag{4.3}$$

where 0.076 mmol m^{-2} is an empirical constant.

Leaf chlorophyll (Chl) and chlorophyll-binding proteins contain a large fraction of foliar nitrogen, and therefore, it is pertinent to express leaf chlorophyll content in nitrogen equivalents (Niinemets and Tenhunen 1997) as:

$$\chi_A = N_M M_A F_L B_C, \tag{4.4}$$

where F_L is the fraction of leaf nitrogen invested in light harvesting, and B_C (mmol Chl (g N)$^{-1}$) is the chlorophyll binding defined as the amount of chlorophyll per unit nitrogen invested in light harvesting. It depends on the nitrogen cost of chlorophyll and specific chlorophyll-binding proteins, on the number of chlorophyll-binding sites in each chlorophyll-binding protein and on the stoichiometry of light-harvesting pigment-binding protein complexes (Hikosaka and Terashima 1996; Niinemets and Tenhunen 1997; Bassi and Caffarri 2000). In particular, B_C increases with increasing the share of chlorophyll associated with light-harvesting complex of photosystem II (LHC II) that

binds more chlorophyll than the centers of photosystems I and II (PS I and PS II) (Bassi and Caffarri 2000; Jackowski et al. 2001; Paulsen 2001). Since the bulk of chlorophyll *b* is associated with LHC II and minor light harvesting complexes of PS II (Bassi and Caffarri 2000), increases in B_C are also associated with decreases in chlorophyll *a*/*b* ratio.

The chlorophyll binding is normally about 2.1–2.5 mmol (g N)$^{-1}$ in vascular plants (Niinemets and Tenhunen 1997; Niinemets et al. 1998b), and it increases and chlorophyll *a*/*b* ratio decreases with decreasing light availability in the canopy (e.g., Evans 1993a, b; Niinemets and Tenhunen 1997; Niinemets et al. 1998b; Pons and Anten 2004), reflecting increases in the amount of chlorophyll associated with LHC II relative to that contained in PS I and PS II. This is an important acclimatory modification as it reduces the N cost of light harvesting (Hikosaka and Terashima 1995). While values of B_C are not routinely reported in the literature, chlorophyll *a*/*b* ratio is characteristically assessed in studies investigating light acclimation, and can be used as a proxy of light-driven modifications in thylakoid stoichiometry.

III. Light-Dependent Variations in Photosynthesis and Underlying Traits Across Plant Canopies

Equations 4.1, 4.2, 4.3, and 4.4 provide a simple means to analyze the effects of variations in foliage structure, nitrogen content and nitrogen partitioning on foliage photosynthetic potentials and initial quantum yield. In this section, I analyze how leaf structural and chemical traits vary in plant canopies and what are the implications for foliage photosynthetic potentials. As realized net assimilation rates are importantly driven by CO_2 diffusion conductances from ambient atmosphere to chloroplasts, I also consider within-canopy variations in stomatal and mesophyll conductances.

This section provides first a meta-analysis of within-canopy variations in leaf traits in the Mediterranean evergreen sclerophyll *Quercus ilex*. This species grows in water-limited open ecosystems where the variation in light availability as a source for foliage functional differentiation has been traditionally neglected. This meta-analysis serves to identify the basic scaling relationships between key foliage traits and irradiance in the canopy and make the general point that even in species growing in open ecosystems, there can be major within-canopy variations in foliage characteristics. This meta-analysis also serves as an example demonstrating how fragmentary information present in multiple studies can be summarized to gain insight into within-species variability. Overall, there is less data available for broad-leaved evergreen woody species than for herbaceous species and needle-leaved evergreen and winter-deciduous woody species (Niinemets and Anten 2009 for a review), making this analysis particularly pertinent. Furthermore, the data summarized in *Q. ilex* include all key functional leaf-level traits covering structural, biochemical and diffusional limits of photosynthesis, making the analysis truly comprehensive. In particular, within-canopy variation in mesophyll diffusion conductance has not been routinely studied with a few exceptions (Niinemets et al. 2006a; Cano et al. 2013; Niinemets 2015).

Although the meta-analysis in *Q. ilex* highlights the basic within-canopy leaf trait variation patterns, evergreens such as *Q. ilex* support multiple age cohorts. This is significant as in evergreens, older foliage becomes gradually shaded with canopy expansion and formation of new leaves. Accordingly, within-canopy trait patterns of older leaves are importantly driven by the capacity of older foliage to reacclimate to new light conditions. Thus, in the following, I analyze the within-canopy trait variations in older leaf age classes in evergreens primarily focusing on modifications in the overall plastic variations and on the strength of trait vs. light climate relationships.

After highlighting the basic within-canopy variation patterns in evergreens, I further ask how do the within-canopy gradients in foliage traits vary among different plant functional types? Different plant

functional types are characterized by varying rates of foliage and canopy growth and turnover and such differences in the rates of canopy expansion and leaf longevity can alter the gradients of light through the canopy, leaf lifetime intercepted light integral and the extent of variation in light availability during leaf lifetime (Schulze 1981; Jarvis and Leverenz 1983; Woodward et al. 1994; Niinemets et al. 2012; Niinemets and Keenan 2012). This may significantly alter the degree of within-canopy variation in different leaf-level traits in different plant functional types.

Finally, I analyze the overall significance of within-canopy variations in photosynthetic potentials for whole-canopy net assimilation rates using a simple modeling approach. This model-based analysis further underscores the importance of within-canopy trait variation and emphasizes the need to include phenotypic plasticity in large-scale photosynthesis models.

A. A Meta-Analysis of Within-Canopy Variations in the Mediterranean Evergreen Quercus ilex

1. Data and Methods

A thorough literature survey identified eight studies that provided information on within-canopy variation in light vs. foliage traits in *Q. ilex* (Eckardt et al. 1975; Rambal 1992; Sala et al. 1994; Rambal et al. 1996; Niinemets et al. 2002b, 2006a; Davi et al. 2008; Vaz et al. 2011). For these studies, average seasonal average incident integrated quantum flux density for 50 days after bud burst (Q_{int}) was used as an estimate of light availability. In studies reporting leaf dry mass per unit area (M_A) in relation to directly measured cumulative leaf area index, relative quantum flux density was derived according to Lambert-Beer's law using an extinction coefficient of 0.5 (Sala et al. 1994), while for optical leaf area index obtained by LAI-2000 instrument (Rambal et al. 1996), an extinction coefficient of 0.8 (Niinemets et al. 2010) was used. The above-canopy Q_{int} was derived for the year of foliage sampling using global radiation databases as in Niinemets and Keenan (2012). Q_{int} vs. foliage trait relationships were fitted by non-linear regressions in the form $y = ax^b$ and $y = a\mathrm{Ln}(x) + b$. As leaf dry mass per unit area is strongly correlated with within-canopy variations in Q_{int} (e.g., Fig. 4.2a and Meir et al. 2002; Niinemets 2007; Niinemets and Anten 2009), M_A was used as a substitute of light for studies explicitly investigating variations in foliage chemistry within the canopy light gradients, but lacking direct light measurements. This analysis only included mature fully-expanded current year foliage. The relationships in older leaf age classes are analyzed in Sect. III.B.

2. Variations in key Functional Traits

Analysis of all published within-canopy patterns of foliage traits in *Q. ilex* highlights several broad trends in plastic modifications in foliage structural, chemical and photosynthetic characteristics. First of all, M_A strongly increased with increasing average quantum flux density during leaf growth, 1.5–2.4-fold between canopy top and bottom (Q_{int}, Fig. 4.2a). Nitrogen content per unit area (N_A) also increased, 1.7–2.7-fold, with increasing Q_{int} ($r^2 = 0.77$–0.93, $P < 0.001$), but nitrogen content per unit dry mass (N_M) varied little within the canopy ($r^2 = 0.00$–0.12, $P > 0.2$, average ± SD = 1.57 % ± 0.25 % across the studies analyzed). Foliage photosynthetic capacity per unit area ($A_{max}{}^A$, $r^2 = 0.64$, $P < 0.001$ for the data of Niinemets et al. 2006a) and foliage photosynthetic potentials, the maximum carboxylase activity of Rubisco ($V_{cmax}{}^A$) and the capacity for photosynthetic electron transport per unit area ($J_{max}{}^A$, Fig. 4.2b) scaled positively with Q_{int} (ca. 2.5-fold change of foliage photosynthetic potentials between canopy top and bottom for the data in Fig. 4.2b and 1.8-fold change in Vaz et al. 2011), but mass-based photosynthetic characteristics varied little within the canopy ($r^2 = 0.00$–0.06 for these three traits). Furthermore, the fractions

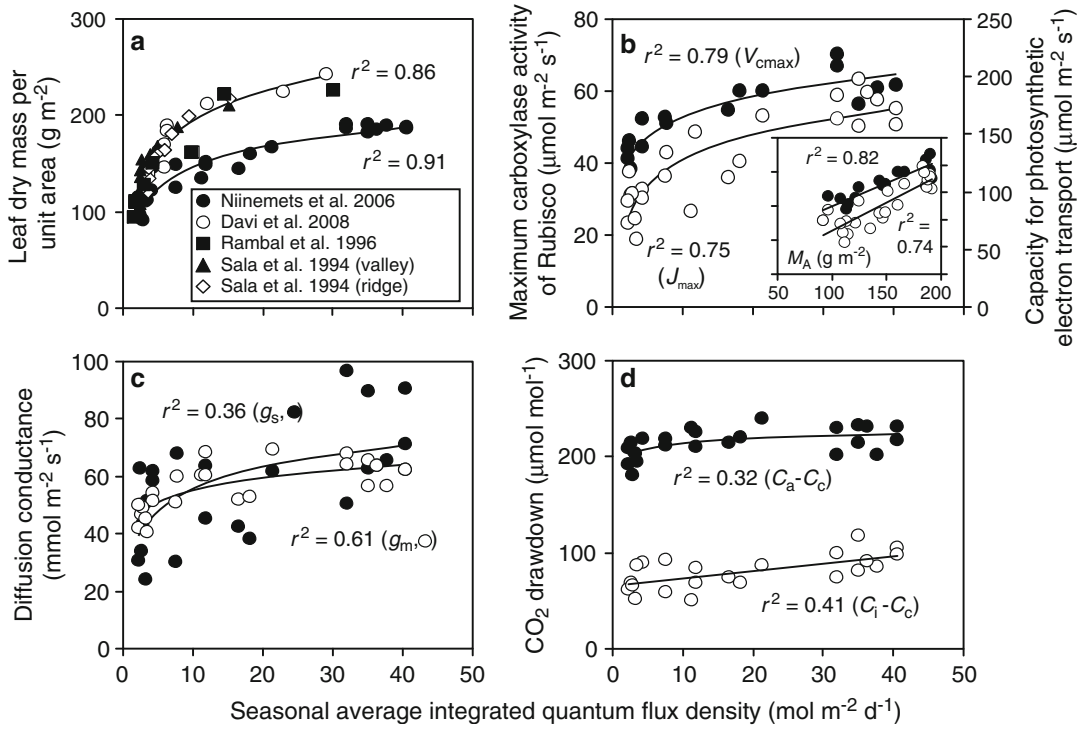

Fig. 4.2. Effects of within-canopy variation in average integrated quantum flux density (Q_{int}) on (**a**) leaf dry mass per unit area (M_A), (**b**) maximum carboxylase activity of Rubisco (V_{cmax}) and capacity for photosynthetic electron transport (J_{max}), (**c**) stomatal conductance to water vapor (g_s) and mesophyll diffusion conductance (g_m) and (d) CO_2 drawdown from ambient air to chloroplasts (C_a-C_i) and from intercellular air space to chloroplasts (C_i-C_c) in current-year leaves of Mediterranean broad-leaved evergreen sclerophyll *Quercus ilex*. The inset in (**b**) demonstrates the correlations of V_{cmax} and J_{max} with leaf dry mass per unit area. The data were fitted by linear (panel inset and C_i-C_c in **d**) and by non-linear regressions in the form $y = ax^b$ and $y = a\text{Ln}(x) + b$, whichever of the two provided a higher r^2 ($P < 0.01$ for all regressions). Data sources in panel **a** as indicated, all other data are from Niinemets et al. (2006a). The sampling locations were: 41.73°N, 3.58°E, elevation 270 m (Davi et al. 2008), 41.25°N, 1°E, elevation 700 m (valley) and 975 m (ridge) (Sala et al. 1994), 43.74°N, 3.59°E, elevation 270 m (Rambal et al. 1996) and 45.88°N, 10.87°E, elevation 300 m (Niinemets et al. 2006a). Q_{int} corresponds to average daily integrated incident quantum flux density for 50 days after bud burst

of nitrogen in Rubisco (Eq. 4.1, average ± SD = 0.154 ± 0.025 for the data of Niinemets et al. 2006a) and in bioenergetics (Eq. 4.2, 0.039 ± 0.007 for the data of Niinemets et al. 2006a and 0.036 ± 0.009 for the data of Rambal et al. 1996) were independent of Q_{int} ($P > 0.1$ for both variables and both datasets). Given the invariability of nitrogen allocation and considering that the area-based traits are the products of mass-based traits and M_A, within-canopy variation in N_A and foliage photosynthetic potentials was mainly driven by light-dependent variations in M_A (Fig. 4.2b inset).

Both stomatal and mesophyll conductances were greater in the upper canopy (Fig. 4.2c). The CO_2 drawdown from ambient air (C_a) to intercellular air space (C_i) was independent of Q_{int} ($r^2 = 0.01$), indicating that stomata limited photosynthesis similarly through the canopy. However, the CO_2 drawdown from intercellular air space to chloroplasts (C_c, C_i-C_c), and the overall drawdown (C_a-C_c) increased with increasing Q_{int} (Fig. 4.2d), demonstrating that g_m limited photosynthesis more in the upper canopy. Thus, increases in M_A were not only associated with stacking of photosynthesizing biomass per unit area,

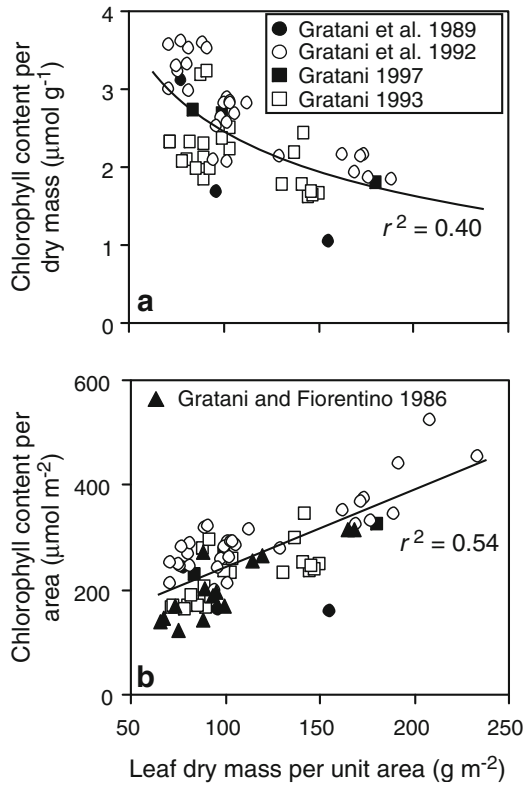

Fig. 4.3. Correlations of leaf chlorophyll content per unit leaf dry mass (**a**) and per unit leaf area (**b**) with leaf dry mass per unit area in current-year leaves of *Quercus ilex*. Variations in dry mass per unit area are due to within-canopy differences in light environment (Fig. 4.2a). Data from multiple studies investigating within-canopy variation in leaf traits (Gratani and Fiorentino 1986, Table 1 for site locations; Gratani et al. 1989, 1992; Gratani 1993, 1997) were pooled and fitted by a non-linear regression in the form $y = ax^b$ (a) and with a linear regression (**b**). $P < 0.001$ for both regressions

but increased foliage robustness also resulted in reduced efficiency of use of resources invested in photosynthetic machinery. Such enhanced diffusion limitations might reflect increases in cell wall thickness, an acclimation response contributing to withstanding low leaf water potentials in the upper canopy (see Sect. I), but also reducing CO_2 diffusion rate through leaf liquid phase (e.g., Terashima et al. 2011; Tosens et al. 2012a, b; Tomás et al. 2013).

As light measurements were not available in studies investigating within-canopy variation in chlorophyll contents, M_A was used as a proxy of within-canopy light conditions. Across these studies, foliage chlorophyll content per unit dry mass (χ_M) scaled negatively with M_A (Fig. 4.3a). Given that N_M was not correlated with within-canopy variation in light, this result also suggests that N in light harvesting (F_L, Eq. 4.4) increases with increasing shading in the canopy. Nevertheless, in this species, within-canopy variation in M_A was greater than the variation in χ_M such that leaf chlorophyll content per unit area was positively correlated with M_A (Fig. 4.3b).

B. Leaf Age-Dependent Variations in Foliage Plasticity in Evergreens

1. Why Should Plasticity Depend on Leaf Age?

Evergreen species support multiple leaf age cohorts, e.g., *Q. ilex* supports leaves up to 6 years old (Niinemets et al. 2005a), and several conifers can support leaves more than 10 years old (Ewers and Schmid 1981; Schoettle 1989; Schoettle and Fahey 1994; Niinemets and Lukjanova 2003). Increases in leaf age are characteristically associated with increases in leaf dry mass per unit area and in reductions in N_M and photosynthetic capacity (Teskey et al. 1984; Brooks et al. 1994, 1996; Niinemets 1997b; Niinemets et al. 2005a). On the other hand, older foliage initially developed at higher light becomes gradually shaded by new foliage and the key question is to what extent the older foliage can reacclimate to the modified light conditions. Although there is some secondary leaf growth at least in conifers (Ewers 1982; Gilmore et al. 1995), rigidification of cell walls after foliage maturation strongly curbs further foliage expansion growth. Thus, foliage structural reacclimation to modified light conditions is inherently limited. However, foliage may reacclimate to altered light conditions by changing nitrogen content and nitrogen allocation among the components of photosynthetic machinery within the leaf (Brooks et al. 1996; Niinemets 1997b; Escudero and Mediavilla 2003; Oguchi et al. 2005, 2006; Muller et al. 2009). Given the structural constraints, it is

plausible that foliage photosynthetic plasticity to light is decreasing with increasing foliage age.

2. Analyzing Plasticity Changes

To compare plastic changes in foliage traits of leaves of different age, I calculated the relative light-dependent change (R_c) of a given trait as (Niinemets et al. 2015):

$$R_c = \frac{V_{i+x} - V_i}{\Delta Q_{int}(V_{i+x} + V_i)/2}, \qquad (4.5)$$

where V_i is the trait value at a seasonal average quantum flux density of i ($Q_{int,i}$) and V_{i+x} is the trait value at $Q_{int,i} + x$ ($Q_{int,i+x}$). R_c is normalized with respect to the average trait value across the given light range, $(V_{i+x} + V_i)/2$, to account for age-dependent changes in absolute trait values. The plasticity to within-canopy variations in light increases with increasing the R_c value. In the following analysis, R_c was calculated with $Q_{int,i} = 6$ mol m^{-2} d^{-1} and $Q_{int,i+x} = 12$ mol m^{-2} d^{-1}. Foliage trait vs. Q_{int} relationships are curvilinear (Fig. 4.2), and this is a moderately high light range positioned in the strongly increasing part of foliage trait vs. Q_{int} relationships. In the following, age-dependent changes in plasticity are analyzed in three species, *Q. ilex* and conifers *Abies amabilis* and *Pinus contorta*.

3. Experimental Evidence of Plasticity Modifications

Examination of R_c values in leaves of different age indicated that the plasticity in N_A (Fig. 4.4a), M_A (data not shown) and $A_{max}{}^A$ (Fig. 4.4b) decreased with increasing leaf age in the three species analyzed. The reduction in plasticity was also associated with reduction in the degree of explained variance (Fig. 4.4c, d), indicating that the relationships became weaker and more scattered with increasing leaf age.

However, the age-dependent reduction in the plasticity in $A_{max}{}^A$ was less than in N_A and M_A (cf. Fig. 4.4a, b). This suggests that differently from structural traits and total nitrogen content, foliage photosynthetic traits of older shaded foliage can adapt to modified light regime (Brooks et al. 1994; Niinemets et al. 2006a). In fact, in *Q. ilex*, photosynthetic capacity of 1-year-old foliage was even more plastic that photosynthetic capacity of current-year foliage (Fig. 4.4b). This was associated with within-leaf changes in nitrogen allocation among proteins limiting photosynthetic capacity. Differently from current-year leaves (Sect. III.A.2), both F_R (Eq. 4.1, $r^2 = 0.29$, $P < 0.05$) and F_B (Eq. 4.2, $r^2 = 0.45$, $P < 0.01$ for the data of Niinemets et al. 2006a) increased with Q_{int} in 1-year-old leaves of *Q. ilex*. Nevertheless, in these leaves, the within-canopy variation in nitrogen allocation, F_R and F_B, 1.4–1.5-fold for the whole canopy, was still less than for nitrogen content and leaf dry mass per unit area.

In *Abies amabilis*, it has been further demonstrated that reacclimation to reduced light conditions results in increased nitrogen allocation to light harvesting (Brooks et al. 1994, 1996). This evidence collectively indicates that older foliage of evergreens can reacclimate to altered light conditions primarily due to modifications in nitrogen allocation within leaves, but also that the overall photosynthetic plasticity to light is lower for older leaves (Fig. 4.4). Thus, the modifications in nitrogen allocation cannot fully compensate for the structural inadequacy of shaded older foliage morphologically acclimated to higher past irradiance.

This analysis indicates that in evergreens, foliage photosynthetic characteristics of any canopy layer depend both on the structural, chemical and physiological acclimation to growth light conditions as well as on the reacclimation capacity. Interactions of leaf age with light availability and limited reacclimation capacity can clearly blur light vs. foliage structure and physiological activity relationships (Niinemets et al. 2006a). For example, such a confounding variation in leaf age and within-canopy light regime might explain why the correlations of leaf structural characteristics with light were weak for Australian broad-leaved evergreens (Wright et al. 2006) and in conifer *Pinus*

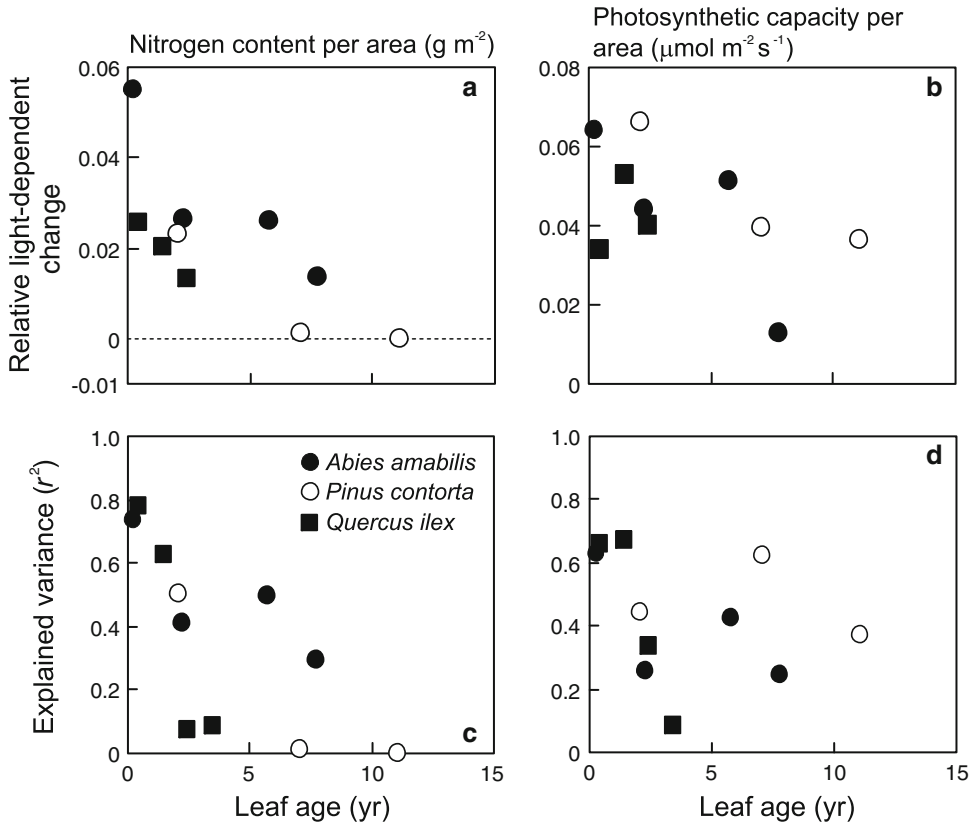

Fig. 4.4. Modifications in relative light-dependent changes in foliage nitrogen content per unit area (**a**) and photosynthetic capacity per unit area (**b**) with leaf age and concomitant changes in the explained variance (r^2, c and d) in the temperate evergreen conifers *Abies amabilis* (Data of Brooks et al. 1996) and *Pinus contorta* (Data of Schoettle and Smith 1999) and in the Mediterranean evergreen broad-leaved species *Quercus ilex* (Data of Niinemets et al. 2006a). Relative light-dependent change (R_c) of a given trait is defined by Eq. 4.5 and characterizes the light-dependent plasticity normalized with respect to the average trait value to directly compare plasticities in species with different average trait values. The plasticity increases with increasing the R_c value. Here R_c was calculated for a moderately high light range (Q_{int}) of 6–12 mol m^{-2} d^{-1} (Fig. 4.2 for the full light responses). Q_{int} is defined as in Fig. 4.2

pinaster (Warren and Adams 2001) when all leaves of different age were analyzed together.

C. Qualitative Differences among Trait Relationships between Plant Functional Types

1. Species with Low to Moderately High Leaf Turnover

The meta-analysis in the broad-leaved evergreen sclerophyll *Q. ilex* underscores the strong within-canopy variation in foliage structural, chemical and photosynthetic characteristics (Figs. 4.2 and 4.3) as is typical in plant canopies (Hirose and Werger 1987a, b; Ellsworth and Reich 1993; Pons et al. 1994; Meir et al. 2002; Niinemets 2007). The overall range of variation in M_A between canopy top and bottom in *Q. ilex* was 1.5–2.4 in the eight studies analyzed (Fig. 4.2a). The within-canopy variation in M_A was associated with similar variations in area-based contents of nitrogen and chlorophyll (Fig. 4.3), mass-based photosynthetic potentials (Fig. 4.2b) and stomatal conductance (Fig. 4.2c). In contrast, mass-based nitrogen content and photosynthetic potentials were not associated with light

availability and chlorophyll content per unit dry mass even decreased with increasing light availability. Overall, this evidence demonstrates that within-canopy increase in area-based characteristics in *Q. ilex* primarily reflected accumulation of tissue with similar chemical composition and physiological activity per unit leaf area (most traits) or that the stacking trend dominated over the trend of dilution of the chemicals (chlorophyll).

These observations in *Q. ilex* are in a broad agreement with past observations in other broad-leaved evergreens. Differently from *Q. ilex*, a moderate increase in N_M with Q_{int} has been observed in temperate evergreen *Ilex aquifolium* (Aranda et al. 2004) and in several temperate *Nothofagus* species (Niinemets et al. 2004b), and in tropical species *Ficus insipida* (Posada et al. 2009). Analogously, photosynthetic capacity per unit dry mass (A_{max}^{M}) (Chazdon and Field 1987; Ishida et al. 1999b; Posada et al. 2009) and nitrogen partitioning coefficients, F_R and F_B (Evans and Poorter 2001), can either moderately decrease or increase in different evergreen species. Nevertheless, all these studies emphasize that the light-dependent increase in M_A is the key factor responsible for within-canopy increases in N_A and A_{max}^{A} in broad-leaved evergreens.

The relationships are analogous in evergreen needle-leaved conifers. In conifers, the variations in foliage nitrogen content and photosynthetic capacity per unit area are also dominated by M_A (Sprugel et al. 1996; Niinemets 1997a; Stenberg et al. 1999; Palmroth and Hari 2001; Han et al. 2003; Leal and Thomas 2003; Han et al. 2004, 2006). Furthermore, similar relationships have been demonstrated in other species with needle-like assimilative organs such as cladodes in the angiosperm *Casuarina* (Niinemets et al. 2005b). However, an increase in N_M with increasing Q_{int} has been observed in some conifers, and this was associated with increased mesophyll volume fraction and enhanced photosynthetic capacity per leaf dry mass at higher Q_{int} (Niinemets et al. 2007). So far, light-dependent modifications in tissue fractional composition have been studied only in a few conifers (e.g., Aussenac 1973; Kovalyev 1980; Niinemets et al. 2007), and clearly more studies on three-dimensional needle anatomy are called for. Furthermore, in conifers with complex three-dimensional leaf cross-section, foliage photosynthetic capacity per unit projected area also depends on modifications in total to projected leaf area ratio (S_T/S_P, Sect. IV.A).

The relationships of leaf traits with Q_{int} are qualitatively similar in broad-leaved deciduous species that form all leaves simultaneously in the beginning of growing season, and thus, are characterized by a relatively high leaf longevity (Ellsworth and Reich 1993; Tjoelker et al. 1995; Niinemets and Kull 1998; Niinemets et al. 1998b; Koike et al. 2001; Meir et al. 2002; Iio et al. 2005). Although in some species, N_M (Niinemets et al. 1998b), A_{max}^{M} (Niinemets et al. 1998b) and nitrogen partitioning in photosynthetic machinery, F_B and F_R (Niinemets et al. 1998b, 2010) increase with increasing Q_{int}, in other species, N_M (Ellsworth and Reich 1993; Niinemets 1995; Fleck et al. 2003), A_{max}^{M} (Ducrey 1981; Ellsworth and Reich 1993; Niinemets et al. 1998b), and nitrogen partitioning coefficients (Niinemets et al. 2010) can also moderately decrease with increasing Q_{int}. Thus, again the overall photosynthetic response to within-canopy variations in Q_{int} primarily results from modifications in M_A. Nevertheless, upon sudden changes in irradiance, woody deciduous species can significantly change foliage photosynthetic capacity through changes in nitrogen partitioning (Naidu and DeLucia 1997; Niinemets et al. 2003; Oguchi et al. 2005, 2006), albeit the acclimation is limited due to anatomical constraints as in evergreen species (Sect. III.B, Oguchi et al. 2005, 2006) and can be relatively time-consuming (Naidu and DeLucia 1997; Kull and Kruijt 1999; Niinemets et al. 2003).

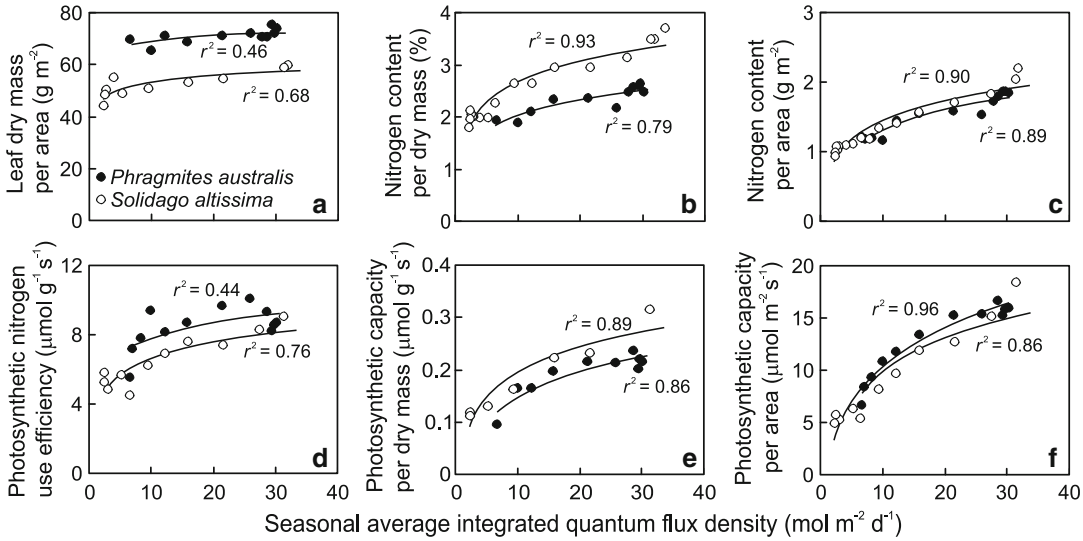

Fig. 4.5. Light-dependent variations in leaf dry mass per unit area (**a**), nitrogen content per unit dry mass (**b**) and area (**c**), photosynthetic nitrogen use efficiency (photosynthetic capacity per unit nitrogen, (**d**), and light-saturated net assimilation rate at ambient CO_2 concentration (photosynthetic capacity) per unit dry mass (**e**) and area (**f**) in the grass *Phragmites australis* (Data of Hirose and Werger 1994, 1995) and in the herb *Solidago altissima* (Data of Hirose and Werger 1987a, b; Werger and Hirose 1988). Data were fitted by non-linear regressions in the form of $y = a\mathrm{Ln}(x) + b$ (all regressions are significant at least at $P < 0.02$). Seasonal average integrated quantum flux density (Q_{int}) is defined as in Fig. 4.2

2. Species with High Leaf Turnover

The situation is qualitatively different for broad-leaved deciduous woody species with continuous canopy expansion such as in fast-growing dense young *Salix* stands or coppice plantations. In such stands, foliage developed earlier becomes shaded by newly developed foliage analogously to different-aged foliage in evergreen canopies (Sect. III.B). Thus, there are strong leaf age and light gradients within the fast-expanding canopies of deciduous species. In fact, in such canopies, most leaves could have been exposed to high light during their development at the top of the canopy. As the result, M_{A} is relatively invariable in fast-growing woody canopies, and the within-canopy variation in N_{A} is primarily driven by a strong gradient in N_{M} (Vapaavuori et al. 1989; Vapaavuori and Vuorinen 1989; Noormets et al. 1996; Kull et al. 1998), while the within-canopy variation in ${A_{\mathrm{max}}}^{\mathrm{A}}$ is driven by increases of ${A_{\mathrm{max}}}^{\mathrm{M}}$ with Q_{int} (Vapaavuori et al. 1989; Vapaavuori and Vuorinen 1989).

The situation is similar in the canopies of herbaceous species where the entire canopy is formed during a single growing season and there is a continuous canopy growth until the onset of inflorescence formation. Examination of leaf trait vs. Q_{int} relationships in representative grass (*Phragmites australis*) and herb (*Solidago altissima*) species (Data of Hirose and Werger 1987a, 1994, 1995, Werger and Hirose 1988) demonstrates that although M_{A} does increase with increasing Q_{int} (Fig. 4.5a), the increase is much less than the corresponding change of N_{M} through the canopy (Fig. 4.5b) such that the increase of N_{A} (Fig. 4.5c) is mainly dependent on within-canopy gradient in N_{M}. In addition to N_{A}, the light-dependent increase of ${A_{\mathrm{max}}}^{\mathrm{A}}$ (Fig. 4.5f) is determined by increases in nitrogen allocation (photosynthetic nitrogen use efficiency, E_{N}, Fig. 4.5d), i.e., ${A_{\mathrm{max}}}^{\mathrm{A}} = E_{\mathrm{N}}N_{\mathrm{A}}$. Increases in both N_{M} and photosynthetic nitrogen use efficiency are responsible for the strong increase of ${A_{\mathrm{max}}}^{\mathrm{M}}$ with Q_{int} (Fig. 4.5e; ${A_{\mathrm{max}}}^{\mathrm{M}} = E_{\mathrm{N}}N_{\mathrm{M}}$). Given further that

$A_{max}^{A} = E_N N_M M_A$, this evidence collectively indicates that nitrogen reallocation among the leaves and modification in nitrogen partitioning within the leaves are the primary mechanisms determining acclimation of herbaceous canopies to within-canopy light gradients, while changes in M_A play a less important role.

Overall, the strong gradients in N_M, photosynthetic nitrogen use efficiency and A_{max}^{M} in species with high leaf turnover partly reflect reacclimation to modified light conditions, but also greater leaf turnover and senescence of older leaves at the bottom of plant canopy (Vapaavuori et al. 1989; Vapaavuori and Vuorinen 1989; Pons and Pearcy 1994; Hikosaka 1996; Anten et al. 1998; Weih 2009). In fact, in species with short leaf life-span and fast leaf turnover, it has been demonstrated that shading, especially shading of individual leaves, can introduce programmed cell death, leading to rapid reductions of leaf photosynthetic capacity and leaf abscission (Burkey and Wells 1991; Pons and Pearcy 1994; Ackerly and Bazzaz 1995; Ono et al. 2001; Vos and van der Putten 2001; Boonman et al. 2006). On the other hand, compared with species with low rate of leaf turnover, photosynthetic capacity in species with high leaf turnover can relatively rapidly respond to increases in light availability (Pons and Pearcy 1994; Boonman et al. 2006).

D. Variations in Photosynthetic Plasticity Among Plant Functional Types

In *Q. ilex*, the relationships of M_A and photosynthetic potentials with Q_{int} were strongly curvilinear, with most of the change in foliage characteristics occurring over the light range of 2–12 mol m^{-2} d^{-1} (Fig. 4.2). In the case of M_A, clear site differences were evident at the saturating part of M_A vs. Q_{int} relationships, at Q_{int} values higher than ca. 12 mol m^{-2} d^{-1} (Fig. 4.2a). Although extensive, the ranges of variation in M_A, N_A and photosynthetic potentials in broad-leaved evergreens are somewhat smaller than the within-canopy variations in these traits of two- to four-fold in the canopies of winter-deciduous forest trees (see Sect. V; e.g., Ellsworth and Reich 1993; Niinemets and Kull 1998; Iio et al. 2005; Niinemets and Anten 2009; Niinemets et al. 2015). In fact, in several deciduous broad-leaved species, there is only a moderate curvilinearity in leaf trait vs. Q_{int} relationships (Niinemets and Kull 1998; Meir et al. 2002; Aranda et al. 2004; Niinemets et al. 2015). The range of variation in trait vs. Q_{int} relationships is also high, more than two- to four-fold in several evergreen shade-tolerant conifers from genera *Abies* and *Picea* (Niinemets 1997a; Stenberg et al. 1998; Cescatti and Zorer 2003). However, there was a low within-canopy plasticity of 1.3–1.7-fold in two *Picea* species in the study of Ishii et al. (2003), and in *Pseudotsuga menziesii* and *Tsuga heterophylla* in the study of Bond et al. (1999). Low foliage plasticity 1.3–2-fold has been reported for several *Pinus* species (Bond et al. 1999; Niinemets et al. 2001, 2002a).

In the case of herbaceous species, high photosynthetic plasticity, typically two- to four-fold (Fig. 4.5f; Hirose and Werger 1994; Anten et al. 1995b; Niinemets et al. 2015), in exceptional cases close to or even more than an order of magnitude (Pons et al. 1993; Hirose and Werger 1994; Anten et al. 1995b, Chap. 5, Pons 2016) has been reported. This high plasticity is associated with moderate changes in leaf dry mass per unit area (Fig. 4.5a) and nitrogen allocation (Fig. 4.5d) and moderate to extensive changes in leaf nitrogen content per unit dry mass (Fig. 4.5b; Hirose et al. 1989; Lemaire et al. 1991; Evans 1993a, b; Hirose and Werger 1994; Niinemets et al. 2015; Chap. 5, Pons 2016).

Overall, there is evidence of greater photosynthetic plasticity in leaves with shorter life-span. The differences among evergreen and deciduous woody species mainly result from the circumstance that evergreens can reduce their M_A when growing in shade conditions less than deciduous species,

resulting in correspondingly narrower range in photosynthetic potentials in evergreens. High photosynthetic plasticity in herbaceous canopies is mainly associated with moderate to high gradients in all three determinants of photosynthetic capacity (Eqs. 4.1 and 4.2): M_A, nitrogen allocation and partitioning. In particular, gradients in nitrogen allocation in herbaceous species reflect the inherent strategy of resource remobilization from shaded leaves undergoing senescence to young developing leaves at the top of the canopy (Werger and Hirose 1988; Hikosaka et al. 1994; Hirose and Werger 1994; Hikosaka 1996; Franklin and Ågren 2002, Chap. 5, Pons 2016).

E. Importance of Within-Canopy Biochemical Modifications in Whole Canopy Photosynthesis

Within-canopy variation in key leaf traits allows for investment of photosynthesizing biomass in environments where the pay-back is higher, and has therefore been considered as an adaptive feature. Several studies have explored the quantitative benefits of trait variation using either numerical integration or optimality analyses (Field 1983; Hirose and Werger 1987b; Gutschick and Wiegel 1988; Farquhar 1989; Sands 1995; Anten 2005; Peltoniemi et al. 2012; Hikosaka 2014; Chap. 13, Anten 2016). There can be several target variables for optimization of canopy photosynthesis: maximization of canopy photosynthesis for given biomass investment in leaves (Gutschick and Wiegel 1988), maximization of canopy photosynthesis for given total canopy nitrogen content (Field 1983; Hirose and Werger 1987b; Farquhar 1989; Anten 2005; Chap. 13, Anten 2016) or maximization of canopy photosynthesis with given nitrogen and water use (Buckley et al. 2002; Farquhar et al. 2002; Peltoniemi et al. 2012). Overall, all optimality analyses have suggested that foliage photosynthetic capacity and nitrogen content should increase with average quantum flux density in the canopy and that such "optimal" distribution of resources results in a higher carbon gain than a constant photosynthetic capacity for all leaves in the canopy (Fig. 4.6; Niinemets 2012 for a review).

Comparisons of predicted and observed canopy gradients, however, indicate that unconstrained optimality analyses predict too strong gradients in nitrogen content and foliage photosynthetic capacity (Niinemets and Anten 2009 and Chap. 13, Anten 2016 for reviews). Various hypotheses have been put forward to explain the discrepancies from full optimality. First of all, the condition of optimality can differ depending on the time scale and light characteristics, e.g., for diffuse and direct light (Hikosaka 2014). Thus, definition of the pertinent light (diffuse vs. direct, incident vs. absorbed, instantaneous vs. integrated) driving within-canopy acclimation can importantly modify the predicted optimal distribution. It has further been hypothesized that changes in foliage traits from canopy top to bottom are not only driven by light, but also by other co-varying environmental characteristics (Sect. I), in particular, by variations in evaporative demand (e.g., Niinemets and Valladares 2004). Meeting the needs for hydraulic and structural adjustment to ensure water flux to photosynthetically more active leaves and cope with potentially enhanced water availability limitations in the upper canopy can compromise full photosynthetic acclimation to high light (Peltoniemi et al. 2012; Chap. 7, Woodruff et al. 2016).

There are also biophysical limitations on the minimum and maximum thickness of leaves and their N content per unit dry mass, constraining leaf M_A and N_A values and ultimately leaf photosynthetic capacity in both high and low light (Gutschick and Wiegel 1988; Dewar et al. 2012; Niinemets 2012). Clearly, including constraints on M_A and N_A has resulted in more realistic predictions of within-canopy gradients in M_A, N_A and photosynthetic capacity (Gutschick and Wiegel 1988; Dewar et al. 2012) than assuming unconstrained variation in leaf traits (e.g., Farquhar 1989; Sands 1995).

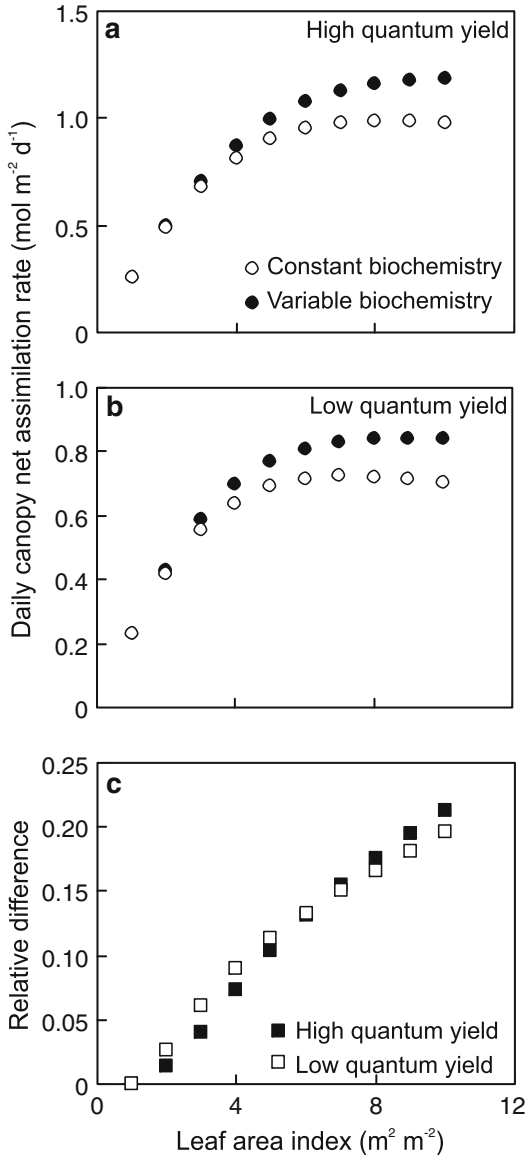

Fig. 4.6. Simulated whole canopy daily integrated photosynthesis (**a**, **b**) in dependence on canopy leaf area index (L) for hypothetical canopies with constant foliage biochemical potentials (canopy photosynthesis, $A_{c,con}$) and in canopies with light-dependent variation in foliage biochemical potentials ($A_{c,var}$), and (**c**) relative differences in daily canopy photosynthesis among canopies with constant and variable biochemistry, $(A_{c,var} - A_{c,con})/A_{c,con}$, in relation to L. The simulations were conducted for canopies with high initial quantum yield for photosynthetic electron transport for an incident light of 0.248 mol mol^{-1} (**a**) and in canopies with a low quantum yield 0.15 mol mol^{-1}. The high quantum yield scenario corresponds to non-photoinhibited leaves with moderately high leaf absorptance of 0.85, while the low quantum yield scenario corresponds to photoinhibited and/or highly reflective leaves. Foliage net assimilation rates were modeled according to Farquhar et al. (1980) photosynthesis model for constant values of leaf temperature of 25 °C and CO_2 concentration in chloroplasts (C_c) of 280 μmol mol^{-1} and using the Rubisco kinetic characteristics as in Niinemets and Tenhunen (1997). In the case of the simulation with constant biochemistry, the maximum carboxylase activity of Rubisco was set at a value of 20 μmol m^{-2} s^{-1} and the capacity for photosynthetic electron transport was scaled as $2.5V_{cmax}$, and non-photorespiratory respiration rate as $0.015V_{cmax}$ (see Niinemets et al. 1998b). A sine function with a maximum quantum flux density (Q) of 1,400 μmol m^{-2} s^{-1} was used to approximate the diurnal variations in above-canopy Q (Q_0). Variation in Q through the canopy was simulated according to a simple Lambert-Beer model assuming that foliage is randomly dispersed (the clumping index $\Omega = 1.0$): $Q = Q_0 e^{-k\Omega L}$, where k is the extinction coefficient ($k = 0.5$ in this simulation). In the case of variable biochemistry, V_{cmax} vs. daily integrated Q (Q_{int}) relationships were fitted for canopies with different L by linear regressions such that the ratio of the values of V_{cmax} at the top of the canopy ($V_{cmax,t}$) and at the bottom ($V_{cmax,b}$) was 2.6 (moderately high within-canopy variation in foliage biochemical potentials) and the whole-canopy leaf area-weighted average V_{cmax} was 20 μmol m^{-2} s^{-1}. All other characteristics of Farquhar et al. (1980) photosynthesis model were varied with V_{cmax} as in the simulations with the constant biochemistry

Using either constrained or unconstrained optimization algorithms, it is possible to analyze what is the possible significance of within-canopy variation in foliage traits in canopies of different leaf area index (L) and structure (Fig. 4.6; Anten et al. 1995a; Anten 2005; Chap. 13, Anten 2016). In the case of constrained optimization, the within-canopy gradient in $A_{max}{}^{A}$ was fixed at a moderately high level of 2.6-fold between canopy top and bottom. In the case of unconstrained optimization, $A_{max}{}^{A}$ was set directly proportional to Q_{int}. In all simulations, the whole-canopy leaf area-weighted average $A_{max}{}^{A}$ was a given fixed constant value ($A_{max,c}{}^{A}$). Thus, the "unconstrained" optimization used the greatest gradient to yield the given $A_{max,c}{}^{A}$ value.

Independent of the way of modeling, these analyses suggest that the possible benefits of foliage acclimation to Q_{int} are greater for canopies with stronger light gradients, i.e.,

in canopies with a larger leaf area index (Fig. 4.6a, b) and in canopies with higher light extinction coefficient (data not shown, see Chap. 9, Hikosaka et al. 2016b for gradients of cumulative L and light). In the case of the constrained optimization, the optimal distribution was expected to increase whole canopy photosynthesis between 1.5 and 21 % compared with all leaves having a constant photosynthetic capacity equal to $A_{max,c}{}^{A}$. The effect of considering within-canopy variation in leaf traits increased with increasing L (Fig. 4.6c). Of course, the stronger the within-canopy gradient in photosynthetic characteristics, the greater is the overall whole-canopy photosynthetic benefit. In the case of "unconstrained" optimization of $A_{max}{}^{A}$, whole-canopy photosynthetic rate was predicted to be ca. 50 % greater than in the simulation with a constant $A_{max}{}^{A}$ (data not shown).

The photosynthetic benefit might seem relatively small for open canopies (Fig. 4.6a), especially when the whole-canopy gradient in $A_{max}{}^{A}$ is moderate as for instance in the Mediterranean evergreen *Q. ilex* (Fig. 4.2). Nevertheless, even a moderate improvement of long-term carbon gain can importantly benefit the plant in highly stressful environments where the annual carbon gain is significantly reduced due to soil drought. Furthermore, drought stress often leads to photoinhibition, importantly reducing the initial quantum yields of photosynthetic electron transport and carbon assimilation (Niinemets and Keenan 2014 for a review). The implication of such a reduction in the initial quantum yields is that the light saturation point of photosynthesis is shifted to higher quantum flux densities, and thus higher quantum flux densities appear limiting to photosynthesis. The overall effect in terms of whole-canopy photosynthesis is that the canopy photosynthesis decreases with a reduction of the quantum yield (cf. Fig. 4.6a, b). However, photosynthesis of canopies with low to moderate L, becomes much more sensitive to within-canopy variations in $A_{max}{}^{A}$ (Fig. 4.6b, c). Thus, within-canopy differences in photosynthetic capacity can importantly benefit photosynthesis in relatively open canopies as well, especially under conditions leading to reduction of quantum yields of photosynthesis such as drought and photoinhibition stresses.

IV. Variations in Traits Improving Light Harvesting and Protecting from Excess Light

Apart from the major within-canopy modifications in foliage functional traits that result in alterations in foliage photosynthetic potentials, variations in a number of leaf traits also alter leaf light harvesting efficiency and/or play a role in avoidance of excess light harvesting. Given the interaction of light with other environmental drivers (Sect. I), there are also significant within-canopy gradients in abiotic stress. In particular, leaves exposed to high irradiances can be severely heat- and drought-stressed, especially in conditions of soil drought, while in the lower canopy, the photosynthetic productivity is still most severely limited by light availability. The interactive effects of environmental drivers are further complicated by highly dynamic nature of light in plant canopies. In this section, I analyze variations in structural and chemical traits responsible for alterations in light harvesting and abiotic stress tolerance, and further consider the dynamic responses of leaf traits to rapid changes in light availability.

A. Structural Traits as Determinants of Light Harvesting and Avoidance

Section III.A indicated that acclimation to low light availability in the bottom of a plant canopy is associated with enhanced investment of nitrogen in chlorophyll and pigment-binding complexes (see Fig. 4.3), and analogous relationships have been observed in a number of species (Niinemets and Anten 2009 for a review). Such enhanced investment of nitrogen in light harvesting within the leaf enhances light harvesting per unit mass, i.e., increases

light availability of an average mesophyll cell (e.g., Niinemets 2007). Although researchers seldom think of light harvesting as a mass-based phenomenon, mass basis characterizes the cost of light harvesting in terms of resource investment.

Differently from the mass basis, area-based chlorophyll contents may increase (Fig. 4.3b), be invariable or decrease with increasing Q_{int} (e.g., Hallik et al. 2009a). Nevertheless, due to non-linear dependence of leaf absorptance on leaf chlorophyll content (Eq. 4.3), effects of such changes in area-based chlorophyll content generally result in minor within-canopy modifications in leaf absorptance (e.g., St-Jacques et al. 1991; St-Jacques and Bellefleur 1993; Poorter et al. 1995). Given this, major reductions in M_A in woody species in low light constitute an important acclimation response leading to greater light intercepting surface area, and thus, enhanced light interception with given biomass investment in leaves.

Light harvesting efficiency in needle-leaved species can also be enhanced by changes in total to projected leaf area ratio (S_T/S_P). S_T/S_P decreases strongly with decreasing Q_{int} in some shade-tolerant conifers such as in *Picea* and *Abies* (Niinemets and Kull 1995; Sprugel et al. 1996; Cescatti and Zorer 2003), increasing the light harvesting surface area at the given total surface area in lower light. However, minor modifications or invariable S_T/S_P have been observed in intolerant conifers from the genus *Pinus* (Niinemets et al. 2001, 2002a) and in the angiosperm *Casuarina* with needle-like cladodes (Niinemets et al. 2005b).

Furthermore, at the shoot scale, the degree of foliage spatial aggregation in shoots decreases with decreasing Q_{int}, implying reduction of within-shoot shading (Stenberg 1996, 1998; Smolander and Stenberg 2001; Cescatti and Zorer 2003; Niinemets et al. 2006b). In addition, foliage inclination angle distributions within shoots become more horizontal in the lower canopy in several shade-tolerant conifers, thereby improving interception of light from vertical inclination angles that constitute a more prevalent source of both diffuse and direct radiation in the lower canopy (Stenberg 1996, 1998; Cescatti and Zorer 2003; Niinemets et al. 2006b). On the other hand, greater foliage aggregation and more vertical foliage inclination angles at higher irradiances reduce mean irradiance on leaf surface, and thus reduce the degree of foliage photoinhibition and severity of heat stress (Cescatti and Zorer 2003; Niinemets et al. 2006b). This implies that modifications in needle and shoot structure play a dual role, improving light harvesting in low light and avoiding excess radiation interception at high light.

In broad-leaved species, there are also classic changes in leaf inclination angle distributions analogous to conifers (Fig. 4.7a; for reviews see Niinemets 2010; Chap. 2, Goudriaan 2016). In addition to changes in average leaf inclination angle from vertical to horizontal with decreasing light availability in the canopy, there are also important modifications in the degree of lamina flatness in several broad-leaved species. In particular, leaves tend to be increasingly rolled at the top of plant canopies (Fig. 4.7b). Such increases in the degree of foliage rolling can strongly reduce leaf light interception and also change the share of light interception by leaf lower and upper surface (Fleck et al. 2003). Consideration of both the within-canopy changes in leaf inclination angle and degree of leaf rolling indicates that the overall efficiency of light interception may vary more than two-fold within the canopy of broad-leaved species due to modifications in these structural traits (Fig. 4.7c). Thus, modifications in inclination angles and degree of rolling play a major role in altering the balance between light interception and avoidance. Overall, these case studies suggest that avoidance of excess light interception leads to a more uniform illumination of foliage in the canopy, i.e., greater penetration of light into deeper canopy layers. Simulations studies indicate that more uniform light distribution strongly benefits the whole canopy carbon gain

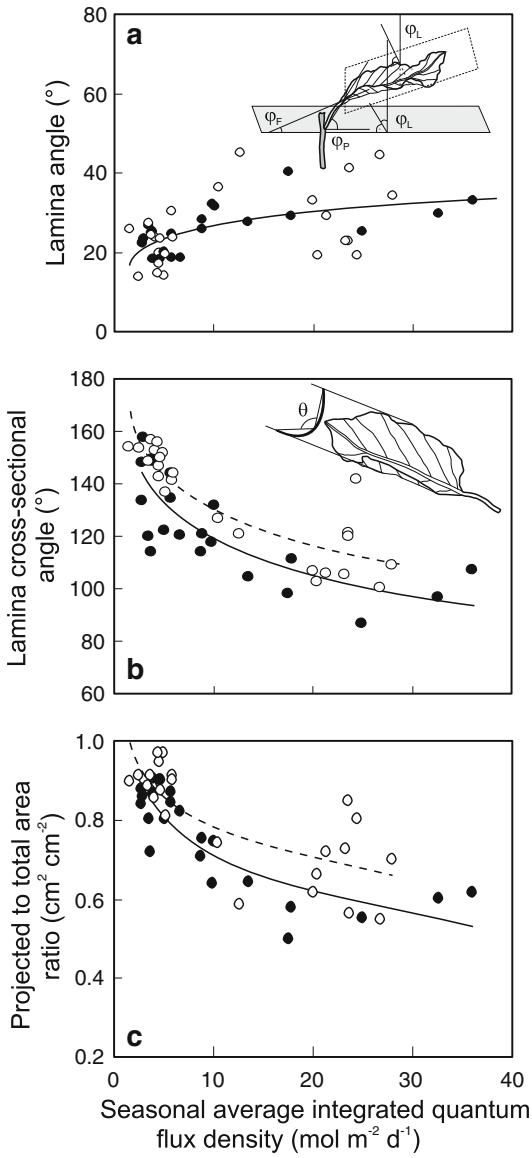

Fig. 4.7. Effects of seasonal average daily integrated quantum flux density (Q_{int}) on (a) the absolute lamina inclination angle, i.e., the average angle between the normal to the leaf plane and the vertical direction ($|\phi_L|$, inset in (**a**) for the definition), (**b**) lamina cross-sectional angle (θ, inset in (**b**) for the definition) and (**c**) lamina projected to total area ratio in a dominant (*filled circles*) and a sub-dominant tree (*open circles*) of the temperate deciduous species *Fagus sylvatica*. Inset in (**a**) also demonstrates the definition of inclination angles of petiole (φ_P) and leaf lamina at leaf fall-line (φ_F). Data fitting as in Fig. 4.5 ($P < 0.001$ for all). In (**a**), the slopes and intercepts of $|\phi_L|$ vs. $\mathrm{Ln}Q_{int}$ relationships did not differ among the trees according to covariation analyses, and thus, the data for both trees were fitted by a common regression. Modified from Fleck et al. (2003)

(Ryel et al. 1994; Hikosaka and Hirose 1997; Werner et al. 2001a; Cescatti and Niinemets 2004; Valladares and Niinemets 2007), and thus, "optimization" of canopy structure constitutes an important means to maximize canopy carbon gain.

B. Chemical Traits Improving Abiotic Stress Tolerance

Excess light intercepted during midday on clear days can result in severe photooxidative damage of photosynthetic apparatus compromising photosynthetic activity in the morning and evening periods and on overcast days when light intensities are lower. Temporal exceeding of leaf heat stress limits during lighflecks and upon sustained exposure to high radiation loads can further result in heat damage of photosynthetic apparatus. All such adverse effects are expected to be more significant in the upper canopy due to greater radiation loads (Sect. I).

Plants cope with excess energy by increasing the capacity for non-photochemical quenching (non-radiative dissipation of excess light energy), in particular, through xanthophyll cycle. In the xanthophyll cycle, the xanthophyll violaxanthin is converted into xanthophylls antheraxanthin and zeaxanthin under strong light by violaxanthin deepoxidaze enzyme (Demmig-Adams and Adams 1994, 1996b, 2006). This process is activated by acidification of chloroplast lumen when photosynthetic electron transport exceeds the capacity for electron use in dark reactions of photosynthesis, and ultimately, zeaxanthin formation together with acidification result in thylakoid conformational changes that lead to enhanced non-radiative dissipation of excess light (Demmig-Adams and Adams 1994, 1996, b, 2006; Gilmore et al. 1994; Arnoux et al. 2009). The capacity for non-radiative energy dissipation depends on the pool size of xanthophyll cycle carotenoids, violaxanthin, antheraxanthin and zeaxanthin (VAZ) (Demmig-Adams and Adams 1996a; Demmig-Adams et al. 1998; Logan et al. 1996).

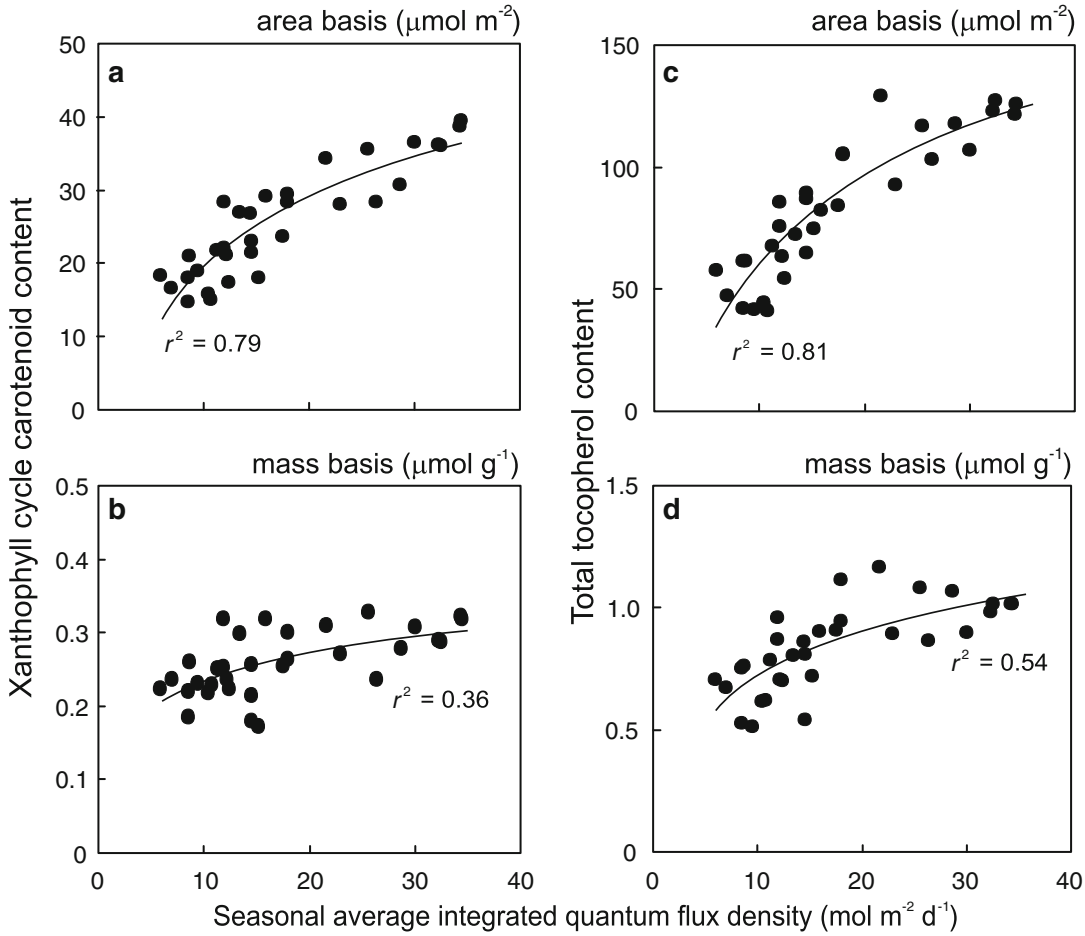

Fig. 4.8. Correlations of xanthophyll cycle carotenoids (VAZ) (**a**, **b**) and total tocopherol (**c**, **d**) contents per unit area (**a**, **c**) and dry mass (**b**, **d**) with seasonal average integrated incident quantum flux density (Q_{int}) in the canopy of the temperate deciduous tree *Populus tremula*. VAZ is the sum of contents of violaxanthin, antheraxanthin and zeaxanthin (Data of Niinemets et al. 2003), and total tocopherol content is the sum of contents of α-, β, δ- and γ-tocopherol (Data of García-Plazaola et al. 2004). Data were fitted by non-linear regressions as in Fig. 4.5 ($P < 0.001$ for all)

Acclimation to high irradiance typically results in increases in VAZ pool size (Fig. 4.8a, b; Demmig-Adams et al. 1999; Demmig-Adams and Adams 2006). The within-canopy range of variation in leaf area-based VAZ pool size is often three- to four-fold (Fig. 4.8a). Since VAZ content per unit dry mass also increases with increasing light availability (Fig. 4.8b), this increase does reflect greater VAZ content and higher capacity for safe dissipation of excess excitation energy of single mesophyll cells at higher light (e.g., Niinemets et al. 1998a, 2003). However, differently from foliage photosynthetic capacity and nitrogen allocation that are relatively invariable during growing season in temperate trees (Niinemets et al. 2004c; Grassi and Magnani 2005; Grassi et al. 2005), the adjustment in VAZ pool size to changed light conditions is much faster, occurring typically in a few days (Sect. IV.C). The pool sizes of other carotenoids, for example β-carotene and lutein pools, can also change along the light gradients, but the changes are typically only moderate compared with modifications in

VAZ. In fact, VAZ to carotenoid ratio also increases with increasing light availability in the canopy (e.g., Niinemets et al. 1998a, 1999a, 2003; Hansen et al. 2002).

Free non-protein-bound, VAZ, in particular zeaxanthin, has also been implicated in direct protection against photooxidative stress (Havaux and Niyogi 1999). In fact, plants have multiple antioxidant systems to cope with oxidative stress, including ascorbate and glutathione in leaf liquid phase and tocopherols in leaf lipid phase (Barclay et al. 1997; Noctor and Foyer 1998; Havaux and Niyogi 1999). In addition to VAZ, the contents of these specific liquid- and lipid-phase antioxidants increase with increasing light in the canopy (Garcia-Plazaola and Becerril 2001; Hansen et al. 2002, 2003; García-Plazaola et al. 2004). However, the within-canopy variation seems to be larger for liphophilic antioxidants than for water-soluble antioxidants (García-Plazaola et al. 2004). For instance, in *Populus tremula*, total tocopherol content per unit area varied more than three-fold within the canopy (Fig. 4.8c), while total ascorbate and glutathione contents per leaf area varied only ca. 1.5-fold within the canopy (García-Plazaola et al. 2004). In fact, the within-canopy variation of total tocopherol content per unit dry mass was more than two-fold (Fig. 4.8d), while no strong canopy gradient was evident for liquid-soluble antioxidants expressed on a dry mass basis (García-Plazaola et al. 2004).

Some of the lipid-phase antioxidant systems have been implicated in heat stress resistance as well. In particular, zeaxanthin has been demonstrated to play an important role in maintaining membrane integrity in heat-stressed leaves (Havaux et al. 1996; Havaux and Tardy 1997). Furthermore, constitutive isoprene emissions have been demonstrated to improve foliage heat stress resistance in isoprene-emitting species (Sharkey and Singsaas 1995; Singsaas et al. 1997). Improvement of heat resistance by isoprene has been suggested to be due to direct involvement of isoprene in stabilization of membranes at higher temperatures or/and due to antioxidative properties of isoprene that avoids peroxidation of membrane lipids in heat-stressed leaves (Sharkey et al. 2008; Vickers et al. 2009; Possell and Loreto 2013). Although isoprene is emitted constitutively only in a few emitting species (Kesselmeier and Staudt 1999; Fineschi et al. 2013), in the emitting species, there are extensive within-canopy gradients in isoprene emission rate (Harley et al. 1996, 1997; Funk et al. 2006; Niinemets et al. 2010). For example, in deciduous broad-leaved trees, the variation between canopy top and bottom was 27-fold for isoprene emission rate per leaf area (Fig. 4.9a) and 17-fold for isoprene emission rate per leaf dry mass (Fig. 4.9b). Furthermore, the fraction of photosynthetic carbon used for isoprene emission varied 12-fold (Fig. 4.9c), indicating that the plasticity in isoprene emission rate was more than a magnitude larger than the plasticity in net assimilation rate.

Taken together, the evidence summarized here demonstrates presence of major gradients in photoprotective pigment and antioxidant pools and isoprene emissions in plant canopies. These gradients in protective chemicals likely play key roles in coping with excess irradiance and recurrent heat stress events, whereas the protective capacity is particularly high at the top of plant canopies where the abiotic stress is often the greatest. Presence of such an extensive array of defenses plays a major role in preserving the integrity of foliage photosynthetic capacity through stress periods and allows for rapid onset of photosynthesis when the stress is relieved.

C. Dynamics in Protective Traits After Rapid Changes in Light Availability

As mentioned in Sect. IV.B, VAZ pool size adjusts to changes in light regime much faster than leaf structure, nitrogen content and allocation and photosynthetic capacity, although the rate of change in photosynthetic traits depends on plant growth form (Sect. III.C). In fact, it seems that the acclimation to potentially damaging high

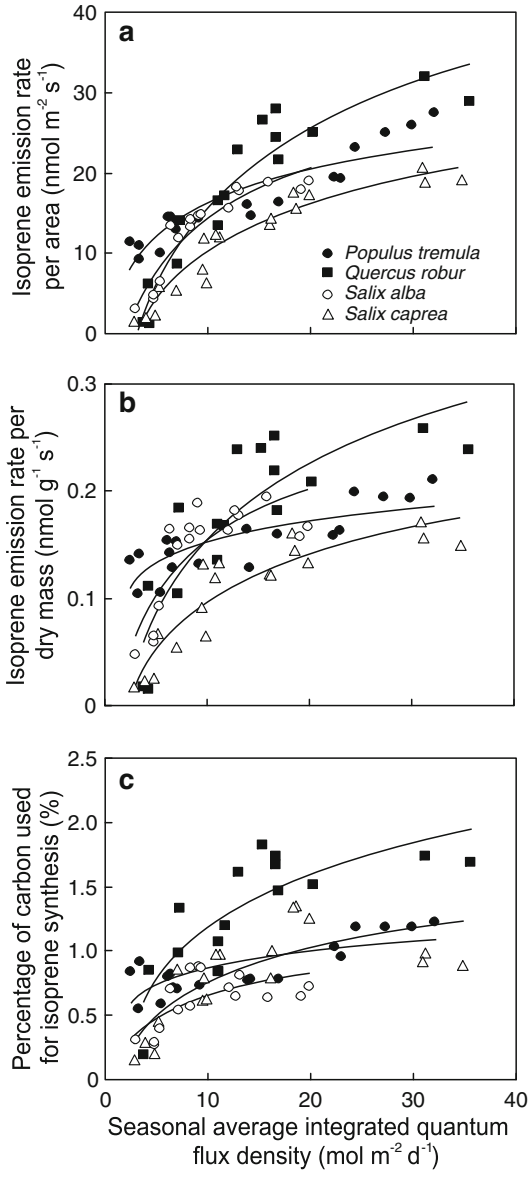

Fig. 4.9. Light-dependent variations in isoprene emission rate per unit leaf area (**a**) and dry mass (**b**) and the percentage of photosynthetic carbon used for isoprene emission (**c**) within the canopies of four temperate deciduous species. Data fitting as in Fig. 4.2 ($P < 0.001$ for all relationships). Measurements of isoprene emission and net assimilation rates were conducted at an ambient CO_2 concentration of 380 μmol mol^{-1}, light intensity of 1000 μmol m^{-2} s^{-1} and leaf temperature of 25 °C. Modified from Niinemets et al. (2010)

irradiances is governed by adjustments in foliar photosynthetic capacity in long-term, while the safe dissipation of excess light energy is accomplished by changes in xanthophyll cycle pool size during short-term weather fluctuations. However, as discussed in the Sect. III.C, acclimation to altered light conditions not always occurs, and either shading or exposure to excessive light can result in a continuous time-dependent decline in foliage photosynthetic rates and pigment contents, and ultimately leaf abscission.

Provided leaves do acclimate to the modified conditions, the key questions are what is the overall capacity for adjustment of VAZ content and antioxidant pools to changes in light conditions and whether the rate of acclimation varies within the canopy? Field data can to some extent be used to study the speed of xanthophyll cycle acclimation in ecosystems with significant day-to-day variations in quantum flux densities. For instance, in temperate humid forests, clear days are commonly intervened with overcast days such that day-to-day variation in above-canopy irradiance is several-fold (Niinemets et al. 2004c). Averaging quantum flux density over various number of days preceding measurement of physiological and chemical characteristics and using these various estimates of average integrated light can be used to test the strength of correlations of integrated light vs. leaf trait relationships in dependence on the length of light integration period (Ögren and Sjöström 1990; Niinemets et al. 1998a, 1999a; Geron et al. 2000; Werner et al. 2001b).

Using such an approach, it was observed that integrated light for 3 days preceding foliage sampling best explained the within-canopy variation in VAZ pool size in a temperate deciduous tree canopy (Niinemets et al. 1998a, 1999a). This result indicates that VAZ pool size can rapidly adjust to day-to-day variations in light conditions, thereby quickly regulating the capacity for non-photochemical quenching of excess

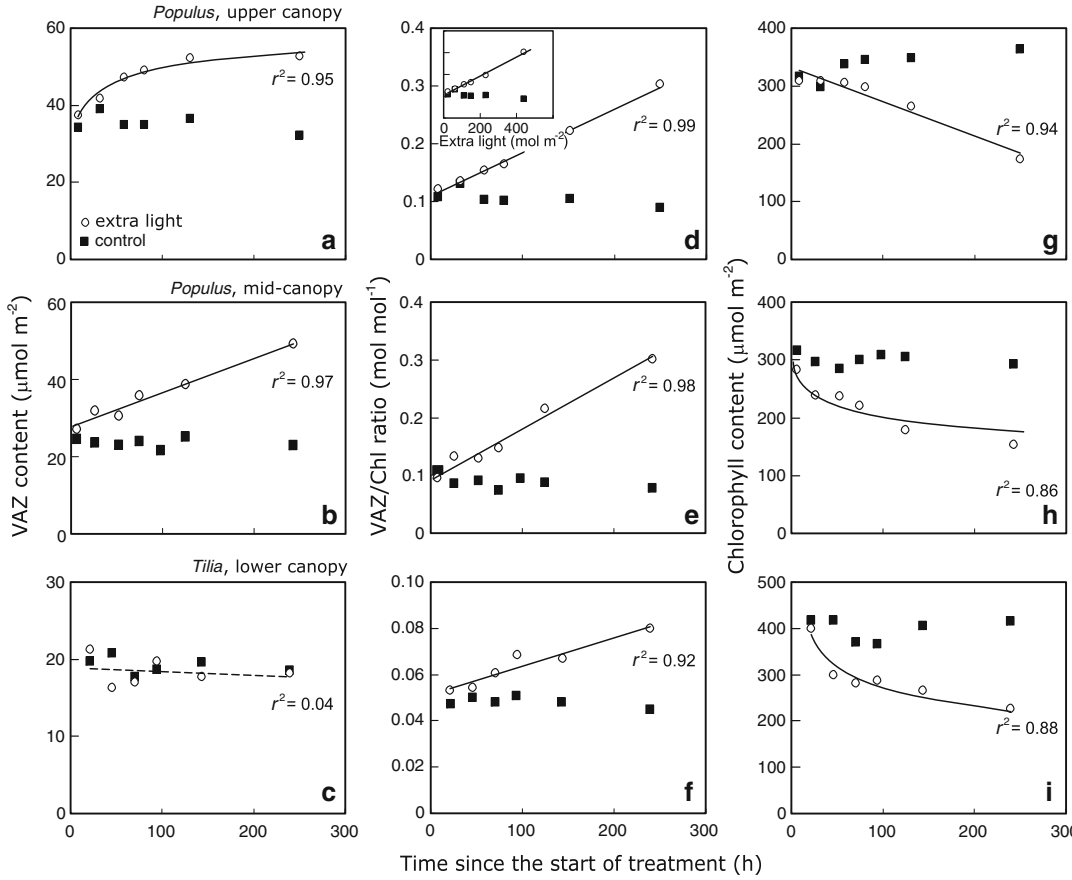

Fig. 4.10. Effects of illumination with extra light of ca. 40–50 mol m^{-2} d^{-1} upon foliage pigment contents at different positions in the tall tree canopy: time-dependent changes in xanthophyll cycle carotenoid (VAZ) content pear unit area (**a–c**), ratio of VAZ to chlorophyll (Chl) content (VAZ/Chl, **d–f**) and chlorophyll content (**g–i**) for representative control and illuminated leaves of temperate deciduous trees *Populus tremula* from the upper (**a, d, g**) and the mid-canopy (**b, e, h**) and *Tilia cordata* from the lower canopy (**c, f, i**). In addition, the inset in (**d**) demonstrates the variation in VAZ/Chl ratio in relation to cumulative extra irradiance in *P. tremula* (the control treatment corresponds to leaves without extra light sampled at the same time as the treated leaves). The data were fitted by non-linear (**a, h, i**) or linear (all others) regressions. The non-significant regression ($P > 0.8$) in (**c**) is drawn by a dashed line. In the upper-canopy leaves of *P. tremula* (height 23 m), the seasonal average natural integrated irradiance (Q_{int}) was 34.4 mol m^{-2} d^{-1} for both the control and the treated leaf, and the extra irradiance was 40.8 mol m^{-2} d^{-1}. In the mid-canopy leaves of *P. tremula* (height 19 m), Q_{int} was 22.5 mol m^{-2} d^{-1} for the control and 18 mol m^{-2} d^{-1} for the treated leaf, and the extra irradiance was 50.6 mol m^{-2} d^{-1}. In the lower canopy leaves of *T. cordata* (height 17 m), Q_{int} was 6.03 mol m^{-2} d^{-1} for the control and 6.10 mol m^{-2} d^{-1} for the treated leaf, and the extra irradiance of the illuminated leaf was 48.0 mol m^{-2} d^{-1}. Data of Niinemets et al. (2003)

light to match the changed light conditions. However, using illumination with extra light, it was further demonstrated that the degree of acclimation in VAZ pool size varies through the canopy and that there are different response kinetics in leaves developed at different light availabilities in the canopy (Niinemets et al. 2003). In particular, VAZ pool size was less responsive in the lower canopy species *Tilia cordata* than in the upper canopy species *Populus tremula*, and the initial increase in VAZ pool size tended to be faster in the upper canopy of *Populus tremula* (Fig. 4.10a–c). Furthermore, the ratio of VAZ to chlorophyll content was more responsive to extra illumination in the

upper canopy leaves in both species (Niinemets et al. 2003; Fig. 4.10d–f), reflecting within-canopy differences in the response of chlorophyll contents to extra illumination (Niinemets et al. 2003, Fig. 4.10g–i). Foliage tocopherol contents responded even stronger to extra illumination than leaf pigments, and the rate of increase of tocopherol content was greater in upper canopy leaves (García-Plazaola et al. 2004). These results together demonstrate that the overall degree of adjustment in pigment pools and foliage antioxidative capacity after light changes can importantly depend on leaf past acclimation status.

Although pigment and antioxidant pool sizes dynamically respond to variations in light input among days, the experiment with extra illumination in the canopies of deciduous trees demonstrated that full acclimation was not reached even after 11 days of exposure to extra light (Fig. 4.10). This delayed response is in agreement with several other experimental studies that have indicated that the response to stepwise increase in light in the field conditions may not even be fully completed in 17 days after start of exposure to enhanced illumination (Logan et al. 1998a, b). This differs from experiments in growth chambers under constant environmental conditions where changes in VAZ and antioxidant pools were completed in 5–7 days after stepwise increases in irradiance (Demmig-Adams et al. 1989; Bilger et al. 1995; Eskling and Åkerlund 1998). This suggests that in natural plant canopies under strongly fluctuating light, temperature and humidity conditions, pigment and antioxidant systems are inherently in non-steady-state conditions. Although pigment pools do rapidly adjust to environmental changes, the period of environmental fluctuations is often shorter than is needed to reach the steady-state pigment and antioxidant pool sizes. Furthermore, the rate of response to altered conditions significantly varies through the canopy, being likely an important factor determining leaf abiotic stress resistance in the canopy.

V. Photosynthetic Acclimation in Relation to Species Shade Tolerance

The term "economics spectrum" characterizes the covariation of foliage traits associated with superior performance in low resource environments such as structurally more robust foliage, and traits that improve fitness in high resource environments such as enhanced photosynthetic capacity (e.g., Wright et al. 2004, 2005). However, shading is associated both with reduced foliage robustness and reduced photosynthetic capacity, especially within single species, but also for several plant functional types (Lusk et al. 2008; Hallik et al. 2009b; Niinemets and Anten 2009). Thus, compared with other stresses, shading constitutes an outlying low resource environment. Here I analyzed within-canopy patterns in key foliage functional traits from the perspective of the leaf economics spectrum with main focus on Northern hemisphere temperate species.

A. Evidence from the Case Studies

Section III demonstrated that there are important differences in the within-canopy variations in different leaf traits among plant functional types and that these differences are associated with differences in leaf turnover. Apart from differences among plant functional types, plant stands are often composed of species with different ecological potentials. Characteristically, species in the lower canopy layers and in dense late-successional communities have greater shade tolerance than species in the upper canopy positions and in more open early-successional communities (Valladares and Niinemets 2008). Differences in community position among shade-tolerant and intolerant species are also associated with differences in leaf trait vs. Q_{int} relationships. In broad-leaved deciduous trees, M_A often responds less plastically to Q_{int} in more shade-tolerant than in less tolerant species (Fig. 4.11, Kull and Niinemets 1998; Niinemets et al. 1998b;

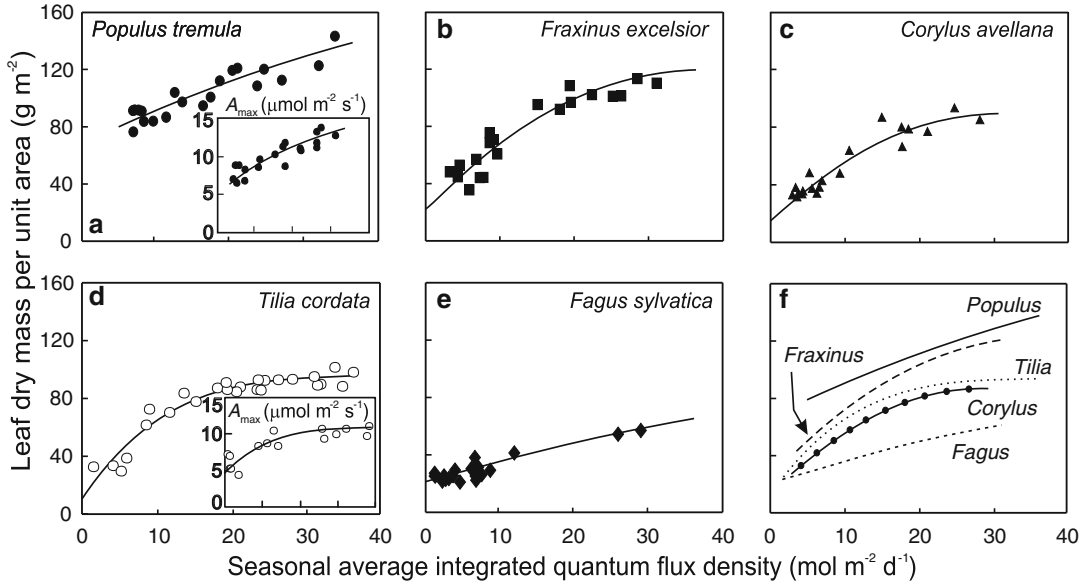

Fig. 4.11. Comparison of light-dependent variations in leaf dry mass per unit area within the canopies of five temperate deciduous woody species of contrasting shade tolerance. The insets demonstrate variations in leaf photosynthetic capacity with Q_{int}. Data fitting as in Fig. 4.5 (all relationships are significant at $P < 0.001$). Species are ranked according to shade tolerance score (SC, Niinemets and Valladares 2006) from the least tolerant to the most tolerant as: *Populus tremula* (SC = 2.3), *Fraxinus excelsior* (2.9), *Corylus avellana* (3.5), *Tilia cordata* (4.2) and *Fagus sylvatica* (4.6). Shade tolerance score is a relative measure varying from 1 (least tolerant) to 5 (most tolerant) that characterizes species capacity to endure shade relative to other species (Niinemets and Valladares 2006 for a detailed definition; Valladares and Niinemets 2008. Data for *Fagus sylvatica* are from Niinemets (1995) and for the four other species from Niinemets et al. (1998b)

Valladares and Niinemets 2008). However, such a pattern is not always observed (e.g., very intolerant *Populus tremula* in Fig. 4.11a vs. very tolerant *Fagus sylvatica* in Fig. 4.11e). Although shade-intolerant species can maintain leaves at low light availabilities when grown in monocultures (Nygren and Kellomäki 1983; Niinemets et al. 2004a), the situation is different in multispecies canopies where shade-tolerant species gradually grow into the upper canopy, and the foliage of intolerant species competes for light availability with foliage of tolerant species in the lower and mid-canopy. Thus, the apparent low plasticity in *P. tremula* in Fig. 4.11a might reflect the general circumstance that in multispecies canopies intermixed with shade-tolerant species, the intolerant species may not simply be able to maintain leaves below a certain Q_{int} value (ca. 7–8 mol m^{-2} d^{-1} for *P. tremula* in Fig. 4.11a).

As in broad-leaved deciduous woody species, within-canopy plasticity in foliage photosynthetic potentials is mainly driven by changes in M_A that result in stacking of rate-limiting photosynthetic proteins per unit leaf area (Sect. III.C), lower within-canopy plasticity in M_A is also associated with lower photosynthetic plasticity in less shade-tolerant species (Kull and Niinemets 1998; Niinemets et al. 1998b). It has further been demonstrated that the sensitivity to photoinhibition is greater in more shade-tolerant species (Lovelock et al. 1994; Chazdon et al. 1996; Naidu and DeLucia 1997) that also generally possess lower photosynthetic capacities (Bazzaz 1979; Lovelock et al. 1994).

On the other hand, shade-tolerant temperate species can support foliage at lower Q_{int} than intolerant species and have both smaller minimum and maximum M_A values (Fig. 4.11). Thus, despite lower

photosynthetic plasticity, shade-tolerant species can form a greater leaf area with given foliage biomass in leaves, improving light interception of the canopy. Such a greater light interception capacity not only improves the whole canopy carbon gain, but the shading by more extensive canopy itself can serve as an important competitive attribute constraining the survival of seedlings and saplings of less shade-tolerant competitors and ultimately leading to dominance of shade-tolerant late-successional plants in the canopy (Küppers 1985; Schieving and Poorter 1999; Anten 2002).

Much less data are available for within-canopy gradients in tropical and southern hemisphere temperate evergreen species. In three tropical species, within-canopy plasticity in M_A, N_A and ${A_{max}}^A$ was greater in shade-intolerant evergreen species *Ficus insipida* than in more tolerant *Luehea seemannii*, whereas the highest plasticity was observed in the shade-intolerant drought-deciduous species *Castilla elastica* (Posada et al. 2009). Among the tropical *Piper* species of varying shade tolerance, the within-canopy plasticity in M_A, N_A and ${A_{max}}^A$ of shade tolerant *P. aequale* and *P. lapathifolium* was less than in moderately tolerant *P. hispidum* and intolerant *P. auritum* and *P. umbellatum* (Chazdon and Field 1987). Among southern hemisphere temperate evergreen *Nothofagus* species, more shade tolerant *Nothofagus solandri* var. *cliffortoides* had a greater within-canopy plasticity in M_A than less tolerant *N. fusca*, but the plasticity in N_A did not differ among species (Niinemets et al. 2004b). In another study in temperate southern hemisphere evergreens, more tolerant *Nothofagus solandri* var. *cliffortoides* had a greater plasticity in M_A than very intolerant species *Kunzea ericoides* (White and Scott 2006). However, in this study, other moderately shade-tolerant species had a similar within-canopy plasticity in M_A as the very intolerant *K. ericoides* (White and Scott 2006). Clearly more comparative studies are needed to gain conclusive insight into the controls of foliage plasticity by shade tolerance in tropics and in southern hemisphere temperate ecosystems.

B. Generalizing the Patterns

The conclusions drawn from the case studies in temperate deciduous broad-leaved species seem to be valid more widely. Broad-scale analyses of structural, chemical and physiological variation in high-light-developed leaves across Northern hemisphere temperate woody flora indicate that M_A decreases with increasing species shade-tolerance also in broad-leaved and needle-leaved evergreen species (Fig. 4.12a). Thus, formation of an extensive leaf area is also the key competitive strategy in shade-tolerant evergreen species (Niinemets 2010; Warren et al. 2012). However, in temperate evergreens, greater canopy leaf area in more tolerant species is also importantly driven by enhanced leaf longevity (Hallik et al. 2009b; Niinemets 2010).

Differently from M_A, nitrogen content per unit area (Fig. 4.12b) and photosynthetic capacity per unit area (Fig. 4.12c) were not correlated with species shade tolerance in temperate evergreens. However, the patterns developed for leaves exposed to high light do not necessarily provide insight into variations in within-canopy plasticity in foliage structure and photosynthetic potentials. Given the higher leaf longevity in shade-tolerant species and reduction in leaf-level plasticity with leaf age (Fig. 4.4), canopy-level photosynthetic plasticity across leaves of different age might be lower in more shade-tolerant species.

Differently from Northern hemisphere temperate species, M_A of tropical evergreens and southern hemisphere temperate evergreens is typically higher in more shade tolerant species than in less tolerant species (Chazdon 1992; Kitajima 1994; Lusk 2004; Lusk et al. 2008; Houter and Pons 2012). Thus, higher biomass investment is needed for a given plastic change in M_A in more shade tolerant species, implying that the high initial M_A may limit both structural and photosynthetic plasticity in shade tolerators. Further studies are needed to generalize within-canopy plastic changes in evergreens of different shade tolerance in both temperate and tropical ecosystems.

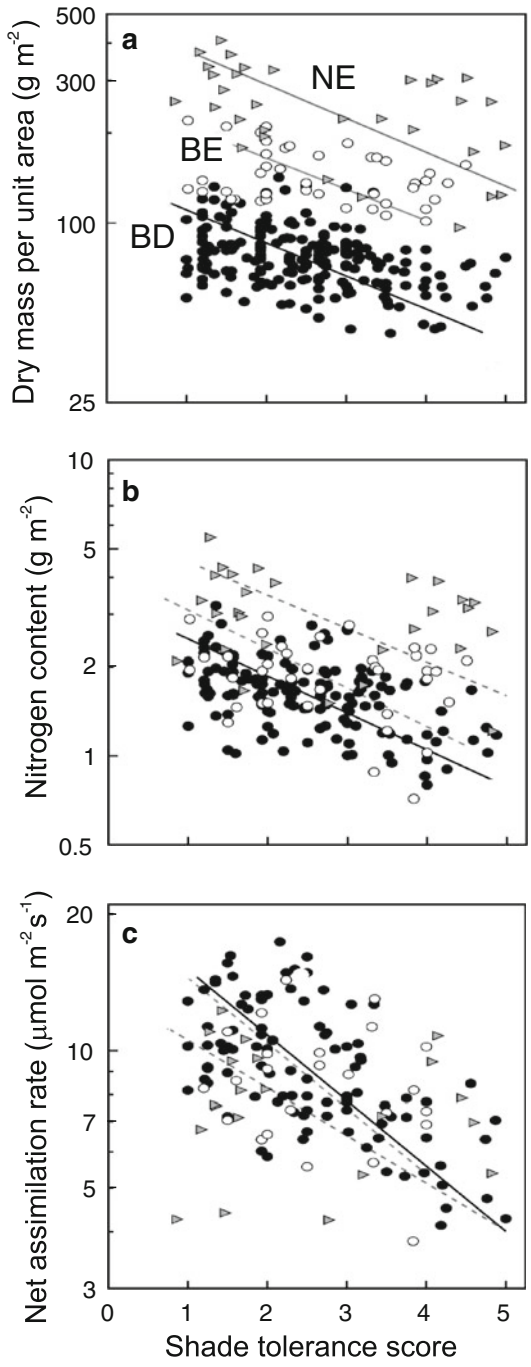

Fig. 4.12. Correlations of leaf dry mass per unit area (**a**), nitrogen content per unit area (**b**) and light-saturated net assimilation rate per unit area (photosynthetic capacity, (**c**) with species shade tolerance score in Northern hemisphere broad-leaved deciduous (BD), broad-leaved evergreen (BE) and needle-leaved evergreen (NE) trees and shrubs (n = 341, modified from Hallik et al. 2009b). Species shade tolerance score defined as in Fig. 4.11. Data were fitted by standardized major axis regressions using SMATR 2.0 (Warton et al. 2006) and non-significant regressions ($P > 0.05$) are shown by *dashed lines*

VI. Conclusions

This review highlights major within-canopy modifications in foliage photosynthetic capacity that improve the whole canopy carbon gain compared with a hypothetical canopy with constant photosynthetic capacity for all leaves in the canopy. While scaling of photosynthetic capacity with long-term average integrated quantum flux density is a ubiquitous response in plants, there are important plant functional type differences in the scaling of key foliage functional traits with light availability. The rate of foliage turnover increases in the sequence evergreens < deciduous woody species with deterministic growth < deciduous woody species with indeterminate growth < herbaceous species. The evidence summarized here indicates that plant functional type differences in canopy growth phenology and differences in leaf turnover importantly alter the significance of various leaf traits in determining the within-canopy acclimation of foliage photosynthetic capacity.

This chapter also emphasizes that environmental gradients are typically complex in plant canopies. Leaves at the top of plant canopies often can suffer from more sever water, photoinhibition and oxidative stresses that can constrain photosynthetic acclimation to canopy light regime. Furthermore, coping with such interacting stresses typically leads to structural adaptations reducing excess light interception in the upper canopy, and chemical modifications improving the stress resistance. In fact, within-canopy variations in protective traits can be much larger than in photosynthetic characteristics, and there are further significant within-canopy variations in the degree and rate of adjustment of the pools of protective chemicals to dynamically changing light conditions.

There is still a limited understanding of species differences in foliage plasticity to within-canopy environmental gradients, but the evidence summarized suggests that shade tolerance is an important driver of species plasticity. Shade-tolerant species growing in understory and in late-successional communities characteristically form a greater foliage area and have superior light harvesting capacity, but their photosynthetic capacity and plasticity seem to be lower than in less tolerant species growing in more open communities and in early-successional habitats where rapid carbon gain capacity is the primary attribute of competition. Further studies are needed to gain insight into the generality of suggested variation patterns of foliage plasticity with species ecological potentials. Understanding such plastic variations is not only fundamentally important, but would allow construction of more realistic carbon gain models capable of simulating ecosystem carbon gain through ecosystem development.

Acknowledgements

I thank Drs. Thijs Pons and Kouki Hikosaka for insightful comments on the manuscript. Author's work on plant acclimation has been financially supported by the Estonian Ministry of Science and Education (institutional grant IUT-8-3) and the European Commission through the European Regional Fund (the Center of Excellence in Environmental Adaptation).

References

Aasamaa K, Sõber A, Hartung W, Niinemets Ü (2004) Drought acclimation of two deciduous tree species of different layers in a temperate forest canopy. Trees 18:93–101

Ackerly DD, Bazzaz FA (1995) Leaf dynamics, self-shading and carbon gain in seedlings of a tropical pioneer tree. Oecologia 101:289–298

Anderson MC (1964) Studies of the woodland light climate. I. The photographic computation of light conditions. J Ecol 52:27–41

Anten NPR (1997) Modelling canopy photosynthesis using parameters determined from simple non-destructive measurements. Ecol Res 12:77–88

Anten NPR (2002) Evolutionarily stable leaf area production in plant populations. J Theor Biol 217:15–32

Anten NPR (2005) Optimal photosynthetic characteristics of individual plants in vegetation stands and implications for species coexistence. Ann Bot 95:495–506

Anten NPR (2016) Optimization and game theory in canopy models. In: Hikosaka K, Niinemets Ü, Anten N (eds) Canopy Photosynthesis: From Basics to Applications. Springer, Berlin, pp 355–377

Anten NPR, Schieving F, Medina E, Werger MJA, Schuffelen P (1995a) Optimal leaf area indices in C_3 and C_4 mono- and dicotyledonous species at low and high nitrogen availability. Physiol Plant 95:541–550

Anten NPR, Schieving F, Werger MJA (1995b) Patterns of light and nitrogen distribution in relation to whole canopy carbon gain in C_3 and C_4 mono- and dicotyledonous species. Oecologia 101:504–513

Anten NPR, Hernandez R, Medina EM (1996) The photosynthetic capacity and leaf nitrogen concentration as related to light regime in shade leaves of a montane tropical forest tree, *Tetrorchidium rubrivenium*. Funct Ecol 10:491–500

Anten NPR, Miyazawa K, Hikosaka K, Nagashima H, Hirose T (1998) Leaf nitrogen distribution in relation to leaf age and photon flux density in dominant and subordinate plants in dense stands of a dicotyledonous herb. Oecologia 113:314–324

Aranda I, Pardo F, Gil L, Pardos JA (2004) Anatomical basis of the change in leaf mass per area and nitrogen investment with relative irradiance within the canopy of eight temperate tree species. Acta Oecol 25:187–195

Arnoux P, Morosinotto T, Saga G, Bassi R, Pignola D (2009) A structural basis for the pH-dependent xanthophyll cycle in *Arabidopsis thaliana*. Plant Cell 21:2036–2044

Aussenac G (1973) Effets de conditions microclimatiques différentes sur la morphologie et la structure anatomique des aiguilles de quelques résineux. (Effect of some different microclimatic conditions

on morphology and anatomic structure of needles). Ann Sci For 30:375–392

Barclay LRC, Antunes F, Egawa Y, McAllister KL, Mukai K, Nishi T, Vinqvist MR (1997) The efficiency of antioxidants delivered by liposomal transfer. Biochimica et Biophysica Acta - Biomembranes 1328:1–12

Bassi R, Caffarri S (2000) Lhc proteins and the regulation of photosynthetic light harvesting function by xanthophylls. Photosynth Res 64:243–256

Bazzaz FA (1979) The physiological ecology of plant succession. Annu Rev Ecol Syst 10:351–371

Bilger W, Fisahn J, Brummet W, Kossmann J, Willmitzer L (1995) Violaxanthin cycle pigment contents in potato and tobacco plants with genetically reduced photosynthetic capacity. Plant Physiol 108:1479–1486

Bond BJ, Farnsworth BT, Coulombe RA, Winner WE (1999) Foliage physiology and biochemistry in response to light gradients in conifers with varying shade tolerance. Oecologia 120:183–192

Boonman A, Anten NPR, Dueck TA, Jordi WJRM, van der Werf A, Voesenek LACJ, Pons TL (2006) Functional significance of shade-induced leaf senescence in dense canopies: an experimental test using transgenic tobacco. Am Nat 168:597–607

Brodribb TJ, Holbrook NM, Zwieniecki MA, Palma B (2005) Leaf hydraulic capacity in ferns, conifers and angiosperms: impacts on photosynthetic maxima. New Phytol 165:839–846

Brooks JR, Hinckley TM, Sprugel DG (1994) Acclimation responses of mature *Abies amabilis* sun foliage to shading. Oecologia 100:316–324

Brooks JR, Sprugel DG, Hinckley TM (1996) The effects of light acclimation during and after foliage expansion on photosynthesis of *Abies amabilis* foliage within the canopy. Oecologia 107:21–32

Buckley TN, Farquhar GD, Miller JM (2002) The mathematics of linked optimisation for water and nitrogen use in a canopy. Silva Fenn 36:639–669

Burkey KO, Wells R (1991) Response of soybean photosynthesis and chloroplast membrane function to canopy development and mutual shading. Plant Physiol 97:245–252

Cano FJ, Sánchez-Gómez D, Rodríguez-Calcerrada J, Warren CR, Gil L, Aranda I (2013) Effects of drought on mesophyll conductance and photosynthetic limitations at different tree canopy layers. Plant Cell Environ 36:1961–1980

Cartechini A, Palliotti A (1995) Effect of shading on vine morphology and productivity and leaf gas exchange characteristics in grapevines in the field. Am J Enol Vitic 46:227–234

Cescatti A, Niinemets Ü (2004) Sunlight capture. Leaf to landscape. In: Smith WK (ed) Photosynthetic Adaptation. Chloroplast to Landscape. Springer, Berlin, pp 42–85

Cescatti A, Zorer R (2003) Structural acclimation and radiation regime of silver fir (*Abies alba* Mill.) shoots along a light gradient. Plant Cell Environ 26:429–442

Chazdon RL (1992) Photosynthetic plasticity of two rain forest shrubs across natural gap transects. Oecologia 92:586–595

Chazdon RL, Field CB (1987) Determinants of photosynthetic capacity in six rainforest *Piper* species. Oecologia 73:222–230

Chazdon RL, Pearcy RW, Lee DW, Fetcher N (1996) Photosynthetic responses of tropical forest plants to contrasting light environments. In: Mulkey SR (ed) Tropical Forest Plant Ecophysiology. Chapman & Hall, New York, pp 5–55

Chiariello N (1984) Leaf energy balance in the wet lowland tropics. In: Medina E (ed) Physiological Ecology of Plants of the Wet Tropics Proceedings of an International Symposium Held in Oxatepec and Los Tuxtlas, Mexico, June 29 to July 6, 1983. Dr. W. Junk Publishers, The Hague, pp 85–98

Davi H, Barbaroux C, Dufrêne E, François C, Montpied P, Bréda N, Badeck F (2008) Modelling leaf mass per area in forest canopy as affected by prevailing radiation conditions. Ecol Model 211:339–349

Demmig-Adams B, Adams WW III (1994) Light stress and photoprotection related to the xanthophyll cycle. In: Foyer CH, Mullineaux PM (eds) Causes of Photooxidative Stress and Amelioration of Defense Systems in Plants. CRC Press, Boca Raton, pp 105–126

Demmig-Adams B, Adams WW (1996a) Chlorophyll and carotenoid composition in leaves of *Euonymus kiautschovicus* acclimated to different degrees of light stress in the field. Aust J Plant Physiol 23:649–659

Demmig-Adams B, Adams WW III (1996b) Xanthophyll cycle and light stress in nature: uniform response to excess direct sunlight among higher plant species. Planta 198:460–470

Demmig-Adams B, Adams WW III (2006) Photoprotection in an ecological context: the remarkable complexity of thermal energy dissipation: Tansley review. New Phytol 172:11–21

Demmig-Adams B, Winter K, Winkelmann E, Krüger A, Czygan FC (1989) Photosynthetic characteristics and the ratios of chlorophyll, ß-carotene, and the components of the xanthophyll cycle upon a sudden

increase in growth light regime in several plant species. Bot Acta 102:319–325

Demmig-Adams B, Moeller DL, Logan BA, Adams WW III (1998) Positive correlation between levels of retained zeaxanthin + antheraxanthin and degree of photoinhibition in shade leaves of *Schefflera arboricola* (Hayata) Merrill. Planta 205:367–374

Demmig-Adams B, Adams WW, Ebbert V, Logan BA (1999) Ecophysiology of the xanthophyll cycle. In: Photochemistry of Carotenoids. Kluwer Academic Publishers, Dordrecht, pp 245–269

Dewar RC, Tarvainen L, Parker K, Wallin G, McMurtrie RE (2012) Why does leaf nitrogen decline within tree canopies less rapidly than light? An explanation from optimization subject to a lower bound on leaf mass per area. Tree Physiol 32:520–534

Disney M (2016) Remote sensing of vegetation: potentials, limitations, developments and applications. In: Hikosaka K, Niinemets Ü, Anten N (eds) Canopy Photosynthesis: From Basics to Applications. Springer, Berlin, pp 289–331

Ducrey M (1981) Étude bioclimatique d'une futaie feuillue (*Fagus silvatica* L. et *Quercus sessiliflora* Salisb.) de l'Est de la France. III. Potentialités photosynthétiques des feuilles à différentes hauteurs dans le peuplement. (Bioclimatological studies in a broad leaf high stand (*Fagus silvatica* L. and *Quercus sessiliflora* Salisb.). III. Photosynthetic rates of leaves from various levels in the stand). Ann Sci For 38:71–86

During H (1999) High light and water stress in grapevines: photoinhibition and photoprotection. In: Proceedings of the First ISHS Workshop on Water Relations of Grapevines. International Society of Horticultural Science, Louvain, pp 45–54

Eckardt F, Heim G, Methy M, Sauvezon R (1975) Interception de l'énergie rayonnante échanges gazeux et croissance dans une forèt méditerranéenne à feuillage persistant (*Quercetum ilicis*). Photosynthetica 9:145–156

Ehleringer J, Björkman O (1977) Quantum yields for CO_2 uptake in C_3 and C_4 plants. Dependence on temperature, CO_2 and O_2 concentration. Plant Physiol 59:86–90

Ehleringer JR, Björkman O (1978) Pubescence and leaf spectral characteristics in a desert shrub, *Encelia farinosa*. Oecologia 36:151–162

Ellsworth DS, Reich PB (1993) Canopy structure and vertical patterns of photosynthesis and related leaf traits in a deciduous forest. Oecologia 96:169–178

Escudero A, Mediavilla S (2003) Decline in photosynthetic nitrogen use efficiency with leaf age and nitrogen resorption as determinants of leaf life span. J Ecol 91:880–889

Eskling M, Åkerlund H-E (1998) Changes in the quantities of violaxanthin de-epoxidase, xanthophylls and ascorbate in spinach upon shift from low to high light. Photosynth Res 57:41–50

Evans JR (1993a) Photosynthetic acclimation and nitrogen partitioning within a lucerne canopy. II. Stability through time and comparison with a theoretical optimum. Aust J Plant Physiol 20:69–82

Evans JR (1993b) Photosynthetic acclimation and nitrogen partitioning within a lucerne canopy. I. Canopy characteristics. Aust J Plant Physiol 20:55–67

Evans JR, Poorter H (2001) Photosynthetic acclimation of plants to growth irradiance: the relative importance of specific leaf area and nitrogen partitioning in maximizing carbon gain. Plant Cell Environ 24:755–767

Ewers FW (1982) Secondary growth in needle leaves of *Pinus longaeva* (bristlecone pine) and other conifers: quantitative data. Am J Bot 69:1552–1559

Ewers FW, Schmid R (1981) Longevity of needle fascicles of *Pinus longaeva* (bristlecone pine) and other North American pines. Oecologia 51:107–115

Ewers BE, Oren R, Kim H-S, Bohrer G, Lai C-T (2007) Effects of hydraulic architecture and spatial variation in light on mean stomatal conductance of tree branches and crowns. Plant Cell Environ 30:483–496

Farquhar GD (1989) Models of integrated photosynthesis of cells and leaves. Philos Trans R Soc Lond Ser B-Biol Sci 323:357–367

Farquhar GD, von Caemmerer S, Berry JA (1980) A biochemical model of photosynthetic CO_2 assimilation in leaves of C_3 species. Planta 149:78–90

Farquhar GD, Buckley TN, Miller JM (2002) Optimal stomatal control in relation to leaf area and nitrogen content. Silva Fenn 36:625–637

Field C (1983) Allocating leaf nitrogen for the maximization of carbon gain: leaf age as a control on the allocation program. Oecologia 56:341–347

Fineschi S, Loreto F, Staudt M, Peñuelas J (2013) Diversification of volatile isoprenoid emissions from trees: evolutionary and ecological perspectives In: Niinemets Ü and Monson RK (eds) Biology, Controls and Models of Tree Volatile Organic Compound Emissions. Springer, Berlin, pp 1–20

Fleck S, Niinemets Ü, Cescatti A, Tenhunen JD (2003) Three-dimensional lamina architecture alters light harvesting efficiency in *Fagus*: a leaf-scale analysis. Tree Physiol 23:577–589

Flexas J, Barbour MM, Brendel O, Cabrera HM, Carriquí M, Diaz-Espejo A, Douthe C, . . ., Warren CR (2012) Mesophyll diffusion conductance to

CO_2: an unappreciated central player in photosynthesis. Plant Sci 193–194:70–84

Franklin O, Ågren GI (2002) Leaf senescence and resorption as mechanisms of maximizing photosynthetic production during canopy development at N limitation. Funct Ecol 16:727–733

Funk JL, Giardina CP, Knohl A, Lerdau MT (2006) Influence of nutrient availability, stand age, and canopy structure on isoprene flux in a *Eucalyptus saligna* experimental forest. J Geophys Res Biogeosci 111: G02012

Garcia-Plazaola JI, Becerril JM (2001) Seasonal changes in photosynthetic pigments and antioxidants in beech (*Fagus sylvatica*) in a Mediterranean climate: implications for tree decline diagnosis. Aust J Plant Physiol 28:225–232

García-Plazaola JI, Becerril JM, Hernández A, Niinemets Ü, Kollist H (2004) Acclimation of antioxidant pools to the light environment in a natural forest canopy. New Phytol 163:87–97

Geron C, Guenther A, Sharkey T, Arnts RR (2000) Temporal variability in basal isoprene emission factor. Tree Physiol 20:799–805

Gilmore AM, Mohanty N, Yamamoto HY (1994) Epoxidation of zeaxanthin and antheraxanthin reverses non-photochemical quenching of photosystem II chlorophyll *a* fluorescence in the presence of trans-thylakoid deltapH. FEBS Lett 350:271–274

Gilmore DW, Seymour RS, Halteman WA, Greenwood MS (1995) Canopy dynamics and the morphological development of *Abies balsamea*: effects of foliage age on specific leaf area and secondary vascular development. Tree Physiol 15:47–55

Goudriaan J (2016) Light distribution. In: Hikosaka K, Niinemets Ü, Anten N (eds) Canopy Photosynthesis: From Basics to Applications. Springer, Berlin, pp 3–22

Grassi G, Magnani F (2005) Stomatal, mesophyll conductance and biochemical limitations to photosynthesis as affected by drought and leaf ontogeny in ash and oak trees. Plant Cell Environ 28:834–849

Grassi G, Vicinelli E, Ponti F, Cantoni L, Magnani F (2005) Seasonal and interannual variability of photosynthetic capacity in relation to leaf nitrogen in a deciduous forest plantation in northern Italy. Tree Physiol 25:349–360

Gratani L (1993) Response to microclimate of morphological leaf attributes, photosynthetic and water relations of evergreen sclerophyllous shrub species. Photosynthetica 29:573–582

Gratani L (1997) Canopy structure, vertical radiation profile and photosynthetic function in a *Quercus ilex* evergreen forest. Photosynthetica 33:139–149

Gratani L, Fiorentino E (1986) Relationship between chlorophyll content and leaf biomass for *Quercus ilex* in a Mediterranean maquis stand. Photosynthetica 20:267–273

Gratani L, Fiorentino E, Kubová A, Marzi P (1989) Effect of microclimate on ecophysiological features of some sclerophyllous species. Photosynthetica 23:230–233

Gratani L, Marzi P, Crescente MF (1992) Morphological adaptions of *Quercus ilex* leaves in the Castelporziano forest. Vegetatio 100:155–161

Gutschick VP, Wiegel FW (1988) Optimizing the canopy photosynthetic rate by patterns of investment in specific leaf mass. Am Nat 132:67–86

Hallik L, Kull O, Niinemets Ü, Aan A (2009a) Contrasting correlation networks between leaf structure, nitrogen and chlorophyll in herbaceous and woody canopies. Basic Appl Ecol 10:309–318

Hallik L, Niinemets Ü, Wright IJ (2009b) Are species shade and drought tolerance reflected in leaf-level structural and functional differentiation in Northern Hemisphere temperate woody flora? New Phytol 184:257–274

Han Q, Kawasaki T, Katahata S, Mukai Y, Chiba Y (2003) Horizontal and vertical variations in photosynthetic capacity in a *Pinus densiflora* crown in relation to leaf nitrogen allocation and acclimation to irradiance. Tree Physiol 23:851–857

Han Q, Kawasaki T, Nakano T, Chiba Y (2004) Spatial and seasonal variability of temperature responses of biochemical photosynthesis parameters and leaf nitrogen content within a *Pinus densiflora* crown. Tree Physiol 25:737–744

Han Q, Araki M, Chiba Y (2006) Acclimation to irradiance of leaf photosynthesis and associated nitrogen reallocation in photosynthetic apparatus in the year following thinning of a young stand of *Chamaecyparis obtusa*. Photosynthetica 44:523–529

Hansen U, Fiedler B, Rank B (2002) Variation of pigment composition and antioxidative systems along the canopy light gradient in a mixed beech/oak forest: a comparative study on deciduous tree species differing in shade tolerance. Trees 16:354–364

Hansen U, Schneiderheinze J, Stadelmann S, Rank B (2003) The α-tocopherol content of leaves of pedunculate oak (*Quercus robur* L.) – variation over the growing season and along the vertical light gradient in the canopy. J Plant Physiol 160:91–96

Harley P, Guenther A, Zimmerman P (1996) Effects of light, temperature and canopy position on net photosynthesis and isoprene emission from sweetgum (*Liquidambar styraciflua*) leaves. Tree Physiol 16:25–32

Harley P, Guenther A, Zimmerman P (1997) Environmental controls over isoprene emission in deciduous oak canopies. Tree Physiol 17:705–714

Havaux M, Niyogi KK (1999) The violaxanthin cycle protects plants from photooxidative damage by more than one mechanism. Proc Natl Acad Sci U S A 96:8762–8767

Havaux M, Tardy F (1997) Photoacoustically monitored thermal energy dissipation and xanthophyll cycle carotenoids in higher plant leaves. J Photochem Photobiol B: Biol 40:68–75

Havaux M, Tardy F, Ravenel J, Chanu D, Parot P (1996) Thylakoid membrane stability to heat stress studied by flash spectroscopic measurements of the electrochromic shift in intact potato leaves: influence of the xanthophyll content. Plant Cell Environ 19:1359–1368

Hikosaka K (1996) Effects of leaf age, nitrogen nutrition and photon flux density on the organization of the photosynthetic apparatus in leaves of a vine (*Ipomoea tricolor* Cav.) grown horizontally to avoid mutual shading of leaves. Planta 198:144–150

Hikosaka K (2014) Optimal nitrogen distribution within a leaf canopy under direct and diffuse light. Plant Cell Environ 37:2077–2085

Hikosaka K, Hirose T (1997) Leaf angle as a strategy for light competition: optimal and evolutionary stable light extinction coefficient within a leaf canopy. Écoscience 4:501–507

Hikosaka K, Terashima I (1995) A model of the acclimation of photosynthesis in the leaves of C_3 plants to sun and shade with respect to nitrogen use. Plant Cell Environ 18:605–618

Hikosaka K, Terashima I (1996) Nitrogen partitioning among photosynthetic components and its consequence in sun and shade plants. Funct Ecol 10:335–343

Hikosaka K, Terashima I, Katoh S (1994) Effects of leaf age, nitrogen nutrition and photon flux density on the distribution of nitrogen among leaves of a vine (*Ipomoea tricolor* Cav.) grown horizontally to avoid mutual shading of leaves. Oecologia 97:451–457

Hikosaka K, Hanba YT, Hirose T, Terashima I (1998) Photosynthetic nitrogen-use efficiency in leaves of woody and herbaceous species. Funct Ecol 12:896–905

Hikosaka K, Noguchi K, Terashima I (2016a) Modeling leaf gas exchange. In: Hikosaka K, Niinemets Ü, Anten N (eds) Canopy Photosynthesis: From Basics to Applications. Springer, Berlin, pp 61–100

Hikosaka K, Kumagai T, Ito A (2016b) Modeling canopy photosynthesis. In: Hikosaka K, Niinemets Ü, Anten N (eds) Canopy Photosynthesis: From Basics to Applications. Springer, Berlin, pp 239–268

Hirose T, Bazzaz FA (1998) Trade-off between light- and nitrogen-use efficiency in canopy photosynthesis. Ann Bot 82:195–202

Hirose T, Werger MJA (1987a) Nitrogen use efficiency in istantaneous and daily photosynthesis of leaves in the canopy of a *Solidago altissima* stand. Physiol Plant 70:215–222

Hirose T, Werger MJA (1987b) Maximizing daily canopy photosynthesis with respect to the leaf nitrogen allocation pattern in the canopy. Oecologia 72:520–526

Hirose T, Werger MJA (1994) Photosynthetic capacity and nitrogen partitioning among species in the canopy of a herbaceous plant community. Oecologia 100:203–212

Hirose T, Werger MJA (1995) Canopy structure and photon flux partitioning among species in a herbaceous plant community. Ecology 76:466–474

Hirose T, Werger MJA, Pons TL, van Rheenen JWA (1988) Canopy structure and leaf nitrogen distribution in a stand of *Lysimachia vulgaris* L. as influenced by stand density. Oecologia 77:145–150

Hirose T, Werger MJA, van Rheenen JWA (1989) Canopy development and leaf nitrogen distribution in a stand of *Carex acutiformis*. Ecology 70:1610–1618

Houter NC, Pons TL (2012) Ontogenetic changes in leaf traits of tropical rainforest trees differing in juvenile light requirement. Oecologia 169:33–45

Hubbard RM, Bond BJ, Senock RS, Ryan MG (2002) Effects of branch height on leaf gas exchange, branch hydraulic conductance and branch sap flux in open-grown ponderosa pine. Tree Physiol 22:575–581

Iio A, Fukasawa H, Nose Y, Kato S, Kakubari Y (2005) Vertical, horizontal and azimuthal variations in leaf photosynthetic characteristics within a *Fagus crenata* crown in relation to light acclimation. Tree Physiol 25:525–536

Ishida A, Toma T, Marjenah (1999a) Leaf gas exchange and chlorophyll fluorescence in relation to leaf angle, azimuth, and canopy position in the tropical pioneer tree, *Macaranga conifera*. Tree Physiol 19:117–124

Ishida A, Uemura A, Koike N, Matsumoto Y, Hoe AL (1999b) Interactive effects of leaf age and self-shading on leaf structure, photosynthetic capacity and chlorophyll fluorescence in the rain forest tree, *Dryobalanops aromatica*. Tree Physiol 19:741–747

Ishii H, Ooishi M, Maruyama Y, Koike T (2003) Acclimation of shoot and needle morphology and photosynthesis of two *Picea* species to differences in soil nutrient availability. Tree Physiol 23:453–461

Jackowski G, Kacprzak K, Jansson S (2001) Identification of Lhcb1/Lhcb2/Lhcb3 heterotrimers of the main light-harvesting chlorophyll *a/b*-protein complex of photosystem II (LHC II). Biochim Biophys Acta 1504:340–345

James SA, Bell DT (2000) Leaf orientation, light interception and stomatal conductance of *Eucalyptus globulus* ssp. *globulus* leaves. Tree Physiol 20:815–823

Jarvis PG, Leverenz JW (1983) Productivity of temperate, deciduous and evergreen forests. In: Lange OL (ed) Physiological Plant Ecology. Springer, Berlin, pp 233–280

Joffre R, Rambal S, Damesin C (2007) Functional attributes of Mediterranean-type ecosystems. In: Pugnaire FI, Valladares F (eds) Handbook of Functional Plant Ecology. CRC Press, Boca Raton, pp 285–312

Joyce BJ, Steiner KC (1995) Systematic variation in xylem hydraulic capacity within the crown of white ash (*Fraxinus americana*). Tree Physiol 15:649–656

Kesselmeier J, Staudt M (1999) Biogenic volatile organic compounds (VOC): an overview on emission, physiology and ecology. J Atmos Chem 33:23–88

Kitajima K (1994) Relative importance of photosynthetic traits and allocation patterns as correlates of seedling shade tolerance of 13 tropical trees. Oecologia 98:419–428

Koike T, Kitao M, Maruyama Y, Mori S, Lei TT (2001) Leaf morphology and photosynthetic adjustments among deciduous broad-leaved trees within the vertical canopy profile. Tree Physiol 21:951–958

Kovalyev AG (1980) Vozrast dereva i anatomomorfologicheskoye stroyeniye hvoi sosny obyknovennoi. (The age of a tree and anatomomorphological structure of needles in *Pinus sylvestris* L.). Lesovedeniye 6:30–35

Krédl Z, Středa T, Pokorný R, Kmoch M, Brotan J (2012) Microclimate in the vertical profile of wheat, rape and maize canopies. Acta Universitatis Agriculturae et Silviculturae Mendelianae Brunensis 60:79–90

Kull O, Kruijt B (1999) Acclimation of photosynthesis to light: a mechanistic approach. Funct Ecol 13:24–36

Kull O, Niinemets Ü (1998) Distribution of leaf photosynthetic properties in tree canopies: comparison of species with different shade tolerance. Funct Ecol 12:472–479

Kull O, Koppel A, Noormets A (1998) Seasonal changes in leaf nitrogen pools in two *Salix* species. Tree Physiol 18:45–51

Küppers M (1985) Carbon relations and competition between woody species in a Central European hedgerow. IV. Growth form and partitioning. Oecologia 66:343–352

Le Roux X, Sinoquet H, Vandame M (1999) Spatial distribution of leaf dry weight per area and leaf nitrogen concentration in relation to local radiation regime within an isolated tree crown. Tree Physiol 19:181–188

Leal DB, Thomas SC (2003) Vertical gradients and tree-to-tree variation in shoot morphology and foliar nitrogen in an oldgrowth *Pinus strobus* stand. Can J For Res 33:1304–1314

Lemaire G, Onillon B, Gosse G, Chartier M, Allirand JM (1991) Nitrogen distribution within a lucerne canopy during regrowth: relation with light distribution. Ann Bot 68:483–488

Lemoine D, Cochard H, Granier A (2002) Within crown variation in hydraulic architecture in beech (*Fagus sylvatica* L.): evidence for a stomatal control of xylem embolism. Ann For Sci 59:19–27

Leverenz JW (1987) Chlorophyll content and the light response curve of shade-adapted conifer needles. Physiol Plant 71:20–29

Leverenz JW (1988) The effects of illumination sequence, CO_2 concentration, temperature and acclimation on the convexity of the photosynthetic light response curve. Physiol Plant 74:332–341

Leverenz JW (1994) Factors determining the nature of the light dosage response curve of leaves. In: Baker NR, Bowyer JR (eds) Photoinhibition of Photosynthesis: From Molecular Mechanisms to the Field. Bios Scientific Publishers Ltd, Oxford, pp 239–254

Logan BA, Barker DH, Demmig-Adams B, Adams WW III (1996) Acclimation of leaf carotenoid composition and ascorbate levels to gradients in the light environment within an Australian rainforest. Plant Cell Environ 19:1083–1090

Logan BA, Demmig-Adams B, Adams WW III (1998a) Antioxidants and xanthophyll cycle-dependent energy dissipation in *Cucurbita pepo* L. and *Vinca major* L. upon a sudden increase in growth PPFD in the field. J Exp Bot 49:1881–1888

Logan BA, Demmig-Adams B, Adams WW III, Grace SC (1998b) Antioxidants and xanthophyll cycle-dependent energy dissipation in *Cucurbita pepo* L. and *Vinca major* L. acclimated to four growth PPFDs in the field. J Exp Bot 49:1869–1879

Long SP, Postl WF, Bolhár-Nordenkampf HR (1993) Quantum yields for uptake of carbon dioxide in C_3 vascular plants of contrasting habitats and taxonomic groupings. Planta 189:226–234

Lovelock CE, Jebb M, Osmond CB (1994) Photoinhibition and recovery in tropical plant species: response to disturbance. Oecologia 97:297–307

Lusk CH (2004) Leaf area and growth of juvenile temperate evergreens in low light: species of contrasting shade tolerance change rank during ontogeny. Funct Ecol 18:820–828

Lusk CH, Reich PB, Montgomery RA, Ackerly DD, Cavender-Bares J (2008) Why are evergreen leaves so contrary about shade? Trends Ecol Evol 23:299–303

Meir P, Kruijt B, Broadmeadow M, Barbosa E, Kull O, Carswell F, Nobre A, Jarvis PG (2002) Acclimation of photosynthetic capacity to irradiance in tree canopies in relation to leaf nitrogen concentration and leaf mass per unit area. Plant Cell Environ 25:343–357

Muller O, Oguchi R, Hirose T, Werger MJ, Hikosaka K (2009) The leaf anatomy of a broad-leaved evergreen allows an increase in leaf nitrogen content in winter. Physiol Plant 136:299–309

Naidu SL, DeLucia EH (1997) Acclimation of shade-developed leaves on saplings exposed to late-season canopy gaps. Tree Physiol 17:367–376

Niinemets Ü (1995) Distribution of foliar carbon and nitrogen across the canopy of *Fagus sylvatica*: adaptation to a vertical light gradient. Acta Oecol 16:525–541

Niinemets Ü (1997a) Distribution patterns of foliar carbon and nitrogen as affected by tree dimensions and relative light conditions in the canopy of *Picea abies*. Trees 11:144–154

Niinemets Ü (1997b) Acclimation to low irradiance in *Picea abies*: influences of past and present light climate on foliage structure and function. Tree Physiol 17:723–732

Niinemets Ü (1999) Research review. Components of leaf dry mass per area – thickness and density – alter leaf photosynthetic capacity in reverse directions in woody plants. New Phytol 144:35–47

Niinemets Ü (2007) Photosynthesis and resource distribution through plant canopies. Plant Cell Environ 30:1052–1071

Niinemets Ü (2010) A review of light interception in plant stands from leaf to canopy in different plant functional types and in species with varying shade tolerance. Ecol Res 25:693–714

Niinemets Ü (2012) Commentary. Optimization of foliage photosynthetic capacity in tree canopies: towards identifying missing constraints. Tree Physiol 32:505–509

Niinemets Ü (2015) Is there a species spectrum within the world-wide leaf economics spectrum? Major variations in leaf functional traits in the Mediterranean sclerophyll *Quercus ilex*. New Phytol 205:79–96

Niinemets Ü, Anten NPR (2009) Packing the photosynthesis machinery: from leaf to canopy. In: Laisk A (ed) Photosynthesis in Silico: Understanding Complexity from Molecules to Ecosystems. Springer, Berlin, pp 363–399

Niinemets Ü, Keenan TF (2012) Measures of light in studies on light-driven plant plasticity in artificial environments. Front Plant Sci 3:156

Niinemets Ü, Keenan TF (2014) Photosynthetic responses to stress in Mediterranean evergreens: mechanisms and models. Environ Exp Bot 103:24–41

Niinemets Ü, Kull O (1995) Effects of light availability and tree size on the architecture of assimilative surface in the canopy of *Picea abies*: variation in shoot structure. Tree Physiol 15:791–798

Niinemets Ü, Kull O (1998) Stoichiometry of foliar carbon constituents varies along light gradients in temperate woody canopies: implications for foliage morphological plasticity. Tree Physiol 18:467–479

Niinemets Ü, Kull O (2001) Sensitivity to photoinhibition of photosynthetic electron transport in a temperate deciduous forest canopy: Photosystem II centre openness, non-radiative energy dissipation and excess irradiance under field conditions. Tree Physiol 21:899–914

Niinemets Ü, Lukjanova A (2003) Total foliar area and average leaf age may be more strongly associated with branching frequency than with leaf longevity in temperate conifers. New Phytol 158:75–89

Niinemets Ü, Tenhunen JD (1997) A model separating leaf structural and physiological effects on carbon gain along light gradients for the shade-tolerant species *Acer saccharum*. Plant Cell Environ 20:845–866

Niinemets Ü, Valladares F (2004) Photosynthetic acclimation to simultaneous and interacting environmental stresses along natural light gradients: optimality and constraints. Plant Biol 6:254–268

Niinemets Ü, Valladares F (2006) Tolerance to shade, drought and waterlogging in the temperate dendroflora of the Northern hemisphere: tradeoffs, phylogenetic signal and implications for niche differentiation. Ecol Monogr 76:521–547

Niinemets Ü, Bilger W, Kull O, Tenhunen JD (1998a) Acclimation to high irradiance in temperate deciduous trees in the field: changes in xanthophyll cycle pool size and in photosynthetic capacity along a canopy light gradient. Plant Cell Environ 21:1205–1218

Niinemets Ü, Kull O, Tenhunen JD (1998b) An analysis of light effects on foliar morphology, physiology, and light interception in temperate deciduous woody species of contrasting shade tolerance. Tree Physiol 18:681–696

Niinemets Ü, Bilger W, Kull O, Tenhunen JD (1999a) Responses of foliar photosynthetic electron transport, pigment stoichiometry, and stomatal conductance to interacting environmental factors in a mixed species forest canopy. Tree Physiol 19:839–852

Niinemets Ü, Oja V, Kull O (1999b) Shape of leaf photosynthetic electron transport versus temperature response curve is not constant along canopy light gradients in temperate deciduous trees. Plant Cell Environ 22:1497–1514

Niinemets Ü, Sõber A, Kull O, Hartung W, Tenhunen JD (1999c) Apparent controls on leaf conductance by soil water availability and via light-acclimation of foliage structural and physiological properties in a mixed deciduous, temperate forest. Int J Plant Sci 160:707–721

Niinemets Ü, Tenhunen JD, Canta NR, Chaves MM, Faria T, Pereira JS, Reynolds JF (1999d) Interactive effects of nitrogen and phosphorus on the acclimation potential of foliage photosynthetic properties of cork oak, *Quercus suber*, to elevated atmospheric CO_2 concentrations. Global Change Biol 5:455–470

Niinemets Ü, Ellsworth DS, Lukjanova A, Tobias M (2001) Site fertility and the morphological and photosynthetic acclimation of *Pinus sylvestris* needles to light. Tree Physiol 21:1231–1244

Niinemets Ü, Ellsworth DS, Lukjanova A, Tobias M (2002a) Dependence of needle architecture and chemical composition on canopy light availability in three North American *Pinus* species with contrasting needle length. Tree Physiol 22:747–761

Niinemets Ü, Hauff K, Bertin N, Tenhunen JD, Steinbrecher R, Seufert G (2002b) Monoterpene emissions in relation to foliar photosynthetic and structural variables in Mediterranean evergreen *Quercus* species. New Phytol 153:243–256

Niinemets Ü, Kollist H, García-Plazaola JI, Hernández A, Becerril JM (2003) Do the capacity and kinetics for modification of xanthophyll cycle pool size depend on growth irradiance in temperate trees? Plant Cell Environ 26:1787–1801

Niinemets Ü, Al Afas N, Cescatti A, Pellis A, Ceulemans R (2004a) Petiole length and biomass investment in support modify light-interception efficiency in dense poplar plantations. Tree Physiol 24:141–154

Niinemets Ü, Cescatti A, Christian R (2004b) Constraints on light interception efficiency due to shoot architecture in broad-leaved *Nothofagus* species. Tree Physiol 24:617–630

Niinemets Ü, Kull O, Tenhunen JD (2004c) Within canopy variation in the rate of development of photosynthetic capacity is proportional to integrated quantum flux density in temperate deciduous trees. Plant Cell Environ 27:293–313

Niinemets Ü, Sonninen E, Tobias M (2004d) Canopy gradients in leaf intercellular CO_2 mole fractions revisited: interactions between leaf irradiance and water stress need consideration. Plant Cell Environ 27:569–583

Niinemets Ü, Cescatti A, Rodeghiero M, Tosens T (2005a) Leaf internal diffusion conductance limits photosynthesis more strongly in older leaves of Mediterranean evergreen broad-leaved species. Plant Cell Environ 28:1552–1566

Niinemets Ü, Lukjanova A, Sparrrow AD, Turnbull MH (2005b) Light-acclimation of cladode photosynthetic potentials in *Casuarina glauca*: trade-offs between physiological and structural investments. Funct Plant Biol 32:571–582

Niinemets Ü, Cescatti A, Rodeghiero M, Tosens T (2006a) Complex adjustments of photosynthetic capacity and internal mesophyll conductance to current and previous light availabilities and leaf age in Mediterranean evergreen species *Quercus ilex*. Plant Cell Environ 29:1159–1178

Niinemets Ü, Tobias M, Cescatti A, Sparrow AD (2006b) Size-dependent variation in shoot light-harvesting efficiency in shade-intolerant conifers. Int J Plant Sci 167:19–32

Niinemets Ü, Lukjanova A, Turnbull MH, Sparrow AD (2007) Plasticity in mesophyll volume fraction governs the light-acclimation in needle photosynthesis in two pines. Tree Physiol 27:1137–1151

Niinemets Ü, Copolovici L, Hüve K (2010) High within-canopy variation in isoprene emission potentials in temperate trees: implications for predicting canopy-scale isoprene fluxes. J Geophys Res Biogeosci 115: G04029

Niinemets Ü, García-Plazaola JI, Tosens T (2012) Photosynthesis during leaf development and ageing. In: Flexas J (ed) Terrestrial Photosynthesis in a Changing Environment. A Molecular, Physiological and Ecological Approach. Cambridge University Press, Cambridge, pp 353–372

Niinemets Ü, Keenan T, Hallik L (2015) Tansley review. A worldwide analysis of within-canopy variations in leaf structural, chemical and

physiological traits across plant functional types. New Phytol 205: 973–993

Noctor G, Foyer CH (1998) Ascorbate and glutathione: keeping active oxygen under control. Annu Rev Plant Physiol Plant Mol Biol 49:249–279

Noormets A, Kull O, Koppel A (1996) Nitrogen dynamics in *Salix* leaves during the first production year. In: Perttu K, Koppel A (eds) Short Rotation Willow Coppice for Renewable Energy and Improved Environment. Proceedings of a Joint Swedish-Estonian Seminar on Energy Forestry and Vegetation Filters Held in Tartu 24–26 September 1995. Swedish University of Agricultural Sciences, Uppsala, pp 51–59

Nygren M, Kellomäki S (1983) Effect of shading on leaf structure and photosynthesis in young birches, *Betula pendula* Roth. and *Betula pubescens* Ehrh. For Ecol Manage 7:119–132

Oberhuber W, Dai Z-Y, Edwards GE (1993) Light dependence of quantum yields of photosystem II and CO_2 fixation in C_3 and C_4 plants. Photosynth Res 35:265–274

Ögren E, Sjöström M (1990) Estimation of the effect of photoinhibition on the carbon gain in leaves of a willow canopy. Planta 181:560–567

Oguchi R, Hikosaka K, Hirose T (2005) Leaf anatomy as a constraint for photosynthetic acclimation: differential responses in leaf anatomy to increasing growth irradiance among three deciduous trees. Plant Cell Environ 28:916–927

Oguchi R, Hikosaka K, Hiura T, Hirose T (2006) Leaf anatomy and light acclimation in woody seedlings after gap formation in a cool-temperate forest. Oecologia 149:571–582

Ono K, Nishi Y, Watanabe A, Terashima I (2001) Possible mechanisms of adaptive leaf senescence. Plant Biol 3:234–243

Osmond CB, Anderson JM, Ball MC, Egerton JG (1999) Compromising efficiency: the molecular ecology of light-resource utilization in plants. In: Press MC (ed) Physiological Plant Ecology. The 39th Symposium of the British Ecological Society Held at the University of York, 7–9 September 1998. Blackwell Science, Oxford, pp 1–24

Palmroth S, Hari P (2001) Evaluation of the importance of acclimation of needle structure, photosynthesis, and respiration to available photosynthetically active radiation in a Scots pine canopy. Can J For Res 31:1235–1243

Patrick LD, Ogle K, Tissue DT (2009) A hierarchical Bayesian approach for estimation of photosynthetic parameters of C_3 plants. Plant Cell Environ 32:1695–1709

Paulsen H (2001) Pigment assembly – transport and ligation. In: Aro E-M, Andersson B (eds) Regulation of Photosynthesis. Kluwer Academic Publishers, Dordrecht, pp 219–233

Peltoniemi M, Duursma R, Medlyn B (2012) Co-optimal distribution of leaf nitrogen and hydraulic conductance in plant canopies. Tree Physiol 32:510–519

Pinheiro Prado M, de Oliveira Filho JA, França S, Márcio Amorim A, Schramm Mielke M (2013) Annual variation in canopy openness, air temperature and humidity in the understory of three forested sites in southern Bahia State, Brazil. Ciência Florestal 23:107–116

Pons TL (2016) Regulation of leaf traits in canopy gradients. In: Hikosaka K, Niinemets Ü, Anten N (eds) Canopy Photosynthesis: From Basics to Applications. Springer, Berlin, pp 143–168

Pons TL, Anten NPR (2004) Is plasticity in partitioning of photosynthetic resources between and within leaves important for whole-plant carbon gain in canopies? Funct Ecol 18:802–811

Pons TL, Pearcy RW (1994) Nitrogen reallocation and photosynthetic acclimation in response to partial shading in soybean plants. Physiol Plant 92:636–644

Pons TL, Westbeek MHM (2004) Analysis of differences in photosynthetic nitrogen-use efficiency between four contrasting species. Physiol Plant 122:68–78

Pons TL, van Rijnberk H, Scheurwater I, van der Werf A (1993) Importance of the gradient in photosynthetically active radiation in a vegetation stand for leaf nitrogen allocation in two monocotyledons. Oecologia 95:416–424

Pons TL, van der Werf A, Lambers H (1994) Photosynthetic nitrogen use efficiency of inherently slow- and fast-growing species: possible explanations for observed differences. In: Roy J, Garnier E (eds) A Whole Plant Perspective on Carbon-Nitrogen Interactions. SPB Academic Publishing bv, The Hague, pp 61–77

Poorter L, Oberbauer SF, Clark DB (1995) Leaf optical properties along a vertical gradient in a tropical rain forest canopy in Costa Rica. Amer J Bot 82:1257–1263

Posada JM, Lechowicz MJ, Kitajima K (2009) Optimal photosynthetic use of light by tropical tree crowns achieved by adjustment of individual leaf angles and nitrogen content. Ann Bot 103:795–805

Possell M, Loreto F (2013) The role of volatile organic compounds in plant resistance to abiotic stresses: responses and mechanisms. In: Niinemets Ü, Monson RK (eds) Biology, Controls and Models of

Tree Volatile Organic Compound Emissions. Springer, Berlin, pp 209–235
Ramalho JC, Lauriano JA, Nunes MA (2000) Changes in photosynthetic performance of *Ceratonia siliqua* in summer. Photosynthetica 38:393–396
Rambal S (1992) *Quercus ilex* facing water stress: a functional equilibrium hypothesis. Vegetatio 99–100:147–153
Rambal S (2001) Productivity of Mediterranean-type ecosystems. In: Mooney HA (ed) Terrestrial Global Productivity: Past, Present, and Future. Academic Press Inc, San Diego, pp 315–344
Rambal S, Damesin C, Joffre R, Méthy M, Lo Seen D (1996) Optimization of carbon gain in canopies of Mediterranean evergreen oaks. Ann Sci For 53:547–560
Rasmuson KE, Anderson JE, Huntly N (1994) Coordination of branch orientation and photosynthetic physiology in the Joshua tree (*Yucca brevifolia*). Great Basin Natur 54:204–211
Renninger HJ, Meinzer FC, Gartner BL (2006) Hydraulic architecture and photosynthetic capacity as constraints on release from suppression in Douglas-fir and western hemlock. Tree Physiol 27:33–42
Ryel RJ, Beyschlag W, Caldwell MM (1994) Light field heterogeneity among tussock grasses: theoretical considerations of light harvesting and seedling establishment in tussocks and uniform tiller distributions. Oecologia 98:241–246
Sala A, Sabaté S, Gracia C, Tenhunen JD (1994) Canopy structure within a *Quercus ilex* forested watershed: variations due to location, phenological development, and water availability. Trees 8:254–261
Sands PJ (1995) Modelling canopy production. I. Optimal distribution of photosynthetic resources. Aust J Plant Physiol 22:593–601
Sands PJ (1996) Modelling canopy production. III. Canopy light-utilisation efficiency and its sensitivity to physiological and environmental variables. Aust J Plant Physiol 23:103–114
Schieving F, Poorter H (1999) Carbon gain in a multispecies canopy: the role of specific leaf area and photosynthetic nitrogen-use efficiency in the tragedy of the commons. New Phytol 143:201–211
Schoettle AW (1989) Potential effect of premature needle loss on the foliar biomass and nutrient retention of lodgepole pine. In: Olson RK, Lefohn AS (eds) Transactions of Air Pollution on Western Forests. Air & Waste Management Association, Anheim, pp 443–454
Schoettle AW, Fahey TJ (1994) Foliage and fine root longevity of pines. In: Gholz HL (ed) Environmental Constraints on the Structure and Productivity of Pine Forest Ecosystems: A Comparative Analysis. Munksgaard International Booksellers and Publishers, Copenhagen, pp 136–153
Schoettle AW, Smith WK (1999) Interrelationships among light, photosynthesis and nitrogen in the crown of mature *Pinus contorta* ssp. *latifolia*. Tree Physiol 19:13–22
Schulze ED (1981) Carbon gain and wood production in trees of deciduous beech (*Fagus sylvatica*) and trees of evergreen spruce (*Picea excelsa*). Mitt Forstl Bundesvers Wien 142:105–123
Sellin A, Kupper P (2004) Within-crown variation in leaf conductance in Norway spruce: effects of irradiance, vapour pressure deficit, leaf water status and plant hydraulic constraints. Ann For Sci 61:419–429
Sharkey TD, Singsaas EL (1995) Why plants emit isoprene. Nature 374:769
Sharkey TD, Wiberley AE, Donohue AR (2008) Isoprene emission from plants: why and how. Ann Bot 101:5–18
Singsaas EL, Lerdau M, Winter K, Sharkey TD (1997) Isoprene increases thermotolerance of isoprene-emitting species. Plant Physiol 115:1413–1420
Smolander S, Stenberg P (2001) A method for estimating light interception by a conifer shoot. Tree Physiol 21:797–803
Sprugel DG, Brooks JR, Hinckley TM (1996) Effects of light on shoot geometry and needle morphology in *Abies amabilis*. Tree Physiol 16:91–98
Stenberg P (1996) Simulations of the effects of shoot structure and orientation on vertical gradients in intercepted light by conifer canopies. Tree Physiol 16:99–108
Stenberg P (1998) Implications of shoot structure on the rate of photosynthesis at different levels in a coniferous canopy using a model incorporating grouping and penumbra. Funct Ecol 12:82–91
Stenberg P, Smolander H, Sprugel DG, Smolander S (1998) Shoot structure, light interception, and distribution of nitrogen in an *Abies amabilis* canopy. Tree Physiol 18:759–767
Stenberg P, Kangas T, Smolander H, Linder S (1999) Shoot structure, canopy openness, and light interception in Norway spruce. Plant Cell Environ 22:1133–1142
St-Jacques C, Bellefleur P (1993) Light requirements of some broadleaf tree seedlings in natural conditions. For Ecol Manage 56:329–341
St-Jacques C, Labrecque M, Bellefleur P (1991) Plasticity of leaf absorptance in some broadleaf tree seedlings. Bot Gaz 152:195–202
Terashima I, Hikosaka K (1995) Comparative ecophysiology of leaf and canopy photosynthesis. Plant Cell Environ 18:1111–1128

Terashima I, Hanba YT, Tholen D, Niinemets Ü (2011) Leaf functional anatomy in relation to photosynthesis. Plant Physiol 155:108–116

Teskey RO, Grier CC, Hinckley TM (1984) Change in photosynthesis and water relations with age and season in *Abies amabilis*. Can J For Res 14:77–84

Tjoelker MG, Volin JC, Oleksyn J, Reich PB (1995) Interaction of ozone pollution and light effects on photosynthesis in a forest canopy experiment. Plant Cell Environ 18:895–905

Tomás M, Flexas J, Copolovici L, Galmés J, Hallik L, Medrano H, Tosens T, …, Niinemets Ü (2013) Importance of leaf anatomy in determining mesophyll diffusion conductance to CO_2 across species: quantitative limitations and scaling up by models. J Exp Bot 64:2269–2281

Tosens T, Niinemets Ü, Vislap V, Eichelmann H, Castro-Díez P (2012a) Developmental changes in mesophyll diffusion conductance and photosynthetic capacity under different light and water availabilities in *Populus tremula*: how structure constrains function. Plant Cell Environ 35:839–856

Tosens T, Niinemets Ü, Westoby M, Wright IJ (2012b) Anatomical basis of variation in mesophyll resistance in eastern Australian sclerophylls: news of a long and winding path. J Exp Bot 63:5105–5119

Valladares F (2003) Light heterogeneity and plants: from ecophysiology to species coexistence and biodiversity. In: Esser K (ed) Progress in Botany. Springer, Berlin, pp 439–471

Valladares F, Niinemets Ü (2007) The architecture of plant crowns: from design rules to light capture and performance. In: Pugnaire FI, Valladares F (eds) Handbook of Functional Plant Ecology. CRC Press, Boca Raton, pp 101–149

Valladares F, Niinemets Ü (2008) Shade tolerance, a key plant feature of complex nature and consequences. Annu Rev Ecol Evol Syst 39:237–257

Valladares F, Dobarro I, Sánchez-Gómez D, Pearcy RW (2005) Photoinhibition and drought in Mediterranean woody saplings: scaling effects and interactions in sun and shade phenotypes. J Exp Bot 56:483–494

Vapaavuori EM, Vuorinen AH (1989) Seasonal variation in the photosynthetic capacity of a willow (*Salix* cv. *Aquatica gigantea*) canopy. I. Changes in the activity and amount of ribulose 1,5-bisphosphate carboxylase-oxygenase and the content of nitrogen and chlorophyll at different levels in the canopy. Tree Physiol 5:423–444

Vapaavuori EM, Nurmi A, Vuorinen AH, Kangas T (1989) Seasonal variation in the photosynthetic capacity of a willow (*Salix* cv. *Aquatica gigantea*) canopy. 2. Comparison of the structure and function of chloroplasts at different levels in the canopy. Tree Physiol 5:445–457

Vaz M, Maroco J, Ribeiro N, Gazarini LC, Pereira JS, Chaves MM (2011) Leaf-level responses to light in two co-occurring *Quercus* (*Quercus ilex* and *Quercus suber*): leaf structure, chemical composition and photosynthesis. Agrofor Syst 82:173–181

Vickers CE, Gershenzon J, Lerdau MT, Loreto F (2009) A unified mechanism of action for volatile isoprenoids in plant abiotic stress. Nat Chem Biol 5:283–291

Vos J, van der Putten PEL (2001) Effects of partial shading of the potato plant on photosynthesis of treated leaves, leaf area expansion and allocation of nitrogen and dry matter in component plant parts. Eur J Agron 14:209–220

Warren CR, Adams MA (2001) Distribution of N, Rubisco and photosynthesis in *Pinus pinaster* and acclimation to light. Plant Cell Environ 24:597–609

Warren CR, García-Plazaola JI, Niinemets Ü (2012) Ecophysiology of photosynthesis in temperate forests. In: Flexas J (ed) Terrestrial Photosynthesis in a Changing Environment a Molecular, Physiological and Ecological Approach. Cambridge University Press, Cambridge, pp 465–487

Warton DI, Wright IJ, Falster DS, Westoby M (2006) Bivariate line-fitting methods for allometry. Biol Rev Camb Philos Soc 81:259–291

Weih M (2009) Genetic and environmental variation in spring and autumn phenology of biomass willows (*Salix* spp.): effects on shoot growth and nitrogen economy. Tree Physiol 29:1479–1490

Werger MJA, Hirose T (1988) Effects of light climate and nitrogen partitioning on the canopy structure of stands of a dicotyledonous, herbaceous vegetation. In: Werger MJA (ed) Plant Form and Vegetation Structure. Adaptation, Plasticity and Relation to Herbivory. SPB Academic Publishing, The Hague, pp 171–181

Werner C, Ryel RJ, Correia O, Beyschlag W (2001a) Structural and functional variability within the canopy and its relevance for carbon gain and stress avoidance. Acta Oecol 22:129–138

Werner C, Ryel RJ, Correia O, Beyschlag W (2001b) Effects of photoinhibition on whole-plant carbon gain assessed with a photosynthesis model. Plant Cell Environ 24:27–40

Werner C, Correia O, Beyschlag W (2002) Characteristic patterns of chronic and dynamic photoinhibition of different functional groups in a Mediterranean ecosystem. Funct Plant Biol 29:999–1011

White JD, Scott NA (2006) Specific leaf area and nitrogen distribution in New Zealand forests:

species independently respond to intercepted light. For Ecol Manage 226:319–329

Woodruff DR, McCulloh KA, Meinzer FC (2016) Forest canopy hydraulics. In: Hikosaka K, Niinemets Ü, Anten N (eds) Canopy Photosynthesis: From Basics to Applications. Springer, Berlin, pp 187–217

Woodward FI, Smith TM, Shugart HH (1994) Defining plant functional types: the end view. In: Smith TM (ed) Plant Functional Types. Their Relevance to Ecosystem Properties and Global Change. Cambridge University Press, Cambridge/New York/Melbourne, pp 355–359

Wright IJ, Reich PB, Westoby M, Ackerly DD, Baruch Z, Bongers F, Cavender-Bares J, . . ., Villar R (2004) The world-wide leaf economics spectrum. Nature 428:821–827

Wright IJ, Reich PB, Cornelissen JHC, Falster DS, Garnier E, Hikosaka K, Lamont BB, . . ., Westoby M (2005) Assessing the generality of global leaf trait relationships. New Phytol 166:485–496

Wright IJ, Leishman MR, Read C, Westoby M (2006) Gradients of light availability and leaf traits with leaf age and canopy position in 28 Australian shrubs and trees. Funct Plant Biol 33:406–419

Yasumura Y, Hikosaka K, Matsui K, Hirose T (2002) Leaf-level nitrogen-use efficiency of canopy and understorey species in a beech forest. Funct Ecol 16:826–834

Zhang G, Leclerc MY, Karipot A (2010) Local flux-profile relationships of wind speed and temperature in a canopy layer in atmospheric stable conditions. Biogeosciences 7:3625–3636

Zhang J, Guo B, Jiang Qo RH, Wang Z (2013) Study on microclimate characteristics and vertical variation of potential evapotranspiration of the *Robinia pseudoacacia* forest in the loess plateau of China. Adv Meteorol 2013:748418

Chapter 5

Regulation of Leaf Traits in Canopy Gradients

Thijs L. Pons*
Department Plant Ecophysiology, Institute of Environmental Biology, Utrecht University, Padualaan 8, Utrecht 3508 CH, Netherlands

Summary

The gradient of leaf traits in a canopy from sunlit upper regions to shaded lower ones is regulated in response to the density of its leaf area. The gradients of environmental factors act as signals for the regulation. The result is improved resource use efficiency for carbon gain at the whole plant level. Herbaceous species with relatively fast leaf turnover typically grow new leaves at the top in high light that are subsequently progressively shaded in developing dense canopies. Export of resources associated with photosynthetic capacity accompanies the progressive shading, later on followed by degradation of light harvesting components when senescence is induced. The red:far-red ratio of the light gradient is involved in the reallocation of resources and the induction of leaf senescence, but the irradiance component of the light gradient dominates the canopy effect. It impacts a multitude of physiological processes. Their effect can operate locally such as perception by photoreceptors and excitation pressure implicated in chloroplast organization. Other effects impact processes operating at the whole plant level such as the distribution of signaling compounds in the transpiration stream and the supply of assimilates to developing young leaves. These systemically operating pathways are at the basis of a coordinated response of plants to the shading effect in a canopy gradient, which is different from

*Author for correspondence, e-mail: T.L.Pons@uu.nl

K. Hikosaka, Ü. Niinemets, and N.P.R. Anten (eds.), *Canopy Photosynthesis: From Basics to Applications*, DOI 10.1007/978-94-017-7291-4_5

whole plant shading. The available evidence for mechanisms involved in the regulation of leaf traits in canopies is discussed.

Keywords Chloroplast organization • Cytokinin • Photoreceptors • Photosynthetic capacity • Reallocation • Senescence • Sugar sensing • Systemic signaling • Transpiration stream

I. Introduction

Early models of canopy photosynthesis assumed a uniform distribution of leaf traits in canopies (de Wit 1965; Monsi and Saeki 1953). However, real canopies display a gradient of leaf traits with depth parallel to environmental gradients (Chap. 4, Niinemets 2016). Resources required for the photosynthetic apparatus are often limiting, and metabolic costs are involved in their acquisition and processing in a plant. Since photosynthetic rates are low in the shaded parts of the canopy, equal investments in the photosynthetic apparatus across the canopy light gradient would not be efficient (Mooney and Gulmon 1979). Canopy photosynthesis models were developed taking into account resource use efficiency. These predicted that the distribution of resources, and thus photosynthetic capacity, over the leaf area of plants growing in a canopy should more or less follow the distribution of light (Field 1983; Hirose and Werger 1987a; Farquhar et al. 1989; Anten 2005). The distribution of leaf N was selected as representative for the resources required for the photosynthetic apparatus because it is the most abundant nutrient element with the largest costs involved and is often available in limited supply. Furthermore, a large fraction of leaf N is involved in the photosynthetic apparatus (Evans and Seemann 1989). Leaf N thus generally scales with photosynthetic capacity (Field and Mooney 1986; Evans 1989) and its distribution in a canopy is then representative for the distribution of photosynthetic capacity.

The actual distribution of leaf N over the leaf area across plant height in canopies was indeed roughly according to the predictions of these optimality models (Hirose and Werger 1987b; Grindlay 1997), but deviations of the actual distribution from the predictions were typically found (Pons et al. 1989; Anten 2005). This is probably because other selection pressures and constraints are not taken into account (Niinemets 2012; Peltoniemi et al. 2012; Buckley et al. 2013). The distribution of leaf N and thus photosynthetic capacity appeared to be dependent on the density of leaf area in canopies (Hirose et al. 1988; Anten et al. 1998; Fig. 5.1f, i). Also other leaf traits that contribute to resource use efficiency such as leaf mass per unit area (LMA) (Fig. 5.1g) and photosynthetic capacity per unit chlorophyll showed gradients with depth in canopies, which are steeper with increasing leaf area density (Chap. 4, Niinemets 2016; Pons and Anten 2004). This illustrates that plants can perceive the density of canopies and can adjust their leaf trait values in a functional manner. Gradients in

Abbreviations: ABA – Abscisic acid; A_{day} – Daily net carbon gain; A_{sat} – Light saturated rate of photosynthesis per unit leaf area at atmospheric CO_2 concentration; A_{chl} – A_{sat} per unit chlorophyll; Chl a/b – Molar chlorophyll a/b ratio; Chl_{LA} – Chlorophyll content per unit leaf area; CKs – Cytokinins; FR – Far-red radiation (730 nm); J_{max} – Electron transport capacity; LAI – Leaf area index; LHCII – Light harvesting complex associated with PSII; LMA – Leaf mass per unit area; N_{LA} – Nitrogen per unit leaf area; N_{DM} – Nitrogen per unit leaf mass; PAR – Photosynthetically active radiation; PPFD – Photosynthetic photon flux density; PSI – Photosystem I; PSII – Photosystem II; R – Red light (660 nm); R:FR – Red:far-red quantum flux ratio; ROS – Reactive oxygen species; V_{cmax} – Carboxylation capacity

irradiance (Fig. 5.1a) and other environmental factors (Chap. 1, Goudriaan 2016) are correlated with the gradients in leaf traits (Chap. 4, Niinemets 2016). The environmental cues used by plants for the perception of canopy density are likely to be associated with these environmental gradients in the canopy. The question that will be addressed in this chapter is what the perception and response mechanisms are for the regulation of the gradient of leaf trait values in canopies.

The regulation of leaf traits and more in particular photosynthetic traits can operate at different levels of organization. At the chloroplast level, the organization of the photosynthetic apparatus changes with the local light environment (Anderson et al. 1995; Hüner et al. 2012) and other factors such as temperature (Hüner et al. 1998). This form of photosynthetic acclimation is evident from chloroplast structure such as grana stacking and from the partitioning between compartments of the photosynthetic apparatus that determine for instance light harvesting relative to carboxylation capacity and electron transport capacity. Given the chloroplast traits, leaf structure further determines traits at the leaf level. For instance the thickness of the mesophyll packed with chloroplasts determines photosynthetic capacity per unit area (Terashima et al. 2011). The proportion of reinforcing structures, such as sclerenchyma, thickness of cell walls and epidermis, further influences LMA (van Arendonk and Poorter 1994; Niinemets 1999; Wright et al. 2004), which determines photosynthetic capacity expressed per unit dry mass.

Signaling mechanisms pertaining to the classical shade avoidance response of plants, which includes the hyponasty (upward bending) of petioles and their elongation and the elongation of internodes (Fig. 5.1d), are better understood than the regulation of leaf traits (Chap. 6, deWit and Pierik 2016). The reallocation of resources for the photosynthetic apparatus away from leaves in the shaded parts of the canopy to leaves in more favorable light conditions can also be considered as a form of shade avoidance. However, evidence indicates that the mechanisms of its regulation are to a large extent different. Furthermore, the acclimation at the chloroplast level is not comparable to a shade avoidance response and is likely to be subject to its own form of regulation. Several mechanisms have been proposed for the regulation of leaf traits in canopies including developmental leaf ageing, photoreceptors, redox and ROS signaling, sugar signaling and systemic signaling with cytokinins (CKs) and other messengers in the transpiration stream (see also reviews by Anten et al. 2000; Ono et al. 2001; Terashima et al. 2005; Niinemets and Anten 2009). These will be discussed in the following sections. Most experimental work on these regulation mechanisms has been done with relatively fast growing herbaceous plants. The question will also be addressed to what extent the mechanisms could be different for plants belonging to other functional groups.

II. Environmental Gradients

The distribution of short wave solar radiation in canopies is at the basis of most of the environmental gradients. It consists of several spectral regions that are of importance in this respect. The gradient in the 400–700 nm wavelength band (photosynthetically active radiation; PAR) is strong as a result of absorption by chlorophyll (Fig. 5.1a). The extinction of PAR in a canopy is a complicated function of direct and diffuse light in the overhead light environment, and canopy characteristic such as leaf area index, leaf angle distribution and aggregation of foliage (Chap. 1, Goudriaan 2016). Plants growing in dense canopies thus experience strong gradients of photosynthetic photon flux density (PPFD) over their height, which apart from photosynthetic activity, drives also other physiological processes such as transpiration (Fig. 5.1c, k).

Short wave infrared (700–3,000 nm), which comprises about half of the energy in the daylight spectrum, is partly absorbed by leaves where it generates heat and thus forms an important component of the energy balance of leaves together with absorbed PAR. This contributes to elevated temperatures in

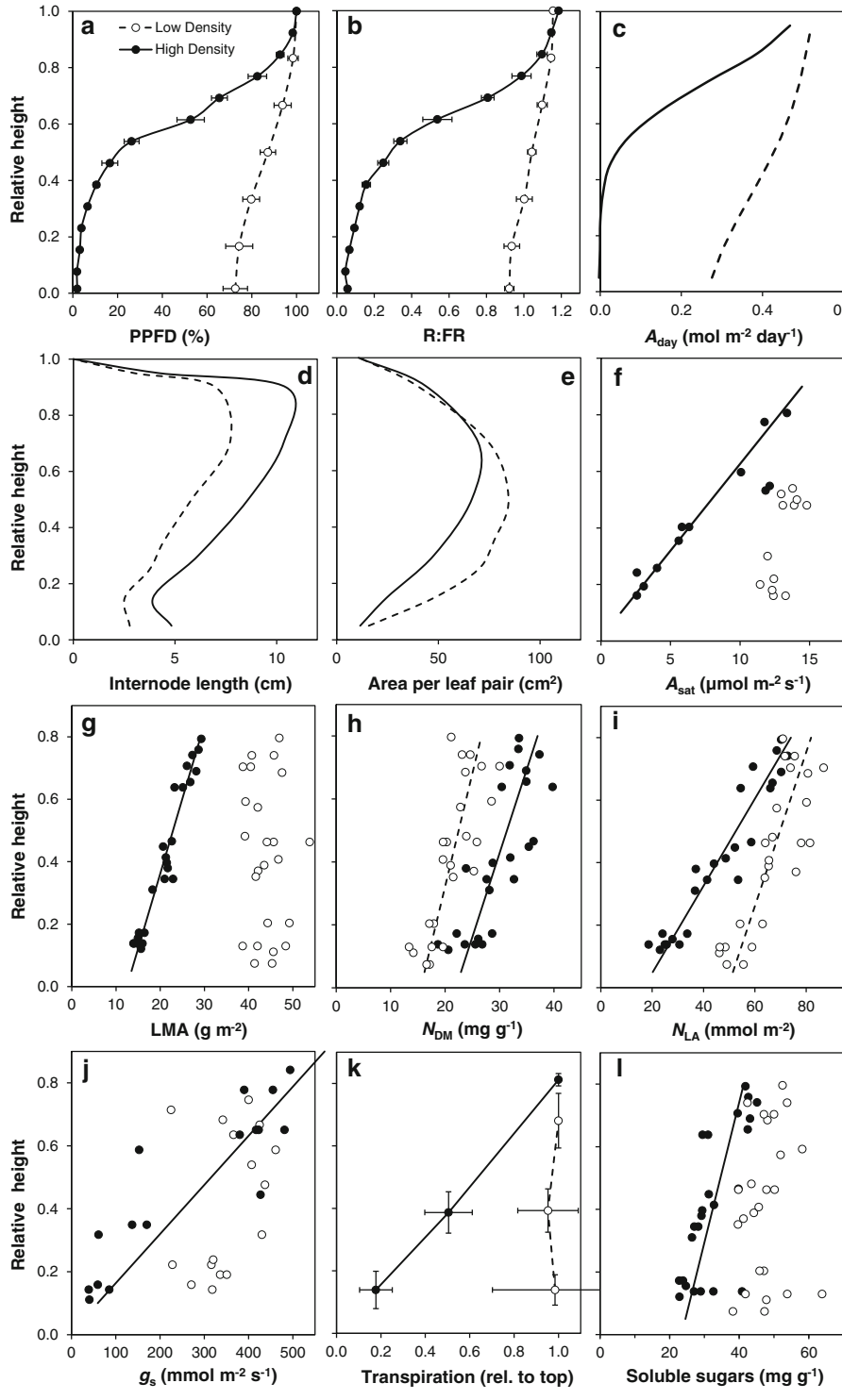

Fig. 5.1. Distribution over plant height of light, leaf traits and physiological activity variables at low and high plant density in *Lysimachia vulgaris*. Height was expressed relative to the tallest plant in the canopy. (**a**) photon flux density of photosynthetically active radiation (PPFD) expressed relative to above the canopy, (**b**) red:far-red

the upper leaves and thus to a gradient in leaf temperatures (Chap. 2, Gutschick 2016). The 700 nm to about 1,000 nm region of the short wave infrared is much less absorbed by leaves. The differential absorption between this spectral region and PAR can be perceived by plants using the phytochrome system (Chap. 6, de Wit and Pierik 2016). The spectral composition of the light with respect to phytochrome action is characterized by the red:far-red ratio (R:FR), the quantum flux ratio between the 660 nm (R) and 730 nm (FR) wavelength bands. This ratio decreases with intensity of canopy shade as the absorption of R increases stronger compared to FR. Canopy gradients in R:FR are thus similar to PPFD gradients (Fig. 5.1a, b).

Wind speeds are reduced inside canopies. As a result, strong gradients in air turbulence exist that parallel the light gradient. Leaves at the top of the canopy can thus be exposed to much stronger mechanical forces than inside the canopy. Another effect is that on quiet days, gaseous compounds can be trapped inside the canopy. Water vapor from evaporation from a moist soil surface and from transpiring leaves can accumulate to some extent. However, the above mentioned gradient in leaf temperature is generally more important for generating a gradient in leaf–to–air vapor pressure difference. Similarly, CO_2 can significantly accumulate under canopies near the ground from soil and plant respiration (Buchman et al. 1997). Depletion around photosynthetically active upper leaves can occur as well (Kruijt et al. 1996). Other gasses that can accumulate in a similar manner are volatile organic compounds. The gaseous phytohormone ethylene is produced by plants and escapes to the atmosphere. Its production can be stimulated by exposure to a low R:FR as found inside canopies. Accumulation to physiologically active levels has been found for *Nicotiana tabacum* (Pierik et al. 2004), which was related to petiole hyponasty and internode elongation. It could also be involved in leaf trait adjustment, but evidence is lacking.

These gradients in environmental factors across canopy height are potential signals for the regulation of leaf traits in response to canopy density. Perception can be direct such as the R:FR ratio by phytochrome, or more indirect through an effect on a physiological process that generates the signal such as photosynthesis and transpiration that are under control of irradiance and leaf-to-air vapor pressure difference respectively.

III. Leaf Age or the Light Gradient

Fast growing herbaceous dicots are generally characterized by leaf development at the top of a canopy. Their leaves thus typically develop in high light and are shaded by new leaves with further growth. The older leaves tend to senesce within one growth season. This developmental pattern is particularly evident in dense canopies. These plants show a gradient with height of leaf N per unit area (N_{LA}) and associated photosynthetic capacity per unit leaf area (the light saturated rate of photosynthesis (A_{sat}) is often used as a measure), which runs parallel

Fig. 5.1. (continued) ratio (R:FR), (**c**) calculated daily net carbon gain per unit leaf area (A_{day}), (**d**) mean internode length, (**e**) mean leaf size, (**f**) the light saturated rate of net photosynthesis per unit leaf area at ambient CO_2 concentration (A_{sat}), (**g**) leaf dry mass per unit area (LMA), (**h**) organic nitrogen concentration in leaf dry matter (N_{DM}), (**i**) organic nitrogen per unit leaf area (N_{LA}), (**j**) stomatal conductance (g_s), (**k**) transpiration rate expressed relative to that of the highest leaf, (**l**) soluble sugar concentration in leaf dry matter. Panels c, d, e and f are results of the high nutrient treatment in an experiment described in Pons and Jordi (1998) and Pons and Anten (2004). Panels a, b, g, h, i, j, k and l show unpublished results of a similar experiment also carried out in a greenhouse in natural daylight (June 2003). The distribution of light was measured with line sensors containing an array of filtered photodiodes (Pons and van der Toorn 1988; Boonman et al. 2006).The g_s was measured with a Licor gas exchange system (LI-6400) and transpiration rate was measured as weight loss of detached leaves held in the original canopy position as described in Boonman et al. (2007)

to the light gradient (Fig. 5.1a, f, i; Chap. 4, Niinemets 2016). The gradient in leaf age runs thus parallel with these traits. As aging leaves show a decline in N_{LA} (Thomas and Stoddart 1980), the gradient may, at least partly, be constitutively generated by this age gradient. The question therefore arises to what extent the N_{LA} gradient in canopies is the result of the parallel age gradient the perception of canopy density. To investigate this, plants growing in dense canopies were compared with solitary growing plants or plants in more open canopies. A small light gradient across the foliage of these plants is unavoidable, but particularly in herbaceous plants with short-lived leaves, the gradient in N_{LA} and A_{sat} was stronger than expected on the basis of this small light gradient (Hirose et al. 1988; Anten et al. 1998; Boonman et al. 2007). It is thus likely that leaf age can indeed contribute to the leaf trait gradient in canopies, but there is an added canopy density effect. These observations indicate that plants can indeed perceive the leaf area density of the canopy where they grow, which adds to the age gradient effect. They respond with reallocation of resources for the photosynthetic apparatus from shaded lower leaves to among others the top leaves for building a high photosynthetic capacity in more favorable light conditions.

Situations where the light and age gradient are not parallel provide an opportunity to investigate the possible involvement of leaf age further. Ackerly (1992) studied a vine in tropical rainforest (*Syngonium podophyllum*) that grows horizontally towards dark tree stems where it starts to grow upwards towards the light. The light and age gradient are thus to some extent independent, and N_{LA} appeared to be related to PPFD and not age. The sedge *Carex acutiformis* was studied in the vegetative phase in a marsh where it dominates the canopy (Hirose et al. 1989; Schieving et al. 1992; Pons et al. 1993). These plants have erect leaves that span the whole light gradient. The leaves grow from the bottom and the age gradient is therefore opposite to the light gradient in each individual leaf. The N_{LA} and associated A_{sat} appeared to be parallel to the light gradient except for the leaf tips that showed signs of senescence. These observations support the notion that the distribution of light over a plant is more important than leaf age for induction of a gradient in leaf N and photosynthetic capacity in a canopy.

Experimental manipulation of the light environment can give more conclusive evidence. The above mentioned *Carex* species was grown with lighting from the sides, thus creating a homogeneous distribution of PPFD across the vertical leaves (Pons et al. 1993). This resulted in a much more homogeneous distribution of N_{LA} across plant height as compared to plants growing in an experimental light gradient, although the higher N_{LA} in the lower leaf sections did not result in an equivalently higher photosynthetic capacity. Hikosaka et al. (1994) grew the vine *Ipomoea tricolor* horizontally, thus creating a homogeneous distribution of light across the plant. Leaves of plants grown at high nutrient availability showed little difference in photosynthetic capacity along the stem. However, when grown at low nutrient availability, a gradient from the top to the base of the plant was evident, which was explained from leaf age.

Further manipulation of the light gradient independent of leaf age showed also that the light environment was much more important for the distribution of leaf N. Pons and Pearcy (1994) applied shading to single leaves on soybean (*Glycine max*) plants. These showed the decline in N_{LA} and the A_{sat} as expected from the effect of progressive shading of plants growing in canopies. Control leaves on separate plants showed some decline in these trait values, particularly on plants grown at low nutrient availability. Shading of leaves on plants that remained in high light conditions has been applied to several other species and yielded similar results (Pons and Bergkotte 1996; Pons and Jordi 1998; Frak et al. 2001, 2002; Vos and van der Putten 2001; Pons and de Jong – van Berkel 2004; Boonman et al. 2007). These experiments collectively show that leaf ageing when parallel to the

environmental gradient in a canopy can contribute to the development of a gradient in N_{LA} and A_{sat}. However, the light gradient is in most cases dominant for the induction of a leaf trait gradient.

When comparing plants in a dense stand with border plants or solitarily growing ones, it is often observed that their lower leaves prematurely senesce (Rousseaux et al. 1996; Boonman et al. 2006). Earlier senescence was also induced experimentally by shading individual soybean leaves at low nutrient availability (Pons and Pearcy 1994), and leaves of *Helianthus annuus* (Rousseaux et al. 1996), *Solanum tuberosum* (Vos and van der Putten 2001), *Phaseolus vulgaris* (Pons and de Jong – van Berkel 2004) and *Arabidopsis thaliana* (Weaver and Amasino 2001; Booman et al. 2007; Brouwer et al. 2012). Apparently, the environmental gradient in a canopy induces a decrease in leaf N that contributes to an efficient distribution of photosynthetic capacity in the canopy gradient. This ultimately leads to accelerated leaf senescence in herbaceous plants with short-lived leaves. The induction of leaf senescence is typical for the effect of shading a part of the foliage of a plant as in a canopy gradient. When whole plants were shaded (Pons and Pearcy 1994) or darkened (Weaver and Amasino 2001) this was not observed. This difference between the effect of a light gradient over a plant's foliage and whole plant shading indicates that the responses to these light conditions are regulated differently. The reallocation of resources from shaded leaves of plants growing in canopies to upper leaves in more favorable light conditions is thus not just a response to the local light conditions in a particular canopy position, but is regulated at the whole plant level.

The shade-induced senescence in lower leaves is involved in the regulation of the leaf area index (LAI) in a growing canopy. New leaves grow at the top and lower ones are dropped at the bottom, maintaining a more or less constant LAI. As LAI is lower at low nutrient availability (Anten 2002; Hikosaka 2003), induction of senescence occurs before the light compensation is reached under these conditions (Oikawa et al. 2006). Earlier induction of leaf senescence at low compared to high nutrient availability was also found in leaf shading experiments (Pons and Pearcy 1994). The functional significance of shade induced senescence in canopies was shown in an experiment with P_{SAG12}-*IPT* tobacco (*Nicotiana tabacum*) that has delayed leaf senescence (Boonman et al. 2006). In these genetically modified plants, CK synthesis is induced in tissues at the onset of senescence, which delays it (Gan and Amasino 1995). Growing under nutrient limitation, wild type plants performed better when grown in competition with these plants because they formed more leaf area at the top of the canopy, but not additional photosynthetic capacity per unit leaf area, and did not have the negative effect of respiring leaves in deep shade on the carbon balance.

The above description of regulation of leaf senescence by the canopy gradient pertains to fast-growing herbaceous plant species that continuously form new relatively short-lived leaves at the top. The export of resources from shaded leaves originally developed in high light causes that the decrease in N_{LA} is largely the result of a decrease in N per unit dry mass (N_{DM}) rather than a decrease in LMA (Niinemets et al. 2015). The situation is likely to be comparable for pioneer trees that have a similar pattern of leaf growth and senescence as observed in tropical (Ackerly and Bazzaz 1995; Ackerly 1996) and in temperate forests (Vapaavuori and Vuorinen 1989; Kull et al. 1998). However, more late-successional deciduous trees form their canopies mostly in a single flush of leaf growth at the beginning of the growth season. The light environment for individual leaves is thus much less dynamic. As in herbaceous plants, canopies of late successional trees have gradients in leaf traits that contribute to efficient utilization of resources for whole plant carbon gain (Chap. 4, Niinemets 2016). However, shade-induced export of resources and leaf senescence is much less important in this functional

group. Consequently, the gradient in N_{LA} is more associated with a gradient in LMA and much less with N_{DM} (Niinemets et al. 2015).

IV. Perception of and Response to Canopy Density

Plants have a multitude of sensory mechanisms for the detection of the proximity of neighbors. This has been mainly studied in the context of shade avoidance, i.e. morphological responses that avoid shading of a plant's leaves (Chap. 6, de Wit and Pierik 2016). Much less is known about the mechanisms involved in the perception of leaf area density of canopies with respect to effects on leaf traits. Reallocation of resources for the photosynthetic apparatus from shaded leaves to among others sunlit ones can also be seen as a form of shade avoidance, but this term is normally reserved for morphological aspects. The change in spectral composition of the light with depth in a canopy is dominant with morphological shade avoidance, and is perceived by the phytochrome system (Smith and Whitelam 1997). Most effects of the environmental gradient in canopies on leaf traits can be simulated by spectrally neutral shading of a leaf or part of the foliage of a plant, but as discussed in Sect. IV.A, the spectral component of the light climate is involved as well. Also other components of environmental gradients in canopies can be involved. Several perception mechanisms for reallocation of resources and acclimation of leaf traits in canopies have been proposed. These will be discussed with respect to possible involvement in the regulation of canopy gradients in leaf traits in the following sections.

A. The Light Gradient; Spectrally Neutral Shading or Low R:FR Effects

Most experiments on partial shading of the foliage of plants are done with spectrally neutral shading. This treatment simulates most shading effects in a canopy gradient. As in canopies (Fig. 5.1), experimental reduction of PPFD incident on one or more leaves attached to a plant that remains in high light causes decreases in LMA, N_{DM}, N_{LA} and A_{sat} or other measures of photosynthetic capacity per unit leaf area (Pons and Pearcy 1994; Pons and Bergkotte 1996; Ono et al. 2001; Vos and van der Putten 2001; Pons and de Jong – van Berkel 2004; Boonman et al. 2007; Brouwer et al. 2012). These variables are associated with reallocation of resources at the whole plant level and acclimation at the leaf level. Only the content of chlorophyll per unit leaf area (Chl_{LA}) is more or less maintained initially (Fig. 5.2a). This means that when A_{sat} per unit leaf area decreases, A_{sat} per unit chlorophyll (A_{chl}) decreases as well (Fig. 5.2b, c), which is evidence of acclimation at the chloroplast level. It involves a shift from photosynthetic capacity to light harvesting and is typical for plants acclimating at low irradiance (Hikosaka et al. 2006). Most important is an increase in the size of the light harvesting complex associated with photosystem II (LHCII) that is rich in chlorophyll b. The result is a decrease in the chlorophyll a/b ratio (Chl a/b). Chloroplast-level photosynthetic acclimation in canopies contributes to substantially improved resource use efficiency for carbon gain (Evans 1993, Pons and Anten 2004). Reduced PPFD on lower leaves thus causes photosynthetic acclimation in chloroplasts while reallocation of resources proceeds (Pons and Pearcy 1994; Pons and de Jong – van Berkel 2004). At a certain point senescence is induced, which results in further reallocation of all resource that can be mobilized. The mechanisms that can be involved in the regulation of these effects of the PPFD gradient are discussed below.

Far-red radiation (FR) is known to induce leaf senescence through phytochrome action (DeGreef and Butler 1971; Biswal and Biswal 1984). It is thus likely that the decrease in R:FR ratio in canopies is also involved in reallocation of resources away from shaded leaves. Guiamet et al. (1989) investigated this by irradiating attached

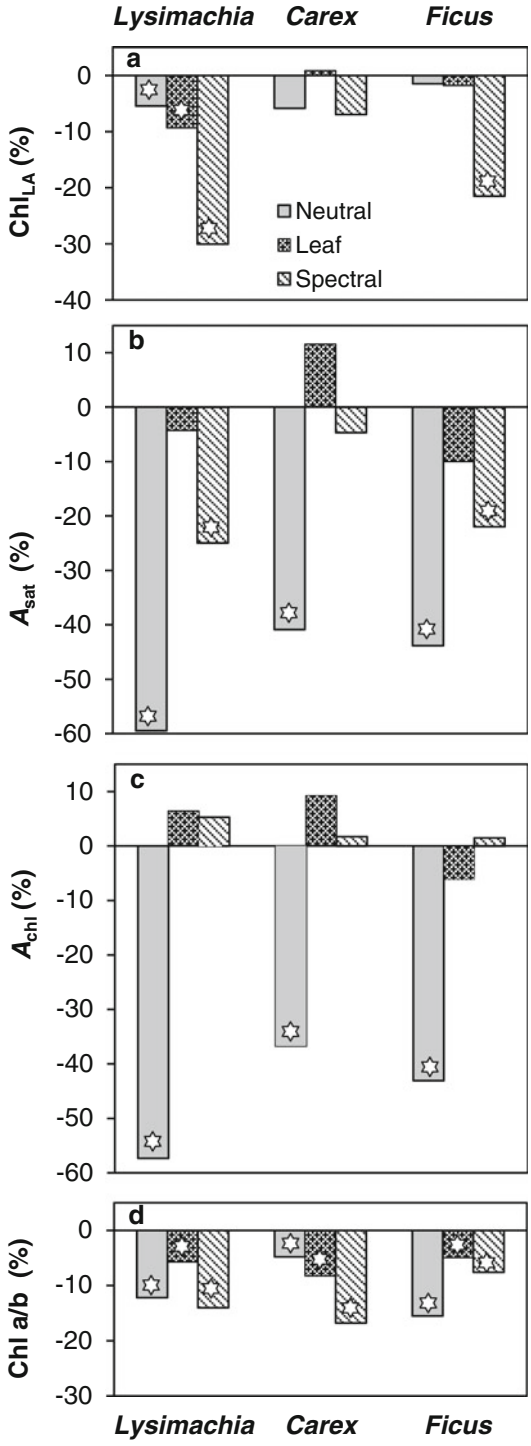

Fig. 5.2. Effect of spectrally neutral shading and/or reduced red:far-red ratio (R:FR) treatment on leaf traits. One leaf was subjected to the treatment during two weeks and the other leaves on the plant remained in the moderately high light and high R:FR growth conditions. Spectrally neutral shading to 7 % of daylight in a greenhouse (Neutral); shading by another leaf with the same effect on PPFD (7 %) and additionally a reduced R:FR to 0.08 (Leaf); a strong beam of supplemental FR on a leaf in a growth chamber at PPFD 250 μmol m^{-2} s^{-1} that reduced R:FR to 0.05 (Spectral). Treatment effects are expressed relative to leaves on control plants (Neutral and Spectral), or relative to the spectrally neutral shading treatment (Leaf). Three species are shown, the herbaceous dicot *Lysimachia vulgaris*, the monocot *Carex acutiformis* and the evergreen tree *Ficus benjamina*. (**a**) chlorophyll per leaf area (Chl_{LA}); (**b**) light saturated photosynthesis per leaf area (A_{sat}); (**c**) A_{sat} per unit chlorophyll (A_{chl}); (**d**) chlorophyll a/b ratio (Chl a/b). A star in a bar refers to a significant effect. Calculated from Pons and de Jong – van Berkel (2004)

primary bean leaves (*Phaseolus vulgaris*) using light with different R:FR ratios. Low ratios resulted in loss of chlorophyll and protein, which was interpreted as induction of leaf senescence. This is evidence of effects of the spectral component of shade light on resource reallocation in canopies. But is it additional to the effect of reduced PPFD?

Pons and de Jong – van Berkel (2004) compared the effect of shade from a spectrally neutral filter with shade from another leaf. Both had the same PAR transmission. The treatment periods for *Phaseolus vulgaris* and *Lysimachia vulgaris* were one and two weeks respectively. There were only small spectrally neutral effects on Chl_{LA}, but effects on A_{sat} and A_{chl} were large, whereas the spectral component did not have much additional effect within the treatment period (Fig. 5.2; Pons and de Jong – van Berkel 2004). This suggests that before the onset of senescence, reallocation of resources and acclimation is largely regulated by PPFD. However, when the treatment period with *Phaseolus* was extended, shading by a leaf caused an earlier decline in Chl_{LA} end subsequent senescence compared to spectrally neutral shade (Pons and de Jong – van Berkel 2004). This is evidence of and effect of the R:FR in shade light on the induction of senescence in addition to a PPFD effect. The results were different when only

additional FR was applied at a relatively high irradiance. N_{LA}, N_{DM}, A_{sat} and Chl_{LA} were reduced, but not LMA and A_{chl} (Fig. 5.2; Pons and de Jong – van Berkel 2004), showing that the R:FR can have an effect on reallocation of resources at the whole plant level when operating as a single factor. Chl a/b ratio was reduced at low R:FR irrespective of the neutral shading treatment (Fig. 5.2d). A low R:FR increases the PSII: PSI ratio, and thus the chlorophyll b rich LHCII, which re-establishes the balance in excitation of the two photosystems as a result of absorbance of FR by PSI (Anderson et al. 1995). Rousseaux et al. (1996, 2000) investigated the role of spectral shade by manipulating the spectrum with filters and mirrors in a canopy of *Helianthus annuus*. FR enrichment accelerated senescence, whereas FR-depleted and R-enriched shade light delayed it. These experiments demonstrate that the R:FR ratio in canopy gradients is involved in the reallocation of resources and the induction of leaf senescence, but not in chloroplast-level acclimation to reduced irradiance in shade.

Apart from the two herbaceous dicots mentioned above, two monocots, *Brachypodium pinnatum* and *Carex acutiformis*, were included in the experiments of Pons and de Jong – van Berkel (2004). The effects of spectrally neutral shading and supplemental FR, and the additional spectral effect from a leaf were essentially the same for *Brachypodium* compared to the two dicots. However, *Carex* showed no response to a spectral change on Chl_{LA} and A_{sat} (Fig. 5.2a–c). Only Chl a/b was reduced at low R:FR (Fig. 5.2d). The spectral component is thus involved in the perception of the canopy gradient with respect to photosynthetic resource reallocation in many but not all species.

B. The Temperature Gradient

A gradient of leaf temperature in canopies runs parallel with the light gradient (Niinemets et al. 1999; Zweifel et al. 2002). Photosynthetic acclimation to temperature shows similarities with acclimation to irradiance (Hüner et al. 1998), but in opposite direction. A higher temperature causes a shift to light harvesting at the expense of photosynthetic capacity, thereby decreasing A_{chl} and Chl a/b, and also LMA (Hikosaka et al. 2006). This would then counteract the effect of the PPFD gradient on these traits. However, the PPFD gradient is much larger than the temperature gradient in dense canopies and dominates the leaf trait gradient.

Upper canopy leaves can reach high temperatures when high air temperature, exposure to direct sunlight, stomatal closure and low air turbulence coincide. Niinemets et al. (1999) found better heat tolerance in these leaves in two deciduous tree species. Bauerle et al. (2007) manipulated temperature independently of canopy position. They found evidence of temperature acclimation of photosynthetic capacity and respiration. Also the ratio between the electron transport and carboxylation capacities (J_{max}/V_{cmax}) was adjusted (Hikosaka et al. 1999). Irradiance and temperature can interact in their effect on photosynthetic acclimation (Pons 2012), which further complicates interpretation of acclimation in the canopy gradient context. The temperature gradient can thus modify the effect of the PPFD gradient on leaf traits in canopies.

C. Photoreceptors

Plants have a multitude of photoreceptors for the perception of the light environment. As mentioned above, phytochromes are involved in the perception of spectral canopy shade, but they can also be involved in the perception of other aspects of the light environment. Phototropins and cryptochromes are involved in responses to irradiance of blue light (Casal 2013). Hence, photoreceptors are important candidates for the perception of canopy light gradients and the regulation of the response.

The involvement of photoreceptors in the perception of the spectrally neutral irradiance component of the canopy light gradient

for acclimation of leaf traits has received little attention. Working with a limited number of photoreceptor mutants in *Arabidopsis thaliana*, Walters et al. (1999) found little evidence for an important role of photoreceptors in photosynthetic acclimation when whole plants were exposed to spectrally neutral shading. Weaver and Amasino (2001) simulated the canopy light gradient by darkening individual *Arabidopsis* leaves, which caused induction of senescence as with shading. The phytochrome and cryptochrome mutants that they used all showed essentially the wild type response with respect to this trait. *Arabidopsis* photoreceptor mutants were also used by Boonman et al. (2009). They included also phototropin mutants for the spectrally neutral shade effect on single leaves. Photosynthetic capacity was down-regulated in all mutants as in the wild type. They concluded that, or photoreceptors are not essential for canopy PPFD gradient effect on photosynthetic resource reallocation and senescence, or there is a high degree of redundancy, which means that several photoreceptors are involved that can take over when one or more others are lacking. There was one exception, the mutant of *Arabidopsis* deficient in phytochrome D (*phyD*) and the *phyAphyBphyD* triple mutant lacked the decrease in Chl a/b that is normally associated with shade (Boonman et al. 2009). PhyD is thus important in this species for the acclimation of pigment composition in the canopy light gradient.

The phytochrome family of photoreceptors is very important for the perception of the spectral component of canopy shade (Smith and Whitelam 1997). Of these PhyB is the most important member involved in the morphological shade avoidance response with other phytochromes playing a role as well (Chap. 6 de Wit and Pierik 2016). What species of phytochrome is involved in the perception of the spectral canopy gradient effect on leaf traits has not been extensively investigated. Contrary to wild type tobacco plants (*Nicotiana tabacum*), senescence was not induced in low R:FR light when phyA was overexpressed (Rousseaux et al. 1997). Phytochrome A levels are low in green plants at high irradiance and high R:FR ratios as a result of degradation of PHYA in the Pfr form (Casal et al. 1997). An *Arabidopsis phyA* mutant showed a similar reduction of A_{sat} and Chl_{LA} in response to supplemental FR at moderately high irradiance compared to wild type *Arabidopsis*, whereas a *phyB* mutant showed no response (unpublished results). This is consistent with the notion that phyA is not active at high PPFD, whereas phyB appears to be the main player in the regulation of resource reallocation in response to the R:FR ratio in these conditions. However, *phy*A mutants showed accelerated loss of chlorophyll in shaded leaves irrespective of spectral composition (Brouwer et al. 2012), indicating that phyA is involved in the maintenance of chlorophyll in shade, counteracting the effect of phyB. The maintenance of chlorophyll is achieved by up-regulation of chlorophyll synthesis rather than the down-regulation of its degradation (Brouwer et al. 2014).

D. Redox and ROS Signaling

Signals are generated in the chloroplast in response to light and other environmental factors that interfere with chloroplast functioning. These can operate in the chloroplast itself, where they trigger pathways for adjustment to altered conditions. The signals can also exit the chloroplast where they can be involved in intracellular communication between organelles and systemic signaling. These processes have recently been reviewed (e.g. Rochaix 2011; Suzuki et al. 2012; Hüner et al. 2012).

A redox signal is generated at the level of the plastoquinon (PQ) pool between photosystem II (PSII) and photosystem I (PSI). Changes in light spectrum and irradiance alter the balance between excitation of PSII end PSI and the excitation pressure of the electron transport system as a whole. This affects the redox state of PQ that generates adjustments, which restores the balance between the two photosystems and light

harvesting (Mittler et al. 2011). The redox signaling system is thus involved in acclimation at the chloroplast level (Hüner et al. 2012).

Over-excitation of the photosynthetic membrane can cause the generation of reactive oxygen species (ROS) such as singlet oxygen ($^1O_2$) and H_2O_2. Scavenging systems are induced in high irradiance conditions for protection against oxidative damage. However, ROS is also implicated in signaling, not only locally but evidence is accumulating for a role in systemic signaling as well (Mullineaux et al. 2006; Mittler et al. 2011). At moderately high irradiance, H_2O_2 is specifically generated by chloroplasts in the bundlesheath cells possibly as a consequence of dependence on malate for their CO_2 supply (Hibberd and Quick 2002). It is suggested that the H_2O_2 is excreted in the transpiration stream. The available evidence points to the implication of this pathway in wounding and pathogen responses (Suzuki et al. 2012). The pathway could also be involved in light signaling in canopy gradients, but that requires further investigation.

E. Assimilate Supply

The gradient in PPFD is clearly the most important environmental factor for the regulation of leaf traits in the canopy gradient as discussed above. Apart from perception by photoreceptors, other processes are under control of irradiance. This is the photosynthetic rate in the first place. As a consequence of the difference in irradiance gradient, solitary plants have a much smaller gradient of photosynthesis across their height compared to plants in dense canopies (Fig. 5.1c). The possible involvement of a signal associated with the rate of photosynthesis in individual leaves is discussed next.

The lower leaves in a dense canopy are often exposed to a PPFD around the light compensation point. Photosynthesis approaching the rate of respiration has been suggested to be a signal for the induction of senescence, resulting in shedding of leaves as soon as assimilate export approaches zero (Kull 2002). This happens indeed at high nutrient availability, but senescence is known to be induced at higher irradiance when growing at low nutrient availability (Anten et al. 1995; Oikawa et al. 2006), which reduces LAI. Senescence at higher irradiance than light compensation is also known from early successional shade intolerant trees (Ackerly 1996; Kitajima et al. 2005), whereas late successional species tend to keep leaves at a lower irradiance resulting in a higher LAI (Niinemets 2010). Induction of senescence by a zero carbon balance can thus not be universal. Although a switch of a leaf from a source of carbohydrates to a sink could be a signal, no experimental evidence has been reported for such a regulation mechanism.

Associated with the gradient in irradiance and photosynthetic rate, there is a parallel gradient in availability of non-structural carbohydrates (Boonman et al. 2007). This is reflected in high concentrations of sugars en/or starch in the upper leaves of dense canopies (Fig. 5.1l). Several studies have explored the potential for the regulation of leaf traits in dense canopies by the availability of sugars (Kull and Kruijt 1999; Ono et al. 2001; Kull 2002; Niinemets et al. 2004). High sugar concentrations are known to down-regulate photosynthetic genes and induce senescence (Krapp et al. 1993), although the effect depends on leaf age (Araya et al. 2006). However, export of resources and induction of senescence occurs in the lower leaves in canopies that have low sugar concentrations (Fig. 5.1l), which is thus not consistent with a role for this form of sugar sensing in its regulation in canopy gradients. Other sugar signaling pathways have been identified more recently that interact with hormonal networks (Smeekens et al. 2010). They serve to monitor the sugar status of the plant and adjust growth and development to external factors such as light and nutrient availability. There is evidence that sugar starvation is involved in the induction of senescence (Buchanan-Wollaston et al. 2005; Baena-Gonzalez and

Sheen 2008). The sensing of the sugar status could be involved in the adjustment of leaf traits to progressive shading in fast growing canopies. However, no direct evidence is available for such a role in lower canopy leaves. Nevertheless, this possibility deserves further investigation.

Sugar insensitive and hypersensitive mutants of *Arabidopsis* were used by Boonman et al. (2009) to investigate whether sugar signaling is important for reduction of photosynthetic capacity in response to shading of a leaf. The four mutants that were included in the study responded similarly to the wild type with respect to a reduction of photosynthetic capacity either expressed per unit chlorophyll or per unit area in response to spectrally neutral shading. This is not conclusive evidence that sugar signaling is not involved in the leaf shading effect on photosynthetic capacity. There can be redundancy of signaling pathways, meaning that when the normal operation of sugar signaling is disturbed, its action could be taken over by other pathways.

F. Cytokinins and Resource Reallocation

Stomata respond to irradiance, resulting in a gradient of stomatal conductance parallel to the PPFD gradient in canopies (Fig. 5.1j). As explained above, air turbulence is less in dense canopies, which decreases the conductance of the a leaf's boundary layer for water vapor diffusion. Water vapor can accumulate in the canopy and the temperature of sun-exposed upper leaves tends to be higher than the lower shaded leaves, causing a canopy gradient in leaf-to-air vapor pressure difference. These factors generate a gradient in transpiration rates parallel to the light gradient (Fig. 5.1k). It was hypothesized by Pons and Bergkotte (1996) that the environmental gradient in a dense canopy is perceived by a signal in the transpiration stream, which is used for the regulation of the reallocation of nitrogen and other resources for the photosynthetic apparatus.

Experimental shading one leaf of a plant with its other leaves at higher irradiance reduces the transpiration rate of the shaded leaf relative to the unshaded leaves (Pons and Bergkotte 1996). This is similar as found in lower canopy leaves that transpire less compared to upper leaves (Fig. 5.1k). When reducing the transpiration rate of a leaf experimentally without altering irradiance by increasing the humidity around that leaf, many effects of shading could be simulated (Pons and Bergkotte 1996; Pons and Jordi 1998; Pons et al. 2001; Boonman et al. 2007, 2009). After one or two weeks of incubation at a high humidity, the leaves had a reduced N_{LA} and A_{sat} (Figs. 5.3 and 5.4), which is similar to the shading effect. These traits pertain to resource partitioning at the whole plant level. But also the traits pertaining to shade acclimation at the chloroplast level, chlorophyll per unit leaf N, A_{chl} and Chl a/b, changed in a similar way as with shading (Fig. 5.4; Pons and Bergkotte 1996; Pons and Jordi 1998). The humidity effects were pronounced in several herbaceous species (*Phaseolus vulgaris, Lysimachia vulgaris, Humulus lupulus, Nicotiana tabacum, Arabidopsis thaliana*). In *Arabidopsis*, leaf senescence was also induced by the high humidity treatment, similar to the shading effect (Boonman et al. 2007). A difference with shading was that LMA was hardly reduced (Figs. 5.3 and 5.4). The photosynthetic rate of a leaf as manipulated with the CO_2 concentration had a large effect on LMA of *Phaseolus* leaves (Pons and Bergkotte 1996). The presence of a shading effect on LMA and its absence in the case of high humidity is thus likely due to the fact that photosynthesis had decreased in the former, but had not changed much in the latter. The simulation of many shading effects by experimental reduction of the transpiration rate relative to that of the other leaves on the same plant is strong evidence that a signal carried in the transpiration stream regulates resource partitioning at the whole plant level in response to partial shading of a plant's foliage. The data also show evidence

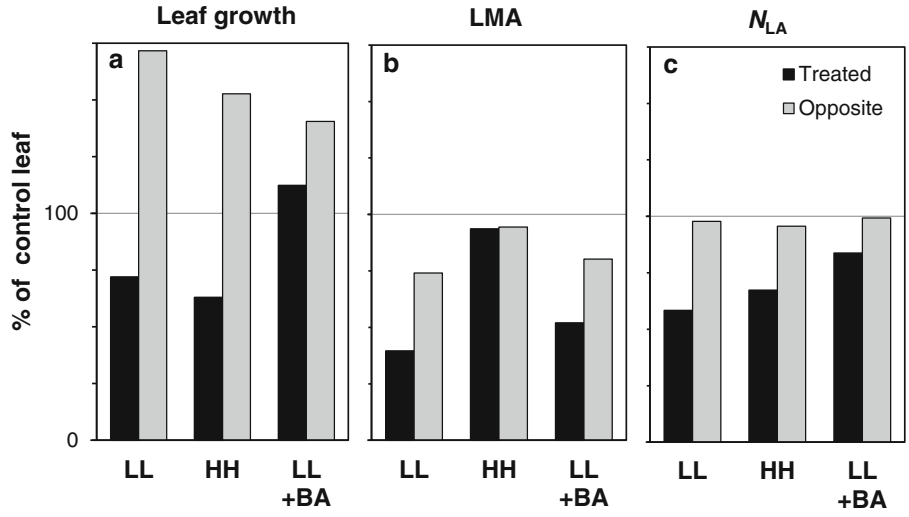

Fig. 5.3. The effects on both primary bean leaves (*Phaseolus vulgaris*) of experimental manipulation of one leaf. The leaf was shaded to 7 % of growth irradiance (300 μmol m^{-2} s^{-1}) at the growth humidity (70 %) (low PPFD and low humidity, LL); the leaf was enclosed in a transparent cuvette that was flushed with high humidity air at the growth irradiance that reduced transpiration (high PPFD and high humidity, HH); application of the synthetic cytokinin benzyl adenine (+BA) on a LL treated leaf. The rest of the plant remained at the growth irradiance and humidity. (**a**) leaf growth, (**b**) leaf mass per area (LMA) and (**c**) N per leaf area (N_{LA}). Values of the variables are expressed relative to leaves on control plants without a treatment (LL and LL + BA) or relative to control leaves in a cuvette flushed with low humidity air (HH). Calculated from Pons and Bergkotte (1996) and Pons et al. (2001)

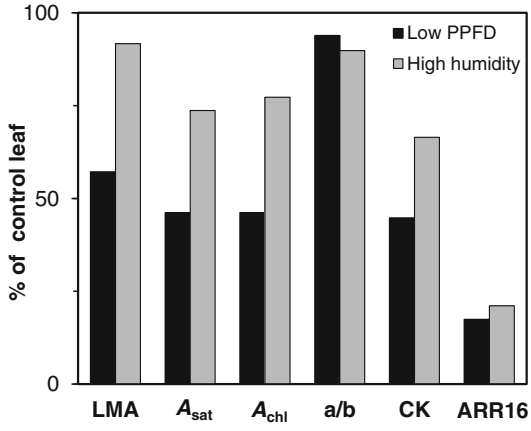

Fig. 5.4. The effect of the treatment of one *Arabidopsis* leaf with spectrally neutral shading (low PPFD) or with high humidity air in a cuvette. Variables are expressed relative to leaves on control plants at growth room conditions (PPFD 200 μmol m^{-2} s^{-1}, RH 70 %) (low PPFD) or leaves in a cuvette flushed with growth chamber air at the growth chamber PPFD (high humidity). Variables are: leaf mass per unit area (LMA), the light saturated rate of photosynthesis per unit leaf area (A_{sat}), A_{sat} per unit chlorophyll (A_{chl}), the chlorophyll a/b ratio (a/b), total cytokinin content per unit fresh mass (CK), and transcript levels of the Arabidopsis response regulator 16 (ARR16). Calculated from Boonman et al. (2007, 2009)

for a role of a xylem-carried signal in photosynthetic acclimation at the chloroplast level.

Cytokinins (CKs) carried in the transpiration stream are a candidate signaling compound and its distribution could operate as a measure of relative differences in transpiration rate between leaves, which is representative of differences in irradiance. Several lines of evidence are in favor of this proposed signaling mechanism. An important place of synthesis of CKs is the root system where they are loaded into the xylem and transported to the shoot (Mathysse and Scott 1982). Although CKs may be modified along the xylem pathway (Jameson et al. 1987; Singh et al. 1992) no differences were found in the CK composition in xylem sap collected from the midrib of a tobacco leaf whether it was shaded or not (Boonman et al. 2007). The spectrum of CKs is thus likely to be delivered to the leaves in proportion to their transpiration rates. The phytohormone increases synthesis of photosynthetic proteins (Flores and Tobin 1988;

Chory et al. 1994; Kusnetsov et al. 1994), decreases protease activity (Li et al. 2000) and delays senescence (Gan and Amasio 1995), and consequently increases sink strength (Mothes and Engelbrecht 1963; Jordi et al. 2000). These known characteristic of CKs are consistent with a role in resource partitioning at the whole plant level.

The distribution of CKs between leaves provides another line of evidence. In *Phaseolus* canopies, CKs with dihydrozeatin as the dominant type showed higher concentrations in lower leaves of an open canopy compared to a dense one (Pons et al. 2001). The measurement of the full spectrum of CKs in *Nicotiana* canopies resulted in a complicated picture (Boonman et al. 2009). There was a tendency that the CKs transported in the xylem in this species, the isopentenyl adenine types, were somewhat more homogeneously distributed in the open canopy compared to the dense one. However, the interpretation of CK concentrations in leaf tissue in canopies in terms of import rates is not straightforward as there is also *de novo* synthesis, oxidation and transformation, which is different in young and old leaves (Nordstrom et al. 2004). Comparison of CKs in experimentally manipulated leaves of the same age gave more consistent results. Concentrations were generally higher in high light and low humidity exposed leaves compared to low light and high humidity (Pons et al. 2001; Boonman et al. 2007). This supports a role for the partitioning of xylem carried CKs in canopy signaling.

Using *Phaseolus* (Pons et al. 2001), *Nicotiana* and *Arabidopsis* (Boonman et al. 2007) it was shown that the effects of shading and high humidity could at least partly be rescued by external application of CK. This was true for leaf traits pertaining to the regulation of the reallocation of resources between leaves, such as LMA, N_{LA}, A_{sat}, Chl_{LA} and senescence, and the transcript levels of the small subunit of Rubisco (rbcS). The most convincing evidence that imported CKs are involved, however, comes from the transcription of two genes that are highly responsive to CK action. The transcription of the type A Arabidopsis response regulators ARR7 and ARR16 was strongly down-regulated in shaded and high humidity treated *Arabidopsis* leaves (Fig. 5.4), whereas CK application rescued the effect on these regulators completely (Boonman et al. 2007). However, the variables pertaining to acclimation at the chloroplast level, Chl a/b and A_{chl}, were not affected by CK application (Pons et al. 2001; Boonman et al. 2007). The evidence from these experiments point to an important role of CKs carried in the transpiration stream and their distribution between leaves proportional to their transpiration rate for the regulation of leaf traits in canopies. This is particularly so for the reallocation of resources for the photosynthetic apparatus away from shaded leaves to leaf area in favorable light conditions, but not for chloroplast level photosynthetic acclimation.

Most leaf shading effects could be simulated by a reduction in transpiration, but application of CK could not rescue all the transpiration effects. This points to signals carried in the transpiration stream other than CKs that are also involved in the regulation of shading effects on leaf traits in canopies. There is cross talk between CK and other signaling pathways, including the phytochrome pathway (Werner and Schmüling 2009). Wild type leaf shading effects on A_{sat} were also present in mutant and transgenic *Arabidopsis* plants impaired in CK perception and synthesis (Boonman et al. 2009). Apparently, other signaling pathways can take over the full response when the CK pathway is impaired. The picture emerges of a complicated signaling network ultimately resulting in the canopy gradient effect on leaf traits.

G. Systemic Signaling Involved in Leaf Growth and Structure

Several cases have been described where the light conditions of one leaf affects other leaves on the same plant as will be discussed below. It is likely that such systemic effects also play a role in canopies. This is suggested by the comparison of leaves from *Lysimachia vulgaris* growing in open canopies with those from dense canopies at

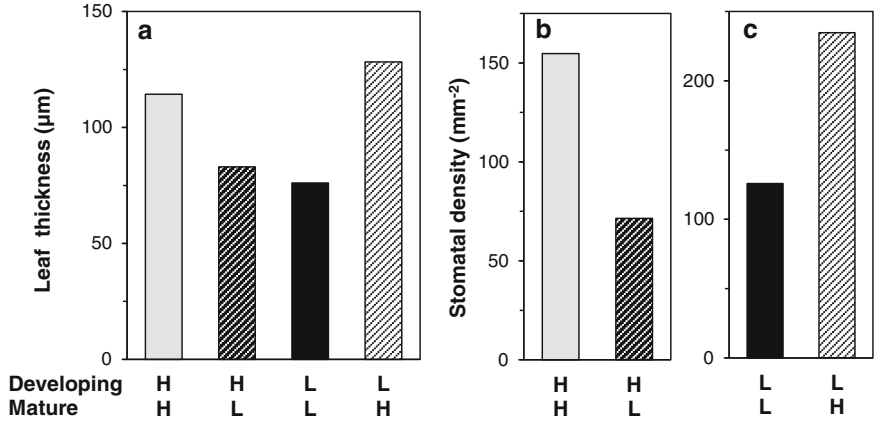

Fig. 5.5. The effect of irradiance incident on mature and developing leaves on leaf thickness and adaxial stomatal density of developing leaves. Exposure of mature leaves to low PPFD (L) resulted in shade leaf trait values and exposure to high PPFD (H) gave sun leaf values in developing leaves, irrespective of the PPFD on the developing leaves themselves. (**a**) leaf thickness of *Chenopodium album* (Yano and Terashima 2001); (**b**) and (**c**) stomatal density of *Nicotiana tabacum* (Thomas et al. 2004)

the same irradiance. The latter have a lower LMA compared to the open canopy leaves (Fig. 5.1g; Hirose et al. 1988). However, the lower LMA was not at the expense of the photosynthetic capacity of these leaves, since N_{DM} was higher resulting in a similar N_{LA} (Fig. 5.1h, i; Hirose et al. 1988; Pons and Jordi 1998). Apparently, LMA is not only determined by the local irradiance, but also by the irradiance conditions and thus photosynthetic rate of other leaves.

When mature leaves of tobacco (*Nicotiana tabacum*) were shaded, the young developing leaves in high light had a reduced stomatal density, just as in shade-grown whole plants (Fig. 5.5b, c; Thomas et al. 2004). Similar results were obtained for *Arabidopsis* using CO_2 as an environmental factor that regulates photosynthetic rate (Lake et al. 2001). Yano and Terashima (2001, 2004) also manipulated the light environment of mature leaves of *Chenopodium album* independently of young developing leaves. The sun or shade type anatomy of young developing leaves appeared also to be determined by the light environment of mature leaves (Fig. 5.5a). Only the chloroplast structure was determined by the local light climate. Similar results were found for the C_4 species *Sorghum bicolor*. The leaf anatomy including stomatal density and also the tolerance to high light of developing leaves was under control of the light conditions of mature leaves, but not the grana stacking in the chloroplasts (Jiang et al. 2011). Apparently, a systemic signal generated in the mature leaves by shading is transported to the meristem where it regulates leaf development.

Yano and Terashima (2001) and Araya et al. (2008) hypothesized that the availability of assimilates from the mature leaves, as determined by the light environment, is a good candidate for the signal involved in the regulation. This is supported by the regulation of stomatal density of developing leaves by the CO_2 environment of mature leaves. A high CO_2 concentration, and thus photosynthetic rate, resulted in a high stomatal density in developing leaves (Lake et al. 2001). Sugar levels were transiently high in the meristem (Coupe et al. 2006). Although direct evidence is lacking, sugar levels in the meristem can respond to the light environment, and thus photosynthetic rate, of mature leaves and could be a signal for the development of a sun- or shade-type anatomy and other traits in young leaves.

Shading a leaf can also affect the growth of other leaves. Not only resources were

reallocated as a result of shading of one leaf of the pair of primary bean leaves (*Phaseolus vulgaris*) (Sect. IV.F), but when applied to a growing leaf, the expansion was reduced in the shaded leaf and increased in the opposite leaf (Pons and Bergkotte 1996) (Fig. 5.3a). This shading effect was also simulated by exposing the target leaf to a high humidity. Counterintuitively, the growth of the leaf that was enclosed in a chamber at high humidity was reduced, whereas growth of the opposite leaf remaining in a lower humidity had increased. Pons and Bergkotte (1996) hypothesized that CKs are involved. They are known to stimulate leaf expansion (Leopold and Kawase 1964; van Volkenburgh 1999), which was also true for the primary bean leaves (Pons et al. 2001). As argued in Sect. IV.F, the distribution of CKs carried in the xylem is likely to follow the transpiration rates of the leaves. The opposite leaf would then receive more CKs compared to the leaf treated with shade or high humidity, which then regulates the expansion of these leaves. Other compounds carried in the transpiration stream could also be involved, including resources for growth.

Preferential leaf area expansion in more favorable light conditions is also found in canopies. The largest leaf area was present higher in a dense canopy compared to a more open spacing of *Lysimachia vulgaris* (Fig. 5.1e). Upper leaves were also larger relative to lower leaves in a dense canopy of tobacco (*Nicotiana tabacum*) compared to leaves from plants grown in an open canopy (Boonman et al. 2007). When wild-type tobacco was grown in competition with genetically modified plants where CK synthesis is induced before the onset of leaf senescence (P_{SAG12}-*IPT*), they developed more leaf area in the upper canopy layers, which gave them a competitive advantage (Boonman et al. 2006). The CKs in the lower leaves of the modified plants apparently increase their sink strength relative to the upper leaves of the P_{SAG12}-*IPT* plants, thus decreasing the transport of resources for leaf expansion to the latter. The available evidence indicates that, at least in herbaceous plants, the distribution of CKs and the availability of assimilates possibly supplemented with other signaling mechanisms act together in the systemic regulation of the distribution of leaf area growth in canopies.

V. Comparison Between Functional Groups

Most studies on the regulation of leaf traits in canopy gradients were done with relatively fast growing herbaceous species. They show continuous growth of leaves mostly at the top when growing in dense canopies. These are then progressively shaded with further canopy development, at least in the vegetative phase, and ultimately the lower leaves senesce. Similar canopy development with high leaf turnover is found in woody species with continuous leaf growth (Chap. 4, Niinemets 2016). The previous sections show that the top leaves that developed in high light acclimate to the progressive shading when fully developed. But differently from leaves on a plant that grows in low light, the shaded leaves in a canopy gradient show induced leaf senescence. However, growth forms with different canopy development have different patterns of acclimation and senescence that may be regulated by a different mechanism. Relevant growth forms in this respect are deciduous trees that form their canopies in a single flush at the beginning of the growth season and evergreen trees that have different cohorts of leaves that are progressively shaded over several years (Chap. 4, Niinemets 2016).

Leaves of single flush deciduous trees experience progressive shading to a much lesser extent compared to plants with a fast leaf turnover. They show a canopy gradient in sun – shade leaf anatomy, and induction of senescence in shaded leaves hardly occurs. The anatomy can already have been determined in the bud that developed in the previous year depending on light conditions (Roy et al. 1986; Esrich et al. 1989; Uemura et al. 2000). This limits acclimation capacity to changes in light conditions as may occur

with disturbance. The canopy gradient in N_{LA} is largely based on the gradient in LMA at a rather constant N_{DM} (Chap. 4, Niinemets 2016). This contrasts with fast leaf turnover plants where N_{DM} decreases with canopy depth, whereas LMA decreases much less (Niinemets et al. 2015). The canopy position of developing leaf primordia in the buds on single-flush deciduous trees is likely perceived by the surrounding leaves. The light signal would then be transferred from the mature leaves to the buds on the same branch. This shows resemblance with the systemic signaling from mature to developing leaves found in herbaceous plants as discussed in Sect. IV.G (Fig. 5.5). This mechanism could thus be more important in deciduous trees for the development of the canopy gradient than in herbaceous species, but needs further investigation.

Clear canopy gradients in N_{LA} and J_{max} were found in *Populus tremula* and *Tilia cordata*, two deciduous temperate trees. However, spectrally neutral shading and additional lighting of leaves throughout the canopy for 11 days hardly changed these leaf traits (Niinemets et al. 2003). Resource reallocation at the whole plant level in response to short term experimental modification of the light environment of leaves was thus not evident in these trees. More detailed experiments on the regulation of leaf traits in canopies were done with young *Juglans* trees (walnut). They grow their leaves in a single flush in spring. Their buds had developed in high light and one branch of the two on a plant was subjected to treatments representative for a shaded canopy position (Frak et al. 2001, 2002). Shading for several months showed decreases in non-structural carbohydrates and LMA with parallel decreases in N_{LA} and photosynthetic capacity (Frak et al. 2001). These effects are similar as found for herbaceous plants when shaded for shorter periods, except that senescence was not induced. The question is whether similar regulation mechanisms are involved. Spectrally neutral shading had similar effects as spectral shade (Frak et al. 2001). These effects can be simulated by reduced transpiration in many herbaceous plants (Sect. IV.F), but reduced transpiration rate had no effect in *Juglans*. The treatment may not have been representative for the decrease in transpiration as a result of shading since it was applied to already shaded leaves that have a low transpiration rate. An attempt to reduce transpiration rate of *Acer pseudoplatanus* leaves in full daylight by increasing of air humidity was not very successful (unpublished results). Temperature changes throughout the day caused condensation that prevented the generation of the high humidity necessary for reduce transpiration significantly (Pons and Bergkotte 1996) as adjustments of stomatal conductance tends to keep transpiration rate independent of vapor pressure over a broad range (Franks and Farquhar 1999). Reduced R:FR in addition to spectrally neutral shading of the *Juglans* leaves had small additional effects on LMA, N_{LA} and photosynthetic capacity (Frak et al. 2002). Phytochrome is thus likely to be involved in resource reallocation between leaves, but not to the extent that senescence is induced as in herbaceous plants (Sect. IV.A). Responses to altered light environment take probably more time in deciduous trees compared to herbs. No evidence is available for the involvement of the distribution of CKs in the xylem along the transpiration gradient in deciduous tree canopies, but that may be due to insufficiently critical experimentation. Leaf traits could be also be influenced by low water potentials as a result of hydraulic limitation such as found in upper leaves of tall trees (Peltoniemi et al. 2012). Cell walls can become thicker in these leaves that limits the conductance of the mesophyll for CO_2 transport and hence photosynthesis (Niinemets 2007). Abscisic acid (ABA) is known as a negative regulator of the conductance for water transport in a leaf (Prado and Maurel 2013). Photosynthetic capacity was also down regulated after ABA application (Aasama et al. 2002). A gradient of decreasing ABA concentration from bottom to top was observed in the xylem of two deciduous tree species (Niinemets et al. 1999). This

suggests that ABA could be involved as a negative regulator of leaf trait values in the canopy gradient. Further work on the regulation of leaf traits in single-flush deciduous tree canopies should distinguish between the generation of canopy gradients in undisturbed canopies that are largely determined in the previous season, and modification of it in response to changes in light availability during the current growth season.

Most evergreen trees with a leaf longevity of more than a year have also leaves appearing in cohorts. This is at the beginning of the growth season for trees in strongly seasonal climates or at regular intervals as in tropical rain forest trees. The difference with deciduous trees is that younger cohorts shade older leaves. These trees show also gradients in leaf traits parallel to the light gradient (Chap. 4, Niinemets 2016). A shade acclimation potential in mature leaves can thus be expected. Applying spectrally neutral shade to branches of *Abies amabilis*, a temperate evergreen conifer, caused indeed strong acclimation at the chloroplast level. However, reallocation of resources after a season of shading was limited as judged from only a small reduction in N_{LA}. This resulted in reduced A_{sat} but increased Chl_{LA} (Brooks et al. 1994). As evident from N_{LA}, resource reallocation was found as a result of experimental shading across the canopy of the broad leaved temperate evergreen tree *Notofagus fusca* (Hollinger 1996). Spectrally neutral shade applied to single leaves of *Ficus benjamina*, a tropical broadleaved evergreen with flushed leaf growth, resulted also in complete chloroplast level shade acclimation as evident from similar values for A_{chl} and Chl a/b compared to plant grown in shade (Fig. 5.2; Pons and Jordi 1998). However, N_{LA} was strongly reduced, even in the short experimental period of two weeks. Contrary to herbaceous species, a reduced transpiration rate and application of CKs had little effect (Pons and Jordi 1998). Spectral shade had no effect additional to spectrally neutral shade except on Chl a/b, but a low R:FR alone reduced also Chl_{LA} but not A_{chl} (Fig. 5.2), which was similar to the response of herbaceous species. Juvenile *Hedera helix*, an evergreen climber with continuous leaf growth, was also included in the experiments and gave similar responses to the treatments (Pons and Jordi 1998; Pons and de Jong – van Berkel 2004). These experiments tentatively indicate that the evergreens described above achieve complete photosynthetic acclimation in response to shading of a part of the foliage. That a signal associated with spectrally neutral shading is involved in the reallocation of resources, but only to a limited extent in *Abies*. However, the distribution of CKs in the transpiration stream may not be as important as in herbaceous plants if involved at all. The lower R:FR ratio in shade light has also an effect on resource reallocation at the whole plant level, but the experiments did not last long enough for the evaluation of a possible effect on the induction of senescence. The results for evergreen species were obtained with a limited number of species and they are comparable to the results for a deciduous tree as discussed above. The results obtained so far cannot be generalized for the whole group of evergreens. Questions to be answered with further studies are if mechanisms of the regulation of leaf traits in canopies, or their relative importance, are the same for all trees. When not identical, whether there is association of variation with evergreen trees from different climates, such as conifers, Mediterranean evergreens and tropical trees.

VI. Concluding Remarks

Analysis of environmental and leaf trait gradients in canopies of plants grown at different densities has generated hypotheses about mechanisms of regulation. Experimentally manipulating the environment of attached leaves further elucidated several aspects of the regulation. Most experimental work was done with herbaceous species with relatively fast leaf turnover. Conclusions based on these experiments pertain to mechanisms in this functional group in the

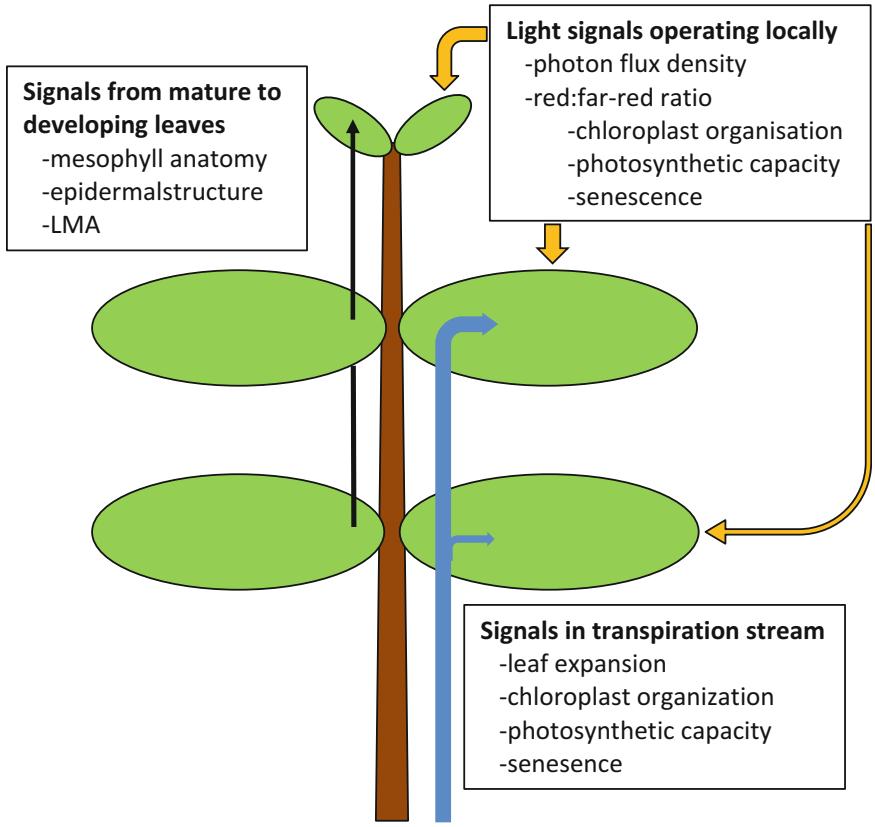

Fig. 5.6. A schematic representation of three groups of signaling mechanisms involved in the regulation of leaf traits in canopy gradients. The transpiration stream is partitioned in proportion to the transpiration rate of leaves and carries a signal that regulates sink strength. Leaf expansion and photosynthetic capacity are stimulated at the high transpiration rates of upper leaves, and reallocation of resources and senescence is induced at the low transpiration rates of shaded lower leaves. An important signaling compound carried in the transpiration stream is cytokinin, but other signaling and resource compound can be involved as well. The irradiance incident upon mature leaves generates a signal that is transported to the young developing leaves that regulates the sun/shade anatomy of the mesophyll and stomatal frequency and other epidermal traits. The carbohydrate status of the leaves and/or whole plant could be involved that also influences LMA independently of local irradiance. Irradiance can generate these systemic signals through its effect on transpiration and photosynthetic rate, but light can also operate locally by redox signaling and ROS generation in chloroplasts. A reduced red:far-red ratio is perceived by the phytochrome system that down-regulates photosynthetic capacity and can induce senescence. Also other photoreceptors can be involved in the perception of the local light environment in the canopy gradient. The scheme shows evidence for redundancy and supplementarity between signaling mechanisms

first place. The most important mechanisms of the regulation of leaf traits in canopies as discussed in this chapter are summarized in a tentative scheme (Fig. 5.6) that is described below.

The R:FR of light penetrating a canopy decreases with depth and depends on its leaf area density. This spectral component is perceived by the phytochrome family of photoreceptors. The low R:FR values to which shaded leaves are exposed cause mobilization of resources leading to accelerated senescence. However, the irradiance gradient dominates the regulation of leaf traits in canopies. Reduced PPFD incident on lower leaves has similar effects as a low R:FR, but when senescence has not been induced yet, the mobilization of resources goes largely at the expense of photosynthetic capacity and not so much chlorophyll. This reflects photosynthetic

acclimation at the chloroplast level in the phases of shading in a canopy gradient before senescence is induced. Several mechanisms are involved in the irradiance effect.

PPFD can operate directly on the photosynthetic apparatus and generate redox signals and ROS that can initiate signaling pathways having a local or systemic effect. The distribution of irradiance over the foliage of a plant can also operate more indirectly by its effect on the distribution of the transpiration stream. Signaling compounds carried in the transpiration stream are distributed accordingly. CKs were identified as such a group of compounds. They are involved in resource partitioning at the whole plant level and in induction of senescence in shaded foliage. They are also implicated in the stimulation of leaf expansion in favorable light conditions. There is evidence that the distribution of the transpiration stream is involved in the regulation of chloroplast organization as well. However, there is no evidence for a role of CKs in chloroplast organization, indicating that other signaling compounds in the transpiration stream could be involved. Assimilate production depends on PPFD and sugar signaling can thus be involved. The supply of assimilates from nearby leaves influence structural traits such as LMA of surrounding leaves. More specifically, the light conditions of mature leave determine the anatomy of mesophyll and epidermis of developing leaves. The assimilate supply from mature leaves to the apex is a good candidate for the regulation. These systemically operating regulation mechanisms are important for a coordinated response of plants to the leaf area density of the canopy where they grow. It clarifies why shading of a part of the foliage of a plant has different effects compared to shading a whole plant.

Several of the pathways described above target the same process. They can thus act redundantly, or cross talk between signaling pathways can be involved, further complicating the interpretation of observed phenomena. The first steps in elucidating the mechanisms how leaf traits are regulated in dependence of canopy density are illustrated here. They can serve as a basis for further studies on the regulation mechanisms.

Acknowledgments

Alex Boonman and Ülo Niinemets are thanked for their valuable comments on earlier versions of this chapter.

References

Aasamaa K, Sober A, Hartung W, Niinemets Ü (2002) Rate of stomatal opening, shoot hydraulic conductance and photosynthetic characteristics in relation to leaf abscisic acid concentration in six temperate deciduous trees. Tree Physiol 22:267–276

Ackerly DD (1992) Light, leaf age, and leaf nitrogen concentration in a tropical vine. Oecologia 89:596–600

Ackerly DD (1996) Canopy structure and dynamics: integration of growth processes in tropical pioneer trees. In: Mulkey SS, Chazdon RL, Smith AP (eds) Tropical Forest Plant Ecophysiology. Chapman & Hall, New York, pp 619–658

Ackerly DD, Bazzaz FA (1995) Leaf dynamics, self-shading and carbon gain in seedlings of a tropical pioneer tree. Oecologia 101:289–298

Anderson JM, Chow WS, Park YI (1995) The grand design of photosynthesis: acclimation of the photosynthetic apparatus to environmental cues. Photosynth Res 46:129–139

Anten NPR (2002) Evolutionarily stable leaf area production in plant populations. J Theor Biol 217:15–32

Anten NPR (2005) Optimal photosynthetic characteristics of individual plants in vegetation stands and implications for species coexistence. Ann Bot 95:495–506

Anten NPR, Schieving F, Medina E, Werger MJA, Schuffelen P (1995) Optimal leaf area indices in C3 and C4 mono- and dicotyledonous species at low and high nitrogen availability. Physiol Plant 95:541–550

Anten NPR, Miyazawa K, Hikosaka K, Nagashima H, Hirose T (1998) Leaf nitrogen distribution in relation to leaf age and photon flux density in dominant and subordinate plants in dense stands of a dicotyledonous herb. Oecologia 113:314–324

Anten NPR, Hikosaka K, Hirose T (2000) Nitrogen utilisation and the photosynthetic system. In: Marshall B, Roberts JA (eds) Leaf Development and Canopy Growth. Sheffield Academic Press, Boca Raton, pp 171–203

Araya T, Noguchi K, Terashima I (2008) Manipulation of light and CO_2 environments of the primary leaves of bean (*Phaseolus vulgaris* L.) affects photosynthesis in both the primary and the first trifoliate leaves: involvement of systemic regulation. Plant Cell Environ 31:50–61

Baena-Gonzalez E, Sheen J (2008) Convergent energy and stress signaling. Trends Plant Sci 13:474–482

Bauerle WL, Bowden JD, Wang GG (2007) The influence of temperature on within-canopy acclimation and variation in leaf photosynthesis: spatial acclimation to microclimate gradients among climatically divergent *Acer rubrum* L. genotypes. J Exp Bot 58:3285–3298

Biswal UC, Biswal B (1984) Photocontrol of leaf senescence. Photochem Photobiol 39:875–879

Boonman A, Anten NPR, Dueck TA, Jordi WJRM, Van der Werf A, Voesenek LACJ, Pons TL (2006) Functional significance of shade-induced leaf senescence in dense canopies: an experimental test using transgenic tobacco. Am Nat 168:597–607

Boonman A, Prinsen E, Gilmer F, Schurr U, Peeters AJM, Voesenek LACJ, Pons TL (2007) Cytokinin import rate as a signal for photosynthetic acclimation to canopy light gradients. Plant Physiol 143:1841–1852

Boonman A, Prinsen E, Voesenek LACJ, Pons TL (2009) Redundant roles of photoreceptors and cytokinins in regulating photosynthetic acclimation to canopy density. J Exp Bot 60:1179–1190

Brooks JR, Hinckley TM, Sprugel DG (1994) Acclimation responses of mature *Abies amabilis* sun foliage to shading. Oecologia 100:316–324

Brouwer B, Ziolkowska A, Bagard M, Keech O, Gardestrom P (2012) The impact of light intensity on shade-induced leaf senescence. Plant Cell Environ 35:1084–1098

Brouwer B, Gardestrom P, Keech O (2014) In response to partial plant shading, the lack of phytochrome A does not directly induce leaf senescence but alters the fine-tuning of chlorophyll biosynthesis. J Exp Bot 65:4037–4049

Buchanan-Wollaston V, Page T, Harrison E, Breeze E, Lim PO, Nam HG, Lin JF, …, Leaver CJ (2005) Comparative Transcriptome Analysis Reveals Significant Differences in Gene Expression and Signalling Pathways Between Developmental and Dark/Starvation-induced Senescence in Arabidopsis. Plant J 42:567–585

Buchmann N, Guehl JM, Barigah TS, Ehleringer JR (1997) Interseasonal comparison of CO_2 concentrations, isotopic composition, and carbon dynamics in an Amazonian rain forest (French Guiana). Oecologia 110:120–131

Buckley TN, Cescatti A, Farquhar GD (2013) What does optimization theory actually predict about crown profiles of photosynthetic capacity when models incorporate greater realism? Plant Cell Environ 36:1547–1563

Casal JJ (2013) Photoreceptor signaling networks in plant responses to shade. Annu Rev Plant Biol 64:403–427

Casal JJ, Sanchez RA, Yanovsky MJ (1997) The function of phytochrome A. Plant Cell Environ 20:813–819

Chory J, Reinecke D, Sim S, Washburn T, Brenner M (1994) A role for cytokinins in de-etiolation in Arabidopsis. Plant Physiol 104:339–347

Coupe SA, Palmer BG, Lake JA, Overy SA, Oxborough K, Woodward FI, Gray JE, Quick WP (2006) Systemic signalling of environmental cues in Arabidopsis leaves. J Exp Bot 57:329–341

de Wit CT (1965) Photosynthesis of leaf canopies. Agric Res Rep 663:1–56

de Wit M, Pierik R (2016) Photomorphogenesis and photoreceptors. In: Hikosaka K, Niinemets Ü, Anten N (eds) Canopy Photosynthesis: From Basics to Applications. Springer, Berlin, pp 171–186

Degreef J, Butler WL, Roth TF, Frederic H (1971) Control of senescence in *Marchantia* by phytochrome. Plant Physiol 48:407–412

Esrich W, Burchardt R, Essiahmah S (1989) The induction of sun and shade leaves of European beech (*Fagus sylvatica* L.): anatomical studies. Trees 3:1–10

Evans JR (1989) Photosynthesis and nitrogen relationships in leaves of C3 plants. Oecologia 78:9–19

Evans JR (1993) Photosynthetic acclimation and nitrogen partitioning within a lucerne canopy II. Stability through time and comparison with a theoretical optimum. Aust J Plant Physiol 20:69–82

Evans JR, Seemann JR (1989) The allocation of protein nitrogen in the photosynthetic apparatus: costs, consequences, and control. In: Briggs W (ed) Towards a Broad Understanding of Photosynthesis. Alan R. Liss, New York, pp 183–205

Farquhar GD (1989) Models of integrated photosynthesis of cells and leaves. Philos Trans R Soc Lond B-Biol Sci 323:357–367

Field C (1983) Allocating leaf nitrogen for the maximization of carbon gain: leaf age as a control on the allocation program. Oecologia 56:341–347

Field CB, Mooney HA (1986) The photosynthesis – nitrogen relationship in wild plant. In: Givnish TJ (ed) On the Economy of Plant Form and Function. Cambridge University Press, New York/Cambridge, pp 25–55

Flores S, Tobin EM (1988) Cytokinin modulation of LCHP mRNA levels: the involvement of post-transcriptional regulation. Plant Mol Biol 11:409–415

Frak E, Le Roux X, Millard P, Dreyer E, Jaouen G, Saint-Joanis B, Wendler R (2001) Changes in total leaf nitrogen and partitioning, of leaf nitrogen drive photosynthetic acclimation to light in fully developed walnut leaves. Plant Cell Environ 24:1279–1288

Frak E, Le Roux X, Millard P, Adam B, Dreyer E, Escuit C, Sinoquet H, …, Varlet-Grancher C (2002) Spatial Distribution of Leaf Nitrogen and Photosynthetic Capacity Within the Foliage of Individual Trees: disentangling the Effects of Local Light Quality, Leaf Irradiance, and Transpiration. J Exp Bot 53:2207–2216

Franks PJ, Farquhar GD (1999) A relationship between humidity response, growth form and photosynthetic operating point in C3 plants. Plant Cell Environ 22:1337–1349

Gan S, Amasino RM (1995) Inhibition of leaf senescence by autoregulated production of cytokinin. Science 270:1986–1988

Goudriaan J (2016) Light distribution. In: Hikosaka K, Niinemets Ü, Anten N (eds) Canopy Photosynthesis: From Basics to Applications. Springer, Berlin, pp 3–22

Grindlay DJC (1997) Towards an explanation of crop nitrogen demand based on the optimization of leaf nitrogen per unit leaf area. J Agric Sci 128:377–396

Guiamet JJ, Willemoes JG, Montaldi ER (1989) Modulation of progressive leaf senescence by the red:far-red ratio of incident light. Bot Gaz 150:148–151

Gutschick VP (2016) Leaf energy balance: basics, and modeling from leaves to Canopies. In: Hikosaka K, Niinemets Ü, Anten N (eds) Canopy Photosynthesis: From Basics to Applications. Springer, Berlin, pp 23–58

Hibberd JM, Quick WP (2002) Characteristics of C4 photosynthesis in stems and petioles of C3 flowering plants. Nature 415:451–454

Hikosaka K (2003) A model of dynamics of leaves and nitrogen in a plant canopy: an integration of canopy photosynthesis, leaf life span, and nitrogen use efficiency. Am Nat 162:149–164

Hikosaka K, Terashima I, Katoh S (1994) Effects of leaf age, nitrogen nutrition and photon flux density on the distribution of nitrogen among leaves of a vine (*Ipomoea tricolor* Cav.) grown horizontally to avoid mutual shading of leaves. Oecologia 97:451–457

Hikosaka K, Murakami A, Hirose T (1999) Balancing carboxylation and regeneration of ribulose-1,5-bisphosphate in leaf photosynthesis temperature acclimation of an evergreen tree, Quercus myrsinaefolia. Plant Cell Environ 22:841–849

Hikosaka K, Ishikawa K, Borjigidai A, Muller O, Onoda Y (2006) Temperature acclimation of photosynthesis: mechanisms involved in the changes in temperature dependence of photosynthetic rate. J Exp Bot 57:291–302

Hirose T, Werger MJA (1987a) Nitrogen use efficiency in instantaneous and daily photosynthesis of leaves in the canopy of a *Solidago altissima* stand. Physiol Plant 70:215–222

Hirose T, Werger MJA (1987b) Maximising daily canopy photosynthesis with respect to the leaf nitrogen allocation pattern in the canopy. Oecologia 72:520–526

Hirose T, Werger MJA, Pons TL, Van Rheenen JWA (1988) Canopy structure and leaf nitrogen distribution in a stand of *Lysimachia vulgaris* L. as influenced by stand density. Oecologia 77:145–150

Hirose T, Werger MJA, Van Rheenen WA (1989) Canopy development and leaf nitrogen distribution in a stand of *Carex acutiformis*. Ecology 70:1610–1618

Hollinger DY (1996) Optimality and nitrogen allocation in a tree canopy. Tree Physiol 16:627–634

Hüner NPA, Oquist G, Sarhan F (1998) Energy balance and acclimation to light and cold. Trends Plant Sci 3:224–230

Hüner NPA, Bode R, Dahal K, Hollis L, Rosso D, Krol M, Ivanov AG (2012) Chloroplast redox imbalance governs phenotypic plasticity: the "grand design of photosynthesis" revisited. Front Plant Sci 3:255

Jameson PE, Letham DS, Zhang R, Parker CW, Badenoch-Jones J (1987) Cytokinin translocation and metabolism in Lupin species. I. Zeatin Riboside introduced into the xylem at the base of *Lupinus angustifolius* stems. Aust J Plant Physiol 14:695–718

Jiang CD, Wang X, Gao HY, Shi L, Chow WS (2011) Systemic regulation of leaf anatomical structure, photosynthetic performance, and high-light tolerance in sorghum. Plant Physiol 155:1416–1424

Jordi W, Schapendonk A, Davelaar E, Stoopen GM, Pot CS, de Visser R, van Rhijn JA, . . ., Amasino RM (2000) Increased Cytokinin Levels in Transgenic

P_{SAG12}-*IPT* Tobacco Plants have Large Direct and Indirect Effects on Leaf Senescence, Photosynthesis and N Partitioning. Plant Cell Environ 23:279–289

Kitajima K, Mulkey SS, Wright SJ (2005) Variation in crown light utilization characteristics among tropical canopy trees. Ann Bot 95:535–547

Krapp A, Hofmann B, Schafer C, Stitt M (1993) Regulation of the expression of Rbcs and other photosynthetic genes by carbohydrates – a mechanism for the sink regulation of photosynthesis. Plant J 3:817–828

Kruijt B, Lloyd J, Grace J, McIntyre JA, Farquhar GD, Miranda AC, McCracken P (1996) Sources and sinks of CO_2 in Rondonia tropical rainforest. In: Gash JHC, Nobr CA, Roberts JM, Victoria RL (eds) Amazonian Deforestation and Climate. Wiley, Chichester, pp 331–351

Kull O (2002) Acclimation of photosynthesis in canopies: models and limitations. Oecologia 133:267–279

Kull O, Kruijt B (1999) Acclimation of photosynthesis to light a mechanistic approach. Funct Ecol 13:24–36

Kull O, Koppel A, Noormets A (1998) Seasonal changes in leaf nitrogen pools in two Salix species. Tree Physiol 18:45–51

Kusnetsov VV, Oelmuller R, Sarwat MI, Porfirova SA, Cherepneva GN, Herrmann RG, Kulaeva ON (1994) Cytokinins, abscisic acid and light affect accumulation of chloroplast proteins in *Lupinus luteus* cotyledons without notable effect on staedy-state mRNA levels. Planta 194:318–327

Lake JA, Quick WP, Beerling DJ, Woodward FI (2001) Plant development – signals from mature to new leaves. Nature 411:154

Leopold AC, Kawase M (1964) Benzyladenine on bean leaf growth and senescence. Amer J Bot 51:294–298

Li Q, Bettany AJE, Donnison I, Griffiths CM, Thomas H, Scott IM (2000) Characterisation of a cysteine protease cDNA from *Lolium multiflorum* leaves and its expression during senescence and cytokinin treatment. Biochim Biophys Acta 1492:233–236

Matthyse AG, Scott TK (1982) Functions of hormones at the whole plant level of organisation. In: Pirson IA, Zimmerman MH (eds) Encyclopedia of Plant Physiology, vol 10, Hormonal regulation of development. Springer, Berlin, pp 219–235

Mittler R, Vanderauwera S, Suzuki N, Miller G, Tognetti VB, Vandepoele K, Gollery M, . . ., Van Breusegem F (2011) ROS Signaling: the New Wave? Trends Plant Sci 16:300–309

Monsi M, Saeki T (1953) Über den Lichtfaktor in den Pflanzengeselschaften und seine Bedeutung für die Stoffproduktion. Jpn J Bot 14:22–52. *Translated as* Monsi M, Saeki T (2005) On the factor light in plant communities and its importance for matter production. Ann Bot 95:549–567

Mooney HA, Gulmon SL (1979) Environmental and evolutionary constraints on the photosynthetic characteristics of higher plants. In: Solbrig OT, Jain S, Johnson GB, Raven PH (eds) Topics in Plant Population Biology. Columbia University Press, New York, pp 316–337

Mothes K, Engelbrecht L (1963) On the activity of a kinetin-like root factor. Life Sci 2:852–857

Mullineaux PM, Karpinski S, Baker NR (2006) Spatial dependence for hydrogen peroxide-directed signaling in light-stressed plants. Plant Physiol 141:346–350

Niinemets Ü (1999) Components of leaf dry mass per area thickness and density alter leaf photosynthetic capacity in reverse directions in woody plants. New Phytol 144:35–47

Niinemets Ü (2007) Photosynthesis and resource distribution through plant canopies. Plant Cell Environ 30:1052–1071

Niinemets Ü (2010) A review of light interception in plant stands from leaf to canopy in different plant functional types and in species with varying shade tolerance. Ecol Res 25:693–714

Niinemets Ü (2012) Optimization of foliage photosynthetic capacity in tree canopies: towards identifying missing constraints. Tree Physiol 32:505–509

Niinemets Ü (2016) Within-canopy variations in functional leaf traits: structural, chemical and ecological controls and diversity of responses. In: Hikosaka K, Niinemets Ü, Anten N (eds) Canopy Photosynthesis: From Basics to Applications, Berlin. Springer, Berlin, pp 101–141

Niinemets Ü, Anten NPR (2009) Packing the photosynthetic machinery: from leaf to canopy. In: Laisk A, Nedbal L, Govindjee (eds) Photosynthesis in Silico: Understanding Complexity from Molecules to Ecosystems. Springer, Netherlands, pp 363–399

Niinemets Ü, Oja V, Kull O (1999) Shape of leaf photosynthetic electron transport versus temperature response curve Is not constant along canopy light gradients in temperate deciduous trees. Plant Cell Environ 22:1497–1513

Niinemets Ü, Kollist H, Garcia-Plazaola JI, Hernandez A, Becerril JM (2003) Do the capacity and kinetics for modification of xanthophyll cycle pool size depend on growth irradiance in temperate trees? Plant Cell Environ 26:1787–1801

Niinemets Ü, Kull O, Tenhunen JD (2004) Within-canopy variation in the rate of development of

photosynthetic capacity is proportional to integrated quantum flux density in temperate deciduous trees. Plant Cell Environ 27:293–313

Niinemets Ü, Keenan TF, Hallik L (2015) A worldwide analysis of within-canopy variations in leaf structural, chemical and physiological traits across plant functional types. New Phytol 205:973–993 doi:10.1111/nph.13096

Nordstrom A, Tarkowski P, Tarkowska D, Norbaek R, Astot C, Dolezal K, Sandberg G (2004) Auxin regulation of cytokinin biosynthesis in *Arabidopsis thaliana*: a factor of potential importance for auxin-cytokinin-regulated development. Proc Natl Acad Sci U S A 101:8039–8044

Oikawa S, Hikosaka K, Hirose T (2006) Leaf lifespan and lifetime carbon balance of individual leaves in a stand of an annual herb, *Xanthium canadense*. New Phytol 172:104–116

Ono K, Nishi Y, Watanabe A, Terashima I (2001) Possible mechanisms of adaptive leaf senescence. Plant Biol 3:234–243

Peltoniemi MS, Duursma RA, Medlyn BE (2012) Co-optimal distribution of leaf nitrogen and hydraulic conductance in plant canopies. Tree Physiol 32:510–519

Pierik R, Whitelam GC, Voesenek LACJ, de Kroon H, Visser EJW (2004) Canopy studies on ethylene-insensitive tobacco identify ethylene as a novel element in blue light and plant-plant signalling. Plant J 38:310–319

Pons TL (2012) Interaction of temperature and irradiance effects on photosynthetic acclimation in two accessions of *Arabidopsis thaliana*. Photosynth Res 113:207–219

Pons TL, Bergkotte M (1996) Nitrogen allocation in response to partial shading of a plant: possible mechanisms. Physiol Plant 98:571–577

Pons TL, de Jong-van Berkel YEM (2004) Species-specific Variation in the Importance of the spectral quality gradient in canopies as a signal for photosynthetic resource partitioning. Ann Bot 94:725–732

Pons TL, Jordi W (1998) Induction of leaf senescence and shade acclimation in leaf canopies – variation with leaf longevity. In: Lambers H, Poorter H, Van Vuuren MMI (eds) Inherent Variation in Plant Growth. Physiological Mechanisms and Ecological Consequences. Backhuys Publishers, Leiden, pp 121–137

Pons TL, Pearcy RW (1994) Nitrogen reallocation and photosynthetic acclimation in response to partial shading in soybean plants. Physiol Plant 92:636–644

Pons TL, van der Toorn J (1988) Establishment of *Plantago lanceolata* L. and *Plantago major* L. among grass. I Significance of light for germination. Oecologia 75:394–399

Pons TL, Schieving F, Hirose T, Werger MJA (1989) Optimization of leaf nitrogen allocation for canopy photosynthesis in *Lysimachia vulgaris*. In: Lambers H, Cambridge ML, Konings H, Pons TL (eds) Causes and Consequences of Variation in Growth Rate and Productivity of Higher Plants. SPB Publishing, The Hague, pp 175–186

Pons TL, Van Rijnberk H, Scheurwater I, Van der Werf A (1993) Importance of the gradient in photosynthetically active radiation in a vegetation stand for leaf nitrogen allocation in two monocotyledons. Oecologia 95:416–424

Pons TL, Jordi W, Kuiper D (2001) Acclimation of plants to light gradients in leaf canopies: evidence for a possible role for cytokinins transported in the transpiration stream. J Exp Bot 52:1563–1574

Pons TL, Anten NPR (2004) Is plasticity in partitioning of photosynthetic resources between and within leaves important for whole-plant carbon gain in canopies? Funct Ecol 18:802–811

Prado K, Maurel C (2013) Regulation of leaf hydraulics: from molecular to whole plant levels. Front Plant Sci 4:255

Rochaix JD (2011) Regulation of photosynthetic electron transport. Biochem Biophys Acta 1807:375–383

Rousseaux MC, Hall AJ, Sánchez RA (1996) Far-red enrichment and photosynthetically active radiation level influence leaf senescence in field-grown sunflower. Physiol Plant 96:217–224

Rousseaux MC, Ballaré CL, Jordan ET, Vierstra RD (1997) Directed overexpression of PHYA locally suppresses stem elongation and leaf senescence responses to far-red radiation. Plant Cell Environ 20:1551–1558

Rousseaux MC, Hall AJ, Sanchez RA (2000) Basal leaf senescence in a sunflower (*Helianthus annuus*) canopy: responses to increased R/FR ratio. Physiol Plant 110:477–482

Roy J, Thiebaut B, Watson MA (1986) Physiological and anatomical consequences of morphogenetic polymorphism: leaf response to light intensity in young beech trees (*Fagus sylvatica* L.). In: Naturalia Monspeliensia – Colloque International sur l'Arbre, pp 431–449

Schieving F, Pons TL, Werger MJA, Hirose T (1992) The vertical distribution of nitrogen and photosynthetic activity at different plant densities in *Carex acutiformis*. Plant Soil 14:9–17

Singh S, Letham DS, Palni LMS (1992) Cytokinin biochemistry in relation to leaf senescence.8. translocation, metabolism and biosynthesis of cytokinins in relation to sequential leaf senescence of tobacco. Physiol Plant 86:398–406

Smeekens S, Ma JK, Hanson J, Rolland F (2010) Sugar signals and molecular networks controlling plant growth. Curr Opin Plant Biol 13:274–279

Smith H, Whitelam GC (1997) The shade avoidance syndrome: Multiple responses mediated by multiple phytochromes. Plant Cell Environ 20:840–844

Suzuki N, Koussevitzky S, Mittler R, Miller G (2012) ROS and redox signalling in the response of plants to abiotic stress. Plant Cell Environ 35:259–270

Terashima I, Araya T, Miyazawa S, Sone K, Yano S (2005) Construction and maintenance of the optimal photosynthetic systems of the leaf, herbaceous plant and tree: an eco-developmental treatise. Ann Bot 95:507–519

Terashima I, Hanba YT, Tholen D, Niinemets Ü (2011) Leaf functional anatomy in relation to photosynthesis. Plant Physiol 155:108–116

Thomas H, Stoddart JL (1980) Leaf senescence. Annu Rev Plant Physiol 31:83–111

Thomas PW, Woodward FI, Quick WP (2004) Systemic irradiance signalling in tobacco. New Phytol 161:193–198

Uemura A, Ishida A, Nakano T, Terashima I, Tanabe H, Matsumoto Y (2000) Acclimation of leaf characteristics of *Fagus* species to previous-year and current-year solar irradiances. Tree Physiol 20:945–951

van Arendonk JJCM, Poorter H (1994) The chemical composition and anatomical structure of leaves of grass species differing in relative growth rate. Plant Cell Environ 17:963–970

van Volkenburgh E (1999) Leaf expansion an integrating plant behavior. Plant Cell Environ 22:1463–1473

Vapaavuori EM, Vuorinen AH (1989) Seasonal variation in the photosynthetic capacity of a willow (Salix cv. Aquatica gigantea) canopy.1. Changes in the activity and amount of ribulose 1,5-bisphosphate carboxylase-oxygenase and the content of nitrogen and chlorophyll at different levels in the canopy. Tree Physiol 5:423–444

Vos J, van der Putten PEL (2001) Effects of partial shading of the potato plant on photosynthesis of treated leaves, leaf area expansion and allocation of nitrogen and dry matter in component plant parts. Eur J Agron 14:209–220

Walters RG, Rogers JJM, Shephard F, Horton P (1999) Acclimation of *Arabidopsis thaliana* to the light environment: the role of photoreceptors. Planta 209:517–527

Weaver LM, Amasino RM (2001) Senescence is induced in individually darkened *Arabidopsis* leaves but inhibited in whole darkened plants. Plant Physiol 127:876–886

Werner T, Schmülling T (2009) Cytokinin action in plant development. Curr Opin Plant Biol 12:527–538

Wright IJ, Reich PB, Westoby M, Ackerly DD, Baruch Z, Bongers F, Cavender-Bares J, . . ., Villar R (2004) The Worldwide Leaf Economics Spectrum. Nature 428:821–827

Yano S, Terashima I (2001) Seperate localization of light signal perception for sun or shade type chloroplast and palisade tissue differentiation on *Chenopodium album*. Plant Cell Physiol 41:1303–1310

Yano S, Terashima I (2004) Developmental process of sun and shade leaves in *Chenopodium album* L. Plant Cell Environ 27:781–793

Zweifel R, Bohm JP, Hasler R (2002) Midday stomatal closure in Norway spruce – reactions in the upper and lower crown. Tree Physiol 22:1125–1136

Part III

Whole-Plant Processes in Leaf Canopies

Chapter 6

Photomorphogenesis and Photoreceptors

Mieke de Wit
Centre for integrative genomics, Faculty of biology and medicine, University of Lausanne, CH-1015 Lausanne, Switzerland

and

Ronald Pierik*
Plant Ecophysiology, Institute of Environmental Biology, Utrecht University, Padualaan 8, Utrecht 3584 CH, The Netherlands

Summary

Plants use light as their main source of energy and to gather information about their surroundings. The light environment is monitored through an extensive set of photoreceptors and largely dictates plant development through induction of processes such as germination and flowering, entrainment of the circadian clock and photomorphogenic responses. Plants display remarkable phenotypic plasticity upon perception of changes in the light, ranging from seedling de-etiolation to shade avoidance and phototropic responses in competition for light. Here, we describe photomorphogenic responses and their underlying mechanisms such as they occur in a leaf canopy. This shade avoidance review will largely focus on the model plant species *Arabidopsis thaliana* as the underlying mechanisms controlling shade avoidance are particularly well elucidated in this species.

Keywords Shade avoidance • Plant architecture • Photoreceptor • Light • Photomorphogenesis

*Author for correspondence, e-mail: r.pierik@uu.nl

K. Hikosaka, Ü. Niinemets, and N.P.R. Anten (eds.), *Canopy Photosynthesis: From Basics to Applications*, DOI 10.1007/978-94-017-7291-4_6

I. Competition for Light: Shade Tolerance and Shade Avoidance

Plants growing at high density are at risk of becoming shaded and have to compete for light to prevent losing access to their main source of energy. The consequence of becoming overgrown is clearly demonstrated by the life style of several (sub)tropical species of *Ficus*. These "strangler" figs can avoid germination at the dark forest floor by starting their life as an epiphyte, which then grows its roots downward and envelops the host tree's stem (Athreya 1999). When these plants reach the light at the top of the canopy they establish a large crown shading the host tree, which eventually dies from lack of light. When plants are growing in dense canopies, size inequalities between individual plants increase with increasing density (Weiner 1985). This shows that a small initial difference in size can have a huge competitive advantage leading to suppression of smaller individuals, whose light capture will be diminished as their taller neighbours start to grow. To conserve energy and enhance fitness in adverse conditions, plants can employ different types of stress responses. Stresses that cannot be outgrown might require a quiescent response, while other stresses can be overcome by an escape strategy (Voesenek and Pierik 2008). In competition for light, both strategies can be found.

Plants that are adapted to completing their life cycle under shade conditions are considered to be shade tolerant. For example, plants living in the forest understory will not be able to outgrow the tall neighbouring trees and a shade tolerance strategy is therefore more adaptive. A photosynthetically optimal strategy in low light environments is to form leaves with a high specific leaf area (SLA: leaf area / leaf dry weight). A high SLA indicates leaves with a relatively large surface area per unit invested dry weight and usually represents relatively thin leaves. This is highly suitable under low light conditions since these leaves will be able to intercept the majority of photons available and have low respiration per unit leaf area due to fewer cell layers. Such acclimated leaves, therefore, have a low light compensation of photosynthesis. These leaf morphological acclimations, combined with photosynthetic adjustments such as reduced chlorophyll a / b ratio's and increased photosystem (PS)II:I ratio's (Meils and Harvey 1981) constitute the so-called carbon gain hypothesis of shade tolerance (reviewed in Givnish 1988; Valladares and Niinemets 2008). Although these leaf traits optimize carbon acquisition in low light, leaves with a high SLA tend to be more prone to mechanical damage and herbivory. In low light conditions, however, plants cannot always afford to lose biomass quite so easily. Therefore, it is observed that very shade tolerant species in deep forest shade produce well-protected, tough and relatively thick leaves rather than the photosynthetically optimal thin leaves (Kitajima and Poorter 2010; Poorter and Bongers 2006). This constrained SLA development is typical of true shade tolerant species. Many shade avoiding species show an even stronger increase of SLA in response to shade to optimize light harvesting but would not be shade tolerant because of a relatively short leaf longevity. It has been proposed that shade tolerant species are therefore less plastic for various morphological traits than are shade avoiding species and invest more in leaf longevity. This hypothesis has been coined the stress tolerance hypothesis of shade tolerance (Kitajima 1994); reviewed in (Valladares and Niinemets 2008).

Another category of plants displays an array of escape responses that serve to ensure light capture in a competitive light environment and collectively are called the shade avoidance syndrome (SAS) (Casal 2012; Franklin 2008; Vandenbussche et al. 2005).

Abbreviations: ABA – Abscisic acid; B – Blue light; BR – Brassinosteroid; Cry – Cryptochrome; ET – Ethylene; FR – Far-red light; GA – Gibberellin; PAR – Photosynthetically Active Radiation; Phot – Phototropin; Phy – Phytochrome; PIF – Phytochrome-interacting Factor; R – Red light; R:FR – Red: Far-red light ratio; UV – Ultraviolet light; VOC – Volatile Organic Compound

Fig. 6.1. Shade avoidance in low R:FR-exposed (*right*) sunflower (*Helianthus annuus*) versus control light conditions (*left*). Three weeks old plants that have been exposed to high (1.8) or low (0.2) R:FR light conditions from 4 day after sowing onwards. Plants were grown at 180 μmol m^{-2} s^{-1} PAR (16 h light, 8 h dark), 21 °C and 70 % RH

These include changes in morphology to position the leaves in a more competitive position through increased leaf angles (hyponasty), elongation of hypocotyls, internodes, petioles and stems (Fig. 6.1), reduced shoot branching due to reduced bud outgrowth (Finlayson et al. 2010; Kebrom et al. 2006), and adjustment of the photosynthetic apparatus. The effect of shade signals on leaf surface area varies between species and both growth stimulation and inhibition have been reported (Bittebiere et al. 2012; Carabelli et al. 2007; Chitwood et al. 2012; Liu et al. 2012). As an ultimate escape response, shade also induces accelerated flowering. Shade avoidance responses are influenced by environmental conditions. Shade-induced flowering and changes in leaf architecture are highly temperature-dependent (Franklin 2009; Halliday et al. 2003) and the effect of light quality on branching is dependent on the light intensity (Su et al. 2011).

Shade avoidance responses have great impact on patterns and species distribution of natural plant communities and plant biodiversity (Goldberg and Barton 1992; Hautier et al. 2009) and can have a major impact on agricultural yield. In homogeneous crop fields shade avoidance negatively affects yield because resources are invested in non-harvestable organs such as stems at the expense of crops. Furthermore, the reduced branching (tillering) in cereals, strongly affects the yield potential, while stem elongation and apical dominance may lead to crop lodging. Expression of shade avoidance responses reduces plant fitness in the absence of competition, but has great adaptive value when plants have to compete for light (Ballaré et al. 1988; Casal and Smith 1989; Casal et al. 1994; Pierik et al. 2003; Schmitt et al. 1995). Thus, to avoid unnecessary fitness costs on one hand and small size differences that may cause great competitive imbalance on the other, it is essential that plants adjust their growth to neighbours exactly at the right time.

II. Perception of Neighbour-Derived Signals

To perceive the presence of proximate neighbours plants make use of the qualitative changes in the spectral composition of the light that occur in the transmitted and reflected light in a canopy (see Chap. 1, Goudriaan 2016). Red (R) and blue (B) light are absorbed for photosynthesis and thus depleted from the transmitted light, whereas far-red (FR) wavelengths are reflected by green issues. The different light components are signalled through a variety of photoreceptors, notably phytochromes, cryptochromes and phototropins (Fig. 6.2). Besides these plant-specific light signals plants may also perceive nearby competitors through touching neighbouring leaves, accumulation of the plant hormone ethylene and possibly other volatile components.

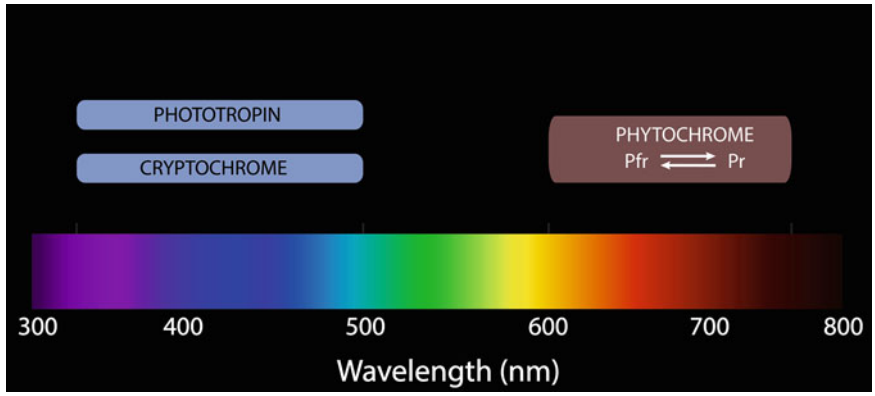

Fig. 6.2. Solar spectrum and the wavebands at which the three major plant photoreceptor classes (phytochromes, cryptochromes and phototropins) display their activities

A. Low R:FR Perception and Signal Transduction

As R light (wavelength 600–700 nm) is absorbed by plant tissues while FR (700–800 nm) light is mostly reflected, the ratio between R and FR (R:FR) decreases in the vertically incoming light inside a canopy (Ballaré et al. 1987b). Since it is reflected by plants, a FR signal can lower the R:FR even before actual shading takes place and thus play an important role as an early neighbour detection signal. A low R:FR in high PAR background was indeed shown to induce shade avoidance responses in plants grown without neighbours (Morgan and Smith 1978; Morgan et al. 1980). Final proof that plants can detect remote vegetation through reflected FR radiation came from plants that failed to respond to neighbours with increased stem elongation at an early stage of competition when they were blinded to FR by a $CuSO_4$ filter around individual internodes (Ballaré et al. 1990).

The R:FR is perceived by the phytochrome photoreceptors, which exist in two photo-convertible conformation states. Photoconversion of phytochromes is brought about by cis-trans isomerisation of the associated tetrapyrrole bilin chromophore called the phytochromobilin (Rockwell et al. 2006). The inactive Pr form absorbs R light and has an absorption peak at 665 nm, whereas the active Pfr form absorbs FR light with an absorption peak at 730 nm (Smith 2000; Fig. 6.2). *PhyB* mutants in various plant species show a constitutive shade avoidance phenotype (Devlin et al. 1992; Reed et al. 1993; Somers et al. 1991), indicating that this is the main regulating photoreceptor in low R:FR signalling. The phytochrome B photoequilibrium thus reflects the R:FR and acts as a sensor for qualitative changes in the red spectrum of the light environment (Holmes and Smith 1975; Smith and Holmes 1977). The Pfr form of phytochrome A is rapidly degraded (Clough et al. 1997; Hennig et al. 1999), making it mostly active in FR. In low R:FR, phyA can inhibit shade-induced elongation growth (Fairchild et al. 2000; Johnson et al. 1994; Reed et al. 1994; Rousseaux et al. 1997).

Upon activation of phytochrome by R light the Pfr form translocates from the cytosol, where it resides in its inactive Pr form, to the nucleus (Kircher et al. 1999; Sakamoto and Nagatani 1996; Yamaguchi et al. 1999), where it is required for regulation of growth inhibition (Huq et al. 2003). In the nucleus, Pfr interacts with several members of the BASIC HELIX-LOOP-HELIX (bHLH) family of transcription factors called PIF or PIL for phytochrome interacting factor (−like) (Duek and Fankhauser 2005). Of these, the positive regulators of elongation

growth PIF4, PIF5 and PIF7 play an important role in shade avoidance signalling, as shown by attenuated hypocotyl elongation of *pif* mutants in low R:FR (Li et al. 2012; Lorrain et al. 2008). PIF4 and PIF5 are targeted for proteasome-mediated degradation in red light, which is dependent on their active phytochrome binding (APB) domain (Lorrain et al. 2008). This suggests that in low R:FR conditions inactivation of phytochrome releases phytochrome-mediated degradation of these PIFs, allowing for their interaction with downstream components of growth regulation. PIF7 action on the other hand seems to involve its de-phosporylation upon detection of shade (Li et al. 2012).

Perception of low R:FR leads to rapid induction of gene expression (Salter et al. 2003; Sessa et al. 2005). Among the first identified genes regulated by changes in R:FR was the homeobox transcription factor *ATHB2* (Carabelli et al. 1993, 1996), which was later confirmed to be important for expression of a shade avoidance phenotype (Steindler et al. 1999). Another well-characterised shade avoidance marker gene is the bHLH transcription factor *PIL1*, whose expression is upregulated within minutes of exposure to low R:FR (Salter et al. 2003). The expression of negative regulators of growth such as the bHLH transcription factors *PHY RAPILY REGULATED (PAR)1* and *2*, and *LONG HYPOCOTYL IN FR (HFR)1* are also induced by a low R:FR signal (Roig-Villanova et al. 2007; Sessa et al. 2005). HFR1 was shown to form heterodimers with PIF4 and PIF5, thereby preventing their DNA-binding capacity and limiting the PIF-modulated growth response (Hornitschek et al. 2009). Further downstream, low R:FR-induced elongation growth through cell expansion is enabled by regulation of cell wall modifying proteins, which involve several members of the xyloglucan endotransglucosylase/hydrolase (XTH) family in Arabidopsis (Sasidharan et al. 2010).

B. Blue Light Perception and Signalling

Like R light, B light (length 400–500 nm) is absorbed for photosynthesis and thus reduced in the light environment inside a canopy. Although reduction of B fluence rates cannot be detected as early as an increase in reflected FR it can induce shade avoidance responses, suggesting that low B serves as a light signal at later stages of competition. Depletion of B light was first shown to affect growth responses in *Datura ferox* monocultures, which showed enhanced internode elongation when blue light was filtered out of the light spectrum (Ballaré et al. 1991). Internode elongation in response to attenuated B has furthermore been shown in the herbaceous perennial *Stellaria longipes* (Sasidharan et al. 2008). Cultivated tobacco (*Nicotiana tabacum*) displays enhanced elongation as well as hyponasty in response to a reduced B environment obtained through low pressure sodium light (Pierik et al. 2004). In Arabidopsis seedlings, low B induces strong hypocotyl elongation (Djakovic-Petrovic et al. 2007; Keuskamp et al. 2011; Pierik et al. 2009). In adult Arabidopsis plants, low B can induce hyponasty and enhanced petiole elongation (Keller et al. 2011), although the latter response is not always apparent (Djakovic-Petrovic et al. 2007; Pierik et al. 2009) and may be dependent on total PAR and duration of treatment.

UV-A/blue light (320–500 nm) is perceived through distinct types of photoreceptors involved in the regulation of different responses; the cryptochromes, the phototropins and the zeitlupe family of photoreceptors. Low B-induced shade avoidance responses in adult Arabidopsis plants have been reported to be dependent on the blue light photoreceptor cryptochrome (cry) 1 (Keller et al. 2011) and hypocotyl elongation in response to reduced B light was shown to be regulated by both cry1 and cry2 (Ahmad et al. 1995; Lin et al. 1998; Pierik et al. 2009). The phototropic response, which is especially important for growth

towards canopy-gaps and thus optimisation of light capture in high density (Ballaré et al. 1987a), is regulated through the phototropins.

Cryptochrome (cry)1 and 2, like the phytochromes, play a role in photoperiodic flowering, entrainment of the circadian clock and in photomorphogenesis through regulation of stem elongation and leaf expansion (Lin and Shalitin 2003; Losi and Gartner 2012). *Cry1* mutants have elongated hypocotyls in both high and low fluence rates of B light. *Cry2* mutants only show this phenotype under low B fluence rates due to rapid blue-light induced degradation of cry2, which is therefore though to act only in low B conditions (Lin et al. 1998). The cryptochromes are localised in the nucleus, where they are best known to directly interact with the E3 ubiquitin ligase CONSTITUTIVE PHOTOMORPHOGENIC (COP)1 in the regulation of light-induced inhibition of hypocotyl growth called photomorphogenesis (Wang et al. 2001; Yang et al. 2001). In darkness, COP1 interacts with the positive regulator of photomorphogenesis HY5 (long hypocotyl 5), thereby targeting this basic leucine zipper (bZIP) transcription factor for proteasome-mediated degradation (Ang et al. 1998; Osterlund et al. 2000). In light, COP1 translocates to the cytosol, thereby rescuing HY5 from degradation and allowing it to inhibit growth (Osterlund et al. 2000). The light-induced nuclear depletion of COP1 is believed to be established through its interaction with cry, which undergoes structural changes upon light perception (Chen et al. 2004). Although phyA and phyB have also been found to directly bind to COP1 (Seo et al. 2004; Yang et al. 2001), it is not known how this affects COP1 binding activity to HY5. COP1 interaction may however be a point of convergence between the phytochrome and cryptochrome signalling pathways. A second point of convergence might be the earlier mentioned PIF proteins since PIFs are also required for low blue-mediated petiole elongation (Keller et al. 2011). It remains to be studied if interaction between cryptochromes and PIFs indeed occur.

Another type of blue light receptors are the phototropins (phot)1 and 2. Phototropins are involved in phototropism (directional growth towards a unilateral light source), stomatal opening and chloroplast movement; responses that serve to optimise photosynthesis upon changes in light intensity (Christie 2007). *Phot1* mutants do not show phototropism in low B fluence rates and both *phot1* and *phot2* show a normal phototropic response in higher light intensities (Liscum and Briggs 1995; Sakai et al. 2000, 2001). Phototropism however is completely abolished in the *phot1phot2* double mutant (Sakai et al. 2001), which implies that phot1 is important for low fluence rates while both phototropins act redundantly at high fluence rates. The phototropins are localised at the plasmamembrane (Kong et al. 2006; Sakamoto and Briggs 2002), where they might regulate the distribution of auxin efflux carriers. Phot1 was found to interact with NONPHOTOTROPIC HYPOCOTYL (NPH)3, by which a lateral auxin gradient is established to allow for growth on the shaded side of the stem (Haga et al. 2005; Motchoulski and Liscum 1999). NPH3-like proteins were shown to regulate directional auxin transport through PIN-FORMED (PIN) auxin efflux carriers (Furutani et al. 2011). In relation to this, the auxin efflux carriers PIN1 and PIN3 have been shown to be required for a proper phototropic response (Blakeslee et al. 2004; Ding et al. 2011; Friml et al. 2002). Upon illumination, PIN3 trafficking to all cell sides by the PINOID (PID) kinase is repressed and unidirectional trafficking is brought about by the GNOM ARF GTPase GUANINE NUCLEOTIDE EXCHANGE FACTOR (GEF) (Ding et al. 2011). This directional targeting of PIN3 is likely to induce the differential auxin concentration between the illuminated and shaded side, leading to bending of hypocotyls and stems. Furthermore, the auxin-regulated transcription factors NPH4/ARF7 and MASSUGU (MSG)2/IAA19 have been involved in phototropism (Stowe-Evans et al. 1998; Tatematsu et al. 2004), emphasizing the importance of auxin

signalling in this response. Other signalling components implemented in the regulation of phototropic responses are PHYTOCHROME KINASE SUBSTRATE (PKS)1 and 2 (Boccalandro et al. 2008; de Carbonnel et al. 2010; Lariguet et al. 2006). PKS1 was found to bind both phot1 and NPH3 (Lariguet et al. 2006), and might thus play an essential role in phototropin signal transduction. As PKSs also interact with phytochromes and since phyA and phyB have been shown to be required for red-light-induced enhancement of phototropism (Janoudi et al. 1997; Parks et al. 1996; Whippo and Hangarter 2004), they might cross-talk between the two different photoreceptor pathways.

More recently, a novel class of blue light photoreceptors has been described. The zeitlupe family of photoreceptors consists of three members (ZTL, FKF1, and LKP2) with a photosensory domain similar to that of the phototropins (Christie 2007; Demarsy and Fankhauser 2009). So far, this type of photoreceptor has been described to play a role in regulation of photoperiodic flowering and the circadian clock, although ZTL might also be involved in photomorphogenesis (Kiba et al. 2007).

C. Other Light Signals: Low PAR and Enriched Green Light

In a closing canopy total light intensity at the lower levels of the vegetation will decrease, even when the leaves might still be in full sunlight (Ballaré et al. 1991). Perception of drastically reduced light intensity induces a hyponastic response and petiole elongation in Arabidopsis even when the spectral composition of the light is similar to sunlight, which is dependent on both phyA and phyB, cry1 and cry2 and photosynthesis-derived signals (Kozuka et al. 2005; Millenaar et al. 2009). Although spectral-neutral reduction of photosynthetically active radiation (PAR) also enhanced stem elongation in tobacco (Pierik et al. 2004) it does not affect internode lengths in *Datura ferox* monocultures (Ballaré et al. 1991), indicating that the role for reduced PAR may be species-specific.

Like FR, green light is reflected by plant tissues containing chlorophyll, making them appear green to the human eye. In a canopy, this results in enrichment of green wavelengths in the light environment. Green light irradiation indeed increased hypocotyl elongation in Arabidopsis seedlings, and addition of green light to constant red and blue light induced the shade avoidance phenotype of increased leaf angles and enhanced petiole elongation in adult Arabidopsis plants (Folta 2004; Zhang et al. 2011). Cryptochromes have been shown to have a green-sensing state with biological activity (Banerjee et al. 2007; Bouly et al. 2007), but other modes of green light perception may exist.

D. Light-Independent Signals

Various plant species are known to have increased emissions of the volatile plant hormone ethylene (ET) upon perception of low R:FR (Finlayson et al. 1999; reviewed in Kegge and Pierik 2010). ET is known to be the main regulator of hyponasty and subsequent petiole elongation in de semi-aquatic species *Rumex palustris* upon submergence stress (Peeters et al. 2002; Voesenek et al. 2003), a response that much resembles the growth adjustments that occur upon shading (Pierik et al. 2011). Indeed, ET has been found to accumulate inside the atmosphere of tobacco canopies to a level in which it induces shade avoidance-like growth responses in single-grown plants (Pierik et al. 2004). ET can induce elevated leaf angles even at very low concentrations (Polko et al. 2012) and it was mainly due to a retarded hyponastic response that ET-insensitive tobacco plants were outcompeted by wild-type plants when grown in high density (Pierik et al. 2003, 2004). These results show that ET can be an important player in neighbour detection.

In Arabidopsis, ethylene is perceived through a family of five redundant receptors (ETR1-2, ERS1-2 and EIN4) divided into two subfamilies based on structural similarities (Bleecker 1999; Chang and

Stadler 2001). All five receptors interact with the Raf-like kinase CONSTITUTIVE TRIPLE RESPONSE (CTR)1 upon binding of ethylene, thereby releasing its inhibition of EIN2 and other downstream signalling components in the ethylene pathway (Hall et al. 2007). Recent progress in the field of plant volatile signalling has shown that emissions of plant-produced volatile organic compounds (VOCs) are light-dependent and are affected by competition (reviewed in Kegge and Pierik 2010). Recently, it was shown that the composition of the VOC blend emitted by Arabidopsis plants is affected by R:FR signalling, leading to altered multitrophic interactions (Kegge et al. 2013). Although not much is known about the perception of the different biogenic volatile organic compounds, it is possible that they are used as a neighbour detection signal in competition for light.

The earliest response to neighbours in Arabidopsis, hyponasty, was found to be induced through touching leaf tips (de Wit et al. 2012). This touch-induced hyponasty is driven by an unidentified touch mechanism and occurs prior to a reduction in the R:FR. In fact, hyponasty was shown to be required to create a low R:FR in an Arabidopsis canopy (de Wit et al. 2012). Touch thus appears to be an especially important detection signal in rosette species, but may also play a role at later stages of competition for light in stem-forming species.

III. Hormonal Regulation of Shade Avoidance

Besides ethylene, several other hormones play a role in the shade avoidance response. Gibberellin (GA) is a key regulator of many growth processes in plants and was shown to be essential for low R:FR-induced elongation. Auxin is involved in phototropism as described previously, but also plays an important role in phytochrome-mediated shade avoidance responses. More recently brassinosteroids (BR), which have partly overlapping functions with auxin, have been implicated in low R:FR signalling as well. Besides their linear pathways these hormones are known to interact, which adds another level of complexity to understanding their actions. Here, it is described how these hormones are involved in regulation of the shade avoidance response.

A. Gibberellin

In the 1990s, it was shown that the constitutively elongated phenotype of *phyB* mutants was related to increased sensitivity to GA (Lopez-Juez et al. 1995; Reed et al. 1996) and could be suppressed by GA deficiency and insensitivity (Peng and Harberd 1997). GA deficient and insensitive mutants have indeed been found to show reduced low R:FR-induced responses (Djakovic-Petrovic et al. 2007; Pigliucci and Schmitt 2004). In an unbiased microarray approach, GA-related genes were found to be upregulated in response to low R:FR and in the *cry1* mutant (Devlin et al. 2003; Folta et al. 2003). Furthermore, *GA20ox2* expression is increased by an end-of-day (EOD) pulse of FR light while mutants with impaired *GA20ox2* expression showed a reduced elongation response to EOD-FR (Hisamatsu et al. 2005), suggesting that the shade avoidance response requires de-novo synthesis of GA.

Binding of GA to its receptor GID1 (GA insensitive dwarf 1; a-c in Arabidopsis) leads to interaction between the receptor and the nuclear growth-inhibiting DELLA proteins, which are subsequently targeted for proteasome-mediated degradation through the SCF^{sly1} complex (Dill et al. 2004; Fu et al. 2004; Nakajima et al. 2006; Ueguchi-Tanaka et al. 2005). Degradation of DELLAs relieves their suppression of genes sensitive to GA, thereby allowing for GA-induced growth responses. The discovery of DELLAs allowed for further understanding of the role GA has in shade avoidance. Abundance of the DELLA protein RGA, which has been implicated in GA-induced vegetative growth (Fleet and Sun 2005), was shown to be strongly reduced in petioles in response to

neighbours, low R:FR and low B (Djakovic-Petrovic et al. 2007). RGA was found to interact with PIF3 and PIF4, thereby preventing their transcriptional activity (De Lucas et al. 2008; Feng et al. 2008). Besides nuclear depletion of active phytochrome upon perception of low R:FR, GA-regulated degradation of DELLAs thus contributes to the release of PIF suppression to allow for growth during the shade avoidance response.

B. Auxin and BR

Many auxin-regulated genes were found to be regulated during shade avoidance-inducing conditions (Devlin et al. 2003; Folta et al. 2003; Roig-Villanova et al. 2007), suggesting the importance of this hormone for the response. Expression of auxin-inducible genes is, like for the GA pathway, dependent on relieved suppression of transcriptional inhibitors (Aux/IAAs) that are targeted for 26S proteasome-mediated degradation when auxin binds to its receptor (the F-box protein TRANSPORT INHBITOR RESPONSE (TIR)1). Auxin binding to the SCF^{TIR1} complex thus stimulates the removal of Aux/IAAs from the ARF (auxin response family) transcription factors that are already bound to the promoter of auxin-responsive genes, allowing for their expression (Benjamins and Scheres 2008; Teale et al. 2006).

Auxin biosynthesis was shown to be rapidly induced by low R:FR through the TRYPTOPHAN AMINOTRANSFERASE OF ARABIDOPSIS (TAA)1 and YUCCA-dependent auxin biosynthetic pathway (Li et al. 2012; Stepanova et al. 2008; Tao et al. 2008; Won et al. 2011). This increase of auxin production proved to be essential for full induction of a shade avoidance response, as was shown by two allelic mutants for the *TAA1* gene; *sav3-1* and *wei8-1* (Keuskamp et al. 2010; Moreno et al. 2009; Tao et al. 2008). Apart from enhanced auxin biosynthesis, lateral redistribution of auxin was proposed to be important for a shade avoidance phenotype (Morelli and Ruberti 2000). Indeed, the auxin efflux carriers *PIN3* and *PIN7* were found to be upregulated in low R:FR (Devlin et al. 2003). Besides its previously described role in phototropism (Friml et al. 2002), auxin redistribution through PIN3 was reported to be required for shade avoidance responses to both neighbours and low R:FR (Keuskamp et al. 2010).

A microarray study on leaves of EOD-FR-treated plants revealed a strong overrepresentation of both auxin and BR-related genes (Kozuka et al. 2010). BR-regulated gene expression is brought about when active BR (brassinolide) binds to the leucine-rich repeat receptor-like kinase BRASSINOSTEROID INSENSITIVE (BRI)1, followed by a number of (de)phosphorylation events leading to accumulation and DNA-binding of the transcription factors BES1 (BRI1 EMS SUPPRESSOR1) and BZR1 (BRASSINAZOLE RESISTANT1) (Clouse 2011; Kim and Wang 2010). The same study on EOD-FR reported a reduced petiole elongation response in the auxin-deficient mutant *doc1* and the BR-deficient mutant *rot3* (Kozuka et al. 2010). Another study on low B-induced hypocotyl elongation showed that this response requires both auxin and BR action (Keuskamp et al. 2011), further confirming a role for BR in shade avoidance.

C. Hormone Physiological Control of Shoot Branching

The above described modes of molecular regulation have been researched for low R:FR-mediated shoot elongation responses. Very little research has been devoted to low R:FR-induced inhibition of shoot branching and tillering. Therefore, it remains mostly unknown if the above-mentioned regulatory network also controls signalling toward branching control. A few recent studies have identified Abscisic acid (ABA), auxin and strigolactones as candidate regulators of phytochrome control of shoot branching (Finlayson et al. 2010; Reddy et al. 2013). The latter two hormones are also implied in phytochrome control of shoot elongation,

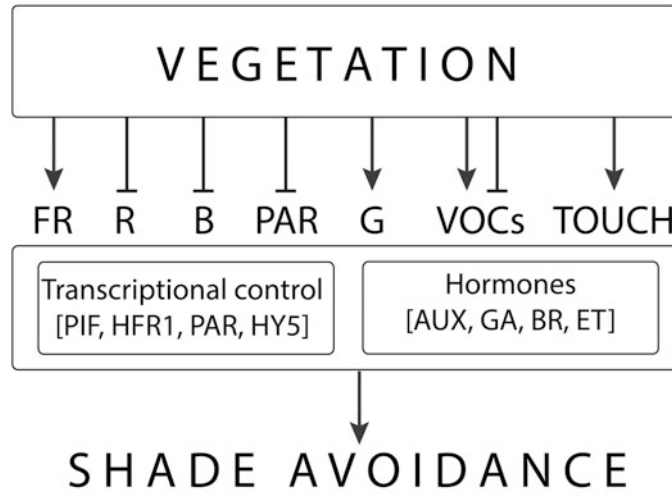

Fig. 6.3. Simplified schematic of regulation of shade avoidance responses to different neighbour detection cues. For more detailed schematic representations of signal transduction component interactions we suggest the following recent reviews: Casal (2012) and Pierik and Testerink (2014)

which may imply that branching and elongation are phytochrome-controlled through at least some shared regulators.

IV. Future Perspective

The majority of studies on shade avoidance have focussed on internode, petiole or hypocotyl elongation in Arabidopsis. These studies have provided breakthrough insights into molecular and physiological regulation of light signalling and signal transduction towards these responses (summarized in Fig. 6.3). Nevertheless, several aspects of how shade avoidance signals alter plant architecture are less intensively studied. For example, the phytochrome-mediated signalling mechanisms that drive changes in leaf blade morphology and shoot branching, important traits for crop yield, remain largely unknown. Phytochrome control of shoot branching is known to involve two TCP domain proteins, called BRANCHED (BRC)1 and BRC2 (Finlayson et al. 2010), but much more in-depth knowledge is needed on this trait. Although Arabidopsis flowering stems do show branching and this is controlled by phytochromes (Finlayson et al. 2010; Reddy et al. 2013), inclusion of other species might facilitate such research. Current technological developments such as high-throughput phenotyping and next generation RNA sequencing enable the characterization of shade avoidance responses with unprecedented resolution and facilitate the use of non-model species. This furthermore opens up possibilities to study the molecular mechanisms behind the alternative strategy of shade tolerance (Gommers et al. 2013). Filling in such gaps will provide a more complete understanding of plant responses to competition for light in both natural and agricultural environments.

References

Ahmad M, Lin C, Cashmore AR (1995) Mutations throughout an arabidopsis blue-light photoreceptor impair blue-light-responsive anthocyanin accumulation and inhibition of hypocotyl elongation. Plant J 8:653–658

Ang LM, Chattopadhyay S, Wei N, Oyama T, Okada K, Batschauer A, Deng XW (1998) Molecular interaction between COP1 and HY5 defines a regulatory switch for light control of arabidopsis development. Mol Cell 1:213–222

Athreya VR (1999) Light or presence of host trees: which is more important for the strangler fig? J Trop Ecol 15:589–602

Ballaré CL, Scopel AL, Sánchez RA (1987a) Plant photomorphogenesis in canopies, crop growth and yield. HortScience 30:1172–1181

Ballaré CL, Sánchez RA, Scopel AL, Casal JJ, Ghersa CM (1987b) Early detection of neighbour plants by

phytochrome perception of spectral changes in reflected sunlight. Plant Cell Environ 10:551–557

Ballaré CL, Sanchez RA, Scopel AL, Ghersa CM (1988) Morphological responses of *Datura ferox* L. seedlings to the presence of neighbors – their relationships with canopy microclimate. Oecologia 76:288–293

Ballaré CL, Scopel AL, Sánchez RA (1990) Far-red radiation reflected from adjacent leaves: an early signal of competition in plant canopies. Science 247:329–332

Ballaré CL, Scopel AL, Sánchez RA (1991) Photocontrol of stem elongation in plant neighbourhoods: effects of photon fluence rate under natural conditions of radiation. Plant Cell Environ 14:57–65

Banerjee R, Schleicher E, Meier S, Viana RM, Pokorny R, Ahmad M, Bittl R, Batschauer A (2007) The signaling state of arabidopsis cryptochrome 2 contains flavin semiquinone. J Biol Chem 282:14916–14922

Benjamins R, Scheres B (2008) Auxin: the looping star in plant development. Annu Rev Plant Biol 59:443–465

Bittebiere A, Renaud N, Clement B, Mony C (2012) Morphological response to competition for light in the clonal *Trifolium repens* (fabaceae). Am J Bot 99:646–654

Blakeslee JJ, Bandyopadhyay A, Peer WA, Makam S, Murphy AS (2004) Relocalization of the PIN1 auxin efflux facilitator plays a role in phototropic responses. Plant Physiol 134:28–31

Bleecker AB (1999) Ethylene perception and signaling: an evolutionary perspective. Trends Plant Sci 4:269–274

Boccalandro HE, De Simone SN, Bergmann-Honsberger A, Schepens I, Fankhauser C, Casal JJ (2008) Phytochrome kinase substrate1 regulates root phototropism and gravitropism. Plant Physiol 146:108–115

Bouly JP, Schleicher E, Dionisio-Sese M, Vandenbussche F, Van Der Straeten D, Bakrim N, Meier S, . . ., Ahmad M (2007) Cryptochrome blue light photoreceptors are activated through interconversion of flavin redox states. J Biol Chem 282:9383–9391

Carabelli M, Sessa G, Baima S, Morelli G, Ruberti I (1993) The arabidopsis athb-2 and −4 genes are strongly induced by far-red-rich light. Plant J 4:469–479

Carabelli M, Morelli G, Whitelam G, Ruberti I (1996) Twilight-zone and canopy shade induction of the athb-2 homeobox gene in green plants. Proc Natl Acad Sci U S A 93:3530–3535

Carabelli M, Possenti M, Sessa G, Ciolfi A, Sassi M, Morelli G, Ruberti I (2007) Canopy shade causes a rapid and transient arrest in leaf development through auxin-induced cytokinin oxidase activity. Genes Dev 21:1863–1868

Casal JJ (2012) Shade avoidance. Arabidopsis Book 10:e0157

Casal JJ, Smith H (1989) The function, action and adaptive significance of phytochrome in light-grown plants. Plant Cell Environ 12:855–862

Casal JJ, Ballaré CL, Tourn M, Sánchez RA (1994) Anatomy, growth and survival of a long-hypocotyl mutant of cucumis sativus deficient in phytochrome B. Ann Bot 73:569–575

Chang C, Stadler R (2001) Ethylene hormone receptor action in arabidopsis. Bioessays 23:619–627

Chen M, Chory J, Fankhauser C (2004) Light signal transduction in higher plants. Annu Rev Genet 38:87–117

Chitwood DH, Headland LR, Filiault DL, Kumar R, Jimenez-Gomez JM, Schrager AV, Park DS, . . ., Maloof JN (2012) Native environment modulates leaf size and response to simulated foliar shade across wild tomato species. PLoS One 7:e29570

Christie JM (2007) Phototropin blue-light receptors. Annu Rev Plant Biol 58:21–45

Clough RC, Lohman KN, Vierstra RD (1997) Sequences within both the N- and C-terminal domains of phytochrome are required for Pfr-specific degradation. Plant Physiol 114:1476

Clouse SD (2011) Brassinosteroid signal transduction: from receptor kinase activation to transcriptional networks regulating plant development. Plant Cell 23:1219–1230

de Carbonnel M, Davis P, Roelfsema MRG, Inoue S, Schepens I, Lariguet P, Geisler M, . . ., Fankhauser C (2010) The Arabidopsis PHYTOCHROME KINASE SUBSTRATE2 protein is a phototropin signaling element that regulates leaf flattening and leaf positioning. Plant Physiol 152:1391–1405

De Lucas M, Davière JM, Rodríguez-Falcón M, Pontin M, Iglesias-Pedraz JM, Lorrain S, Fankhauser C, . . ., Prat S (2008) A molecular framework for light and gibberellin control of cell elongation. Nature 451:480–484

de Wit M, Kegge W, Evers JB, Vergeer-van Eijk MH, Gankema P, Voesenek LACJ, Pierik R (2012) Plant neighbor detection through touching leaf tips precedes phytochrome signals. Proc Natl Acad Sci U S A 109:14705–14710

Demarsy E, Fankhauser C (2009) Higher plants use LOV to perceive blue light. Curr Opin Plant Biol 12:69–74

Devlin PF, Rood SB, Somers DE, Quail PH, Whitelam GC (1992) Photophysiology of the elongated internode (ein) mutant of *Brassica rapa*: ein mutant lacks a detectable phytochrome B-like polypeptide. Plant Physiol 100:1442–1447

Devlin PF, Yanovsky MJ, Kay SA (2003) A genomic analysis of the shade avoidance response in arabidopsis. Plant Physiol 133:1617–1629

Dill A, Thomas SG, Hu J, Steber CM, Sun T (2004) The arabidopsis F-box protein SLEEPY1 targets gibberellin signaling repressors for gibberellin-induced degradation. Plant Cell 16:1392–1405

Ding Z, Galvan-Ampudia CS, Demarsy E, Langowski L, Kleine-Vehn J, Fan Y, Morita MT, . . ., Friml (2011) Light-mediated polarization of the PIN3 auxin transporter for the phototropic response in Arabidopsis. Nat Cell Biol 13:447–453

Djakovic-Petrovic T, de Wit M, Voesenek LACJ, Pierik R (2007) DELLA protein function in growth responses to canopy signals. Plant J 51:117–126

Duek PD, Fankhauser C (2005) bHLH class transcription factors take centre stage in phytochrome signalling. Trends Plant Sci 10:51–54

Fairchild CD, Schumaker MA, Quail PH (2000) HFR1 encodes an atypical bHLH protein that acts in phytochrome A signal transduction. Genes Dev 14:2377–2391

Feng S, Martinez C, Gusmaroli G, Wang Y, Zhou J, Wang F, Chen L, . . ., Deng XW (2008) Coordinated regulation of *Arabidopsis thaliana* development by light and gibberellins. Nature 451:475479

Finlayson SA, Lee IJ, Mullet JE, Morgan PW (1999) The mechanism of rhythmic ethylene production in sorghum. The role of phytochrome B and simulated shading. Plant Physiol 119:1083–1089

Finlayson SA, Krishnareddy SR, Kebrom TH, Casal JJ (2010) Phytochrome regulation of branching in arabidopsis. Plant Physiol 152:1914–1927

Fleet CM, Sun TP (2005) A DELLAcate balance: the role of gibberellin in plant morphogenesis. Curr Opin Plant Biol 8:77–85

Folta KM (2004) Green light stimulates early stem elongation, antagonizing light-mediated growth inhibition. Plant Physiol 135:1407–1416

Folta KM, Pontin MA, Karlin-Neumann G, Bottini R, Spalding EP (2003) Genomic and physiological studies of early cryptochrome 1 action demonstrate roles for auxin and gibberellin in the control of hypocotyl growth by blue light. Plant J 36:203–214

Franklin KA (2008) Shade avoidance. New Phytol 179:930–944

Franklin KA (2009) Light and temperature signal crosstalk in plant development. Curr Opin Plant Biol 12:63–68

Friml J, Wiśniewska J, Benková E, Mendgen K, Palme K (2002) Lateral relocation of auxin efflux regulator PIN3 mediates tropism in arabidopsis. Nature 415:806–809

Fu X, Richards DE, Fleck B, Xie D, Burton N, Harberd NP (2004) The Arabidopsis mutant sleepy1gar2-1 protein promotes plant growth by increasing the affinity of the SCFSLY1 E3 ubiquitin ligase for DELLA protein substrates. Plant Cell 16:1406–1418

Furutani M, Sakamoto N, Yoshida S, Kajiwara T, Robert HS, Friml J, Tasaka M (2011) Polar-localized NPH3-like proteins regulate polarity and endocytosis of PIN-FORMED auxin efflux carriers. Development 138:2069–2078

Givnish TJ (1988) Adaptation to sun and shade – a whole-plant perspective. Aust J Plant Physiol 15:63–92

Goldberg DE, Barton AM (1992) Patterns and consequences of interspecific competition in natural communities: a review of field experiments with plants. Am Nat 139:771–801

Gommers CMM, Visser EJW, St. Onge KR, Voesenek LACJ, Pierik R (2013) Shade tolerance: when growing tall is not an option. Trends Plant Sci 18:65–71

Goudriaan J (2016) Light distribution. In: Hikosaka K, Niinemets Ü, Anten N (eds) Canopy photosynthesis: from basics to applications. Springer, Berlin, pp 3–22

Haga K, Takano M, Neumann R, Iino M (2005) The rice coleoptile phototropism1 gene encoding an ortholog of Arabidopsis NPH3 is required for phototropism of coleoptiles and lateral translocation of auxin. Plant Cell 17:103–115

Hall BP, Shakeel SN, Schaller GE (2007) Ethylene receptors: ethylene perception and signal transduction. J Plant Growth Regul 26:118–130

Halliday K, Salter M, Thingnaes E, Whitelam G (2003) Phytochrome control of flowering is temperature sensitive and correlates with expression of the floral integrator FT. Plant J 33:875–885

Hautier Y, Niklaus PA, Hector A (2009) Competition for light causes plant biodiversity loss after eutrophication. Science 324:636–638

Hennig L, Buche C, Eichenberg K, Schafer E (1999) Dynamic properties of endogenous phytochrome A in Arabidopsis seedlings. Plant Physiol 121:571–577

Hisamatsu T, King RW, Helliwell CA, Koshioka M (2005) The involvement of gibberellin 20-oxidase genes in phytochrome-regulated petiole elongation of Arabidopsis. Plant Physiol 138:1106–1116

Holmes MG, Smith H (1975) The function of phytochrome in plants growing in the natural environment. Nature 254:512–514

Hornitschek P, Lorrain S, Zoete V, Michielin O, Fankhauser C (2009) Inhibition of the shade avoidance response by formation of non-DNA binding bHLH heterodimers. EMBO J 28:3893–3902

Huq E, Al-Sady B, Quail PH (2003) Nuclear translocation of the photoreceptor phytochrome B is necessary for its biological function in seedling photomorphogenesis. Plant J 35:660–664

Janoudi A, Konjević R, Whitelam G, Gordon W, Poff KL (1997) Both phytochrome A and phytochrome B are required for the normal expression of phototropism in *Arabidopsis thaliana* seedlings. Physiol Plant 101:278–282

Johnson E, Bradley M, Harberd NP, Whitelam GC (1994) Photoresponses of light-grown phya mutants of Arabidopsis – phytochrome-a is required for the perception of daylength extensions. Plant Physiol 105:141–149

Kebrom TH, Burson BL, Finlayson SA (2006) Phytochrome B represses teosinte Branched1 expression and induces sorghum axillary bud outgrowth in response to light signals. Plant Physiol 140:1109–1117

Kegge W, Pierik R (2010) Biogenic volatile organic compounds and plant competition. Trends Plant Sci 15:126–132

Kegge W, Weldegergis BT, Soler R, Vergeer – van Eijk M, Dicke M, Voesenek LACJ, Pierik R (2013) Canopy light cues affect emission of constitutive and methyl jasmonate-induced volatile organic compounds in *Arabidopsis thaliana*. New Phytol 200:861–874

Keller MM, Jaillais Y, Pedmale UV, Moreno JE, Chory J, Ballaré CL (2011) Cryptochrome 1 and phytochrome B control shade-avoidance responses in arabidopsis via partially independent hormonal cascades. Plant J 67:195–207

Keuskamp DH, Pollmann S, Voesenek LACJ, Peeters AJM, Pierik R (2010) Auxin transport through PIN-FORMED 3 (PIN3) controls shade avoidance and fitness during competition. Proc Natl Acad Sci U S A 107:22740–22744

Keuskamp DH, Sasidharan R, Vos I, Peeters AJM, Voesenek LACJ, Pierik R (2011) Blue-light-mediated shade avoidance requires combined auxin and brassinosteroid action in arabidopsis seedlings. Plant J 67:208–217

Kiba T, Henriques R, Sakakibara H, Chua NH (2007) Targeted degradation of PSEUDO-RESPONSE REGULATOR5 by an SCFZTL complex regulates clock function and photomorphogenesis in *Arabidopsis thaliana*. Plant Cell 19:2516–2530

Kim TW, Wang ZY (2010) Brassinosteroid signal transduction from receptor kinases to transcription factors. Annu Rev Plant Biol 61:681–704

Kircher S, Kozma-Bognar L, Kim L, Adam E, Harter K, Schäfer E, Nagy F (1999) Light quality-dependent nuclear import of the plant photoreceptors phytochrome A and B. Plant Cell 11:1445–1456

Kitajima K (1994) Relative importance of photosynthetic traits and allocation patterns as correlates of seedling shade tolerance of 13 tropical trees. Oecologia 98:419–428

Kitajima K, Poorter L (2010) Tissue-level leaf toughness, but not lamina thickness, predicts sapling leaf lifespan and shade tolerance of tropical tree species. New Phytol 186:708–721

Kong SG, Suzuki T, Tamura K, Mochizuki N, Hara-Nishimura I, Nagatani A (2006) Blue light-induced association of phototropin 2 with the golgi apparatus. Plant J 45:994–1005

Kozuka T, Horiguchi G, Kim GT, Ohgishi M, Sakai T, Tsukaya H (2005) The different growth responses of the *Arabidopsis thaliana* leaf blade and the petiole during shade avoidance are regulated by photoreceptors and sugar. Plant Cell Physiol 46:213–223

Kozuka T, Kobayashi J, Horiguchi G, Demura T, Sakakibara H, Tsukaya H, Nagatani A (2010) Involvement of auxin and brassinosteroid in the regulation of petiole elongation under the shade. Plant Physiol 153:1608–1618

Lariguet P, Schepens I, Hodgson D, Pedmale UV, Trevisan M, Kami C, De Carbonnel M, …, Fankhauser C (2006) Phytochrome kinase substrate 1 is a phototropin 1 binding protein required for phototropism. Proc Natl Acad Sci USA 103:10134–10139

Li L, Ljung K, Breton G, Schmitz RJ, Pruneda-Paz J, Cowing-Zitron C, Cole BJ, …, Chory J (2012) Linking photoreceptor excitation to changes in plant architecture. Genes Dev 26:785790

Lin C, Shalitin D (2003) Cryptochrome structure and signal transduction. Annu Rev Plant Biol 54:469–496

Lin C, Yang H, Guo H, Mockler T, Chen J, Cashmore AR (1998) Enhancement of blue-light sensitivity of arabidopsis seedlings by a blue light receptor cryptochrome 2. Proc Natl Acad Sci U S A 95:2686–2690

Liscum E, Briggs WR (1995) Mutations in the NPH1 locus of arabidopsis disrupt the perception of phototropic stimuli. Plant Cell 7:473–485

Liu J, Zhang F, Zhou J, Chen F, Wang B, Xie X (2012) Phytochrome B control of total leaf area and stomatal density affects drought tolerance in rice. Plant Mol Biol 78:289–300

Lopez-Juez E, Kobayashi M, Sakurai A, Kamiya Y, Kendrick RE (1995) Phytochrome, gibberellins, and hypocotyl growth. A study using the cucumber (*Cucumis sativus* L.) long hypocotyl mutant. Plant Physiol 107:131–140

Lorrain S, Allen T, Duek PD, Whitelam GC, Fankhauser C (2008) Phytochrome-mediated inhibition of shade avoidance involves degradation of growth-promoting bHLH transcription factors. Plant J 53:312–323

Losi A, Gartner W (2012) The evolution of flavin-binding photoreceptors: an ancient chromophore serving trendy blue-light sensors. Annu Rev Plant Biol 63:49–72

Meils A, Harvey G (1981) Regulation of photosystem stoichiometry, chlorophyll a and chlorophyll b content and relation to chloroplast ultrastructure. Biochim Biophys Acta 637:138–145

Millenaar FF, Van Zanten M, Cox MCH, Pierik R, Voesenek LACJ, Peeters AJM (2009) Differential petiole growth in *Arabidopsis thaliana*: photocontrol and hormonal regulation. New Phytol 184:141–152

Morelli G, Ruberti I (2000) Shade avoidance responses. Driving auxin along lateral routes. Plant Physiol 122:621–626

Moreno JE, Tao Y, Chory J, Ballaré CL (2009) Ecological modulation of plant defense via phytochrome control of jasmonate sensitivity. Proc Natl Acad Sci U S A 106:4935–4940

Morgan DC, Smith H (1978) The relationship between phytochrome-photoequilibrium and development in light grown *Chenopodium album* L. Planta 142:187–193

Morgan DC, O'Brien T, Smith H (1980) Rapid photomodulation of stem extension in light-grown *Sinapis alba* L. – studies on kinetics, site of perception and photoreceptor. Planta 150:95–101

Motchoulski A, Liscum E (1999) Arabidopsis NPH3: a NPH1 photoreceptor-interacting protein essential for phototropism. Science 286:961–964

Nakajima M, Shimada A, Takashi Y, Kim YC, Park SH, Ueguchi-Tanaka M, Suzuki H, . . ., Yamaguchi I (2006) Identification and characterization of arabidopsis gibberellin receptors. Plant J 46:880–889

Osterlund MT, Hardtke CS, Ning W, Deng XW (2000) Targeted destabilization of HY5 during light-regulated development of *Arabidopsis*. Nature 405:462–466

Parks BM, Quail PH, Hangarter RP (1996) Phytochrome A regulates red-light induction of phototropic enhancement in Arabidopsis. Plant Physiol 110:155–162

Peeters AJM, Cox MCH, Benschop JJ, Vreeburg RAM, Bou J, Voesenek LACJ (2002) Submergence research using *Rumex palustris* as a model; looking back and going forward. J Exp Bot 53:391–398

Peng J, Harberd NP (1997) Gibberellin deficiency and response mutations suppress the stem elongation phenotype of phytochrome-deficient mutants of Arabidopsis. Plant Physiol 113:1051–1058

Pierik R, Testerink C (2014) The art of being flexible: how to escape from shade, salt and drought. Plant Physiol 166:5–22

Pierik R, Visser EJW, De Kroon H, Voesenek LACJ (2003) Ethylene is required in tobacco to successfully compete with proximate neighbours. Plant Cell Environ 26:1229–1234

Pierik R, Whitelam GC, Voesenek LACJ, De Kroon H, Visser EJW (2004) Canopy studies on ethylene-insensitive tobacco identify ethylene as a novel element in blue light and plant-plant signalling. Plant J 38:310–319

Pierik R, Djakovic-Petrovic T, Keuskamp DH, de Wit M, Voesenek LACJ (2009) Auxin and ethylene regulate elongation responses to neighbor proximity signals independent of gibberellin and DELLA proteins in Arabidopsis. Plant Physiol 149:1701–1712

Pierik R, de Wit M, Voesenek LACJ (2011) Growth-mediated stress escape: convergence of signal transduction pathways activated upon exposure to two different environmental stresses. New Phytol 189:122–134

Pigliucci M, Schmitt J (2004) Phenotypic plasticity in response to foliar and neutral shade in gibberellin mutants of *Arabidopsis thaliana*. Evol Ecol Res 6:243–259

Polko JK, van Zanten M, van Rooij JA, Maree AFM, Voesenek LACJ, Peeters AJM, Pierik R (2012) Ethylene-induced differential petiole growth in *Arabidopsis thaliana* involves local microtubule reorientation and cell expansion. New Phytol 193:339–348

Poorter L, Bongers F (2006) Leaf traits are good predictors of plant performance across 53 rain forest species. Ecology 87:1733–1743

Reddy SK, Holalu SV, Casal JJ, Finlayson S (2013) Abscisic acid regulates axillary bud outgrowth responses to the ratio of red to far-red light. Plant Physiol 163:1047–1058

Reed JW, Nagpal P, Poole DS, Furuya M, Chory J (1993) Mutations in the gene for the red/far-red light receptor phytochrome B alter cell elongation and physiological responses throughout Arabidopsis development. Plant Cell 5:147–157

Reed JW, Nagatani A, Elich TD, Fagan M, Chory J (1994) Phytochrome-a and phytochrome-B have overlapping but distinct functions in Arabidopsis development. Plant Physiol 104:1139–1149

Reed JW, Foster KR, Morgan PW, Chory J (1996) Phytochrome B affects responsiveness to gibberellins in arabidopsis. Plant Physiol 112:337–342

Rockwell NC, Su Y, Lagarias JC (2006) Phytochrome structure and signaling mechanisms. Annu Rev Plant Biol 57:837–858

Roig-Villanova I, Bou-Torrent J, Galstyan A, Carretero-Paulet L, Portolés S, Rodríguez-Concepción M, Martínez-García JF (2007) Interaction of shade avoidance and auxin responses: a role for two novel atypical bHLH proteins. EMBO J 26:4756–4767

Rousseaux MC, Ballaré CL, Jordan ET, Vierstra RD (1997) Directed overexpression of PHYA locally suppresses stem elongation and leaf senescence responses to far-red radiation. Plant Cell Environ 20:1551–1558

Sakai T, Wada T, Ishiguro S, Okada K (2000) RPT2: a signal transducer of the phototropic response in Arabidopsis. Plant Cell 12:225–236

Sakai T, Kagawa T, Kasahara M, Swartz TE, Christie JM, Briggs WR, Wada M, Okada K (2001) Arabidopsis nph1 and npl1: blue light receptors that mediate both phototropism and chloroplast relocation. Proc Natl Acad Sci U S A 98:6969–6974

Sakamoto K, Briggs WR (2002) Cellular and subcellular localization of phototropin 1. Plant Cell 14:1723–1735

Sakamoto K, Nagatani A (1996) Nuclear localization activity of phytochrome B. Plant J 10:859–868

Salter MG, Franklin KA, Whitelam GC (2003) Gating of the rapid shade-avoidance response by the circadian clock in plants. Nature 426:680–683

Sasidharan R, Chinnappa CC, Voesenek LACJ, Pierik R (2008) The regulation of cell wall extensibility during shade avoidance: a study using two contrasting ecotypes of *Stellaria longipes*. Plant Physiol 148:1557–1569

Sasidharan R, Chinnappa CC, Staal M, Elzenga JTM, Yokoyama R, Nishitani K, Voesenek LACJ, Pierik R (2010) Light quality-mediated petiole elongation in arabidopsis during shade avoidance involves cell wall modification by xyloglucan endotransglucosylase/hydrolases. Plant Physiol 154:978–990

Schmitt J, McCormac AC, Smith H (1995) A test of the adaptive plasticity hypothesis using transgenic and mutant plants disabled in phytochrome-mediated elongation responses to neighbors. Am Nat 146:937–953

Seo HS, Watanabe E, Tokutomi S, Nagatani A, Chua NH (2004) Photoreceptor ubiquitination by COP1 E3 ligase desensitizes phytochrome A signaling. Genes Dev 18:617–622

Sessa G, Carabelli M, Sassi M, Ciolfi A, Possenti M, Mittempergher F, Becker J, . . ., Ruberti I (2005) A dynamic balance between gene activation and repression regulates the shade avoidance response in arabidopsis. Genes Dev 19:2811–2815

Smith H (2000) Phytochromes and light signal perception by plants – an emerging synthesis. Nature 407:585–591

Smith H, Holmes MG (1977) The function of phytochrome in the natural environment? III. Measurement and calculation of phytochrome photoequilibria. Photochem Photobiol 25:547–550

Somers DE, Sharrock RA, Tepperman JM, Quail PH (1991) The hy3 long hypocotyl mutant of arabidopsis is deficient in phytochrome B. Plant Cell 3:1263–1274

Steindler C, Matteucci A, Sessa G, Weimar T, Ohgishi M, Aoyama T, Morelli G, Ruberti I (1999) Shade avoidance responses are mediated by the ATHB-2 HD-zip protein, a negative regulator of gene expression. Development 126:4235–4245

Stepanova AN, Robertson-Hoyt J, Yun J, Benavente LM, Xie DY, Doležal K, Schlereth A, . . ., Alonso JM (2008) TAA1-mediated auxin biosynthesis is essential for hormone crosstalk and plant development. Cell 133:177–191

Stowe-Evans EL, Harper RM, Motchoulski AV, Liscum E (1998) NPH4, a conditional modulator of auxin-dependent differential growth responses in Arabidopsis. Plant Physiol 118:1265–1275

Su H, Abernathy SD, White RH, Finlayson SA (2011) Photosynthetic photon flux density and phytochrome B interact to regulate branching in Arabidopsis. Plant Cell Environ 34:1986–1998

Tao Y, Ferrer JL, Ljung K, Pojer F, Hong F, Long JA, Li L, . . ., Chory J (2008) Rapid synthesis of auxin via a new tryptophan-dependent pathway is required for shade avoidance in plants. Cell 133:164–176

Tatematsu K, Kumagai S, Muto H, Sato A, Watahiki MK, Harper RM, Liscum E, Yamamoto KT (2004) Massugu2 encodes Aux/IAA19, an auxin-regulated protein that functions together with the transcriptional activator NPH4/ARF7 to regulate differential growth responses of hypocotyl and formation of lateral roots in *Arabidopsis thaliana*. Plant Cell 16:379–393

Teale WD, Paponov IA, Palme K (2006) Auxin in action: signalling, transport and the control of plant growth and development. Nat Rev Mol Cell Bio 7:847–859

Ueguchi-Tanaka M, Ashikari M, Nakajima M, Itoh H, Katoh E, Kobayashi M, Chow TY, . . ., Matsuoka M (2005) GIBBERELLIN INSENSITIVE DWARF1 encodes a soluble receptor for gibberellin. Nature 437:693–698

Valladares F, Niinemets Ü (2008) Shade tolerance, a key plant feature of complex nature and consequences. Annu Rev Ecol Evol Syst 39:237–257

Vandenbussche F, Pierik R, Millenaar FF, Voesenek LACJ, Van Der Straeten D (2005) Reaching out of the shade. Curr Opin Plant Biol 8:462–468

Voesenek LACJ, Pierik R (2008) Plant science: plant stress profiles. Science 320:880–881

Voesenek LACJ, Jackson MB, Toebes AHW, Huibers W, Vriezen WH, Colmer TD (2003) De-submergence-induced ethylene production in *Rumex palustris*: regulation and ecophysiological significance. Plant J 33:341–352

Wang H, Ma LG, Li JM, Zhao HY, Deng XW (2001) Direct interaction of *Arabidopsis* cryptochromes with COP1 in light control development. Science 294:154–158

Weiner J (1985) Size hierarchies in experimental populations of annual plants. Ecology 66:743–752

Whippo CW, Hangarter RP (2004) Phytochrome modulation of blue-light-induced phototropism. Plant Cell Environ 27:1223–1228

Won C, Shen X, Mashiguchi K, Zheng Z, Dai X, Cheng Y, Kasahara H, . . ., Zhao Y (2011) Conversion of tryptophan to indole-3-acetic acid by TRYPTOPHAN AMINOTRANSFERASES OF *ARABIDOPSIS* and YUCCAs in *Arabidopsis*. Proc Natl Acad Sci USA 108:18518–18523

Yamaguchi R, Nakamura M, Mochizuki N, Kay SA, Nagatani A (1999) Light-dependent translocation of a phytochrome B-GFP fusion protein to the nucleus in transgenic Arabidopsis. J Cell Biol 145:437–445

Yang HQ, Tang RH, Cashmore AR (2001) The signaling mechanism of Arabidopsis CRY1 involves direct interaction with COP1. Plant Cell 13:2573–2587

Zhang T, Maruhnich SA, Folta KM (2011) Green light induces shade avoidance symptoms. Plant Physiol 157:1528–1536

Chapter 7

Forest Canopy Hydraulics

David R. Woodruff* and Frederick C. Meinzer
USDA Forest Service, Forestry Sciences Laboratory, Corvallis, OR 97331, USA

and

Katherine A. McCulloh
Department of Botany, University of Wisconsin-Madison, Madison, WI 53705, USA

*Author for correspondence, e-mail: dwoodruff@fs.fed.us

e-mail: rick.meinzer@oregonstate.edu

e-mail: kmcculloh@wisc.edu

K. Hikosaka, Ü. Niinemets, and N.P.R. Anten (eds.), *Canopy Photosynthesis: From Basics to Applications*, DOI 10.1007/978-94-017-7291-4_7

Summary

Water and carbon cycles are strongly coordinated and water availability is a primary limiting factor in many terrestrial ecosystems. Photosynthesis requires sufficient water supply to leaves and constraints on delivery at any point in the hydraulic continuum can lead to stomatal closure and reduced photosynthesis. Thus, maximizing water transport enhances assimilation and can provide plants with a competitive advantage. Unregulated water transport, however, can lead to excessive gradients in xylem tension that result in the development of air or vapor bubbles (i.e. embolisms) that block xylem water transport, potentially leading to permanent loss of function of the xylem. As such there can be a tradeoff between maximizing water transport and minimizing the risk of xylem embolism. This tradeoff has led to the development of a variety of hydraulic mechanisms to maximize efficiency and reduce vulnerability. Although several of these were first described centuries ago (such as stomatal control of transpiration), research in this field continues to uncover previously unrecognized processes employed by plants for maintaining hydraulic safety and/or efficiency. The hydraulic traits described in this chapter include xylem structural characteristics that enhance resistance to embolism such as pit and cell wall architecture; a continuum of strategies for constraining xylem tension to avoid embolism including isohydric and anisohydric control of leaf water potential; and safety and recovery mechanisms such as the capacitive discharge of stored water, hydraulic "circuit breakers" and the ability to repair xylem embolisms. Each of these will be discussed in terms of the variation in their use by contrasting tree types, their variability across organs and species, and their plasticity across environmental gradients. Beyond providing information about the means by which trees currently compete and survive, understanding the hydraulic mechanisms described in this chapter may provide insight into ways that trees are affected by, and the degree to which they may acclimate to rapidly changing climatic conditions.

I. Introduction

Ecosystem productivity is largely determined by the capacity for photosynthetic carbon assimilation and it is therefore heavily influenced by the hydraulic characteristics of the plants within the ecosystem. Hydraulic architecture, which we define as: "the structural and physiological characteristics that regulate the movement of water within a plant" is a means to explain plant water relations in the context of the cohesion tension theory of water movement in plants and the electrical analogy used to characterize water transport within the soil-plant water continuum using flow, water potential (Ψ), capacitance and resistance. Martin Zimmermann coined the term "hydraulic architecture" in the 1970s to describe patterns of hydraulic resistances in plants (Zimmermann 1978). Since then,

Symbols and Definitions: A_l:A_s – Leaf area to sapwood area ratio; d_a – Pit aperture depth; D_a – Pit aperture diameter; D_l – Conduit lumen diameter; g_s – Stomatal conductance; HR – Hydraulic redistribution; k – Hydraulic conductivity; k_l – Leaf specific hydraulic conductivity; k_s – Sapwood specific hydraulic conductivity; K_h – Hydraulic conductance; K_{leaf} – Leaf hydraulic conductance; K_{plant} – Whole plant hydraulic conductance; L – Conduit length; l_a – Pit aperture length; n_{pi} – Total number of pits per conduit; P_{50} – 50 % loss of hydraulic conductivity/conductance; P_e – Threshold pressure for conduit air entry; R_b – Radius of a bubble; R_h – Hydraulic resistance; R_{lum} – Conduit lumen resistance; R_{pit} – Conduit end wall pit resistance; $R_{pit\text{-}total}$ – Total conduit pit resistance; R_{tot} – Total conduit resistance; T – Surface tension of water; ρ – Density of water; υ – Viscosity of water; Ψ – Water potential; Ψ_{leaf} – Leaf water potential; Ψ_{soil} – Soil water potential

hydraulic architecture has come to include a broad range of mechanisms that plants have developed to maintain efficient and safe water transport and new discoveries are being made continuously. In order to understand the significance of these mechanisms it is helpful to recognize that the different components of a plant's hydraulic system face distinct challenges, just as they each play different roles in water transport. Although many of the principles in this chapter are applicable to all plants; hydraulics in woody plants, and in particular trees, involves additional challenges and adaptations that influence the transport of water from roots to leaves. It is for this reason that our focus in this chapter is on trees. To a great extent, the components of hydraulic architecture described in this chapter that are associated with leaves are likely applicable to herbaceous canopies (Meinzer and Grantz 1990; Mencuccini 2003).

A. Components of the Hydraulic Transport System

Water moves through trees via a continuous water column from the soil to the site of evaporation within the leaves. The transport of water through xylem generally occurs under tension (or negative pressure) and along a gradient of increasing tension, i.e. along a gradient of water potential (Ψ) from less to more negative. The ability of water to be transported through xylem is described in terms of hydraulic conductance (K_h). K_h is the change in flow rate of liquid water through a system per change in hydraulic pressure driving the flow, and the inverse of K_h is hydraulic resistance (R_h). Leaves, stems and roots comprise different components of a plant's hydraulic system and stomata are intimately linked to the function of each of these through their control of transpiration. Each of these is influenced by different constraints on water transport and each is characterized by different attributes that mitigate these constraints. Stomata maintain the integrity of the soil-to-leaf hydraulic continuum by regulating transpiration of water vapor, and stomatal resistance to transpiration is typically at least two orders of magnitude greater than the hydraulic resistance to bulk water flow of the entire plant (Sack and Tyree 2005). Although transpiration rate is largely determined by stomatal conductance (g_s), leaf water potential (Ψ_{leaf}) has a direct impact on g_s and Ψ_{leaf} at a given transpiration rate is strongly influenced by whole plant hydraulic conductance (K_{plant}; Tyree and Zimmermann 2002). As such, transpiration is strongly influenced by a number of aspects of hydraulic architecture along the hydraulic continuum from roots to leaves.

The response of stomata to changes in plant water status has been described as that of a "pressure regulator" (Sperry et al. 2002). Just as a pressure regulator limits pressure by controlling flow rate, stomata limit the degree of xylem tension due to soil moisture depletion and evaporative demand by reducing transpiration. Stomata will reduce transpiration, and thus photosynthesis, when declining leaf water status decreases the turgor in the guard cells (relative to epidermal cells) leading to stomatal closure and a reduction in g_s. The immediate link between changes in g_s and the ability of plants to acquire carbon makes stomatal function a critically important factor in the water and carbon cycles of terrestrial ecosystems (Farquhar and Sharkey 1982). The precise mechanisms of stomatal control of plant water balance can be difficult to resolve because at any given moment stomata may be responding to an intricate array of environmental factors including light level, light quality, vapor pressure deficit and CO_2 concentration. Although root mediated signals of hormones such as ABA and cytokinin strongly influence stomatal conductance by changing the permeability of guard cell membranes (Wilkinson and Davies 2002), the rapid response of stomata to reduced root area (Meinzer and Grantz 1990), increased root xylem embolism (Alder et al. 1996), decreased shoot conductivity (Salleo et al. 2000) and increased xylem embolism within leaves (Nardini et al. 2001) illustrates that stomatal conductance responds to signals within the plant that are related to changes in hydraulic architecture, and which are able to travel more rapidly than root mediated hormone signals.

Leaf hydraulic conductance (K_{leaf}) is a measure of the rate of water flow through the xylem and extraxylary pathways to the sites of evaporation within the leaf, divided by the water potential difference across the leaf ($\Delta\Psi_{leaf}$), which is the driving force for flow. Leaves comprise an estimated 25 % (Sack et al. 2003) to 80 % (Nardini et al. 2001) of the total hydraulic resistance within plants. Although leaves exist at the terminal end of the hydraulic transport system and are therefore prone to experience higher xylem tensions than other plant organs, they are generally, although not always, more vulnerable to embolism than stems (Johnson et al. 2011). As such, leaves invariably represent a potential hydraulic bottleneck. K_{leaf} is strongly correlated with both maximum photosynthesis and stomatal conductance in temperate deciduous trees (Aasamaa et al. 2001), which highlights the importance of K_{leaf} in influencing gas exchange and therefore productivity of individual plants and ecosystems. Research examining the connections between leaf structural characteristics and transport efficiency has begun to identify the ways in which trade-offs between efficiency and safety manifest themselves in leaf anatomical characteristics (Aasamaa et al. 2005; Sack and Frole 2006; Woodruff et al. 2008).

In addition to transporting water from roots to leaves, stems also provide mechanical support to resist the forces of wind, snow loading and gravity. One way that the xylem conduits of conifers (tracheids) differ from those of angiosperms (generally vessels) is that tracheids are the sole source of mechanical support for the stem, whereas vessels are surrounded by sclerenchyma tissues that contribute mechanical support. In tracheids the increased wall thickness to span ratio that is needed to provide stems with sufficient mechanical strength represents an increased construction cost that is consistent with a trade-off between safety and efficiency (Pittermann et al. 2006). Roots play less of a role in providing mechanical support relative to stems, however roots tend to be very efficient at transporting water. Root xylem conduits tend to have larger lumen diameters and higher conductivity per sapwood cross-sectional area (specific conductivity, k_s) than other tissues (McElrone et al. 2004). They are also more prone to reaching minimum xylem pressures that are closer to levels that are associated with relatively high losses of conductance (i.e. they tend to operate under narrower safety margins than stems; Sperry and Saliendra 1994; Alder et al. 1996; Martínez-Vilalta et al. 2002). Although the narrow safety margins under which roots operate make them potentially more vulnerable to high levels of embolism, it has been argued that root conduits are easier to refill due to the relatively high water potentials of surrounding soil (Sperry and Saliendra 1994), and that they are easier to replace and "less expensive" in terms of carbon investment than stems (Kolb and Sperry 1999; Hacke et al. 2000).

B. Constraints on Hydraulic Transport

The overall water transport pathway from the root-soil interface to the atmosphere can be characterized as consisting of a series of resistances (Fig. 7.1). Each plant organ along this hydraulic continuum is composed of water conducting structures that vary functionally and anatomically across species, ontogeny and location (i.e. root, stem, leaf) within an individual plant. The water conducting portion of a tree's vascular system is composed of tracheids for conifers and vessels in angiosperms (except for some vessel-less species), collectively referred to as conduits. Hydraulic conductance is strongly influenced by the structural characteristics of xylem conduits such as lumen diameter, conduit length and pit characteristics such as pit aperture size and pit membrane pore characteristics. According to the Hagen-Poiseuille equation, even minor changes in conduit lumen diameter (D_l) lead to substantial changes in transport efficiency:

$$R_{lum} = 128\ \upsilon L/\pi\rho D_l^4, \qquad (7.1)$$

where R_{lum} is resistance associated with conduit lumens, υ is the viscosity of water (1.002×10^{-9} MPa s at 20 °C), L is conduit length, and ρ is the density of water

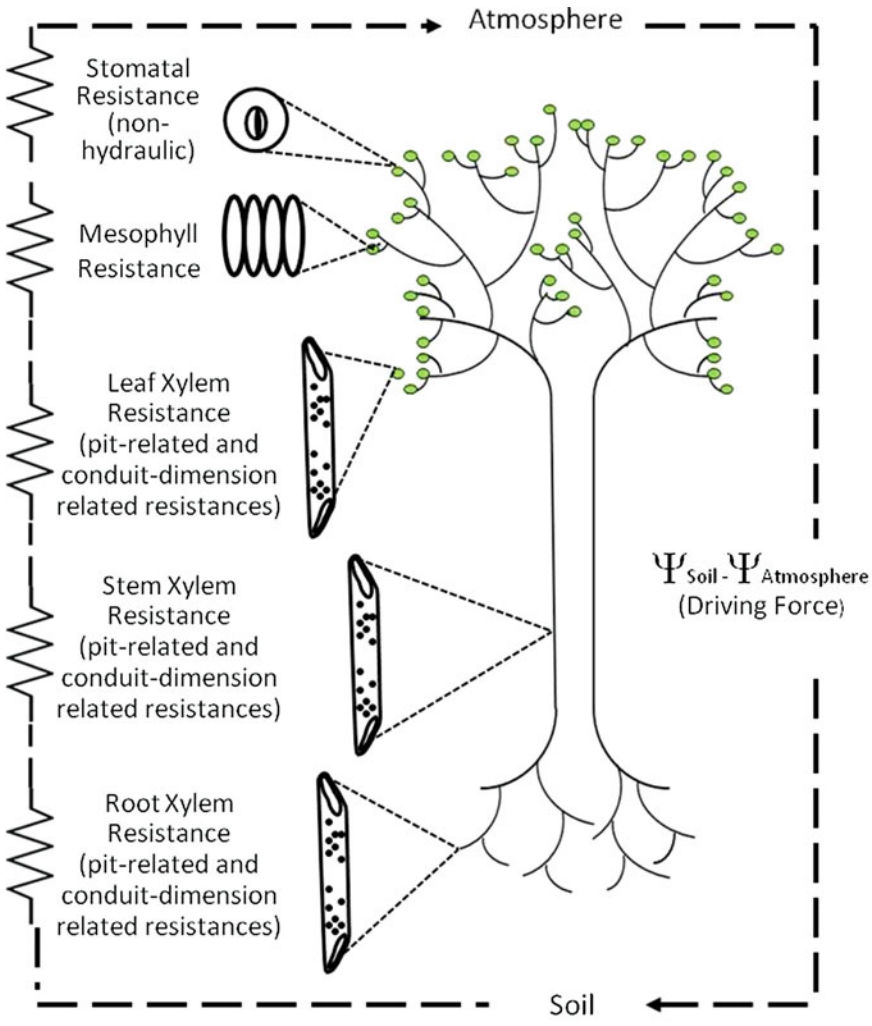

Fig. 7.1. A schematic of hydraulic resistances in series within a tree from soil to the stomata and the driving force for transport

(5.55×10^7 mmol m^{-3}). Because of the fourth power relationship between lumen diameter and hydraulic resistance, a doubling of lumen diameter for example results in a 16-fold increase in hydraulic conductance.

Xylem hydraulic conductance is also substantially impacted by the pitted walls that separate adjacent conduits. Although evaluating hydraulic characteristics at the pit level is inherently difficult due to the small size of pits, a great deal of progress has been made in evaluating the role of pits in maintaining hydraulic safety and constraining hydraulic efficiency. Pit resistivity is largely determined by pit aperture resistance (R_{pit}) (Hacke et al. 2004; Domec et al. 2006a), and the resistance of a conduit's pit aperture can be modeled as a circular opening, the length of which is equivalent to the depth of the pit aperture. Dagan et al. (1982) adapted the following relationship from the Hagen Poiseuille equation to provide an approximate solution for the hydraulic resistance of circular pit pores of finite length:

$$R_{pit} = 24\upsilon/\left(D_a^3\right) + 128 l_a \ \upsilon/\left(\pi D_a^4\right), \qquad (7.2)$$

where D_a is pit aperture diameter and l_a is pit aperture length, taken as half the difference between the thickness of the whole pit and the thickness of the pit chamber. Resistances

are additive in a series by Ohm's law analogy so a conduit's total resistance (R_{tot}) is determined by both R_{lum} and the total contribution of conduit pits to conduit resistance ($R_{pit\text{-}total}$):

$$R_{tot} = R_{lum} + R_{pit\text{-}total}, \quad (7.3)$$

with $R_{pit\text{-}total}$ being determined by both R_{pit} and the total number of pits per conduit (n_{pi}):

$$R_{pit\text{-}total} = R_{pit}/n_{pi}. \quad (7.4)$$

The hydraulic resistance associated with pits has been estimated to represent between 14 and 84 % of the total hydraulic resistance across a number of species (Schulte and Gibson 1988), and other studies have provided estimates of approximately 50 % for the proportion of hydraulic resistance associated with conduit end walls across a range of xylem structures in both tracheid and vessel-bearing species (Sperry et al. 2005; Choat et al. 2008). Conduit length can also have a significant impact on transport efficiency because a decrease in conduit length increases the total number of conduit end-walls that are traversed for a given distance of water transport in the xylem. As such, any increase in mean conduit length results in a decrease in cumulative end-wall resistance for a given pit structure.

C. Hydraulic Vulnerability

As stated earlier, the transport of water through xylem generally occurs under tension (or negative pressure) and along a gradient of increasing tension. The tension results from both frictional resistance during water transport as well as gravitational forces that lead to a 0.01 MPa increase in tension per meter increase in height. If this tension exceeds a critical level, air can be pulled in from adjacent tissues resulting in embolism. Surface tension and the structure and function of the membranes in the pitted end-walls that connect conduits typically block embolisms from moving to adjacent conduits, but not always. Embolisms can substantially decrease the hydraulic conductivity of a plant organ thereby limiting the ability for trees to transpire and assimilate carbon. Figure 7.2 illustrates the relationships between xylem tension, conduit embolism and water transport (in this case in leaves). Figure 7.2a–c are cryo-scanning electron microscope images of Douglas-fir leaf tracheids that show tracheids that are full of water at the time of freezing ($\Psi_{leaf} = -0.5$ MPa), tracheids that are devoid of water ($\Psi_{leaf} = -2.1$ MPa) and what appears to be a transitional phase where tracheids are partially filled with water ($\Psi_{leaf} = -1.5$ MPa), respectively. Panel D represents a hydraulic vulnerability curve of foliage from the same branch as the images in Fig. 7.2a–c in which the y-axis represents K_{leaf} and the x-axis represents Ψ_{leaf}. As the xylem tension increases (represented by increasingly negative Ψ_{leaf}) K_{leaf} declines. The levels of Ψ_{leaf} represented by the images in Fig 7.2a–2c are indicated by arrows in the vulnerability curve. The ability of xylem to avoid or resist cavitation and embolism is a measure of hydraulic safety and it is broadly recognized that enhanced safety often comes at the price of reduced efficiency (Zimmermann 1983; Tyree et al. 1994; Sperry et al. 2008).

II. Safety and Efficiency of Hydraulic Architecture

The metastable state under which water is transported in the xylem means that there is a risk of an air bubble, or embolism, disrupting the flow. If constructing a xylem that is safer from these embolisms means that the hydraulic conductance of the network is reduced, there is a tradeoff between hydraulic safety and efficiency. The focus of this section is on causes and consequences of embolism propagation, recovery from embolisms, and the integration of stomatal control and hydraulic function.

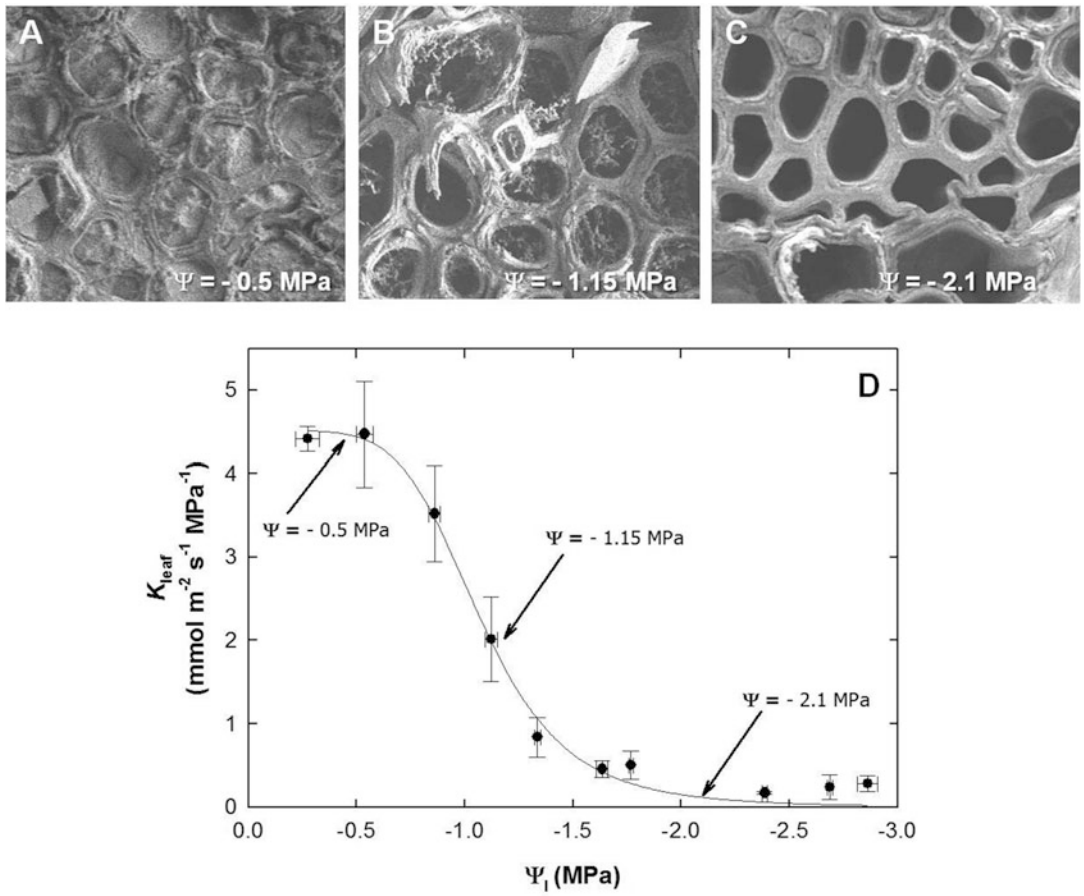

Fig. 7.2. Cryo-scanning electron microscopy (Cryo-SEM) images of Douglas-fir leaf tracheids frozen at a range of leaf water potentials (**a, b, c**) and the relationship between leaf hydraulic conductance and leaf water potential (**d**). Leaf water potential = −0.05 MPa with leaf tracheids predominantly full (**a**). Leaf water potential = −1.15 MPa with leaf tracheids partially full (**b**); and leaf water potential = −2.1 MPa with leaf tracheids predominantly empty (**c**). The three leaf water potentials represented in the Cryo-sem images are indicated by arrows in panel D. Adapted from Woodruff et al. (2007)

A. Embolism Formation and Avoidance

The functional consequence of embolism proliferation is a drop in the hydraulic conductance of the network, and this propagation occurs primarily in two ways. The first cause is due to air-seeding from one conduit to a neighboring conduit and is due to a decline in the xylem pressure because of drought stress. The sites of air-seeding between neighboring conduits are pit membranes (Crombie et al. 1985; Cochard et al. 1992), which are passageways for water to pass when both conduits are functional. These two-way valves are made of primary wall material, and are not "membranes" in the lipid-bilayer sense of the term. The pit membrane rests in the center of the pit chamber when both conduits are water-filled, but gets sucked over to cover the pit aperture by the negative pressure of the water in the functional conduit when the neighboring conduit becomes embolized (Siau et al. 1984). When water stress causes the pressure in the functional conduit to drop below the threshold value that pulls a bubble across the membrane (in angiosperms) or pulls part of the pit membrane into the aperture and

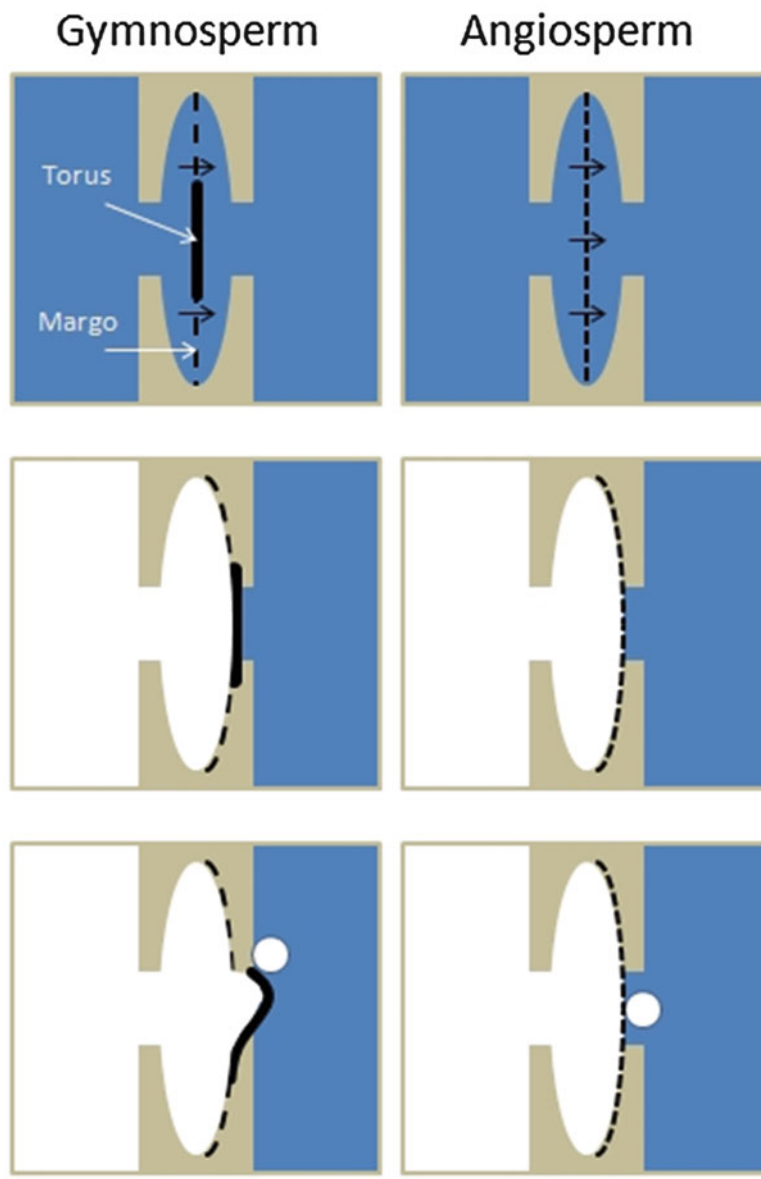

Fig. 7.3. Pit membranes connecting neighboring conduits in gymnosperms and angiosperms. The *top panels* show that water can flow through the pores throughout the homogeneous angiosperm pit and through the porous margo in the gymnosperm pit, but not through its thickened torus. The *middle panels* depict how the pits of each group seal the pit aperture when the conduit on the *left* becomes embolized and the conduit on the *right* remains functional. The *bottom panels* illustrate how a bubble can propagate from one embolized conduit to a functional one through a process called air-seeding. Adapted from Hacke et al. (2004) with permission

allows an air bubble to follow (in conifers), the functional conduit embolizes and becomes non-functional.

The distinction in how the air-seeding occurs in angiosperms vs. conifers is due to the differences in their pit membrane morphology (Fig. 7.3). In angiosperms, the membrane is a homogenous mesh-like network of primary cell wall material, and the air-seeding pressure is only limited by the tensile strength of water. Thus, one theory of what determines air-seeding in angiosperms is the "pit area" or "rare pit" hypothesis, which postulates that the vulnerability of a conduit to water-stress induced embolism increases with the proportion of the conduit wall that is covered by pits (Hargrave et al. 1994; Wheeler et al. 2005; Sperry et al. 2006; Choat et al. 2008; Christman et al. 2009, 2012). This correlation is not due to the collective area of pits, but instead because a greater pit area

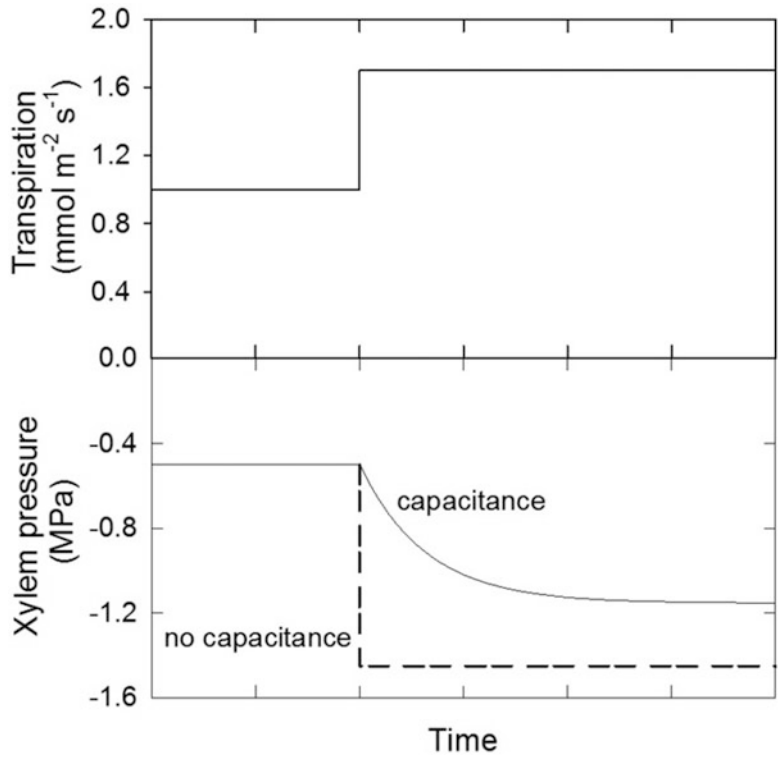

Fig. 7.4. A theoretical example showing the impact of an increase in transpiration (*top panel*) on the xylem pressure in a species with capacitance and a hypothetical one without capacitance (*bottom panel*)

increases the likelihood of having a rare pit pore that is larger than the others and therefore allows air to seed at a smaller pressure difference. A tradeoff exists between hydraulic safety and conducting efficiency because the smaller proportion of wall covered in pits in safer vessels reduces the hydraulic conductance of the network. Conifers, in contrast, have pits with two distinct regions (Bauch et al. 1972). The central region, which is very tightly knit primary cell wall material and does not allow water or air to pass through it, is called the torus. Surrounding the torus is the margo, which is made up of very loosely organized microfibrils. It is through this region that the water passes when both tracheids are functional. The division of labor between the sealing torus and the porous margo means that air-seeding is not the result of a rare, large pit pore as in angiosperms. Instead, the ratio of the torus diameter to the pit aperture diameter seems to determine the vulnerability of a pit to seeding air (Burgess et al. 2006; Domec et al. 2006a, 2008; Hacke and Jansen 2009; Delzon et al. 2010). In conduits that have a large overlap of torus to aperture, greater pressure difference is required between the tracheids to dislodge the pit membrane and allow air to be sucked into the functional tracheid. A tradeoff exists between hydraulic safety and conducting efficiency because the smaller pit aperture of a safer pit has a lower hydraulic conductance (Domec et al. 2008).

At the tissue scale, there are three main parameters that correlate with safety from embolism propagation due to drought stress. First, the ability of a tissue to store water, or its capacitance, buffers the speed of declines in xylem pressure with increases in transpiration (Fig. 7.4), which may provide stomata the time needed to limit transpiration, thus protecting the xylem from embolism-inducing negative pressures (Fig. 7.4). Species with greater capacitance tend to experience milder leaf water potentials at midday (Meinzer et al. 2003; Santiago et al. 2004;

Borchert and Pockman 2005; McCulloh et al. 2012), have lower wood density (Pratt et al. 2007; Meinzer et al. 2003, 2008a), and less negative xylem pressures that result in 50 % loss of hydraulic conductivity (P_{50}, see below) (Domec and Gartner 2001; Pratt et al. 2007; Meinzer et al. 2009). See Sect. III.C of this chapter for further discussion on capacitance.

The second parameter that correlates with drought safety is wood density. Stems with higher wood density tend to have more negative P_{50}s (Hacke et al. 2001; Pratt et al. 2007; Chave et al. 2009; Hoffmann et al. 2011; Markesteijn et al. 2011; Ogasa et al. 2013), yet wood density does not, inherently, provide any known protection against air seeding. The mechanistic link between hydraulic safety and wood density seems to be the result of the thicker walls needed to withstand the lower operating pressures that drought-tolerant species experience. Specifically, species with more negative P_{50}s have a wider double-wall thickness between neighboring conduits for a given mean hydraulic diameter, which is a hydraulic conductivity-weighted average lumen diameter (Hacke et al. 2001). Compared with angiosperms, conifers are able to tolerate a more negative P_{50} with a given wood density. Although robust support for this correlation exists across species, within a species the pattern is not always observed (Bucci et al. 2006; Domec et al. 2009).

The third tissue-level factor is the link between the degree of inter-connectedness of vessels and hydraulic safety, and this is the most causal of the three parameters. Given that air seeding occurs at the level of the pit, the safest vessels are ones that have no or very few pit connections. Indeed, where it has been examined, greater resistance to embolism has been observed in species with fewer vessels in contact with one another, and this drought resistance has come at the cost of reduced hydraulic conductivity (Zanne et al. 2006; Ewers et al. 2007a; Loepfe et al. 2007; Schenk et al. 2008; Lens et al. 2011; Martínez-Vilalta et al. 2012; Brodersen et al. 2012). Due to their short conduits and inherently interconnected xylem network, tracheid bearing species like conifers, cannot alter this parameter.

The second way that emboli form in conduits is because of freeze-thaw cycles (Sucoff 1969; Robson et al. 1988). The "thaw-expansion" hypothesis posits that air that had been dissolved in xylem water forms bubbles in conduits when that water freezes. When the ice thaws, that bubble can either redissolve or expand to fill the conduit and form an embolism. Which of these two options occurs depends on the pressure of the xylem water (Pittermann and Sperry 2006) as described by La Place's law (Yang and Tyree 1992). The bubble will expand or collapse if the xylem pressure is, respectively, less than or greater than $-2\ T/R_b$, where T is the surface tension of water (0.0728 Pa m) and R_b is the radius of the bubble, which in xylem conduits is roughly the diameter of the conduit (Tyree and Zimmermann 2002). The link between the conduit diameter, bubble diameter and the pressure required to dissolve bubbles means two things. First, it means that narrower conduits tend to be less susceptible to loss of hydraulic conductivity from single freeze-thaw events, and this pattern has been observed in both conifers (Sperry and Robson 2001; Pittermann and Sperry 2003, 2006) and angiosperms (Davis et al. 1999; Feild et al. 2002). Second, it means that more negative xylem pressure prior to freezing leads to more embolisms, and a number of studies have observed a large drop in hydraulic conductivity caused by freeze-thaw cycles coupled with drought (Lemoine et al. 1999; Sparks and Black 2000; Sparks et al. 2001; Mayr et al. 2002, 2003). Seemingly wet environments can create more drought-like stress than expected in cold months, because the hydraulic conductance of water through the soil is severely reduced as water becomes more viscous (Wan et al. 2001; Pregitzer and King 2005), and membrane transport properties are altered because of the impact of reduced aquaporin production (Yu et al. 2006; Murai-Hatano et al. 2008).

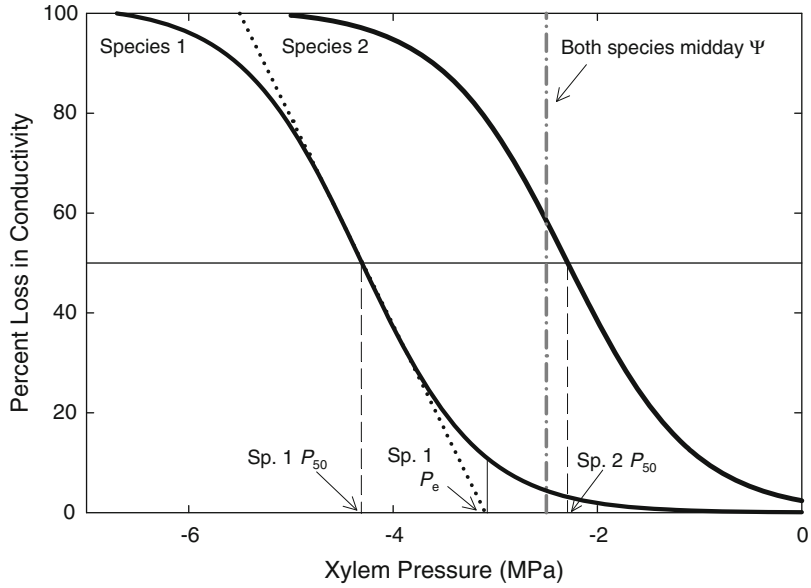

Fig. 7.5. Two theoretical vulnerability curves from organs (e.g., roots, stems or leaves) of two species. The horizontal line shows the point of 50 % loss of hydraulic conductivity, and the x-axis value where this line intersects with each vulnerability curve is the P_{50} (*dashed drop lines*). The *vertical dot-dash line* is the midday water potential value (Ψ), which for simplicity is the same for both species in this example. The difference between the midday water potential and the P_{50} for each species is an example of a hydraulic safety margin. The *vertical solid line* indicates the P_e for Species 1, which indicates an inflection point on the curve after which the percent loss in conductivity increases rapidly. The P_e for Species 2 is not shown for simplicity

Embolisms caused by freeze-thaw cycles may be avoided by having small diameter conduits, or they can be tolerated by one of two solutions. First, some species refill embolized conduits in the spring either through stem pressure, root pressure, or possibly by absorbing water through distal plant parts. Stem pressure has been well documented in species in which the sap is economically important, such as in maples, but the details of the mechanism are still a matter of dispute (Tyree and Zimmermann 2002). Other species, such as grapevine, create substantial root pressure in the spring to refill vessels (Sperry et al. 1987). Four species of conifer showed substantial recovery from freeze-thaw-induced loss of hydraulic conductivity that could not be explained by stem or root pressure, or growth of new wood (McCulloh et al. 2011a, b). The second solution is to simply grow new vessels. Ring-porous species, which grow 1–2 rings of very wide vessels in the spring and then fibers and much smaller vessels for the rest of the growing season, use this approach. Ring-porosity is a uniquely northern hemisphere solution to the problem of freeze-thaw induced emboli (Wheeler et al. 2007).

B. Functional Implications of the Loss and Recovery of Hydraulic Function

Although plants have many mechanisms to avoid embolism propagation, loss of hydraulic conductance or conductivity does occur. We measure the decline of hydraulic function with water stress by creating vulnerability curves (Fig. 7.5). There are various metrics used to compare these curves across species, but two commonly used ones are the P_{50} (see above) and P_e, which is the threshold pressure for air entry. The P_e is particularly important, because pressures even slightly more negative than it result in large increases in the percent loss of hydraulic conductivity. Although some species attempt

to avoid loss of hydraulic conductance during normal daily cycles of water stress by employing the structural features described above, others tend to lose conductance in one or more distal organs (i.e., leaves, twigs, or rootlets) every day and then regain function overnight (Zwieniecki and Holbrook 1998; Bucci et al. 2003; Trifilò et al. 2003; Brodribb and Holbrook 2004; Stiller et al. 2005; Johnson et al. 2009, 2011). The latter strategy effectively creates a circuit breaker that hydraulically isolates the downstream portions of the plant and causes stomatal closure (Johnson et al. 2012). This idea of a circuit breaker signaling stomatal closure was well characterized in Douglas-fir needle-bearing shoots in which a strong correlation was found between the water potentials at which shoot hydraulic conductance drops to its minimum value and at which stomata close (Woodruff et al. 2007).

One way to determine the threat of hydraulic failure is with hydraulic safety margins (Fig. 7.5; Meinzer et al. 2009; Johnson et al. 2012; Choat et al. 2012). These metrics represent the difference between the xylem tension (or negative pressure) at a specified loss of xylem hydraulic conductivity (e.g., the P_{50} of a root, stem or leaf) and the point where a physiological mechanism engages to limit transpiration and xylem tension (e.g., the midday water potential of that organ). Some species operate under wide margins of hydraulic safety (e.g., Species 1 in Fig. 7.5) and others under narrow margins (Pockman and Sperry 2000; Brodribb et al. 2003; Brodribb and Holbrook 2004; Pratt et al. 2007; Meinzer et al. 2009; Bucci et al. 2012; Johnson et al. 2012; Choat et al. 2012). Safety margins can also differ in organs such as leaves, stems and roots within a species, and the pattern among organs can vary considerably among species with some species exhibiting smaller margins in the leaves than stems and other species showing the opposite pattern (e.g., Hao et al. 2008; Chen et al. 2009). However, it is crucial to bear in mind that some species are able to refill embolized conduits on daily or seasonal bases, and, thus, these safety margins may not accurately reflect the inherent risk that loss of hydraulic conductivity was previously thought to cause.

As described above, embolisms can be refilled when the pressure in the xylem is less negative than the pressure required to dissolve a bubble in a conduit as described by La Place's law (Yang and Tyree 1992). Relatively recently it has also become clear that bubbles can be dissolved when the surrounding xylem pressure is below what La Place's law would predict to be necessary. This "novel refilling" (Hacke and Sperry 2003) was first described after *Laurus nobilis* was shown to regain hydraulic conductivity after emboli were induced by injecting air into stems of intact plants (Salleo et al. 1996; Tyree et al. 1999) and in situ in three species of different wood type that experienced normal daily cycles of water stress (Zwieniecki and Holbrook 1998). Since then, it has been observed extensively in leaves (Bucci et al. 2003; Trifilò et al. 2003; Brodribb and Holbrook 2004; Stiller et al. 2005; Nardini et al. 2008; Johnson et al. 2009, 2011), roots (McCully et al. 1998; McCully 1999; Domec et al. 2006b), and stems (Brodersen et al. 2010; Hacke and Sperry 2003; Taneda and Sperry 2008; Christman et al. 2012). While the mechanism of this refilling remains uncharacterized, it is thought that sugars are imported into embolized conduits, which creates an osmotic gradient that draws water into the conduit from the surrounding tissue (Zwieniecki and Holbrook 2009; Nardini et al. 2011a).

The extent to which plants can recover from embolisms differs between species as well as between different plant parts. When the hydraulic safety margins of angiosperm and conifer small diameter stems are compared, angiosperms tend to have narrower or even negative margins (indicating that the midday water potential should result in significant losses of conductivity; e.g., Species 2 in Fig. 7.5) compared with the wider margins of conifers (Meinzer et al. 2009; Johnson et al. 2012; Choat et al. 2012). Thus, stems of many angiosperm species seem to undergo daily cycles of hydraulic

conductance loss and recovery (Zwieniecki and Holbrook 1998; Taneda and Sperry 2008; Brodersen et al. 2010; Christman et al. 2012; Ogasa et al. 2013), while conifer stems may only lose small amounts or no hydraulic conductivity daily (Zwieniecki and Holbrook 1998). One proposed explanation for this difference is the smaller fraction of living cells in conifer than angiosperm wood, which may limit the ability of conifer stems to quickly or efficiently deliver the sugars necessary to refill under negative pressure (Johnson et al. 2012). It is worth noting that the distinction of whether a species commonly undergoes cycles of conductivity loss and recovery in stems or not is not clearly delineated by taxa (i.e., conifers vs. angiosperms). Instead, there appears to be a continuum of the fraction of wood devoted to living cells, and this correlates negatively with hydraulic safety margin. However, in contrast to the often wide safety margins in their stems, the needles of many conifer species undergo daily cycles of hydraulic conductance loss and recovery (Woodruff et al. 2007; Johnson et al. 2009, 2011). Given the ability of plants to recover from embolisms, it is becoming increasingly clear that static variables such as P_{50} are not adequate to characterize a plant's response to water stress. Indeed, Ogasa et al. (2013) found that species with less negative P_{50}s had a greater ability to recover from embolism than those with more negative P_{50}s.

Although considerable research is currently focused on novel refilling, many questions remain. An obvious area of research focus is on the actual mechanism of novel refilling (Salleo et al. 2004, 2006, 2009; Zwieniecki and Holbrook 2009; Nardini et al. 2011a). Another open question is whether there are trends with respect to the location of hydraulic circuit breakers that correlate with wood type or with plant phylogeny. The Pinaceae that have been examined, for instance, all lose nearly all or their entire leaf hydraulic conductance on a daily basis (Woodruff et al. 2007; Johnson et al. 2009, 2011). Finally, how does the continuum of embolism avoidance vs. tolerating cycles of embolism formation and recovery relate to the continuum of leaf water potential regulation (i.e., iso vs. anisohydry; see next Section)?

C. Linking Stomatal Control of Leaf Water Potential to Xylem Functioning

A continuum exists in the degree to which stomata regulate the minimum leaf water potential. Isohydric plants represent one end of the continuum and their stomata adjust to keep the leaf water potential from dropping below a set value. Alternatively, anisohydric plants exist at the other end of the spectrum and their stomata do not act to regulate the leaf water potential at a specific value, but instead allow leaf water potential to decline as the soil dries out or the vapor pressure deficit increases. Although generalizations are often made about what types of plants exist at each end of the spectrum, a great deal of taxonomic diversity is actually observed throughout the range (Tardieu and Davies 1992; Loewenstein and Pallardy 1998a, b; Tardieu and Simonneau 1998; Bonal and Guehl 2001; West et al. 2008; Zhang et al. 2012; Pou et al. 2012). Another generalization about the spectrum is that anisohydric plants dominate arid environments. However, there are examples of species at both ends of the spectrum co-occurring in arid regions (Linton et al. 1998; McDowell et al. 2008; West et al. 2008).

There are many advantages to isohydry: the predictability of maintaining leaf water potentials at a set value (1) may keep the rest of the plant from experiencing potentially embolism-inducing xylem pressures. This could minimize construction costs of the xylem if the species depends on structural avoidance of embolism. (2) This strategy may also be associated with greater reliance on capacitance. Capacitance can be calculated as the mass of water released per unit tissue volume per change in water potential. Tissue-specific capacitance can be estimated from the slope of the initial, essentially linear portion of the tissue water release curve.

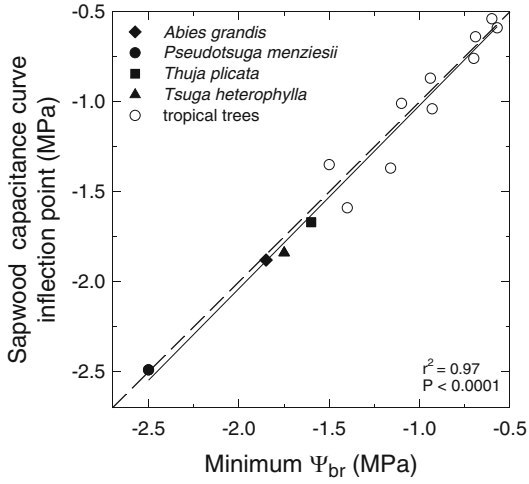

Fig. 7.6. Branch minimum water potential (Ψ_{br}) vs. the inflection point on the sapwood capacitance curve. Water potentials more negative than the inflection point experience diminished returns in terms of water released for a given drop in water potential, and these species-specific set-points for daily minimum branch water potential optimize reliance on capacitance. The data from tropical trees are from Meinzer et al. (2008a), and conifer data are from McCulloh et al. (2014)

Many plants act to maintain their leaf water potentials at milder values than the inflection point on the tissue water release curve (Fig. 7.6). (3) Furthermore, the leaves of isohydric plants would not have to undergo osmotic adjustment to maintain turgor in their living cells, which would avoid energy costs associated with solute accumulation. The obvious drawback to isohydry is that stomata must close to maintain the set leaf water potential, which prevents assimilation of new carbon. In a direct comparison of iso vs. anisohydric crops, the cost of osmotically adjusting vs. stomatal limitation on assimilation were not different (McCree and Richardson 1987), but to our knowledge this has not been examined under natural conditions.

One of the intermediaries along this continuum that has been characterized in *Eucalyptus gomphocephala* was dubbed "isohydrodynamic" (Franks et al. 2007). The stomata of these trees regulate their leaf water potentials in such a way that the pressure gradient between the soil and leaves is constant throughout the growing season. Franks et al. (2007) provided convincing evidence that the degree of stomatal regulation was adjusted based on the whole plant hydraulic conductance. This strategy has also been documented in a grapevine cultivar (Zhang et al. 2012).

There is considerable interest in determining if species at one end of the spectrum vs. the other are more likely to die during severe droughts. McDowell et al. (2008) speculate that isohydric species are more likely to die during long-term droughts because of their inability to open their stomata and capture new carbon. Species that tend to behave more anisohydrically often have more drought-resistant xylem, and this can lead to maintenance of gas exchange during mild drought stress (Pou et al. 2012). However, using a quite comprehensive dataset, Mitchell et al. (2012) showed that container-grown saplings of the more isohydric *Pinus radiata* were able to survive roughly twice as long as two more anisohydric *Eucalyptus* species during an imposed long-term drought. How these results apply to naturally growing plants is not yet clear, but is the focus of considerable current research.

III. Dynamic Responses of Tree Hydraulic Architecture

Early and ongoing research on plant hydraulic architecture have focused primarily on characterizing more or less static properties associated with specific xylem structural attributes. It is now known that constraints on photosynthetic gas exchange and growth imposed by plant hydraulic properties can be dynamic over relatively short timescales from minutes to hours. The dynamic components of hydraulic architecture present both challenges and opportunities for incorporating hydraulic traits into models that predict canopy photosynthesis. Here we discuss four dynamic phenomena whose

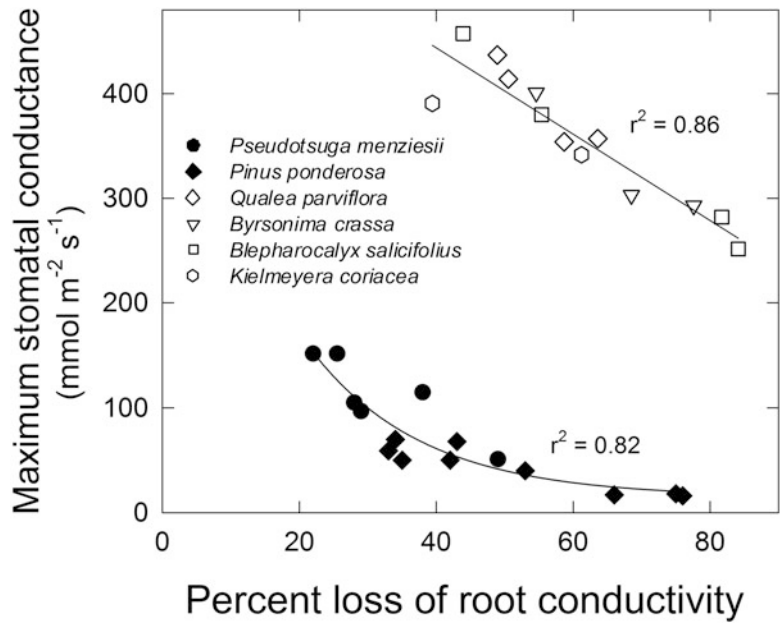

Fig. 7.7. Daily maximum stomatal conductance in relation to loss of hydraulic conductivity in shallow roots (<50 cm depth) for mature trees of two temperate coniferous species and four Brazilian savanna tree species. Data adapted from Domec et al. (2004, 2006b)

impacts on plant hydraulics are becoming increasingly well documented and understood: embolism formation and reversal, ionic effects on xylem conductance, hydraulic capacitance, and hydraulic redistribution of soil water by roots.

A. Embolism Formation and Reversal

Diurnal and seasonal cycles of embolism formation and reversal are a common source of dynamic variation in hydraulic conductance of leaves, stems and roots. Refilling of embolized xylem conduits occurs even when nearby functional conduits are still under considerable tension (McCully et al. 1998; Zwieniecki and Holbrook 1998; McCully 1999; Zwieniecki et al. 2000; Holbrook et al. 2001; Melcher et al. 2001; Bucci et al. 2003; Domec et al. 2006b; Johnson et al., 2009; Brodersen et al. 2010) implying that embolism formation and reversal are two independent, competing processes with the degree of recovery depending on the balance between the two (Bucci et al. 2003; Zwieniecki and Holbrook 2009; Nardini et al. 2011a). Daily loss and recovery of leaf hydraulic conductance has been characterized as a hydraulic circuit breaker function that triggers stomatal closure to provide an adequate safety margin for preserving the hydraulic integrity of the stem upstream (Brodribb and Holbrook 2003; Johnson et al. 2012). However, species that do not experience daily loss and recovery of leaf hydraulic function still exhibit stomatal regulation that minimizes risk of excessive embolism in stems. Although stems show formation and reversal of embolism over different time scales (Holbrook et al. 2001; Lovisolo et al. 2008; Brodersen et al. 2010; McCulloh et al. 2011a), much remains to be learned about species-specific variation in the capacity for embolism reversal in stems, especially critical levels of embolism beyond which conduit refilling does not occur (Ogasa et al. 2013). Roots are usually the most vulnerable portion of the plant hydraulic pathway and can show substantial diurnal and seasonal variation in the degree of embolism, which constrains stomatal conductance (Fig. 7.7; Domec et al. 2004, 2006b, 2009).

B. Ionic Response

The impact of certain ions, particularly K^+, on xylem conductance was apparently first noted by Zimmermann (1978) who reported

that declining flow rates of distilled water through stem segments held under a constant pressure differential could be rapidly reversed by addition of KCl to the perfusion solution. Flow rates of KCl solutions remained constant and were typically higher than initial rates observed with distilled water. These observations led to the use of dilute KCl solutions rather than distilled water as part of the standard protocol for measuring xylem hydraulic conductivity of plant segments. However, the potential significance of ionic modulation of xylem conductivity for dynamic regulation of hydraulic properties in vivo went largely unrecognized for about two decades until researchers began to systematically characterize the ionic effect in excised plant parts. They found that the ionic response is rapid, completely reversible and can result in more than a two-fold increase in xylem conductivity at higher ion concentrations and substantial increases in conductivity at concentrations representative of those in vivo (Van Ieperen et al. 2000; Zwieniecki et al. 2001; Gascò et al. 2006; Domec et al. 2007; Trifilo et al. 2008; Nardini et al. 2010, 2011b; Gortan et al. 2011; Jansen et al. 2011). The ionic effect has been attributed to the shrinkage and swelling of hydrogels in xylem vessel pit membranes (Zwieniecki et al. 2001), vessel grouping characteristics and the fraction of the vessel wall area occupied by intervessel pits (Jansen et al. 2011). Several studies have provided evidence for an ecological role of the ionic effect in intact, field grown plants. Nardini et al. (2010) observed that K^+ concentration was four times higher in xylem sap of illuminated branches than in shaded branches of *Laurus nobilis* and that this concentration difference significantly increased hydraulic conductivity of excised branches. Subsequently, Trifilo et al. (2011) reported that K^+ in xylem sap had a buffering effect on embolism-induced loss of hydraulic conductance in droughted *Laurus nobilis* plants, consistent with an earlier report of an embolism-dependent enhancement of conductivity by K^+ in three other species (Trifilo et al. 2008). The magnitude of ion-mediated enhancement of xylem conductivity may also be associated with species' ecological distributions. Nardini et al. (2012) found greater ionic enhancement of xylem conductivity in *Acer* species native to higher irradiance or lower water availability habitats than in *Acer* species from shady, humid habitats.

C. Capacitance

In addition to its buffering effect on xylem tension, hydraulic capacitance transiently increases apparent whole-tree leaf-specific hydraulic conductance through direct release of water from storage compartments into the transpiration stream, thereby partially circumventing cumulative axial resistances (Andrade et al. 1998; Meinzer et al. 2004a, 2008a). Stomatal regulation of leaf gas exchange is coordinated dynamically with transient capacitance-induced changes in apparent hydraulic conductance over the course of the day. In large tropical trees, crown conductance is highest when capacitive discharge of water into the transpiration stream is greatest and lowest when capacitance is being recharged (Fig. 7.8; Andrade et al. 1998; Meinzer et al. 2008a). This dynamic coordination of vapor and apparent liquid phase conductances in the intact plant cannot be predicted from measurements of steady state hydraulic properties on excised plant segments. Discharge and recharge of capacitance causes lags between rates of change in transpiration and stem sap flux, which can be quantified in terms of hydraulic time constants (Phillips et al. 1997, 2004; Ward et al. 2013).

The sapwood itself appears to be a major source of capacitance and sapwood capacitance on a tissue volume basis can vary dramatically among co-occurring species (e.g. Meinzer et al. 2003, 2008a, b; Scholz et al. 2007) leading to contrasting behaviors in terms of stomatal regulation of gas exchange and tree water status (Goldstein et al. 1998; Meinzer et al. 2003, 2008a). Parenchyma, fibers and the xylem conduits themselves

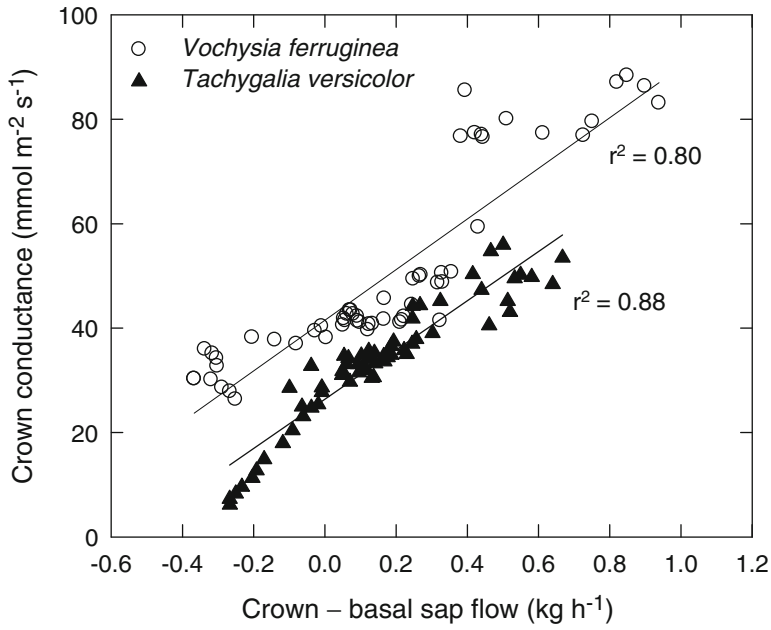

Fig. 7.8. Crown conductance estimated from branch transpiration and vapor pressure deficit in relation to daily patterns of withdrawal and recharge of internal water storage for two tropical forest canopy tree species. Positive values of crown – basal sap flow indicate withdrawal of water from storage compartments located between upper branches and the base of the trunk. Negative values indicate recharge of storage. Adapted from Meinzer et al. (2008a)

may serve as sources of sapwood capacitance (Goldstein et al. 1984; Holbrook and Sinclair 1992; Hölttä et al. 2009). Although cavitation or embolism would be required for capacitive release of water from xylem conduits, modeling exercises suggest that under a range of conditions, the positive effects on plant water status and gas exchange would outweigh the negative effects on xylem conductance, especially if conduits are refilled overnight (Hölttä et al. 2009).

D. Hydraulic Redistribution

Plant root systems passively redistribute water within the soil profile according to gradients of soil water potential. This process, commonly referred to as hydraulic redistribution (HR), can result in upward, downward and lateral movement of water from moist to drier regions of soil via the root xylem, a pathway that typically has substantially greater hydraulic conductivity than that of unsaturated soil (Neumann and Cardon 2012). The fraction of hydraulically redistributed water that passes from shallow roots into the surrounding soil can markedly reduce rates of soil drying during periods of drought (Brooks et al. 2002; Domec et al. 2004; Meinzer et al. 2004b). Additionally, hydraulically redistributed water is available for uptake by roots of neighboring plants either directly or via the soil mycorrhizal network (Querejeta et al. 2003; Plamboek et al. 2007; Warren et al. 2008). Perhaps more importantly from the standpoint of maintenance of plant hydraulic function and shoot gas exchange, the reverse flow of water from roots to soil can partially uncouple the water potential of shallow roots from that of the surrounding dry soil (Domec et al. 2004, 2006b). This phenomenon, combined with reduced rates of soil drying associated with HR, can delay the onset of drought-induced embolism, catastrophic hydraulic dysfunction and ultimately death of shallow roots. Consistent with this, the percent loss of hydraulic conductivity in shallow lateral roots of Brazilian savanna trees during the dry season decreased linearly with increasing rates of reverse sap flow in those roots (Scholz et al. 2008) and internal hydraulic redistribution in *Vitis* root systems has been shown to prolong root lifespan (Bauerle et al. 2008). Thus, given the relatively small

quantities of water redistributed from moist to drier soil via HR (Meinzer et al. 2004b; Warren et al. 2007), the direct contribution of hydraulically redistributed water to maintenance of transpiration during dry periods is likely to be marginal compared to the impact of internal HR on maintenance of root hydraulic function. Because shallow roots and the aerial portion of the plant act as competing sinks for water taken up by deeper roots in moist soil, processes such as nocturnal transpiration inhibit HR (Howard et al. 2009) with potential negative consequences for functioning and survival of shallow roots during dry periods. If warmer nights and higher vapor pressure deficits predicted under future climate regimes enhance nocturnal transpiration or delay nocturnal rehydration of the aerial portion of the plant, the mitigation of drought-induced root embolism by HR is likely to be impaired.

IV. Environmental Plasticity

Numerous studies have documented trends in various components of hydraulic architecture along gradients of aerial and belowground environmental variables. Most of these studies involve comparisons of selected hydraulic traits of multiple species representative of contrasting vegetation types, whereas relatively few have focused on intraspecific trends across broad environmental gradients. In single species studies, the relative roles of genetic versus environmental determinants of hydraulic traits may be unclear unless work has been carried out under a common garden design. Another constraint on interpretation of environmental trends in hydraulic architecture arises when comparisons are based on individual traits from excised plant segments. Inferences drawn from patterns of variation traits such as P_{50} of terminal branches may be limited because selection for suites of hydraulic traits that confer adequate plant fitness under given conditions is likely to occur at the organismal level (Meinzer et al. 2010). Here we discuss selected examples of variation in hydraulic architecture along gradients of aridity, temperature, soil texture and nutrient availability.

A. Aridity

Aridity is expected to be a key determinant of the hydraulic architecture of woody perennials. Consistent with this, in a study of 167 species representing five vegetation types Maherali et al. (2004) found that P_{50} of branch segments ranged from a median value of about −5.3 MPa in Mediterranean climates species to only −0.8 MPa in tropical rainforest species. At the individual species level, a common garden study of *Pseudotsuga menziesii* seedlings from coastal and interior wet and dry climates found that both roots and shoots tended to be more resistant to embolism in populations from dry sites (Kavanagh et al. 1999). However, other studies of hydraulic adjustments of individual species across aridity gradients suggest that maintenance of integrity of water transport and homeostasis of leaf level gas exchange in mature, field-grown trees may be attained largely via changes in tree allometry. A survey of hydraulic traits of *Pinus sylvestris* across a gradient of climate dryness in Europe yielded no significant trend in branch P_{50}, but significant trends of decreasing branch level leaf area to sapwood area ratio (A_L:A_S) and increasing leaf specific conductivity (k_L) with increasing dryness (Martinez-Vilalta et al. 2009). Thus, shifts in branch allometry that resulted in increased k_L apparently compensated for the tendency for xylem tension to increase with aridity. Similarly, tree allometric adjustments in *Pinus palustris* resulted in homeostasis of whole-tree leaf-specific hydraulic conductance and stomatal control of gas exchange in trees growing xeric and mesic sites (Addington et al. 2006). Allometric trends in *Pinus ponderosa* trees caused whole-tree k_L and canopy conductance to be substantially greater in desert populations than in montane populations (Maherali and DeLucia 2001).

B. Freezing

Climatic gradients of increasing frequency and severity of freezing temperatures imply an increased risk of disruption of water transport from freeze-thaw-induced embolism (see section two above), especially in overwintering evergreen species. Xylem vulnerability to freeze-thaw-induced embolism increases with conduit diameter (Davis et al. 1999; Pittermann and Sperry 2003), yet many species growing in frost-prone climates have xylem conduits large enough to experience freezing induced embolism and consequent reduction of water transport capacity probably because smaller conduits would unduly restrict water transport and gas exchange (Davis et al. 1999). The effects of freezing-induced embolism can be overcome by production of new xylem conduits in the spring as in winter-deciduous species or refilling of conduits during periods of above-freezing temperatures as in many evergreen species (Mayr et al. 2006; McCulloh et al. 2011a, b). Nevertheless, if freezing temperatures are low enough, embolism will spread to progressively smaller conduits and become essentially irreversible resulting in plant mortality. Relationships between xylem vulnerability to and capacity for recovery from freezing-induced embolism are likely to be important determinants of latitudinal (Pockman and Sperry 1997) and altitudinal (Feild and Brodribb 2001; Choat et al. 2011) distributions of species. In drought-prone climates with freezing temperatures, drought hardening can contribute to avoidance of freezing-induced loss of hydraulic function (Medeiros and Pockman 2011).

C. Soil Texture

Soil texture and its impact on pore size distribution are major determinants of the moisture releasing characteristics of soils (Brooks and Corey 1964; Warren et al. 2005). It is not surprising therefore, that plants would exhibit a range of structural and physiological features that optimize soil water extraction along gradients of soil texture independent of gradients in other environmental variables such as aridity (Sperry et al. 1998). In a study of *Pinus taeda* growing in a loamy versus sandy soil, Hacke et al. (2000) found that trees growing in sandy soil had substantially higher root area to leaf area ratios, were more deeply rooted, and were more vulnerable to xylem embolism than trees growing in a loamy soil with its much higher clay fraction. Structural and physiological adjustments in both soil types served to maintain soil water extraction at about 86 % of its potential value in both soils. Populations of *Pinus ponderosa* and *Pseudotsuga menziesii* growing in sites with a semi-arid continental climate east of the Cascade Mountains had trunk sapwood with higher specific hydraulic conductivity, higher capacitance and greater vulnerability to embolism than sapwood of the same species growing in sites with a moist maritime climate west of the mountains (Barnard et al. 2011). This somewhat counter-intuitive pattern was attributed to greater soil porosity in the semi-arid sites where about 90 % of the available water is extracted over a relatively narrow range of soil water potential, suggesting little selective pressure for xylem structural reinforcements that would allow greater xylem tension to be sustained without increased risk of embolism. In contrast, the finer textured soils in the maritime climate sites show a broader range of water potential over which it would be physiologically feasible to extract water through xylem structural adjustments that enhance resistance to embolism.

D. Nutrient Availability

The availability of nutrients, particularly N and P can have pronounced effects on tree hydraulic architecture and photosynthetic gas exchange mediated by adjustments in both tree allometry and in the structure and properties of the xylem. Five years of N fertilization in a Brazilian savanna ecosystem resulted in increased whole-tree leaf areas and leaf area to sapwood area ratios

among five dominant species differing in leaf phenology (Bucci et al. 2006). Despite their increased leaf area, whole-tree transpiration was not significantly greater in N-fertilized trees because stomatal conductance on a unit leaf area basis was significantly lower. Adjustments in sapwood hydraulic and biophysical properties induced by N fertilization included higher xylem specific conductivity, more negative values of P_{50} and lower wood density. This combination of sapwood traits was not consistent with frequently observed trade-offs of hydraulic safety against efficiency (see above) or with some reported relationships between wood density and xylem vulnerability to embolism (Hacke et al. 2001). Despite higher sapwood specific conductivity in N-fertilized trees, their daily minimum values of leaf water potential were significantly lower, probably as a result of higher leaf area to sapwood area ratios and lower root to shoot ratios. In *Pinus taeda* trees, increased growth rates in an N fertilization treatment were associated with greater stand leaf area index, but lower root to leaf area ratios, lower leaf-specific hydraulic conductance and lower values of reference stomatal conductance (Ewers et al. 2000). In dwarf stands of the mangrove *Rhizophora mangle*, growth rates of trees fertilized with N were several times higher than in unfertilized trees, but rates of photosynthesis and stomatal conductance were similar to those in unfertilized trees (Lovelock et al. 2004). Taken together, the preceding observations suggest that growth enhancement by N fertilization may often be the result of adjustments in hydraulic architecture that allow increases in whole-crown photosynthesis with increasing leaf area rather than increased rates of photosynthesis per unit leaf area.

V. Scaling from Leaf to Canopy

Stomatal regulation of photosynthetic gas exchange at the leaf level is a manifestation of dynamic coordination between vapor and liquid phase conductances, particularly apparent K_L, which represents the integration of static properties and dynamic processes along the plant hydraulic continuum. Therefore, the role of tree hydraulics in regulation of stomatal behavior and photosynthesis cannot be fully understood unless hydraulic properties and dynamic processes are studied over a range of scale at various points along the root-to-leaf continuum. Scaling of stomatal conductance and photosynthesis with k_L is often strikingly similar among co-occurring species (Fig. 7.9; Meinzer et al. 1995; Brodribb and Feild 2000; Santiago et al. 2004).

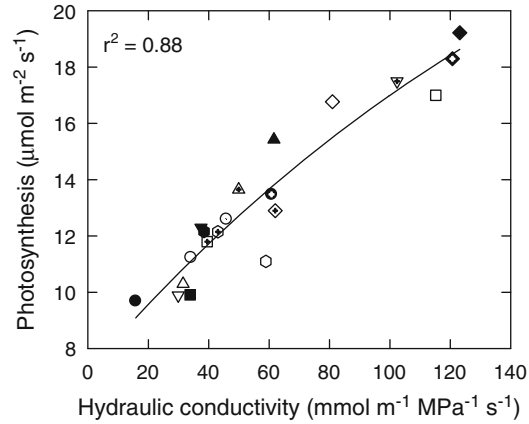

Fig. 7.9. Daily maximum rates of photosynthesis in relation to maximum leaf-specific conductivity in upper branches of 20 Panamanian forest canopy tree species. Adapted from Santiago et al. (2004)

The specific signals involved in stomatal responses to variation in k_L are unclear. Much work has focused on leaf water potential as a physiological set-point for stomatal regulation of gas exchange. However, there is increasing evidence that stomatal regulation of transpiration is coordinated with species-specific set-points for minimum stem water potential such that a relatively constant hydraulic safety margin is maintained in terminal branches (Jones and Sutherland 1991; Sparks and Black 1999; Meinzer et al. 2008a; 2009; Choat et al. 2012; Johnson et al. 2012; Zhang et al. 2013). There is also evidence that diurnal fluctuations in leaf hydraulic capacity are

involved (Brodribb and Holbrook 2003; Bucci et al. 2003; Johnson et al. 2009, 2011).

A. Dynamic Scaling Relationships

Strictly speaking, k_L refers to fixed properties of the hydraulic pathway observed under steady state conditions. However, a number of processes operating at different temporal and spatial scales can cause dynamic variation in apparent k_L leading to adjustments in stomatal control of gas exchange. As described above, daily time courses of crown level stomatal conductance are coordinated with discharge and recharge of capacitance, which transiently influences whole-tree apparent k_L (Fig. 7.8; Andrade et al. 1998; Meinzer et al. 2008a) and species with higher intrinsic sapwood capacitance tend to have higher whole-tree hydraulic conductance estimated under quasi-steady state conditions (Meinzer et al. 2003; Scholz et al. 2007). Stomatal conductance of fully illuminated leaves can also increase rapidly in response to reductions in transpiring leaf area resulting from events such as partial shading (Whitehead et al. 1996) and defoliation (Pataki et al. 1998) of portions of tree crowns, presumably because of concomitant increases in whole-tree k_L. An extreme example of stomatal responses to changes in the ratio of leaf area to hydraulic capacity would be high rates of gas exchange observed in new leaves of recently coppiced trees (Tschaplinski and Blake 1989).

B. Impacts of Tree Size

As trees increase in height, stomatal conductance and photosynthesis are increasingly constrained by frictional resistances associated with path-length and gravitational effects on xylem tension. Although path-length resistances can be partially compensated by increases in trunk xylem specific conductivity (Domec and Gartner 2003) and reductions in the leaf area to sapwood area ratio (McDowell et al. 2002), height-related changes in the gravitational component of xylem tension (0.01 MPa m^{-1}) are inescapable and therefore not an inherently hydraulic influence. Compensatory adjustments in hydraulic architecture can to some extent mitigate the impact of increasing height on photosynthetic gas exchange. Nevertheless, maximum tree height may be ultimately limited by unavoidable conflicts between increased resistance to tension-induced embolism and decreasing hydraulic conductivity in terminal branches (Domec et al. 2008).

Measurements of height-related trends in whole-tree k_L appear to be relatively rare, but the available literature suggests that the relative decline in k_L with increasing height varies dramatically among species. Ryan et al. (2000) reported a 50 % decline in k_L of *Pinus ponderosa* trees over a 24 m height increase from 12 to 36 m, whereas McDowell et al. (2002) found a 50 % decline in k_L of *Pseudotsuga menziesii* trees with a 45 m height increase from 15 to 60 m but with a decline of less than 10 % between height classes of 32 and 60 m. Changes in hydraulic architecture with increasing tree size can also be considerably more abrupt. Specific conductivity of branch xylem decreased by more than 50 % between mean height classes of 4.6 and 9 m in the tropical savanna tree *Sclerolobium paniculatum* (Zhang et al. 2009). This was partially compensated by a decline in branch leaf area to sapwood area ratio such that leaf-specific conductivity declined by only 25 %, but at the cost of reduced photosynthetic leaf area in relation to carbon allocated to branch wood. As expected, height-related declines in k_L are associated with corresponding declines in stomatal conductance and transpiration that modulate vertical gradients of leaf water potential (Niinemets 2002).

Height-related changes in foliar stable carbon isotope composition have been used as an integrated measure of hydraulic constraints on photosynthetic gas exchange. Carbon isotope discrimination of fully illuminated foliage typically decreases with increasing height consistent with increasing relative stomatal limitation of photosynthesis (Koch et al. 2004; Martinez-Vilalta et al. 2007;

Ambrose et al. 2009). However, mesophyll conductance also decreases with increasing height (Woodruff et al. 2008), implying that the height-related decline in carbon isotope discrimination is likely to result from the combined influence of dynamic hydraulic constraints on stomatal conductance and leaf structural constraints on CO_2 diffusion (Niinemets 2002; Ishii et al. 2008; Woodruff et al. 2008).

C. Tree to Stand Scaling

Coordinated adjustments in tree hydraulic architecture and stomatal control of gas exchange are observable at the stand level and often result in partial or complete homeostasis of certain functional attributes across scales. Following thinning treatments that resulted in a five-fold difference in spacing among *Pinus sylvestris* trees in two adjacent plots, differences in stomatal and canopy conductance and canopy transpiration were less than twofold and leaf water potential was nearly identical in the two plots (Whitehead et al. 1984). Seasonal adjustments in canopy conductance and leaf area in Brazilian savanna sites caused canopy transpiration to be similar between the dry and wet seasons despite substantially greater atmospheric vapor pressure deficits during the dry season (Bucci et al. 2008). Coordinated adjustments in tree hydraulic architecture and stomatal control of transpiration have been shown to result in a high degree of homeostasis of minimum leaf water potential among stands of different ages (Ewers et al. 2007b), stands experiencing different levels of water availability (Fisher et al. 2006) and stands experiencing interannual climate variation (Ewers et al. 2007a).

D. Simple Biophysical and Architectural Proxies for Scaling

Simple biophysical and architectural traits of trees can often be used as proxies for more difficult to characterize hydraulic architectural traits that influence photosynthetic gas exchange. Among the simplest of these traits is wood density, which can serve as a proxy for xylem specific conductivity because wood density reflects the relative volumes of solid material and xylem conduits responsible for water transport. Thus conductivity would be expected to decrease with increasing wood density. Dense ring-porous wood is a potential exception because the presence of relatively few large vessels could compensate for the impact of a dense fiber matrix. Functional traits that have been shown to scale uniformly with wood density among co-occurring species include xylem specific conductivity and k_L (Bucci et al. 2004, 2009; Meinzer et al. 2008b), minimum leaf water potential (Bucci et al. 2004, 2009), sapwood hydraulic capacitance (Scholz et al. 2007; Meinzer et al. 2008b), maximum photosynthetic rate (Santiago et al. 2004), total daily transpiration per unit leaf area (Bucci et al. 2004) and whole-tree k_L (McCulloh et al. 2011a, b). Although sapwood capacitance has been reported to scale uniformly with wood density among co-occurring species, scaling relationships between capacitance and wood density appear to vary across sites (Scholz et al. 2007; Meinzer et al. 2008b). Positive correlations between wood density and xylem resistance to embolism are frequently (Hacke et al. 2001; Pratt et al. 2007) but not always (Bucci et al. 2006) observed.

VI. Conclusions

The inextricable links between water use, carbon gain and survival of plants means that to understand plant responses to environmental and competitive pressures one needs a comprehensive understanding of the mechanisms that plants have developed to maximize water transport capacity and to minimize vulnerability to hydraulic failure; as well as the trade-offs involved in balancing these two necessities. Understanding these mechanisms and traits is particularly important when attempting to predict how ecosystems will respond to changes in climate, or to expanding human activities and

land use. The responses of plants to climate extremes, for example, vary from one species to another depending on the different combinations of traits that species possess to cope with these pressures. Although substantial progress has been made in characterizing plant responses to environmental parameters across a range of scales, current models have fallen short in their ability to accurately predict responses to climate extremes. The recent wide-scale drought-induced mortality of piñon pine, and the relatively limited mortality of juniper in the southwest United States (up to 95 and 25 % mortality for piñon and juniper, respectively; Breshears et al. 2005), for example, would not have been predicted with current models such as those which are parameterized by plant functional type (i.e. evergreen needle-leaf forests). Because the two species which exhibit very different strategies in response to climate extremes are indistinguishable within the plant functional type concept, an improved functional trait-based approach is needed that can more effectively describe specific plant adaptive strategies in response to competition and stressors. We believe that the development and application of models that effectively incorporate the hydraulic mechanisms and traits described in this chapter (plus those which have yet to be characterized) will represent a substantial advancement in our ability to more accurately predict plant responses to environmental and competitive stressors.

Acknowledgements

This work was supported in part by NSF grant IBN 09-19871.

References

Aasamaa K, Sber A, Rahi M (2001) Leaf anatomical characteristics associated with shoot hydraulic conductance and stomatal sensitivity to changes of leaf water status in temperate and deciduous trees. Aust J Plant Physiol 28:765–774

Aasamaa K, Niinemets Ü, Sõber A (2005) Leaf hydraulic conductance in relation to anatomical and functional traits during *Populus tremula* leaf ontogeny. Tree Physiol 25:1409–1418

Addington RN, Donovan LA, Mirchell RJ, Vose JM, Pecot SD, Jack SB, Hacke UG, . . ., Oren R (2006) Adjustments in hydraulic architecture of *Pinus palustris* maintain similar stomatal conductance in xeric and mesic habitats. Plant Cell Environ 29:535–545

Alder NN, Sperry JS, Pockman WT (1996) Root and stem xylem embolism, stomatal conductance, and leaf turgor in *Acer grandidentatum* populations along a soil moisture gradient. Oecologia 105:293–301

Ambrose AR, Sillett SC, Dawson TE (2009) Effects of tree height on branch hydraulics, leaf structure and gas exchange in California redwoods. Plant Cell Environ 32:743–757

Andrade JL, Meinzer FC, Goldstein G, Holbrook NM, Cavelier J, Jackson P, Silvera K (1998) Regulation of water flux through trunks, branches and leaves in trees of a lowland tropical forest. Oecologia 115:463–471

Barnard D, Meinzer FC, Lachenbruch B, McCulloh KA, Johnson DM, Woodruff DR (2011) Climate-related trends in sapwood biophysical properties in two conifers: avoidance of hydraulic dysfunction through coordinated adjustments in xylem efficiency, safety and capacitance. Plant Cell Environ 34:643–654

Bauch JW, Liesea W, Schultze R (1972) The morphological variability of the bordered pit membranes in gymnosperms. Wood Sci Tech 6:165–184

Bauerle TL, Richards JH, Smart DR, Eissenstat DM (2008) Importance of internal hydraulic redistribution for prolonging the lifespan of roots in dry soil. Plant Cell Environ 31:177–186

Bonal D, Guehl JM (2001) Contrasting patterns of leaf water potential and gas exchange responses to drought in seedlings of tropical rainforest species. Funct Ecol 15:490–496

Borchert R, Pockman WT (2005) Water storage and xylem tension in isolated branches of temperate and tropical trees. Tree Physiol 25:457–466

Breshears DD, Cobb NS, Rich PM, Price KP, Allen CD, Balice RG, Romme WH, . . ., Meyer CW (2005) Regional vegetation die-off in response to global-change type drought. Proc Natl Acad Sci USA 102:15144–15148

Brodersen CR, McElrone AJ, Choat B, Matthews MA, Shackel KA (2010) The dynamics of embolism repair in xylem: in vivo visualizations using high-resolution computed tomography. Plant Physiol 154:1088–1095

Brodersen CR, Roark LC, Pittermann J (2012) The physiological implications of primary xylem organization in two ferns. Plant Cell Environ 35:1898–1911

Brodribb TJ, Feild TS (2000) Stem hydraulic supply is linked to leaf photosynthetic capacity: evidence from New Caledonian and Tasmanian rainforests. Plant Cell Environ 23:1381–1388

Brodribb TJ, Holbrook NM (2003) Stomatal closure during leaf dehydration, correlation with other leaf physiological traits. Plant Physiol 132:2166–2173

Brodribb TJ, Holbrook NM (2004) Diurnal depression of leaf hydraulic conductance in a tropical tree species. Plant Cell Environ 27:820–827

Brodribb TJ, Holbrook NM, Edwards EJ, Gutierrez MV (2003) Relations between stomatal closure, leaf turgor and xylem vulnerability in eight tropical dry forest trees. Plant Cell Environ 26:443–450

Brooks RH, Corey AT (1964) Hydraulic properties of porous media. Hydrol Pap No. 3. Colorado State University, Fort Collins

Brooks JR, Meinzer FC, Coulombe R, Gregg J (2002) Hydraulic redistribution of soil water during summer drought in two contrasting Pacific Northwest coniferous forests. Tree Physiol 22:1107–1117

Bucci SJ, Scholz FG, Goldstein G, Meinzer FC, Sternberg LDSL (2003) Dynamic changes in hydraulic conductivity in petioles of two savanna tree species: factors and mechanisms contributing to the refilling of embolized vessels. Plant Cell Environ 26:1633–1645

Bucci SJ, Goldstein G, Meinzer FC, Scholz FG, Franco AC, Bustamante M (2004) Functional convergence in hydraulic architecture and water relations of tropical savanna trees: from leaf to whole-plant. Tree Physiol 24:891–899

Bucci SJ, Scholz FG, Goldstein G, Meinzer FC, Franco AC, Campanello PI, Villalobos-Vega R, . . ., Miralles-Wilhelm F (2006) Nutrient availability constrains the hydraulic architecture and water relations of savanna trees. Plant Cell Environ 29:2153–2167

Bucci SJ, Scholz FG, Goldstein G, Hoffmann WA, Meinzer FC, Franco AC, Giambelluca T, Miralles-Wilhelm F (2008) Controls on stand transpiration and soil water utilization along a tree density gradient in a neotropical savanna. Agric For Meteorol 148:839–849

Bucci SJ, Scholz FG, Goldstein G, Meinzer FC, Arce ME (2009) Soil water availability and rooting depth as determinants of hydraulic architecture of Patagonian woody species. Oecologia 160:631–641

Bucci SJ, Scholz FG, Campanello PI, Montti L, Jimenez-Castillo M, Rockwell FA, La Manna L, . . ., Goldstein G (2012) Hydraulic differences along the water transport system of South American *Nothofagus* species: do leaves protect the stem functionality. Tree Physiol 32:880–893

Burgess SO, Pittermann J, Dawson TE (2006) Hydraulic efficiency and safety of branch xylem increases with height in *Sequoia sempervirens* (D.Don) crowns. Plant Cell Environ 29:229–239

Chave J, Coomes D, Jansen S, Lewis SL, Swenson NG, Zanne AE (2009) Towards a worldwide wood economics spectrum. Ecol Lett 12:351–366

Chen J-W, Zhang Q, Li X-S, Cao K-F (2009) Independence of stem and leaf hydraulic traits in six Euphorbiaceae tree species with contrasting leaf phenology. Planta 230:459–468

Choat B, Cobb AR, Jansen S (2008) Structure and function of bordered pits: new discoveries and impacts on whole-plant hydraulic function. New Phytol 177:608–626

Choat B, Medek DE, Stuart SA, Pasquet-Kok J, Egerton JJG, Salari H, Sack L, Ball MC (2011) Xylem traits mediate a trade-off between resistance to freeze-thaw-induced embolism and photosynthetic capacity in overwintering evergreens. New Phytol 191:996–1005

Choat B, Jansen S, Brodribb TJ, Cochard H, Delzon S, Bhaskar R, Bucci SJ, . . ., Zanne AE (2012) Global convergence in the vulnerability of forests to drought. Nature 491:752–755

Christman MA, Sperry JS, Adler FR (2009) Testing the "rare pit" hypothesis in three species of *Acer*. New Phytol 182:664–674

Christman MA, Sperry JS, Smith DD (2012) Rare pits, large vessels, and extreme vulnerability to cavitation in a ring-porous tree species. New Phytol 193:713–720

Cochard H, Cruziat P, Tyree MT (1992) Use of positive pressures to establish vulnerability curves: further support for the air seeding hypothesis and implications for pressure-volume analysis. Plant Physiol 100:205–209

Crombie DS, Hipkins MF, Milburn JA (1985) Gas penetration of pit membranes in the xylem of Rhododendron as the cause of acoustically detectable sap cavitation. Aust J Plant Physiol 12:445–454

Dagan Z, Weibaum S, Pfeffer R (1982) An infinite-series solution for the creeping motion through an orifice of finite length. J Fluid Mech 115:505–523

Davis SD, Sperry JS, Hacke UG (1999) The relationship between xylem conduit diameter and cavitation caused by freezing. Am J Bot 86:1367–1372

Delzon S, Douthe C, Sala A, Cochard H (2010) Mechanism of water-stress induced cavitation in conifers: bordered pit structure and function support the

hypothesis of seal capillary-seeding. Plant Cell Environ 33:2101–2111

Domec JC, Gartner BL (2001) Cavitation and water storage in bole xylem segments of mature and young Douglas-fir trees. Trees 15:204–214

Domec JC, Gartner BL (2003) Relationship between growth rates and xylem hydraulic characteristics in young, mature and old-growth ponderosa pine trees. Plant Cell Environ 26:471–483

Domec JC, Warren JM, Meinzer FC, Brooks JR, Coulombe R (2004) Native root xylem embolism and stomatal closure in stands of Douglas-fir and ponderosa pine: mitigation by hydraulic redistribution. Oecologia 141:7–16

Domec JC, Lachenbruch B, Meinzer FC (2006a) Bordered pit structure and function determine spatial patterns of air-seeding thresholds in xylem of Douglas-fir (*Pseudotsuga menziezii*; Pinaceae) trees. Am J Bot 93:1588–1600

Domec JC, Scholz FG, Bucci SJ, Meinzer FC, Goldstein G, Villalobos-Vega R (2006b) Diurnal and seasonal variation in root xylem embolism in neotropical savanna woody species: impact on stomatal control of plant water status. Plant Cell Environ 29:26–35

Domec JC, Meinzer FC, Lachenbruch B, Housset J (2007) Dynamic variation in sapwood specific conductivity in six woody species. Tree Physiol 27:1389–1400

Domec JC, Lachenbruch B, Meinzer FC, Woodruff DR, Warren JM, McCulloh KA (2008) Maximum height in a conifer is associated with conflicting requirements for xylem design. Proc Natl Acad Sci U S A 105:12069–12074

Domec JC, Noormets A, King JS, Sun G, McNulty SG, Gavazzi MJ, Boggs JL, Treasure EA (2009) Decoupling the influence of leaf and root hydraulic conductances on stomatal conductance and its sensitivity to vapour pressure deficit as soil dries in a drained loblolly pine plantation. Plant Cell Environ 32:980–991

Ewers BE, Oren R, Sperry JS (2000) Influence of nutrient versus water supply on hydraulic architecture and water balance in *Pinus taeda*. Plant Cell Environ 23:1055–1066

Ewers B, Mackay DS, Samanta S (2007a) Interannual consistency in canopy stomatal conductance control of leaf water potential across seven tree species. Tree Physiol 27:11–24

Ewers FW, Ewers JM, Jacobsen AL, Lopez-Portillo J (2007b) Vessel redundancy: modeling safety in numbers. IAWA J 28:373–388

Farquhar GD, Sharkey TD (1982) Stomatal conductance and photosynthesis. Annu Rev Plant Physiol 33:317–345

Feild TS, Brodribb TJ (2001) Stem water transport and freeze-thaw xylem embolism in conifers and angiosperms in a Tasmanian treeline heath. Oecologia 127:314–320

Feild TS, Brodribb TJ, Holbrook NM (2002) Hardly a relict: freezing and the evolution of vesselless wood in Winteraceae. Evolution 56:464–478

Fisher RA, Williams M, Do Vale RL, Da Costa AL, Meir P (2006) Evidence from Amazonian forests is consistent with isohydric control of leaf water potential. Plant Cell Environ 29:151–165

Franks PJ, Drake PL, Froend RH (2007) Anisohydric but isohydrodynamic: seasonally constant plant water potential gradient explained by a stomatal control mechanism incorporating variable plant hydraulic conductance. Plant Cell Environ 30:19–30

Gascò A, Nardini A, Gortan E, Salleo S (2006) Ion-mediated increase in the hydraulic conductivity of Laurel stems: role of pits and consequences for the impact of cavitation on water transport. Plant Cell Environ 29:1946–1955

Goldstein G, Meinzer F, Monasterio M (1984) The role of capacitance in the water balance of Andean giant rosette species. Plant Cell Environ 7:179–186

Goldstein G, Andrade JL, Meinzer FC, Holbrook NM, Cavelier J, Jackson P, Celis A (1998) Stem water storage and diurnal patterns of water use in tropical forest canopy trees. Plant Cell Environ 21:397–406

Gortan E, Nardini A, Salleo S, Jansen S (2011) Pit membrane chemistry influences the magnitude of ion-mediated enhancement of xylem hydraulic conductance in four Lauraceae species. Tree Physiol 31:48–58

Hacke UG, Jansen S (2009) Embolism resistance of three boreal conifer species varies with pit structure. New Phytol 182:675–686

Hacke UG, Sperry JS (2003) Limits to xylem refilling under negative pressure in *Laurus nobilis* and *Acer negundo*. Plant Cell Environ 26:303–311

Hacke UG, Sperry JS, Ewers BE, Ellsworth DS, Schafer KVR, Oren R (2000) Influence of soil porosity on water use in *Pinus taeda*. Oecologia 124:495–505

Hacke UG, Sperry JS, Pockman WT, Davis SD, McCulloh KA (2001) Trends in wood density and structure are linked to prevention of xylem implosion by negative pressure. Oecologia 126:457–461

Hacke UG, Sperry JS, Pittermann J (2004) Analysis of circular bordered pit function. II. Gymnosperm tracheids with torus-margo pit membranes. Am J Bot 91:386–400

Hao G, Hoffmann WA, Scholz FG, Bucci SJ, Meinzer FC, Franco AC, Cao K, Goldstein G (2008) Stem

and leaf hydraulics of congeneric tree species from adjacent tropical savanna and forest ecosystems. Oecologia 155:405–415

Hargrave KR, Kolb KJ, Ewers FW, Davis SD (1994) Conduit diameter and drought-induced embolism in *Salvia mellifera* greene (labiatae). New Phytol 126:695–705

Hoffmann WA, Marchin RM, Abit P, Lau OL (2011) Hydraulic failure and tree dieback are associated with high wood density in a temperate forest under extreme drought. Glob Change Biol 17:2731–2742

Holbrook NM, Sinclair TR (1992) Water balance in the arborescent palm, *Sabal palmetto.* I. Stem structure, tissue water release properties and leaf epidermal conductance. Plant Cell Environ 15:393–399

Holbrook NM, Ahrens ET, Burns MJ, Zwieniecki MA (2001) In vivo observation of cavitation and embolism repair using magnetic resonance imaging. Plant Physiol 126:27–31

Hölttä T, Cochard H, Nikinmaa E, Mencuccini M (2009) Capacitive effect of cavitation in xylem conduits: results from a dynamic model. Plant Cell Environ 32:10–21

Howard AR, Van Iersel MW, Richards JH, Donovan LA (2009) Night-time transpiration can decrease hydraulic redistribution. Plant Cell Environ 32:1060–1070

Ishii HT, Jennings GM, Sillett SC, Koch GW (2008) Hydrostatic constraints on morphological exploitation of light in tall *Sequoia sempervirens* trees. Oecologia 156:751–763

Jansen S, Gortan E, Lens F, Lo Gullo MA, Salleo S, Scholz A, Stein A, . . ., Nardini A (2011) Do quantitative vessel and pit characters account for ion-mediated changes in the hydraulic conductance of angiosperm xylem? New Phytol 189:218–228

Johnson DM, Woodruff DR, McCulloh KA, Meinzer FC (2009) Leaf hydraulic conductance, measured in situ, declines and recovers daily: leaf hydraulics, water potential and stomatal conductance in four temperate and three tropical tree species. Tree Physiol 29:879–887

Johnson DM, McCulloh KA, Meinzer FC, Woodruff DR, Eissenstat DM (2011) Hydraulic patterns and safety margins from stem to stomata, in three eastern US tree species. Tree Physiol 31:659–668

Johnson DM, McCulloh KA, Woodruff DR, Meinzer FC (2012) Hydraulic safety margins and embolism reversal in stems and leaves: why are conifers and angiosperms so different? Plant Sci 195:48–53

Jones HG, Sutherland RA (1991) Stomatal control of xylem embolism. Plant Cell Environ 14:607–612

Kavanagh KL, Bond BJ, Aitken SN, Gartner BL, Knowe S (1999) Shoot and root vulnerability to xylem cavitation in four populations of Douglas-fir seedlings. Tree Physiol 19:31–37

Koch GW, Sillett SC, Jennings GM, Davis SD (2004) The limits to tree height. Nature 428:851–854

Kolb KJ, Sperry JS (1999) Transport constraints on water use by the Great Basin shrub, *Artemisia tridentata*. Plant Cell Environ 22:925–935

Lemoine D, Granier A, Cochard H (1999) Mechanism of freeze-induced embolism in *Fagus sylvatica* L. Trees 13:206–210

Lens F, Sperry JS, Christman MA, Choate B, Rabaey D, Jansen S (2011) Testing hypotheses that link wood anatomy to cavitation resistance and hydraulic conductivity in the genus *Acer*. New Phytol 190:709–723

Linton MJ, Sperry JS, Williams DG (1998) Limits to water transport in *Juniperus osteosperma* and *Pinus edulis*: implications for drought tolerance and regulation of transpiration. Funct Ecol 12:906–911

Loepfe L, Martinez-Vilalta J, Piñol J, Mencuccini M (2007) The relevance of xylem network structure for plant hydraulic efficiency and safety. J Theor Biol 247:788–803

Loewenstein NJ, Pallardy SG (1998a) Drought tolerance, xylem sap abscisic acid and stomatal conductance during soil drying: a comparison of young plants of four temperate deciduous angiosperms. Tree Physiol 18:421–430

Loewenstein NJ, Pallardy SG (1998b) Drought tolerance, xylem sap abscisic acid and stomatal conductance during soil drying: a comparison of canopy trees of three temperate deciduous angiosperms. Tree Physiol 18:431–439

Lovelock CE, Feller IC, McKee KL, Engelbrecht BMJ, Ball MC (2004) The effect of nutrient enrichment on growth, photosynthesis and hydraulic conductance of dwarf mangroves in Panama. Funct Ecol 18:25–33

Lovisolo C, Perrone I, Hartung W, Schubert A (2008) An abscisic acid-related reduced transpiration promotes gradual embolism repair when grapevines are rehydrated after drought. New Phytol 180:642–651

Maherali H, DeLucia EH (2001) Influence of climate-driven shifts in biomass allocation on water transport and storage in ponderosa pine. Oecologia 129:481–491

Maherali H, Pockman WT, Jackson RB (2004) Adaptive variation in the vulnerability of woody plants to xylem cavitation. Ecology 85:2184–2199

Markesteijn L, Poorter L, Paz H, Sack L, Bongers F (2011) Ecological differentiation in xylem

cavitation resistance is associated with stem and leaf structural traits. Plant Cell Environ 34:137–148

Martínez-Vilalta JJ, Prat E, Oliveras I, Piñol J (2002) Xylem hydraulic properties of roots and stems of nine Mediterranean woody species. Oecologia 133:19–29

Martinez-Vilalta J, Vanderklein D, Mencuccini M (2007) Tree height and age-related decline in growth in Scots pine (*Pinus sylvestris* L.). Oecologia 150:529–544

Martinez-Vilalta J, Cochard H, Mencuccini M, Sterck F, Herrero A, Korhonen JFJ, Llorens P, . . ., Zweifel R (2009) Hydraulic adjustment of Scots pine across Europe. New Phytol 184:353–364

Martínez-Vilalta JJ, Mencuccini M, Alvarez X, Camacho J, Loepfe L, Piñol L (2012) Spatial distribution and packing of xylem conduits. Am J Bot 99:1189–1196

Mayr S, Wolfschwenger M, Bauer H (2002) Winter-drought induced embolism in Norway spruce (*Picea abies*) at the Alpine timberline. Physiol Plant 115:74–80

Mayr S, Gruber A, Bauer H (2003) Repeated freeze-thaw cycles induce embolism in drought stressed conifers (Norway spruce, stone pine). Planta 217:436–441

Mayr S, Hacke U, Schmid P, Schwienbacher F, Gruber A (2006) Frost drought in conifers at the alpine timberline: xylem dysfunction and adaptations. Ecology 87:3175–3185

McCree KJ, Richardson SG (1987) Stomatal closure vs. osmotic adjustment: a comparison of stress response. Crop Sci 27:539–543

McCulloh KA, Johnson DM, Meinzer FC, Lachenbruch B (2011a) An annual pattern of native embolism in upper branches of four tall conifer species. Am J Bot 98:1007–1015

McCulloh KA, Meinzer FC, Sperry JS, Lachenbruch B, Voelker SL, Woodruff DR, Domec JC (2011b) Comparative hydraulic architecture of tropical tree species representing a range of successional stages and wood density. Oecologia 167:27–37

McCulloh KA, Johnson DM, Meinzer FC, Voelker SL, Lachenbruch B, Domec JC (2012) Hydraulic architecture of two species differing in wood density: opposing strategies in co-occurring tropical pioneer trees. Plant Cell Environ 35:116–125

McCulloh KA, Johnson DM, Meinzer FC, Woodruff DR (2014) The dynamic pipeline: hydraulic capacitance and xylem hydraulic safety in four tall conifer species. Plant Cell Environ 37:1171–1183

McCully ME (1999) Root xylem embolisms and refilling in relation to water potentials of soil, roots and leaves and osmotic potentials of xylem sap. Plant Physiol 119:1001–1008

McCully ME, Huang CX, Ling LE (1998) Daily embolism and refilling of xylem vessels in the roots of field-grown maize. New Phytol 138:327–342

McDowell NG, Phillips N, Lunch CK, Bond BJ, Ryan MG (2002) Hydraulic limitation and compensation in large, old Douglas-fir trees. Tree Physiol 22:763–774

McDowell N, Pockman WT, Allen CD, Breshears DD, Cobb N, Kolb T, Plaut J, . . ., Yepez EA (2008) Mechanisms of plant survival and mortality during drought: why do some plants survive while others succumb to drought? New Phytol 178:719–739

McElrone AJ, Pockman WT, Martinez-Vilalta J, Jackson RB (2004) Variation in xylem structure and function in stems and roots of trees to 20 m depth. New Phytol 163:507–51

Medeiros JS, Pockman WT (2011) Drought increases freezing tolerance of both leaves and xylem of *Larrea tridentata*. Plant Cell Environ 34:43–51

Meinzer FC, Grantz DA (1990) Stomatal and hydraulic conductance in growing sugarcane: Stomatal adjustment to water transport capacity. Plant Cell Environ 13:383–388

Meinzer FC, James SA, Goldstein G, Woodruff DR (2003) Whole-tree water transport scales with sapwood capacitance in tropical forest canopy trees. Plant Cell Environ 26:1147–1155

Meinzer FC, James SA, Goldstein G (2004a) Dynamics of transpiration, sap flow and use of stored water in tropical forest canopy trees. Tree Physiol 24:901–909

Meinzer FC, Brooks JR, Bucci S, Goldstein G, Scholz FG, Warren JM (2004b) Converging patterns of uptake and hydraulic redistribution of soil water in contrasting vegetation types. Tree Physiol 24:919–928

Meinzer FC, Woodruff DR, Domce J-C, Goldstein G, Campanello P, Gatti MG, Villalobos-Vega R (2008a) Coordination of leaf and stem water transport properties in tropical forest trees. Oecologia 156:31–41

Meinzer FC, Campanello PI, Domec J-C, Gatti MG, Goldstein G, Villalobos-Vega R, Woodruff DR (2008b) Constraints on physiological function associated with branch architecture and wood density in tropical forest trees. Tree Physiol 28:1609–1617

Meinzer F, Goldstein G, Jackson P, Holbrook N, Gutierrez M, Cavelier J (1995) Environmental and physiological regulation of transpiration in tropical forest gap species: the influence of boundary layer and hydraulic properties. Oecologia 101:514–522

Meinzer FC, Johnson DM, Lachenbruch B, McCulloh KA, Woodruff DR (2009) Xylem hydraulic safety margins in woody plants: coordination of stomatal

control of xylem tension with hydraulic capacitance. Funct Ecol 23:922–930

Meinzer FC, McCulloh KA, Lachenbruch B, Woodruff DR, Johnson DM (2010) The blind men and the elephant: the impact of context and scale in evaluating conflicts between plant hydraulic safety and efficiency. Oecologia 164:287–296

Melcher PJ, Goldstein G, Meinzer FC, Yount DE, Jones TJ, Holbrook NM, Huang CX (2001) Water relations of coastal and estuarine Rhizophora mangle: xylem pressure potential and dynamics of embolism formation and repair. Oecologia 126:182–192

Mencuccini M (2003) The ecological significance of long-distance water transport: short-term regulation, long-term acclimation and the hydraulic costs of stature across plant life forms. Plant Cell Environ 26:163–182

Mitchell PJ, O'Grady AP, Tissue DT, White DA, Ottenschlaeger ML, Pinkard E (2012) Drought response strategies define the relative contributions of hydraulic dysfunction and carbohydrate depletion during tree mortality. New Phytol 197:862–872

Murai-Hatano M, Kuwagata T, Sakurai J, Nonami H, Ahamed A, Nagasuga K, Matsunami T, . . ., Okada M (2008) Effect of low root temperature on hydraulic conductivity of rice plants and the possible role of aquaporins. Plant Cell Physiol 49:1294–1305

Nardini A, Tyree MT, Salleo S (2001) Xylem cavitation in the leaf of *Prunus laurocerasus* and its impact on leaf hydraulics. Plant Physiol 125:1700–1709

Nardini A, Ramani M, Gortan E, Salleo S (2008) Vein recovery from embolism occurs under negative pressure in leaves of sunflower (*Helianthus annuus*). Physiol Plant 133:755–764

Nardini A, Grego F, Trifilo P, Salleo S (2010) Changes of xylem sap ionic content and stem hydraulics in response to irradiance in *Laurus nobilis*. Tree Physiol 30:628–635

Nardini A, Lo Gullo MA, Salleo S (2011a) Refilling embolized xylem conduits: is it a matter of phloem unloading? Plant Sci 180:604–611

Nardini A, Salleo S, Jansen S (2011b) More than just a vulnerable pipeline: xylem physiology in the light of ion-mediated regulation of plant water transport. J Exp Bot 62:4701–4718

Nardini A, Dimasi F, Klepsch M, Jansen S (2012) Ion-mediated enhancement of xylem hydraulic conductivity in four Acer species: relationships with ecological and anatomical features. Tree Physiol 32:1434–1441

Neumann RB, Cardon ZG (2012) The magnitude of hydraulic redistribution by plant roots: a review and synthesis of empirical and modeling studies. New Phytol 194:337–352

Niinemets Ü (2002) Stomatal conductance alone does not explain the decline in foliar photosynthetic rates with increasing tree age and size in *Picea abies* and *Pinus sylvestris*. Tree Physiol 22:515–535

Ogasa M, Miki N, Murakami Y, Yoshikawa K (2013) Recovery performance in xylem hydraulic conductivity is correlated with cavitation resistance for temperate deciduous tree species. Tree Physiol 33:335–344

Pataki DE, Oren R, Phillips N (1998) Responses of sap flux and stomatal conductance of *Pinus taeda* L. trees to stepwise reductions in leaf area. J Exp Bot 49:871–878

Phillips NG, Nagchaudhuri A, Oren R, Katul G (1997) Time constant for water transport in loblolly pine trees estimated from time series of evaporative demand and sap flow. Trees 11:412–419

Phillips NG, Oren R, Licata J, Linder S (2004) Time series diagnosis of tree hydraulic characteristics. Tree Physiol 24:879–890

Pittermann J, Sperry JS (2003) Tracheid diameter is the key trait determining the extent of freezing-induced embolism in conifers. Tree Physiol 23:907–914

Pittermann J, Sperry JS (2006) Analysis of freeze-thaw embolism in conifers. The interaction between cavitation pressure and tracheid size. Plant Physiol 140:374–382

Pittermann J, Sperry JS, Wheeler JK, Hacke UG, Sikkema EH (2006) Mechanical reinforcement of tracheids compromises the hydraulic efficiency of conifer xylem. Plant Cell Environ 29:1618–1628

Plamboek AH, Dawson TE, Egerton-Warburton LM, North M, Bruns TD, Querejeta JI (2007) Water transfer via ectomycorrhizal fungal hyphae to conifer seedlings. Mycorrhiza 17:439–447

Pockman WT, Sperry JS (1997) Freezing-induced xylem cavitation and the northern limit of *Larrea tridentata*. Oecologia 109:19–27

Pockman WT, Sperry JS (2000) Vulnerability to cavitation and the distribution of Sonoran Desert vegetation. Am J Bot 87:1287–1299

Pou A, Medrano H, Tomàs M, Martorell S, Ribas-Carbó M, Flexas J (2012) Anisohydric behaviour in grapevines results in better performance under moderate water stress and recovery than isohydric behavior. Plant Soil 359:335–349

Pratt RB, Jacobsen AL, Ewers FW, Davis SD (2007) Relationships among xylem transport, biomechanics and storage in stems and roots of nine *Rhamnaceae* species of the California chaparral. New Phytol 174:787–798

Pregitzer KS, King JS (2005) Effects of soil temperature on nutrient uptake. In: BassiriRad H (ed) Nutrient Acquisition by Plants: an Ecological Perspective. Springer, Berlin, pp 277–310

Querejeta, J.I., Egerton-Warburton, L.M., Allen, M.F., (2003). Direct nocturnal water transfer from oaks to their mycorrhizal symbionts during severe soil drying. Oecologia 134:55–64

Robson DJ, McHardy WJ, Petty JA (1988) Freezing in conifer xylem. II. Pit aspiration and bubble formation. J Exp Bot 39:1617–1621

Ryan MG, Bond BJ, Law BE, Hubbard RM, Woodruff D, Cienciala E, Kucera J (2000) Transpiration and whole-tree conductance in ponderosa pine trees of different heights. Oecologia 124:553–560

Sack L, Frole K (2006) Leaf structural diversity is related to hydraulic capacity in tropical rainforest trees. Ecology 87:483–491

Sack L, Tyree MT (2005) Leaf hydraulics and its implications in plant structure and function. In: Holbrook NM, Zwieniecki MA (eds) Vascular Transport in Plants. Elsevier/Academic Press, Oxford, pp 93–114

Sack L, Cowan PD, Jaikumar N, Holbrook NM (2003) The 'hydrology' of leaves: co-ordination of structure and function in temperate woody species. Plant Cell Environ 26:1343–1356

Salleo S, LoGullo MA, DePaoli D, Zippo M (1996) Xylem recovery from cavitation induced embolism in young plants of *Laurus nobilis*: a possible mechanism. New Phytol 132:47–56

Salleo S, Nardini A, Pitt F, Lo Gullo MA (2000) Xylem cavitation and hydraulic control of stomatal conductance in Laurel (*Laurus nobilis* L.). Plant Cell Environ 23:71–79

Salleo S, Lo Gullo MA, Trifilo P, Nardini A (2004) New evidence for a role of vessel-associated cells and phloem in the rapid xylem refilling of cavitated stems of *Laurus nobilis* L. Plant Cell Environ 27:1065–1076

Salleo S, Trifilo P, Lo Gullo MA (2006) Phloem as a possible major determinant of rapid cavitation reversal in stems of *Laurus nobilis* (laurel). Funct Plant Biol 33:1063–1074

Salleo S, Trifilo P, Esposito S, Nardini A, Lo Gullo MA (2009) Starch-to-sugar conversion in wood parenchyma of field-growing *Laurus nobilis* plants: a component of the signal pathway for embolism repair? Funct Plant Biol 36:815–825

Santiago LS, Goldstein G, Meinzer FC, Fisher JB, Machado K, Woodruff DR, Jones T (2004) Leaf photosynthetic traits scale with hydraulic conductivity and wood density in Panamanian forest canopy trees. Oecologia 140:543–550

Schenk HJ, Espino S, Goedhart CM, Nordenstahl M, Martinez Cabrera HI, Jones CS (2008) Hydraulic integration and shrub growth form linked across continental aridity gradients. Proc Natl Acad Sci U S A 105:11248–11253

Scholz FG, Bucci SJ, Goldstein G, Meinzer FC, Franco AC, Miralles-Wilhelm F (2007) Biophysical properties and functional significance of stem water storage tissues in neotropical savanna trees. Plant Cell Environ 30:236–248

Scholz FG, Bucci SJ, Goldstein G, Moreira MZ, Meinzer FC, Domec J-C, Villalobos-Vega R, Franco AC, Miralles-Wilhelm F (2008) Biophysical and life-history determinants of hydraulic lift in Neotropical savanna trees. Funct Ecol 22:773–786

Schulte PJ, Gibson AC (1988) Hydraulic conductance and tracheid anatomy in six species of extant seed plants. Can J Bot 66:1073–1079

Siau JF, Davidson RW, Meyer JA, Skaar C (1984) Transport Processes in Wood. Springer, Berlin

Sparks JP, Black RA (1999) Regulation of water loss in populations of Populus trichocarpa: the role of stomatal control in preventing xylem cavitation. Tree Physiol 19:453–459

Sparks JP, Black RA (2000) Winter hydraulic conductivity and xylem cavitation in coniferous trees from upper and lower treeline. Arct Antarct Alp Res 32:397–403

Sparks JP, Campbell GS, Black RA (2001) Water content, hydraulic conductivity, and ice formation in winter stems of *Pinus contorta*: a TDR case study. Oecologia 127:468–475

Sperry JS, Robson DJ (2001) Xylem cavitation and freezing in conifers. In: Bigras FJ, Colombo SJ (eds) Conifer Cold Hardiness. Kluwer, Dordrecht, pp 121–136

Sperry JS, Saliendra NZ (1994) Intra- and inter-plant variation in xylem cavitation in *Betula occidentalis*. Plant Cell Environ 17:1233–1241

Sperry JS, Holbrook NM, Zimmermann MH, Tyree MT (1987) Spring filling of xylem vessels in wild grapevine. Plant Physiol 83:414–417

Sperry JS, Adler FR, Campbell GS, Comstock JP (1998) Limitation of plant water use by rhizosphere and xylem conductance: results from a model. Plant Cell Environ 21:347–359

Sperry JS, Hacke UG, Oren R, Comstock JP (2002) Water deficits and hydraulic limits to leaf water supply. Plant Cell Environ 25:251–263

Sperry JS, Hacke UG, Wheeler JK (2005) Comparative analysis of end wall resistivity in xylem conduits. Plant Cell Environ 28:456–465

Sperry JS, Hacke UG, Pittermann J (2006) Size and function in conifer tracheids and angiosperm vessels. Am J Bot 93:1490–1500

Sperry JS, Meinzer FC, McCulloh KA (2008) Safety and efficiency conflicts in hydraulic architecture: scaling from tissues to trees. Plant Cell Environ 31:632–645

Stiller V, Sperry JS, Lafitte R (2005) Embolized conduits of rice (*Oryza sativa*, Poaceae) refill despite negative xylem pressure. Am J Bot 92:1970–1974

Sucoff E (1969) Freezing of conifer xylem and the cohesion – tension theory. Physiol Plant 22:424–431

Taneda H, Sperry JS (2008) A case-study of water transport in co-occurring ring versus diffuse-porous trees: contrasts in water-status, conducting capacity, cavitation and vessel refillings. Tree Physiol 28:1641–1651

Tardieu F, Davies WJ (1992) Stomatal response to abscisic acid is a function of current plant water status. Plant Physiol 98:540–545

Tardieu F, Simonneau T (1998) Variability of species among stomatal control under fluctuating soil water status and evaporative demand: modeling isohydric and anisohydric behaviours. J Exp Bot 49:419–432

Trifilò P, Gascò A, Raimondo F, Nardini A, Salleo S (2003) Kinetics of recovery of leaf hydraulic conductance and vein functionality from cavitation-induced embolism in sunflower. J Exp Bot 54:2323–2330

Trifilo P, Lo Gullo MA, Salleo S, Callea K, Nardini A (2008) Xylem embolism alleviated by ion-mediated increase in hydraulic conductivity of functional xylem: insights from field measurements. Tree Physiol 28:1505–1512

Trifilo P, Nardini A, Raimondo F, Lo Gullo MA, Salleo S (2011) Ion-mediated compensation for drought-induced loss of xylem hydraulic conductivity in field-growing plants of *Laurus nobilis* L. Funct Plant Biol 38:606–613

Tschaplinski TJ, Blake TJ (1989) Photosynthetic reinvigoration of leaves following shoot decapitation and accelerated growth of coppice shoots. Physiol Plant 75:157–165

Tyree MT, Zimmermann MH (2002) Xylem Structure and the Ascent of Sap. Springer, Berlin

Tyree M, Davis S, Cochard H (1994) Biophysical perspectives of xylem evolution – is there a tradeoff of hydraulic efficiency for vulnerability to dysfunction? IAWA J 15:335–360

Tyree MT, Salleo S, Nardini A, Lo Gullo MA, Mosca R (1999) Refilling of embolized vessels in young stems of Laurel. Do we need a new paradigm? Plant Physiol 120:11–21

Van Ieperen W, Van Meeteren U, Van Gelder H (2000) Fluid ionic composition influences hydraulic conductance of xylem conduits. J Exp Bot 51:769–776

Wan X, Zwiazek JJ, Lieffers VJ, Landhausser M (2001) Hydraulic conductance in aspen (*Populus tremuloides*) seedlings exposed to low root temperatures. Tree Physiol 21:691–696

Ward EJ, Bell DM, Clark JS, Oren R (2013) Hydraulic time constants for transpiration of loblolly pine at a free-air carbon dioxide enrichment site. Tree Physiol 33:123–134

Warren JM, Meinzer FC, Brooks JR, Domec J-C (2005) Vertical stratification of soil water storage and release dynamics in Pacific Northwest coniferous forests. Agric For Meteorol 130:39–58

Warren JM, Meinzer FC, Brooks JR, Domec JC, Coulombe R (2007) Hydraulic redistribution of soil water in two old-growth coniferous forests: quantifying patterns and controls. New Phytol 173:753–765

Warren JM, Brooks JR, Meinzer FC, Eberhart JL (2008) Hydraulic redistribution of water from Pinus ponderosa trees to seedlings: evidence for an ectomycorrhizal pathway. New Phytol 178:382–394

West AG, Hultine KR, Sperry JS, Bush SE, Ehleringer JR (2008) Transpiration and hydraulic strategies in a piñon–juniper woodland. Ecol Appl 18:911–927

Wheeler JK, Sperry JS, Hacke UG, Hoang N (2005) Inter-vessel pitting and cavitation in wood Rosaceae and other vesselled plants: a basis for a safety versus efficiency trade-off in xylem transport. Plant Cell Environ 28:800–812

Wheeler EA, Baas P, Rodgers S (2007) Variations in dicot wood anatomy: a global analysis based on the Insidewood database. IAWA J 28:229–258

Whitehead D, Jarvis PG, Waring RH (1984) Stomatal conductance, transpiration, and resistance to water uptake in a *Pinus sylvestris* spacing experiment. Can J For Res 14:692–700

Whitehead D, Livingston NJ, Kelliher FM, Hogan KP, Pepin S, McSeveny TM, Byers JN (1996) Response of transpiration and photosynthesis to a transient change in illuminated foliage area for a *Pinus radiata* D. Don tree. Plant Cell Environ 19:949–957

Wilkinson S, Davies WJ (2002) ABA-based chemical signaling: the coordination of responses to plants in stress. Plant Cell Environ 25:195–210

Woodruff DR, McCulloh KA, Warren JM, Meinzer FC, Lachenbruch B (2007) Impacts of tree height on leaf hydraulic architecture and stomatal control in Douglas-fir. Plant Cell Environ 30:559–569

Woodruff DR, Meinzer FC, Lachenbruch B (2008) Height related trends in leaf xylem anatomy and hydraulic characteristics in a tall conifer: safety versus efficiency in foliar water transport. New Phytol 180:90–99

Yang S, Tyree MT (1992) A theoretical model of hydraulic conductivity recovery from embolism with comparison to experimental data on *Acer saccharum*. Plant Cell Environ 15:633–643

Yu X, Peng YH, Zhang MH, Shao YJ, Su WA, Tang ZC (2006) Water relations and an expression analysis of plasma membrane intrinsic proteins in sensitive and tolerant rice during chilling and recovery. Cell Res 16:599–608

Zanne AE, Sweeney K, Sharma M, Orians CM (2006) Patterns and consequences of differential vascular sectoriality in 18 temperate tree and shrub species. Funct Ecol 20:200–206

Zhang Y-J, Meinzer FC, Hao G-Y, Scholz FG, Bucci SJ, Takahashi FSC, Villalobos-Vega R, . . ., Goldstein G (2009) Size-dependent mortality in a Neotropical savanna tree: the role of height-related adjustments in hydraulic architecture and carbon allocation. Plant Cell Environ 32:1456–1466

Zhang Y, Oren R, Kang S (2012) Spatiotemporal variation of crown-scale stomatal conductance in an arid *Vitis vinifera* L. cv. Merlot vineyard: direct effects of hydraulic properties and indirect effects of canopy leaf area. Tree Physiol 32:262–279

Zhang YJ, Meinzer FC, Qi JH, Goldstein G, Cao KF (2013) Midday stomatal conductance is more related to stem rather than leaf water status in subtropical deciduous and evergreen broadleaf trees. Plant Cell Environ 36:149–158

Zimmermann MH (1978) Hydraulic architecture of some diffuse-porous trees. Can J Bot 56:2286–2295

Zimmermann MH (1983) Xylem Structure and the Ascent of Sap. Springer, Berlin

Zwieniecki MA, Holbrook NM (1998) Short term changes in xylem water conductivity in white ash, red maple and Sitka spruce. Plant Cell Environ 21:1173–1180

Zwieniecki MA, Holbrook NM (2009) Confronting Maxwell's demon: biophysics of xylem embolism repair. Trends Plant Sci 14:530–534

Zwieniecki MA, Hutyra L, Thompson MV, Holbrook NM (2000) Dynamic changes in petiole specific conductivity in red maple (*Acer rubrum* L.), tulip tree (*Liriodendron tulipifera* L.) and northern fox grape (*Vitis labrusca* L.). Plant Cell Environ 23:407–414

Zwieniecki MA, Melcher PJ, Holbrook NM (2001) Hydrogel control of xylem hydraulic resistance in plants. Science 291:1059–1062

Chapter 8

Simulating Crop Growth and Development Using Functional-Structural Plant Modeling

Jochem B. Evers*
Centre for Crop Systems Analysis, Wageningen UR, Droevendaalsesteeg 1, Wageningen 6708 PB, The Netherlands

Summary

Crop canopies are composed of individual plants. Yet, in the analysis of crop characteristics such as canopy photosynthesis, growth and performance, plants are normally not considered as individual entities with their own developmental pattern and plastic responses to their environment. Therefore, in research questions that implicitly or explicitly contain aspects of individual plant development, modelling tools that scale up processes at the level of the plant to the level of the canopy can be used. In this chapter, the functional-structural plant (FSP) modelling approach will be introduced. FSP modelling provides the possibilities to simulate individual plants in a stand setting, and their architecture in 3D over time. It can take into account light interception and scattering at the level of the leaf as a function of leaf size, angle and optical properties, and use this information to determine photosynthesis, photomorphogenesis, and overall plant growth and development. Therefore, FSP modelling can be used to translate individual plant behaviour to whole canopy performance while taking into account phenotypic variation between individuals and plastic responses to local conditions, as well as the consequences of active manipulation of plant architecture such as pruning or herbivory.

This chapter will treat the underlying principles of FSP modelling as well as the calibration and validation of such models. It will subsequently describe how the interaction

*Author for correspondence, e-mail: jochem.evers@wur.nl

K. Hikosaka, Ü. Niinemets, and N.P.R. Anten (eds.), *Canopy Photosynthesis: From Basics to Applications*, DOI 10.1007/978-94-017-7291-4_8

between light and a canopy composed of individual plants with their own architecture can be simulated, and how the feedback of photosynthesis, carbon allocation and growth as well as photomorphogenetic processes on light capture can be included.

Keywords Plant architecture • Simulation • Leaf photosynthesis • Sink strength • Crop performance

I. Introduction

The plant kingdom contains an extremely rich variety in plant shape and structure. Plant shape varies from compact and dense to wide and open, from single stemmed to bushy, from crawling to erect. Even individuals within one species can adopt contrasting shapes depending on the variety or on the environmental conditions. The more formal term for plant shape or structure, plant architecture, has been defined as the three-dimensional (3D) organisation of the plant body (Reinhardt and Kuhlemeier 2002). Important components of plant architecture are leaf angle, shape and curvature, branching frequency and orientation, shoot and root length and thickness, *etc*. Together they determine what the plant looks like throughout its development. Plant architecture can be regarded as a concept central in plant growth and development. On the one hand, the genetic make-up of a plant, its internal physiological processes, and environmental factors such as light interception, water uptake, herbivory and competition for resources with other plants determine development of plant architecture. On the other hand, plant architecture itself determines to what extent light can be intercepted, assimilates can be transported from a leaf to a growing tip, water and nutrients can be taken up from the soil by the roots, above- and below-ground signals can be perceived and broadcast. In other words, there is an important feedback loop between plant architecture itself and its determinants. Therefore, to better understand how plants with a specific genetic basis grow and develop in specific environmental conditions, it is essential to take plant architecture into account.

In plant and crop science many research questions are related to one or more aspects of plant architecture. Examples include the distribution of light interception in a canopy (Hirose and Werger 1995), optimal pruning strategies in orchards (Grossman and DeJong 1998), and grass branching in relation to plant population density (Casal et al. 1986). To help address such questions, simulation models have been developed during the last few decades that take into account plant architecture and its development as an integral component. Early models of plant architecture were created mainly with the purpose to descriptively recreate plant architecture itself, mostly based on elegant and robust mathematical algorithms (Prusinkiewicz and Lindenmayer 1990). Soon it was realized that the ability to simulate plant architecture opened up possibilities for problems in plant

Abbreviations: a – Moment of blade appearance; FSP – Functional-Structural Plant; k_1 – Maximum slope of blade length curve; k_2 – Maximum slope of the final blade length curve; l – Normalized blade length; l_f – Final blade length; $l_{f,m}$ – Maximum final blade length on a stem; LAI – Leaf area index; LED – Light emitting diode; p – Phytomer rank; p_o – Phytomer rank at first emerging leaf; PAR – Photosynthetically active radiation; *phyl* – Phyllochron; R:FR – Red to far-red ratio; p_m – Phytomer rank at maximum final blade length; SLA – Specific leaf area; SVAT – Soil-vegetation-atmosphere transfer; tt – Blade age at the inflection point of the relationship between final blade length and phytomer rank; Z – Slope of the phytochrome status to red far-red curve; ϕ – The phytochrome status ζ – Red to far-red ratio; ϕ_r – Phytochrome status at saturating red light; ϕ_{fr} – Phytochrome status at saturating far-red light.

and crop research related to plant architecture (Room et al. 1996; Vos et al. 2007). The resulting modelling approach is called functional-structural plant (FSP) modelling (Godin and Sinoquet 2005). New studies on refinement of FSP modelling in terms of concepts and technicalities, as well as studies that apply FSP modelling to specific plant or crop research problems are currently being conducted at a high rate. Initially these studies were done mostly by researchers with background in modelling, but lately also more and more by plant and crop scientists, who increasingly see simulation modelling as a valuable tool to complement and support experimental research. This chapter focuses on the use of FSP modelling in plant and crop science, with special attention to simulation of light interception, photosynthesis, and photomorphogenesis in herbaceous crops.

II. Functional-Structural Plant Modelling

FSP modelling is used to simulate "the development over time of the 3D architecture or structure of plants as governed by physiological processes which, in turn, depend on environmental factors" (Vos et al. 2010). *Sensu stricto*, models that simulate plant architecture without any mechanistic foundation, *i.e.* purely architectural models, are not FSP models. However in general the term is used for any simulation method that explicitly includes plant architecture. A frequently used synonym of FSP modelling is virtual-plant modelling (Room et al. 1996). FSP models have a rich history of variation in methods of implementation, in degree of complexity and biological realism, as well as in the associated simulation platforms such as L-Studio (Prusinkiewicz et al. 2007), GroIMP (Kniemeyer et al. 2007; Hemmerling et al. 2008), OpenAlea (Pradal et al. 2008), GreenLab (Guo et al. 2006) and L-Py (Boudon et al. 2012), among other platforms. The common denominator of all FSP modelling approaches is the explicit inclusion of (aspects of) plant architecture, which results from the general philosophy behind FSP modelling that plant architecture is a concept central in plant growth and development, as outlined in the introduction of this chapter.

To be able to support research on plant and crop growth and development, FSP modeling has several distinctive properties to offer. Simulation of plant topology, *i.e.* the (2D) structure of the network of interconnected organs, allows simulation of transport of compounds such as assimilates or hormones through the plant from source to sink organs, taking into account the number of nodes to travel and the number of ramifications to encounter. Additionally, simulation of (3D) geometry of the plant and its organs enables simulation of light interception from any direction on leaves and other organs. This enables calculation of local and whole-plant light absorption, which is vital for simulation of photosynthesis and photomorphogenetic processes. Simulation of root system geometry also supports studies for instance on uptake of water and nutrients from spatially heterogeneous soils (Dunbabin et al. 2013). Finally, a property of FSP modelling crucial for questions on plant growth and development in crop sciences is the ability to include external factors such as environmental variables (light, water, nutrients, herbivores, volatiles, *etc.*) and management (plant manipulation, planting pattern or density, biocide spraying, *etc.*).

Typically, an FSP model is defined and calibrated at the level of plant organs such as leaves, internodes, root segments, *etc.* Alternatively, an FSP model is defined at lower levels such as the tissue or cell level (Roeder et al. 2011). In such cases model output is not a whole plant or plant stand, but a tissue or organ such as a developing leaf (Bilsborough et al. 2011) or meristem (Barbier de Reuille et al. 2006). For a comprehensive review of the different types of plant models and aggregation levels, see Prusinkiewicz and Runions (2012).

Most FSP modelling approaches use specific rules to define both plant development (creation of new organs, break of lateral

buds, the switch from vegetative to generative development, etc.) as well as plant growth (the increase in length, size, and/or biomass of existing organs). By repeated application of such so-called string-rewriting rules (Lindermayer systems, Prusinkiewicz and Lindenmayer 1990) or extensions like graph-rewriting rules (Kurth et al. 2005), realistic growth and development of a plant is simulated over time. To illustrate the principle of rewriting, we consider the creation of new organs during the development of a shoot. A shoot can be decomposed into phytomers, the 'building blocks' of a stem that typically consist of an internode, a leaf petiole/sheath, a leaf blade, and a lateral meristem. In classic L-system notation (Prusinkiewicz and Lindenmayer 1990) a phytomer can be represented by a string of characters:

$$\mathrm{I}\,[\mathrm{M}][\mathrm{L}]$$

with an internode I, a meristem M and a leaf L. M and L are placed within square brackets to indicate the structures they represent branch off the main axis (note this makes [M] a lateral meristem). An L-system rewriting rule that codes for the production of new phytomers by a meristem could look like:

$$\mathrm{M} ==> \mathrm{I}\,[M][\mathrm{L}]\;\;\mathrm{M}$$

This rule dictates that in one time step, every M should be replaced (==>) by a phytomer with a meristem M on top. Assuming a starting situation in which only one M is present, applying this rule several times give rise to an exponentially developing structure:

Start: M
Step 1: I [M] [L] M
Step 2: I [I [M] [L] M] [L] I [M] [L] M
Step 3: I [I [I [M] [L] M] [L] I [M] [L] M] [L] I [I [M] [L] M] [L] I [M] [L] M

Figure 8.1 illustrates the development of this structure visually. Plant components can be given variables (such as age) and application of rewriting rules can be made dependent on those variables, using conditions. For instance, the above-mentioned rewriting rule could be provided with the condition that a new phytomer should only be formed if the age of the apical meristem has reached a certain value. Also, a lateral meristem could be prevented from developing a branch unless a number of conditions for bud break are met. This way, a network of plant organs can be created that represent the topology over time of actual plants. To introduce the second important component of FSP modelling, geometry, primitive shapes such as those shown in Fig. 8.1 are replaced with more realistic ones, and variables for organ dimensions, orientation, angle, curvature can be provided to the plant components. Similar to rewriting rules, updating rules can be applied every time step to increase organ size, change the angle, etc. Finally, the combination of plant topology and geometry results in accurate descriptive representations of actual plant architectural development over time.

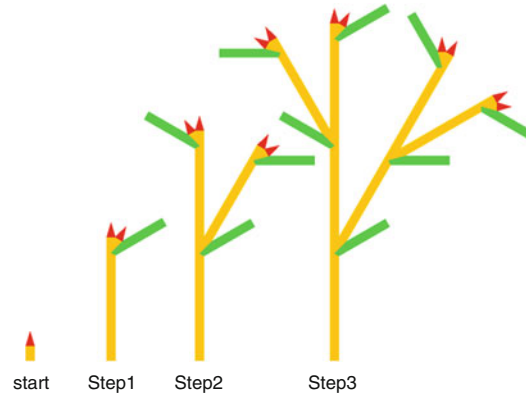

Fig. 8.1. Visual representation of applying the rewriting rule M == > I [M] [L] M three times to a starting situation with only an apical meristem. The *red triangles* represent apical or lateral meristems (M), the *green* objects are leaves (L), and the *orange* objects are internodes (I). The orientation of the organs is chosen such that clarity of the illustration is optimised. The visualisation for each step corresponds to the strings of characters in the main text

To be able to perform meaningful scenario studies using such a model of plant architecture, it needs to be calibrated and validated for

the species and conditions of interest in terms of rate of development, organ sizes and positions, *etc*. The following section will deal with calibration and validation of a descriptive model of plant architecture. However, the true power of FSP modeling emerges when the physiological and environmental processes that actually drive growth and development are added. For instance, by replacing rules that describe organ growth with routines for assimilate acquisition and allocation, and by adding calculation of light absorption and nutrient uptake, above- and below-ground growth can be simulated mechanistically, as an emergent property of the model (Allen et al. 2005; Evers et al. 2010b; Cieslak et al. 2011; Xu et al. 2011; Dunbabin et al. 2013). Therefore, in Sect. IV onwards, gradually the addition of several external factors and physiological processes will be outlined, leading to a mechanistic simulation model of plant growth and development. Note that it is generally not recommended to implement a great number of internal and external factors regulating plant growth and development in one FSP model. This could lead to simulation output that is hard to interpret. Only the factors of interest should be incorporated, leaving the remaining parts of the model descriptive.

III. Calibration of an Architectural Model

Including realistic plant architecture in simulation modelling requires this architecture to be calibrated. As mentioned above, calibration of an architectural plant model usually occurs at the level of the organ. Therefore, experimental data acquisition and interpretation should be done for individual organs. In contrast, validation of an architectural model is usually done at the level of the whole plant or the plant canopy, requiring data at those levels to be acquired. Due to the focus of this book on light interception and photosynthesis, this chapter will be limited to above-ground plant parts only.

A. Architectural Data

Data gathering at the organ level implies careful labelling and tracking of individual organs from the start, since in advanced stages of plant development it is easy to lose track and confuse organs. Organs are identified using their phytomer rank. All organs that belong to a phytomer share a phytomer rank value. Phytomers are usually counted from the bottom upwards, *i.e.* the bottom-most leaf has rank 1, the third internode from the bottom has rank 3, etc. Phytomers on branches are identified by their rank number within the branch as well as the rank number of the phytomer that carries the branch. For instance, the third leaf on a branch that grows on the fourth phytomer of the main stem has rank 4.3.

Architectural variables that need to be collected for calibration can be categorized as follows: (a) rates of organ initiation, appearance, maturity and death; (b) organ extension; (c) final organ size; (d) geometrical organ features such as angle, orientation and shape; (e) probability of branch formation by individual buds. In case the architectural model is used for simulation of light interception and scattering, also data on (f) optical properties of the leaves and stems need to be collected.

(a) Organ initiation on the apex can be determined by microscopic inspection of the shoot apex, whereas organ appearance, maturity and death can be monitored non-destructively simply by scoring. For simplicity and depending on the species of interest, organ appearance can often be used as a proxy for organ initiation, although in grasses and cereals the rate of organ initiation and appearance may differ substantially McMaster (2005). Figure 8.2 shows typical relationships between these four variables and thermal time; in a descriptive architectural model these relationships would serve as input. Note that in many cases these relationships may not be linear, in contrast to what is shown in Fig. 8.2. Bilinear, exponential, and sigmoid relationships are also found and may vary with species, variety and/or environmental conditions.

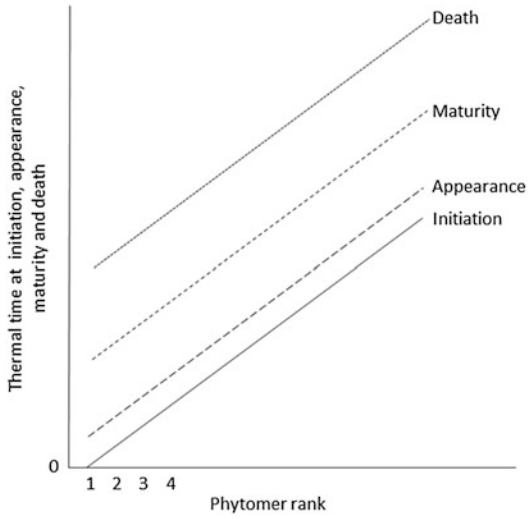

Fig. 8.2. Typical relationships between moments of initiation, appearance, maturity and death of organs and their phytomer rank. Note that these relationships are not necessarily applicable to all organs. For example, leaves may die at some stage but internodes remain alive much longer. The time between appearance and death of a leaf is the 'functional time' of a leaf, *i.e.* the period of time in which a leaf can photosynthesize and contribute carbon to the plant. The time between initiation and death is the organ life span. The time between initiation and maturity is the extension period of the organ. In the case of the linear relationships shown here, the slope of the initiation line is called the 'plastochron', and the slope of the appearance line is called the 'phyllochron'. Here, thermal time was set to 0 at initiation of the first organ

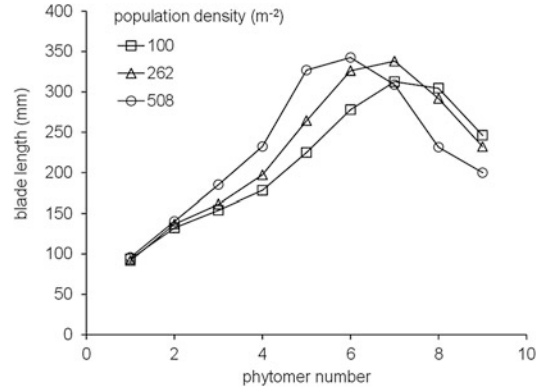

Fig. 8.3. Final blade length *vs.* phytomer rank for spring wheat grown at three population densities. At all three population densities the bell-shaped curve can be observed (J.B. Evers, unpublished)

(b) Organ extension can be monitored non-destructively or obtained from sampled plants. Like most growth processes the relationship between organ extension and time is bell-shaped and the corresponding relationship between organ size and time is sigmoidal (for example Fournier et al. 2005). By normalizing all size data with the final size of the organ, curve characteristics of organ extension independent of organ size can be obtained. Extension data is best gathered using a simple ruler or by analysis of digital images.

(c) Final organ size can be obtained non-destructively in the case of leaf blades and petioles. For partially hidden organs like sheaths and internodes, plant sampling is usually necessary. The type of relationships between final organ size and phytomer rank heavily depends on the organ type. For example, in cereals the leaf blade, leaf sheath and internode size relationships with phytomer rank are usually bell-shaped, linear to slightly sigmoidal and linear, respectively. Also, environmental conditions may effect final organ size. Figure 8.3 shows the effect of population density on the final size distribution of wheat blades along a stem. Although the shape of the three curves are similar, the steepness and the location and value of the peak differ between population densities.

(d) Organ geometry is a key aspect for plant architectural models: it determines the overall shape of the plant but more importantly, it determines light interception which is crucial for computation of light interception and light signal perception by individual plants, as well as for computation of light penetration in a canopy. Geometrical features can be obtained using an array of methods. A protractor can very directly deliver data on leaf and branch angles and phyllotaxis (the angle between successive leaves on a stem). The same information can also be obtained from digital photos in combination with analysis software. More sophisticated methods allow capturing 3D plant skeletons or dense point clouds, which can be analysed to derive geometrical

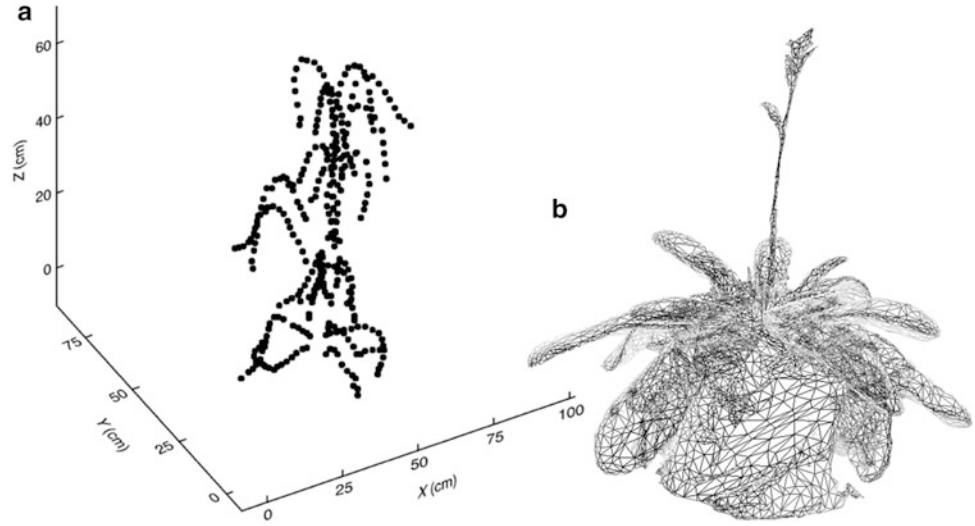

Fig. 8.4. Visual output of 3D digitising. (**a**) X, Y and Z coordinates expressed in distance (cm) to the reference point for the leaves of one spring wheat plant at booting stage. Data obtained using a magnetic digitiser. From Evers et al. (2005), reprinted with permission from Wiley-Blackwell. (**b**) Wireframe model of an Arabidopsis rosette and primary stem, obtained using the profiling method

features as well as sizes of visible organs. Such methods include sonic or magnetic touch-probe digitizing (for example Sinoquet et al. 1998; Evers et al. 2005) (Fig. 8.4a), laser scanning and profiling (Fig. 8.4b). In the latter method, photos taken from all sides of the plant are combined to reconstruct the plant in 3D. Additionally, leaf shape can be obtained from top-down photos of flattened leaves or using a flatbed scanner. An advantage of methods that produce point clouds from which the relevant parameters can be determined is that it will remain possible to return to the data to extract other parameters, long after the original plants ceased to exist.

(e) Bud fate, *i.e.* the decision whether a bud remains dormant or produces a branch, is a highly plastic plant trait, influenced by a multitude of internal and external factors (Domagalska and Leyser 2011). Therefore, in purely descriptive models of plant architecture, branching is best captured by collecting probabilities of buds to grow out into a branch, in relation to some canopy variable such as leaf area index, light interception or population density. In more mechanistic models processes that drive shoot branching can be incorporated, see Sect. VI on simulation of photomorphogenesis.

(f) Optical properties of organs include reflectance, transmittance and absorbance, and can be collected for any wavelength or waveband of interest (*e.g.* photosynthetically active radiation, 400–700 nm, or only red, green, blue, or far-red light) using a spectrophotometer. Ideally, the optical properties should be gathered for organs of different ages, as the properties are affected by chlorophyll content.

Architectural data for model validation needs to be collected from independent experiments. Variables of interest for validation are for example plant leaf area, leaf area index, ground cover fraction and light penetration at soil level. These plant or canopy-level variables are the combined results of organ-level variables. For example, plant leaf area combines leaf appearance, extension and death as well as branching. Canopy light penetration at soil level adds to this internode extension and size, leaf angles, curvature and phyllotaxis, as well as organ optical properties.

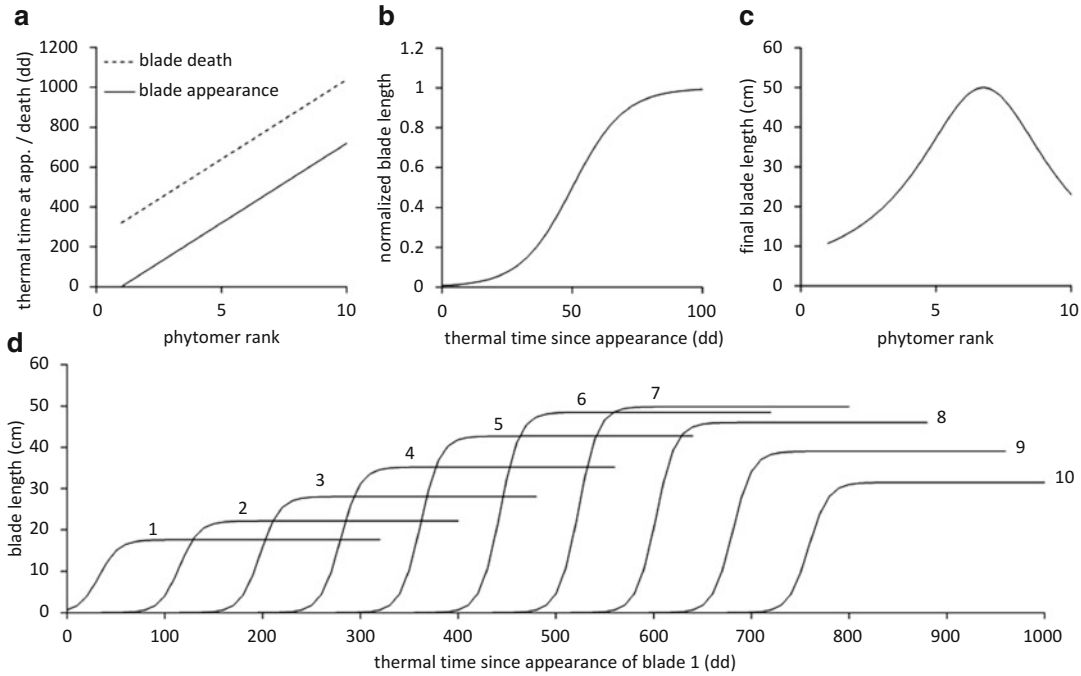

Fig. 8.5. Relationships that can be used to calibrate leaf blade development in an architectural model. (**a**) Moment of appearance of new leaf blades and moment of death. (**b**) Elongation of leaf blades in time. (**c**) Final blade length distribution along an axis. (**d**) Combining the relationships from (**a**), (**b**) and (**c**) yields the kinetics of leaf blade appearance, elongation to a certain size and death. The numbers at the individual lines indicate the phytomer rank of the blade the line represents

B. The Calibration Process

All architectural data gathered should be analysed and proper functions should be chosen to fit the data against phytomer rank or (thermal) time. As an example, we consider leaf blade development. Blade appearance can be calibrated using simple linear function (Eq. 8.1):

$$a = phyl \cdot (p - p_o) \tag{8.1}$$

where a is the moment of blade appearance (degree days), *phyl* is phyllochron (the thermal time between the appearances of two consecutive blades, degree days), p is phytomer rank of the blade, and p_o is the phytomer rank at which a should be 0 (*i.e.* plant emergence). Figure 8.5a shows this relationship for parameter values $phyl = 80$ dd and $p_0 = 1$.

Blade length increase can be calibrated using a sigmoid relationship between normalized blade length and blade age (Eq. 8.2):

$$l = \frac{1}{1 + e^{-k_1 \cdot (tt - tt_i)}} \tag{8.2}$$

where l is normalized blade length (in cm), k_1 is the maximum slope of the curve (*i.e.* the slope at the inflection point), tt is blade age since appearance (degree days) and tt_i is age at the inflection point of the curve. Note that many other equations with an equal or higher number of parameters give similar sigmoid relationships (Yin et al. 2003) depending on the flexibility needed to fit the data well. An example is shown in Fig. 8.5b for parameter values $k_1 = 0.1$ and $tt_i = 50$ dd. In architectural models that include external influences on blade extension, it is more appropriate to

calculate blade extension per time step (*i.e.* the first derivative of Eq. 8.2) and to add this to the current length using a differential equation, instead of calculating length directly.

To simulate the actual length of a blade at a certain phytomer rank instead of its normalized length, the result of Eq. 8.2 needs to be multiplied with the result of an equation that calculates final blade length as a function of phytomer rank. An equation that would be appropriate to fit the final blade length data shown in Fig. 8.3 could be the Cauchy-Lorentz distribution function (Eq. 8.3):

$$l_f = \frac{l_{f,m}}{1 + \left(\frac{p - p_m}{k_2}\right)^2} \tag{8.3}$$

where l_f is final blade length (cm), $l_{f,m}$ is maximum final blade length on a stem, p_m is the phytomer rank at which the maximum final blade length is found (*i.e.* the location of the peak of the curve), and k_2 represents the maximum slope of the curve. Figure 8.5c shows Eq. 8.3 for the parameter values $l_{f,m} = 50$ cm, $p_m = 6.75$ and $k_2 = 3$. Blade death is modelled taking a blade longevity of 4 phyllochrons (dashed lines in Fig. 8.5a). Combining all relationships shown in Fig. 8.5a–c allows calculation of the kinetics of all individual leaves on a stem, as shown in Fig. 8.5d. After implementing the relationships in Fig. 8.5a–c, running the model will provide output as shown in Fig. 8.5d. Comparable methods of calibration can be used to calibrate all other aspects of plant architecture, including phyllotaxis and the progressive change in leaf angle or curvature as a leaf develops.

An important consideration in the calibration of a model of plant architecture lies in the use of stochastic elements. If parameter values obtained through fitting or otherwise show great variability, the modeller may decide not to include one parameter value but a probability distribution of values for a particular parameter. Each model run a value will then be picked from this probability distribution randomly. This results in model stochasticity, which gives different plant architectures each new simulation. Also the use of probabilities for bud fate, as discussed above, gives this result. When simulating plant stands, this stochasticity results in canopies composed of plants differing in terms of their architecture, which resembles the actual situation in crop canopies in which no plants are identical.

IV. Simulation of Light

One of the most well-developed and frequently used environmental drivers in FSP model simulations is light. The explicit inclusion of plant architecture in FSP modelling allows for the simulation of absorption and scattering of radiation of various wavelengths by individual organs or even parts of organs (for example in case of long or compound leaves) – crucial for simulation of photosynthesis or photomorphogenesis. At least two components need to be specified. (I) The source of light, and its characteristics such as direct and/or diffuse, its intensity, its spectral composition, its location in the virtual sky or greenhouse/growth chamber, and the degree of divergence of the radiation. (II) The optical properties of the plant organs, *i.e.* the absorbance, reflectance and transmittance of the radiation incident on the organ, as a function of wavelength or waveband.

Depending on the type of study the modeller may choose to use only one single light source of constant intensity in all wavelengths directly above the plant or canopy. For very realistic conditions the modeller may choose for a combination of light sources that represent direct sunlight and diffuse skylight at an intensity and location depending on time of the day, day of the year, and geographical location, and possibly greenhouse lamps and even additional light-emitting diodes (LEDs) above or in between the plants mimicking actual setups. An example of such a realistic greenhouse light environment in FSP modelling can be

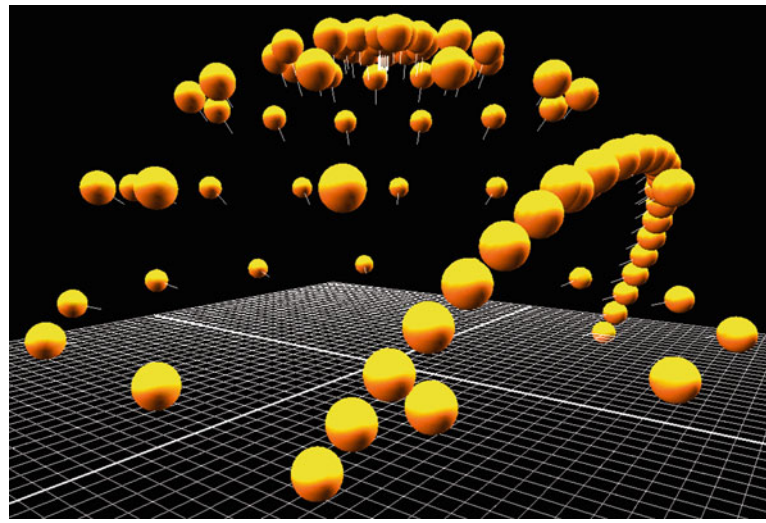

Fig. 8.6. Location of direct and diffuse light sources (represented by *spheres* for visualisation) as used in an FSP model that runs at a daily time step. The arc of light sources represents the direct light during a day, and the dome of light sources represents diffuse light. The *thin line* sticking out of each sphere indicates the direction of the radiation path

found in Buck-Sorlin et al. (2011). For a typical field crop situation, both direct sunlight and diffuse skylight can be included. For simulation models that use an hourly time step, direct sunlight can be approximated by a single light source that changes position and intensity every hour of the day. For models with a daily time step, an arc of light sources of different radiation intensity can be used that represent the daily course of the sun. In both cases, day of the year and location on the globe further determine the location of the light source(s) with respect to the simulated plants. Simulation of diffuse light is somewhat less straight-forward, due to the fact that diffuse light comes from all directions instead of from a (moving) point source. In many cases, diffuse light is approximated by a dome of weak light sources, arranged in rings at different elevations (Chelle and Andrieu 1999; Evers et al. 2007, 2010b; Buck-Sorlin et al. 2011). Figure 8.6 shows an example of a combination of an arc of light sources representing direct light during a day, and a dome of light sources representing diffuse light. The intensity of the light sources can be taken from actual weather data, or can be calculated using mathematical approximations (Spitters 1986; Spitters et al. 1986; Goudriaan and Van Laar 1994).

In FSP modelling several methods are available to simulate light. A well-known method is the so-called radiosity method (Borel et al. 1991; Chelle and Andrieu 1998) which is used in a number of FSP modelling studies (for example Chelle et al. 2007; Evers et al. 2010b; Sarlikioti et al. 2011). The radiosity method enables calculation of radiation on plants using a system of linear equations, under the assumption that all plant elements are diffusely reflecting (*i.e.* Lambertian) surfaces (Chelle 2006). Another frequently used method to simulate light in FSP modelling is ray tracing (Cieslak et al. 2008; Hemmerling et al. 2008). The ray tracing method entails casting of millions of rays from the light sources and tracing of those rays as they interact with canopy elements in terms of reflection, transmission and absorption. By taking the number of rays high enough, a representative distribution of radiation in the canopy can be obtained, and the light absorbed or perceived by organs can be calculated (Hemmerling et al. 2008; Buck-Sorlin et al. 2011; Cieslak et al. 2011).

In FSP modelling, light characteristics of a developing canopy can be simulated at the (sub-)organ level. Visual simulation output as shown in Fig. 8.7 displays the extent of the variability between light interception by individual leaves depending on their orientation and location in the canopy (bright *vs.* dark

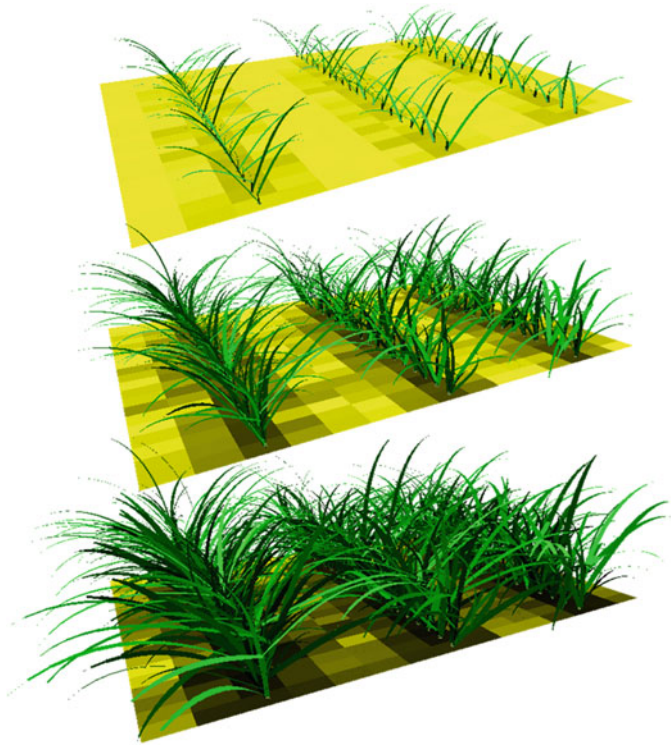

Fig. 8.7. Visual output of the FSP model of wheat development at three stages of early development. The brightness of the soil tiles below the simulated plants represent the PAR (photosynthetically active radiation) intensity at each tile, which decreases as the crop canopy develops and intercepts an increasing amount of light. The brightness of the leaves represent the amount of light intercepted by each individual leaf (J.B. Evers, N.I. Huth and M. Renton, unpublished). Wheat model based on Evers et al. (2005)

leaves), as well as the variation in light penetration at soil level (bright *vs.* dark tiles). This highlights a fundamental difference between FSP modelling and the more traditional crop models, which approach the plant canopy as a homogeneous layer of leaves. In such crop models, interception of light as a function of LAI (m^2 leaf per m^2 ground area) is usually calculated using the classical Lambert-Beer equation (Monsi and Saeki 1953) that has a parameter called the extinction coefficient, denoted by k. The value of k highly depends on architectural characteristics of the canopy (Goudriaan 1988) and the state of canopy development. Also, its value differs between direct and diffuse light. Chapter 1 (Goudriaan 2016) deals with these aspects of light interception in homogenized canopies in detail. In FSP modelling on the other hand, k can be calculated based on the simulated interception of light by the canopy, making k an output rather than an input. This opens up the possibility to use an FSP model to calculate k values for specific species, architectural characteristics and plant configuration, and to use the k values found and their variation through the growing season as input in traditional crop models (Evers et al. 2010a).

The combination of an architectural model of plant development and a light model to simulate interception and scattering of light, as discussed in this section, basically acts one-way: the architecture of the plants determines to what extent light is intercepted and scattered, and not *vice versa*. To be able to simulate the feedback between light interception or light signal perception and plant growth and development, functional relationships or underlying mechanisms on photosynthesis or photomorphogenesis need to be included. This leads to a model construct that fully follows the definition of an FSP model.

V. Simulation of Photosynthesis and Carbon Allocation at the Organ Level

As described in Sect. III, the growth rates and final sizes of organs in architectural models of plant development are directly calibrated. Such models are descriptive. However, in FSP models aiming at simulation of growth and development of plants driven by light, growth rate and organ size should be an output of the model rather than an input. Such models are mechanistic, because they are based on the underlying mechanisms that drive growth.

The first step towards simulation of plant growth driven by light is the incorporation of photosynthesis routines. As each organ has its own individual level of photosynthetically active radiation (PAR) intercepted each time step, photosynthesis can also be calculated at the level of the plant organ each time step. A relatively straight-forward way to accomplish this is to use a photosynthesis-light-response curve to convert the amount of PAR absorbed to an instantaneous rate of photosynthesis. This rate can be scaled up to the level of the simulation time step (*e.g.* 1 h) and multiplied by the area of the leaf, leading to a value of assimilated CO_2 per hour for each individual leaf. However, the most popular model implementation of photosynthesis, also in FSP models, is the biochemical model of Farquhar et al. (1980), used in FSP models of tomato (Sarlikioti et al. 2011), rice (Xu et al. 2011), cucumber (Wiechers et al. 2011), rose (Buck-Sorlin et al. 2011), wheat (Evers et al. 2010b) and several others. Due to the fact that the Farquhar model was originally designed as a leaf photosynthesis model, it can be directly implemented at the level of the leaf (and other organs) in an FSP model, without any leaf area upscaling or other conversions. Leaf photosynthesis modelling is extensively covered in Chap. 3 (Hikosaka et al. 2016a).

The parameters of any implementation of organ-level photosynthesis can be coupled to relevant organ variables such as organ nitrogen content, temperature, stomatal conductance, CO_2-concentration, and transpiration (Müller et al. 2005; Yin and Van Laar 2005). For example, in the wheat FSP model presented in Evers et al. (2010b) organ photosynthesis rate was calculated using a combined model of photosynthesis, stomatal conductance and chloroplast CO_2-concentration. The parameters of this coupled model were made functions of PAR absorbed, organ nitrogen content (taken from measurements) and organ temperature. Due to the mutual dependence of organ temperature on one side and organ photosynthesis and transpiration on the other, an iterative procedure was used, taking air temperature instead of organ temperature in the first round of estimation of photosynthesis and transpiration. This procedure led to converging values for the three variables. In theory, accuracy of the calculation of such organ-level variables can be improved by combining the architectural detail of FSP models with the microclimatic detail of soil-vegetation-atmosphere (SVAT) models (Duursma and Medlyn 2012; Kobayashi et al. 2012). To date, this task has not been taken up.

Once the amount of assimilated CO_2 in an organ is calculated, the amount of substrates available for plant growth can be calculated taking into account the mitochondrial and maintenance respiration rates. From this point onwards, there are several ways to model allocation of substrates to growing organs (Marcelis and Heuvelink 2007). The organ may use the substrates it requires to grow itself, and export the remainder. Its substrate may be allocated to nearby growing organs first and the remainder to more remote ones. Alternatively, all new substrates may be gathered in a plant-wide pool from which substrates are distributed throughout the plant. This central-pool hypothesis is part of the so-called relative-sink-strength principle (Heuvelink 1996), which dictates that substrates are allocated to growing organs according to their relative sink strength, *i.e.* their potential growth rate (in units of substrate demanded per unit of

time) proportional to the potential growth rate of the whole plant. Taking into account growth respiration, the amount of substrates allocated to an organ is either equal to their demand in the case in the case substrate availability is sufficient, or a fraction of the available substrates equal to their relative sink strength, in the case the amount of available substrates is insufficient to meet total plant demand. In the former case, excess substrates can be stored in the pool and used in the next model time step. Finally, organ growth can be calculated by using empirical relationships between organ size and organ biomass. For leaf blades, this could be SLA (specific leaf area), which may be taken as a constant or dependent on phytomer rank. In the next model time step, the updated organ sizes determine light interception, and the cycle continues.

At each point during the simulation, canopy characteristics such as canopy photosynthesis can be calculated. This can be done simply by adding photosynthesis rates of the individual organs. In contrast to models approximating a canopy as a homogeneous layer, there is no need to make calculations such as the fraction of sunlit leaves in the canopy, or PAR extinction as a function of canopy depth. In FSP modelling, PAR absorption and photosynthesis are calculated at the organ level, making up-scaling to the canopy level straight-forward. The downside of FSP models versus for instance single or multi-layer models and big-leaf models (see Chap. 9, Hikosaka et al. 2016b) is the much larger parameter demand of FSP models.

VI. Simulation of Photomorphogenesis

Next to simulation of photosynthesis and organ growth, another powerful application of a model of plant architecture interacting with incoming light is simulation of photomorphogenesis (see Chap. 6, de Wit and Pierik 2016). Light signals at any location in the virtual canopy can be simulated. Of special interest for FSP modelling is the ratio between the intensities of red and far-red light (R:FR). As a component of PAR, red light is mostly absorbed by plant tissues whereas far-red light is mostly reflected and transmitted. This results in scattering of light with a low R:FR among the leaves and stems within a canopy. Due to the high variability of R:FR in a canopy (Chelle et al. 2007), an approach such as the Lambert-Beer relationship between PAR and LAI is not possible for R:FR. Figure 8.8 illustrates this variability in R:FR for a simulated Arabidopsis canopy. Therefore, to simulate canopy R:FR properly, an approach that takes into account the spatial and temporal heterogeneity in canopy architecture such as FSP modelling is indispensable (Bongers et al. 2014). For example, in a study on leaf angle effects on R:FR signalling in Arabidopsis (de Wit et al. 2012), leaf-level R:FR simulations (Fig. 8.8) supported experimental evidence that R:FR is not responsible for early changes in leaf angle as observed in Arabidopsis canopies.

Similar to photosynthesis, photomorphogenesis can be simulated either descriptively using empirical relationships between light signals and plant response (dose-response

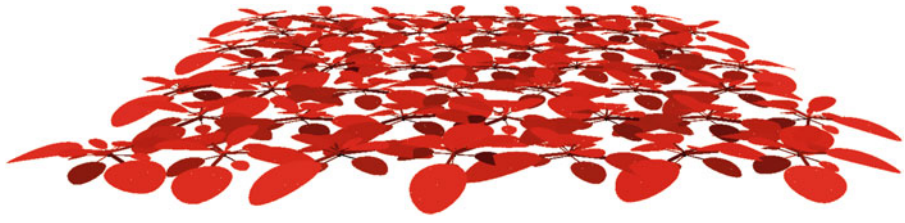

Fig. 8.8. Simulated canopy of 49 hexagonally placed Arabidopsis rosettes. The brightness of the leaves represents R:FR on the leaf, ranging from 0 (*black*) to 1.2 (*bright red*)

curves), or more mechanistically by implementing physiological processes driving the plant's response to a light signal. For example, a model of white clover development (Gautier et al. 2000) included empirical relationships between PAR intensity, R:FR and responses in internode length, petiole length and branching. In Evers et al. (2007) a number of possible relationships between R:FR and the growth rate of axillary buds was implemented in a simulation model of wheat development. Models like these allow simulation of plant plasticity, with (aspects of) plant architecture representing the response to light signals the plant encountered during development. When simulating canopies of plants, this results in differences between individual plant architectures depending on their local light conditions, e.g. a plant at the border of a stand vs. a plant in the center.

Light signals are perceived by photoreceptors such as phytochromes (for details see Chap. 6, de Wit and Pierik 2016). In mechanistic simulation models of photomorphogenesis, including the effect of light signals on the status of such photoreceptors is the step that translates an environmental signal into a plant physiological state. For instance, the relationship between R:FR and phytochrome status can be described by the following equation (Burema 2007):

$$\phi = 1 - \frac{\zeta + Z}{\frac{\zeta}{1-\phi_r} + \frac{Z}{1-\phi_{fr}}} \qquad (8.4)$$

In Eq. 8.4, ϕ is the phytochrome status, expressed as the fraction of phytochrome in its active form, ζ is R:FR, ϕ_r is phytochrome status at very high R:FR (saturating red light), ϕ_{fr} is phytochrome status when R:FR is 0 (saturating far-red light), and Z determines the slope of the curve. Suitable parameter values are $\phi_r = 0.75$, $\phi_{fr} = 0.03$ and $Z = 1.7$, all dimensionless (Smith and Holmes 1977; Burema 2007). The hyperbolic shape of this relationship is shown in Fig. 8.9. R:FR simulated at the level of the organ can thus be converted into phytochrome status of that organ. Subsequently, organ phytochrome status can drive specific physiological processes such as hormone biosynthesis and/or transport, or even expression of plasticity-related genes (Kebrom et al. 2006; Tao et al. 2008; Keuskamp et al. 2010). For example, the production of branches from dormant axillary buds is known to be regulated by such internal factors (McSteen 2009; Domagalska and Leyser 2011) as well as by R:FR perceived by the plant (Casal et al. 1987; Finlayson et al. 2010). An FSP model could be constructed that combines simulation of hormonal regulation of shoot branching (Prusinkiewicz et al. 2009) with simulation of light signalling within a developing plant canopy as described above. This would lead to an environmentally sensitive mechanistic simulation model of shoot branching (Evers et al. 2011).

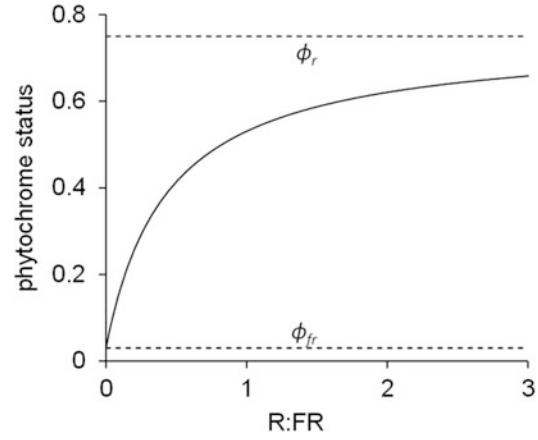

Fig. 8.9. Relationship between phytochrome status (ϕ in Eq. 8.4) and R:FR (ζ in Eq. 8.4). Values of parameters ϕ_r and ϕ_{fr} are shown as *dashed lines*

Applied to crops, such a modelling approach potentially predicts branching behaviour of individual plants in a crop canopy, responding to competition for light with conspecific individuals or weeds. Similar mechanisms could be implemented to simulate other aspects of photomorphogenesis, such as adjustments of leaf angle and orientation or stem extension. Especially when combined with photosynthesis and carbon

allocation, detailed simulation of plants responding to above-ground competition for light in terms of both growth and development can be conducted. However, such complex models require all components to be parameterized well and implemented in a balanced way. Taking into account the fact that modelling only above-ground competition represents really only half of the total picture, a more reliable way of approaching competition processes is to focus on individual mechanisms that play a role, keeping the remainder of the model descriptive.

VII. Conclusions

Being able to simulate plant architecture and processes that play a role in its determination opens up exciting possibilities. Many research questions that deal with crop development, competition, physiology, microclimate, but also crop management (row spacing and density, pruning, spraying of biocides, *etc.*) are related to the architecture of the plants, making an FSP modelling approach to these questions potentially valuable (Zhu et al. 2015). However, applying FSP modelling comes at a cost. As mentioned before, its parameter requirement is generally higher than of conventional types of simulation modelling due to the inclusion of architecture. Also, computational requirements are not modest, especially when including simulation of light and/or transport processes in the simulated plants (not covered in this chapter). Nevertheless, if these obstacles can be overcome, FSP modelling offers a wealth of possibilities in plant and crop science at various levels of biological integration.

References

Allen MT, Prusinkiewicz P, DeJong TM (2005) Using L-systems for modeling source-sink interactions, architecture and physiology of growing trees: the L-PEACH model. New Phytol 166:869–880

Barbier de Reuille P, Bohn-Courseau I, Ljung K, Morin H, Carraro N, Godin C, Traas J (2006) Computer simulations reveal properties of the cell-cell signaling network at the shoot apex in Arabidopsis. Proc Natl Acad Sci U S A 103:1627–1632

Bilsborough GD, Runions A, Barkoulas M, Jenkins HW, Hasson A, Galinha C, . . ., Tsiantis M (2011) Model for the regulation of *Arabidopsis thaliana* leaf margin development. Proc Natl Acad Sci USA 108:3424–3429

Bongers FJ, Evers JB, Anten NPR, Pierik R (2014) From shade avoidance responses to plant performance at vegetation level: using virtual plant modelling as a tool. New Phytol: 204, 268–272.

Borel CC, Gerstl SAW, Powers BJ (1991) The radiosity method in optical remote sensing of structural 3-D surfaces. Remote Sens Environ 36:13–44

Boudon F, Pradal C, Cokelaer T, Prusinkiewicz P, Godin C (2012) L-Py: an L-System simulation framework for modeling plant development based on a dynamic language. Front Plant Sci 3:76

Buck-Sorlin GH, de Visser PHB, Henke M, Sarlikioti V, van der Heijden GWAM, Marcelis LFM, Vos J (2011) Towards a functional-structural plant model of cut-rose – simulation of light environment, light absorption, photosynthesis and interferences with the plant structure. Ann Bot 108:1121–1134

Burema BS (2007) *Arabidopsis silicana*, Shade Avoidance Responses in a Virtual Plant Model. MSc Thesis Plant Sciences, Wageningen UR, Wageningen

Casal JJ, Sánchez RA, Deregibus VA (1986) The effect of plant density on tillering: the involvement of R/FR ratio and the proportion of radiation intercepted per plant. Environ Exp Bot 26:365–371

Casal JJ, Sánchez RA, Deregibus VA (1987) Tillering responses of *Lolium multiflorum* plants to changes of red/far-red ratio typical of sparse canopies. J Exp Bot 38:1432–1439

Chelle M (2006) Could plant leaves be treated as Lambertian surfaces in dense crop canopies to estimate light absorption? Ecol Model 198:219–228

Chelle M, Andrieu B (1998) The nested radiosity model for the distribution of light within plant canopies. Ecol Model 111:75–91

Chelle M, Andrieu B (1999) Radiative models for architectural modelling. Agronomie 19:225–240

Chelle M, Evers JB, Combes D, Varlet-Grancher C, Vos J, Andrieu B (2007) Simulation of the three-dimensional distribution of the red:far-red ratio within crop canopies. New Phytol 176:223–234

Cieslak M, Lemieux C, Hanan J, Prusinkiewicz P (2008) Quasi-Monte Carlo simulation of the light environment of plants. Funct Plant Biol 35:837–849

Cieslak M, Seleznyova AN, Hanan J (2011) A functional–structural kiwifruit vine model integrating architecture, carbon dynamics and effects of the environment. Ann Bot 107:747–764

de Wit M, Pierik R (2016) Photomorphogenesis and photoreceptors. In: Hikosaka K, Niinemets Ü, Anten N (eds) Canopy Photosynthesis: From Basics to Applications. Springer, Berlin, pp 171–186

de Wit M, Kegge W, Evers JB, Vergeer-van Eijk MH, Gankema P, Voesenek LACJ, Pierik R (2012) Plant neighbor detection through touching leaf tips precedes phytochrome signals. Proc Natl Acad Sci U S A 109:14705–14710

Domagalska MA, Leyser O (2011) Signal integration in the control of shoot branching. Nat Rev Mol Cell Biol 12:211–221

Dunbabin VM, Postma JA, Schnepf A, Pagès L, Javaux M, Wu L, Leitner D, . . ., Diggle AJ (2013) Modelling root-soil interactions using three-dimensional models of root growth, architecture and function. Plant Soil 372:93124

Duursma RA, Medlyn BE (2012) MAESPA: a model to study interactions between water limitation, environmental drivers and vegetation function at tree and stand levels, with an example application to $[CO_2] \times$ drought interactions. Geosci Model Dev 5:919–940

Evers JB, Vos J, Fournier C, Andrieu B, Chelle M, Struik PC (2005) Towards a generic architectural model of tillering in Gramineae, as exemplified by spring wheat (*Triticum aestivum*). New Phytol 166:801–812

Evers JB, Vos J, Chelle M, Andrieu B, Fournier C, Struik PC (2007) Simulating the effects of localized red:far-red ratio on tillering in spring wheat (*Triticum aestivum*) using a three-dimensional virtual plant model. New Phytol 176:325–336

Evers JB, Huth NI, Renton M (2010a) Light extinction in spring wheat canopies in relation to crop configuration and solar angle. In: Li B, Jaeger M, Guo Y (eds) Plant Growth Modelling, Simulation, Visualization and Applications – PMA09. IEEE, Beijing, China, pp 107–110

Evers JB, Vos J, Yin X, Romero P, van der Putten PEL, Struik PC (2010b) Simulation of wheat growth and development based on organ-level photosynthesis and assimilate allocation. J Exp Bot 61:2203–2216

Evers JB, van der Krol AR, Vos J, Struik PC (2011) Understanding shoot branching by modelling form and function. Trends Plant Sci 16:464–467

Farquhar GD, von Caemmerer S, Berry JA (1980) A biochemical model of photosynthetic CO_2 assimilation in leaves of C_3 species. Planta 149:78–90

Finlayson SA, Krishnareddy SR, Kebrom TH, Casal JJ (2010) Phytochrome regulation of branching in arabidopsis. Plant Physiol 152:1914–1927

Fournier C, Durand JL, Ljutovac S, Schaufele R, Gastal F, Andrieu B (2005) A functional-structural model of elongation of the grass leaf and its relationships with the phyllochron. New Phytol 166:881–894

Gautier H, Měch R, Prusinkiewicz P, Varlet-Grancher C (2000) 3D Architectural modelling of aerial photomorphogenesis in white clover (*Trifolium repens* L.) using L-systems. Ann Bot 85:359–370

Godin C, Sinoquet H (2005) Functional-structural plant modelling. New Phytol 166:705–708

Goudriaan J (1988) The bare bones of leaf-angle distribution in radiation models for canopy photosynthesis and energy exchange. Agric For Meteorol 43:155–169

Goudriaan J (2016) Light distribution. In: Hikosaka K, Niinemets Ü, Anten N (eds) Canopy Photosynthesis: From Basics to Applications. Springer, Berlin, pp 3–22

Goudriaan J, Van Laar HH (1994) Modelling Potential Crop Growth Processes. Kluwer Academic Publishers, Dordrecht

Grossman YL, DeJong TM (1998) Training and pruning system effects on vegetative growth potential, light interception, and cropping efficiency in peach trees. J Am Soc Hortic Sci 123:1058–1064

Guo Y, Ma Y, Zhan Z, Li B, Dingkuhn M, Luquet D, De Reffye P (2006) Parameter optimization and field validation of the functional-structural model GREENLAB for maize. Ann Bot 97:217–230

Hemmerling R, Kniemeyer O, Lanwert D, Kurth W, Buck-Sorlin GH (2008) The rule-based language XL and the modelling environment GroIMP illustrated with simulated tree competition. Funct Plant Biol 35:739–750

Heuvelink E (1996) Dry matter partitioning in tomato: validation of a dynamic simulation model. Ann Bot 77:71–80

Hikosaka K, Noguchi K, Terashima I (2016a) Modeling leaf gas exchange. In: Hikosaka K, Niinemets Ü, Anten N (eds) Canopy Photosynthesis: From Basics to Applications. Springer, Berlin, pp 61–100

Hikosaka K, Kumagai T, Ito A (2016b) Modeling canopy photosynthesis. In: Hikosaka K, Niinemets Ü, Anten N (eds) Canopy Photosynthesis: From Basics to Applications. Springer, Berlin, pp 239–268

Hirose T, Werger MJA (1995) Canopy structure and photon flux partitioning among species in a herbaceous plant community. Ecology 76:466–474

Kebrom TH, Burson BL, Finlayson SA (2006) Phytochrome B represses Teosinte Branched1 expression and induces Sorghum axillary bud outgrowth in response to light signals. Plant Physiol 140:1109–1117

Keuskamp DH, Pollmann S, Voesenek LACJ, Peeters AJM, Pierik R (2010) Auxin transport through PIN-FORMED 3 (PIN3) controls shade avoidance and fitness during competition. Proc Natl Acad Sci U S A 107:22740–22744

Kniemeyer O, Buck-Sorlin GH, Kurth W (2007) GroIMP as a platform for functional-structural modelling of plants. In: Vos J, Marcelis LFM, de Visser PHB, Struik PC, Evers JB (eds) Functional-Structural Plant Modelling in Crop Production. Springer, Dordrecht, pp 43–52

Kobayashi H, Baldocchi DD, Ryu Y, Chen Q, Ma S, Osuna JL, Ustin SL (2012) Modeling energy and carbon fluxes in a heterogeneous oak woodland: a three-dimensional approach. Agric For Meteorol 152:83–100

Kurth W, Kniemeyer O, Buck-Sorlin G (2005) Relational growth grammars – a graph rewriting approach to dynamical systems with a dynamical structure. In: Banâtre J-P, Fradet P, Giavitto J-L, Michel O (eds) Unconventional Programming Paradigms. Springer, Berlin/Heidelberg, p 97

Marcelis LFM, Heuvelink E (2007) Concepts of modelling carbon allocation among plant organs. In: Vos J, Marcelis LFM, de Visser PHB, Struik PC, Evers JB (eds) Functional-Structural Plant Modelling in Crop Production. Springer, Dordrecht, pp 103–111

McMaster GS (2005) Phytomers, phyllochrons, phenology and temperate cereal development. J Agr Sci 143:137–150.

McSteen P (2009) Hormonal regulation of branching in grasses. Plant Physiol 149:46–55

Monsi M, Saeki T (1953) Uber den Lichtfaktor in den Pflanzengesellschaften und seine Bedeutung fur die Stoffproduktion. Jpn J Bot 14:22–52. *Translated as*: Monsi M, Saeki T (2005) On the factor light in plant communities and its importance for matter production. Ann Bot 95:549–567

Müller J, Wernecke P, Diepenbrock W (2005) LEAFC3-N: a nitrogen-sensitive extension of the CO_2 and H_2O gas exchange model LEAFC3 parameterised and tested for winter wheat (*Triticum aestivum* L.). Ecol Model 183:183–210

Pradal C, Dufour-Kowalski S, Boudon F, Fournier C, Godin C (2008) OpenAlea: a visual programming and component-based software platform for plant modelling. Funct Plant Biol 35:751–760

Prusinkiewicz P, Lindenmayer A (1990) The Algorithmic Beauty of Plants. Springer, New York

Prusinkiewicz P, Runions A (2012) Computational models of plant development and form. New Phytol 193:549–569

Prusinkiewicz P, Karwowski R, Lane B (2007) Modelling architecture of crop plants using L-systems. In: Vos J, Marcelis LFM, de Visser PHB, Struik PC, Evers JB (eds) Functional-Structural Plant Modelling in Crop Production. Springer, Dordrecht, pp 27–42

Prusinkiewicz P, Crawford S, Smith RS, Ljung K, Bennett T, Ongaro V, Leyser O (2009) Control of bud activation by an auxin transport switch. Proc Natl Acad Sci U S A 106:17431–17436

Reinhardt D, Kuhlemeier C (2002) Plant architecture. EMBO Rep 3:846–851

Roeder AHK, Tarr PT, Tobin C, Zhang X, Chickarmane V, Cunha A, Meyerowitz EM (2011) Computational morphodynamics of plants: integrating development over space and time. Nat Rev Mol Cell Biol 12:265–273

Room PM, Hanan JS, Prusinkiewicz P (1996) Virtual plants: new perspectives for ecologists, pathologists and agricultural scientists. Trends Plant Sci 1:33–38

Sarlikioti V, de Visser PHB, Marcelis LFM (2011) Exploring the spatial distribution of light interception and photosynthesis of canopies by means of a functional–structural plant model. Ann Bot 107:875–883

Sinoquet H, Thanisawanyangkura S, Mabrouk H, Kasemsap P (1998) Characterization of the light environment in canopies using 3D digitising and image processing. Ann Bot 82:203–212

Smith H, Holmes MG (1977) The function of phytochrome in the natural environment. 3. Measurement and calculation of phytochrome photoequilibria. Photochem Photobiol 25:547–550

Spitters CJT (1986) Separating the diffuse and direct component of global radiation and its implications for modeling canopy photosynthesis Part II. Calculation of canopy photosynthesis. Agric For Meteorol 38:231–242

Spitters CJT, Toussaint HAJM, Goudriaan J (1986) Separating the diffuse and direct component of global radiation and its implications for modeling canopy photosynthesis Part I. Components of incoming radiation. Agric For Meteorol 38:217–229

Tao Y, Ferrer JL, Ljung K, Pojer F, Hong F, Long JA, Li L, …, Chory J (2008) Rapid synthesis of auxin via a new tryptophan-dependent pathway is required for shade avoidance in plants. Cell 133:164176

Vos J, Marcelis LFM, de Visser PHB, Struik PC, Evers JB (2007) Functional-Structural Plant Modelling in Crop Production. Springer, Dordrecht

Vos J, Evers JB, Buck-Sorlin GH, Andrieu B, Chelle M, de Visser PHB (2010) Functional-structural plant modelling: a new versatile tool in crop science. J Exp Bot 61:2102–2115

Wiechers D, Kahlen K, Stützel H (2011) Dry matter partitioning models for the simulation of individual fruit growth in greenhouse cucumber canopies. Ann Bot 108:1075–1084

Xu L, Henke M, Zhu J, Kurth W, Buck-Sorlin G (2011) A functional–structural model of rice linking quantitative genetic information with morphological development and physiological processes. Ann Bot 107:817–828

Yin X, Van Laar HH (2005) Crop Systems Dynamics – An Ecophysiological Simulation Model for Genotype-by-Environment Interactions. Wageningen Academic Publishers, Wageningen

Yin X, Goudriaan J, Lantinga EA, Vos J, Spiertz HJ (2003) A flexible sigmoid function of determinate growth. Ann Bot 91:361–371

Zhu J, Van der Werf W, Anten NPR, Vos J, Evers JB (2015) The contribution of phenotypic plasticity to complementary light capture in plant mixtures. New Phytol 207:1213–1222

Part IV

Assessments of Vegetation Functioning

Chapter 9

Modeling Canopy Photosynthesis

Kouki Hikosaka*
Graduate School of Life Sciences, Tohoku University, Sendai 980-8578, Japan

CREST, JST, Tokyo, Japan

Tomo'omi Kumagai
Institute for Space-Earth Environmental, Nagoya University, Chikusa-ku, Nagoya 464-8601, Japan

and

Akihiko Ito
National Institute for Environmental Studies, Tsukuba, Ibaraki 305-8506, Japan

*Author for correspondence, e-mail: hikosaka@m.tohoku.ac.jp

e-mail: tomoomikumagai@gmail.com

e-mail: itoh@nies.go.jp

K. Hikosaka, Ü. Niinemets, and N.P.R. Anten (eds.), *Canopy Photosynthesis: From Basics to Applications*, DOI 10.1007/978-94-017-7291-4_9

Summary

Canopy photosynthesis models (CPMs) calculate canopy photosynthetic rate as a sum of leaf photosynthetic rate. Here we focus on one-dimensional CPMs and show that simulated rates of canopy photosynthesis vary depending on whether multiple layers or a monolayer are considered and on whether direct and diffuse light sources are considered. We discuss how canopy photosynthetic rates vary depending on plant traits, which can differ within and among species; canopy photosynthetic rates are sensitive to leaf area index, light extinction coefficient, leaf photosynthetic capacity (photosynthetic nitrogen use efficiency), and nitrogen allocation between leaves. CPMs can predict exchange rates not only for carbon but also for water and energy. The predicted rates are consistent with observations. Finally, we describe how CPMs have been utilized for vegetation and global studies.

Keywords Atmosphere-ecosystem interaction • Big-leaf model • Canopy photosynthesis • Diffuse light • Direct light • Energy balance • Global environmental change • Leaf area index • Light extinction coefficient • Multi-layer model • Thermally produced turbulence effect • Uncertainty and model validation

I. Introduction

By definition, canopy photosynthesis is the sum of the photosynthetic rates of all leaves in the canopy. The complexity of canopy photosynthesis was first described by Boysen-Jensen (1932), who demonstrated that light dependence of canopy photosynthesis differs from that of leaves isolated from the canopy (see also Hirose 2005). It differs because leaves are exposed to different environmental conditions depending on their position in the canopy, and have different morphological and physiological traits depending on their environment and ontogeny, as has been discussed in previous Chaps. 1, 2, 3, 4, 5 (Goudriaan 2016; Gutschick 2016; Hikosaka et al. 2016; Niinemets 2016; Pons 2016). Current canopy photosynthesis models (CPMs) have incorporated these issues and photosynthetic performance of each leaf in the canopy, and permit the estimation of canopy gas exchange rate, such that predicted values are close to observations. Here we review the development of CPMs, focusing mainly on one-dimensional models and how they show the dependence of canopy photosynthetic rates on environmental variables and on plant or canopy traits. We also highlight how CPMs play important roles in terrestrial carbon cycle models and dynamic

Abbreviations (See Table 9.1 for Model Parameters in Box 9.2): A – Photosynthetic rate; a_l – Albedo; a_V – Slope of V_{cmax}-N relationship; BLM – Big-leaf model; C_i – Intercellular CO_2 partial pressure; c_p – Specific heat of air; CPM – Canopy photosynthesis model; d – Zero-plane displacement; E – Evapotranspiration rate; e – Vapor pressure; G – Heat flux into thermal storage; g – Conductance; GPP – Gross primary production; H – Sensible heat flux; I_c – Absorbed light per unit leaf area; IBP – International Biological Programme; k – Extinction coefficient; L – Cumulative leaf area index; LUE – Light use efficiency; l – Monin-Obukhov length; LAI – Leaf area index; m_a – and m_e Molecular weights of air and water; MDDM – Multilayer model under direct-diffuse light; MSM – Multilayer model with simple light extinction; N – Nitrogen content; NDVI – Normalized difference vegetation index; NEE – Net ecosystem CO_2 exchange; NPP – Net primary production; P – Atmospheric pressure; PFD – Photosynthetially active photon flux density; R – Radiation; RE – Ecosystem respiration; SS – Sunshade big-leaf model; T – Temperature; u – Wind velocity; V_{cmax} – Maximum rate of carboxylation; z – Height; z_{0H} – and z_{0M} Roughness lengths for heat and momentum; γ – Psychrometric constant in Eq. 9.6; κ – von Karman constant; ρ – Density of air; λ – Heat of vaporization; θ – Convexity of photosynthetic curves; χ_H – and χ_M Dimensionless temperature and velocity profiles; X_{dif} – X for diffuse light; X_{dir} – X for direct light; X_{sca} – X for scattering light; X_{sh} – X for shade leaf; X_{sca} – X for sunlit leaf; n – Value of X at the top of the canopy; X_t – Value of X per ground area

vegetation models and how they have contributed to the understanding and projection of global carbon balance.

II. Advances in Canopy Photosynthesis Models

The first CPM was developed by Monsi and Saeki (1953). They assessed canopy structure using a stratified clipping method and determined vertical profiles of leaf and light distribution. They found that light distribution can be described by an exponential function like the Beer–Lambert law, and the slope (extinction coefficient, k) can differ among stands depending mainly on leaf angle. A rectangular hyperbola was used to express the light-response curve of photosynthesis, and the canopy photosynthetic rate was calculated as the sum of leaf photosynthetic rates. This model successfully included the essential parts of canopy photosynthesis in a mathematical manner.

Models of light distribution were further developed, for instance, by separate distributions of direct and diffuse light, solar angle, and leaf angle distributions (de Wit 1965; Gourdriaan 1977, see Chap. 1, 2016).

Leaf canopies are characterized by vertical gradients in leaf photosynthetic properties (Saeki 1959; see Chap. 4, Niinemets 2016). However, until the early 1980s, such gradients were ignored in CPMs (i.e., all leaves in the canopy were assumed to have the same characteristics), owing mainly to limitation in computation abilities. To incorporate such variation, Hirose and Werger (1987a) introduced a two-step process first determining the relationships between the parameters of the light-response curve of photosynthesis (maximum rate, respiration rate, initial slope, and convexity of the curve), and leaf nitrogen content and then calculating the leaf N distribution in the canopy.

For leaf photosynthesis, earlier models incorporated only light as an environmental variable. Farquhar et al. (1980) developed a biochemical model of leaf photosynthesis in which CO_2 assimilation rates are expressed as the function of light, CO_2 concentration, and temperature. Ball et al. (1987) proposed an empirical model of stomatal conductance as a function of air humidity, CO_2 concentration, and photosynthetic rate. Combining these models permits the estimation of gas exchange rates under fluctuating environmental conditions (Harley and Tenhunen 1991; Harley et al. 1992; Baldocchi 1994; Harley and Baldocchi 1995; see Chap. 3, Hikosaka et al. 2016).

During the 1990s, several CPMs that incorporated light distribution, leaf property gradient, and leaf physiology were developed (e.g., MAESTRO: Wang and Jarvis 1990). Some of them incorporated heat fluxes (e.g., CANOAK: Baldocchi and Harley 1995). The predicted gas exchange rate was strongly correlated with the rate measured by the eddy covariance method (Baldocchi and Harley 1995). Nowadays, we can accurately predict canopy gas exchange if canopy characteristics and environmental variables are given.

Alternative efforts have been made to describe canopy photosynthesis using simpler models that minimize calculation time and the need for parameterization. The simplest model expresses canopy productivity as the product of light use efficiency (or radiation use efficiency), interception efficiency and solar radiation (Monteith 1972).

Farquhar (1989) showed that an equation describing whole-leaf photosynthesis has the same form as one for individual chloroplasts across a leaf, provided the distribution of chloroplast photosynthetic capacity is in proportion to the profile of absorbed irradiance and that the shape of the response to irradiance is identical in all layers. This led to a new generation of big-leaf models (BLMs; see Sect. III.B) for canopy photosynthesis. BLMs treat the canopy as a layer of one big leaf. Some studies have simply applied a leaf photosynthesis model to calculation of canopy photosynthetic rates (e.g., Lloyd et al. 1995). However, most BLMs did not separate direct from diffuse light in the canopy. de Pury and Farquhar (1997) developed a single layered model that separately accounts for beam and diffuse lights, and is as accurate as, but simpler than, multi-layer models. Several ecosystem models use the

model of de Pury and Farquhar (1997) for calculating canopy photosynthesis.

CPMs have been incorporated into terrestrial ecosystem models (Table 9.2), which play important roles for understanding the present processes and in making future projections under global environmental change. For example, terrestrial carbon cycle models, such as the Vegetation Integrated SImulator for Trace gases (VISIT: Ito et al. 2005) and the Biosphere Model integrating Eco-physiology and Mechanistic approaches using Satellite data (BEAMS: Sasai et al. 2005), use canopy models to estimate ecosystem carbon uptake from the atmosphere. Similarly, several dynamic vegetation models, such as the Lund–Potsdam–Jena (LPJ: Sitch et al. 2003) and the Organized Carbon and Hydrology in Dynamic Ecosystems (ORCHIDEE: Krinner et al. 2005) models, include canopy models but in a relatively simple manner. Because these vegetation canopy models are used to estimate carbon and water budgets of ecosystems, their uncertainty eventually influences estimation of future ecosystem responses and feedback to global change.

CPMs have also been incorporated into crop models (van Ittersum et al. 2003). Simple models used relationships between radiation and crop growth based on the light use efficiency (e.g., LINTUL: Spitters and Schapendonk 1990). Some models are a mechanistic models that consider CO_2 assimilation and respiration as a function of environmental conditions (e.g., SUCROS: Goudriaan and van Laar 1994). Recent models consider the spatiotemporal dynamics of growth and development of plants, where complex three-dimensional structures of individual plants are combined with physiological mechanisms (functional–structural plant models, FSPM; see Chap. 8, Evers 2016).

III. Models of One-Dimensional Canopy Photosynthesis

A. Multi-layer Model

In most multi-layer models, the canopy comprises many horizontal layers. Light from top to bottom of the canopy is modeled, and absorbed light by leaves in each layer is calculated as described in Chap. 1 (Goudriaan 2016). In earlier models, light availability was assumed to be identical among leaves within each layer, whereas more advanced models consider sunlit and shaded leaves separately (Fig. 9.1). Sunlit leaves receive both direct and diffuse light, whereas shaded leaves receive only diffuse light. In general, leaf angle is assumed to be identical, or mean values are used, but some models consider leaves with different angles separately (e.g., Anten and Hirose 2003). In earlier models, leaf photosynthetic traits were assumed to be identical among leaves, whereas recent models incorporate vertical distributions of photosynthetic capacity or nitrogen content as an exponential or linear functions of canopy depth (normally expressed as cumulative leaf area index from the top of the canopy). In some models, differences in leaf traits among individuals or species are taken into account (Anten and Werger 1996; Hikosaka et al. 1999; Anten and Hirose 2003; See Chap. 14, Anten and Bastiaans 2016). Canopy photosynthetic rate is calculated as the sum of photosynthetic rates of leaves (Fig. 9.1).

B. Big-Leaf Model

BLMs treat the canopy as if it were a single-layer leaf. There are several types of BLMs. The simplest one applies a leaf photosynthesis model to the canopy (Amthor 1994; Lloyd et al. 1995), with assimilation rates expressed per unit ground area instead of per unit leaf area. This model is used when data of environmental dependence of stand CO_2 exchange are available for parameter calibration, by which model estimates are adjusted to observations.

A slightly more elaborate BLM derives canopy photosynthesis A_t as an integral of photosynthesis from top leaves with some assumptions:

$$A_t = A_o \frac{1 - \exp(-kL)}{k} \qquad (9.1)$$

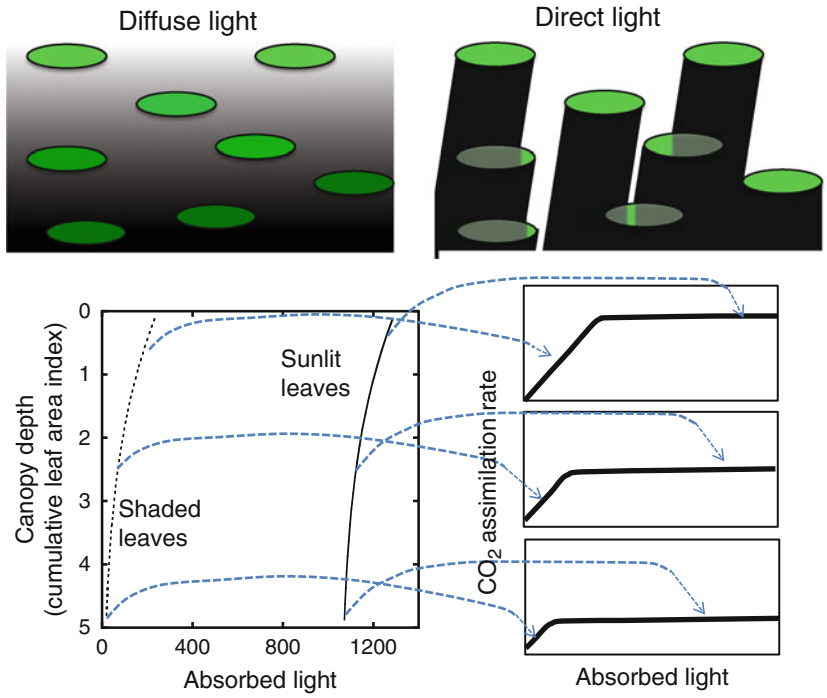

Fig. 9.1. Principle of the canopy photosynthesis model. Diffuse light diminishes in intensity with canopy depth, whereas direct light diminishes in area with canopy depth. Sunlit leaves receive direct and diffuse light whereas shaded leaves receive only diffuse light. CO_2 assimilation rates are calculated for sunlit and shaded leaves in each layer

where A_o denotes the photosynthetic rate of the top leaf in the canopy. The term $1 - \exp(-kL)$ is the fraction of the incident light that is absorbed by the canopy. This equation assumes the photosynthetic capacity (light-saturated rate of photosynthesis, $A_{\max}$) of a leaf to be proportional to the relative light availability that it receives; for example, if a leaf receives only 50 % of the light, its $A_{\max}$ is also 50 % of $A_{\max}$ of top leaves. It further assumes other environmental factors (such as humidity and temperature) to be identical among layers (See Box 9.1 for how this equation is derived). The environmental response of A_o can be simulated by the biochemical model of the photosynthesis as shown in Chap. 3 (Hikosaka et al. 2016).

Box 9.1 Derivation of Big-Leaf Model

Here we apply a rectangular hyperbola for gross leaf photosynthesis A.

$$A = \frac{A_{\max}\phi I_c}{A_{\max} + \phi I_c} \qquad \text{(B9.1.1)}$$

where $A_{\max}$, ϕ, I_c are light-saturated rate, the initial slope and the absorbed light by the leaf, respectively.

Light extinction is described by Beer's law.

$$I = I_o \exp(-kL) = I_o q \qquad \text{(B9.1.2)}$$

(continued)

Box 9.1 (continued)

where I_o, k, L and q is the light intensity above the canopy, light extinction coefficient, cumulative leaf area index from the top, and relative light intensity. Ignoring light scattering by leaves, I_c is derived from the differentiate of I.

$$I_c = I_o k \exp(-kL) \qquad \text{(B9.1.3)}$$

Here we assume that A_{max} of a leaf is proportional to q.

$$A_{max} = A_{omax} q \qquad \text{(B9.1.4)}$$

where A_{omax} is A_{max} of the top leaf. Canopy photosynthesis A_t is give as the integral of leaf photosynthesis.

$$A_t = \int_0^{L_{max}} A \; dL \qquad \text{(B9.1.5)}$$

Substituting Eqs. B9.2.2 and B9.2.5 to Eq. B9.2.6, A_t is derived as follows

$$\begin{aligned} A_t &= \int_0^{L_{max}} \frac{A_{omax} q \phi I_c}{A_{omax} q + \phi I_c} dL \\ &= \int_0^{L_{max}} \frac{A_{omax} \exp(-kL) \phi k I_o \exp(-kL)}{A_{omax} \exp(-kL) + \phi k I_o \exp(-kL)} dL \\ &= \frac{A_{omax} \phi I_{oc}}{A_{omax} + \phi I_{oc}} \int_0^{L_{max}} \exp(-kL) dL \\ &= A_o \frac{1 - \exp(-kL)}{k} \end{aligned} \qquad \text{(B9.1.6)}$$

where A_o is A of the top leaf.

C. Sun–Shade Model

One of the shortcomings of BLMs is that they consider only average light level at each layer and ignore direct and diffuse light, which have different canopy-transfer and photosynthetic properties. Given that the light-response curve of photosynthesis is concave, an increase in light intensity increases photosynthesis in low light but not in high light. Thus, a difference in frequency of light intensity affects photosynthetic rates even when average light intensities are similar. de Pury and Farquhar (1997) developed an adjustment to the above-mentioned BLM that considered the difference between direct (beam) and diffuse light and scattering within the canopy. The model divides the canopy into two components: sunlit and shaded leaves. Shaded leaves receive only diffuse light, whereas sunlit leaves receive both direct and diffuse light. Canopy photosynthesis is calculated as the sum of photosynthesis of sunlit and shade leaves.

D. Comparison of Calculated Rates Between Canopy Photosynthesis Models

Here we use five CPMs.

1. Multi-layer Model Under Direct–Diffuse Light (MDDM)

In this model, solar geometry and photosynthetically active photon flux density (PFD) above the canopy were modeled as described in Box 1.1 of Chap. 1 (Goudriaan 2016) (equations are shown in Box 9.2; Eqs. B9.2.1, B9.2.2, B9.2.3, B9.2.4 and B9.2.5). The canopy comprised multiple layers (in this example, 20 layers) in which leaves were randomly distributed. Leaves received direct PFD $I_{c,dir}$, diffuse PFD $I_{c,dif}$, and scattered direct PFD $I_{c,sca}$. An example is shown in Fig. 9.2. $I_{c,dir}$ was constant across the layers (Eq. B9.2.7), but the fraction of leaves receiving direct PFD decreased with canopy depth (Eq. B9.2.6). $I_{c,dif}$ decreased with canopy depth (Eq. B9.2.8). $I_{c,sca}$ was calculated as the difference between light interception by black (no scattering) and actual leaves (Eq. B9.2.9). Sunlit leaves received $I_{c,dir}$, $I_{c,dif}$, and $I_{c,sca}$ whereas shade leaves received $I_{c,dif}$, and $I_{c,sca}$ (Eqs. B9.2.10 and B9.2.11). The light extinction coefficient for direct light was calculated as a function of leaf angle and solar angle (Anten 1997; Kamiyama et al. 2010; Eqs. B9.2.12, B9.2.13 and B9.2.14). The light extinction coefficient for diffuse light k_{dif} was assumed to depend on the leaf inclination angle: 0.5, 0.7, and 0.9 when this angle was 75°, 45°, and 15°, respectively.

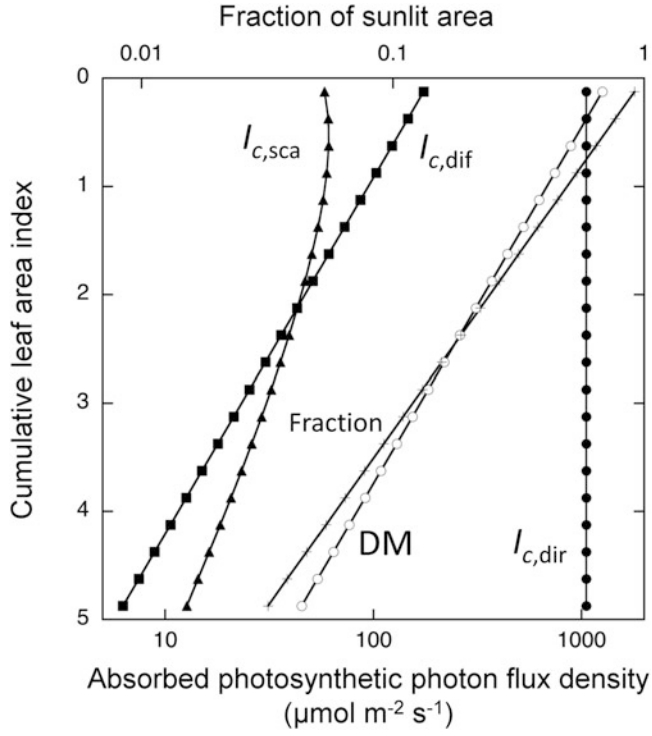

Fig. 9.2. An example of a vertical profile of photosynthetically active photon flux density (PFD). Assumptions include 1200 on a cloudless vernal equinox day at the equator in and leaf angle of 45°. A canopy with leaf area index of 5 was divided into 20 layers and absorbed PFD was calculated. $I_{c,\mathrm{dir}}$ is absorbed PFD of direct light per unit sunlit leaf area. $I_{c,\mathrm{dif}}$ and $I_{c,\mathrm{sca}}$ denote absorbed PFD of diffuse and scattered direct light per unit total leaf area in each layer, respectively. MSM (diffuse-light model) denotes the absorbed PFD per leaf area when all the light above the canopy is assumed to be diffuse light (see text). Fraction is the fraction of sunlit area in each layer

For simplicity, leaf angle was assumed to be constant within the canopy. PFD absorption was calculated assuming that it was identical among sunlit leaves and among shade leaves within each layer (Eqns B9.2.6′, B9.2.8′, and B9.2.9′).

Box 9.2 Equations Used in the Models

See Table 9.1 for abbreviations and units.

1. Solar geometry (see Chap. 1 Goudriaan 2016)

$$\sin\delta = -\frac{23.44\pi}{180}\cos\frac{2\pi\left(t_{\mathrm{day}}+10\right)}{365.24} \qquad \text{(B9.2.1)}$$

$$\sin\beta = \sin\lambda\sin\delta + \cos\lambda\cos\delta\cos\frac{2\pi(t_h-12)}{24} \qquad \text{(B9.2.2)}$$

2. Multi-layer model under direct-diffuse light (MDDM)

2.1 PFD above the canopy

$$I_{\mathrm{dir}} = a^m I_e \sin\beta \qquad \text{(B9.2.3)}$$

$$m = \frac{P}{P_o\sin\beta} \qquad \text{(B9.2.4)}$$

$$I_{\mathrm{dif}} = f_a(1-a^m)I_e\sin\beta \qquad \text{(B9.2.5)}$$

2.2 Light absorption at depth L (see Chap. 1 Goudriaan 2016)

(continued)

Box 9.2 (continued)

$$f_{su} = \exp\left(-k'_{dir}L\right) \quad \text{(B9.2.6)}$$

$$I_{c,dir} = (1-\sigma)k'_{dir}I_{dir} \quad \text{(B9.2.7)}$$

$$I_{c,dif} = (1-\rho_{dif})k_{dif}I_{dif,0}\exp(-k_{dif}L) \quad \text{(B9.2.8)}$$

$$I_{c,sca} = I_{dir}(1-\rho_{dir})k_{dir}\exp(-k_{dir}L) - I_{dir}(1-\sigma)k'_{dir}\exp\left(-k'_{dir}L\right) \quad \text{(B9.2.9)}$$

$$I_{c,su} = I_{c,dir} + I_{c,dif} + I_{c,sca} \quad \text{(B9.2.10)}$$

$$I_{c,sh} = I_{c,dif} + I_{c,sca} \quad \text{(B9.2.11)}$$

$$k_{dir} = \frac{O_{av}}{\sin\beta} \quad \text{(B9.2.12)}$$

$$O_{av} = \sin\beta\cos\alpha \quad \beta > \alpha \quad \text{(B9.2.13a)}$$

$$O_{av} = \frac{2}{\pi}\left(\sin\beta\ \cos\alpha \arcsin\frac{\tan\beta}{\tan\alpha} + \sqrt{\sin^2\alpha - \sin^2\beta}\right) \quad \alpha > \beta \quad \text{(B9.2.13b)}$$

$$k_{dir} = k'_{dir}\sqrt{1-\sigma} \quad \text{(B9.2.14a)}$$

$$k_{dif} = k'_{dif}\sqrt{1-\sigma} \quad \text{(B9.2.14b)}$$

2.3 Nitrogen content at depth L

$$N_l = \frac{k_b N_t \exp(-k_b L)}{1-\exp(-k_b L_t)} + N_b \quad \text{(B9.2.15)}$$

2.4 Light absorption and nitrogen content per unit leaf area in a layer between Ln+1 and Ln

$$f_{su} = \frac{\exp\left(-k'_{dir}L_n\right) - \exp\left(-k'_{dir}L_{n+1}\right)}{k'_{dir}(L_{n+1}-L_n)} \quad \text{(B9.2.6′)}$$

$$I_{c,dif} = (1-\rho_{dif})I_{dif,0}\frac{\exp(-k_{dif}L_n) - \exp(-k_{dif}L_{n+1})}{L_{n+1}-L_n} \quad \text{(B9.2.8′)}$$

$$I_{c,sca} = I_{dir}\frac{(1-\rho_{dir})[\exp(-k_{dir}L_n) - \exp(-k_{dir}L_{n+1})] - (1-\sigma)\left[\exp\left(-k'_{dir}L_n\right) - \exp\left(-k'_{dir}L_{n+1}\right)\right]}{L_{n+1}-L_n} \quad \text{(B9.2.9′)}$$

$$N_l = (N_o - N_b)\frac{\exp(-k_b L_n) - \exp(-k_b L_{n+1})}{k_b(L_{n+1}-L_n)} + N_b \quad \text{(B9.2.15′)}$$

where $N_o = \frac{k_b N_t}{1-\exp(-k_b L_t)} + N_b$.

2.5 Gas exchange (see Chap. 3)

$$\theta_{cj}A^2 - A\left(A_c + A_j\right) + A_c A_j = 0 \quad \text{(B9.2.16)}$$

$$A_c = \frac{V_{cmax}\left(C_i - \Gamma^*\right)}{C_i + K_c(1+O/K_o)} - R_d \quad \text{(B9.2.17)}$$

$$A_j = \frac{J\left(C_i - \Gamma^*\right)}{4C_i + 8\Gamma^*} - R_d \quad \text{(B9.2.18)}$$

$$J = \frac{\phi_j I_c + J_{max} - \sqrt{\left(\phi_j I_c + J_{max}\right)^2 - 4\phi_j I_c J_{max}\theta_j}}{2\theta_j} \quad \text{(B9.2.19)}$$

$$V_{cmax} = V_{cmax25}\exp\left[\frac{E_{aV}(T_k - 298)}{298\boldsymbol{R}T_k}\right] \quad \text{(B9.2.20)}$$

$$R_d = R_{d25}\exp\left[\frac{E_{aR}(T_k - 298)}{298\boldsymbol{R}T_k}\right] \quad \text{(B9.2.21)}$$

$$J_{max25} = \frac{J_{max25}\exp\left[\frac{E_{aJ}(T_k-298)}{298\boldsymbol{R}T_k}\right]\left[1+\exp\left(\frac{298\Delta S - H_d}{298\boldsymbol{R}}\right)\right]}{1+\exp\left(\frac{T_k\Delta S - H_d}{\boldsymbol{R}T_k}\right)} \quad \text{(B9.2.22)}$$

$$V_{cmax25} = a_V(N_l - N_b) \quad \text{(B9.2.23)}$$

$$J_{max25} = a_J V_{cmax25} \quad \text{(B9.2.24)}$$

$$R_{25} = a_R V_{cmax25} \quad \text{(B9.2.25)}$$

$$A_t = \sum A \quad \text{(B9.2.26)}$$

(continued)

Box 9.2 (continued)

3. Multi-layer model with simple light extinction (MSM)
   3.1 PFD above the canopy

$$I_{\mathrm{dir}} = 0 \qquad \text{(B9.2.3}')$$

$$I_{\mathrm{dif}} = f_a(1-a^m)I_e \sin\beta + a^m I_e \sin\beta \qquad \text{(B9.2.5}')$$

Other equations are same as those in MDDM

4. Big-leaf model 2 (BLM2; de Pury and Farquhar 1997 with some modifications)
   PFD above the canopy is modeled as in MDDM
   4.1 Light absorption by the canopy

$$I_t = \int_0^{L_t} I_c dL = I_{\mathrm{dir}}(1-\rho_{\mathrm{dir}}) \{1-\exp(-k_{\mathrm{dir}}L_t)\} + I_{\mathrm{dif}}(1-\rho_{\mathrm{dif}}) \{1-\exp(-k_{\mathrm{dif}}L_t)\} \qquad \text{(B9.2.27)}$$

   4.2 Canopy gas exchange

$$\theta_{cj}A_t^2 - A_t(A_{ct}+A_{jt}) + A_{ct}A_{jt} = 0 \qquad \text{(B9.2.16}')$$

$$A_{ct} = \frac{V_{\mathrm{cmax}t}(C_i-\Gamma^*)}{C_i + K_c(1+O/K_o)} - R_{dt} \qquad \text{(B9.2.17}')$$

$$A_{jt} = \frac{J_t(C_i-\Gamma^*)}{4C_i+8\Gamma^*} - R_{dt} \qquad \text{(B9.2.18}')$$

$$J_t = \frac{\phi_j I_t + J_{\mathrm{max}t} - \sqrt{(\phi_j I_t + J_{\mathrm{max}t})^2 - 4\phi_j I_t J_{\mathrm{max}t}\theta_j}}{2\theta_j} \qquad \text{(B9.2.19}')$$

$$V_{\mathrm{cmax}t25} = a_V(N_t - L_t N_b) \qquad \text{(B9.2.23}')$$

$$J_{\mathrm{max}t25} = a_J V_{\mathrm{cmax}t25} \qquad \text{(B9.2.24}')$$

$$R_{dt25} = a_R V_{\mathrm{cmax}t25} \qquad \text{(B9.2.25}')$$

5. Sun–shade BLM (SSM, de Pury and Farquhar 1997 with some modifications)
   PFD above the canopy is modeled as in MDDM
   5.1 LAI of sunlit leaves

$$L_{\mathrm{su}} = \int_0^{L_t} f_{\mathrm{su}} dL = \frac{1-\exp(-k'_{\mathrm{dir}}L_t)}{k'_{\mathrm{dir}}} \qquad \text{(B9.2.28)}$$

Light absorption by the canopy is defined by B9.2.27.

   5.2 Light absorption of sunlit leaves

$$I_{t,\mathrm{su}} = \int_0^{L_t} I_{c,\mathrm{su}} f_{\mathrm{su}} dL = \int_0^{L_t} I_{c,\mathrm{dir}} f_{\mathrm{su}} dL + \int_0^{L_t} I_{c,\mathrm{dif}} f_{\mathrm{su}} dL + \int_0^{L_t} I_{c,\mathrm{sca}} f_{\mathrm{su}} dL \qquad \text{(B9.2.29)}$$

$$\int_0^{L_t} I_{c,\mathrm{dir}} f_{\mathrm{su}} dL = I_{\mathrm{dir}}(1-\sigma)\left[1-\exp\left(-k'_{\mathrm{dir}}L_t\right)\right] \qquad \text{(B9.2.29a)}$$

$$\int_0^{L_t} I_{c,\mathrm{dif}} f_{\mathrm{su}} dL = I_{\mathrm{dif}}(1-\rho_{\mathrm{dif}}) k_{\mathrm{dif}} \frac{1-\exp\left[-\exp\left(-k_{\mathrm{dif}}L_t - k'_{\mathrm{dir}}L_t\right)\right]}{k_{\mathrm{dif}}+k'_{\mathrm{dir}}} \qquad \text{(B9.2.29b)}$$

$$\int_0^{L_t} I_{c,\mathrm{sca}} f_{\mathrm{su}} dL = I_{\mathrm{dir}}(1-\rho_{\mathrm{dir}}) k_{\mathrm{dir}} \frac{1-\exp\left[-\exp\left(-k_{\mathrm{dir}}L_t - k'_{\mathrm{dir}}L_t\right)\right]}{k_{\mathrm{dir}}+k'_{\mathrm{dir}}} - I_{\mathrm{dir}}(1-\sigma)\frac{1-\exp\left(-2k'_{\mathrm{dir}}L_t\right)}{2} \qquad \text{(B9.2.29c)}$$

   5.3 Light absorption of shaded leaves

$$I_{t,\mathrm{sh}} = I_t - I_{t,\mathrm{su}} \qquad \text{(B9.2.30)}$$

(continued)

Box 9.2 (continued)

5.4 Total canopy photosynthetic capacity is calculated by B9.2.23′ Photosynthetic capacity of sunlit leaves

$$V_{cmaxf25,su} = \int_0^{L_t} V_{cmaxf25} f_{su} dL = a_V (N_o - N_b) \frac{1 - \exp\left(-k_b L_t - k'_{dir} L_t\right)}{k_b + k'_{dir}} \quad \text{(B9.2.31)}$$

5.5 Photosynthetic capacity of shaded leaves

$$V_{cmaxt,sh} = V_{cmaxt} - V_{cmaxt,su} \quad \text{(B9.2.32)}$$

5.6 Canopy photosynthesis

$$A_t = A_{t,su} + A_{t,sh} \quad \text{(B9.2.33)}$$

where $A_{t,su}$ and $A_{t,sh}$ are calculated using $V_{cmaxt,su}$ and $V_{cmaxt,sh}$, respectively, as A_t in BLM2.

Table 9.1. Abbreviations, units, and values used in the models

Symbol	Definition	Unit	Value
a	atmospheric transmission coefficient of PFD	–	0.72
A	Assimilation rate	μmol m^{-2} s^{-1}	–
A_c	RuBP-saturated A	μmol m^{-2} s^{-1}	–
Aj	RuBP-limited A	μmol m^{-2} s^{-1}	–
a_J	Ratio of J_{max25} to V_{cmax25}	–	2.1
a_R	Ratio of R_{d25} to V_{cmax25}	–	0.0089
a_V	Ratio of V_{cmax25} to photosynthetic nitrogen	s^{-1}	1.16×10^{-3}
C_i	Intercellular CO_2 partial pressure	Pa	25
E_{aJ}	Activation energy of J_{max}	J mol^{-1}	37,000
E_{aV}	Activation energy of V_{cmax}	J mol^{-1}	64,800
E_{aR}	Activation energy of R_d	J mol^{-1}	66,400
f_a	Forward scattering coefficient of PFD in atmosphere	–	0.426
f_{su}	Fraction of sunlit area	–	–
H_d	Deactivation energy	J mol^{-1}	220,000
LAI	Leaf area index	m^2 m^{-2}	–
I_c	Absorbed PFD	μmol m^{-2} s^{-1}	–
I_e	extra-terrestrial PFD	μmol m^{-2} s^{-1}	2413
J_{max}	Maximal rate of electron transport	μmol m^{-2} s^{-1}	–
k	Light extinction coefficient		
k'	Light extinction coefficient for 'black' leaves		
k_b	Nitrogen distribution coefficient		
K_c	Michaelis constant for CO_2	Pa	29.16 (at 21 °C)
K_o	Michaelis constant for O_2	kPa	20.35 (at 21 °C)
L	Cumulative leaf area index	m^2 m^{-2}	–
m	Optical air mass	–	–
N_b	Leaf structural nitrogen content	mmol m^{-2}	–
N_l	Leaf nitrogen content	mmol m^{-2}	–
O	O_2 partial pressure	kPa	20.5
O_{av}	Average projection of leaves in the direction of direct PFD	–	–
P	Air pressure	kPa	98.7
PFD	Photosynthetically active photon flux density	μmol m^{-2} s^{-1}	–
P_o	Air pressure at sea level	kPa	101.3

(continued)

Table 9.1. (continued)

Symbol	Definition	Unit	Value
R_d	Day respiration rate	μmol m^{-2} s^{-1}	–
$\boldsymbol{R}$	Gas constant	J mol^{-1} K^{-1}	8.314
t_{day}	Day of year	day	264
t_h	Time of day	hour	–
T_k	Leaf temperature	K	21 °C
V_{cmax}	Maximal rate of carboxylation	μmol m^{-2} s^{-1}	–
α	Leaf inclination angle	radians	–
β	Solar elevation angle	radians	–
δ	Solar declination angle	radians	–
ΔS	Entropy term for J_{max}	J mol^{-1} K^{-1}	710
ϕ_j	Initial slope of light-response curve of electron transport rate	mol mol^{-1}	0.425
Γ*	CO_2 compensation point in the absence of day respiration	Pa	3.0 (at 21 °C)
ρ_{dif}	Reflection coefficient for diffuse light	–	0.036
ρ_{dir}	Reflection coefficient for direct light	–	0.027
λ	Latitude	radians	0
θ_{cj}	Curvature factor for A_c–A_j transition	–	0.99
θ_j	Curvature factor for light-response of electron transport	–	0.7
σ	Leaf scattering coefficient	–	0.15
X_0	X of top leaves		
X_{25}	X at 25 °C		
X_{dif}	X of diffuse light		
X_{dir}	X of direct light		
X_{sca}	X of scattered light		
X_{sh}	X in shaded leaves		
X_{su}	X in sunlit leaves		
X_t	Amount of X in the canopy per unit ground area		

2. Multi-layer Model With Simple Light Extinction (MSM)

In this model we estimated the effect of not separating direct and diffuse light on canopy photosynthesis. To this end, PFD above and within the canopy was assumed to be diffuse light (without direct light). Total PFD above the canopy was the same as that in the MDDM. Other variables were same as for MDDM.

3. Big-Leaf Model 1 (BLM1)

In this model, we calculated photosynthesis of top leaves A_0 using PFD above the canopy ($I_{c,dir} + I_{c,dir,o}$) and nitrogen content of top leaves (N_o; see Eq. B9.2.15). A_t was derived by Eq. 9.1.

4. Big-Leaf Model 2 (BLM2)

The BLM2 is a type of modified BLM described by de Pury and Farquhar (1997). In this model, the variation in nitrogen content in the canopy is taken into account. PFD absorbed by the canopy on a ground-area basis was calculated by Eq. B9.2.27. Canopy photosynthetic capacity V_{cmaxt} was calculated from total canopy nitrogen content N_t (B9.2.23′) and other rates were simply obtained as that for leaves (Eqs. B9.2.24′ and B9.2.25′). A_t was calculated in the

same way for leaf photosynthetic rate (Eqs. B9.2.16′ and B9.2.19′).

5. Sun–Shade Big-Leaf Model (SSM)

This model was developed by de Pury and Farquhar (1997). The sunlit fraction of leaf area index (LAI) is given by Eq. B9.2.28. Total PFD absorbed by sunlit leaves comprises direct, diffuse, and scattered direct light (Eq. B9.2.29). Total PAR absorbed by shaded leaves was obtained as the difference between PFD absorbed by the canopy and PFD absorbed by sunlit leaves (Eq. 9.2.30). Photosynthetic capacity of sunlit leaves expressed per unit ground area, $V_{cmaxt,su}$, was calculated as the integral of V_{cmax} of sunlit leaves, which was calculated as a function of leaf nitrogen content (Eq. 9.2.31). Photosynthetic capacity of shaded leaves was calculated as the difference between canopy photosynthetic capacity and the photosynthetic capacity of sunlit leaves (Eq. B9.2.32).

In calculation of all these models, CO_2 assimilation rates were calculated based on the biochemical model of Farquhar et al. (1980) as shown in Eqs. B9.2.16, B9.2.17, B9.2.18, B9.2.19, B9.2.20′, B9.2.21 and B9.2.22. Maximal carboxylation (V_{cmax}), maximal electron transport (J_{max}), and respiration rates (R_d) were assumed as linear functions of leaf nitrogen content per unit leaf area (N_l; Eqs. B9.2.23′, B9.2.24′ and B9.2.25′). Most parameters of leaf gas exchange were taken from data obtained from a wheat canopy (de Pury and Farquhar 1997). To evaluate the effects of interspecific variation in leaf traits, we adopted higher, middle, and lower values of the V_{cmax} to photosynthetic nitrogen ratio (a_V; 1.16, 0.58, and 0.29), corresponding roughly to PNUE of herbaceous, deciduous tree, and evergreen tree species (Hikosaka and Shigeno 2009; see Chap. 3, Hikosaka et al. 2016 for details of the gas exchange model).

The distribution of leaf photosynthetic nitrogen content was described with an exponential function (Eq. B9.2.15) and the slope (nitrogen distribution coefficient, k_b) was assumed to be half of the light extinction coefficient for diffuse light (Anten et al. 2000; K. Hikosaka, unpublished data; discussed below). However, as described in Box 9.1, BLM1 assumes that A_{max} is proportional to the relative PFD. This proportionality is achieved when the value of k_b is identical to that of the light extinction coefficient. Thus, BLM1 implicitly assumes that nitrogen distribution is steeper than that in other models.

The model simulation was performed for the vernal equinox day at the equator in which no cloud in the sky was assumed. Leaf temperature and intercellular CO_2 partial pressure were fixed at 21 °C and 25 Pa, respectively, meaning that the effect of stomatal limitation was not considered (see Sect. V for incorporating stomatal functions). Canopy photosynthetic rate was calculated every 30 min from dawn (0600) to dusk (1800) and daily carbon gain was obtained by the trapezoidal rule. The nighttime respiration rate is assumed to be twice as high as the day respiration rate (see Chap. 3, Hikosaka et al. 2016).

Figure 9.3 shows the light-response curves of canopy photosynthetic rate per unit ground area. BLM1 and BLM2 simulated a convex curve in which the rate was saturated at lower irradiance because this light response was identical to that in leaves. The difference in the light-saturated rate of canopy photosynthesis between BLM1 and BLM2 resulted from the difference in canopy nitrogen content. As mentioned above, BLM1 assumed a steeper nitrogen distribution than the other models, but the nitrogen content of top leaves was identical in all models so that total canopy nitrogen content was lower in BLM1 than in other models, leading to its lower canopy photosynthetic capacity.

The light response of the multi-layer models (MDDM and MSM) was less convex than that of the BLMs. This difference arose because light saturation of photosynthesis was not synchronized among layers;

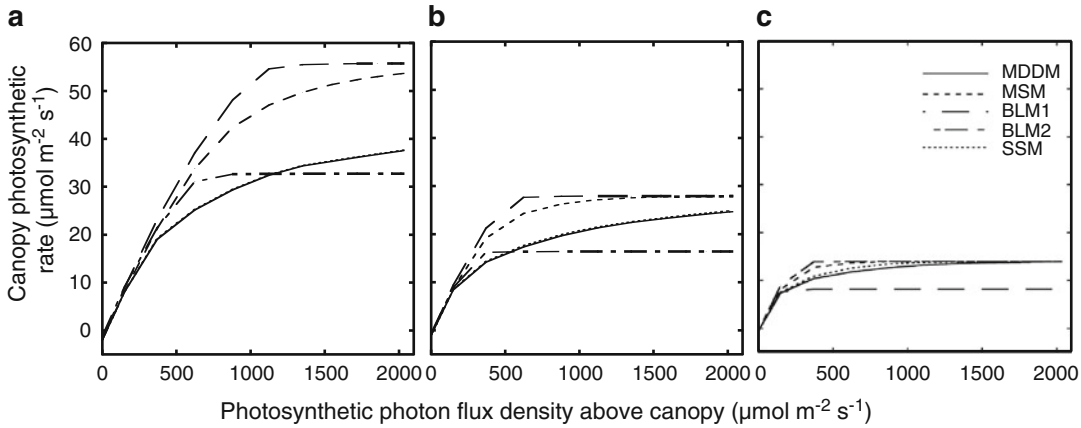

Fig. 9.3. Light-response curves of the canopy photosynthetic rate in five canopy photosynthesis models. MDDM, multi-layer model under direct–diffuse light; MSM, Multi-layer model with simple light extinction; BLM1 and BLM2, Big-leaf model 1 and 2; SSM, sun–shade big-leaf model. See text for detailed explanation of each model. Different levels of photon active radiation above the canopy assume the temporal PFD change from morning to noon in the cloudless vernal equinox day at the equator. Leaf angle was 45° in all models. Canopy nitrogen per unit ground area (N_t) was 400 mmol m^{-2} except for BLM1. In BLM1, leaf nitrogen content of the top layer (N_o) was identical to other models. The ratio of V_{cmax} to leaf photosynthetic nitrogen content (a_V) was 1.16, 0.58, and 0.29 × 10^{-3} s^{-1} in a, b, and c, respectively

photosynthesis in lower leaves was not saturated, whereas in upper leaves it was saturated (see Terashima and Saeki 1985). Canopy photosynthetic rate at high irradiance was higher in MSM than in MDDM. Furthermore, canopy photosynthetic rate in MDDM increased gradually, even at very high irradiance. These trends occurred because photosynthesis of all leaves was nearly light-saturated in MSM, but photosynthesis of shaded leaves in lower layers was not saturated in MDDM.

The light response of canopy photosynthesis in SSM was quite similar to that in MDDM. Give that SSM is a single-layer model, the computation effort is much lower than that in multi-layer models. Thus, SSM is a more accurate and useful morel.

The variation in the light-response of canopy photosynthesis among the five models was large when the V_{cmax} to photosynthetic nitrogen ratio a_V was high, but it was diminished when the ratio was small (Fig. 9.3). This is because most leaves were saturated at relatively lower irradiance when a_V is low. Therefore, the error in BLMs associated with ignoring direct light, may increase with the photosynthetic nitrogen-use efficiency of the plants considered.

IV. Effect of Canopy Traits on Canopy Photosynthesis

In addition to the effects of environmental factors, canopy photosynthesis of a given vegetation stand depends on the characteristics of the canopy. CPMs can analyze the dependencies of canopy photosynthesis on such characteristics as total leaf area index, light extinction, total leaf nitrogen in the canopy, nitrogen distribution among leaf layers, and leaf photosynthesis, including environmental response and nitrogen use (a_V). Environmental response of leaf photosynthesis is described in Chap. 3 (Hikosaka et al. 2016). The decrease in a_V results in a decrease in the maximum rate of canopy photosynthesis (Fig. 9.3). Here we analyze effect of other variables on canopy photosynthesis using MDDM.

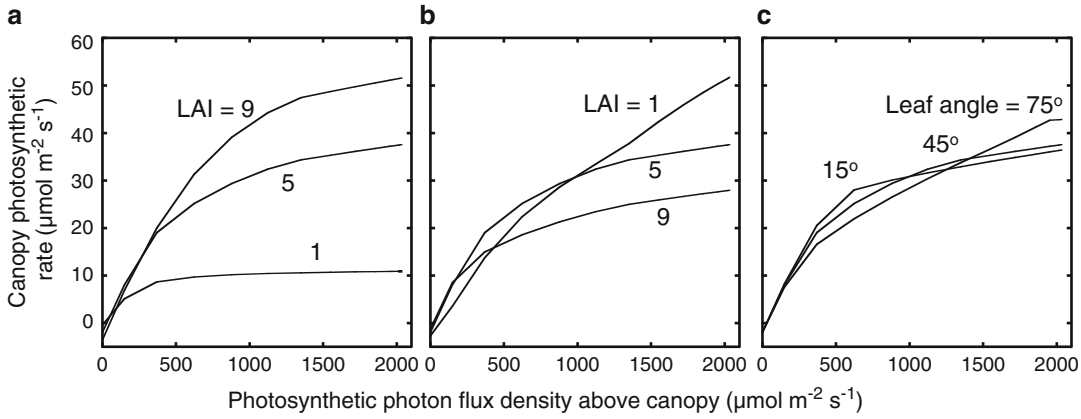

Fig. 9.4. Light-response curves of the canopy photosynthetic rate in the multi-layer model under direct–diffuse light (MDDM). (**a**) Leaf area index (LAI) was different with constant mean leaf nitrogen content per unit leaf area ($N_l = 80$ mmol m^{-2}); (**b**) LAI was different with constant canopy nitrogen content per unit ground area ($N_t = 400$ mmol m^{-2}); and (**c**) leaf angle was different. In a and b, leaf angle was 45°. In c, LAI and N_t was 5 m^2 m^{-2} and 400 mmol m^{-2}, respectively. The ratio of V_{cmax} to leaf photosynthetic nitrogen content (a_V) was 1.16×10^{-3} s^{-1} in every case

Figure 9.4a and b shows the light-response curve of the photosynthetic rates of canopies with different leaf area indices. In Figure 9.4a, b, the mean leaf nitrogen content per leaf area N_l and total leaf nitrogen content in the canopy per unit ground area N_t were constant, respectively. When the mean N_l was constant, the canopy photosynthetic rate was higher in a canopy with higher LAI irrespective of light (Fig. 9.4a). This difference occurs mainly because of the greater light absorption at higher LAI. In contrast, when N_t was constant, the effect of LAI on canopy photosynthesis is not simple; the photosynthetic rate of canopy with lower LAI was higher at high irradiance, but lower at low irradiance, compared with a canopy with a higher LAI (Fig. 9.4b). This complex result is owed to a trade-off between leaf area and leaf nitrogen content. Give that total nitrogen content (N_t) is assumed to be fixed, mean leaf nitrogen content per area (N_l) decreases with increasing LAI. Under high light, increasing N_l is advantageous because leaves have higher photosynthetic capacity. Under low light, increasing N_l is not beneficial because photosynthesis is limited by light rather than by nitrogen (see also Anten et al. 1995b). Decreasing LAI decreases light absorption, which lowers canopy photosynthesis. Consequently, when nitrogen is limited, extremely high or low LAI is disadvantageous. Fig. 9.5 shows simulation results of daily carbon gain of a canopy in which both LAI and canopy nitrogen were altered. When canopy nitrogen content was fixed, there was an optimal LAI that maximizes daily carbon gain (Anten et al. 1995b; Hirose et al. 1997). The optimal LAI increased with increasing canopy nitrogen content (Anten et al. 2004). Optimal LAI is discussed in Chap. 13 (Anten 2016).

Figure 9.4c shows light-response curves of photosynthetic rate in canopies with different leaf angles. The canopy with more-horizontal leaves (15°) had higher photosynthetic rates at lower irradiance but lower rates at higher irradiance. The higher rates occurs because more-horizontal leaves absorb more light under the same irradiance, owing to the higher associated k values. However, as the light increases, horizontal leaves that are exposed to light become light-saturated and this saturation dampens the response of canopy photosynthesis to light. In contrast, vertical leaves let more light through to lower canopy layers where it is efficiently used for photosynthesis. Thus, light is more homogenously used by

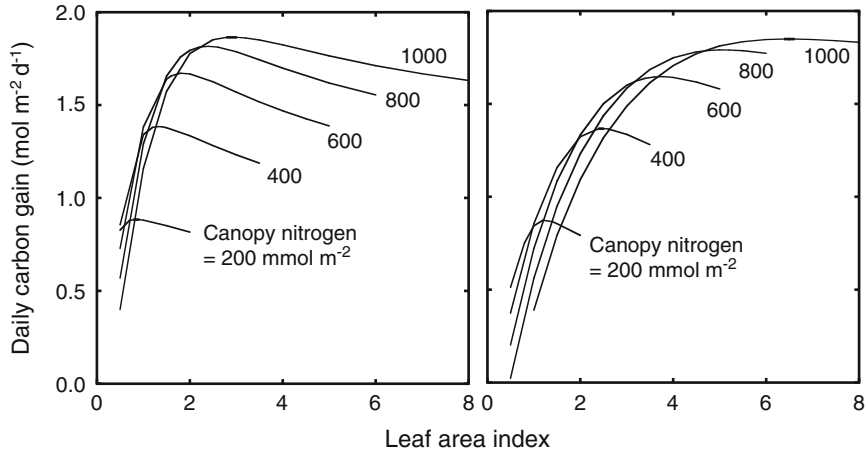

Fig. 9.5. Daily carbon gain as a function of leaf area index and canopy nitrogen content in a canopy with leaf angle of 15° (**a**) or 75° (**b**) in the multi-layer model under direct–diffuse light (MDDM). The ratio of V_{cmax} to leaf photosynthetic nitrogen content was 1.16×10^{-3} s^{-1}

different layers in the canopy. Compared at the same N_t, the optimal LAI was greater in a canopy with more vertical leaves (Fig. 9.5; Saeki 1960; Anten et al. 1995b).

Compared at the same N_t value, daily carbon gain of the canopy was similar between different leaf angles (Fig. 9.5). This result is inconsistent with simulation results of earlier models. For example, Saeki (1960) showed that maximal daily carbon gain was lower in canopies with higher k values (see also Hirose 2005). The result of Saeki (1960) was consistent with experimental results. For example, Tanaka (1972) manipulated the leaf inclination angle of a rice stand and found that canopy photosynthetic rate at high irradiance decreased with decreasing leaf angle (see also Monsi et al. 1973). Why does a canopy with horizontal leaves have low photosynthetic capacity in earlier studies? As mentioned above, earlier CPMs assumed a constant value for photosynthetic capacity. Thus, in a canopy with higher k values, photosynthesis of the topmost leaves is light-saturated, and absorbed light is not efficiently used for photosynthesis. Why then is canopy carbon gain similar between horizontal and vertical leaves in the present simulation? This is probably because we did not assume any constraint on increasing N_l or photosynthetic capacity. In this model, canopies with more horizontal leaves have steeper nitrogen distributions (higher k_b), leading to a higher N_l and associated light-saturated photosynthesis in upper leaves than those with more vertical leaves. However, the convexity of light-response curve of photosynthesis (θ, θ_j, or θ_{cj}), one of the other characteristics of the light-response curve of photosynthesis, often decreases with increasing N_l (Hirose and Werger 1987a; Hikosaka et al. 1999), which was ignored in the present model. Furthermore, increasing photosynthetic capacity of a leaf may be constrained by the availability of other resources such as water; if an increase in V_{cmax} is not accompanied by a proportionate increase in stomatal and mesophyll conductance, CO_2 concentration at the carboxylation site decreases. This response may lead to a smaller increase in photosynthetic capacity with an increase in leaf nitrogen content, and thus to a saturating relationship between photosynthetic capacity and leaf nitrogen content. To increase stomatal conductance, additional biomass may need to be invested in the root system to improve hydraulics. Otherwise, plants may suffer from a risk of water deficit in the leaf canopy (such as by embolism; see Chap. 7, Woodruff et al. 2016). Therefore, having very high leaf photosynthetic rates

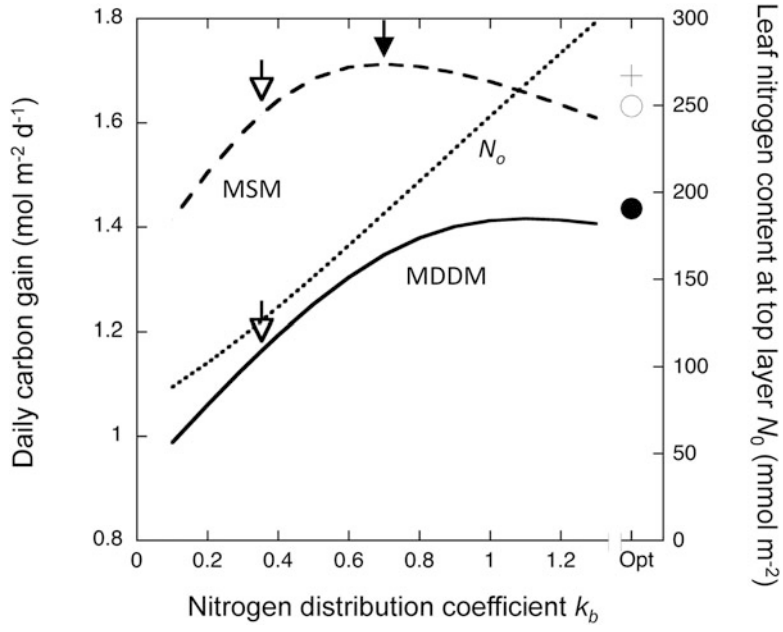

Fig. 9.6. Effects of nitrogen distribution on the daily carbon gain of the canopy. *Continuous* and *broken lines* denote carbon gain under direct–diffuse light and under diffuse light only, respectively, plotted against the nitrogen distribution coefficient (k_b). The *dotted line* describes leaf nitrogen content at the top layer. *Closed* and *open circles* show carbon gain of the canopy under direct–diffuse light and under diffuse light only, respectively, where nitrogen distribution is optimized under direct–diffuse light. The cross shows nitrogen content at the top layer in the canopy optimized under direct–diffuse light. *Open arrows* show carbon gain at actual nitrogen distribution, which is assumed to be half of k_{dif}. The *closed arrow* shows carbon gain when nitrogen distribution is optimized under diffuse light only. Redrawn from Hikosaka (2014)

may be costly. If water supply is saved, higher N content may be wasteful. Such constraints on increasing photosynthetic capacity lead to an upper limit of leaf nitrogen content, and horizontal leaves may be unable to achieve high canopy photosynthesis.

Figure 9.6 shows the effect of nitrogen distribution on daily carbon gain in as simulated by the MDDM and MSM (Hikosaka 2014). Open arrows denote the value of k_b (nitrogen distribution coefficient) observed in actual canopies (half of the light extinction coefficient; Anten et al. 2000, K. Hikosaka et al., unpublished data). Dependence of daily carbon gain on k_b was considerably different between MDDM and MSM. In MSM, daily carbon gain was maximized when the value of k_b was the same as that of the light extinction coefficient. When k_b was optimal in MSM, nitrogen content was proportional to light availability (Anten et al. 1995a; see Chap. 13, Anten 2016 for details). In contrast, optimal k_b in MDDM was much higher than that in MSM. MSM assumes that light availability is identical among leaves within the same canopy layer. Thus, plants can allocate an appropriate amount of nitrogen to leaves so that the nitrogen content is proportional to light availability. In contrast, under direct–diffuse light conditions, some leaves receive both direct and diffuse light, whereas others receive only diffuse light. Furthermore, light availability of a leaf fluctuates depending on the solar position and other factors, leading to optimal nitrogen allocation being different from that shown in MSM.

V. Canopy Photosynthesis Models with Heat Exchange

CPMs described above can simulate CO_2 exchange rates as a function of environmental variables. However, these models need

leaf temperature and intercellular CO_2 partial pressure C_i (or stomatal conductance) as input data (note that simulations in Sect. IV used fixed leaf temperature and C_i). Furthermore, leaf temperature generally differs from air temperature as a result of energy exchanges in the surroundings. For this reason, a complete canopy photosynthesis model needs to incorporate energy balances.

The surface energy balance for both an individual leaf surface and a vegetated land surface is:

$$R_{\mathrm{S\_ab}} + R_{\mathrm{L\_ab}} - R_{\mathrm{L\_out}} = H + \lambda E + G \quad (9.2)$$

where R_{S_ab} and R_{L_ab} are total solar and thermal radiation absorbed by leaves and bulk vegetation surface, respectively, R_{L_out} is outgoing thermal radiation from a surface, H and E are sensible heat and water vapor fluxes from this surface, respectively, λ is the latent heat of vaporization of water, and G is the heat flux into thermal storage depending on surface temperature (T_c) in a way that can be determined precisely only by solving the heat diffusion equation. At the leaf-scale, R_{S_ab} and R_{L_ab} are the computation results from the formulation of radiative transfer within the canopy (see Kumagai et al. 2006). In contrast, on land surface-scale, R_{S_ab} is calculated as $(1 - a_l) \times R_S$, where a_l is the albedo (the reflection of solar radiation) and R_S is solar radiation, and incident thermal radiation can be substituted for R_{L_ab}. R_{L_out} is expressed as a function of T_c according to the Stefan–Boltzmann law at the leaf-scale. Two-sided evolution and probability of no contact within a given canopy layer must be considered (see Kumagai et al. 2006).

When we consider heat balance in each canopy layer, H and λE depend on T_k, and from a leaf surface, giving:

$$H = 2\Delta L m_a c_p g_H (T_k - T_a) \quad (9.3)$$

$$\lambda E = \lambda \Delta L m_e g_E \frac{e_{\mathrm{sat}}(T_k) - e}{P} \quad (9.4)$$

where ΔL is the LAI in a given canopy layer, m_a and m_e are the molecular weights of air and water, respectively, c_p is the specific heat of air at constant pressure, g_H and g_E are the leaf-scale heat and the vapor conductances, respectively, T_k and T_a are the leaf and air temperatures, $e_{sat}(T_k)$ and e are the saturation vapor pressures at T_k, which can be represented by a function of T_k, and atmospheric water vapor pressure, respectively, and P is the atmospheric pressure.

Equations 9.2, 9.3, and 9.4 are to be solved for one unknown, individual leaf-scale T_k. As may be seen, the T_k is among the most critical factors in computing both biological and physical aspects in the atmosphere-leaf exchange models. For example, the T_k influences a computation result of leaf-scale photosynthetic rate (A) via computation of biocatalytic reactions in the photosynthesis model, and thus, controls the stomatal conductance (see Chap. 3, Hikosaka et al. 2016). Also, T_k modulates the turbulent heat and moisture transfer by controlling thermal convection above the leaf surface, resulting in alteration of the leaf boundary layer conductance. Because H and λE in Eq. 9.2 are altered through these processes, the energy balance model (Eq. 9.2) with the flux models (Eqs. 9.3 and 9.4), the photosynthesis coupled with stomatal conductance model, and the boundary layer conductance model taking into consideration the effects of both forced and free convection (see Campbell and Norman 1998), must be solved simultaneously for all unknowns by numerical iteration.

When we consider the whole vegetation, fluxes from a vegetation surface are given by:

$$H = \rho c_p g_{Ht} (T_k - T_a) \quad (9.5)$$

$$\lambda E = \frac{c_p \rho}{\gamma} g_{Et} (e_{sat}(T_k) - e) \quad (9.6)$$

where ρ is the density of air, γ is the psychrometric constant, T_k is canopy-scale leaf temperature and g_{Ht} and g_{Et} are the canopy-scale heat and the vapor conductances, respectively. Note that the reciprocal of the total conductance is the sum of the reciprocals of the component conductances, namely the stomatal and boundary layer conductances.

Equations 9.2, 9.5, and 9.6 are formulations from a BLM (see Sect. III.B) to be solved for one unknown, canopy-scale T_k. Practically, the T_k is the canopy surface temperature denoting radiative temperature above the canopy, which can be derived using observed upward long-wave radiation and inversion of the Stefan–Boltzmann equation. Thus, note that the canopy-scale T_k cannot be related to the leaf-scale T_k by a simple equation. However, as with the leaf-scale T_k, the canopy-scale T_k alters a computation result of canopy-scale A and stomatal conductance, resulting in modifications of surface energy partitioning (i.e., H and λE) and atmospheric stability above the canopy.

Hence, we can define local feedbacks between the T_k formation and the atmosphere-land fluxes including a carbon flux such as A. Among the feedbacks, this section discusses "aerodynamic feedback," impacts of atmospheric convective motion induced by the T_k formation on the fluxes using canopy-scale theory (Raupach 1998). It should also be noted that when the leaf-scale theory is used, formulations describing fluxes within atmospheric surface layers (see Chap. 10, Kumagai 2016) are almost the same between the two theories. As mentioned above, g_{Et} (and also the canopy-scale CO_2 conductance, g_{Ct}) can be represented as:

$$\frac{1}{g_{Et}} = \frac{1}{g_{at}} + \frac{1}{g_{st}} \tag{9.7}$$

where g_{at} is the aerodynamic conductance, and g_{st} is the canopy stomatal conductance, whose formulation is described in Chap. 2 (Gutschick 2016). For computing g_{Ct}, g_{at} and g_{st} should be adjusted to be appropriate for the CO_2 transfer. g_{at} is usually expressed using Monin-Obukhov similarity theory (Garratt 1992):

$$g_{at} = \frac{\kappa^2 u}{\chi_H(z-d, z_{0H}, l)\chi_M(z-d,\ z_{0M}, l)} \tag{9.8}$$

where κ is the von Karman constant, u is wind velocity measured at a height of z, χ_H and χ_M are dimensionless temperature and velocity profiles, respectively, d is the zero-plane displacement, z_{0H} and z_{0M} are the roughness lengths for heat and momentum, respectively, and l is the Monin-Obukhov length. The aerodynamic feedback denotes the modulations of turbulent heat and moisture transfer by alteration of g_{at} through atmospheric stability (l) and thereby through the surface energy balance (Eq. 9.2), feeding back on Eq. 9.2 itself (Raupach 1998).

Raupach (1998) incorporated the convective boundary layer (see Chap. 10, Kumagai 2016) slab model (McNaughton and Spriggs 1986) into the surface energy balance model (Eq. 9.2) and investigated the impact of aerodynamic feedback on computations of water vapor and CO_2 fluxes (Fig. 9.7). Here, the effect of soil water stress on photosynthetic rate (s_W values in Fig. 9.7) was also considered. Without aerodynamic feedback, surface temperature reaches up to around 40 °C even under the moistest conditions, and the high surface temperature reduces the magnitudes of water vapor and CO_2 fluxes through the effect of stomatal closure in the hottest part of the day. When aerodynamic feedback is considered, turbulent heat and moisture transfer enhanced by unstable stratification induces a cooling effect on the surface, resulting in attenuating the tendency to heat-induced stomatal closure. Thus, assessing and describing surface temperature formation and the atmospheric convective motion above the surface are necessary for building a canopy exchange model.

VI. Validation

A. Plant Growth and Model Prediction

Given that assimilated carbon that is not respired is utilized for plant growth, we can test the validity of predicted gas exchange rates by comparing them with plant growth rates. Previous studies have shown that the estimated canopy carbon exchange rate is closely related to plant growth rate.

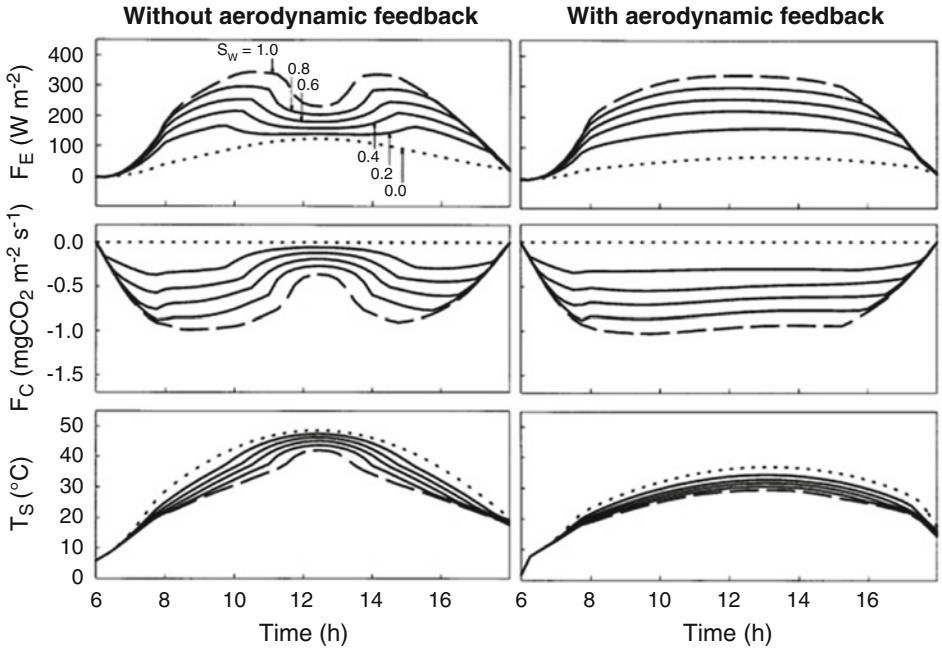

Fig. 9.7. Temporal variations in water vapor (F_E) and CO_2 (F_C) fluxes, and surface temperature (T_S) computed by the surface energy balance model incorporated into the convective boundary layer slab model without (*left panels*) and with (*right panels*) aerodynamic feedback. Different curves represent different values of water stress parameter s_W, which can vary between 0 (highly water-stressed) and 1 (least water-stressed). Redrawn from Raupach (1998 with modification)

For example, Hirose et al. (1997) established stands of annual plants under two CO_2 concentrations in greenhouses with natural sunlight. Although they did not determine the respiration rates of stems and roots, canopy photosynthetic rates estimated with MSM (multilayer model using simple light extinction) were significantly correlated with stand growth rates. Borjigidai et al. (2009) established stands of *Chenopodium album* under two CO_2 concentrations using open-top chambers. Growth rates were estimated using biomass and dead parts of plants harvested four times during the growing season. Canopy photosynthesis was estimated using MSM with environmental variables determined near the open-top chambers and respiration rates of stems and roots were determined. The estimated carbon balance was not only strongly correlated but also showed a 1:1 relationship with stand growth (Fig. 9.8a), suggesting that CPMs predict quantitatively correct rates of CO_2 exchange rates. See also Chap. 12 (Ohtsuka et al. 2016) for the case of a forest ecosystem.

CPMs are useful for estimation of carbon exchange of individuals in a plant stand (See Chap. 14, Anten and Bastiaans 2016 for their principle). Hikosaka et al. (1999, 2003) estimated growth rates of aboveground part of individuals in a dense stand of annual plants using allometric relationships between size and mass of individual plants. The calculated plant growth rates were strongly correlated with leaf daily carbon gain of individuals (Fig. 9.8b), suggesting that CO_2 exchange rates can also be estimated correctly even at an individual level.

B. Eddy Covariance and Model Prediction

Measurements of CO_2 flux by the eddy covariance method allow us to examine terrestrial carbon cycle models in terms of canopy- and ecosystem-scale net carbon

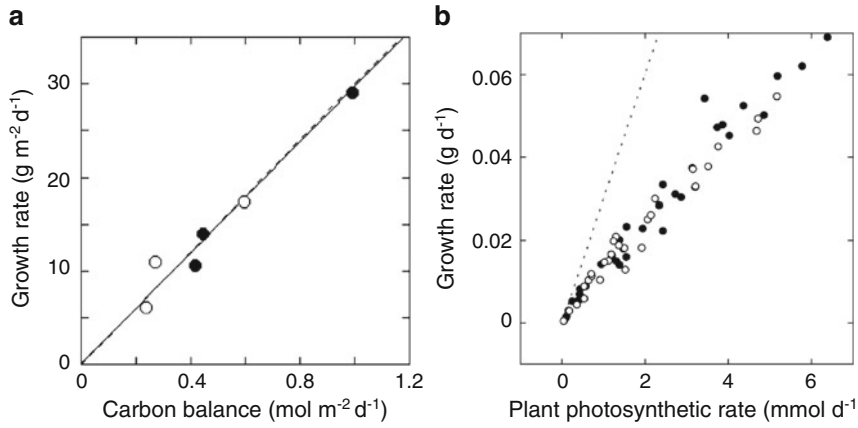

Fig. 9.8. Comparison between plant growth and estimated carbon balance. (**a**) Growth rate per unit ground area of *Chenopodium album* stands as a function of estimated daily carbon balance (canopy photosynthesis minus respiration). Stands were established at two CO_2 concentrations (*open* and *closed circle* denotes ambient and 700 μmol mol^{-1}, respectively). The plant density was 93 m^{-2} and top leaves of all individuals were exposed to the canopy top. The whole plant body was harvested four times and the growth rate for each interval was determined. Carbon balance was calculated as a mean of the interval. See Borjigidai et al. (2009) for details. (**b**) Growth rate of individuals in *C. album* stands as a function of estimated daily carbon gain. Stands were established at two CO_2 concentrations (*open* and *closed circles* show ambient and 700 μmol mol^{-1}, respectively). The plant density was 400 m^{-2} and there was a large variation in plant size. Aboveground mass of each individual in the census quadrat was estimated in the first census using the allometric relationship of length and diameter of stems and aboveground mass of harvested individuals from another quadrat. In the second census aboveground part of individuals in the census quadrat was estimated. Carbon gain was estimated as average for leaves of each individual in the two census (allocation of assimilates to stems and roots was not considered). See Hikosaka et al. (2003) for details

budget at fine temporal resolutions (see Chap. 10, Kumagai 2016). The eddy-covariance method directly measures net ecosystem CO_2 exchange (NEE), which can be separated into photosynthetic and respiratory components on the basis of the nighttime temperature–NEE (respiration only) relationship (Reichstein et al. 2005). Thus, it is possible to compare gross primary production (GPP, which is essentially same as the gross canopy photosynthesis), ecosystem respiration (RE), and NEE (= GPP − RE) between model estimations and flux measurements at typically 30-min time steps. Until the mid-1990s, it was impossible to evaluate NEE directly; in most cases, field-measured net primary production (NPP) and carbon stock data at annual time steps were used for model validation. Development of the flux measurement method allowed model validation in a novel and more accurate manner. At present, flux measurement sites constitute a worldwide network, called FLUXNET (Baldocchi et al. 2001); 732 sites as of July 2015. Since the establishment of the first tower site in Harvard Forest, U.S., in 1992, more than 20 years of records have accumulated and are accessible to researchers, allowing us to explore not only micrometeorological but also ecological aspects of CO_2 fluxes (Baldocchi 2008).

Although increasing amounts of flux measurement data are available, several limitations should be considered when model validation is performed with these data. First, there are some biases and errors associated with measurements by the eddy covariance method, especially during nighttime and in mountainous areas, owing to hilly terrain. The fundamental micrometeorological theory on which the eddy covariance method is based was developed for a sufficiently turbulent condition over a flat

surface and cannot adequately consider the effect of advection (transport by air mass flow). Second, the quality of flux data depends heavily on the methods used for bias correction, data selection, and gap-filling. For example, Papale et al. (2006) showed that threshold friction velocity of wind (u^*, an index of atmospheric turbulence) is one of the critically important factors for data selection and quality. Third, the spatial scale usually differs between the ecosystem model and the flux measurement. In general, the upwind area contributing to the flux measured by instruments (in micrometeorology, this area is called a footprint) depends on wind condition and covers up to a few square kilometers (km^2), whereas ecosystem models are often applied to broader areas. In particular, the spatial resolution of global terrestrial ecosystem models is typically hundreds to thousands of km^2 (e.g., $0.5^\circ \times 0.5^\circ$, a typical global-model grid size, covers about 3000 km^2 on the equator) often containing diverse land cover types. In addition, the footprint of flux measurement varies with wind direction. Accordingly, when flux data are used for model validation, care about such data limitations and scale-gaps is essential.

During the last 10 years, more and more studies have used flux measurement data for validation of terrestrial carbon cycle models including CPMs. Sitch et al. (2003) validated the LPJ dynamic global vegetation model at six sites in Europe. Krinner et al. (2005) validated the ORCHIDEE model at 28 sites in Europe, not only for NEE but also for energy exchange fluxes. Ito et al. (2005) and Sasai et al. (2005) applied the VISIT and the BEAMS models, respectively, to the Takayama flux measurement site in Japan; Fig. 9.9 shows examples of the site-scale validation using flux measurement data.

Recently, flux measurement data have been used for model validation in other ways as well, especially as benchmarking data for model intercomparison. Several studies have compared ecosystem models at multiple sites (e.g., Kramer et al. 2002; Morales et al. 2005; Schwalm et al. 2010; Richardson et al. 2012; Ichii et al. 2013). These studies indicated that the present models worked poorly in several regions;

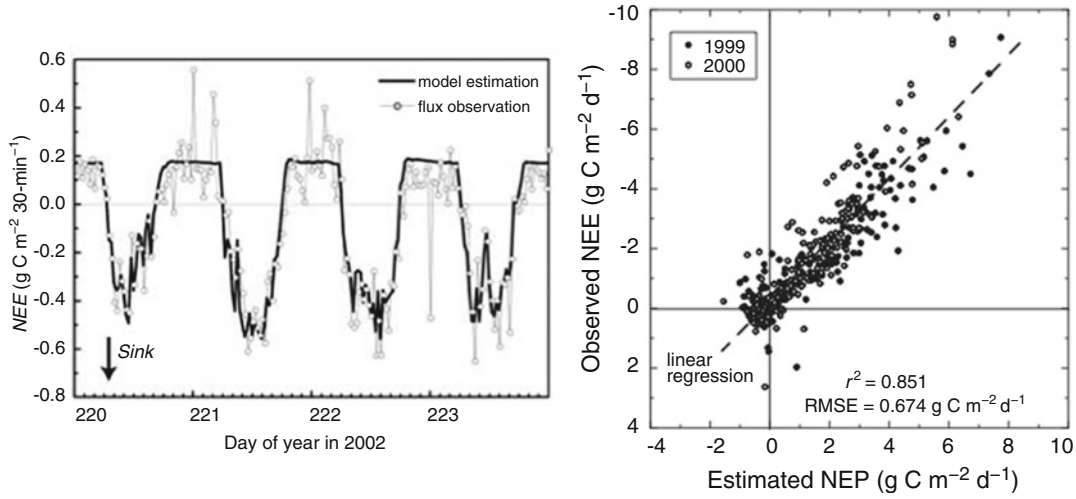

Fig. 9.9. Comparison of net CO_2 exchange (NEE) between eddy-covariance measurement and model estimation at the Takayama site. A process-based terrestrial ecosystem model, VISIT (Ito et al. 2006), was applied to the site, using the sun–shade canopy scheme of de Pury and Farquhar (1997). (*Left*) Time-series of 30-min step simulation in mid-summer of 2002, and (*right*) 1:1 comparison for daily NEE in 1999 and 2000. Note that seasonal change in leaf photosynthetic parameters is included in an empirical manner

for example, Morales et al. (2005) showed that most models failed in simulating CO_2 fluxes at Mediterranean sites, where water stress is a key factor. Also, these comparison studies are effective for identifying key processes. For example, Richardson et al. (2012) suggested that the present ecosystem models have difficulty in simulating leaf phenology.

These validations show that the present models have improved in capturing canopy photosynthesis in various ecosystems. Incorporating biochemical photosynthesis models and canopy radiation models (mentioned above) into ecosystem models make them highly mechanistic, allowing researchers to interpret observational data from an ecophysiological point of view and to conduct various sensitivity analyses to identify key parameters. However, it is also apparent that uncertainties remain in the present models, as implied by model intercomparison studies. As shown by the canopy-model comparison (Fig. 9.3), differences in model structure, parameter values, and assumptions can result in remarkably different simulation results. To improve simulation credibility, we need further refinement of process models including CPMs and broad-scale validation using data from multiple sites.

VII. Application of Canopy Photosynthesis Models to Larger Scales

Because quantification of primary productivity of the biosphere has received much interest from ecologists and geochemists, many researchers have attempted to evaluate global GPP and NPP (Ito 2011). For example, the International Biological Programme (IBP, 1965–1972) collected a large number of field data of NPP from various ecosystems and estimated global total NPP. During the IBP period, empirical models (statistical regression) were used; for example, the Miami model estimates annual NPP of any terrestrial ecosystems as a function of annual mean temperature and annual precipitation (Lieth 1975). Although these models captured the geographic variability of mean annual NPP well, they were unable to simulate seasonal and interannual variability and environmental impacts, such as for land-use change.

During the last few decades, global environmental issues have gained increasing awareness from the general public and scientific community as one of the urgent issues. In particular, temporal variability and spatial heterogeneity of the carbon cycle, including terrestrial CO_2 uptake has received attention from many researchers. Accordingly, canopy or vegetation models have been used at large spatial scales, including the global scale. Table 9.2 summarizes the canopy parameterization approaches used in several global terrestrial ecosystem models. Additionally, several recent models have adopted individual-based approaches to simulating vegetation dynamics (e.g., Levy et al. 2004; Sato et al. 2007) in conjunction with some photosynthetic scheme. Because observational data of ecosystem properties are quite limited at these scales, the models are expected to work at as little input of a priori information as possible. As mentioned above, empirical models have been widely used to estimate terrestrial primary productivity. During the early period of global studies (the 1980s and early 1990s), only a few datasets of global climatology and land cover were available. In the 1990s, many different kinds of global terrestrial models were developed in accordance with the increase of global datasets.

In particular, global satellite remote sensing data became available, enabling us to evaluate vegetation activity at broader scales. Importantly, Monteith (1977) developed a fundamental relationship between canopy-observed solar energy and vegetation productivity; the conversion coefficient was termed light-use efficiency (LUE; carbon exchange per unit absorbed light). Using the satellite-derived vegetation absorption of solar energy (PFD) and the LUE principle, it was possible to estimate NPP by remote

Table 9.2. Summary of canopy schemes in several global terrestrial ecosystem models

Model	Biome-BGC	CASA	CLM ver.4	LPJ	ORCHIDEE	VISIT
References	Running and Hunt (1993)	Potter et al. (1993)	Bonan et al. (2011)	Sitch et al. (2003)	Krinner et al. (2005)	Ito et al. (2005)
Canopy structure	Mono-layer	Mono-layer	Mono-layer (tree/grass)	Mono-layer (tree/grass)	Mono-layer (tree/grass)	Overstory/understory
Leaf photosynthesis	Asymptotic light-response curve	Light-use efficiency model	Biochemical model (Farquhar)	Biochemical model (Haxeltin and Prentice)	Biochemical model (Farquhar)	Biochemical model (Farquhar)
Scaling-up method	Big-leaf	Big-leaf	Sun/shade, N distribution	Optimal leaf N distribution	Optimal leaf N distribution	Sun/shade, N distribution
C_3/C_4 plants	No	No	Yes	Yes	Yes	Yes
Stomata	Nobel	No	Ball et al.	Haxeltin and Prentice	Ball et al.	Leuning

sensing. Since 1982, continuous monitoring data of global terrestrial vegetation are available such as NOAA-AVHRR, Terra/Aqua-MODIS, and SPOT-VEGETATION for the purposes of various analytical and modeling studies. Time-series of vegetation indices (e.g., NDVI, Normalized Difference Vegetation Index) have revealed seasonal and interannual variation of vegetation activity (Myneni et al. 1997; Nemani et al. 2003). The vegetation indices are also useful for characterizing the photosynthetic properties of vegetation stands. For example, Sellers (1985) estimated the fraction of canopy-absorbed PFD from the simple ratio of visible red to near-infrared reflectance. Subsequently, Potter et al. (1993) adopted this approach and developed a new terrestrial ecosystem model, the Carnegie-Ames-Stanford Approach (CASA). Similar methodology was employed by several models (e.g., Ruimy et al. 1996; Goetz et al. 1999). These models are simple and reasonably capture the present vegetation productivity. However, they have several shortcomings: (1) these models are driven by satellite-observed data and so are not applicable for future projections; (2) it is difficult to include ecophysiological findings to improve this kind of model, although Sasai et al. (2005) has developed a mechanistic satellite-driven model. More recently, new sensors, such as synthetic aperture radar and lidar, are used to assess canopy structure from the space.

To improve future projections, process-based models of terrestrial ecosystems are effective because these models consider ecophysiological factors such as different environmental responsiveness between C_3 and C_4 plants. Several process-based models have been developed on the basis of stand-scale carbon cycle models and tested using field data. Running and Hunt (1993) developed a global model, the Biome-BGC, on the basis of the Forest-BGC model developed for pine forest studies in Montana, U.S. Similarly, Ito and Oikawa (2002) developed the Simulation model of Carbon cYCle in Land Ecosystem (Sim-CYCLE) on the basis of a carbon cycle model that was developed for tropical forest studies in Pasoh, Malaysia. Figure 9.10 shows the global annual NPP and its water-use efficiency estimated by VISIT (Ito and Inatomi 2012), developed from Sim-CYCLE. Earlier global terrestrial models adopted the "big-leaf" canopy approach for simplicity, and it is notable that these models are able to predict LAI and estimate impacts of environmental change. For global application, these models should estimate leaf phenology in deciduous forests and grasslands, which is determined by temperature, water, and radiation (for example, day-length) conditions. Many models include some phenological scheme, in which leaf seasonal display and shedding occur on the basis of cumulative temperatures above/below certain threshold

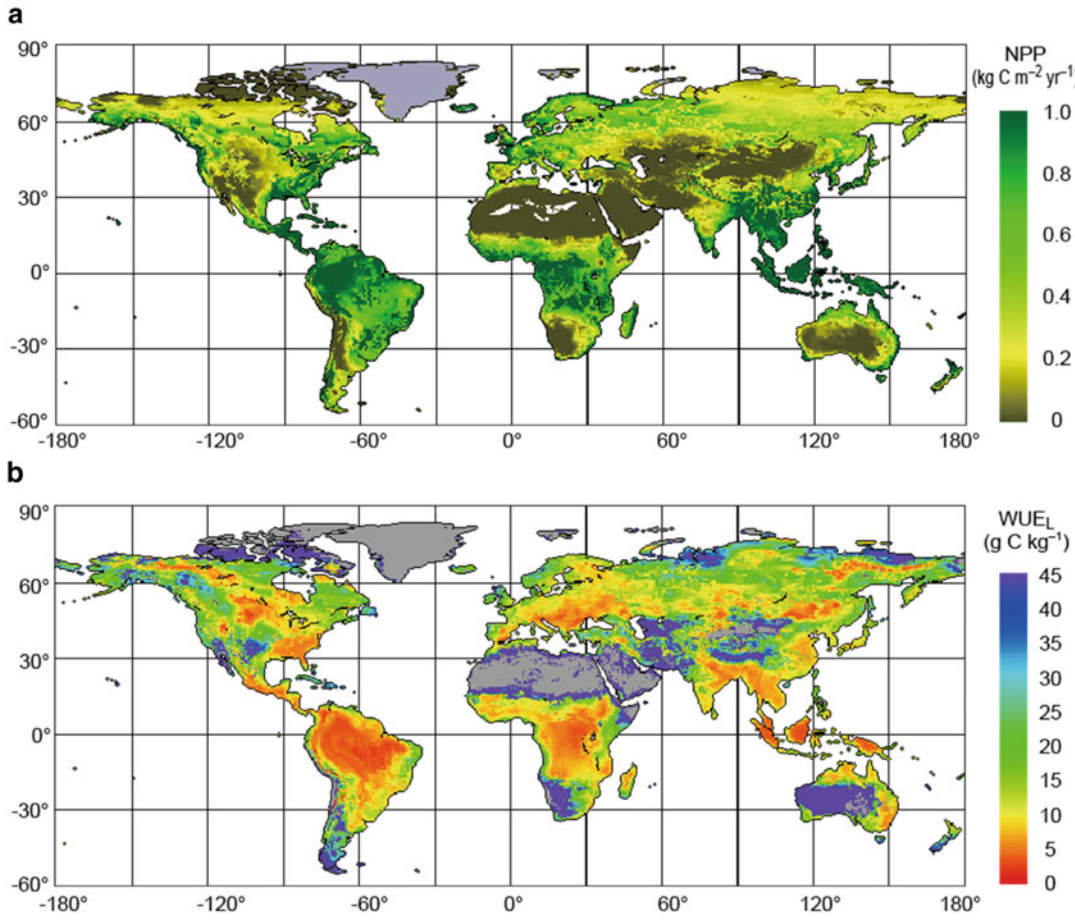

Fig. 9.10. Global distribution of (**a**) net primary production (NPP) of terrestrial ecosystems and (**b**) water-use efficiency (WUE, carbon assimilation per unit later loss) in 1995–2004, estimated by VISIT model (Ito and Inatomi 2012)

temperatures. The "big-leaf" scheme in earlier process-based models considers vertical attenuation of PFD within canopy but in most cases neglects the difference between direct and diffuse radiation as discussed earlier (see Sect. III.B. BLM). Using the Monsi–Saeki theory, leaf-level photosynthesis is integrated to canopy-level gross primary production (GPP), considering environmental factors (ambient CO_2, temperature, and moisture) in empirical but ecophysiological ways. For example, the leaf modules estimate stomatal conductance using several semi-empirical models (e.g., Ball et al. 1987; Leuning 1995; see Chap. 3, Hikosaka et al. 2016), which respond directly to atmospheric humidity and CO_2 concentration. A similar approach was adopted by land-surface parameterization schemes (such as the second version of Simple Biosphere [SiB2]; Sellers et al. 1997) used in climate models, which need to estimate surface energy and gas exchange including stomatal regulation. In most cases, the temperature and moisture limitations were included by developing empirical scholar functions (i.e., multipliers; from zero under severe conditions to one under standard condition) for maximum photosynthetic rate. Because terrestrial models differ in canopy integration (for example, assumption of light attenuation coefficient) and

environmental functions, their simulation results are not always consistent, implying estimation uncertainty.

Since the late 1990s, advances in CPMs have made it easier to conduct simulations of global terrestrial production and the carbon cycle. On the other hand, model validations in comparison with observation data have indicated that there remain large uncertainties and insufficiencies in the present models. One evident example is the anomalous CO_2 uptake after the huge eruption of Mt. Pinatubo, Philippines, in June 1991. After the eruption, a massive amount of volcanic ash was ejected into the atmosphere, as far as to the stratosphere, resulting in unusual scattering of solar radiation. This event was associated with anomalous cooling of Earth's surface by about 0.5 °C, affecting terrestrial ecosystems including croplands. Simultaneously, the atmospheric CO_2 growth rate slowed down notably, but the mechanism causing this slowdown has not been clear. Several model studies implied a reduction of respiratory emissions due to cooling, but it was insufficient to explain the phenomenon fully. Gu et al. (2003) pointed out that net CO_2 uptake of the Harvard Forest increased apparently after the Mt. Pinatubo eruption and proposed a hypothesis that increase of diffuse radiation after the event enhanced photosynthetic CO_2 uptake by the vegetation canopy at broad scale (Roderick et al. 2001). Because the "big-leaf" canopy scheme could not evaluate the effect of different radiation components (direct and diffuse radiation), the anomalous event enhanced use of the more mechanistic canopy radiation transfer and photosynthetic scheme to adequately capture the interannual variability of terrestrial CO_2 budget. Also, Mercado et al. (2009) implied that the diffuse-radiation fraction would increase as a result of human-emitted aerosols, indicating the importance of an improved canopy scheme for global terrestrial ecosystem models. Accordingly, several recent terrestrial models employ sun–shade canopy schemes (SSM) to include biochemical photosynthetic responses and canopy absorption of direct–diffuse light as discussed in Sect. III.

More than 30 terrestrial ecosystem models applicable to global scale have been developed. They are used for simulating not only current states but also past and future changes in response to environmental change. Process-based models are expected to work reasonably well under different conditions because they take account of ecophysiological factors (such as CO_2 fertilization effects on photosynthesis) determining ecosystem responsiveness. For example, Melillo et al. (1993) estimated that global NPP would increase by about 20 % under doubled atmospheric CO_2 and climate change condition using the Terrestrial Ecosystem Model (TEM). More recently, Friend et al. (2014) assessed the future change in vegetation carbon budget on the basis of simulation results of seven terrestrial ecosystem models.

As shown in Table 9.2, current terrestrial models adopt different canopy schemes in terms of complexity and environmental responsiveness. Another important feature is the inclusion of nitrogen effects on canopy photosynthesis. Using the model sensitivity analysis, Friend (2001) found that realistic nitrogen allocation should be taken into account for improving model simulations, in comparison with classical "big-leaf" models. This finding is consistent with field-scale ecophysiological and modeling studies (e.g., Hirose and Werger 1987b; Hikosaka 2014). The current models differ in approach and complexity in parameterization of canopy processes (Table 9.2), leading to considerable intermodel difference in estimated results. For example, Cramer et al. (1999) compared global terrestrial NPP estimated by 17 models and found that the results ranged from 39.9 to 80.5 Pg C $year^{-1}$ (Pg = 10^{15} g), even using common input climate data and simulation protocols. Such estimation uncertainty has not been reduced until recently. In the Multi-scale Terrestrial Model Intercomparison Project (MsTMIP; Huntzinger et al. 2013), it was found that 10 terrestrial models

differ in estimates of global terrestrial NPP from 36 to 67 Pg C $year^{-1}$ at the present time. A similar range of variability was also found among the terrestrial models embedded in Earth System Models (Todd-Brown et al. 2013), which are used for climate projection. Apparently, such uncertainty exerts serious influences on future projections under global environmental change, including the climatic feedback by the terrestrial biosphere through CO_2 exchange. Further studies are needed to improve vegetation canopy models and to reduce estimation uncertainty.

VIII. Conclusion

Current CPMs can predict land–atmosphere exchange rates of carbon, water, and energy almost correctly. Not only detailed models but also simplified models, some of which provide quite accurate predictions, have been developed. Scaling up from leaf to canopy level contributes to the understanding of mechanisms that cause variation in canopy exchange rates of gas and energy. CPMs also contribute to future projections of responses in ecosystem functions to future global climate change. For accurate prediction, however, we need detailed information of plant traits such as LAI, light extinction coefficient, leaf biochemical characteristics, and vertical variation in leaf traits, all of which vary considerably between species and as a function of environmental factors. Since part of environmental responses of such plant traits are not fully known, some projections involve large uncertainties. The increasing amounts of flux measurement data, ecophysiological findings, and the improvement of data–model fusion, especially in a collaborative manner, will bring new and deeper insights and eventually allow advanced prediction.

Acknowledgments

We thank Niels Anten for valuable comments. This work was supported by Grants-in-Aid for Scientific Research on Innovative Areas (Nos. 21114009 and 21114010), by KAKENHI (Nos. 20677001, 25291095, 20323503 and 25660113) and by CREST, JST, Japan.

References

Amthor JS (1994) Scaling CO_2-photosynthesis relationships from the leaf to the canopy. Photosynth Res 39:321–350

Anten NPR (1997) Modelling canopy photosynthesis using parameters determined from simple non-destructive measurements. Ecol Res 12:77–88

Anten NPR (2016) Optimization and game theory in canopy models. In: Hikosaka K, Niinemets Ü, Anten N (eds) Canopy Photosynthesis: From Basics to Applications. Springer, Berlin, pp 355–377

Anten NPR, Bastiaans L (2016) The use of canopy models to analyze light competition among plants. In: Hikosaka K, Niinemets Ü, Anten N (eds) Canopy Photosynthesis: From Basics to Applications. Springer, Berlin, pp 379–398

Anten NPR, Hirose T (2003) Shoot structure, leaf physiology and carbon gain of species in a grassland. Ecology 84:955–968

Anten NPR, Werger MJA (1996) Canopy structure and nitrogen distribution in dominant and subordinate plants in a dense stand of *Amaranthus dubius* (L.) with a size hierarchy of individuals. Oecologia 105:30–37

Anten NPR, Schieving F, Werger MJA (1995a) Patterns of light and nitrogen distribution in relation to whole canopy carbon gain in C_3 and C_4 mono- and dicotyledonoous species. Oecologia 101:504–513

Anten NPR, Schieving F, Medina E, Werger MJA, Schuffelen P (1995b) Optimal leaf area indices in C_3 and C_4 mono- and dicotyledonous species at low and high nitrogen availability. Physiol Plant 95:541–550

Anten NPR, Hikosaka K, Hirose T (2000) Nitrogen utilization and the photosynthetic system. In: Marshal B, Roberts J (eds) Leaf Development and Canopy Growth. Sheffield Academic, Sheffield, pp 171–203

Anten NPR, Hirose T, Onoda Y, Kinugasa T, Kim HY, Okada M, Kobayashi K (2004) Elevated CO_2 and nitrogen availability have interactive effects on canopy carbon gain in rice. New Phytol 161:459–471

Baldocchi D (1994) An analytical solution for coupled leaf photosynthesis and stomatal conductance models. Tree Physiol 14:1069–1079

Baldocchi D (2008) 'Breathing' of the terrestrial biosphere: lessons learned from a global network of carbon dioxide flux measurement systems. Aust J Bot 56:1–26

Baldocchi DD, Harley PC (1995) Scaling carbon dioxide and water vapor exchange from leaf to canopy in a deciduous forest: model testing and application. Plant Cell Environ 18:1157–1173

Baldocchi D, Falge E, Gu L, Olson R, Hollinger D, Running S, Anthoni P, ..., Wofsy S (2001) FLUXNET: a new tool to study the temporal and spatial variability of ecosystem-scale carbon dioxide, water vapor, and energy flux densities. Bull Am Meteorol Soc 82:2415–2434

Ball JT, Woodrow IE, Berry JA (1987) A model predicting stomatal conductance and its contribution to the control of photosynthesis under different environmental conditions. In: Biggins I (ed) Progress in Photosynthesis Research. Martinus Nijhoff, La Hague, pp 221–224

Bonan GB, Lawrence PJ, Oleson KW, Levis S, Jung M, Reichstein M, Lawrence DM, Swenson SC (2011) Improving canopy processes in the Community Land Model version 4 (CLM4) using global flux fields empirically inferred from FLUXNET data. J Geophys Res 116, G02014. doi:10.1029/2010JG001593

Borjigidai A, Hikosaka K, Hirose T (2009) Carbon balance in a monospecific stand of an annual, *Chenopodium album*, at an elevated CO_2 concentration. Plant Ecol 203:33–44

Boysen Jensen P (1932) Die Stoffproduktion der Pflanzen. Gustav Fischer, Jena

Campbell GS, Norman JM (1998) An Introduction to Environmental Biophysics. Springer, New York

Cramer W, Kicklighter DW, Bondeau A, Moore BI, Churkina G, Nemry B, Ruimy A, ..., Potsdam-NPP-model-intercomparison-participants (1999) Comparing global NPP models of terrestrial net primary productivity (NPP): overview and key results. Global Change Biol 5(Suppl 1): 1–15

de Pury DGG, Farquhar GD (1997) Simple scaling of photosynthesis from leaves to canopies without the errors of big-leaf models. Plant Cell Environ 20:537–557

de Wit CT (1965) Photosynthesis of Leaf Canopies. Pudoc, Wageningen

Evers JB (2016) Simulating crop growth and development using functional-structural plant modeling. In: Hikosaka K, Niinemets Ü, Anten N (eds) Canopy Photosynthesis: From Basics to Applications. Springer, Berlin, pp 219–236

Farquhar GD (1989) Models of integrated photosynthesis of cells and leaves. Philos Trans R Soc B 323:357–367

Farquhar GD, von Caemmerer S, Berry JA (1980) A biochemical model of photosynthetic CO_2 assimilation in leaves of C_3 species. Planta 149:78–90

Friend AD (2001) Modeling canopy CO_2 fluxes: are 'big-leaf' simplifications justified? Glob Ecol Biogeogr 10:603–619

Friend AD, Lucht W, Rademacher TT, Keribin RM, Betts R, Cadule P, Ciais P, ..., Woodward FI (2014) Carbon residence time dominates uncertainty in terrestrial vegetation responses to future climate and atmospheric CO_2. Proc Nat Acad Sci USA 111:3280–3285

Garratt JR (1992) The Atmospheric Boundary Layer. Cambridge University Press, Cambridge

Goetz SJ, Prince SD, Goward SN, Thawley MM, Small J (1999) Satellite remote sensing of primary production: an improved production efficiency modeling approach. Ecol Model 122:239–255

Goudriaan J (1977) Crop Micrometeorology: A simulation study, Simulation monographs. Pudoc, Wageningen

Goudriaan J (2016) Light distribution. In: Hikosaka K, Niinemets Ü, Anten N (eds) Canopy Photosynthesis: From Basics to Applications. Springer, Berlin, pp 3–22

Goudriaan J, van Laar HH (1994) Modelling Potential Crop Growth Processes. Kluwer Academic Publishers, Dordrecht

Gu L, Baldocchi DD, Wofsy SC, Munger JW, Michalsky JJ, Urbanski S, Boden TA (2003) Response of a deciduous forest to the Mount Pinatubo eruption: enhanced photosynthesis. Science 299:2035–2038

Gutschick VP (2016) Leaf energy balance: basics, and modeling from leaves to canopies. In: Hikosaka K, Niinemets Ü, Anten N (eds) Canopy Photosynthesis: From Basics to Applications. Springer, Berlin, pp 23–58

Harley PC, Baldocchi DD (1995) Scaling carbon dioxide and water vapour exchange from leaf to canopy in a deciduous forest. I. Leaf model parameterization. Plant Cell Environ 18:1146–1156

Harley PC, Tenhunen JD (1991) Modelling the photosynthetic response of C_3 leaves to environmental factors. In: Boote KJ, Loomis RS (eds) Modelling Crop Photosynthesis – From Biochemistry to Canopy. CSSA, Madison, pp 17–39

Harley PC, Thomas RB, Reynolds JF, Strain BR (1992) Modelling the effects of growth in elevated CO2 on photosynthesis in cotton. Plant Cell Environ 15:271–282

Hikosaka K (2014) Optimal nitrogen distribution within a leaf canopy under direct and diffuse light. Plant Cell Environ 9:2077–2085

Hikosaka K, Shigeno A (2009) The role of Rubisco and cell walls in the interspecific variation in photosynthetic capacity. Oecologia 160:443–451

Hikosaka K, Sudoh S, Hirose T (1999) Light acquisition and use of individuals competing in a dense stand of an annual herb, *Xanthium canadense*. Oecologia 118:388–396

Hikosaka K, Yamano T, Nagashima H, Hirose T (2003) Light-acquisition and use of individuals as influenced by elevated CO_2 in even-aged monospecific stands of *Chenopodium album*. Funct Ecol 17:786–795

Hikosaka K, Noguchi K, Terashima I (2016) Modeling leaf gas exchange. In: Hikosaka K, Niinemets Ü, Anten N (eds) Canopy Photosynthesis: From Basics to Applications. Springer, Berlin, pp 61–100

Hirose T (2005) Development of the Monsi–Saeki theory on canopy structure and function. Ann Bot 95:483–494

Hirose T, Werger MJA (1987a) Nitrogen use efficiency in instantaneous and daily photosynthesis of leaves in the canopy of a *Solidago altissima* stand. Physiol Plant 70:215–222

Hirose T, Werger MJA (1987b) Maximizing daily canopy photosynthesis with respect to the leaf nitrogen allocation pattern in the canopy. Oecologia 72:520–526

Hirose T, Ackerly DD, Traw MB, Ramseier D, Bazzaz FA (1997) CO_2 elevation, canopy photosynthesis, and optimal leaf area index. Ecology 78:2339–2350

Huntzinger DN, Schwalm C, Michalak AM, Schaefer K, King AW, Wei Y, Jacobson A, . . ., Zhu Q (2013) The North American carbon program multi-scale synthesis and terrestrial model intercomparison project: part 1: overview and experimental design. Geosci Model Dev 6:2121–2133

Ichii K, Kondo M, Lee Y-H, Wang S-Q, Kim J, Ueyama M, Lim H-J, . . ., Zaho F-H (2013) Site-level model-data synthesis of terrestrial carbon fluxes in the CarboEastAsia eddy-covariance observation network: toward future modeling efforts. J For Res 18:13–20

Ito A (2011) A historical meta-analysis of global terrestrial net primary productivity: are estimates converging? Glob Chang Biol 17:3161–3175

Ito A, Inatomi M (2012) Water-use efficiency of the terrestrial biosphere: a model analysis on interactions between the global carbon and water cycles. J Hydrometeorol 13:681–694

Ito A, Oikawa T (2002) A simulation model of the carbon cycle in land ecosystems (Sim-CYCLE): a description based on dry-matter production theory and plot-scale validation. Ecol Model 151:147–179

Ito A, Saigusa N, Murayama N, Yamamoto S (2005) Modeling of gross and net carbon dioxide exchange over a cool-temperate deciduous broad-leaved forest in Japan: analysis of seasonal and interannual change. Agric For Meteorol 134:122–134

Kamiyama C, Oikawa S, Kubo T, Hikosaka K (2010) Light interception in species with different functional types coexisting in moorland plant communities. Oecologia 164:591–599

Kramer K, Leinonen KI, Bartelink HH, Berbigier P, Borghetti M, Bernhofer C, Cienciala E, . . ., Vesala T (2002) Evaluation of six process-based forest growth models using eddy-covariance measurements of CO_2 and H_2O fluxes at six forest sites in Europe. Glob Chang Biol 8:213–230

Krinner G, Viovy N, de Noblet-Ducoudré N, Ogée J, Polcher J, Friedlingstein P, Ciais P, . . ., Prentice IC (2005) A dynamic global vegetation model for studies of the coupled atmosphere-biosphere system. Global Biogeochem Cycles 19: GB1015

Kumagai T (2016) Observation and modeling of net ecosystem carbon exchange over canopy. In: Hikosaka K, Niinemets Ü, Anten N (eds) Canopy Photosynthesis: From Basics to Applications. Springer, Berlin, pp 269–287

Kumagai T, Ichie T, Yoshimura M, Yamashita M, Kenzo T, Saitoh TM, Ohashi M, . . ., Komatsu H (2006) Modeling CO_2 exchange over a Bornean tropical rain forest using measured vertical and horizontal variations in leaf-level physiological parameters and leaf area densities. J Geophys Res 111:D10107

Leuning R (1995) A critical appraisal of a combined stomatal-photosynthesis model for C_3 plants. Plant Cell Environ 18:339–355

Levy PE, Cannell MGR, Friend AD (2004) Modelling the impact of future changes in climate, CO_2 concentration and land use on natural ecosystems and the terrestrial carbon sink. Glob Environ Chang 14:21–30

Lieth H (1975) Modeling the primary productivity of the world. In: Lieth H, Whittaker RH (eds) Primary Productivity of the Biosphere. Springer, Berlin, pp 237–263

Lloyd J, Grace J, Miranda AC, Meir P, Miranda HS, Wright IR, Gash JHC, McIntyre J (1995) A simple calibrated model of Amazon rainforest productivity based on leaf biochemical properties. Plant Cell Environ 18:1129–1145

McNaughton KG, Spriggs TW (1986) A mixed layer model for regional evaporation. Bound Lay Meteorol 34:243–262

Melillo JM, McGuire AD, Kicklighter DW, Moore B III, Vörösmarty CJ, Schloss AL (1993) Global climate change and terrestrial net primary production. Nature 363:234–240

Mercado LM, Bellouin N, Sitch S, Boucher O, Huntingford C, Wild M, Cox PM (2009) Impact of

changes in diffuse radiation on the global land carbon sink. Nature 458:1014–1017

Monsi M, Saeki T (1953) Über den Lichtfaktor in den Pflanzengesellschaften und seine Bedeutung für die Stoffproduktion. Jpn J Bot 14:22–52. *Translated as*: Monsi M, Saeki T (2005) On the factor light in plant communities and its importance for matter production. Ann Bot 95:549–567

Monsi M, Uchijima Z, Oikawa T (1973) Structure of foliage canopies and photosynthesis. Annu Rev Ecol Syst 4:301–327

Monteith JL (1972) Solar radiation and productivity of terrestrial ecosystems. J Appl Ecol 9:747–766

Monteith JL (1977) Climate and efficiency of crop production in Britain. Phil Trans R Soc London Ser B 281:277–294

Morales P, Sykes MT, Prentice IC, Smith P, Smith B, Bugmann H, Zierl B, . . ., Ogee J (2005) Comparing and evaluating process-based ecosystem model predictions of carbon and water fluxes in major European forest biomes. Glob Chang Biol 11:2211–2233

Myneni RB, Keeling CD, Tucker CJ, Asrar G, Nemani RR (1997) Increased plant growth in the northern high latitudes from 1981 to 1991. Nature 386:698–702

Nemani RR, Keeling CD, Hashimoto H, Jolly WM, Piper SC, Tucker CJ, Myneni RB, Running SW (2003) Climate-driven increases in global terrestrial net primary production from 1982 to 1999. Science 300:1560–1563

Niinemets Ü (2016) Within-canopy variations in functional leaf traits: structural, chemical and ecological controls and diversity of responses. In: Hikosaka K, Niinemets Ü, Anten N (eds) Canopy Photosynthesis: From Basics to Applications. Springer, Berlin, pp 101–141

Ohtsuka T, Saigusa N, Imura Y, Muraoka H, Koizumi H (2016) Biometric-based estimations of net primary production (NPP) in forest ecosystems. In: Hikosaka K, Niinemets Ü, Anten N (eds) Canopy Photosynthesis: From Basics to Applications. Springer, Berlin, pp 333–351

Papale D, Reichstein M, Aubinet M, Canfora E, Bernhofer C, Kutsch W, Longdoz B, . . ., Yakir D (2006) Towards a standardized processing of net ecosystem exchange measured with eddy covariance technique: algorithms and uncertainty estimation. Biogeosci 3:571–583

Pons TL (2016) Regulation of leaf traits in canopy gradients. In: Hikosaka K, Niinemets Ü, Anten N (eds) Canopy Photosynthesis: From Basics to Applications. Springer, Berlin, pp 143–168

Potter CS, Randerson JT, Field CB, Matson PA, Vitousek PM, Mooney HA, Klooster SA (1993) Terrestrial ecosystem production: a process model based on global satellite and surface data. Global Biogeochem Cycles 7:811–841

Raupach MR (1998) Influences of local feedbacks on land-air exchanges of energy and carbon. Glob Chang Biol 4:477–494

Reichstein M, Falge E, Baldocchi D, Papale D, Aubinet M, Berbigier P, Bernhofer C, . . ., Valentini R (2005) On the separation of net ecosystem exchange into assimilation and ecosystem respiration: review and improved algorithm. Glob Chang Biol 11:1424–1439

Richardson AD, Anderson RS, Arain MA, Barr AG, Bohrer G, Chen G, Chen JM, . . ., Xue Y (2012) Terrestrial biosphere models need better representation of vegetation phenology: results from the North American carbon program site synthesis. Glob Chang Biol 18:566–584

Roderick ML, Farquhar GD, Berry SL, Noble IR (2001) On the direct effect of clouds and atmospheric particles on the productivity and structure of vegetation. Oecologia 129:21–30

Ruimy A, Dedieu G, Saugier B (1996) TURC: a diagnostic model of continental gross primary productivity and net primary productivity. Global Biogeochem Cycles 10:269–285

Running SW, Hunt ERJ (1993) Generalization of a forest ecosystem process model for other biomes, BIOME-BGC, and an application for global-scale models. In: Ehleringer JR, Field CB (eds) Scaling Physiological Processes. Academic Press, San Diego, pp 141–158

Saeki T (1959) Variation of photosynthetic activity with aging of leaves and total photosynthesis in a plant community. Bot Mag Tokyo 72:404–408

Saeki T (1960) Interrelationships between leaf amount, light distribution and total photosynthesis in a plant community. Bot Mag Tokyo 73:55–63

Sasai T, Ichii K, Yamaguchi Y, Nemani R (2005) Simulating terrestrial carbon fluxes using the new biosphere model BEAMS: biosphere model integrating eco-physiological and mechanistic approaches using satellite data. J Geophys Res 110, G02014. doi:10.1029/2005JG000045

Sato H, Ito A, Kohyama T (2007) SEIB–DGVM: a new Dynamic Global Vegetation Model using a spatially explicit individual-based approach. Ecol Model 200:279–307

Schwalm CR, Williams CA, Schaefer K, Anderson R, Arain MA, Baker I, Barr A, . . ., Verma SB (2010) A model-data intercomparison of CO_2 exchange across North America: Results from the North American carbon program site synthesis. J Geophys Res 115:G00H05. doi:10.1029/2009JG001229

Sellers PJ (1985) Canopy reflectance, photosynthesis and transpiration. Int J Remote Sens 6:1335–1372

Sellers PJ, Dickinson RE, Randall DA, Betts AK, Hall FG, Berry JA, Collatz GJ, . . ., Henderson-Sellers A (1997) Modeling the exchanges of energy, water, and carbon between continents and the atmosphere. Science 275:502–509

Sitch S, Smith B, Prentice IC, Arneth A, Bondeau A, Cramer W, Kaplan JO, . . ., Venevsky S (2003) Evaluation of ecosystem dynamics, plant geography and terrestrial carbon cycling in the LPJ dynamic global vegetation model. Glob Chang Biol 9:161–185

Spitters CJT, Schapendonk AHCM (1990) Evaluation of breeding strategies for drought tolerance in potato by means of crop growth simulation. Plant Soil 123:193–203

Tanaka T (1972) Studies on the light-curves of carbon assimilation of rice plants – the interrelation among the light-curves, the plant type and the maximizing yield of rice. Bul Nat Inst Agri Sci A 19:1–100

Terashima I, Saeki T (1985) A new model for leaf photosynthesis incorporating the gradients of light environment and of photosynthetic properties of chloroplasts within a leaf. Ann Bot 56:489–499

Todd-Brown KEO, Randerson JT, Post WM, Hoffman FM, Tarnocai C, Schuur EAG, Allison SD (2013) Causes of variation in soil carbon simulations from CMIP5 Earth system models and comparison with observations. Biogeosciences 10:1717–1736

van Ittersum MK, Lefferlaar PA, van Keulen H, Kropff MJ, Bastiaans L, Goudriaan J (2003) On approaches and applications of the Wageningen crop models. Eur J Agron 18:201–234

Wang YP, Jarvis PG (1990) Description and validation of an array model-MAESTRO. Agr For Meteor 51:257–280

Woodruff DR, McCulloh KA, Meinzer FC (2016) Forest canopy hydraulics. In: Hikosaka K, Niinemets Ü, Anten N (eds) Canopy Photosynthesis: From Basics to Applications. Springer, Berlin, pp 187–217

Chapter 10

Observation and Modeling of Net Ecosystem Carbon Exchange Over Canopy

Tomo'omi Kumagai*
Institute for Space-Earth Environmental, Nagoya University, Chikusa-ku, Nagoya 464-8601, Japan

Summary

Eddy covariance, which is the most common micrometeorological flux measurement method, can estimate ecosystem-scale and fine time-resolution carbon dioxide (CO_2) exchange between the upper vegetation surface and atmosphere. Given no lateral CO_2 advection, the sum of eddy covariance measurements and CO_2 storage in the underlying air represents net ecosystem-atmosphere CO_2 exchange (N_E). Although observation, analysis and prediction of N_E are major concerns in terms of terrestrial ecosystem carbon balance, there are many difficulties in obtaining reasonable observation values. N_E observation is based on fluid dynamics principles and turbulence theory; thus, model computations to reproduce N_E observation should reflect the theory for N_E mechanisms and processes. The Soil-Vegetation-Atmosphere Transfer (SVAT) model is a promising tool for validation of magnitude and analysis of N_E formation.

Keywords Energy, H_2O, and CO_2 exchange between land and atmosphere • Eddy covariance measurement • Flux observation • Boundary layer meteorology

*Author for correspondence, e-mail: tomoomikumagai@gmail.com

K. Hikosaka, Ü. Niinemets, and N.P.R. Anten (eds.), *Canopy Photosynthesis: From Basics to Applications*, DOI 10.1007/978-94-017-7291-4_10

I. Introduction

Energy and materials exchange between the vegetation canopy and atmosphere can be directly measured using the basics of fluid dynamics, called micrometeorological methods (Moncrieff et al. 2000). In general, the micrometeorological flux measurement methods are conducted with installation of automatic and frequent-sampling sensors above the canopy. These report temporal flux variations at intervals of several tens of minutes and integrate the fluxes over horizontal length scales between 100 m and several kilometers.

Eddy covariance typically provides a direct and sequential estimate of carbon dioxide (CO_2) flux absorbed/released by the vegetation canopy from/to the atmosphere with fine temporal resolution. The CO_2 flux referred to here denotes exchange between the canopy and atmosphere resulting from the integration of CO_2 absorption (leaf photosynthesis) and evolution (leaf, branch, stem and root respiration, and soil organic matter decomposition) within the canopy (Fig. 10.1). Reliable and reasonable flux

Abbreviations: ABL – Atmospheric boundary layer; A_l – Leaf photosynthesis rate; $A_{lsh} - A_l$ for shaded leaves; $A_{lsl} - A_l$ for sunlit leaves; a_{leaf} – Leaf area density; a_{sh} – Shaded leaf area density; a_{sl} – Sunlit leaf area density; ASL – Atmospheric surface layer; b_L – Intercept of the stomatal conductance model (Ball et al. 1987; Collatz et al. 1991); c – CO_2 concentration in the air; CBL – Convective boundary layer; C_d – Drag coefficient; C_i – CO_2 concentration within the stomatal cavity; c_p – Specific heat of air at constant pressure; C_s – CO_2 concentration of air inside the laminar boundary layer of leaves; CSL – Canopy sub-layer; e – Atmospheric water vapor pressure; E_l – Water vapor flux per unit of leaf area; $E_{lsh} - E_l$ for shaded leaves; $E_{lsh} - E_l$ for sunlit leaves; $e_{sat}(T_l)$ – Saturation vapor pressure at leaf temperature (T_l); e_{tk} – Turbulent kinetic energy; F_A – CO_2 flux without soil respiration; F_c – Vertical CO_2 flux; FLUXNET – Global network of flux tower sites; g_{ac} – Boundary conductance for CO_2; g_{ah} – Boundary conductance for heat; g_{aw} – Boundary layer conductance for water vapor; g_{sc} – Stomatal conductance for CO_2; g_{sw} – Stomatal conductance for water vapor; GSWP – Global Soil Wetness Project; g_w – Total conductance for water vapor; h_c – Forest canopy height; H_l – Sensible heat flux per unit of leaf area; $H_{lsh} - H_l$ for shaded leaves; $H_{lsh} - H_l$ for sunlit leaves; h_s – Relative humidity of air inside the boundary layer of a leaf; H_{soil} – Sensible heat flux at the soil surface; J_C – Ribulose bisphosphate (RuBP) carboxylase/oxygenase activity; J_E – Rate of RuBP regeneration through electron transport; J_{max} – Potential rate of whole-chain electron transport; $J_{max\_25} - J_{max}$ at 25 °C; J_S – Export rate of synthesized sucrose; K_t – Eddy turbulent diffusivity; L – Long-wave radiation at the given height; LAI – Leaf area index; LE – Latent heat flux; LT – Local time; m_a – Molecular weight of air; m_e – Molecular weight of water; m_L – Slope of the stomatal conductance model (Ball et al. 1987; Collatz et al. 1991); NCEP-NCAR – National Centers for Environmental Prediction – National Center for Atmospheric Research; N_a – Leaf nitrogen per unit area; N_E – Net ecosystem-atmosphere CO_2 exchange; NIR – Near-infrared radiation; p – Atmospheric pressure; P_b – Probability of no contact within a canopy layer for beam irradiance; P_d – Probability of no contact within a canopy layer for diffuse irradiance; PAR – Photosynthetic active radiation; q – Specific humidity; R_d – Respiration rate during the day but in the absence of photorespiration; $R_{d\_25} - R_d$ at 25 °C; R_{Lab} – Absorbed longwave radiation within a canopy layer; $R_{Labsl} - R_{Lab}$ of the sunlit leaves; $R_{Labsh} - R_{Lab}$ of the shaded leaves; R_s – Global solar radiation; R_{sabsl} – Total R_s absorbed by sunlit leaves; R_{sabsh} – Total R_s absorbed by shaded leaves; R_{sab_soil} – Total R_s absorbed by the soil surface; RSL – Roughness sub-layer; S_b – PAR or NIR at the given height for beam irradiance; S_c – Source strength for CO_2; S_d – PAR or NIR at the given height for diffuse irradiance; S_q – Source strength for water vapor; S_T – Source strength for heat; S_u – Momentum source; SVAT – Soil-vegetation-atmosphere transfer; t – Time; T – Air temperature at a given height; T_l – Leaf temperature; T_{soil} – Soil temperature; u – Wind speed; V_{cmax} – Maximum carboxylation rate when RuBP is saturated; $V_{cmax\_25} - V_{cmax}$ at 25 °C; w – Vertical wind speed; z – Height above the ground; z_r – Reference height; ε_l – Leaf emissivity; ε_s – Soil emissivity; η – Leaf transmissivity; λ – Latent heat of vaporization of water; λ_1 – Characteristic length scale for turbulent transport; λ_4 – Characteristic length scale for t pressure-scalar gradient correlation; λE_{soil} – Latent heat flux at the soil surface; ξ – Leaf reflectivity; ρ_a – Air density; σ – Stefan-Boltzmann constant; Ω – Clumping factor

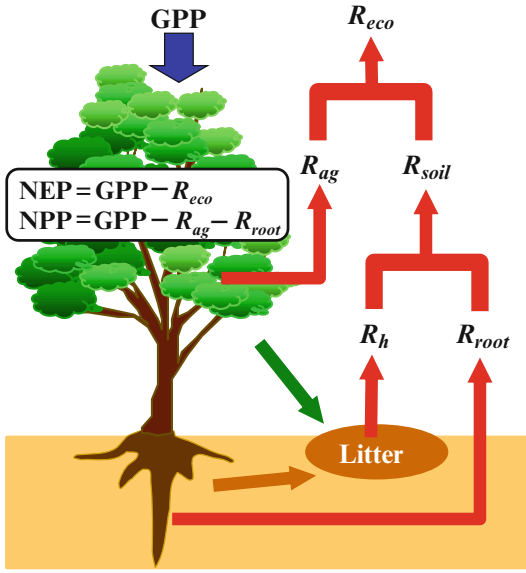

Fig. 10.1. Schematic representation of carbon flow in a forest. R_h, R_{root}, R_{ag}, R_{soil} and R_{eco} are respiratory fluxes from soil carbon, root, aboveground biomass, soil as a whole and ecosystem as a whole. Gross primary productivity (GPP) denotes carbon absorbed by the ecosystem as a whole. Thus, net ecosystem productivity (NEP; shown as GPP − R_{eco}) is ecosystem carbon sequestration, which can be directly measured by micrometeorological methods. Net primary productivity (NPP; shown as GPP − R_{ag} − R_{root}) means production (including litter) in the ecosystem

estimates can be compared with the ecosystem carbon budget estimated by summation of carbon flux components, which represents a valuable tool to clarify carbon flow processes in the ecosystem. Further, an appropriate period of flux observation reveals characteristics of diurnal, seasonal, interannual and interannual variations of CO_2 flux (i.e. vegetation productivity).

A combination of detailed observation of atmospheric and ecophysiological variables and the flux enables investigation of which factors control ecosystem CO_2 exchange. Furthermore, outputs from global and local models are independently validated using eddy covariance flux measured at the top of the canopy. We emphasize that such models were parameterized by independently collected ecophysiological measurements and were driven by observed or generated meteorological variables, and were not calibrated or parameterized by canopy-level flux measurements. After validation, such models can be used to examine how vegetation responds to climate change and, in turn, how functional vegetation changes induced by that change alter global and local climates.

In this review, I briefly describe eddy covariance measurement as the representative micrometeorological flux measurement method and its theory supporting measurements, with an explanation of their practice and limitations. In addition, I introduce the application of the Soil-Vegetation-Atmosphere Transfer (SVAT) model, which considers canopy microclimate processes such as radiation transfer, leaf-scale physiology, and turbulence within the canopy.

II. Theory of Measurement

A. Atmospheric Boundary Layer

Vertical profiles of wind speed, air temperature, and material concentrations vary drastically near the earth surface relative to their horizontal gradients, because of transport processes at the boundary of the domain of the atmosphere (Stull 1988). The atmospheric boundary layer (ABL) can be defined as the lowest part of the troposphere that is directly influenced by the earth surface characteristics (Fig. 10.2). ABL thickness is variable in time and space, ranging from a few tens of meters to several kilometers. All micrometeorological methods should be applied to the ABL, which can be divided into layers according to controlling factors of turbulent transport in each layer. Thus, examination of each ABL layer characteristics is useful for considering exchange processes between the surface and atmosphere.

Under neutral conditions, the convective boundary layer (CBL) is influenced by synoptic and mesoscale processes, whereas under unstable conditions, turbulence in the CBL is convectively driven. The intense

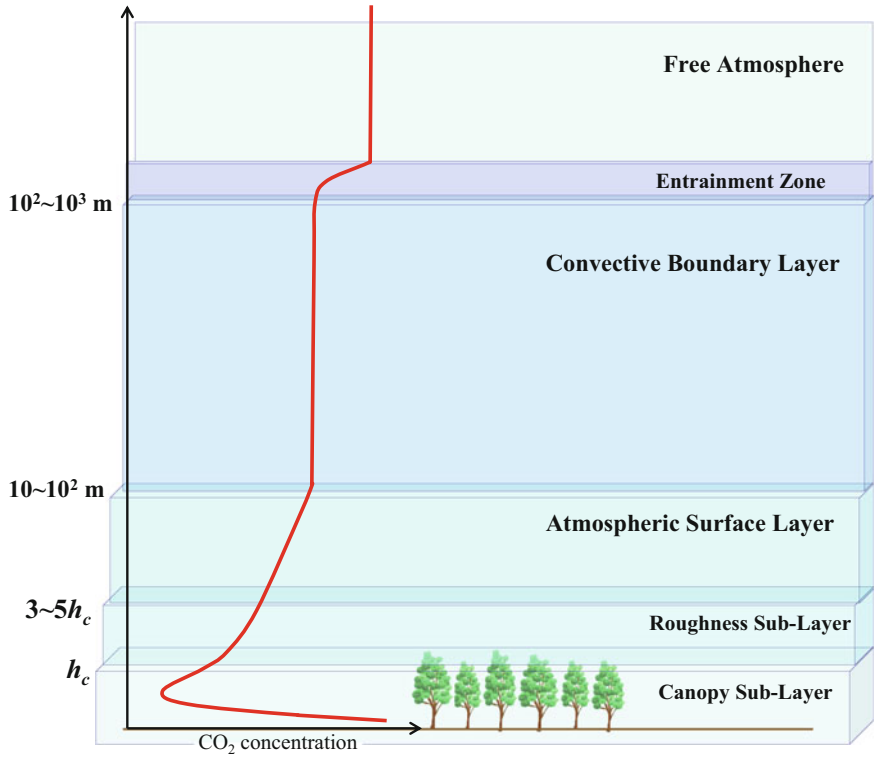

Fig. 10.2. The atmospheric boundary layer (*ABL*), consisting of two major layers, the convective boundary layer (*CBL*) and atmospheric surface layer (*ASL*). The remainder of the air in the troposphere is the free atmosphere. The ASL is subdivided into several sublayers, such as the roughness sublayer (*RSL*), canopy sublayer (*CSL*, where h_c is canopy height), and the remainder (referred to as the inertial sublayer). Typical daytime profile of mean CO_2 concentration is also shown

turbulence in the CBL tends to mix materials promptly and uniformly in the vertical (CO_2 concentration profile in Fig. 10.2). Such mixing causes weak vertical gradients of wind speed and direction and potential temperature. A stable layer at the CBL top is called the inversion layer or entrainment zone, which acts as a lid on convection in the CBL and is where entrainment from the free atmosphere into the CBL occurs.

There are vertical gradients of variables such as wind speed and materials concentration within the bottom 10 % of the ABL, which is called the atmospheric surface layer (ASL). The ASL is often referred to as the "constant flux layer," because vertical turbulent fluxes vary by less than 10 % of their magnitude in this layer. The height of the ASL bottom is about 3–5 times the representative height of the roughness element (h_c in Fig. 10.2; the forest canopy height here). The layer between heights h_c and 3–5 times h_c is called the roughness sublayer (RSL). In the layer beneath the RSL, the so-called canopy sublayer (CSL), turbulence is strongly influenced by the roughness element (i.e. trees) and reduced by viscosity. The CO_2 concentration profile in the CSL (Fig. 10.2) reveals the strongest sink of CO_2 at the mid-canopy position; a strong source, caused by soil respiration, is at the soil surface.

B. Eddy Flux

Fluid motion such as turbulence can transport materials in the atmosphere, resulting in fluxes. The turbulence is generated by eddies on various scales in the ABL. At a point where one observes an eddy flowing in a

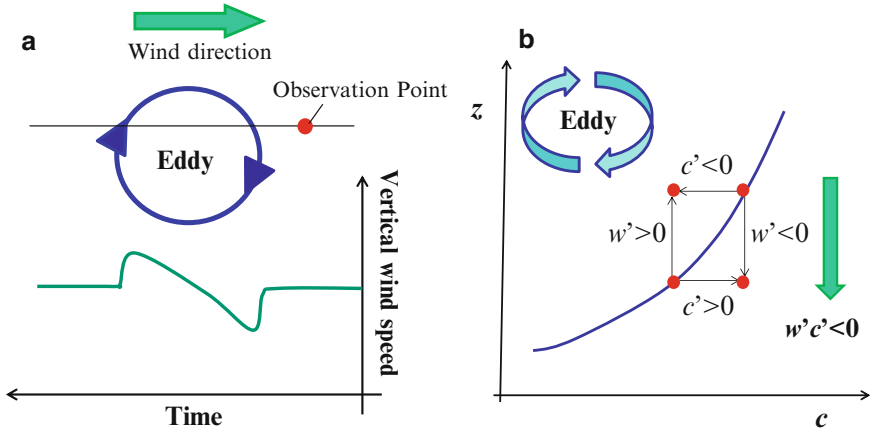

Fig. 10.3. (**a**) An eddy flowing to a given wind direction causes perturbations of vertical wind speed observed at a given position. (**b**) Schematic representation of the small eddy mixing process, showing net downward turbulent CO_2 flux. z, c, w, and prime denote height, CO_2 concentration, vertical wind speed, and perturbation part, respectively

direction, vertical wind speed fluctuates (Fig. 10.3a). This is the turbulence, which drives the vertical transport of materials. As seen in the figure, even though the materials are transported vertically, the dominant air parcel flow containing the materials is horizontal. Thus, the vertical flux at a given measurement height results from integration of the source/sink distribution of the flux on vegetation surfaces (Schuepp et al. 1990). Measurement over an extensive flat area upwind at a height sufficiently close to the vegetated surface would minimize the problem induced by a heterogeneous source/sink distribution on the surface, which is called the fetch problem.

Micrometeorological flux measurement methods were established based on eddy diffusivities. Thus, for appropriate measurements, one needs to take them above the RSL (where diffusivities are enhanced), so that the effect of heterogeneous terrain may not violate the assumption of a flat extensive area upwind (described later). However, by doing so, the fetch problem arises and small gradients of material concentration complicate flux measurement using eddy diffusivity theory. I emphasize that one cannot help in practice conducting tower-based flux measurement over tall vegetation (i.e. a forest canopy) within the RSL. Nonetheless, before commencing full-scale flux observation, one should consider a balance between measurement height and the fetch problem (Lloyd 1995).

Intrinsically, the vertical CO_2 flux (F_c: μmol m^{-2} s^{-1}) can be expressed as

$$F_c = \rho_a c \times w \tag{10.1}$$

where ρ_a, c, and w are air density (mol m^{-3}), CO_2 concentration (μmol mol^{-1} = ppmv) in the air, and vertical wind speed (m s^{-1}), respectively. Both c and w have fine fluctuations in their nature, and thus it is expedient to estimate net turbulent material flux by averaging the flux over a given period:

$$F_c = \overline{\rho_a w c} = \rho_a \overline{w c} \tag{10.2}$$

where the overbar denotes time averaging over a given period. c and w during the period are expressed by

$$\begin{aligned} c &= \overline{c} + c' \\ w &= \overline{w} + w' \end{aligned} \tag{10.3}$$

where the prime denotes a departure from the temporal averaging operator. The overbar

and prime components are called the mean and turbulent part, respectively. Substituting Eq. 10.3 for Eq. 10.2 gives

$$F_c = \rho_a \overline{(\overline{w} + w')(\overline{c} + c')} = \rho_a \left(\overline{wc} + \overline{w'}\overline{c} + \overline{w}\overline{c'} + \overline{w'c'} \right) \quad (10.4)$$

Assuming a flat extensive and heterogeneous terrain upwind and/or measurements above the RSL, one can make $\overline{w} = 0$ and $\overline{w'} = 0$ to obtain

$$F_c = \rho_a \overline{w'c'} \quad (10.5)$$

Application of Eq. 10.5 to the flux estimate is called the eddy covariance method, and requires fast response and high-frequency sampling sensors such as a supersonic anemometer and closed-path or open-path analyzers. To understand the meaning of instantaneous product $w'c'$ and net flux $\overline{w'c'}$, it is instructive to examine a small idealized eddy near the vegetation surface during daylight hours (Fig. 10.3b). Average CO_2 concentration usually decreases toward the surface because of active absorption of CO_2 from the vegetation, i.e., photosynthesis. Assuming that the eddy is a swirling motion, some air parcels are mixed upward (positive w') and some mixed downward (negative w'). The upward ($w' > 0$) and downward ($w' < 0$) moving air parcels make the CO_2 concentration lower ($c' < 0$) or higher ($c' > 0$) than their surroundings, respectively. In both cases, the instantaneous product $w'c'$ is negative, indicating that both the upward and downward moving air parcels contribute negatively to the flux $w'c'$. Thus, the average eddy CO_2 flux $\overline{w'c'}$ is negative for this small eddy mixing process.

In practice, F_c cannot be obtained from simple calculation such as $\overline{w'c'}$, because there are some cases in which we cannot assume $\overline{w} = 0$. For example, complex terrain and vegetation structure (Kaimal and Finnigan 1994; Lee 1998; Lee et al. 2004) and changes of dry air density (Webb et al. 1980; Leuning 2007) cause nonzero $\overline{w}$ effects, and draw attention to the need to consider corrections of the measured flux. Hereafter in this chapter for simplicity, the notation $\overline{w'c'}$ will be used for F_c.

C. Above-Canopy Flux, Storage Flux, and Net Ecosystem Exchange

Since micrometeorological methods are based on fluid mechanics, one should begin with its fundamentals, i.e. an equation for scalar conservation (Baldocchi et al. 2000):

$$\frac{\partial \overline{\rho_a c}}{\partial t} = -\frac{\partial \left(\rho_a \overline{w'c'} \right)}{\partial z} + S_c(t, z) \quad (10.6)$$

where t is time (s), z is height (m) above the ground, and S_c is the source term (μmol m^{-3} s^{-1}) from mass absorption/release (i.e. net photosynthesis). Here, no lateral advection of CO_2 out of the sampling area is assumed. As delimited by the canopy height h_c, integrating Eq. 10.6 from the ground to reference height z_r gives

$$\int_0^{z_r} \rho_a \frac{\partial \overline{c}}{\partial t} dz = -\rho_a \left(\overline{w'c'}(z_r) - \overline{w'c'}(0) \right) + \int_0^{h_c} S_c(t, z) dz \quad (10.7)$$

where $\overline{w'c'}(z_r)$ and $\overline{w'c'}(0)$ are observed CO_2 fluxes at height z_r, called the above-canopy flux, and ground surface (i.e. soil respiration), respectively. The balance between the vertical integration of net photosynthesis and soil respiration is called net ecosystem CO_2 exchange N_E, and is given by

$$\rho_a \overline{w'c'}(0) + \int_0^{h_c} S_c(t, z) dz = N_E = \rho_a \overline{w'c'}(z_r) + \int_0^{z_r} \rho_a \frac{\partial \overline{c}}{\partial t} dz \quad (10.8)$$

Equation 10.8 suggests that N_E can be estimated from observation of the above-canopy flux (first term on right side of

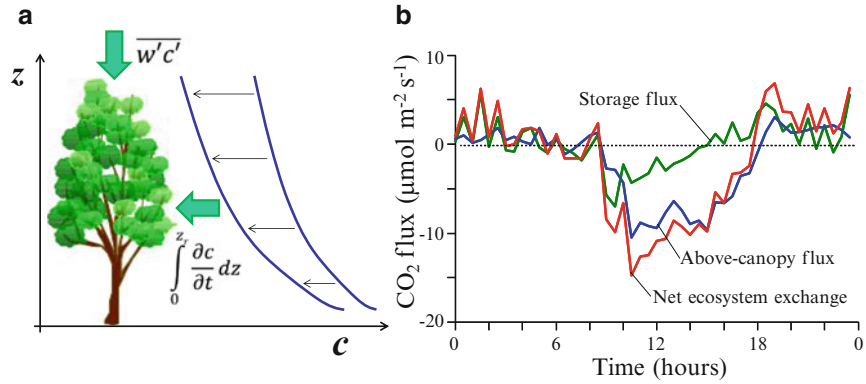

Fig. 10.4. (**a**) Representation of above-canopy flux and storage flux induced by change in vertical CO_2 concentration (c) profile. (**b**) Diurnal variations in above-canopy flux, storage flux, and net ecosystem exchange, observed in a Bornean tropical rainforest

Eq. 10.8) using the eddy covariance system on the canopy top and within-canopy storage flux (second term on right side of Eq. 10.8). The latter term is determined by quantifying the rate of change of CO_2 concentration in the air column within the canopy (Fig. 10.4a).

Observation in a Bornean tropical rainforest showed diurnal variations in the above-canopy flux, storage flux, and their sum, i.e. N_E (Fig. 10.4b). Most of the nocturnal-respired CO_2 at the rainforest site was stored within the canopy until morning, and was reabsorbed into the canopy through photosynthesis around 0800–1000 local time (LT). N_E represents a diurnal cycle of vegetation activity, and thus I address the physiological interpretation of N_E in relation to environmental factors, using the SVAT model.

III. Modeling

A. Soil-Vegetation-Atmosphere Transfer (SVAT) Model

Vegetation affects the within-canopy microclimate by intercepting radiation, attenuating wind, and distributing sources/sinks of materials and energy at each position within the canopy. These source/sink distributions and canopy turbulence form scalar distributions (air temperature, humidity, and CO_2 concentration) and above-canopy fluxes such as heat, H_2O, and CO_2. These scalar distributions in turn influence the within-canopy microclimate and scalar source/sink strength.

In reality, vegetation canopy fluxes form as a result of the aforementioned within-canopy processes (cf. Chap. 9, Hikosaka et al. 2016b). Therefore, I focus on a one-dimensional (vertical-only) multilayer SVAT model (Kumagai et al. 2006) that attempts to faithfully reproduce the formation process of eddy flux described in the previous part of this chapter. The model explicitly considers three major within-canopy processes: (1) radiative transfer and leaf-scale energy conservation; (2) leaf-scale ecophysiological status for stomatal opening and carbon assimilation; and (3) turbulent diffusion of materials (Baldocchi 1992). Detailed description of the turbulent transport process enables the SVAT model to reproduce the eddy flux measurements. For model computation, the canopy is divided into layers and all equations describing the within-canopy processes (1–3) are solved for each layer. The model used here was parameterized with independently collected ecophysiological measurements and was not calibrated or parameterized with canopy-level flux measurements.

1. Radiative Transfer and Energy Balance at Both Leaf and Soil-Surface Levels

When considering leaf-scale energy balance (cf. Chap. 2, Gutschick 2016) together with photosynthesis in a forest canopy, radiative transfer through the canopy (cf. Chap. 1, Goudriaan 2016) must be determined. Then, direct beam and diffuse irradiance must be considered separately, owing to their different attenuation in the canopy. The probability of no contact within a canopy layer for beam irradiance (P_b) must be formulated for describing direct irradiance transfer within the canopy. This formulation includes leaf area density (a_{leaf} in $m^2\ m^{-3}$), the beam extinction function of solar elevation, and leaf angle distribution within a given layer. When considering the effect of clumped foliage and crowns, we should incorporate a clumping factor (Ω) in the P_b equation by replacing a_{leaf} with Ωa_{leaf} (see Kumagai et al. 2013). The probability of no contact within a canopy layer for diffuse irradiance (P_d) is calculated by integrating P_b over the solid angles of the sky hemisphere.

Both direct and diffuse solar radiation can be further separated into photosynthetic active radiation (PAR) and near-infrared radiation (NIR), according to their different absorptions by leaves. Fortunately, approximately half the global solar radiation (R_s: W m^{-2}) over the canopy is in the form of PAR, while the other half is in the form of NIR. This enables estimates of R_s penetration inside the canopy. The absorbed PAR or NIR within a canopy layer between z (height above ground) and $z + \Delta z$, ΔS (W m^{-2}), is defined as

$$\Delta S_b = (1 - \eta - \xi)(1 - P_b)S_b(z + \Delta z) \quad (10.9)$$

$$\Delta S_d^{\downarrow} = (1 - \eta - \xi)(1 - P_d)S_d^{\downarrow}(z + \Delta z) \quad (10.10)$$

$$\Delta S_d^{\uparrow} = (1 - \eta - \xi)(1 - P_d)S_d^{\uparrow}(z) \quad (10.11)$$

where η and ξ are leaf transmissivity and reflectivity, respectively, for PAR or NIR. S is PAR or NIR at the given height (W m^{-2}). Subscripts b and d denote direct beam and diffuse irradiation, respectively, and superscript arrows indicate the direction of the irradiation. Although it appears that Eqs. 10.9, 10.10, and 10.11 are simple formulations of the two-stream model, P_b and P_d are complex functions of a_{leaf}, leaf angle distribution and Ω within a given canopy layer and solar geometric direction. Therefore, this shortwave radiative transfer model can be considered a semi-3D model (see Kumagai et al. 2006). Total absorbed solar radiation within the canopy layer is then calculated as the sum of absorbed PAR and NIR, both of which are calculated by Eqs. 10.9, 10.10 and 10.11. Sunlit leaves receive the beam and upward and downward diffuse radiation, while shaded leaves receive only upward and downward diffuse radiation. Therefore, irradiance absorption and energy balance must be computed separately for sunlit and shaded leaves.

The absorbed long-wave radiation within a canopy layer between z and $z + \Delta z$, R_{Lab} (W m^{-2}), is defined as

$$R_{Lab} = (1 - P_d)L^{\uparrow}(z) + (1 - P_d)L^{\downarrow}(z + \Delta z) \quad (10.12)$$

Here, L is long-wave radiation at the given height (W m^{-2}), calculated using leaf temperature (T_l in K) and the theory for diffuse irradiance transfer within the canopy layer between z and $z + \Delta z$ (Kumagai et al. 2006).

Energy balance at the soil surface for computing soil temperature (T_{soil} in K) is expressed by

$$R_{sab\_soil} + L^{\downarrow}(0) - \varepsilon_s \sigma {T_{soil}}^4 = \lambda E_{soil} + H_{soil} \quad (10.13)$$

where R_{sab_soil} is the total R_s absorbed by the soil surface (W m^{-2}), ε_s is soil emissivity, σ is the Stefan-Boltzmann constant (5.67×10^{-8} W m^{-2} K^{-4}), and λE_{soil} and H_{soil} are latent (W m^{-2}) and sensible (W m^{-2}) heat fluxes at the soil surface, respectively. λE_{soil} and H_{soil} are functions of T_{soil}, as described by the products of

transport conductance and concentration difference. In addition, soil-surface moisture availability was used for λE_{soil} conductance. For full computations describing λE_{soil} and H_{soil}, a more complicated soil physics describing soil heat and water motion is needed (Campbell and Norman 1998).

The energy balance on sunlit and shaded leaf surfaces within a canopy layer between z and $z + \Delta z$ is expressed by

$$R_{sabsl} + R_{Labsl} - 2(1 - P_d)\varepsilon_l \sigma {T_{lsl}}^4 a_{sl}/a_{leaf} = \lambda E_{lsl} a_{sl} \Delta z + H_{lsl} a_{sl} \Delta z \quad (10.14)$$

$$R_{sabsh} + R_{Labsh} - 2(1 - P_d)\varepsilon_l \sigma {T_{lsh}}^4 a_{sh}/a_{leaf} = \lambda E_{lsh} a_{sh} \Delta z + H_{lsh} a_{sh} \Delta z \quad (10.15)$$

Here, R_{sabsl} and R_{sabsh} are total R_s absorbed by sunlit and shaded leaves, respectively (W m^{-2}), expressed per unit of ground area. R_{Labsl} and R_{Labsh} are R_{Lab} of the sunlit and shaded leaves (W m^{-2}) within a canopy layer between z and $z + \Delta z$, respectively, expressed per unit of ground area. ε_l is leaf emissivity, and subscripts sl and sh denote sunlit and shaded leaves, respectively. a_{sl} and a_{sh} are sunlit and shaded leaf area densities (m^2 m^{-3}) within a given layer, respectively. λ is the latent heat of vaporization of water (J kg^{-1}), and E_l and H_l respectively represent water vapor (kg m^{-2} s^{-1}) and sensible heat (W m^{-2}) fluxes expressed per unit of leaf area. These are described in the next section. The energy balance Eqs. 10.14 and 10.15 are critical for computation of T_l, which is required for assessing leaf physiological activity as follows.

2. Leaf-Level Physiological Functions

Leaf-level scalar source strengths, i.e., leaf sensible heat (H_l in W m^{-2}), transpiration (E_l in kg m^{-2} s^{-1}) and photosynthesis rate (A_l in μmol m^{-2} s^{-1}), are derived from physiological controls using

$$H_l = 2 m_a c_p g_{ah} (T_l - T) \quad (10.16)$$

$$E_l = m_e g_w \frac{[e_{sat}(T_l) - e]}{p} \quad (10.17)$$

$$A_l = g_{ac}(c - C_s) \quad (10.18)$$

$$= g_{sc}(C_s - C_i) \quad (10.19)$$

where m_a and m_e are the molecular weights of air and water (kg mol^{-1}), respectively, c_p is the specific heat of air at constant pressure (J kg^{-1} K^{-1}), and g_{ah}, g_{ac} and g_w are boundary conductances for heat and CO_2 and total conductance for water vapor (mol m^{-2} s^{-1}), respectively. T is air temperature (K) at a given height, and $e_{sat}(T_l)$ and e are saturation vapor pressure at leaf temperature (T_l) and atmospheric water vapor pressure (Pa), respectively. p is atmospheric pressure (Pa), and C_s, c and C_i are CO_2 concentrations (μmol mol^{-1}) of air inside and outside the laminar boundary layer of leaves and within the stomatal cavity, respectively. g_w is the sum of the reciprocals of the stomatal (g_{sw}, mol m^{-2} s^{-1}) and boundary layer (g_{aw}, mol m^{-2} s^{-1}) conductances for water vapor. Campbell and Norman (1998) gave typical formulations of boundary conductances.

As described by Ball et al. (1987) and Collatz et al. (1991), g_{sc} is stomatal conductance for CO_2 (mol m^{-2} s^{-1}) and is linked to A_l, the relative humidity of air inside the boundary layer of a leaf (h_s), and C_s:

$$g_{sc} = m_L \frac{A_l h_s}{C_s} + b_L \quad (10.20)$$

where m_L and b_L are the slope and intercept, respectively. These were obtained by linear regression of data from leaf-level gas exchange measurements. g_{sw} was obtained from $g_{sw} = 1.6\, g_{sc}$, where 1.6 is the ratio of diffusivities of water and CO_2 in air (von Caemmerer and Farquhar 1981).

A_l was computed using the biochemical model of Farquhar et al. (1980) and Collatz

et al. (1991) as a minimum value of the gross rate of photosynthesis, limited by the rate of ribulose bisphosphate (RuBP) regeneration through electron transport (J_E in μmol m^{-2} s^{-1}), RuBP carboxylase/oxygenase (Rubisco) activity (J_C in μmol m^{-2} s^{-1}), and the export rate of synthesized sucrose (J_S in μmol m^{-2} s^{-1}), as

$$A_l = \min\{J_E, J_C, J_S\} - R_d \tag{10.21}$$

Here, R_d is the respiration rate (μmol m^{-2} s^{-1}) during the day but in the absence of photorespiration. The formulations and parameterizations of J_E, J_C, J_S and R_d as a function of PAR absorbed by the leaf, CO_2 concentration within the stomatal cavity, and leaf temperature (T_l) are given in Chap. 3 (Hikosaka et al. 2016a) of this volume. In those formulations, the maximum carboxylation rate when RuBP is saturated (V_{cmax} in μmol m^{-2} s^{-1}), the potential rate of whole-chain electron transport (J_{max} in μmol m^{-2} s^{-1}), and R_d are critical sub-functions, which are expressed as nonlinear functions of T_l and values at 25 °C (V_{cmax_25}, J_{max_25}, and R_{d_25}, respectively). Practically, both J_{max_25} and R_{d_25} are related to V_{cmax_25}. Hence, V_{cmax_25} is the key parameter in the leaf photosynthesis model.

The aforementioned model calculates A_l for both sunlit and shaded leaves. The A_l calculated in Eq. 10.21 is coupled with g_{sc} using Eq. 10.20. Hence, determination of A_l requires C_s, C_i, h_s and T_l, which result from e, c and T using Eqs. 10.16, 10.17, 10.18, and 10.19. Thus, all three scalar (e, c and T) transport equations and Eqs. 10.16, 10.17, 10.18, and 10.19 must be simultaneously considered, as described in the following.

3. Scalar Transport

Scalar continuity is obtained assuming steady-state planar homogeneity (cf. Eq. 10.6):

$$\frac{d\varphi}{dt} = 0 = -\frac{d\overline{w'\varphi'}}{dz} + S_\varphi(t,z) \tag{10.22}$$

where φ is a variable such as T, specific humidity (q in kg kg^{-1}) or c, and $\overline{w'\varphi'}$ is the vertical turbulent flux. S_φ is a source (or sink) term for φ, attributable to mass release (or uptake) by the ensemble of leaves within the averaging plane, given by

$$S_T = \frac{1}{m_a \rho_a c_p}\left(H_{lsl} a_{sl} + H_{lsh} a_{sh}\right) \tag{10.23}$$

$$S_q = \frac{1}{m_a \rho_a}\left(E_{lsl} a_{sl} + E_{lsh} a_{sh}\right) \tag{10.24}$$

$$S_c = -\frac{1}{\rho_a}\left(A_{lsl} a_{sl} + A_{lsh} a_{sh}\right) \tag{10.25}$$

where S_T, S_q, and S_c are source strengths for heat (K s^{-1}), water vapor (kg kg^{-1} s^{-1}), and CO_2 concentration (μmol mol^{-1} s^{-1}), respectively.

To compute φ, S_φ and $\overline{w'\varphi'}$, use of a turbulent diffusion model is required and two main approaches have been adopted, Lagrangian and Eulerian models (see Katul and Albertson 1999). In the Lagrangian dispersion model, scalar concentration differences between arbitrary and reference heights were computed by summing the contributions of scalar diffusion to or from various canopy heights, expressed by a dispersion matrix calculated using the random walk algorithm (see Baldocchi 1992; Baldocchi and Meyers 1998). The Lagrangian approach has been successfully used to compute the interdependence between scalar sources and concentrations and resultant fluxes (e.g. Raupach 1988; Baldocchi 1992; Lai et al. 2000).

With regard to the Eulerian approach, the closure approximation is required to prevent an increase in the order of the turbulent flux term. Assuming that the turbulent Schmidt number for scalar is unity, one can apply a first-order turbulent closure scheme (see Kumagai et al. 2013):

$$\overline{w'\varphi'} = -K_t \frac{d\varphi}{dz} \tag{10.26}$$

where K_t is eddy turbulent diffusivity ($m^2\ s^{-1}$). In general, the first-order closure principles fail in countergradient flows but are applicable when the production term is balanced by the dissipation term in the scalar flux budget, with minimal contributions from gradients in the turbulent flux transport terms (see Manzoni et al. 2011).

Both Lagrangian and higher-order Eulerian approaches can be formulated to account for the existence of countergradient flow (see Katul and Albertson 1999). Here, assuming steady-state planar homogeneity and high Reynolds number and Peclet number flow, and applying temporal and horizontal averaging, the turbulent vertical flux equation for φ with a second-order closure scheme is (see Katul and Albertson 1999):

$$0 = -\overline{w'^2}\frac{d\varphi}{dz} + 2\frac{d}{dz}\left(e_{tk}\lambda_1\frac{d\overline{w'\varphi'}}{dz}\right) - \frac{e}{3\lambda_4}\overline{w'\varphi'} \tag{10.27}$$

where e_{tk} is a turbulent kinetic energy, and λ_1 and λ_4 are characteristic length scales for turbulent transport and pressure-scalar gradient correlation, respectively (see Watanabe 1993).

To solve Eqs. 10.22, 10.23, 10.24, 10.25, 10.26 or 10.22, 10.23, 10.24, 10.25, and 10.27, velocity statistics within the canopy must be computed. For the first-closure model, we have only to substitute u (wind speed in m s^{-1}) for φ in Eqs. 10.22 and 10.26 and use a momentum source $S_u = C_d\ a_{leaf}\ u^2$, where C_d is the drag coefficient (see Kumagai et al. 2013). For the second-order closure model for turbulent vertical fluxes, the second-order closure model for canopy turbulence formulated by Wilson and Shaw (1977) is generally applied. Then, boundary conditions can be specified in accord with Katul and Albertson (1999), and the closure constants in Wilson and Shaw (1977), Watanabe (1993) and Katul and Albertson (1999) can be used. To solve the second-order closure model, the numerical scheme described in Katul and Albertson (1998, 1999) is applicable.

B. Model Applications

Again, the SVAT model introduced here is parameterized by independently collected data of ecophysiological traits such as V_{cmax_25} and m_L and of canopy structure such as a_{leaf} spatial variation, and is not calibrated or parameterized by canopy-level flux measurements. Model outputs are independently validated using the N_E measurements. After validation, the model can be used to examine how the energy and material fluxes over the forest ecosystems are generated, e.g. how the canopy structure and physiological traits impact CO_2 exchange between the canopy and atmosphere, shown by the following.

It is first necessary to validate the model by examining how sensitive the flux calculations are to micrometeorological factors. Examples of comparisons between modeled and measured N_E in a Bornean tropical rainforest (Kumagai and Kume 2012) are shown under four typical meteorological conditions. These are a rainfall event at noon (Fig. 10.5a, e), rainfall event from midnight to early morning and cloud during daylight hours (Fig. 10.5b, f), cloudy with little rainfall (Fig. 10.5c, g), and midnight rainfall and clear sky during daylight hours (Fig. 10.5d, h). There were two types of abrupt declines of N_E and solar radiation (R_s) at noon on 6 September with rainfall (Fig. 10.5a, e) and 11 September without rainfall (Fig. 10.5c and g). The model accurately reproduced measured N_E for the entire available data period, including periods of the four aforementioned meteorological conditions. Regression statistics for comparisons between measured and modeled values during daylight hours had a slope of 0.79, intercept of –0.80 μmol $m^{-2}\ s^{-1}$, R^2 of 0.62, and a root mean square error of 6.95 μmol $m^{-2}\ s^{-1}$ (Kumagai et al. 2006).

Measurements of horizontal variation of leaf area index (LAI) at the tropical rainforest site revealed values from 4.8 to 6.8 $m^2\ m^{-2}$, with a mean of 6.2 $m^2\ m^{-2}$. Cumulative LAI data measured downwards from the canopy top at 57 observation points

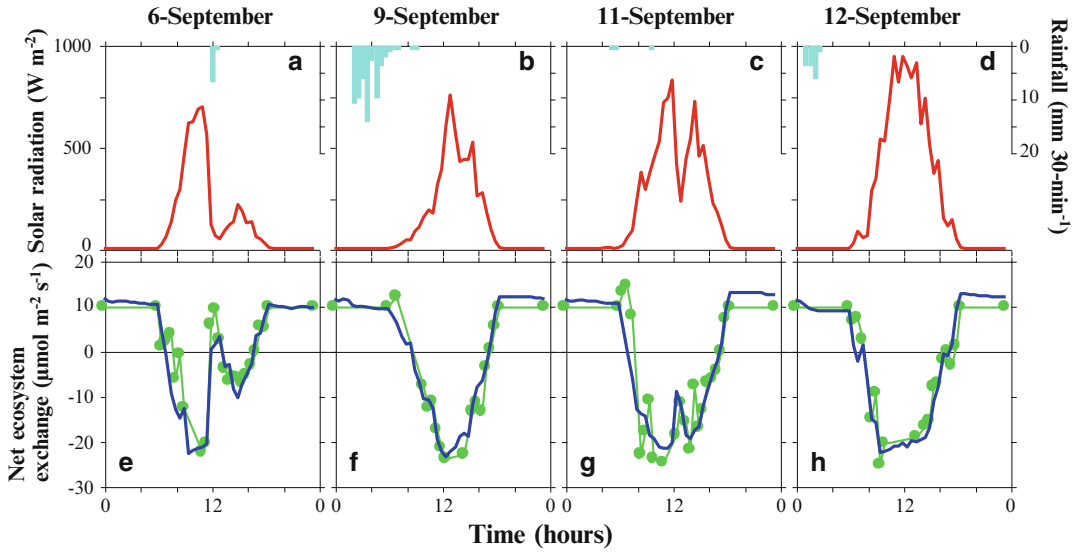

Fig. 10.5. Diurnal patterns of rainfall (*bars*) and solar radiation (*lines*) (**a–d**), and measured (*closed circles*) and modeled (*lines*) net ecosystem CO_2 exchange (**e–h**) in Bornean tropical rainforest from 6 to 12 September 2002 (From Kumagai and Kume 2012)

along four vertical lines showed a strong linear relationship between z and cumulative LAI ($R^2 = 0.82$). A straight line representing this linear relationship, connecting two points (z, cumulative LAI) = (0, LAI) and (h, 0), can be generated by integrating constant vertical distributions of leaf area density. Hence, Kumagai et al. (2006) assumed that LAI varied horizontally at the site between 4.8 and 6.8 $m^2\ m^{-2}$, and that at each horizontal position, leaf area density was vertically constant from the canopy top to forest floor. Because in describing variation of leaf-level physiological parameters we had only to present the one-dimensional vertical variation (Kumagai et al. 2006), how the flux calculations respond to changes in vertical distributions of leaf area density should also be examined. Thus, Kumagai et al. conducted four numerical experiments with consideration of the results of leaf area density. In Case 1, a mean observed LAI of 6.2 $m^2\ m^{-2}$, along with constant leaf area density of 0.123 $m^2\ m^{-3}$ from the canopy top to forest floor, was used in the SVAT model. Cases 2 and 3 assumed LAIs of 6.8 and 4.8 $m^2\ m^{-2}$ (the maximum and minimum observed LAIs), along with constant leaf area densities of 0.136 and 0.096 $m^2\ m^{-3}$, respectively. In most SVAT models, the leaf area density distribution is arbitrarily assumed as a single vertical profile, because a tower is generally used to obtain measurements (however, Kumagai et al. used a canopy crane, which enabled them to obtain a 3D canopy structure). To examine the effect of arbitrarily determined vertical distributions of leaf area density on flux calculations, we also constructed Case 4, assuming a vertical distribution of leaf area density as a single vertical observation line, the LAI of which was 4.8 $m^2\ m^{-2}$.

In the study of Kumagai et al. (2006), all cases recreated the canonical form of measured N_E throughout all photosynthesis periods, implying that efforts to measure the detailed leaf area density distribution within the canopy do not always improve the predictive accuracy of the model. Reproducing both spatial and temporal patterns of the mean concentration field, a state variable influenced by combined source variation and turbulent transport mechanics, is one of the strengths of a multilayer SVAT model (Lai et al. 2000). However, although the

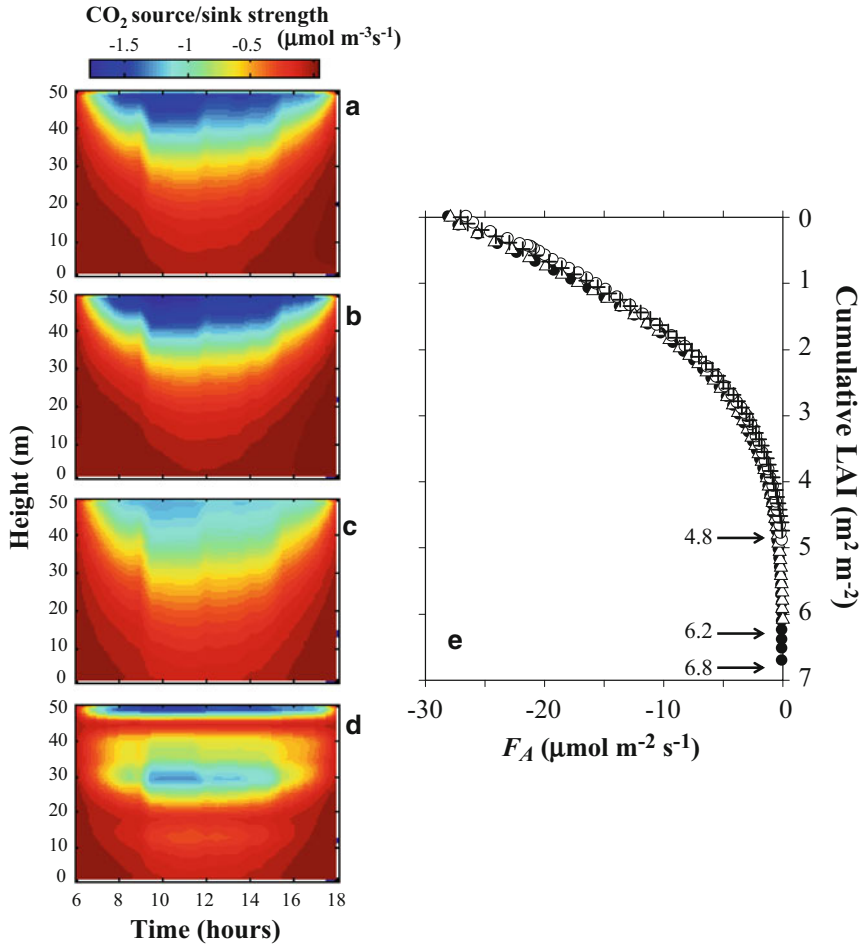

Fig. 10.6. Left panels: contour plots of average CO_2 source/sink distributions within the canopy as a function of height and time of day for Cases 1 (**a**), 2 (**b**), 3 (**c**), and 4 (**d**). *Right panel*: (**e**) vertical profiles of average CO_2 flux without soil respiration (F_A) around noon (1100–1300 LT) as a function of cumulative leaf area index (LAI) modeled from Cases 1 (*open triangles*), 2 (*closed circles*), 3 (*crosses*), and 4 (*open circles*). LAI values (6.8, 6.2 and 4.8) are also shown (From Kumagai et al. 2006)

model calculations of N_E clearly reproduced the measurements, those of the scalar profiles inside the canopy did not match the measured values. This implies that a simpler description of velocity statistics that modulate turbulent transport, like those proposed by Baldocchi and Meyers (1998), might be adequate.

At different levels in the canopy, absorbed radiation altered by changes in the vertical distribution of leaf area density mainly drives variations of physiological sources and sinks. Thus, Kumagai et al. (2006) compared CO_2 source strength distributions estimated with Cases 1–4. Figure 10.6a–d shows contour maps of these distributions as a function of time of day and height. In contrast to the calculated N_E, there were pronounced discrepancies between the estimated source strength distributions. Among Cases 1–3 (Fig. 10.6a–c, respectively), those with higher LAI had greater CO_2 uptake in the upper canopy layers, but less uptake in the lower canopy. In contrast, in Case 4 (Fig. 10.6d), CO_2 uptake was high at heights of about 50 and 30 m, where leaf area densities were also high.

Figure 10.6e compares profiles of average CO_2 flux without soil respiration (F_A) around

noon (1100–1300 LT) modeled from Cases 1–4, described as a function of cumulative LAIs measured downward from the canopy top. F_A denotes CO_2 flux in each canopy layer, expressed per unit area of ground. Therefore, F_A at cumulative LAI = 0 is equal to the above-canopy flux without soil respiration, and decreases with increasing cumulative LAI. The cumulative LAI is not necessarily related to canopy height. In contrast to the source strength distributions, there were no large differences between flux profiles of each case. This figure reveals that in Cases 1 and 2, which had high LAI, CO_2 uptake by leaves in the lower canopy layers contributed little to F_A because of the small contribution of J_E (see Eq. 10.21) in the lower canopy. Therefore, despite the varying distributions of leaf area density, a greater part of the above-canopy flux was generated by a constant cumulative LAI integrated from the canopy top, ~4.8 m^2 m^{-2}. Hence, the above-canopy flux appears robust to changes of leaf area density distributions, and in all cases the results were almost identical.

Given the strong vertical gradients of leaf photosynthetic capacity in tropical forest canopies, it is instructive to investigate the impacts of these vertical gradients on the CO_2 flux. This might be of use in framing a strategy for measuring leaf-level physiological parameters, because it is relatively difficult to access some positions within the canopy. Leaf nitrogen per unit area (N_a in g m^{-2}) is a key physiological parameter in the SVAT model (see Niinements and Tenhunen 1997; Wilson et al. 2001; Kumagai et al. 2006). At the study site, average N_a across species in height classes 0–5 m (30 individuals) and 40–55 m (10 individuals) were 0.68 (±0.25 standard deviation) and 1.41 (±0.14) g m^{-2}, respectively. Using the vertical distribution of leaf area density in Case 1, Kumagai et al. constructed two further numerical experiments, Cases 5A and B, which had constant vertical distributions of N_a (0.68 and 1.41 g m^{-2}, respectively). That is, Cases 5A and B assumed that N_a measured in the lower and upper canopies, respectively, was distributed evenly throughout, and evaluated CO_2 flux variation caused by these two "end-members" of vertical distribution with the assumption that the entire profile represents the N_a in either the lower or upper canopy. Figure 10.7a compares N_E modeled from Cases 1, 5A and 5B, bin-averaged by time of day. Although N_E in Case 5A was about half that in Case 1, that in Case 5B was nearly the same as in Case 1. This result also suggests that the N_a distributed through the canopy in Case 5B had no photosynthetic capacity in the lower canopy layers.

Distinct peaks of the diurnal precipitation cycle at specific times of the day at various locations in the Southeast Asian tropics have been found (Kumagai and Kume 2012). Because exchanges between forest canopy and atmosphere such as assimilation and evapotranspiration are driven mainly by solar radiation, their activities might be influenced by diurnal precipitation timing via the effects of weak incident solar radiation, low vapor-pressure deficit, and leaf wetness. Therefore, Kumagai and Kume investigated potential changes of N_E caused by alteration of diurnal rainfall regime. N_E was computed by the SVAT model with input of a 30-min interval rainfall time series. This series was constructed using rainfall statistics of observation site data (at Lambir) and published data of long-term diurnal precipitation cycles (at Bintulu and Kuching) in Borneo (Fig. 10.7b). For these computations, the authors replaced only rainfall temporal patterns (including rainfall amount) of Lambir with those of Bintulu and Kuching, and retained relationships between rainfall intensity and other environmental factors (such as R_s) as at Lambir. The highest rainfall peak in the diurnal rainfall cycle at Lambir resulted in the lowest N_E around 1300–1400 LT at the three sites, but the difference was very slight. There were also differences in N_E variability among those sites (e.g. at 1030 and 1500 LT), but these were very slight (Fig. 10.7b). As a result, there was little or no difference in the full-year N_E among the sites (Fig. 10.7b). This

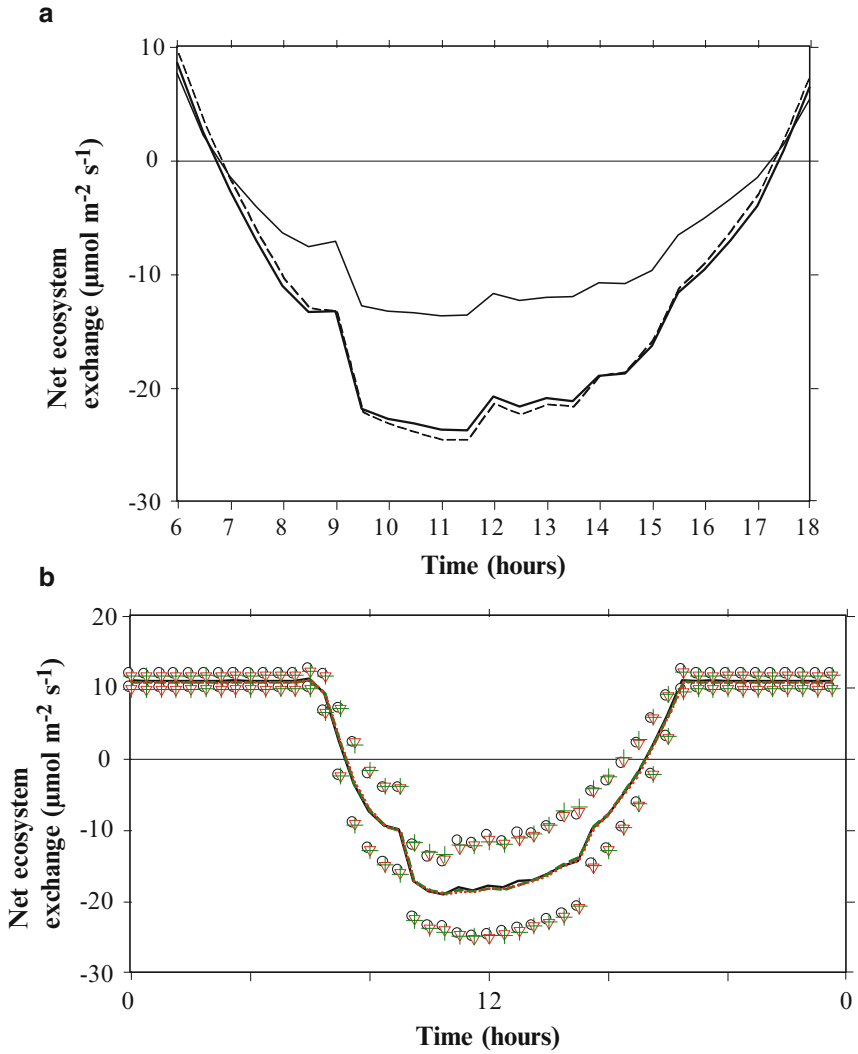

Fig. 10.7. (**a**) Average temporal variation of CO_2 fluxes (F_c) modeled from Cases 1 (*thick solid line*), 5A (*thin solid line*), and 5B (*broken line*). Cases 5A and B included constant vertical distributions of N_a (0.68 and 1.41 g m^{-2}, respectively) (From Kumagai et al. (2006)) (**b**) Average diurnal variations of modeled ecosystem CO_2 exchange for entire year with ± 1 standard deviation (SD) at Lambir (*solid line with circles*), Bintulu (*dotted line with triangles*), and Kuching (*broken line with crosses*) in Sarawak, Malaysia. Upper and lower symbols denote plus and minus one SD, respectively. All three lines almost perfectly overlap (From Kumagai and Kume 2012)

confirms that the diurnal rainfall cycle does not significantly affect the diurnal cycle of incident radiative energy in the studied tropical rainforest region. This is because the contribution of rainfall duration to the total duration is small, and productivity of the tropical rainforest ecosystem may be somewhat conservative in terms of its similarity across that region. This is because of the combined effects of N_E light response saturation at relatively low light intensity and constant cloud cover (Kumagai and Kume 2012).

Finally, to show the impact of canopy structure on atmosphere-canopy exchange, simulations of ecosystem CO_2 (N_E) and latent heat (LE) fluxes at a Cambodian rubber plantation site were conducted with

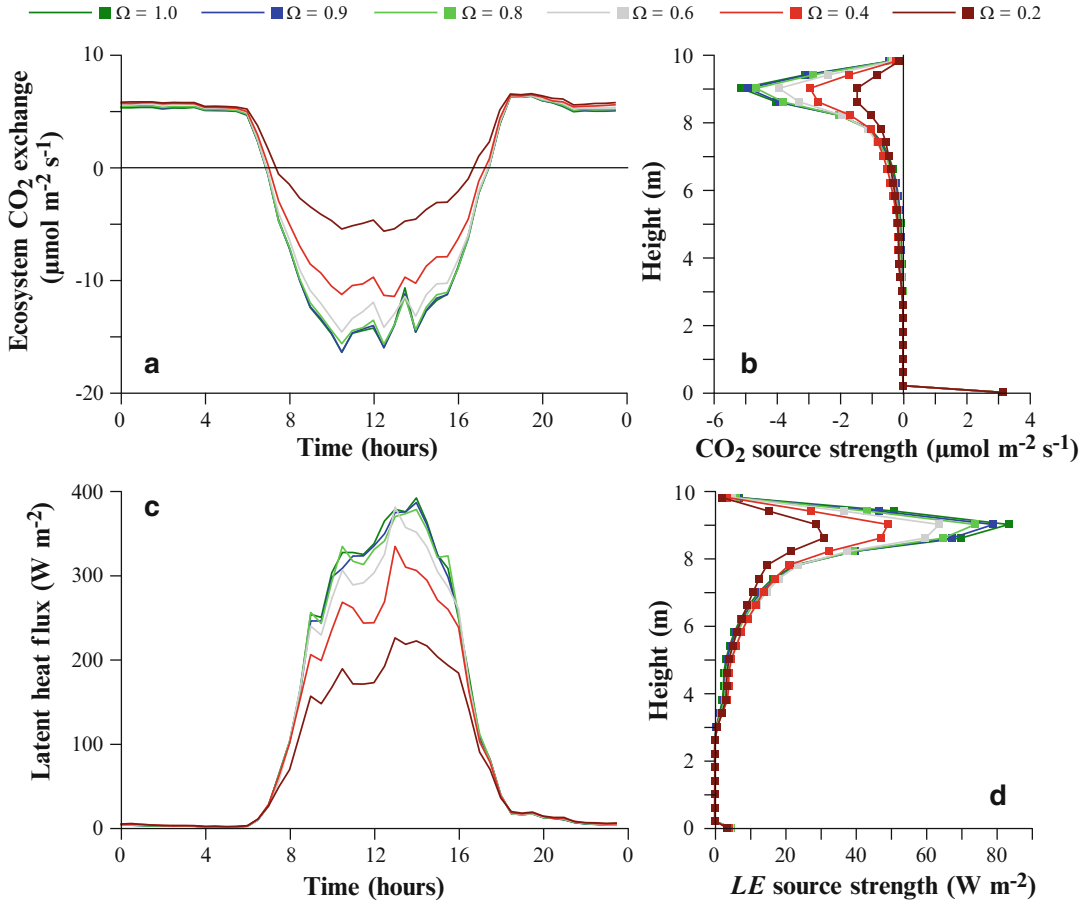

Fig. 10.8. Mean diurnal cycles of modeled ecosystem CO_2 exchange (**a**) and latent heat flux (*LE*) (**c**), along with vertical profiles of average modeled midday (1100–1300 LT) CO_2 (**b**) and *LE* (**d**) source strength as a function of canopy height, for canopy clumping factors (Ω) of 1.0, 0.9, 0.8, 0.6, 0.4 and 0.2. Total leaf area per ground area (LAI) was held constant at 3.89 (From Kumagai et al. 2013)

varying canopy clumping factors (Ω) and constant LAI (Kumagai et al. 2013). A decrease in Ω from 1.0 to 0.8 had little effect on either N_E and *LE* flux, but reducing Ω to less than 0.6 changed them appreciably (Fig. 10.8a, c). With decreasing Ω, fluctuations of N_E and *LE* fluxes at timescales shorter than the diurnal cycle became smaller and larger, respectively. In particular, *LE* flux tended to be depressed in the morning and rose in the afternoon (Fig. 10.8c). Figure 10.8b, d show that decreases in source strengths at their peaks in accord with decreases in Ω reduced N_E and *LE* fluxes. With decreasing Ω, source strengths in the upper canopy declined, while those in the lower canopy slightly increased. This implies that a Ω decrease enables light to penetrate deeper into the canopy. However, in the present study, strong source strengths in the upper canopy controlled the ecosystem fluxes because of dense foliage there (Fig. 10.8b, d).

IV. Future Research Directions

Prediction of carbon sequestration by vegetation under an increased atmospheric CO_2 environment and concomitant modifications to global climate are among the most important issues surrounding global climate

change, because global terrestrial ecosystem CO_2 absorption may impact local and global climate via direct atmospheric CO_2 concentration change. Also, vegetation covers a major part of the land surface and promotes latent heat exchange via transpiration. How the available energy is partitioned between sensible and latent heat fluxes at the air-land interface is critical for the evolution of local and global climate.

There are various relationships between global climatic factors and terrestrial ecosystem CO_2 dynamics. The climatic zone mainly determines vegetation type and thereby regional limitations on vegetation material exchange. The micrometeorological factors alter leaf-scale material exchange through environmental control of assimilation/respiration and stomatal aperture. Furthermore, extreme and drastic climatic shifts induce rapid and large-scale shifts in ecosystem structure and function, such as tree mortality and die-offs. This results in drastic changes in carbon, water and energy exchange between atmosphere and vegetation surfaces.

Again, our main concern is to gain the ability to predict global ecosystem carbon sequestration under climate change. Toward this objective, large-scale and long-term assessments of relationships between net ecosystem exchange (N_E) / net primary productivity and environmental factors are urgently needed. First of all, global investigations of N_E characteristics could be done using tower eddy covariance and meteorological data from the FLUXNET data archive (http://www.fluxnet.ornl.gov/). Also needed are an improved network of observations (e.g. a global network of vegetation inventories), which would be useful to clarify relationships between N_E and vegetation dynamics, and for validation of eddy flux data (see Chap. 12, Ohtsuka et al. 2016).

Combination of the SVAT model and the aforementioned network datasets would be a promising tool to generalize N_E characteristics of each vegetation type at global scale. Global and temporal patterns of environmental factors would permit straightforward construction of a global carbon balance map. Examples of such patterns could be basic climatic variables on a global 0.25° latitude-longitude resolution grid from the National Centers for Environmental Prediction – National Center for Atmospheric Research (NCEP-NCAR) reanalysis (cf. Kistler et al. 2001) and soil moisture outputs from the second Global Soil Wetness Project (GSWP-2) (cf. Dirmeyer et al. 2006).

Acknowledgments

I am grateful to the Forestry Department of Sarawak for their support during data acquisition. I also thank numerous colleagues who helped me with the eddy covariance works that I have ever done. The work was supported in part by a grant from the project "Program for Risk Information on Climate Change" of the Ministry of Education, Science and Culture, Japan.

References

Baldocchi D (1992) A Lagrangian random-walk model for simulating water vapor, CO_2 and sensible heat flux densities and scalar profiles over and within a soybean canopy. Bound Layer Meteorol 61:113–144

Baldocchi D, Meyers T (1998) On using eco-physiological, micrometeorological and biogeochemical theory to evaluate carbondioxide, water vapor and trace gas fluxes over vegetation: a perspective. Agric For Meteorol 90:1–25

Baldocchi D, Finnigan J, Wilson K, Paw UKT, Falge E (2000) On measuring net ecosystem carbon exchange over tall vegetation on complex terrain. Bound Layer Meteorol 96:257–291

Ball JT, Woodrow IE, Berry JA (1987) A model predicting stomatal conductance and its contribution to the control of photosynthesis under different environmental conditions. In: Biggens J (ed) Progress in Photosynthesis Research. Mirtinus Nijhoff Publishers, Dordrecht, pp 221–224

Campbell GS, Norman JM (1998) An Introduction to Environmental Biophysics. Springer, New York

Collatz GJ, Ball JT, Grivet C, Berry JA (1991) Regulation of stomatal conductance and transpiration: a physiological model of canopy processes. Agric For Meteorol 54:107–136

Dirmeyer PA, Gao X, Zhao M, Guo Z, Oki T, Hanasaki N (2006) The Second Global Soil Wetness Project (GSWP-2): multi-model analysis and implications for our perception of the land surface. Bull Am Meteorol Soc 87:1381–1397

Farquhar GD, von Caemmerer S, Berry JA (1980) A biochemical model of photosynthetic CO_2 assimilation in leaves of C3 species. Planta 149:78–90

Goudriaan J (2016) Light distribution. In: Hikosaka K, Niinemets Ü, Anten N (eds) Canopy Photosynthesis: From Basics to Applications. Springer, Berlin, pp 3–22

Gutschick VP (2016) Leaf energy balance: basics, and modeling from leaves to Canopies. In: Hikosaka K, Niinemets Ü, Anten N (eds) Canopy Photosynthesis: From Basics to Applications. Springer, Berlin, pp 23–58

Hikosaka K, Noguchi K, Terashima I (2016a) Modeling leaf gas exchange. In: Hikosaka K, Niinemets Ü, Anten N (eds) Canopy Photosynthesis: From Basics to Applications. Springer, Berlin, pp 61–100

Hikosaka K, Kumagai T, Ito A (2016b) Modeling canopy photosynthesis. In: Hikosaka K, Niinemets Ü, Anten N (eds) Canopy Photosynthesis: From Basics to Applications. Springer, Berlin, pp 239–268

Kaimal JC, Finnigan JJ (1994) Atmospheric Boundary Layers Flows. Their Structure and Measurement. Oxford University Press, New York

Katul GG, Albertson JD (1998) An investigation of higher-order closure models for a forested canopy. Bound Layer Meteorol 89:47–74

Katul GG, Albertson JD (1999) Modeling CO_2 sources, sinks, and fluxes within a forest canopy. J Geophys Res 104:6081–6091

Kistler R, Kalnay E, Collins W, Saha S, White G, Woollen J, Chelliah M, . . ., Fiorino M (2001) The NCEP-NCAR 50-year reanalysis: Monthly means CD-ROM and documentation. Bul Am Met Soc 82:247–267

Kumagai T, Kume T (2012) Influences of diurnal rainfall cycle on CO_2 exchange over Bornean tropical rainforests. Ecol Model 246:91–98

Kumagai T, Ichie T, Yoshimura M, Yamashita M, Kenzo T, Saitoh TM, Ohashi M, . . ., Komatsu H (2006) Modeling CO_2 exchange over a Bornean tropical rain forest using measured vertical and horizontal variations in leaf-level physiological parameters and leaf area densities. J Geophys Res 111:D10107

Kumagai T, Mudd RG, Miyazawa Y, Liu W, Giambelluca TW, Kobayashi N, Lim TK, . . ., Yin S (2013) Simulation of canopy CO_2/H_2O fluxes for a rubber (*Hevea brasiliensis*) plantation in central Cambodia: the effect of the regular spacing of planted trees. Ecol Model 265:124–135

Lai C-T, Katul G, Oren R, Ellsworth D, Schäfer K (2000) Modelling CO_2 and water vapor turbulent flux distributions within a forest canopy. J Geophys Res 105:26333–26351

Lee X-H (1998) On meteorological observations of surface-air exchange over tall vegetation. Agric For Meteorol 91:39–49

Lee X-H, Finnigan J, Paw UKT (2004) Coordinate systems and flux bias error. In: Lee X-H, Massman W, Law B (eds) Handbook of Micrometeorology, A Guide for Surface Flux Measurement and Analysis. Kluwer Academic Publishers, Dordrecht, pp 33–66

Leuning R (2007) The correct form of the Webb, Pearman and Leuning equation for eddy fluxes of trace gases in steady and non-steady state, horizontally homogeneous flows. Bound Layer Meteorol 123:263–267

Lloyd CR (1995) The effect of heterogeneous terrain on micrometeorological flux measurements: a case study from HAPEX-SAHEL. Agric For Meteorol 73:209–216

Manzoni S, Katul G, Fay PA, Polley HW, Porporato A (2011) Modeling the vegetation-atmosphere carbon dioxide and water vapor interactions along a controlled CO_2 gradient. Ecol Model 222:653–665

Moncrieff JB, Jarvis PG, Valentini R (2000) Canopy fluxes. In: Sala OE, Jackson RB, Mooney HA, Howarth RW (eds) Methods in Ecosystem Science. Springer, New York, pp 161–180

Niinements U, Tenhunen JD (1997) A model separating leaf structural and physiological effects on carbon gain along light gradients for the shade-tolerant species *Acer sccharum*. Plant Cell Environ 20:845–866

Ohtsuka T, Saigusa N, Imura Y, Muraoka H, Koizumi H (2016) Biometric-based estimations of net primary production (NPP) in forest ecosystems. In: Hikosaka K, Niinemets Ü, Anten N (eds) Canopy Photosynthesis: From Basics to Applications. Springer, Berlin, pp 333–351

Raupach MR (1988) Canopy transport processes. In: Steffen WL, Denmead OT (eds) Flow and Transport in the Natural Environment. Springer, New York, pp 95–127

Schuepp PH, Leclerc MY, Macpherson JI, Desjardins RL (1990) Footprint prediction of scalar fluxes from analytical solutions of the diffusion equation. Bound Layer Meteorol 50:355–373

Stull RB (1988) An Introduction to Boundary Layer Meteorology. Kluwer Academic Publishers, Dordrecht

von Caemmerer S, Farquhar GD (1981) Some relationships between the biochemistry of photosynthesis and the gas exchange of leaves. Planta 153:376–387

Watanabe T (1993) The bulk transfer coefficients over a vegetated surface based on K-theory and 2nd-order closure model. J Meteor Soc Jpn 71:33–42

Webb EK, Pearman GI, Leuning R (1980) Correction of flux measurements for density effects due to heat and water vapour transfer. Quart J R Meteorol Soc 106:85–100

Wilson NR, Shaw RH (1977) A higher order closure model for canopy flow. J Appl Meteorol 16:1198–1205

Wilson KB, Baldocchi DD, Hanson PJ (2001) Leaf age affects the seasonal pattern of photosynthetic capacity and net ecosystem exchange of carbon in a deciduous forest. Plant Cell Environ 24:571–583

Chapter 11

Remote Sensing of Vegetation: Potentials, Limitations, Developments and Applications

Mathias Disney*
Department of Geography, University College London, Gower Street, London WC1E 6BT, UK

NERC National Centre for Earth Observation

Summary

Earth observation, i.e., gaining information of Earth's physical, chemical and biological characteristics by remote sensing methods, can be used to make a range of quantitative measurements related to vegetation canopy structure and function. The capabilities of Earth observation for mapping, even indirectly, canopy state and function over wide areas and over decadal time-scales allow for studies of phenology, disturbance, anthropogenic impacts and

*Author for correspondence, e-mail: mathias.disney@ucl.ac.uk

K. Hikosaka, Ü. Niinemets, and N.P.R. Anten (eds.), *Canopy Photosynthesis: From Basics to Applications*, DOI 10.1007/978-94-017-7291-4_11

responses to climate change. Key limitations of Earth observation measurements are discussed, in particular how their indirect nature makes them potentially hard to interpret and relate to physically-measurable quantities, as well as assumptions that are made to derive information from Earth observation data. Various Earth observation measurements of vegetation routinely provided from satellite data are introduced and a radiative transfer framework for developing, understanding and exploiting these measurements is outlined. This framework is critical in that it allow us to chart a consistent route from measurements made at the top-of-the atmosphere to estimates of canopy state and function. The impacts of assumptions required to solve the canopy radiative transfer problem in practical applications are discussed. New developments in radiative transfer theory and modelling are introduced, in particular focusing on how incorporating the vegetation structure in these models is key to interpreting many Earth observation measurements. These new techniques help to unpick the nature of the canopy signal from Earth observation measurements. The (key) issue of 'effective' model parameters that are often used to interpret and exploit observations is raised. These simplified or approximate manifestations of measurable physical properties permit development of practical, rapid models of the sort required for global applications but potentially introduce inconsistency between Earth observation measurements and models of vegetation productivity. Methods to overcome these limitations are discussed, such as data assimilation, which is being used to provide consistent model-data frameworks and make best use of both. Lastly, new remote sensing measurements are described that are providing information on 3D

Abbreviations: A_l – Area of a given leaf; ALS – Airborne laser scanning; BRDF – Bidirectional reflectance distribution function; c – Speed of light; d – Sensor-target distance; DA – Data assimilation; DASF – Directional area scattering factor; DEM – Digital elevation model; DGVM – Dynamic global vegetation model; DWEL – Dual-wavelength Echidna laser scanner; E_i – Downwelling surface irradiance; EO – Earth observation; ESA – European Space Agency; ESM – Earth system model; ESS – Earth system science; EVI – Enhanced vegetation index; fAPAR – Fraction of absorbed photosynthetically active radiation; F_s – Solar-induced chlorophyll fluorescence; FTS – Fourier Transform Spectrometer; $g_l(z, \mathbf{\Omega}_l)$ – Angular distribution of leaf normal vectors (leaf angle distribution); $G_l(\mathbf{\Omega})$, $G_l(\mathbf{\Omega}')$ – Leaf projection function in direction $\mathbf{\Omega}$, $\mathbf{\Omega}'$ respectively; GLAS – Geoscience Laser Altimeter System; GO – Geometric optics; GOSAT – Greenhouse Gases Observing Satellite; GPP – Gross primary productivity; $h_l(\phi_l)$ – Azimuthal dependence of leaf angle, ϕ_l; H – Canopy total height; $H(\boldsymbol{x})$ – Observation operator, mapping model state variable vector $\boldsymbol{x}$ to the EO signal; i_0 – Radiation first intercepted in the canopy by leaves; i_L – Leaf interceptance that enters the leaf interior; I_r – Upwelling (reflected) radiance; $I(z, \mathbf{\Omega})$ – Specific energy intensity in direction $\mathbf{\Omega}$ at depth z in a horizontal plane-parallel canopy; $J_s(z, \mathbf{\Omega}')$ – Source term of radiative transfer equation at depth z, in direction $\mathbf{\Omega}'$; κ_e – Volume extinction coefficient; $L(z)$ – Cumulative leaf area index at depth z; LAD – Leaf angle distribution; LAI – Leaf area index; $L\tilde{A}I$ – Effective LAI; lidar – Light detection and ranging; LSM – Land surface model; MCRT – Monte Carlo ray tracing; MERIS – Medium Resolution Imaging Spectrometer; MISR – Multiangle Imaging Spectroradiometer; MODIS – Moderate Resolution Imaging Spectroradiometer; $N_v(z)$ – Number of leaves per unit volume; NASA – National Aeronautics and Space Administration; NDVI – Normalized difference vegetation index; NIR – Near infrared; NPP – Net primary productivity; p – Recollision probability; $P\left(z, \mathbf{\Omega}' \rightarrow \mathbf{\Omega}\right)$ – Volume scattering phase function; PFT – Plant functional type; PILPS – Project for Intercomparison of Land Surface Parameterization Schemes; Q_0 – Uncollided radiation passing through the canopy to the lower boundary layer; $\boldsymbol{R}$ – Vector of EO measurements; RADAR – Radio detection and ranging; RAMI – Radiation Transfer Model Intercomparison; $\boldsymbol{S}$ – Radiation model system state vector; SALCA – Salford Advanced Laser Canopy Analyser; SWIR – Shortwave infrared; t – Time of flight; TANSO – Thermal and Near infrared Sensor for carbon Observation; TLS – Terrestrial laser scanning; z – Canopy depth; $\boldsymbol{Z}$ – Radiation signal modelled by a radiation model with state variable $\boldsymbol{S}$; W_λ – Spectral canopy scattering coefficient; ζ – Canopy clumping factor; λ – Wavelength; μ, μ' – Cosine of the view, illumination direction vectors $\mathbf{\Omega}$, $\mathbf{\Omega}'$ with the local normal; ρ – Reflectance; τ – Transmittance; $\theta_{v,i}$ – View, illumination zenith angles; $\varphi_{v,i}$ – View, illumination azimuth angles; $u_l(z)$ – Canopy leaf area density at depth z; ω – Leaf single scattering albedo; $\hat{\omega}_\lambda$ – Spectral leaf single scattering albedo normalized by leaf interceptance; $\mathbf{\Omega}(\theta_v, \varphi_v)$ and $\mathbf{\Omega}'(\theta_i, \varphi_i)$ – View, illumination vectors

canopy structure, from lidar particularly, and canopy function from fluorescence. These measurements, along with other Earth observation data and model-data fusion techniques are providing new insights into canopy state and function on global scales.

I. Introduction

A. What Is Earth Observation?

Terrestrial vegetation is a key component of the Earth's climate system, via mediation of fluxes of solar radiation, water and atmospheric gases at the land surface, and the resulting interactions with and feedback to the global carbon cycle (Denman et al. 2007; Solomon et al. 2007). Terrestrial vegetation processes operate across a huge range of time-scales, responding from seconds to hourly and daily time-scales to changes in environmental conditions temperature, precipitation and light, and over seasonal and much longer time-scales to cycles of climate and global change. Vegetation is also heterogeneous at a huge range of scales (within leaf, root systems) to composition of savannahs and forests shaped by millennia of evolutionary, climate and more recently anthropogenic influences. Vegetation is of course also intimately connected to human activity in provision of food, shelter, fuel and many other direct and indirect ecosystem services.

The importance of understanding the state and function of vegetation has led to development of a wide range of observational and modelling techniques (Sellers 1985; Liang 2004; Monteith and Unsworth 2008; Jones 2014). Of these, remote sensing (hereafter referred to as Earth observation (EO), to distinguish it from planetary remote sensing) has become a central part of efforts to address many of these issues due to the large spatio-temporal scales that can be covered by satellite and airborne instruments. The developments of EO have seen huge advances in instrument design, accuracy, consistency and the ability to handle large (and ever-growing) datasets (Lynch 2008). These benefits have led to EO becoming ubiquitous in Earth System Science. A wide range of problems at global and regional scales are ideally-suited to the scale and coverage of EO. New observations and models have arisen in tandem, sometimes by design, although more often not. This has led to many new developments for exploiting EO data in understanding and measuring the Earth System (Chapin et al. 2011). This has also raised fundamental questions about how such observations can be used (Pfeifer et al. 2012).

Here, I introduce the problem of how EO is used for understanding and quantifying terrestrial vegetation i.e. what can and can't be measured via EO. A key advantage of remote sensing, its remoteness, is also a key limitation: what we actually *can* measure is rarely what we *want* to measure. To translate the former to the latter, a hierarchy of models has been developed. I outline some of the issues and approaches to modelling across this hierarchy: from scattering and absorption of radiation (EO models), through models that transform radiation into canopy properties (state, productivity, dynamics) and on to large-scale models of ecosystem processes, both of the current state (diagnostic, biogeochemical cycling) and future changes (prognostic, dynamic global vegetation models (DGVMs), and their big brothers, global climate models). If and when these various models interface with EO data, they do so in very different ways due to their underlying assumptions, structure and aims. I discuss some of the consequences of these variations (and inconsistencies) from the point of view of how EO can be used to understand and quantify terrestrial vegetation systems, as well as how models may be developed to better exploit EO data. Clearly, quantifying the state of terrestrial ecosystems and understanding how they will change in the face of uncertain climate and anthropogenic drivers, requires best use of both observations and models.

B. What Earth Observation Can and Can't Measure

The value of an EO measurement is simply the answer to the question: how much

information about the system being observed is contained within the EO measurement of that system? The EO signal is a measure of scattered (reflected, transmitted) or emitted radiation from a target. We measure photons escaping towards a sensor, from a target, either above the atmosphere in the case of a satellite, or at some point lower down in the case of airborne or even ground-based observations. Table 11.1 describes a list of properties that EO can and does provide, along with an assessment of the level of how 'direct' these measurements are in some sense, from the perspective of any additional ground-level measurements or modelling needed to interpret the measurements. Not surprisingly, as EO 'measurements' become less direct, three critical (and related) things occur:

- The number of assumptions underlying an EO measurement becomes larger and the opportunity for these assumptions to become inconsistent at some level increases.
- The uncertainty associated with an EO measurement becomes more difficult to quantify (albeit not necessarily larger), due to the increasing number of assumptions and requirements for ancillary information, and the way uncertainties in each may combine in potentially non-linear ways.
- The more difficult it is likely to be to compare an EO measurement against independent measurements (or model-derived estimates) of what ought to be the same property. This is due to possible differences in underpinning assumptions and ancillary information.

These issues of the limits of remote sensing measurement are identified by Verstraete et al. (1996). They define a physical model relationship between an observation of emitted radiation $\boldsymbol{Z}$ and a system described by model state variables $\boldsymbol{S}$ as

$$\boldsymbol{Z} = f\boldsymbol{S} \tag{11.1}$$

where the $\boldsymbol{S}$ are the smallest set of variables needed to fully describe the physical state of the observed system, at the scale of observation. It is worth repeating the first proposition of Verstraete et al. (1996) on the limitations of remote sensing, as it provides a useful framing for the ensuing discussion: "A physical interpretation of electromagnetic measurements $\boldsymbol{Z}$ obtained from remote sensing can provide reliable quantitative information *only on the radiative state variables* $\boldsymbol{S}$ *that control the emission of radiation from its source and its interaction with all intervening media and the detector*" (emphasis added). We may be able to translate from $\boldsymbol{S}$ to other parameters of interest that may rely on $\boldsymbol{S}$ indirectly (e.g. canopy state or function), but we always require a mapping back to $\boldsymbol{S}$ at some point if we wish to make use of remote sensing.

The last category in Table 11.1 is intended to indicate properties that are either not well-defined (i.e. do not have a clear physically-derived meaning), or perhaps are not directly measurable quantities i.e. in the formalism of Verstraete et al. (1996) we are not able to define a physically-based mapping $\boldsymbol{Z} = f(\boldsymbol{S})$ for these parameters. However, such properties may be used to capture some aspect of the canopy either for (empirical) correlation with some more desirable variable, or for parameterizing more complex models. Examples include vegetation indices such as the normalized difference vegetation index (NDVI) and variants, which have been widely and successfully used to provide surrogate indicators of canopy 'greenness' (Pettorelli et al. 2005). They are attractive due to being easy to calculate and apply, and they may capture key aspects of vegetation 'well enough'. NDVI for example exploits the characteristic high contrast between red and near-infrared (NIR) spectral reflectance, ρ of healthy vegetation as $\mathrm{NDVI} = (\rho_{NIR} - \rho_{RED})/(\rho_{NIR} + \rho_{RED})$. Such indices are clearly useful for capturing particular broad vegetation patterns, in themselves e.g. as indicators of vegetation response to climate, disturbance, insect or fire damage, malaria risk etc. (Pettorelli et al. 2005, Pettorelli 2013; Pfeifer et al. 2012). Vegetation indices can also be used as surrogates for empirically-related variables such as leaf area index (LAI), the (unitless) one sided leaf area per unit

Table 11.1. List of properties of interest to terrestrial ecosystem studies that can be derived from EO data, categorised broadly by their requirement for additional information and assumptions beyond a direct measurement

'Directness'	Measurement (units)	Key additional assumptions
Direct	Top-of-atmosphere at-sensor radiance (W m^{-2} sr^{-1} μm^{-1}) from reflectance (optical), emittance (passive microwave/thermal), backscatter (RADAR); canopy fluorescence (arbitrary units).	Calibrated sensor response, geolocated instantaneous field of view (IFOV)
	Distance from sensor to target i.e. canopy and surface height (m) e.g. from lidar	Accurate time-of-flight of active (generated) signal (pulse), known pulse characteristics and position of sensor in 3D space.
High	Top-of-canopy (surface) radiance (W m^{-2} sr^{-1} μm^{-1})	Known atmospheric path radiance (via models and/or ancillary data)
	Albedo (unitless)	Known incoming radiation distribution in terms of angular and direct-to-diffuse ratio i.e. function of atmosphere; integrable model of surface angular reflectance distribution
	Surface temperature (K)	Well-calibrated sensor; surface emissivity
Medium	Canopy structural properties: Leaf area index (LAI, unitless); canopy cover (unitless %); canopy gap fraction (unitless)	Model relating scattered radiation to structural parameters, assume a degree of clumping/ Inversion must be tractable and not ill-posed.
	Canopy radiometric properties: fraction of photosynthetically active radiation, fAPAR (unitless); canopy-average biochemical constituents (chlorophyll, water, N and dry matter, mass per unit specific leaf area i.e. g m^{-2})	Model relating radiation scattered within and from the canopy to radiometric parameter. Inversion must be tractable and not ill-posed.
	Leaf radiometric properties: biochemical constituents (chlorophyll, water, N and dry matter, mass per unit specific leaf area i.e. g m^{-2})	Model relating radiation scattered within and from the leaf. Often embedded into canopy-level model.
	Standing biomass (kg C m^{-2})	Empirical allometric model relating height to biomass (via time-of-flight from lidar, or interferometric RADAR); requires woody biomass to total carbon ratio.
	Fire radiative power (FRP, W m^{-2} μm^{-1}) and energy (FRE) (J m^{-2})	FRP requires model relating observed temperature to surface emissivity; FRE requires integration of FRE over time.
	Burned area (ha)	Model of surface bidirectional reflectance distribution function (BRDF) allowing prediction of reflectance and detection of change.
Low	Standing biomass (kg C m^{-2}) from scattering	Model of reflectance (optical) or backscatter (RADAR) related to biomass; assumption of leaf to wood ratio in canopy and wood density conversion factor;
	Photosynthetic rate (μmol m^{-2} s^{-1})	Model relating leaf absorption or fluorescence, to measured signal
	Gross primary productivity, GPP (kg C m^{-2} h^{-1})	Incoming radiation, fAPAR, model relating intercepted radiation to gross productivity; ancillary information on biome type, climate (T, P)
	Net primary productivity, NPP (kg C m^{-2} h^{-1})	GPP, autotrophic respiration losses (measured or modelled)
	Net ecosystem productivity, NEP (kg C m^{-2} h^{-1})	NPP, heterotrophic respiration losses (measured or modelled)

(continued)

Table 11.1. (continued)

'Directness'	Measurement (units)	Key additional assumptions
	Net ecosystem exchange, NEE (kg C m^{-2} h^{-1})	NEP, losses due to disturbance (fire, harvest, predation, etc)
	Land cover (km^{-2}), Land use/land use change (LULUC, km^{-2})	Unique mapping of vegetation types (or biome) and other spectrally identifiable cover types to land cover classes; LULUC requires mapping between biome/land cover and land use.
Ambiguous/ surrogate	NDVI (and other empirical spectral indices); 'greenness'; phenology.	Land cover or biome type; spectral; definition of 'greenness' – usually some arbitrary translation of a spectral index to vegetation 'vigour' or state; phenology requires definition of canopy timing, as a function of an EO-derived variable, typically NDVI or LAI.

Key assumptions required to move from more to less direct measurements are outlined. The list is not intended to be exhaustive, and 'directness' is somewhat subjective.

ground area, fraction of absorbed photosynthetically active radiation (fAPAR) and hence productivity (Myneni and Williams 1994; Myneni et al. 1997a; Angert et al. 2005). However, simplicity comes at the cost of ecological meaning (i.e. direct causality) and requirement for site- or biome-specific calibration (e.g. Nagai et al. 2010). Other more general limitations of vegetation indices are the lack of sensitivity with increasing LAI, saturating at values of 4–5, and sensitivity to background effects (soil, haze etc.). Care is also needed when compositing vegetation indices over time to account for variations in view and sun angles in the reflectance observations from which the vegetation indices are derived. These limitations, particularly saturation, are not soluble through taking a particular calibration approach.

The difficulty of interpreting vegetation indices has been seen in the debate over unexpected trends in Amazonian green-up observed during the severe 2005 drought (Saleska et al. 2007; Samanta et al. 2010). Subsequent to this, work relating carefully re-processed estimates of enhanced vegetation index (EVI, another empirical spectral index) to ground-based measures of productivity, water availability and other ecological variables suggested that apparent discrepancies may be due to leaf flushing being mistaken for changes in LAI and productivity (Brando et al. 2010). This debate was rejoined by recent re-analysis of the satellite data, including detailed consideration of vegetation structure and satellite-sun geometry (Morton et al. 2014). This approach accounts for the apparent 'observed' green-up, whilst also ruling out the leaf-flushing hypothesis. Crucially, this re-analysis was carried out on the original satellite spectral reflectance data, rather than the spectral indices derived from those data from which the original 2005 green-up conclusions were drawn.

This debate perhaps illustrates the difficulty of trying to explain variations in empirical spectral indices that can be functions of complex, often mutually compensating biophysical processes. Verstraete et al. (1996) sum up this difficulty by noting that any number of empirical functions relating a parameter of interest $\boldsymbol{Y}$ to observations $\boldsymbol{Z}$ of the form $\boldsymbol{Y} = g(\boldsymbol{Z})$ may be derived. However, these relationships effectively assume that the variable of interest is the main controlling factor of the observations $\boldsymbol{Z}$ to the (near) exclusion of all other factors. Since the same vegetation index is often used to derive different $g(\boldsymbol{Z})$ for different applications, the information contained in $g(\boldsymbol{Z})$ must be the same, regardless of how the vegetation index is interpreted. This is rarely acknowledged in practice.

The problem of ascribing direct meaning to surrogate variables makes them hard (or even impossible) to validate. For example 'greenness' has been used to imply amount (Myneni et al. 1997a), productivity, health (degree of stress) and phenology (Myneni et al. 2007; Pettorelli 2013). This latter

term is also ambiguous; although it implies seasonality, this can be defined to encapsulate a number of different, related things: bud break, leaf emergence, onset of photosynthesis and growth, start of flowering, seasonal LAI profile, onset of senescence, leaf drop, growing season length etc. A further complication is that ecological models that describe plant seasonality typically use some integrated estimate of time such as growing degree days (number of days over a base threshold, T_t multiplied by the excess temperature T-T_t). Recent work by Richardson et al. (2012) has shown that different model representations of phenology tend to introduce overestimates of canopy productivity during spring greenup by 13 %, and during autumn senescence by 8 % of total annual productivity. This problem was exacerbated by the tendency of individual models to compensate for over-estimates during transition periods by under-prediction of summer peak productivity. As a result, Richardson et al. (2012) conclude that current model uncertainties preclude reliable prediction of future phenological response to climate change.

The difference between the ways ecological models treat vegetation amount and state and how these properties can be derived from EO is a key reason for differences between models and observations: both representations may be internally consistent, but inconsistent with each other (of course, either or both may be wrong as well!). Lastly, even when empirically-derived properties appear to correlate well with characteristics we wish to measure, we do not know how the residual unexplained variance arises, or if it is important. For a more detailed discussion I refer to Pfeifer et al. (2012) and Grace et al. (2007) who review a range of ecologically-relevant biophysical properties available from EO, as well as some of the issues in moving from direct to more indirect products.

Perhaps most importantly then, for understanding and interpreting EO-derived measurements of canopy state and function, we require physically-based models of radiation interaction with the canopy. Below, I provide a statement of this problem, lay out some of approaches to solving it, and describe how these approaches are used to exploit the EO signal for remote sensing studies of vegetation. Advances in computing power have meant that highly-detailed modelling approaches which were previously impractical have become increasingly attractive. A good example of this is how photo-realistic 3D modelling techniques developed by the computer graphics community for movie-making and visualisation, have been co-opted for modelling vegetation for scientific applications (Disney et al. 2006; Widlowski et al. 2006). This in turn has led to improved parameter estimation schemes (Disney et al. 2011), allowed assessed of uncertainty, and provided test and benchmark tools for simpler modelling approaches (Widlowski et al. 2008, 2013). Rapid increases in computation speed have also led to changes in the way information can be derived from very large (GB to TBs) satellite datasets. This is almost always a balance between requirements for speed/efficiency, and accuracy or physical realism. Increasingly, statistical tools such as Monte Carlo and Bayesian methods, which had been too slow for these applications, can be employed (Sivia and Skilling 2006).

I discuss some of these developments in canopy modelling in more detail below, before moving on to discussing recent developments in model-data fusion that are pushing the limitations of both, and the advent of new observations that may provide information more directly-related to the problems at hand. I embark on this description with a quote that encapsulates the difficulty that can arise in trying to reconcile models (hypotheses) and measurements, in part due to the different scientific drivers and assumptions that underlie them; this is particularly apposite in remote sensing, where the two are so intimately intertwined.

> A hypothesis is clear, desirable and positive, but is believed by no one but the person who created it. Experimental findings, on the other hand, are messy, inexact things which are already believed by everyone except the person who did the work (Harlow Shapley (1885–1972), *Through Rugged Ways to the Stars*, 1969).

II. Radiative Transfer in Vegetation: The Problem and Some Solutions

We are rarely interested in the most direct EO measurement we can make i.e. in top-of-atmosphere radiance resulting from photons incident on the surface that are scattered in some way back towards the sensor (Pfeifer et al. 2012). In order to relate the above-atmospheric signal to the structural (amount, arrangement) and biochemical (absorbing species and concentrations) properties of the canopy we need a physically-realistic description of the radiation scattering properties of the canopy. This in turn requires understanding of the canopy radiative transfer (RT) regime from the leaf level, across scales to shoot and crown levels, and finally to the whole canopy.

A. Statement of the Radiative Transfer Problem

RT models have been used extensively since the 1960s to model scattering from canopies at optical wavelengths (Ross 1981; Myneni et al. 1989). The models consider energy balance across an elemental volume in terms of the energy arriving into the volume (either energy incident in the propagation direction, or energy that is scattered from other directions) and energy losses from the volume (either scattering out of the propagation direction, or absorption losses). Across optical wavelengths (visible, NIR and shortwave infrared (SWIR) regions of 400–2500 nm) a scalar radiative transfer equation is used. At RADAR wavelengths (cm to m), a slightly different approach is required, incorporating a vector of intensities to allow consideration of polarization (controlled by the sensor design). In this case orthogonal polarizations are coupled so radiative transfer equations must take this into account in a vector solution. Here I focus on radiative transfer in the optical domain, due to the particular relevance to canopy activity.

A widely-applied approach to describing radiation transport in vegetation has been via the so-called turbid medium approximation (Ross 1981; Myneni et al. 1989; Liang 2004). This considers the canopy as a plane parallel homogeneous medium of infinitesimal, oriented scattering elements, suspended over a scattering (soil) background – a 'green gas'. In this case, mutual shading can be ignored (the 'far field' approximation) and the radiance field resulting from single and multiple scattered photons can be described by considering the conservation of energy within a canopy layer, and specifying the sources of radiation external to that layer (boundary conditions). The result is an integro-differential equation describing the change in intensity I along a viewing direction $\mathbf{\Omega}(\theta_v, \varphi_v)$ due to: (i) interactions causing radiation to be scattered out of the illumination direction $\mathbf{\Omega}'(\theta_i, \varphi_i)$ (sink term); and (ii) interactions causing radiation to be scattered from other directions into the viewing direction $\mathbf{\Omega}(\theta_v, \varphi_v)$ (source term), where $\theta_{i,v}$ and $\varphi_{i,v}$ are the illumination and view zenith and azimuth angles respectively. This system is shown schematically in Fig. 11.1.

The far-field approximation allows us to ignore polarization, frequency shifting interactions and emission, in which case the upward and downward energy fluxes within the canopy are described by the (1D) scalar radiative transfer equation. For a plane parallel medium (air) embedded with a low density of small scattering objects the radiative transfer equation is composed of two terms, the (negative) extinction term with depth z that is determined by the path length through the canopy and the extinction along this path, and the source term due to multiple scattering from all directions within an elemental volume in the canopy into direction $\mathbf{\Omega}$ by the objects in the volume. Thus,

$$\mu \frac{\partial I(z,\mathbf{\Omega})}{\partial z} = -\kappa_e I(z,\mathbf{\Omega}) + J_s\left(z,\mathbf{\Omega}'\right) \quad (11.2)$$

where $\partial I(z,\mathbf{\Omega})/\partial z$ is the steady-state radiance distribution function and μ is the cosine of the (illumination) direction vector $\mathbf{\Omega}'$ with the local normal i.e. the viewing zenith

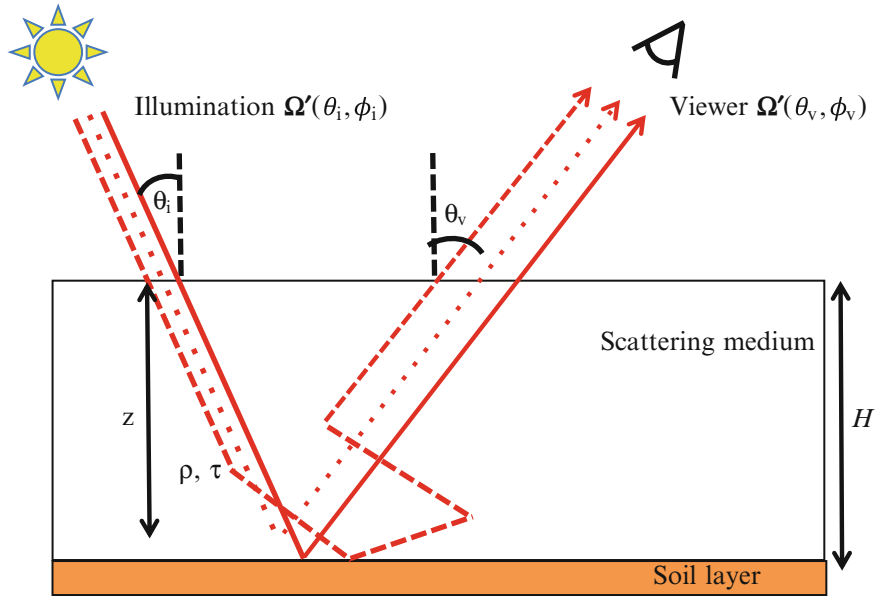

Fig. 11.1. Schematic illustration of radiation incident on a plane parallel homogeneous medium (*solid line*), at a zenith angle θ_i azimuth angle ϕ_i from the surface normal and penetrating to a depth z (marked by *dashed line*). In this example incoming radiation either passes through uncollided to the lower boundary, and back up (*solid line*); is scattered once at depth z by reflectance (*dotted line*); or is scattered multiple times via reflectance and/or transmittance, including the canopy lower boundary (at $z = -H$) before escaping in the viewing direction (*dashed line*)

angle, θ_i used to account for path length through the canopy. The extinction term is given as the product of κ_e, the volume extinction coefficient, and $I(z, \mathbf{\Omega})$, the specific energy intensity in direction $\mathbf{\Omega}$ at depth z within a horizontal plane-parallel canopy of total height H ($0 < z < H$). The source term, $J_s(z, \mathbf{\Omega}')$, is defined as

$$J_s\left(z, \mathbf{\Omega}'\right) = \int_{4\pi} P\left(z, \mathbf{\Omega}' \rightarrow \mathbf{\Omega}\right) I\left(z, \mathbf{\Omega}'\right) d\mathbf{\Omega}' \tag{11.3}$$

where $P\left(z, \mathbf{\Omega}' \rightarrow \mathbf{\Omega}\right)$ is the volume scattering phase function. This defines the (angular) probability of a photon at depth z in the canopy being scattered from the illumination direction $\mathbf{\Omega}'$ through a solid angle $d\mathbf{\Omega}'$ into to the viewing direction, $\mathbf{\Omega}$, integrated over the unit viewing hemisphere. This term depends on the size and orientation of scatterers within the canopy (see below).

When this description is extended to 3D, i.e. the canopy can vary in density in vertical and horizontal directions, the illumination and viewing vectors are functions of both the zenith and azimuth angles $\theta_{i,v}$ and $\varphi_{i,v}$ i.e. $\mathbf{\Omega}'(\theta_i, \varphi_i)$ and $\mathbf{\Omega}(\theta_v, \varphi_v)$ respectively.

A full description of radiative transfer should include the corresponding emission source term $J_s(z, \mathbf{\Omega}')$ for wavelengths where this might be significant e.g. for passive microwave (thermal) emissions from objects at ~300 K (~8–20 μm). In this case each object within the medium may need to be considered as an emission source in its own right. However, for optical and RADAR wavelengths, the emission source term is effectively zero.

Solving Eq. 11.2 requires defining κ_e in terms of canopy biophysical properties, and considering a particular viewing direction $\mathbf{\Omega}'$, for given boundary conditions. In using Eq. 11.2 to model canopy scattering for remote sensing applications, we wish to phrase the scattered radiation as an intrinsic

property of the canopy, rather than as a function of incident intensity. This permits comparison of measurements made under differing illumination intensities. At optical wavelengths this fundamental intrinsic scattering quantity wavelengths is known as the Bidirectional Reflectance Distribution Function (BRDF) i.e.:

$$\mathrm{BRDF}(\boldsymbol{\Omega},\, p, \boldsymbol{\Omega}',\, p';\lambda) = \frac{dI_{\mathrm{r}}(\boldsymbol{\Omega},\, p', F;\lambda)}{dE_{\mathrm{i}}\left(\boldsymbol{\Omega}',\, p;\lambda\right)} \tag{11.4}$$

where p and p' are the polarization of the received/transmitted wave; E_{i} is the downwelling irradiance on the surface (W m^{-2}); and I_r is the upwelling (reflected) radiance (W m^{-2} sr^{-1}). The BRDF of an ideal diffuse (Lambertian) surface is $1/\pi$ (for an unpolarized reflector) and is independent of viewing and illumination angles. As defined, BRDF is an infinitesimal quantity (with respect to solid angle and wavelength), so although it can be modelled, it is not a measurable quantity in this form. In practice, we consider the Bidirectional Reflectance Factor (BRF) $\rho_{\mathrm{c}}(\boldsymbol{\Omega}, \boldsymbol{\Omega}')$, defined as the ratio of radiance leaving the surface around viewing direction $\boldsymbol{\Omega}$, $I(\boldsymbol{\Omega})$ due to irradiance $E(\boldsymbol{\Omega}')$, to the radiance on a flat totally reflective Lambertian surface under the same illumination conditions i.e.

$$\begin{aligned}\rho_{\mathrm{c}}\left(\boldsymbol{\Omega}, \boldsymbol{\Omega}'\right) &= \frac{E\left(\boldsymbol{\Omega}'\right)\mathrm{BRDF}\left(\boldsymbol{\Omega}, \boldsymbol{\Omega}'\right)}{E\left(\boldsymbol{\Omega}'\right)(1/\pi)} \\ &= \pi \mathrm{BRDF}\left(\boldsymbol{\Omega}, \boldsymbol{\Omega}'\right)\end{aligned} \tag{11.5}$$

for an equivalent infinitesimal solid angle definition. As the BRF is defined as the ratio of two radiances, it is a directly measurable quantity and allows for model predictions to be compared with measurements, albeit over instrument finite solid angles (and of course wavelength intervals). Detailed definitions of reflectance nomenclature are given by Nicodemus et al. (1977) and Schaepman-Strub et al. (2006).

B. Solving the Radiative Transfer Problem for Explicit Canopy Structure

To solve the radiative transfer problem for realistic canopies, we need to consider how vegetation structure can be expressed in terms of the equations above, using assumptions that permit physically realistic solutions. Various solutions for the radiative transfer equation have been developed in a range of subjects including astrophysics, particle physics and neutron transport (Chandrasekhar 1960). Most importantly, once we have a solution of Eq. 11.2, if it can be inverted in terms of the canopy parameters it contains, we can then estimate distributions of these parameters from EO measurements of $\rho_{\mathrm{c}}(\boldsymbol{\Omega}, \boldsymbol{\Omega}')$ in the standard inverse problem sense (Twomey 1977; Verstraete et al. 1996; Tarantola 2005). Forward and inverse approaches to canopy modelling have been reviewed in detail by Asrar (1989), Goel and Thompson (2000) and more recently by Liang (2004), among others, and I provide a brief overview here.

Solving the forward radiative transfer problem either requires empirical parameterisations or physically-based approximations of canopy properties including leaf size, leaf angle distribution and 1D or 3D arrangement. Some applications do not require a physically-meaningful interpretation of model parameters, only a reasonable prediction of $\rho_{\mathrm{c}}(\boldsymbol{\Omega}, \boldsymbol{\Omega}')$. For example, many remote sensing applications require comparing observations made over time (and/or using wide-angle sensors). These observations are typically acquired at different view and/or illumination angles, so variations in reflectance caused by these varying view and sun angles (i.e. BRDF effects) must be accounted for, otherwise they may be interpreted as surface changes. A widely-used approach is to fit a simple empirical (or semi-empirical) model of BRDF to observations, and use the resulting (inverted) model parameters to interpolate (or normalize) observations to some fixed view and illumination configuration Dickinson (1983). The simple nature of

semi-empirical BRDF models means they can be inverted rapidly, making them suitable for rapid, large-scale applications. Observations from the NASA MODIS and MISR sensors employ variants of this approach to account for sensor and sun angle variations (Pinty et al. 1989; Wanner et al. 1997).

Physically-based models of BRDF are required to represent three specific processes:

1. Coherent superposition of scattered incident radiation. This is dependent on the mean free path between scattering events within the canopy being of the order of the wavelength of the incident radiation. Coherence is generally ignored for vegetation, but is important for soils.
2. Scattering effects resulting from the arrangement of objects on the surface, i.e. specular reflectance, and reflectance variations caused by geometric-optic shadowing assuming parallel rays of incident radiation.
3. Volume (diffuse) scattering of aggregated canopy elements. This is particularly important for dense vegetation and is modelled using radiative transfer methods as outlined above. As higher orders of photon scattering are considered, the interactions become increasingly random in direction, and the volume scattering component tends to become isotropic.

To solve Eq. 11.2, approximations regarding the leaf scattering properties are often made (e.g. Myneni et al. 1989). Other approaches attempt to include modifications for observed features that occur due to the fact that real vegetation canopies are not turbid media and leaves, branches etc. have finite sizes. The most obvious of these features is the so-called 'hotspot', an increase in reflectance seen when $\mathbf{\Omega}$ and $\mathbf{\Omega}'$ are near-coincident, that arises due to shadowing in the scene being at a minimum (Nilson and Kuusk 1989). An example of this phenomenon is shown in Fig. 11.2 As an example of the importance of considering canopy structure on the EO signal, Morton et al. (2014) demonstrate that the apparent Amazon 'greenup' observed in 2005 can be explained almost entirely as a BRDF effect: most observations made in October in this location are in the hotspot i.e. the observed increase in reflectance is an angular effect.

Perhaps the most difficult problem in solving Eq. 11.2 is that of modelling the source term, $J_s(z, \mathbf{\Omega})$ as this requires keeping a 'scattering history' of each photon from one interaction to the next. This problem is essentially insoluble analytically (Knyazikhin et al. 1992), but numerical approximations can be made or computer simulation models can be used (see below). It is also necessary to define the boundary conditions in the case of a canopy illuminated from above. At the top of the canopy the incident irradiation can be considered as diffuse and direct components of solar irradiation. In addition, some radiation arriving at the base of the canopy re-radiates isotropically back up through the canopy effectively creating a source function at the lower canopy boundary. Modified forms of Eq. 11.2 have been widely used to model canopy reflectance for a range of applications. Further approximations and simplifications have been applied for specific types of canopy, such as row crops or particular tree crown shapes. In these cases, simplifying approximations can be made regarding canopy structure, in particular the vertical and horizontal arrangement of leaves and their angular orientations (distribution functions). Various approaches are summarised by Goel (1988), Strahler (1996), Liang (2004) and Lewis (2007, from http://www2.geog.ucl.ac.uk/~plewis/CEGEG065/rtTheoryPt1v1.pdf and http://www2.geog.ucl.ac.uk/~plewis/CEGEG065/rtTheoryPt2v7-1.pdf).

Separation of canopy fluxes into uncollided and collided intensities of various orders (Kubelka and Munk 1931; Suits 1972; Hapke 1981) has often been employed in order to simplify the radiative transfer approach (Norman et al. 1971; Myneni et al. 1990; Verstraete et al. 1990). The simplest two-stream approach decomposes multiple scattering into total upward and downward diffuse fluxes Meador and Weaver (1980). This can be elaborated in

Fig. 11.2. Illustration of the canopy hotspot effect. The image was captured with the sun directly behind the camera (see shadow of aircraft in the centre) and the scene is brightest at the centre, darkening radially outwards due to shadows becoming increasingly visible (author's own, taken over temperate rainforest canopy, Fraser Island, Queensland, Australia)

e.g. a four-stream approximation into fluxes resulting from reflectance and transmittance interactions respectively. The discrete properties of the canopy, those related to the size and distribution of scatterers, tend to impact only the first few orders of scattering and these features tend to become 'smeared out' by higher order multiple scattering interactions. Dividing the radiation field into collided and uncollided intensities as opposed to following a standard radiative transfer treatment may preserve these features.

As the canopy becomes denser, mutual shading of scattering elements cannot be ignored. It also becomes increasingly difficult to justify the use of convenient values for the scattering phase function i.e. the assumptions that leaf normals are randomly oriented and azimuthally invariant in defining leaf normal distribution and leaf projection function. This is clearly partially or wholly violated for a number of canopies, particularly for row-oriented agricultural crops. Various approaches have been proposed to overcome this. However, Knyazikhin et al. (1998) have shown that accounting for the discrete nature of vegetation within a (continuous) radiative transfer description leads to an apparent paradox: the more accurate the representation of canopy geometry, the less accurate the resulting description of radiative transfer and photosynthesis in the canopy is likely to be. This arises because of the discrepancy between the assumption of a continuous homogeneous scattering medium underpinning the radiative transfer approach, and the macroscopic effects of 3D leaf and branch size and distribution. Knyazikhin et al. (1998) point out that the radiative transfer approach assumes that the number of foliage elements in an elementary volume is proportional to this volume (encapsulated in the leaf area density), but the larger leaves become are in relation to the volume, the less this

assumption holds. The impact of this departure therefore decreases as we look at larger scales/volumes.

One of the most powerful approximations used in radiative transfer modelling is to concentrate on single scattering interactions only. These are in many cases the dominant component of canopy scattering (Myneni and Ross 1990), particularly at visible wavelengths. Considering single scattering interactions within a turbid medium, the radiation intensity in the incident direction $\mathbf{\Omega}'$, at a depth z within the canopy can be described using Beer's (Beer-Bouger-Lambert's) Law (Monsi and Saeki 1953) as follows

$$I\left(z,\mathbf{\Omega}'\right) = I\left(0,\mathbf{\Omega}'\right)e^{-\left(\frac{L(z)G\left(\mathbf{\Omega}'\right)}{\mu'}\right)} \tag{11.6}$$

where $I(0, \mathbf{\Omega}')$ is the incident irradiance at the top of the canopy; $L(z)$ is the cumulative leaf area index (LAI) in the canopy at depth z (m^2 m^{-2}); $G(\mathbf{\Omega}')$ is the leaf projection function i.e. the fraction of leaf area projected in the illumination direction $\mathbf{\Omega}'$; $\mu' = \cos(\theta_i)$.

The exponent in Eq. 11.6 is effectively the extinction coefficient κ_e i.e. a measure of the rate of attenuation of radiation in the canopy, and is a function of two things: (i) the amount of material along the path i.e. the domain-averaged optical thickness of the canopy layer LAI; and (ii) the volume absorption and scattering properties of the media i.e. loss due to absorption by the particles (leaves) and scattering by the particles away from the direction of propagation (Fung 1994). The term $L(z)$ is better defined as $u_l(z)$, the canopy leaf area density i.e. the vertical distribution of one-sided leaf area per unit canopy volume (m^2 of leaf area per m^3 of canopy volume). We will see later in Section III that this exponent implicitly encapsulates the fact that canopies are not homogeneous but are actually clumped at multiple scales from leaf to branch to crown. Assuming a constant leaf area of A_l, and given a leaf number density of $N_v(z)$ (number of leaves per unit volume, m^{-3}), then

$$u_l(z) = N_v(z)A_l \tag{11.7}$$

The integral of $u_l(z)$ over the canopy depth, H, gives the LAI i.e.

$$\mathrm{LAI} = \int_{z=0}^{z=H} u_l(z)dz \tag{11.8}$$

In practice, $u_l(z)$ may vary from top to bottom of a canopy, with more material perhaps in the upper parts than in the lower parts. As a result, $L(z)$ can be modelled in various ways in a radiative transfer scheme, but the simplest is to assume it is constant with canopy height H i.e. $u_l = LAI/H$.

The term $G(\mathbf{\Omega}')$ in Eq. 11.6 is the projection of a unit area of foliage on a plane perpendicular to the illumination direction $\mathbf{\Omega}'$. By extension, $G_i(\mathbf{\Omega})$ is the leaf projection function in the viewing direction $\mathbf{\Omega}$, averaged over elements of all orientations and is a (unitless) canopy-average representation of the effective leaf area encountered by a photon travelling in a direction $\mathbf{\Omega}$ within the canopy. $G_i(\mathbf{\Omega})$ is defined as

$$G_i(\mathbf{\Omega}) = \frac{1}{2\pi}\int_{2\pi+} g_i(\mathbf{\Omega}_i)|\mathbf{\Omega}\cdot\mathbf{\Omega}_i|d\mathbf{\Omega}_i \tag{11.9}$$

where $g_i(z, \mathbf{\Omega}_i)$ is the angular distribution of leaf normal vectors, known as the leaf angle distribution (LAD) and is defined so that its integral over the upper hemisphere is 1 i.e.

$$\int_{2\pi+} g(\mathbf{\Omega}_i)d\mathbf{\Omega}_i = 1 \tag{11.10}$$

A wide range of choices for models of $g_i(z, \mathbf{\Omega}_i)$ have been proposed (Ross 1981; Goel and Strebel 1984). A typical assumption is that leaf azimuth angles are independent of azimuth i.e. $g_i(\mathbf{\Omega}_i) = g_i(\theta_i)h_i(\phi_i)$ where $h_i(\phi_i)$ is the azimuthal dependence and can be specified separately as

$(1/2\pi)\int_{\phi_i=0}^{\phi_i=2\pi} h_i(\phi_i)d\phi_i = 1$. If the azimuthal distribution is assumed to be uniform (i.e. random) then $h_i(\phi_i) = 1$ and this allows for expression of $g_i(z, \mathbf{\Omega}_i)$ as a function of θ_l only and $\int_{\theta_i=0}^{\theta_i=\pi/2} g_i(\theta_i)sin\,\theta_i d\theta_i = 1$. While these assumptions make the formulation of $g_i(\theta_i)$ easier, it is known that many canopies depart from them particularly in the case of strongly-row oriented canopies (crops), or due to environmental factors such as wind and water stress (e.g. wilting) and heliotropism. Tree crowns may also have particular azimuthal arrangement due to branching structure, particularly in conifers. Jones and Vaughan (2010) discuss measured LADs and their departures from radiative transfer assumptions.

Caveats aside, a number of leaf angle archetypes (simple analytical expression representing particular LADs) have been used to model LAD, covering a wide range of observed canopy types (Wang et al. 2007). These include:

- planophile – favouring horizontal leaves
- erectophile – favouring vertical leaves
- spherical – distributed as if leaves were distributed parallel to the surface of a sphere and so favouring vertical over horizontal, but less than erectophile
- plagiophile – favouring leaves with angles mid-way between erect and flat
- extremophile – favouring leaves with angles at either end of the distribution

An alternative, more general approach has been to use ellipsoidal leaf angle distributions (Campbell 1986; Flerchinger and Yu 2007). These tend to give improved solutions for absorption, but at the cost of more complex models. Hence large-scale remote sensing and Earth system model applications strongly favour the simpler approaches due to the requirements for speed.

A more flexible alternative to specifying archetypes, is to use a parameterisation of $g_l(\theta_l)$ which covers the same variation as these archetypes. Bunnik (1978) proposed a simple four-parameter combination of geometric functions; Goel and Strebel (1984) used a two-parameter Gamma function. The Bunnik (1978) model is shown in Eq. 11.11 (assuming $g_l(\theta_l)$ is independent of azimuth)

$$g(\theta_l) = \frac{2}{\pi}[(a + bcos(2c\theta_l)) + dsin\theta_l] \quad (11.11)$$

Examples of the behaviour of the Bunnik model are shown Fig. 11.3. The fixed archetypes of Ross (1981) agree with these parameterisations very closely across all angles. The uniform distribution (not shown in Fig. 11.3) i.e. randomly-distributed leaf normals, is often assumed for simplicity but is rarely seen in practice.

The turbid medium approximation permits a description of canopy scattering as a function of a small number of structural parameters. Various models have been based on the approach outlined above originating from the work of Monsi and Saeki (1953). The major assumption underpinning Beer's Law is that the number of scattering objects in a volume of canopy (leaves, stems etc.) is proportional to its volume. However, Knyazikhin et al. (1998) show that the canopy structure may in some cases be fractal, resulting in non-linear relationships between canopy volume and the density of scattering elements, violating the assumptions of Beer's Law. However, the basic formulation of Beer's Law can be a useful tool in describing single scattering interactions within the canopy (Monsi and Saeki 1953). This issue of non-random spatial distribution of canopy material (clumping) is discussed further below.

A major drawback of the turbid medium approximation is that the size of the scattering objects within the canopy is not considered. By definition, the canopy is assumed to

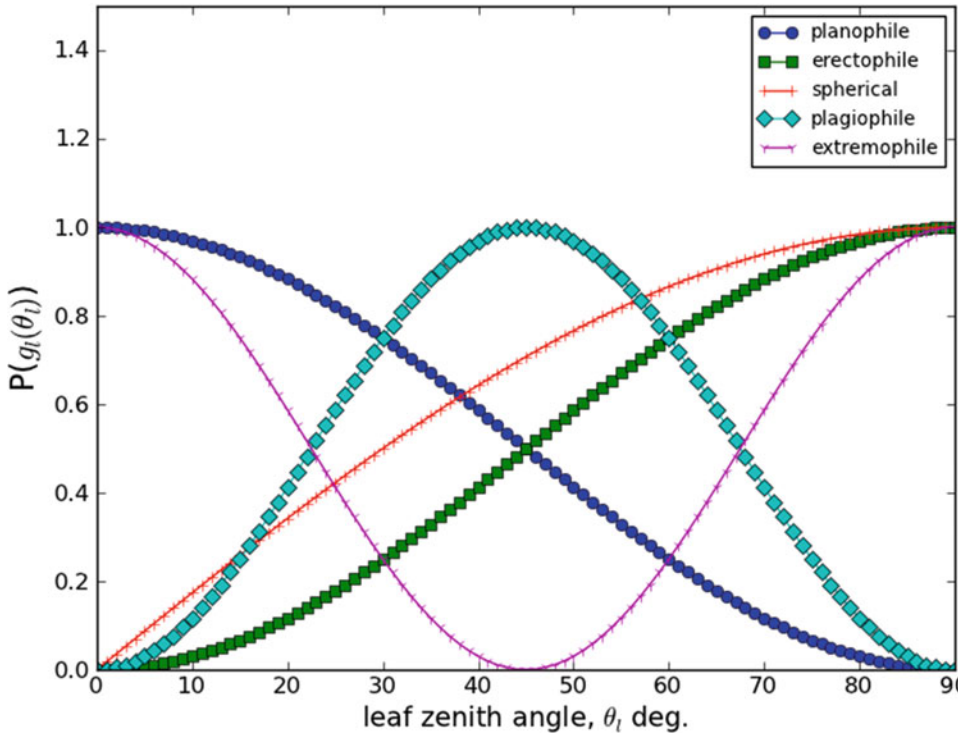

Fig. 11.3. Examples of (normalized) leaf angle distribution functions generated using the Bunnik (1978) four parameter model with parameter value sets: (1, 1, 1, 0), (1, −1, 1, 0), (0, 0, 0, 1), (1, −1, 2, 0) and (1, 1, 2, 0) in legend order

be a homogeneous medium of infinitesimal scatterers (to satisfy the far-field approximation) with mutual shading not permitted. Consequently, expressions describing the reflected radiation from such a canopy do not contain information regarding the size of scattering objects. However, certain properties of observed canopy scattering are directly controlled by the size and orientation of scattering objects (e.g. Pinty et al. 1989). A canopy-level example of this impact of finite leaf size is the hotspot effect. At the leaf level, the penumbra effect is of particular importance to photosynthesis, which depends very strongly on the leaf-level irradiance. The penumbra effect describes the fact that irradiance at the leaf is neither wholly direct nor diffuse, but somewhere in between, a consequence of the finite size of both the solar disk (light rays are never perfectly parallel) and the leaf (Cescatti and Niinemets 2004). Turbid medium approximations will not capture such features, and if the size of scattering objects is to be considered a different approach is needed to model the dimensions of scattering elements explicitly (Myneni et al. 1989).

As we can see, solving the radiative transfer equation in a vegetation canopy is a complex problem. Inverting the resulting models must generally be performed numerically, or using look-up-tables. Additionally, the approximations made in order to solve Eq. 11.2 result in the model driving parameters being relatively 'far-removed' from parameters directly representative of physical canopy properties. This issue of so-called 'effective parameters' is critical to applications of remote sensing and is discussed further below. First, I look at how radiative transfer is considered at the leaf level. Following this, a relatively new approach to radiative transfer modelling is outlined,

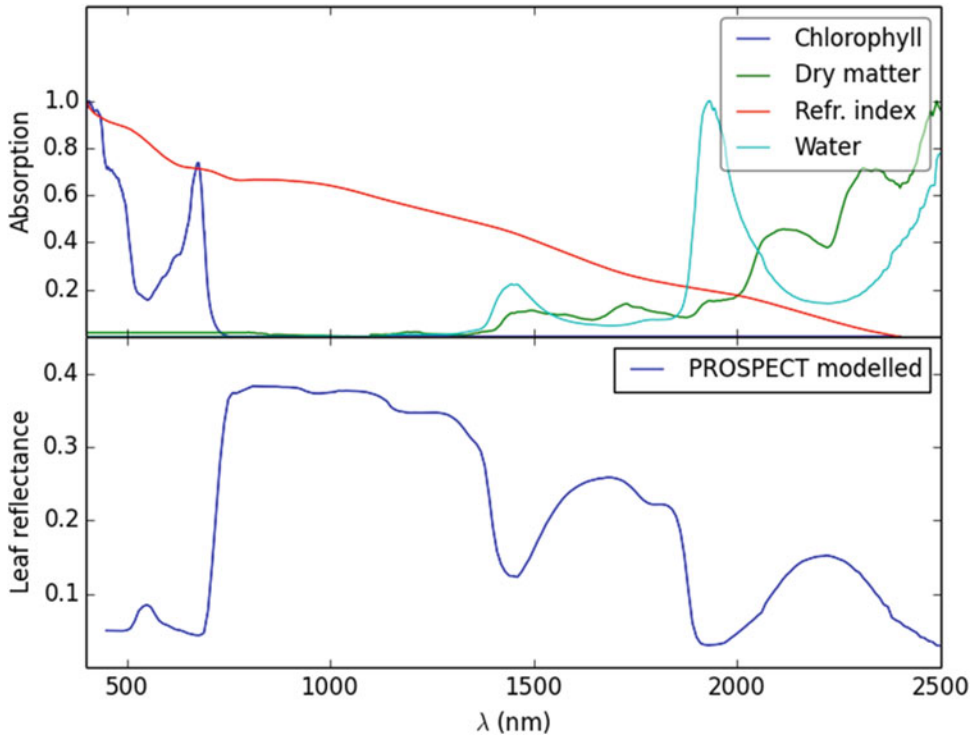

Fig. 11.4. Normalized absorption coefficients used within the PROSPECT model (*upper panel*) and leaf spectral reflectance modelled by PROSPECT from these absorbing constituents (*lower panel*)

which scales from leaf to canopy, and has significant consequences for understanding the links between canopy structure and biochemistry.

C. Radiation Transfer Within the Leaf

Now we have a description of radiation transfer in a canopy, the issue arises of radiation interactions at the scale of leaves. This problem is analogous to the canopy case: radiation can penetrate the air/surface interface depending on the surface properties Ross and Marshak (1989) (waxy, smooth etc.) and can either pass through air gaps within the leaf unimpeded or be scattered, across cell walls into and through cells, as well as at the boundaries between cells and cell/air. Scattering within the leaf will depend on the amount of material encountered by a photon (function of leaf thickness, analogous to leaf area density at the canopy level) and the absorption properties of the materials(s), typically the concentrations of absorbing pigments (chlorophyll, carotenoids, flavonoids), water and other absorbents such as lignin and cellulose. It is the pigments, and their relationships to leaf/canopy state and nutrient concentrations (particularly leaf N), that are often of interest via remote sensing (Ollinger 2011).

Various approaches to modelling radiative transfer within the leaf have been proposed and Jacquemoud and Ustin (2008) provide an excellent overview. Leaf models require at the very least some description of the refractive index (essentially a structural effect, modifying behaviour at boundaries of scattering materials within the leaf such as cell walls, air and water etc.), and the specific absorption coefficients of absorbing constituents within the leaf. Examples of these properties taken from the widely-used PROSPECT model of Jacquemoud et al. (1996) are given in Fig. 11.4 along with a modelled leaf spectrum for comparison.

This illustrates the very specific wavelength ranges over which the absorption properties act: chlorophyll pigment dominates the visible; refractive index (leaf structure) dominates beyond this into the NIR; water and to a lesser extent dry matter (such as cellulose and lignin) dominate beyond 1300 nm. In the UV region, proteins, tannins and lignin are important, but these regions are rarely used in large-scale remote sensing due to the absorption of the solar signal by the atmosphere.

Leaf radiative transfer models essentially follow one of four broad schemes. The first and perhaps simplest approach considers a leaf as a semi-transparent plate with plane parallel surface, and some surface roughness (Allen et al. 1969). Scattering from the leaf is calculated as the total sum of successive orders of scattering from reflections and refractions at the plate boundaries with the air. This approach has been generalised to consider multiple plane parallel plates by decomposing the total upward and downward fluxes (a two-stream approach) into the separate fluxes from each plate (Allen et al. 1970). This latter approach is used in PROSPECT, perhaps the most widely-used leaf radiative transfer model for remote sensing applications. The model has developed over a number of iterations through inclusion of more detailed treatment of absorption coefficients in particular (Feret et al. 2008). PROSPECT has been used to explore the impact of biochemistry on leaf reflectance, to infer optical properties from remote sensing measurements, and been coupled to canopy radiative transfer schemes (Jacquemoud et al. 2009).

An alternative approach for modelling radiative transfer properties of leaves that do not conform to the plane parallel approximation, such as needles, has been to consider scattering from discrete particles such as spheres. The LIBERTY model of Dawson et al. (1998) follows this approach, using the formulation of Melamed (1963) for scattering from suspended powders. Particle size is assumed $\gg\lambda$, and scattering is again a function of successive internal reflections and refractions, but from within spheres in this case, rather than plates.

One of the difficulties in developing and testing leaf models has been the concomitant difficulty of measuring leaf optical properties, either in the lab or the field. Measurement equipment has certainly improved in recent years, with the development of portable field spectrometers and integrating spheres. However, leaf measurements are still challenging as they involve handling and mounting leaf material without damaging it, controlling environmental lighting conditions, making reference measurements etc. Thus the number of high quality leaf measurements that can be used for testing models, particularly for needles, or non-flat leaves is rather small (see for example Hosgood et al. 1995).

A range of more general radiative transfer modelling approaches have been proposed for the particular size problem of leaves. One solution of this class is the development of Kubelka-Munk theory to provide a 2- or 4-stream approximation to represent the upward and downward fluxes (separated into diffuse and direct in the 4-stream case) within a single leaf layer, or multiple layers (Vargas and Niklasson 1997). This type of model has the advantage of allowing analytical solutions in certain specific cases. An alternative is to solve the radiative transfer problem numerically, via Monte Carlo methods (described in Sect. E in more detail). Govaerts and Verstraete (1998) demonstrated the use of a Monte Carlo ray tracing (MCRT) model which considered the internal structure of the leaf explicitly in 3D. Baranoski (2006) developed a variant of MCRT for bifacial leaves that calculates Fresnel coefficients for all interfaces in the leaf (air, adaxial and abaxial epidermis, mesophyll cell walls and cytosol), and uses these coefficients to weight Monte Carlo samples of reflectance and transmittance; scattering within a cell is approximated by Beer's Law. The main advantage of these more structurally detailed approaches is

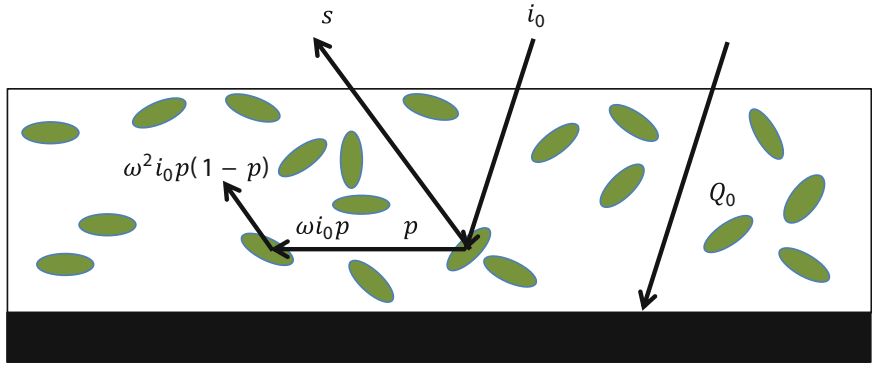

Fig. 11.5. Schematic representation of radiation that passes through the canopy uncollided ($\boldsymbol{Q_0}$), or is first intercepted by the canopy ($\boldsymbol{i_0}$) or escapes in the upward direction ($\boldsymbol{s}$) to be measured. $\boldsymbol{p}$ is the probability of a scattered photon being re-intercepted and $\boldsymbol{\omega}$ is the leaf single scattering albedo (After Lewis, P. http://www2.geog.ucl.ac.uk/~plewis/CEGEG065/rtTheoryPt1v1.pdf)

flexibility. The main limitation is the requirement for information to parameterize the model, such as cell dimensions, air volumes etc. Such models can be used to explore the impact of structure at the canopy level on issues such as the relative absorption of diffuse to direct light (Alton et al. 2007; Brodersen et al. 2008), as well as at the leaf level, where surface and internal properties, such as polarization and focusing may be important (Martin et al. 1989; Combes et al. 2007).

The following section describes relatively new developments in solving the canopy radiative transfer problem that have provided new parameterisations of multiple scattering that apply across scales from within-leaf to canopy. These methods have already been applied successfully to the problem of modelling leaf reflectance (Lewis and Disney 2007) and are providing new insight into the nature of radiative transfer in vegetation more generally.

D. Recollision Probability and Spectral Invariance

As seen above, the key to providing an accurate description of canopy radiative transfer is the multiple scattering component, particularly at NIR wavelengths. Development of the concept of the so-called 'recollision probability' p has seen significant advancement in this area. The approach is summarised in Huang et al. (2007), but is based on the observation that the decrease in scattered energy with increasing scattering interactions is well-behaved and close to linear in log space, at least in canopies with low to moderate LAI (Lewis and Disney 1998). Scattered energy typically decreases dramatically after 1 or 2 interactions, and then proceeds to decrease more slowly with increasing scattering order. This implies that, once the scattering reaches the linearly decreasing portion, the scattering at interaction order $i+1$ is simply p times the scattering at interaction order i. Figure 11.5 illustrates this situation schematically.

From Fig. 11.5 we can see that some proportion of the incoming radiation Q_0 may pass through uncollided to the lower boundary layer. If this layer is assumed completely absorbing (black soil, a reasonable approximation for dense understory and/or dark soil), then multiple scattered radiation can only originate from vegetation. The first interaction with leaves is then $i_0 = 1 - Q_0$. A fraction s of this scattered radiation exits the canopy in the upward direction, and the remaining proportion p interacts further with leaves in the canopy. Therefore the first order scattered radiation is $s_1 = i_0\omega(1\text{-}p)$ where ω is the leaf single scattering albedo. Rearranging, we obtain $s_1/i_0 = \omega(1\text{-}p)$. The probability of being further intercepted is also p, so the second order scattering

$s_2 = \omega p s_1 = i_0 \omega^2 p(1\text{-}p)$. Following the same logic for higher orders we see that

$$\frac{s}{i_0} = \omega(1-p) + \omega^2(1-p)p + \omega^3(1-p)p^2 + \cdots = \omega(1-p)[1 + \omega p + \omega^2 p^2 + \cdots] \tag{11.12}$$

The series in p and ω can be summed as

$$\frac{s}{i_0} = \frac{\omega(1-p)}{1-p\omega} \tag{11.13}$$

This provides for a very compact description of multiple scattering, albeit under the assumptions of total scattering and black soil. Crucially, the resulting scattering is *independent of wavelength* i.e. is spectrally invariant, and is a function of p only, where p is a purely structural term, encapsulating the size and arrangement of scattering elements within the canopy. Recollision theory has been developed over the last decade (Knyazikhin et al. 1998, 2011; Disney et al. 2005; Huang et al. 2007). It has been shown to work well for higher values of LAI when the understory becomes less important (Huang et al. 2007). This is also where optical EO tends to be less sensitive to variations in LAI. The recollision probability approach has now been used for a range of remote sensing applications including in a parameterised canopy model (Rautiainen and Stenberg 2005), to classify forest structural types (Schull et al. 2011), and for providing a structural framework for merging data from various sensors with different spatial and spectral resolutions (Ganguly et al. 2008, 2012). Further, the same behaviour has been observed in atmospheric radiative transfer (Marshak et al. 2011).

Specific insights provided from the spectral invariant approach include that of Smolander and Stenberg (2005) who showed that if the fundamental scattering element within a canopy is considered to be a shoot (a good approximations in conifers for example), then a shoot-level recollision probability p_{shoot}, can be defined. In this case total scattering can be expressed as a nested combination of the within-shoot needle-level recollision probability, p_{needle} and p_{shoot}. This is a key insight into how different scales of clumping interact. Following this, Lewis and Disney (2007) used recollision probability to parameterise the PROSPECT leaf-level radiative transfer model. Their rephrasing in terms of p_{leaf} was able to reproduce the behaviour of PROSPECT with very high accuracy (root mean square error $<$0.4 % across all tested conditions). Lewis and Disney (2007) also showed that the same form of scattering will be nested across multiple scales from within-leaf to shoot to canopy. A key implication of this work was the observation that the structural and radiometric components of the canopy (represented by p and the leaf absorbing constituents such as pigments, cellulose, lignin, and water) are fundamentally coupled. As a result Lewis and Disney (2007) conclude "...it is simply not possible to derive robust estimates of both leaf biochemical concentration and structural parameters such as LAI from (hyperspectral) data ... no matter how narrow the wavebands or how many wavebands there are". Increasing LAI by some factor k and simultaneously decreasing the biochemical concentration per unit leaf area by the same factor (i.e. keeping the total canopy concentration the same) can result in the same total scattering, but for very different values of p, corresponding to very different canopy structures. This implies that without knowledge of either p or the leaf biochemical constituents, independent retrieval of either from total scattering measurements is not possible. An additional implication is that attempts to estimate 'total' canopy biochemical concentration as a coupled measure may contain large errors.

The various developments of recollision probability have important implications for the use of Earth observation data to infer canopy biochemical properties, particularly pigment concentrations. Many studies have observed empirical correlations between canopy biochemical concentrations and observed spectral properties (reviewed by

Ollinger 2011), including observed positive correlations between leaf nitrogen content per area (canopy N) and albedo. Such work suggests a potentially important route for monitoring canopy biochemistry (and hence state) from EO. However, recent work by Knyazikhin et al. (2013) building on recollision probability theory and the observation that p encapsulates scattering across scales, shows quite clearly that some of these correlations e.g. between canopy N and albedo, are in fact entirely explained by canopy structure. As an example, Knyazikhin et al. (2013) show that observed correlations between canopy N and reflectance (e.g. Ollinger et al. 2008) can be almost completely explained by canopy structure. Knyazikhin et al. (2013) also suggest that canopy scattering can be reformulated using recollision probability, as a combination of separate structural and spectral terms as follows:

$$BRF_\lambda(\mathbf{\Omega}) = DASF \cdot W_\lambda \tag{11.14}$$

where $DASF$ is the (structural) Directional Area Scattering Factor and W_λ is the (spectral) canopy scattering coefficient. DASF is defined as:

$$DASF = \rho(\mathbf{\Omega})\frac{i_0}{1-p} \tag{11.15}$$

where $\rho(\mathbf{\Omega})$ is the directional gap density of the canopy, along a given viewing direction $\mathbf{\Omega}$; i_0 is the first interception by the canopy from Eq. 11.14. W_λ is defined as:

$$W_\lambda = \hat{\omega}_\lambda \frac{1-pi_\mathrm{L}}{1-\hat{\omega}_\lambda pi_\mathrm{L}} \tag{11.16}$$

where i_L is the leaf interceptance defined as the fraction of radiation incident on the leaf that enters the leaf interior; and $\hat{\omega}_\lambda = \omega_\lambda / i_\mathrm{L}$. The quantity $\rho(\mathbf{\Omega})LAI$ is the fraction of leaf area inside the canopy visible from outside the canopy along $\mathbf{\Omega}$. For dense canopies in the NIR, $DASF \sim \rho(\mathbf{\Omega})LAI$ and is an estimate of the ratio between the leaf area that forms the canopy boundary as seen along $\mathbf{\Omega}$ and the total (one-sided) leaf area, effectively the 'texture' of the canopy upper boundary. Importantly, calculating $DASF$ allows the impact of structure to be removed from observed hyperspectral reflectance, providing a potential route for re-analysis of empirical relationships between biochemistry and reflectance.

The recollision probability theory has provided new ways to express scattering across scales, and has found a range of potential applications in accounting for structural effects in EO measurements. Ustin (2013) highlights the importance of using a first principles radiative transfer approach to accounting for the impact of structure on EO estimates of biochemistry.

E. 3D Monte Carlo Approaches

The methods outlined above to solve the radiative transfer problem in vegetation involve a range of approximations regarding structural and radiometric properties in order to make the problem tractable. A sub-class of methods exist which solve the radiative transfer problem based on 'brute force' Monte Carlo sampling of the radiation field in a 3D canopy. These methods derive from developments in computer graphics, where they form the basis of modern movie animation and special effects. The aim in these applications is to simulate 'realistic' light environments i.e. scenes that are either convincing and/or aesthetically pleasing to the human eye. For EO applications, the requirement is somewhat different i.e. physical accuracy (including constraints such as energy conservation for example). Monte Carlo methods are computationally intensive, which has tended to limit their application. However, computing power has reached a level where such limitations are no longer so relevant, and these methods have some key advantages for quantitative applications. Niinemets and Anten (2009) discuss the issues of the trade-off between accuracy

and efficiency in radiative transfer modelling approaches.

Monte Carlo methods in remote sensing are reviewed in detail by Disney et al. (2000) and Liang (2004). These methods fall into two broad classes: radiosity (originating from thermal engineering), which requires calculating the viewed areas of each object in a scene in relation to the other objects in the scene (so-called 'view factors'); and ray tracing (MCRT). I will briefly discuss the latter method here, as it is more practical for EO applications where view and illumination configurations change arbitrarily (making radiosity less feasible). MCRT essentially involves calculating the intersections of photons (rays) projected into a 3D scene with the objects in the scene, and determining the behaviour of these photons at each intersection. The subsequent direction and energy of a scattered photon following an intersection is governed by the radiometric properties of absorption, transmission and reflection of the surface at the point of intersection, in addition to the geometric scattering properties (phase function) of the object. Objects are not limited to representation by simple polygons (facets). Volumetric objects can be used, in conjunction with a description of the (volumetric) scattering properties of the materials contained within (North 1996). Diffuse sampling can be used to simulate diffuse light sources (Govaerts 1996; Lewis 1999). The bidirectional reflectance of a given scene (represented as a collection of 3D objects) is simulated by simply repeating the sampling process for every sample (pixel) in the viewing plane (Disney et al. 2000), possibly multiple times.

A key advantage of MCRT models is that they can operate on structurally explicit 3D scenes, often of arbitrary complexity, allowing them to simulate EO signals with the least possible number of assumptions about structure. Some models represent 3D detail in a given scene down to the level of individual needles and leaves (España et al. 1999; Lewis 1999; Govaerts and Verstraete 1998; Widlowski et al. 2006). Other approaches represent larger structural units explicitly such as tree crowns, but then make assumptions regarding the scattering and extinction properties within individual crowns (North 1996). The issue with this latter approach is determining what these within-crown bulk scattering properties ought to be. Other models divide 3D space into voxels, and assign voxel-average scattering properties, such as the Discrete Anisotropic radiative transfer (DART) model of Gastellu-Etchegorry et al. (2004). This has benefits in terms of speed and simplicity, but again at the expense of requiring definitions of bulk (volume) scattering properties. Fully explicit 3D MCRT models avoid these volume scattering approximations, but at the expense of requiring 3D input on all canopy elements, as well as potentially much greater computational demands (Disney et al. 2006; Widlowski et al. 2013).

The ability to deal with 3D canopy structure explicitly means MCRT models are ideally-suited to applications where we wish to know, and have control over, 3D scene properties in order to generate a modelled EO signal e.g. for generating synthetic data sets to test retrieval algorithms based on simpler model approximations or when EO data are not readily available. Disney et al. (2011) show how 3D MCRT model simulations can be used as a surrogate for observations of fire impact. Other applications include simulating the properties of new sensor characteristics (Disney et al. 2009); understanding the impact of structure on observations (España et al. 1999); providing a common structural framework for combining optical and microwave scattering models (Disney et al. 2006); and providing benchmark information for testing simpler radiative transfer models (Widlowski et al. 2007). This latter example is an important one; a question that arises for anyone using any radiative transfer approach to an EO application is: which model is best for my application, and why? The Radiation Transfer Model Intercomparison exercise (RAMI, http://rami-benchmark.jrc.ec.europa.eu/HTML/) has sought to answer this question via intercomparison of radiative transfer models. Over various phases RAMI has shown that detailed 3D MCRT models can

provide the most credible solution to the radiative transfer problem in well-defined, simplified cases (Widlowski et al. 2007). Scenes can be defined for which MCRT models provide exact solutions (within limitations of numerical sampling), and this allows for testing of more approximate radiative transfer models, in particular quantifying the impact of model assumptions on resulting model accuracy. The RAMI work has led to an online benchmarking tool, allowing radiative transfer model developers to test and benchmark their models (Widlowski et al. 2008). The most recent RAMI exercise has shown how detailed 3D MCRT models can represent the effects of structure on the EO signal for very complex (realistic) 3D scenes in ways that simpler models cannot (Widlowski et al. 2013).

There are three main limitations of the MCRT approach. First, they are very slow compared to the more approximate models. This is certainly a problem if speed is absolutely essential, e.g. for large-scale or near real-time applications. MCRT models can of course still be used to quantify the impact of assumptions made in simpler models. Secondly, they cannot be inverted either directly or using standard optimisation routines, given their requirement for explicit location and properties of a (potentially) very large number of 3D objects. However, computation speeds have increased to an extent where it is now feasible to consider using a MCRT model for look-up table-based model inversion. It may take thousands of hours of CPU time to run forward MCRT model simulations over a large range of canopy, view and illumination configurations to populate the pertinent look-up tables, but these need only be run once. The third and perhaps most serious limitation of 3D MCRT models is that they are only as good as the underlying 3D scene descriptions on which they are based; the models require highly-detailed, accurate 3D structural information to generate 3D model scenes. This 3D information can come from various sources, including empirical growth models (e.g. España et al. 1999; Disney et al. 2006), purely parametric models (Widlowski et al. 2006; Disney et al. 2009), and parametric models modified using field measurements (Disney et al. 2011).

A range of models can provide 3D scene information. Growth models provide an accurate description of a 'domain-average' tree structure, but not a specific tree at a particular time (Leersnijder 1992; Perttunen et al. 1998). Parametric models allow a great degree of flexibility over manipulation of tree structure. Various models of this sort exist, e.g. xfrog (Xfrog Inc. xfrog.com) and OnyxTREE (Onyx Computing, onyxtree.com) and they have been used in EO applications (Disney et al. 2010, 2011). However, it can be both time-consuming and difficult to parameterise a model that is designed to 'look right' for computer graphic visualisation (Mêch and Prusinkiewicz 1996), in such a way that it is a structurally accurate representation of a tree for radiative transfer applications (leaf and branch shape and size distributions, leaf angular distributions etc). An alternative approach is the use of growth grammars based on L-systems (Prusinkiewicz and Lindenmayer 1990). These use simple growth rules to produce 'realistic' canopy structure and have been used to drive 3D simulations, particularly of relatively simple crop canopies (Lewis 1999), but may bear little resemblance to real canopies of greater complexity. Functional structural plant modelling (FSPM) overcomes this limitation to a certain extent by considering fundamental rules of plant function due to the genetic and organ level constraints to drive structural development (Godin and Sinoquet 2005). The resulting 3D structure can in turn be expressed via L-systems. FSPM and L-systems approaches suffer from the same problem that the resulting models are accurate instances of a particular species or plant type, rather than specific (observed) plants. Furthermore, additional rules are needed to create a general, 3D scene.

These limitations on 3D structure have led to searches for new ways to derive detailed,

accurate 3D information that can be used to drive 3D simulation models. Some of these methods are outlined below in Sect. IV.

III. Effective Parameters

A. Basics: Definition of Effective Characteristics

Having discussed the various approximations that can be employed to help solve radiative transfer equations in leaves and canopies, a note of caution is required in regard to any biophysical parameters we derive from EO data via such methods.

For real canopies the exponent in Eq. 11.6 implicitly includes a structural term $\zeta(\mu')$ encapsulating the fact that real canopies are not turbid media but are clumped at multiple scales from cm to tens of m. Leaves or needles are arranged around twigs, along branches, within crowns and within stands. Pinty et al. (2004, 2006) suggest adopting an effective LAI value $\widetilde{LAI}\,(\mu')$ i.e.

$$\widetilde{LAI}\,(\mu') = LAI\zeta(\mu') \tag{11.17}$$

This permits a solution to the 1D limiting case of radiative transfer in a 3D canopy that is consistent with the assumptions made in Eq. 11.2. Crucially however, the values of $\tilde{LAI}\,(\mu')$ are not the same as LAI which are in turn, not the same as the actual LAI that would be measured on the ground (unless measured over some large, discrete canopy volume). That is, the resulting radiative transfer model parameters will be 'effective' parameters and will not have a direct physically measurable meaning. These effective parameters allow solution of the 1D radiative transfer problem by representing domain-averaged quantities that are forced to satisfy the constraints associated with a 1D representation of what is an inherently 3D system (Pinty et al. 2006).

The issue of effective parameters is important because it encapsulates the problem of interpreting EO measurements more generally. As an example, a typical use of a 1D radiative transfer scheme is to describe the surface radiation budget in a large-scale Earth System Model (ESM) (Sitch et al. 2003; Best et al. 2011). Developing such a model is inevitably a trade-off between multiple and often competing constraints including computational speed and model robustness vs. providing 'sufficiently accurate' radiant flux values (Pinty et al. 2004). Moreover, introducing a physically-realistic estimate of LAI (for example) may only make things worse, as it will not be consistent with the simplified radiative transfer schemes and will thus introduce errors. If radiative consistency is the key requirement (getting the fluxes right) rather than interpreting the LAI values, then the effective parameters should be used (Pinty et al. 2006, 2011a, b). What is true of LAI is potentially true of other structural and biochemical parameters in radiative transfer schemes.

The issue of consistency between EO-derived biophysical parameters, and their representation in models of vegetation function, biogeochemical cycling and climate is key to making best use of both observations and models. The fusion of EO data with models, particularly via data assimilation (DA), is a rapidly-growing field because EO data can potentially provide information on land cover, plant functional types (PFTs), vegetation state and dynamics, land surface temperature (LST), soil moisture etc. at the scales and frequencies required by the large-scale models (Pfeifer et al. 2012). However, the further an EO-derived parameter is away from a fundamental EO measurement, the more likely it is to be 'effective' rather than directly measurable. This in turn increases the likelihood of inconsistency between EO data and large-scale models that use these parameters (Carrer et al. 2012a; Pfeifer et al. 2012).

B. Data Assimilation

As the spatial detail of the land surface representation within ESMs increases (from ~10^3 to ~10^1 km and finer), the assumption

of canopy homogeneity typically assumed in a simplified radiative transfer approach is violated and potentially becomes an increasing source of error (Knorr and Heimann 2001; Pinty et al. 2006; Brut et al. 2009; Widlowski et al. 2011). Various solutions have been proposed, essentially approaching the problem from opposite directions. From the EO perspective, one approach is to ensure consistency between EO parameters and ESMs as far as possible by coupling a physically-realistic radiative transfer scheme directly to the ESM that will use it. The ESM can then actually predict an EO measurement, which in turn allows direct comparison with EO data. Perhaps more importantly, the model can also be used to assimilate EO data to estimate ESM model state properties (in an inverse scheme). This approach lies at the heart of data assimilation schemes with land surface models (Quaife et al. 2008; Lewis et al. 2012). For a DA scheme, the RT models are referred to as 'observation operators' (denoted $H(\boldsymbol{x})$) which map the model state variable vector $\boldsymbol{x}$ to the EO signal (as a vector) $\boldsymbol{R}$ for a given set of control variables i.e. $\boldsymbol{R} = H(\boldsymbol{x})$. The inverse problem is then to obtain an estimate of some function of $\boldsymbol{x}$, $F(\boldsymbol{x})$ from measurements $\boldsymbol{R}$ (Lewis et al. 2012). An advantage of this approach is that it can utilise much more direct EO measurements (reflectance or even radiance) where the uncertainties in the measurements can be better-characterised. This characterisation of uncertainty (in observation *and* radiative transfer model schemes) is critical for data assimilation. A drawback is that more complex radiative transfer schemes tend to slow the assimilation process, potentially limiting them for large-scale inverse problems (at least currently). However, data assimilation approaches of this sort are being used to assimilate EO data from a range of sources, and have shown great promise in improving and constraining model estimates of C fluxes and photosynthesis (Quaife et al. 2008; Knorr et al. 2010), evapotranspiration (Olioso et al. 2005), surface energy balance (Qin et al. 2007; Pinty et al. 2011a, b) and hydrology (Rodell et al. 2004; Houser et al. 2012).

C. Scale Differences and Model Intercomparisons

From the other direction, we can modify the ESM internal radiative transfer scheme to account for inconsistency with EO measurements and ensure the resulting ESM outputs are consistent at some broader, integrated level e.g. such as total productivity (Brut et al. 2009; Carrer et al. 2012). An example of this is improved representation of canopy diffuse fluxes, which tend to increase C uptake (via increased photosynthesis) with increasing diffuse radiation fraction (Mercado et al. 2009). Carrer et al. (2012) show that introducing clumping to an ESM representation of vegetation (resulting in an effective LAI), even at coarse scale, can improve modelled annual GPP fluxes of various deciduous and conifer forests by up to 15 %. This approach accepts that the resulting internal model parameters are effective and not measurable in practice. Lafont et al. (2012) show that this modification of LAI can have a significant impact on the way fluxes are apportioned within different ESMs.

An additional complication can arise that different internal LAI representations can cause processes such as photosynthesis and transpiration to reach different equilibria (different spatial and temporal distribution of fluxes) in different ESMs while still producing similar net C fluxes i.e. the models can arrive at the same answers for different reasons. This in turn can result in differences in seasonal variations (e.g. timing of peak fluxes) and/or longer-term model divergence that may be hard to identify (Richardson et al. 2012). The effective nature of the model parameters also makes model intercomparison difficult. Clearly, the consideration of scale is not consistent between models.

Recent work by Widlowski et al. (2011) has attempted to address the issue of consistency of radiative transfer schemes in ESMs systematically, by instigating a

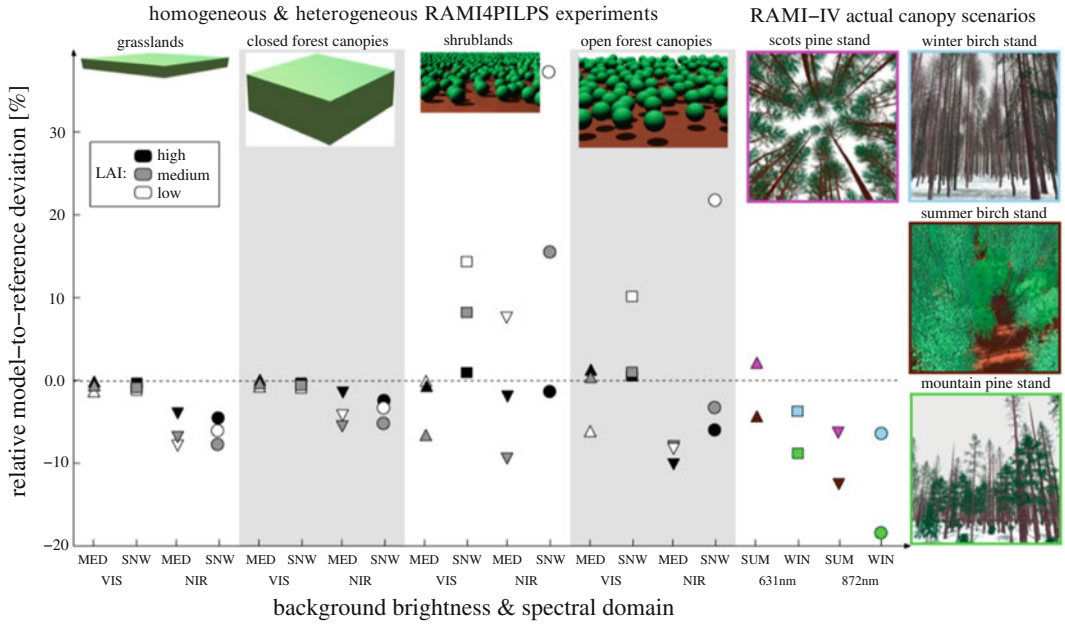

Fig. 11.6. An illustration of differences in canopy absorption as a function of increasing structural complexity (from left to right) for visible and NIR spectral domains. Different grey levels show varying LAI (low = 0.5, medium = 1.5, high = 2.5), over snow-covered (SNW) and medium-bright (MED) backgrounds, with $\theta_i = 60°$ or 27° respectively. The first two panels represent simple 1D radiative transfer models; the second two panels represent the most basic level of 3D heterogeneity; the right-most column includes four reference cases derived via a full 3D Monte Carlo Ray Tracing (MCRT) model description (Modified from Widlowski et al. 2011 © Wiley)

radiative transfer model intercomparison exercise, RAMI4PILPS (http://rami-benchmark.jrc.ec.europa.eu/HTML/RAMI4PILPS/RAMI4PILPS.php). RAMI4PILPS builds on both the RAMI exercise and the Project for Intercomparison of Land Surface Parameterization Schemes (PILPS). PILPS was set up to improve understanding of model processes in coupled climate, atmospheric and ESMs mainly through intercomparison of the various model parameterisation schemes (http://www.pilps.mq.edu.au/). PILPS recognises that for large, complex models, the wide range of approximations and possible parameterisations required makes direct model-to-model comparisons very difficult and instead compares the abilities of the models to reproduce various observed climate and land-surface trends (Henderson-Sellers et al. 2003). RAMI4PILPS is perhaps much closer to RAMI than PILPS in terms of the intercomparison approach. It attempts to isolate the radiative transfer schemes in participating models in such a way as to examine only that part, making like-for-like comparisons much more feasible over specific scenarios. In this case the RAMI results are used to provide a 'known' reference solution. RAMI4PILPS covers quite a large range of model types, from simple land surface model schemes, to very complex models that describe the full range of surface energy, water and C fluxes between the surface and atmosphere. Figure 11.6 shows a comparison of the RAMI4PILPS models against the reference solution for a range of canopy complexities. This comparison demonstrates that the relatively simplistic concept of canopy 'structure' (from varying 1D homogeneous, to a simplified consideration of clumping) can still introduce a large degree of scatter between the models, as well as between the models and the reference solution under different environmental conditions and for different spectral regions.

IV. New Observations of Structure and Function

Lastly, I discuss newer Earth observation techniques that provide rapid and detailed information on canopy structure and function. These new technologies based on lidar (light detection and ranging) and microwave RADAR (radio detection and ranging) are becoming increasingly widely available. I show that lidar is a near-direct remote sensing measurement of canopy height and structure. There is significant promise in merging airborne lidar scanning (ALS) instruments, and terrestrial laser scanning (TLS) instruments, as well as optical and RADAR data in order to maximise structural information. The 3D nature of the lidar signal also raises the possibility of using these data to further extend and exploit the recollision probability approach to the canopy radiative transfer problem.

I also briefly consider the prospects for EO data of this sort over the next decade, and how such observations might be used. Having discussed new structural measurements, I turn lastly to a new measurement related to canopy function based on chlorophyll fluorescence.

A. Structural Information from Lidar and RADAR

Lidar systems have become increasingly common over the last decade. Figure 11.7 illustrates this by highlighting the increase in published papers with the words "lidar" and "vegetation" in the title or abstract, from 1990–2012. The advent of airborne lidar scanning (ALS) instruments, terrestrial laser scanning (TLS) instruments, and the lifespan of the only spaceborne lidar mission to date used for terrestrial applications (NASA ICESAT/Glas) are marked on the figure (Fig. 11.7).

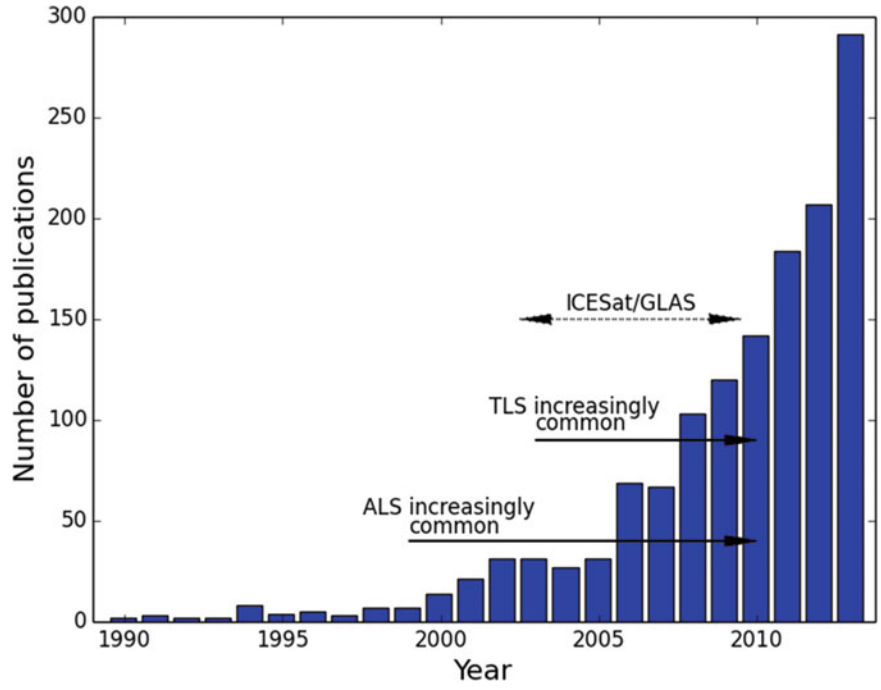

Fig. 11.7. Number of publications containing the words 'lidar' and 'vegetation' in the title or abstract from 1990 to 2013 (Citation information from Thomson Reuters Web of Knowledge ©). ALS and TLS are airborne and terrestrial lidar scanning respectively

Lidar is an active remote sensing method, recording return time-of-flight of a laser pulse between instrument and target. Lidar provides a (near) direct estimate of surface (canopy) height and is in this sense a much more direct measurement than those relying on passive reflected or emitted radiation. Lidar instruments also record returned signal intensity and, in combination with height, this signal can provide unique information on the vertical distribution of canopy structure when operated from above the canopy (e.g. Dubayah and Drake 2000). As discussed above, structure plays a critical role in radiative transfer in vegetation. Thus, structure must be accounted for to allow retrieval of canopy state and function from remote sensing. Lidar has proven extremely useful in addressing this issue (Lefsky et al. 2002; Armston et al. 2013a).

1. Discrete-Return Lidar Systems

Lidar systems broadly fall into one of two categories – discrete-return, or full-waveform (the less widely-used phase-based systems are not discussed here). Discrete return lidar essentially records the distance to the first object from which a return is recorded at the sensor, over some signal threshold, or multiple thresholds. Assuming that emitter and detector are co-located, the time-of-flight to the target is $t = 2d/c$ where d is the distance to the target, and c is the speed of light (and assuming that emitter and detector are co-located). For a sensor above a vegetation canopy returns may come from both the canopy and the ground, depending on canopy cover. It is then possible to determine the height of the vegetation canopy, h, through the difference in travel time between the two returns i.e. $h = (t_1\text{-}t_2)c/2$. Discrete return lidar datasets therefore comprise 'point clouds', each of which has a 3D co-ordinate relating its location to the sensor. Lidar has been widely used in this way to estimate biomass via allometric relationships with canopy height (e.g. Asner et al. 2010; Asner and Mascaro 2014). Lidar measurements can be used to estimate biomass over dense, high biomass (high LAI) tropical forests where passive optical measurements saturate and are thus insensitive to change and/or variation (Saatchi et al. 2011). Canopy height estimation from lidar is now included in routine commercial and forestry measurements (Næsset et al. 2004; Hyyppä et al. 2008).

2. Full-Waveform Lidar Systems

Waveform (often referred to as 'full-waveform') lidar systems record a 'binned' and digitised version of the real intensity return detected by the sensor, resulting from an outgoing pulse of known form (Mallet and Bretar 2009). Waveform instruments record the intensity of the response at a certain sampling rate (this sampling and detector non-linearity mean that the measurement never are true *full*-waveform), while performing minimal pulse-detection methods. Waveform lidar is becoming prevalent in airborne systems, even if they are in practice often used as discrete return systems with much of the intermediate waveform information being ignored. However, the power of waveform lidar is that it has the capability to record detailed information on the vertical distribution of canopy structure, and hence has a range of applications in remote sensing of vegetation including height and biomass (Dubayah et al. 2010), LAI (Tang et al. 2012) and canopy gap fraction (Armston et al. 2013a). The waveform signal can not only identify where there is a surface, but also what the properties of that surface are. This is particularly relevant for example in distinguishing woody from leaf material. Figure 11.8 shows an example of a modelled full-waveform lidar return over a conifer canopy, and highlights the potential information content of the signal.

3. Limitations and Future Developments of Lidar Systems

A current limitation of lidar is the lack of wide area coverage due to reliance on airborne platforms. However, ALS survey costs

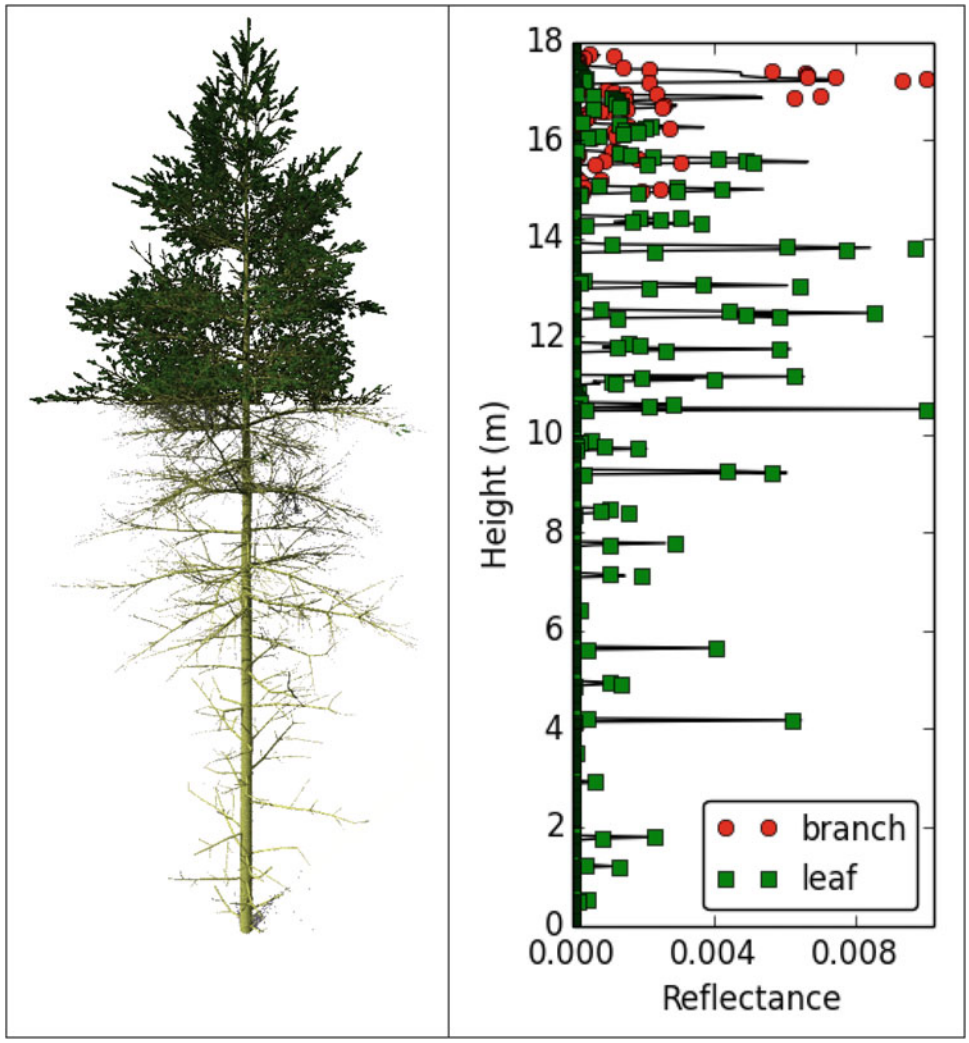

Fig. 11.8. Example of full-waveform lidar signal simulated from a 3D model of a Scots pine (*Pinus sylvestris*) tree (visualised in the *left panel*). The signal shows height-resolved return intensity (*black* impulses), as well as the normalized proportion of the signal in each height bin coming from the leaf and branch objects in the 3D model. Leaf and branch returns can be separated explicitly in the 3D model returns

are coming down (Wulder et al. 2012), and so larger and larger areas are being covered, with a number of countries now aiming to obtain total coverage (e.g. see http://www.gim-international.com/issues/articles/id1664-Swedish_Lidar_Project.html).

Obtaining this coverage is time-consuming (typically months to years) and hence can only provide a temporally fragmented 'snapshot' (note that this is only a limitation for very large areas; smaller regions, even 1000s of ha, where forest height and density will not vary in a few weeks or even months, can be covered rapidly and even revisited). In addition, these relatively large surveys are generally designed for deriving digital elevation models (DEMs) rather than for vegetation applications. As a result the sampling is often at or below 1 pt m^{-2} in order to reduce the survey time, meaning limited sampling of the canopy properties. A further difficulty is differentiating between leaf and woody material, particularly in larger footprint instruments. It has been proposed that this

limitation could be overcome by dual wavelength systems using spectral contrast to distinguish canopy components (Morsdorf et al. 2009). No system of this sort has been flown as yet, although work on laboratory prototypes show great promise (Woodhouse et al. 2011). An ongoing issue in dealing with lidar systems of all types is the often proprietary (and hence generally hidden) nature of the instrument characteristics (Disney et al. 2010). This makes it hard to obtain information on key technical specifications such as the thresholds used to trigger a recorded pulse (Armston et al. 2013a), or the stability of the instrument absolute response (and gain). Lidar instruments are rarely if ever calibrated to provide absolute reflectance, making it hard to make quantitative comparisons of signal returns from different backgrounds and canopy types.

In terms of spaceborne lidar for vegetation applications, unfortunately none currently exist due to perceived cost and technical limitations. This is despite the success of NASA's ICESAT/GLAS mission, which is remarkable given that it was not designed for vegetation applications and had some severe limitations including a large footprint (70 m), limited vertical resolution and relatively poor spatial sampling (hundreds of meters along tracks between footprints and kilometres between tracks horizontally). Despite this, GLAS data have been widely used to derive estimates of canopy height and structure over large areas, particularly for tall boreal and tropical forests (Harding and Carabajal 2005; Lefsky et al. 2005; Rosette et al. 2005) as well as forming the basis of the current best estimates of pan-tropical forest biomass (Saatchi et al. 2011; Baccini et al. 2012). A second ICESAT mission is due to launch in 2017 (http://icesat.gsfc.nasa.gov/icesat2/) but will have a different lidar system to that on ICESAT, and the possibilities for vegetation applications are as yet uncertain. Future prospects for space-based canopy lidar improved in July 2014, when NASA announced plans to launch the Global Ecosystem Dynamics Investigation (GEDI) lidar system on board the International Space Station (ISS) in 2019.

4. Terrestrial Laser Scanning (TLS)

Another development over the last decade has been the rise of terrestrial laser scanning (TLS) instruments. Typically developed for commercial surveying applications, TLS data have proved an interesting source of 3D canopy structure information (Maas et al. 2008). Given the importance of 3D structure for radiative transfer modelling, biomass, canopy state etc., ways to rapidly and accurately characterise structure are obviously attractive. This is particularly true as traditional field-based measurement of structure are hard to make, particularly in remote and tall forests where access may be limited. Under these conditions, even measuring tree height can be problematic. As a result, structural measurements are often limited to diameter-at-breast height, stem number density, with perhaps some estimates of overall height, height-to-crown ratio, and crown extent. Tree height can be estimated using hypsometers or clinometers and even cheap laser ranging devices. However, for these height measurements, the top of a tree has to be visible from the ground. In dense canopies, with tall trees or in steep terrain, this can be problematic. Additional structural measurements are often inferred from indirect techniques, such as gap fraction and cover (and hence LAI) from upward-looking hemispheric photographs. TLS can potentially overcome many of these limitations, allowing rapid estimation of dbh, height and vertical structure and potentially providing information that can be used to develop 3D canopy structural models quickly and accurately (Raumonen et al. 2013).

The value of TLS measurements has seen development of new instruments specifically designed for vegetation applications, including: the use of wavelengths that are eye-safe, but also reflected strongly by vegetation (e.g. 1064 nm); a move from discrete-return to

waveform instruments; full hemisphere scanning; multiple wavelengths. Most of these innovations have been developed in the research community, but commercial manufacturers are now recognising there may be a larger market for robust field-portable vegetation TLS instruments. Perhaps the most exciting of these developments is that of full-waveform, hemispherical scanners, with dual wavelengths. The only currently operational instrument is the Salford Advanced Laser Canopy Analyser (SALCA), which operates at 1040 and 1550 nm (Danson et al. 2014). As for ALS, dual wavelengths have the potential to allow leaf and woody material to be separated in the lidar scans (Woodhouse et al. 2011). Another new instrument is the dual-wavelength Echidna laser scanner (DWEL, Douglas et al. 2012), a development of the Echidna single wavelength instrument that has been deployed successfully for a number of canopy applications (Yao et al. 2011). Both SALCA and DWEL are prototypes and require significant time to set up and carry out full hemisphere scans. A more robust, commercial alternative is the Riegl VZ-400 scanner (http://www.riegl.com/uploads/tx_pxpriegldownloads/DataSheet_VZ-400_18-09-2013.pdf). This is a full waveform hemispherical TLS instrument, albeit with a single wavelength at 1550 nm. It is a robust, field-ready instrument that can carry out high angular resolution hemispherical scans in 1–2 min. It can be used in conjunction with a digital camera to provide image data aligned to the scan data to aid target identification (and even separation of canopy elements). The instrument was not designed for vegetation applications, and so use of the waveform information for this purpose is still in the early stages but is potentially very promising (Disney et al. 2014). Field intercomparisons are being used to test the various strengths and weaknesses of the different instrument approaches (Armston et al. 2013b).

A key obstacle of using TLS for 3D structure is transforming point cloud data into some form of topologically-structured description of individual trees, preferably in a robust, automated way. Estimating tree diameter at breast height and stem number-density is fairly easy; height can be straightforward but requires points to be returned from the top of the canopy, which can be problematic in tall, dense canopies. Topology is much harder, as it requires an association between points and organs within a particular tree (branches, leaves). Various 3D tree reconstruction methods have been proposed for TLS data (e.g. Gorte and Pfeifer 2004). Limitations of these methods have been the speed and the requirement for a large number of heuristic thresholds. Recent work has shown that development of more robust and rapid methods is possible (Raumonen et al. 2013).

An additional problem for any reconstruction method is validation, given the practical difficulty of measuring 3D structure for other than the simplest trees. Detailed 3D radiative transfer models as described above are proving one possible route for overcoming this limitation (Disney et al. 2012). In turn, the resulting tree reconstructions open the way for routine development of 3D scene models for remote sensing simulations. Figure 11.9 shows an example of a single TLS scan collected in an Australian *Eucalyptus* forest. The rich structural nature of the data is immediately apparent. Also shown are lidar 'hits' from a single tree extracted from the resulting point cloud, and a 3D reconstruction of the same tree via the method of Raumonen et al. (2013). It is worth noting that other uses of TLS are in estimating canopy clumping and gap fraction from the ground. TLS is potentially a more accurate way to estimate clumping than e.g. hemiphoto methods, as the effective resolution is generally higher, and few if any assumptions are required to estimate gap fraction (Casella et al. 2013). Reconstruction of tree volume from TLS data allows rapid, accurate and non-destructive estimates of above ground biomass to be made (Calders et al. 2014). The TLS measurement errors are also independent of tree size, unlike biomass estimates inferred indirectly from tree height or diameter measurements.

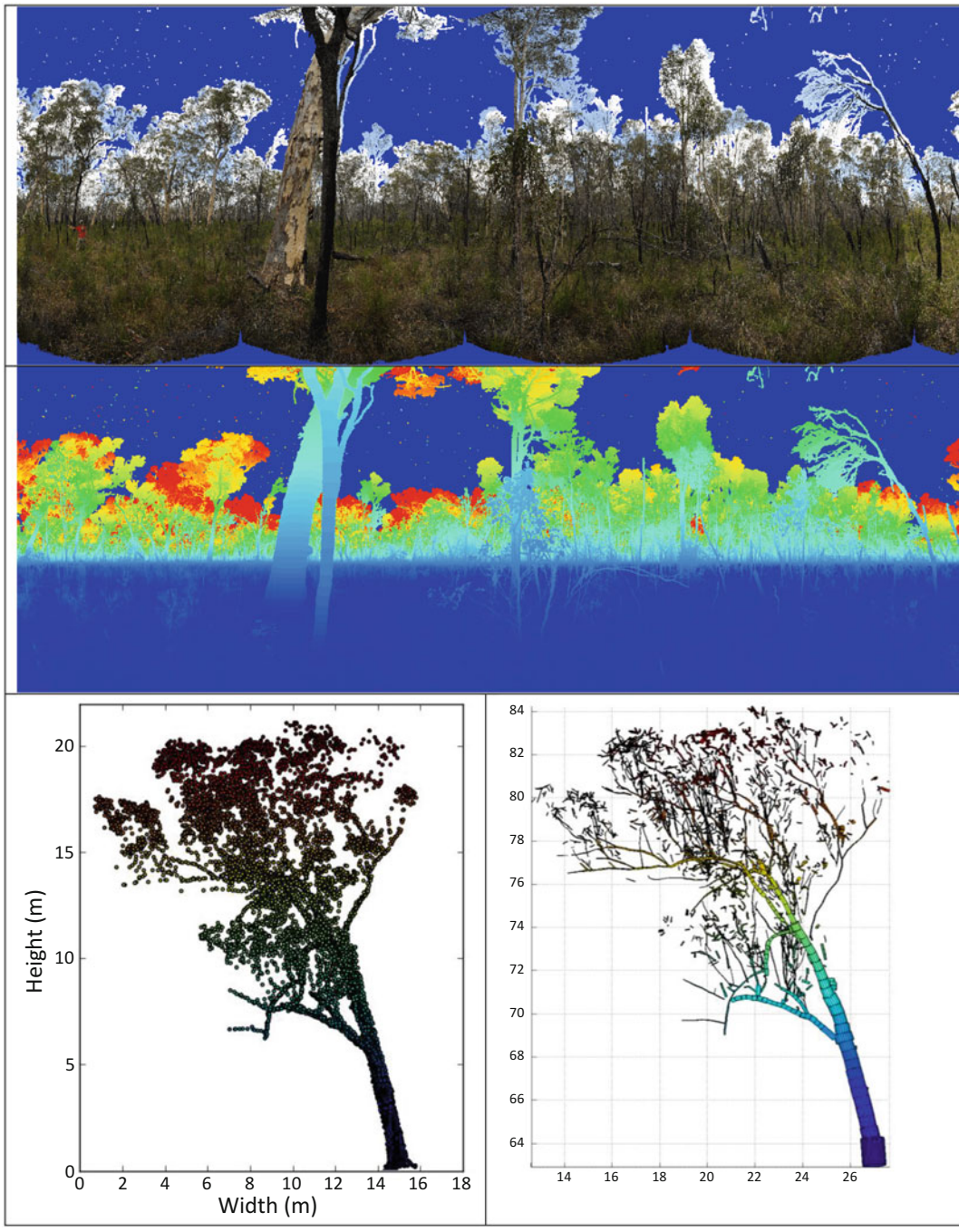

Fig. 11.9. Examples of Riegl VZ-400 terrestrial laser scanning (TLS) data from a bush site in Queensland, Australia and 3D tree structure reconstructed from the resulting scans. *Top*: 360° panorama of individual hemispheric photographs taken from a camera mounted on the TLS instrument. *Centre*: TLS scan, with height mapped to color. *Bottom left*: TLS points from a single tree extracted from the point cloud data (*color* represents height above the ground); *bottom right*: 3D reconstruction of the same tree (*color* again represents height) using the method of Raumonen et al. (2013)

5. RADAR Systems

RADAR is an alternative promising instrument for canopy structure and function observations (Lee and Pottier 2009). In fact, RADAR has the specific, very great, advantage over optical reflected methods of all-weather operation. Longer wavelength (tens of cm) RADAR is potentially sensitive to much higher levels of biomass due to penetration through the upper canopy and interacting only with larger trunks and branches. Unlike lidar systems, scanning imaging RADAR systems are well-advanced from an engineering perspective, allowing for the wide area coverage that is often such an advantage of remote sensing. High-resolution interferometric synthetic aperture RADAR (InSAR) instruments also hold promise for measurements of canopy height and structure (Krieger et al. 2007). However, the radiative transfer problem in the RADAR domain is less well-understood than for optical wavelengths due to complications as a result of phase, polarization and coherence. As a result, exploitation of RADAR for vegetation applications has been primarily via empirical relationships between backscatter and amount/biomass. Yet, these measurements are known to have significant shortcomings in terms of their ability to reliably predict biomass as a function of backscatter. This arises in part due to gaps in understanding of the physical processes governing the observed backscatter (Mitchard et al. 2011; Woodhouse et al. 2012).

B. Fluorescence and Canopy Function

Plant physiological stress studies mainly focus on pulse-modulated chlorophyll fluorescence, but the light levels needed for saturated pulses are far too high such that this method is not practical for EO (Schreiber et al. 1995; Baker 2008). As a potential alternative, there has been major interest in solar-induced chlorophyll fluorescence (F_s). F_s results from the excitation of chlorophyll molecules within assimilating leaves in the canopy and it is produced at the core of Photosystems I and II, primarily at photosystem II. Chlorophyll fluorescence is the remaining part of intercepted light energy, typically less than a few percent, that is not used photochemically nor dissipated non-photochemically. Fluorescence occurs at longer wavelengths than the excitation light wavelength (typically 650–800 nm for sunlight). Although minor, F_s is often inversely related to photosynthesis, except when non-photochemical quenching of fluorescence occurs. Under stress, or in conditions where irradiance exceeds that required for photosynthesis, plant tissues increase heat production to dissipate excess energy. This tends to decrease F_s, at least initially. Therefore, the resulting level of F_s is a balance between the radiation used for photosynthesis, heat production, and chlorophyll fluorescence. Steady-state measurements of F_s are therefore highly responsive to changes in environmental conditions and can be used as a near-direct indicator of plant photosynthetic function (Moya et al. 2004; Guanter et al. 2012, 2014).

This rapid response of F_s to changing environment (temperature, light) and canopy state (water, internal temperature, nutrients etc.) has elicited significant interest in the possibility of relating remotely sensed measurements of F_s to canopy function and stress in particular. However, the induced fluorescence signal is only 1–5 % of the total reflected solar signal in the NIR, making it difficult to separate from the background reflected signal (Meroni et al. 2009). Malenovsky et al. (2009) review some of the challenges of measuring F_s from the solar reflected signal. Despite these issues, there have been several attempts to employ these measurements, including the ESA FLEX (Fluorescence Explorer) mission, primarily based on using narrow, specific dark lines of the solar and atmospheric spectrum in which irradiance is strongly reduced (the so-called Fraunhofer lines). Three main Fraunhofer features have been exploited for F_s estimation: Hα due to

hydrogen (H) absorption (centred at 656.4 nm) and two telluric oxygen (O_2) absorption bands O2-B (687.0 nm) and O2-A (760.4 nm). These lead to variants of the so-called Fraunhofer Line Depth (FLD) methods, in which F_s is estimated from some form of ratio of the measured signal in a Fraunhofer band to that measured in a reference band just outside the Fraunhofer band (see Meroni et al. 2009 for details of these methods). Key limitations for spaceborne applications include the requirement for very accurate spectral calibration, and the removal of atmospheric and directional effects. However, a major advantage of exploiting existing (and future) imaging spectroradiometers is that they have become relatively common and acquire spatial image data over wide areas. Guanter et al. (2007) demonstrated that F_s retrieval was possible from the MERIS sensor aboard ESA's Envisat platform. Their approach incorporated F_s retrieval into an atmospheric radiative transfer scheme so that F_s and surface reflectance were retrieved consistently from measured at-sensor radiance. This holds the promise for more systematic retrievals from newer sensors such as ESA's Sentintel 5 precursor mission, due for launch in 2015 (http://esamultimedia.esa.int/docs/S5-prec_Data_Sheet.pdf).

A new approach to retrieve F_s was recently developed that does not rely on the reflected solar signal, but uses estimates of changes in the depth of solar Fraunhofer lines, which tend to decrease due to in-filling by F_s (Joiner et al. 2011; Frankenberg et al. 2011a, b). These methods rely on high spectral resolution observations in the 755–775 nm range, which can resolve individual Fraunhofer lines overlapping with the F_s emission region. A key advantage of this method is that Fraunhofer line depth is unaffected by atmospheric scattering and absorption in certain narrow spectral windows. If these windows can be observed, then it is possible to estimate the in-filling due to F_s emission, which can of course only arise from vegetation. Such an approach has only become feasible since the launch of the Japanese Greenhouse Gases Observing SATellite "IBUKI" (GOSAT), carrying the Thermal and Near infrared Sensor for carbon Observation (TANSO) (http://www.gosat.nies.go.jp/index_e.html). The TANSO Fourier Transform Spectrometer (FTS) was designed for measuring column-averaged atmospheric CO_2 on global scales. The possibility for retrieving F_s was a serendipitous after-thought. TANSO-FTS observations are by no means ideal for F_s due to their large spatial extent (tens km footprint), and limited spatial and temporal coverage due to the instrument design. Despite these issues, the first retrievals of F_s have shown large-scale patterns consistent with expectations of seasonal and regional variations in productivity (Joiner et al. 2011). An example global map of F_s derived from TANSO-FTS data is shown in Fig. 11.10.

The results suggest that estimates of F_s correlate strongly with independent estimates of GPP (Frankenberg et al. 2011b; Guanter et al. 2012, 2014). Critically, F_s also seems to contain information which is independent of standard satellite reflectance-derived estimates of productivity via NDVI or EVI, for example, that basically measure vegetation 'greenness' i.e. some property related to vegetation amount. In addition, the F_s signal is likely to be much more sensitive to canopy stress due to its origins in the photosynthetic machinery. This might allow exploration of large-scale impacts of stressors on vegetation productivity. As an example of this, Lee et al. (2013) used satellite fluorescence to show that instantaneous midday productivity (GPP) was reduced by as much as 15 % across the Amazon due to severe drought conditions in 2010. This interest in fluorescence as an indicator of GPP has led to new ways to exploit data from sensors primarily aimed at atmospheric trace gas applications. Joiner et al. (2013) have extracted fluorescence from the Japanese GOME-2 instrument, at higher precision and over smaller spatial and temporal scales than is possible with

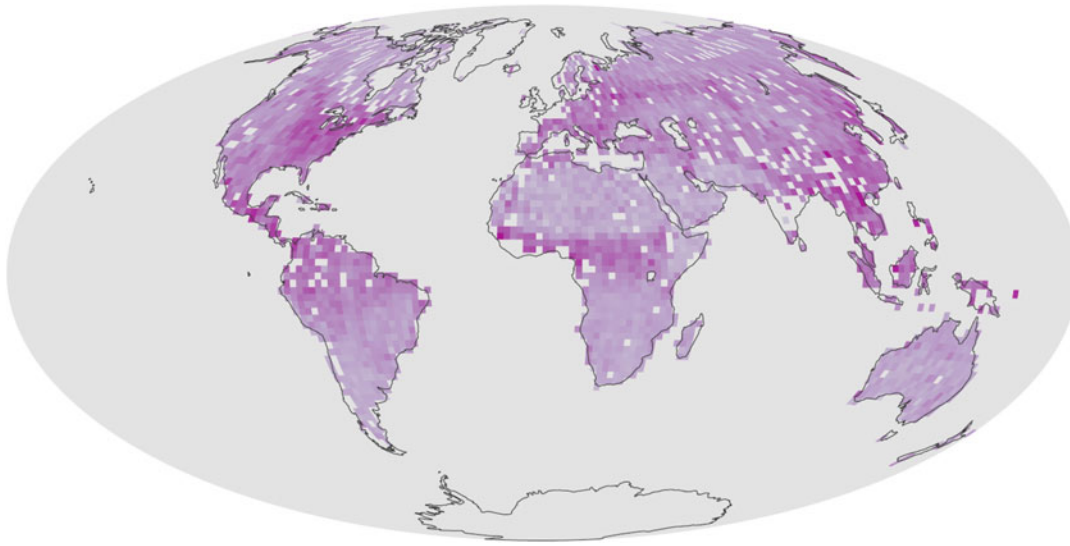

Fig. 11.10. Sun-induced steady-state fluorescence yield (F_s) estimated from GOSAT TANSO-FTS observations composited during July 2009. Color intensity represents intensity of F_s in arbitrary units. Image from NASA Earth Observatory, created by Robert Simmon, using data from GOSAT (http://visibleearth.nasa.gov/view.php?id=51121)

GOSAT. This work holds the promise of more detailed maps of fluorescence from space in the near future, which has in turn led to an increase in interest as to how to understand and exploit this signal using models.

The intriguing and unique information content of F_s has led to work on modelling the signal at the leaf and canopy levels in order to understand the signal and potentially allow parameter retrievals (Miller et al. 2005). F_s models rely on embedding a model of leaf-level fluorescence within a canopy reflectance model. The FLSAIL model (Rosema et al. 1991) was an extension of the SAIL canopy reflectance model (Verhoef 1984) with F_s contributions modelled through a doubling method. The model was primarily developed for describing laser-induced rather than solar-induced fluorescence. Olioso et al. (1992) used a simple Beer's Law approximation for canopy and leaf-level extinction and allowed for within-canopy gradient in chlorophyll content to account for variations in leaf biochemistry. The 3D DART model has also been modified to provide estimates of fluorescence at the canopy level (Miller et al. 2005). FlurMODleaf is perhaps the most sophisticated F_s model, based on the PROSPECT model described above (Miller et al. 2005; Zarco-Tejada et al. 2006). This model has been used in various studies to show the influence of fluorescence on hyperspectral reflectance data (Zarco-Tejada et al. 2006, 2009; Middleton et al. 2008).

Reliable remotely-sensed observations of fluorescence are still in their infancy but they hold out the tantalising prospect of much more direct estimates of canopy function, productivity, and stress than at present, from spaceborne instruments based on visible and near infra-red radiation reflectance (Grace et al. 2007). NASA's Orbiting Carbon Observatory 2 (launched in mid-2014) may be capable of retrieving F_s from solar reflected signal, and there is increasing interest in other ways to retrieve F_s and vegetation productivity from both spaceborne and airborne hyperspectral data.

V. Conclusions

Various issues arise in using remote sensing in estimating vegetation structure and function in a quantitative sense. The primary limitation clearly is the indirect nature of most remote sensing measurements. However, there are also great capabilities that now exist for mapping, even indirectly, canopy state and function over wide areas and with repeated sampling, allowing for studies of phenology, disturbance and anthropogenic impacts. We have explored the key role that vegetation structure plays in providing a link between incoming radiation and how this radiation is subsequently scattered or absorbed within the canopy before exiting to provide the remote sensing signal. New developments in understanding and modelling the fundamental nature of these interactions are allowing us to chart a route from measurements made at the top-of-the atmosphere to estimates of canopy state and function. These developments are allowing us to unpick the relationships between 'effective' canopy parameters, simplified or approximate manifestations of measurable physical parameters, and their real measurable counterparts. Effective parameters allow us to model the radiation signal in practical, rapid models that are required to operate on global scales. The effective nature of the parameters, however, makes such models difficult to test and validate. Increases in the resolution and physical accuracy of large-scale land surface models has highlighted these discrepancies, but also calls for improvements in representations of vegetation. This is critical to reducing uncertainty in modelling the responses of terrestrial vegetation to changes in climate and land use, particularly via the terrestrial carbon cycle.

A range of new remote sensing measurements providing more direct information on canopy structure and function have been discussed. Terrestrial and airborne lidar systems, notably full-waveform and multispectral, are providing new information on canopy structure. Observations of canopy fluorescence have provided promising estimates of canopy function, particularly under stress. These new observations are being exploited through developments in detailed 3D canopy and leaf models, which are making use of the continued increases in computing power to reduce the requirements for approximations.

From 2000 on there has been an unprecedented increase in high quality calibrated consistent and error-quantified satellite measurements of terrestrial vegetation at resolutions of 250 m – 1 km, covering the globe every few days. Notwithstanding limitations, these observations are now central to a huge range of applications. Indeed, many of these observations have been identified as so-called 'essential climate variables' (http://www.wmo.int/pages/prog/gcos/index.php?name=EssentialClimateVariables).

However, the future is perhaps a little more uncertain: current activities by major space agencies include plans for continuation of many, but not all, of the existing observations of the land surface that have proved so useful. Some of these new systems will provide observations with reduced capability and/or scope than their predecessors, for a variety of practical reasons. Given what we have, and what is to come, we should look forward to the coming decade as one that will likely provide as many developments in our ability to measure and understand terrestrial vegetation as the last decade undoubtedly had.

Acknowledgments

I acknowledge the support of UCL Geography and the NERC National Centre for Earth Observation (NCEO), as well as the University of Queensland for hosting me during some of this work. I also acknowledge various colleagues for the numerous and varied discussions over the last few years, that have led to thoughts and collaborations on issues

discussed here, including (inter alia): P Lewis, J Gomez-Dans, MJ Disney, M Barnsley, T Quaife, M DeKauwe, S Hancock, M Williams, S Quegan C Schaaf, A Strahler, Y Knyazkhin, B Pinty, JL Widlowski, J Armston and K Calders among many others. I am grateful to Prof. Vince Gutschick and the Mathematical Biosciences Institute of Ohio State University, for the invitation to the MBI Workshop on Modelling Plant Development which provided initial impetus for this work.

References

Allen WA, Gausman HW, Richardson AJ, Thomas JR (1969) Interaction of isotropic light with a compact plant leaf. J Opt Soc Am 59:1376–1379

Allen WA, Gausman HW, Richardson AJ (1970) Mean effective optical constants of cotton leaves. J Opt Soc Am 60:542–547

Alton PB, North PRJ, Los SO (2007) The impact of diffuse sunlight on canopy light-use efficiency, gross photosynthetic product and net ecosystem exchange in three forest biomes. Glob Chang Biol 13:776–787

Angert A, Biraud S, Henning CC, Bauermann W, Pinzon J, Tucker CJ, Fung I (2005) Drier summers cancel out the CO_2 uptake enhancement induced by warmer springs. Proc Natl Acad Sci U S A 102:10823–10827

Armston J, Disney MI, Lewis P, Scarth P, Phinn S, Lucas R, Bunting P, Goodwin N (2013a) Direct retrieval of canopy gap probability using airborne waveform lidar. Remote Sens Environ 134:24–38

Armston J, Newnham G, Strahler AH, Schaaf C, Danson M, Gaulton R, Zhang Z, . . ., Wu S (2013b) Intercomparison of terrestrial laser scanning instruments for assessing forested ecosystems: a Brisbane field experiment, B11G-0443, In: Proc. AGU San Francisco, Dec. 2013 http://128.197.168.195/wp-content/uploads/2013/11/Armston_Brisbane.pdf

Asner GP, Mascaro J (2014) Mapping tropical forest carbon: Calibrating plot estimates to a simple LiDAR metric. Remote Sens Environ 140:614–624

Asner GP, Powell GV, Mascaro J, Knapp DE, Clark JK, Jacobson J, Kennedy-Bowdoin T, . . ., Hughes RF (2010) High resolution forest carbon stocks and emissions in the Amazon. Proc Natl Acad Sci USA 107:16738–16742

Asrar G (ed) (1989) Theory and Applications of Optical Remote Sensing. Wiley, New York

Baccini A, Goetz SJ, Walker WS, Laporte NT, Sun M, Sulla-Menashe D, Hackler J, . . ., Houghton RA (2012) Estimated carbon dioxide emissions from tropical deforestation improved by carbon-density maps. Nat Clim Change 2:182–185

Baker, Neil R. "Chlorophyll fluorescence: a probe of photosynthesis in vivo."Annu. Rev. Plant Biol. 59 (2008): 89–113

Baranoski GVG (2006) Modeling the interaction of infrared radiation (750 to 2500 nm) with bifacial and unifacial plant leaves. Remote Sens Environ 100:335–347

Best MJ, Pryor M, Clark DB, Rooney GG, Essery RLH, Ménard CB, Edwards JM, . . ., Harding RJ (2011) The Joint UK Land Environment Simulator (JULES), model description – Part 1: Energy and water fluxes. Geosci Model Dev 4:677–699

Brando P, Goetz S, Baccini A, Nepstad DC, Beck PSA, Chiristman MC (2010) Seasonal and interannual variability of climate and vegetation indices across the Amazon. Proc Natl Acad Sci U S A 107:14685–14690

Brodersen CR, Voglemann TC, Williams WE, Gorton H (2008) A new paradigm in leaf-level photosynthesis: direct and diffuse lights are not equal. Plant Cell Environ 31:159–164

Bunnik NJJ (1978) The multispectral reflectance of shortwave radiation of agricultural crops in relation with their morphological and optical properties. PhD Thesis, In Mededelingen Landbouwhogeschool, Wageningen University, Wageningen

Brut A, Rüdiger C, Lafont S, Roujean J-L, Calvet J-C, Jarlan L, Gibelin A-L, . . ., Ceschis E (2009) Modelling LAI at a regional scale with ISBA-A-gs: comparison with satellite-derived LAI over southwestern France. Biogeosciences 6:1389–1404

Calders K, Newnham G, Burt A, Murphy S, Raumonen P, Herold M, Culvenor D, . . ., Kaasalainen M (2014) Non-destructive estimates of above-ground biomass using terrestrial laser scanning. Methods Ecol Evol, in press. doi: 10.1111/2041-210X.12301

Campbell GS (1986) Extinction coefficient for radiation in plant canopies calculated using an ellipsoidal inclination angle distribution. Agric For Meteorol 36:317–321

Carrer D, Roujean JL, Lafont S, Boone A, Calvet, JC (2012) A vegetation radiative transfer scheme in ISBA-A-gs interactive vegetation model. In: Proceedings of IGARSS2012. Munich, Germany, 22–27 July 2012, pp 1151–1154

Casella E, Disney MI, McKay H (2013) tLiDAR methodologies can overcome limitations in

estimating forest canopy LAI from conventional hemispherical photograph analyses. In: Proceedings of Functional Structural Plant Modelling 2013 (FSPM2013), Saariselkä, Finland, 9–14 June, 2013

Cescatti A, Niinemets Ü (2004) Leaf to landscape. In: Smith WK, Vogelmann TC, Critchley C (eds) Ecological Studies: Photosynthetic Adaptation, vol 178. Springer, New York, pp 42–85

Chandrasekhar S (1960) Radiative Transfer. Dover, New York

Chapin FS III, Chapin MC, Matson PA, Vitousek P (2011) Principles of Terrestrial Ecosystem Ecology, 2nd edn. Springer, New York

Combes D, Bousquet L, Jacquemoud S, Sinoquet H, Varlet-Grancher C, Moya I (2007) A new spectrogoniophotometer to measure leaf spectral and directional optical properties. Remote Sens Environ 109:107–117

Danson FM, Gaulton R, Armitage RP, Disney MI, Gunawan O, Lewis PE, Pearson G, Ramirez AF (2014) Developing a dual-wavelength full-waveform terrestrial laser scanner to characterise forest canopy structure. Agric For Meteorol 198–199:7–14

Dawson TP, Curran PJ, Plummer SE (1998) LIBERTY – modeling the effects of leaf biochemical concentration on reflectance spectra. Remote Sens Environ 65:50–60

Denman KL, Brasseur G, Chidthaisong A, Ciais P, Cox PM, Dickinson RE, Hauglustaine D, . . ., Zhang X (2007) Couplings between changes in the climate system and biogeochemistry. In: Solomon S, Qin D, Manning M, Chen Z, Marquis M, Averyt KB, Tignor M, Miller HL (eds) Climate Change 2007: The Physical Science Basis. Contribution of Working Group I to the Fourth Assessment Report of the Intergovernmental Panel on Climate Change. Cambridge University Press, Cambridge, pp 499–587

Dickinson RE (1983) Land surface processes and climate—surface albedos and energy balance. Adv Geophys 25:305–353

Disney MI, Lewis P, North P (2000) Monte Carlo ray tracing in optical canopy reflectance modelling. Remote Sens Rev 18:163–197

Disney MI, Lewis P, Quaife T, Nichol, C (2005) A spectral invariant approach to modeling canopy and leaf scattering. In: Proceedings of the 9th International Symposium on Physical Measurements and Signatures in Remote Sensing (ISPMSRS), 17–-19 October 2005, Beijing, China, Part 1: 318–320

Disney MI, Lewis P, Saich P (2006) 3D modelling of forest canopy structure for remote sensing simulations in the optical and microwave domains. Remote Sens Environ 100:114–132

Disney MI, Lewis P, Bouvet M, Prieto-Blanco A, Hancock S (2009) Quantifying surface reflectivity for spaceborne lidar via two independent methods. IEEE Trans Geosci Remote Sens 47:3262–3271

Disney MI, Kalogirou V, Lewis PE, Prieto-Blanco A, Hancock S, Pfeifer M (2010) Simulating the impact of discrete-return lidar system and survey characteristics over 2 young conifer and broadleaf forests. Remote Sens Environ 114:1546–1560

Disney MI, Lewis P, Gomez-Dans J, Roy D, Wooster M, Lajas D (2011) 3D radiative transfer modelling of fire impacts on a two-layer savanna system. Remote Sens Environ 115:1866–1881

Disney MI, Lewis P, Raumonen P (2012) Testing a new vegetation structure retrieval algorithm from terrestrial lidar scanner data using 3D models. In: Proceedings of Silvilaser 2012, Vancouver, BC, Canada, 16–19 September 2012

Disney MI, Burt A, Calders K, Raumonen P, Gonzalez de Tanago J, Cuni Sanchez A, Herold M, Armston J, Lewis S, Lines S, Lewis P (2014) New applications of 3D measurements and modelling to quantifying forest structure and biomass. In: Global Vegetation Modelling and Measurement (GV2M) meeting, Avignon, France, 3–7 Feb 2014

Douglas ES, Strahler AH, Martel J, Cook T, Mendillo C , Marshall R, Chakrabarti S, . . ., Lovell J (2012) DWEL: a dual-wavelength Echidna lidar for ground-based forest scanning. In: Proceedings of IGARSS2012, 22–27 July 2012, Munich, Germany, pp 4998–5001

Dubayah RO, Drake JB (2000) Lidar remote sensing for forestry. J For 98:44–46

Dubayah RO, Sheldon SL, Clark DB, Hofton MA, Blair JB, Hurtt GC et al (2010) Estimation of tropical forest height and biomass dynamics using lidar remote sensing at La Selva, Costa Rica. J Geophys Res 115

España M, Baret F, Aries F, Andrieu B, Chelle M (1999) Radiative transfer sensitivity to the accuracy of canopy structure description. The case of a maize canopy. Agronomie 19:241–254

Feret JB, François C, Asner GP, Gitelson AA, Martin RE, Bidel LPR, Ustin SL, le Maire G, Jacquemoud S (2008) PROSPECT-4 and 5: advances in the leaf optical properties model separating photosynthetic pigments. Remote Sens Environ 112:3030–3043

Flerchinger GN, Yu Q (2007) Simplified expressions for radiation scattering in canopies with ellipsoidal leaf angle distributions. Agric For Meteorol 144:230–235

Frankenberg C, Butz A, Toon GC (2011a) Disentangling chlorophyll fluorescence from

atmospheric scattering effects in O2A-band spectra of reflected sun-light. Geophys Res Lett 38, L03801

Frankenberg C, Fisher JB, Worden J, Badgley G, Saatchi SS, Lee J-E, Toon GC, . . ., Yokota T (2011b) New global observations of the terrestrial carbon cycle from GOSAT: Patterns of plant fluorescence with gross primary productivity. Geophys Res Lett 38:L17706

Fung AK (1994) Microwave Scattering and Emission Models and Their Applications. Artech House, Norwood

Ganguly S, Schull MA, Samanta A, Shabanov NV, Milesi C, Nemani R, Knyazikhin YV, Myneni RB (2008) Generating vegetation leaf area index earth system data records from multiple sensors. Part 1: Theory. Remote Sens Environ 112:4333–4343

Ganguly S, Nemani R, Zhong G, Hashimoto H, Milesi C, Michaelis M, Wang W, . . ., Myneni RB (2012) Generating global leaf area index from Landsat: algorithm formulation and demonstration. Remote Sens Environ 122:185–202

Gastellu-Etchegorry JP, Martin E, Gascon F (2004) Dart: a 3D model for simulating satellite images and studying surface radiation budget. Int J Remote Sens 25:73–96

Godin C, Sinoquet H (2005) Functional–structural plant modelling. New Phytol 166:705–708

Goel NS (1988) Models of vegetation canopy reflectance and their use in the estimation of biophysical parameters from reflectance data. Remote Sens Rev 4:1–222

Goel NS, Strebel DE (1984) Simple beta distribution representation of leaf orientation in vegetation canopies. Agron J 75:800–802

Goel NS, Thompson RL (2000) A snapshot of canopy reflectance models, and a universal model for the radiation regime. Remote Sens Rev 18:197–225

Gorte B, Pfeifer N (2004) Structuring laser-scanned trees using 3D mathematical morphology. Int Arch Photogramm Remote Sens XXXV:929–933

Govaerts YM (1996) A model of light scattering in three-dimensional plant canopies: a Monte Carlo ray tracing approach. Office for Official Publication of the European Communities

Govaerts Y, Verstraete MM (1998) Raytran: a Monte Carlo ray-tracing model to compute light scattering in three-dimensional heterogeneous media. IEEE Trans Geosci Remote Sens 36:493–505

Grace J, Nichol C, Disney MI, Lewis P, Quaife T, Bowyer P (2007) Can we measure photosynthesis from space? Glob Chang Biol 13:1484–1497

Guanter L, Alonso L, Gomez-Chova L, Amoros-Lopez J, Moreno J (2007) Estimation of solar-induced vegetation fluorescence from space measurements. Geophys Res Lett 34:L08401

Guanter L, Frankenberg C, Dudhia A, Lewis PE, Gomez-Dans J, Kuze A, Suto H, Grainger RG (2012) Retrieval and global assessment of terrestrial chlorophyll fluorescence from GOSAT space measurements. Remote Sens Environ 121:236–257

Guanter L, Zhang Y, Jung M, Joiner J, Voigt M, Berry JA, Frankenberg C, . . ., Griffis TJ (2014) Global and time-resolved monitoring of crop photosynthesis with chlorophyll fluorescence. Proc Natl Acad Sci USA 111:E1327–E1333

Hapke B (1981) Bidirectional reflectance spectroscopy. I. Theory. J Geophys Res 86:3039–3054

Harding DJ, Carabajal CC (2005) ICESat waveform measurements of within-footprint topographic relief and vegetation vertical structure. Geophys Res Lett 32, L21S10

Henderson-Sellers A, Irannejad P, McGuffie K, Pitman A (2003) Predicting land-surface climates: better skill or moving targets? Geophys Res Lett 30:1777

Hosgood B, Jacquemoud S, Andreoli G, Verdebout J, Pedrini G, Schmuck G (1995) LOPEX: Leaf optical properties experiment 93. Technical Report EUR 16095 EN, Joint Research Center, European Commission, Institute for Remote Sensing Applications

Houser P, De Lannoy G, Walker JP (2012) Hydrologic data assimilation. In: Tiefenbacher JP (ed) Approaches to Managing Disaster – Assessing Hazards, Emergencies and Disaster Impacts. InTech, Rijeka, 162 p

Huang D, Knyazikhin Y, Dickinson R, Rautiainen M, Stenberg P, Disney MI, Lewis P, . . ., Myneni RB (2007) Canopy spectral invariants for remote sensing and model applications. Remote Sens Environ 106:106–122

Hyyppä J, Hyyppä H, Leckie D, Gougeonm F, Yu X, Maltamo M (2008) Review of methods of small-footprint airborne laser scanning for extracting forest inventory data in boreal forests. Int J Remote Sens 29:1339–1366

Jacquemoud S, Ustin S (2008) Modelling leaf optical properties. Photobiological Sciences Online (Smith KC , ed.) American Society for Photobiology, http://www.photobiology.info/

Jacquemoud S, Ustin SL, Verdebout J, Schmuck G, Andreoli G, Hosgood B (1996) Estimating leaf biochemistry using the PROSPECT leaf optical properties model. Remote Sens Environ 56:194–202

Jacquemoud S, Verhoef W, Baret F, Bacour C, Zarco-Tejada PJ, Asner GP, Francois C, Ustin SL (2009) PROSPECT + SAIL Models: a review of use for vegetation characterization. Remote Sens Environ 113:56–66

Joiner J, Yoshida Y, Vasilkov AP, Yoshida Y, Corp LA, Middleton EM (2011) First observations of global and seasonal terrestrial chlorophyll fluorescence from space. Biogeosciences 8:637–651

Joiner J, Guanter L, Lindstrot R, Voigt M, Vasilkov AP, Middleton EM, Huemmerich KF, . . ., Franenberg C (2013) Global monitoring of terrestrial chlorophyll fluorescence from moderate spectral resolution near-infrared satellite measurements: methodology, simulations and application to GOME-2. Atmos Meas Tech Discuss 6:3883–3930

Jones HG (2014) Plants and Microclimate: A Quantitative Approach to Environmental Plant Physiology, 3rd edn. CUP, Cambridge

Jones HG, Vaughan RA (2010) Remote Sensing of Vegetation: Principles, Techniques and Applications. OUP, Oxford

Knorr W, Heimann M (2001) Uncertainties in global terrestrial biosphere modeling: 1. A comprehensive sensitivity analysis with a new photosynthesis and energy balance scheme. Glob Biogeochem Cycles 15.1:207–225

Knorr W, Kaminski T, Scholze M, Gobron N, Pinty B, Giering R, Mathieu P-P (2010) Carbon cycle data assimilation with a generic phenology model. J Geophys Res 115, doi:10.1029/2009JG001119

Knyazikhin YV, Marshak AL, Myneni RB (1992) Interaction of photons in a canopy of finite dimensional leaves. Remote Sens Environ 39:61–74

Knyazikhin YV, Kranigk J, Myneni RB, Panfyorov O, Gravenhorst G (1998) Influence of small-scale structure on radiative transfer and photosynthesis in vegetation canopies. J Geophys Res 103:6133–6144

Knyazikhin YV, Schull MA, Liang X, Myneni RB, Samanta A (2011) Canopy spectral invariants. Part 1: A new concept in remote sensing of vegetation. J Quant Spectrosc Radiat Transf 112:727–735

Knyazikhin YV, Schull MA, Stenberg P, Mõttus M, Rautiainen M, Yang Y, Marshak A, . . ., Myneni RB (2013) Hyperspectral remote sensing of foliar nitrogen content. Proc Natl Acad Sci USA 110: E185–E192

Krieger G, Moreira A, Fiedler H, Hajnsek I, Werner M, Younis M, Zink M (2007) TanDEM-X: A satellite formation for high-resolution SAR interferometry. IEEE Trans Geosci Remote Sens 45:3317–3341

Kubelka P, Munk F (1931) Zeit Für Tekn Physik 12:593

Lafont S, Zhao Y, Calvet J-C, Peylin P, Ciais P, Maignan F, Weiss M (2012) Modelling LAI, surface water and carbon fluxes at high-resolution over France: comparison of ISBA-A-gs and ORCHIDEE. Biogeosciences 9:439–456

Lee J-S, Pottier E (2009) Polarimetric radar imaging: from basics to applications. CRC Press, Boca Raton

Lee J-E, Franksnberg C, van der Tol C, Berry JA, Guanter L, Boyce CK, Fisher JB, . . ., Saatchi, S (2013) Forest productivity and water stress across Amazonia: observations from GOSAT chlorophyll fluorescence. Proc Royal Soc B 280:1471–2954

Leersnijder RP (1992) PINOGRAM: A Pine Growth Area Model. WAU dissertation 1499, Wageningen Agricultural University, The Netherlands

Lefsky MA, Cohen WB, Parker GG, Harding DJ (2002) Lidar remote sensing for ecosystem studies. Biogeosciences 52:19–30

Lefsky MA, Harding DJ, Keller M, Cohen WB, Carabajal CC, Espirito-Santo FDB, Hunter MO, de Oliveira R Jr (2005) Estimates of forest canopy height and aboveground biomass using ICESat. Geophys Res Lett 32:L22S02

Lewis P (1999) Three-dimensional plant modelling for remote sensing simulation studies using the Botanical Plant Modelling System (BPMS). Agron Agric Environ 19:185–210

Lewis P, Disney MI (1998) The botanical plant modeling system (BPMS): a case study of multiple scattering in a barley canopy. In: Proceedings of IGARSS'98, Seattle, USA.

Lewis P, Disney MI (2007) Spectral invariants and scattering across multiple scales from within-leaf to canopy. Remote Sens Environ 109:196–206

Lewis P, Gómez-Dans J, Kaminski T, Settle J, Quaife T, Gobron N, Styles J, Berger M (2012) An Earth Observation Land Data Assimilation System (EO-LDAS). Remote Sens Environ 120:219–235

Liang S (2004) Quantitative Remote Sensing of Land Surfaces. Wiley, New York

Lynch C (2008) Big data: How do your data grow? Nature 455:28–29

Maas HG, Bientert A, Scheller S, Keane E (2008) Automatic forest inventory parameter determined from terrestrial laser scanner data. Int J Remote Sens 29:1579–1593

Malenovsky Z, Mishra KB, Zemek F, Rascher U, Nedbal L (2009) Scientific and technical challenges in remote sensing of plant canopy reflectance and fluorescence. J Exp Bot 60:2987–3004

Mallet C, Bretar F (2009) Full-waveform topographic lidar: state-of-the-art. ISPRS J Photogramm Remote Sens 64:1–16

Marshak A, Knyazikhin YV, Chiu JC, Wiscombe WJ (2011) Spectrally invariant approximation within atmospheric radiative transfer. J Atmos Sci 68:3094–3111

Martin G, Josserand SA, Bornman JF, Vogelmann TC (1989) Epidermal focussing and the light microenvironment within leaves of Medicago sativa. Physiol Plant 76:485–492

Meador I, Weaver WR (1980) Two-stream approximations to radiative transfer in planetary atmospheres: a unified description of existing methods and new improvements. J Atmos Sci 37:630–643

Mêch R, Prusinkiewicz P (1996) Visual models of plants interacting with their environment. Proceedings of SIGGRAPH 96. New Orleans, Louisiana, August 4–9 1996. In computer graphics proceedings, annual conference series, ACM SIGGRAPH, pp 397–410

Melamed NT (1963) Optical properties of powders. Part I. Optical absorption coefficients and the absolute value of the diffuse reflectance. Part II. Properties of luminescent powders. J Appl Phys 34:560–570

Mercado LM, Bellouin NM, Sitch S, Boucher O, Huntingford C, Wild M, Cox PM (2009) Impact of changes in diffuse radiation on the global land carbon sink. Nature 458:1014–1018

Meroni M et al (2009) Remote sensing of solar-induced chlorophyll fluorescence: review of methods and applications. Remote Sens Environ 113(10):2037–2051

Middleton E, Corp LA, Campbell PKE (2008) Comparison of measurements and FluorMOD simulations for solar-induced chlorophyll fluorescence and reflectance of a corn crop under nitrogen treatments. Int J Remote Sens 29:5193–5213

Miller J, Berger M, Goulas Y, Jacquemoud S, Louis J, Mohammed G, Moise N, . . ., Zarco-Tejada P (2005) Development of a vegetation fluorescence canopy model, ESTEC Contract No. 16365/02/NL/FF Final Report

Mitchard ETA, Saatchi SS, Woodhouse IR, Feldpausch TR, Lewis SL, Sonké B, Rowland C, Meir P (2011) Measuring biomass changes due to woody encroachment and deforestation/degradation in a forest-savanna boundary region of central Africa using multi-temporal L-band radar backscatter. Remote Sens Environ 115:2861–2873

Monsi M, Saeki T (1953) Über den Lichtfaktor in den Pflanzengesellscahften und seine Bedeutung für die Stoffproduktion. Jpn J Bot 14:22–52. *Translated as*: Monsi M, Saeki T (2005) On the factor light in plant communities and its importance for matter production. Ann Bot 95:549–567

Monteith JL, Unsworth MH (2008) Principles of Environmental Physics, 3rd edn. Academic, Burlington

Morsdorf F, Nichol C, Malthus T, Woodhouse IH (2009) Assessing forest structural and physiological information content of multi-spectral LiDAR waveforms by radiative transfer modelling. Remote Sens Environ 113:2152–2163

Morton DC, Nagol J, Carbajal C, Rosette J, Palace M, Cook BD, Vermote EF, . . ., North PRJ (2014) Amazon forests maintain consistent canopy structure and greenness during the dry season. Nature 506:221–224

Moya I, Camenen L, Evain S, Goulas Y, Cerovic ZG, Latouche L, Flexas J (2004) A new instrument for passive remote sensing: 1. Measurement of sunlight-induced chlorophyll fluorescence. Remote Sens Environ 91:186–197

Myneni RB, Ross J (eds) (1990) Photon-vegetation Interactions: Applications in Optical Remote Sensing and Plant Ecology. Springer, Heidelberg

Myneni RB, Williams DL (1994) On the relationship between fAPAR and NDVI. Remote Sens Environ 49:200–211

Myneni RB, Ross J, Asrar G (1989) A review of the theory of photon transport in leaf canopies. Agric For Meteorol 45:1–153

Myneni RB, Asrar G, Gerstl SAW (1990) Radiative transfer in three-dimensional leaf canopies. Transp Theor Stat Phys 19:205–250

Myneni RB, Keeling CD, Tucker CJ, Asrar G, Nemani RR (1997a) Increased plant growth in the northern high latitudes from 1981 to 1991. Nature 386:698–702

Myneni RB, Nemani RR, Running SW (1997b) Estimation of global leaf area index and absorbed par using radiative transfer models. IEEE Trans Geosci Remote Sens 35:1380–1393

Myneni RB, Hofmann S, Knyazikhin Y, Privette JL, Glassy J, Tian J, Song X, . . ., Running SW (2002) Global products of vegetation leaf area and fraction absorbed PAR from year one of MODIS data. Remote Sens Environ 83:214–231

Myneni RB, Yang W, Nemani R., Huete AR, Dickinson RE, Kynazikhin Y, Didan K, . . ., Salomonson V (2007) Large seasonal swings in leaf area of Amazon rainforests. Proc Natl Acad Sci USA 104:4820–4823

Næsset E, Gobakken T, Holmgren˙ J, Hyyppä˙ H, Hyyppä˙ J, Maltamo˙ M, Nilsson M, . . ., Söderman U (2004) Laser scanning of forests: the Nordic experience. Scand J For Res 19:482–499

Nagai S, Saigusa N, Muraoka H, Nasahara KN (2010) What makes the satellite-based EVI-GPP relationship unclear in a deciduous broad-leaved forest? Ecol Res 25:359–365

Nicodemus FE, Richmond JC, Hsia JJ, Ginsberg IW, Limperis T (1977) Geometrical considerations and nomenclature for reflectance. NBS Monograph 160, National Bureau of Standards, U.S. Department of Commerce, Washington, DC

Niinemets Ü, Anten NPR (2009) Packing the photosynthetic machinery: from leaf to canopy. In: Laisk A, Nedbal L, Govindjee (eds) Photosynthesis in Silico: Understanding Complexity from Molecules to Ecosystems. Springer, Dordrecht, pp 363–399

Nilson T, Kuusk A (1989) A reflectance model for the homogenous plant canopy and its inversion. Remote Sens Environ 27:157–167

Norman JM, Miller EE, Tanner CB (1971) Light intensity and sunfleck size distribution in plant communities. Agron J 63:743–748

North PRJ (1996) Three-dimensional forest light interaction model using a Monte Carlo method. IEEE Trans Geosci Remote Sens 34:946–956

Olioso A, Méthy M, Lacaze B (1992) Simulation of canopy fluorescence as a function of canopy structure and leaf fluorescence. Remote Sens Environ 41:239–247

Olioso A, Inoue Y, Ortega-Farias S, Demarty J, Wigneron JP, Braud I (2005) Future directions for advanced evapotranspiration modeling: Assimilation of remote sensing data into crop simulation models and SVAT models. Irrig Drain Syst 19:377–412

Ollinger SV (2011) Sources of variability in canopy reflectance and the convergent properties of plants. New Phytol 189:375–394

Ollinger SV, Richardson AD, Martin ME, Hollinger DY, Frolking SE, Reich PB, Plourde LC, . . ., Schmid HP (2008) Canopy nitrogen, carbon assimilation, and albedo in temperate and boreal forests: Functional relations and potential climate feedbacks. Proc Natl Acad Sci USA 105:19336–19341

Perttunen J, Sievänen R, Nikinmaa E (1998) LIGNUM: a model combining the structure and the functioning of trees. Ecol Model 108:189–198

Pettorelli N (2013) The Normalized Difference Vegetation Index. OUP, Oxford. ISBN 978-0-19-969316-0

Pettorelli N, Vik JO, Mysterud A, Gaillard J-M, Tucker CJ, Stenseth NC (2005) Using the satellite-derived NDVI to assess ecological responses to environmental change. Trend Ecol Evol 20:503–510

Pfeifer M, Disney MI, Quaife T, Marchant R (2012) Terrestrial ecosystems from space: a review of earth observation products or macroecology applications. Glob Ecol Biogeogr 21:603–624

Pinty B, Verstraete MM, Dickinson RE (1989) A physical model for predicting bidirectional reflectances over bare soil. Remote Sens Environ 27:273–288

Pinty B, Gobron N, Widlowski J-L, Lavergne T, Verstraete MM (2004) Synergy between 1-D and 3-D radiation transfer models to retrieve vegetation canopy properties from remote sensing data. J Geophys Res 109: D21205

Pinty B, Lavergne T, Dickinson R, Widlowski J-L, Gobron N, Verstraete MM (2006) Simplifying the interaction of land surfaces with radiation for relating remote sensing products to climate models. J Geophys Res 111: D02116

Pinty B, Andredakis I, Clerici M, Kaminski T, Taberner M, Verstraete MM, Gobron N, . . ., Widlowski JL (2011a) Exploiting the MODIS albedos with the Two-stream Inversion Package (JRC-TIP). 1. Effective leaf area index, vegetation, and soil properties. J Geophys Res 116:D09105

Pinty B, Andredakis I, Clerici M, Kaminski T, Taberner M, Verstraete MM, Gobron N, . . ., Widlowski JL (2011b) Exploiting the MODIS albedos with the Two-stream Inversion Package (JRC-TIP): 2. Fractions of transmitted and absorbed fluxes in the vegetation and soil layers. J Geophys Res 116:D09106

Prusinkiewicz P, Lindenmayer A (1990) The Algorithmic Beauty of Plants. Springer, New York

Qin J, Liang S, Liu R, Zhang H, Hu B (2007) A weak-constraint-based data assimilation scheme for estimating surface turbulent fluxes. IEEE Geosci Remote Sens Lett 4:649–653

Quaife T, Lewis P, De Kauwe M, Williams M, Law BE, Disney MI (2008) Assimilating canopy reflectance data into an ecosystem model with an Ensemble Kalman Filter. Remote Sens Environ 112:1347–1364

Raumonen P, Kaasalainen M, Åkerblom M, Kaasalainen S, Kaartinen H, Vastaranta M, Holopainen M, . . ., Lewis P (2013) Comprehensive quantitative tree models from terrestrial laser scanner data. Remote Sens 5:491–520

Rautiainen M, Stenberg P (2005) Application of photon recollision probability in coniferous canopy reflectance model. Remote Sens Environ 96:98–107

Richardson AD, Anderson RS, Arain MA, Barr AG, Bohrer G, Chen G, Chen JM, . . ., Xue Y (2012) Terrestrial biosphere models need better representation of vegetation phenology: results from the North American Carbon Program Site Synthesis. Glob Chang Biol 18:566–584

Rodell M, et al (2004) Basin scale estimates of evapotranspiration using GRACE and other observations. Geophys Res Lett 31(20)

Rosema A, Verhoef W, Schroote J, Snel JFH (1991) Simulating fluorescence light-canopy interaction in support of laser-induced fluorescence measurements. Remote Sens Environ 37:117–130

Rosette JAB, North PRJ, Suarez JC (2005) Vegetation height estimates for a mixed temperate forest using

satellite laser altimetry. Int J Remote Sens 29:1475–1493
Ross JK (1981) The Radiation Regime and The Architecture of Plant Stands. Dr. W. Junk Publ, The Hague
Ross JK, Marshak AL (1989) The influence of leaf orientation and the specular component of leaf reflectance on the canopy bidirectional reflectance. Remote Sens Environ 27:251–260
Saatchi SS, Harris N, Brown S, Lefsky M, Mitchard E, Salas W, Zutta B, . . ., Morel A (2011) Benchmark map of forest carbon stocks in tropical regions across three continents. Proc Natl Acad Sci USA, 108:9899–9904
Saleska SR, Didan K, Huete AR, da Rocha HR (2007) Amazon forests green-up during 2005 drought. Science 318:612
Samanta A, Ganguly S, Hashimoto H, Devadiga S, Vermote E, Knyazikhin Y, Nemani RR, Myneni, RB (2010) Amazon forests did not green-up during the 2005 drought. Geophys Res Lett 37: L05401
Schaepman-Strub G, Schaepman ME, Painter TH, Dangel S, Martonchik JV (2006) Reflectance quantities in optical remote sensing – definitions and case studies. Remote Sens Environ 103:27–42
Schreiber U, Bilger W, Neubauer C (1995) Chlorophyll fluorescence as a nonintrusive indicator for rapid assessment of in vivo photosynthesis. In: Ecophysiology of photosynthesis. Springer, Berlin/Heidelberg, pp 49–70
Schull MA, Knayzikhin YV, Xu L, Samanta A, Carmona PL, Lepine L, Jenkins JP, . . ., Myneni RB (2011) Canopy spectral invariants, Part 2: Application to classification of forest types from hyperspectral data. J Quant Spectrosc Radiat Transf 112:736–750
Sellers PJ (1985) Canopy reflectance, photosynthesis and transpiration. Int J Remote Sens 6:1335–1372
Sitch S, Smith B, Prentice IC, Arneth A, Bondeau A, Cramer W, Kaplan JO, . . ., Venevsky S (2003) Evaluation of ecosystem dynamics, plant geography and terrestrial carbon cycling in the LPJ dynamic global vegetation model. Glob Chang Biol 9:161–185
Sivia D, Skilling J (2006) Data Analysis: A Bayesian Tutorial, 2nd edn. Oxford University Press, Oxford
Smolander S, Stenberg P (2005) Simple parameterizations of the radiation budget of uniform broadleaved and coniferous canopies. Remote Sens Environ 94:355–363
Solomon SD, Qin M, Manning M, Chen M, Marquis MB, Averyt M, Tignor M, Miller HL (eds) (2007) Contribution of Working Group I to the Fourth Assessment Report of the Intergovernmental Panel on Climate Change, 2007
Strahler AH (1996) Vegetation canopy reflectance modeling: recent developments and remote sensing perspectives. Remote Sens Rev 15:179–194
Suits GH (1972) The calculation of the directional reflectance of a vegetative canopy. Remote Sens Environ 2:117–125
Tang H, Dubayah R, Swatantran A, Hofton M, Sheldon S, Clark D, Blair B (2012) Retrieval of vertical LAI profiles over tropical rain forests using waveform lidar at La Selva, Costa Rica. Remote Sens Environ 124:242–250
Tarantola A (2005) Inverse Problem Theory and Methods for Model Parameter Estimation, Society for the Industrial and Applied Mathematics (SIAM), Philadelphia, PA
Twomey S (1977) Introduction to the Mathematics of Inversion in Remote Sensing and Indirect Measurements. Elsevier, Amsterdam
Ustin S (2013) Remote sensing of canopy chemistry. Proc Natl Acad Sci USA 110: 804–805
Vargas I, Niklasson GA (1997) Applicability conditions of the Kubelka-Munk theory. Appl Opt 36:5580–5586
Verhoef W (1984) Light-scattering by leaf layers with application to canopy reflectance modeling – the SAIL model. Remote Sens Environ 16:125–141
Verstraete, MM, Pinty B, Dickinson RE (1990) A physical model of the bidirectional reflectance of vegetation canopies. 1. Theory. J Geophys Res 95. D8:11
Verstraete MM, Pinty B, Myneni RB (1996) Potential and limitations for information extraction from remote sensing. Remote Sens Environ 58:201–214
Wang WM, Li ZL, Su HB (2007) Comparison of leaf angle distribution functions: effects on extinction coefficient and fraction of sunlit foliage. Agric For Meteorol 143:106–122
Wanner W, Strahler AH, Hu B, Lewis P, Muller JP, Li X, Barker-Schaaf CL, Barnsley MJ (1997) Global retrieval of bidirectional reflectance and albedo over land from EOS MODIS and MISR data: theory and algorithm. J Geophys Res 102:17143–17161
Widlowski JL, Lavergne T, Pinty B, Verstraete MM, Gobron N (2006) Rayspread: A virtual laboratory for rapid BRF simulations over 3-D plant canopies. In: Frank G (ed) Computational Methods in Transport, Lecture Notes in Computational Science and Engineering Series, 48. Springer, Berlin, pp 211–231
Widlowski JL, Taberner M, Pinty B, Bruniquel-Pinel V, Disney MI, Fernandes R, Gastellu-Etchegorry JP, . . ., Xie D (2007) The third Radiation transfer Model Intercomparison (RAMI) exercise: Documenting progress in canopy reflectance modelling, J Geophys Res 112: D09111

Widlowski JL, Robustelli M, Disney MI, Gastellu-Etchegorry JP, Lavergne T, Lewis P, North PRJ, . . ., Verstraete MM (2008) The RAMI On-line Model Checker (ROMC): A web-based benchmarking facility for canopy reflectance models. Remote Sens Environ 112:1144–1150

Widlowski JL, Pinty B, Clerici M, Dai Y., De Kauwe M, de Ridder K, Kallel A, . . ., Yuan H (2011) RAMI4PILPS: An intercomparison of formulations for the partitioning of solar radiation in land surface models. J Geophys Res 116: G02019, 25

Widlowski JL, Pinty B, Lopatka M, Aztberger C, Buzica D, Chelle M, Disney MI, . . ., Xie D (2013) The fourth Radiation transfer Model Intercomparison (RAMI-IV): Proficiency testing of canopy reflectance models with ISO-13528, J Geophys Res 118:1–22

Woodhouse IH, Nichol C, Sinclair P, Jack J, Morsdorf F, Malthus TJ, Patenaude G (2011) A multispectral canopy LiDAR demonstrator project. IEEE Geosci Remote Sens Lett 8:839–843

Woodhouse IH, Mitchard ETA, Brolly M, Maniatis D, Ryan CM (2012) Radar backscatter is not a 'direct measure' of forest biomass. Nat Clim Change 2:556–557

Wulder M, White J, Nelson R, Næsset E, Ørka H, Coops N, Hilker T, . . ., Gobakken T (2012) Lidar sampling for large-area forest characterization: A review. Remote Sens Environ 121:196–209

Yao T, Yang X, Zhao F, Wang Z, Zhang Q, Jupp D, Lovell J, . . ., Strahler A (2011) Measuring forest structure and biomass in New England forest stands using Echidna ground-based lidar. Remote Sens Environ 115:1144–1150

Zarco-Tejada P, Miller JR, Pedros R, Verhoef W, Berger M (2006) FluorMODgui V3.0: a graphic user interface for the spectral simulation of leaf and canopy chlorophyll fluorescence. Comput Geosci 32:577–591

Zarco-Tejada PJ, Bernia JAJ, Suárez L, Sepulcre-Cantó G, Morales F, Miller JR (2009) Imaging chlorophyll fluorescence with an airborne narrow-band multispectral camera for vegetation stress detection. Remote Sens Environ 113:1262–1275

Chapter 12

Biometric-Based Estimations of Net Primary Production (NPP) in Forest Ecosystems

Toshiyuki Ohtsuka*, Hiroyuki Muraoka
River Basin Research Center, Gifu University, Gifu, Gifu 501-1193, Japan

Nobuko Saigusa
Center of Global Environmental Research, National Institute for Environmental Study, Tsukuba, Ibaraki 305-8506, Japan

Yasuo Iimura
School of Environmental Science, The University of Shiga Prefecture, Hikone, Shiga 522-8533, Japan

and

Hiroshi Koizumi
Faculty of Education and Integrated Arts and Sciences, Waseda University, Shinjuku, Tokyo 162-8480, Japan

*Author for correspondence, e-mail: toshi@green.gifu-u.ac.jp

e-mail: muraoka@green.gifu-u.ac.jp

e-mail: n.saigusa@nies.go.jp

e-mail: iimura.y@ses.usp.ac.jp

e-mail: hkoizumi@waseda.jp

K. Hikosaka, Ü. Niinemets, and N.P.R. Anten (eds.), *Canopy Photosynthesis: From Basics to Applications*, DOI 10.1007/978-94-017-7291-4_12

Summary

Net primary production (NPP) refers to the net amount of the carbon and energy fixed by green plants through photosynthetic activity. Estimates of NPP are of fundamental human importance, because food supply is predominantly dependent on plant productivity. Moreover, measurements of spatiotemporal variations of forest NPP provide important information for understanding and projecting the global carbon cycle, because forest ecosystems are a major terrestrial carbon sink. Here we discuss methods for estimating NPP in forest ecosystems using inventory data, and describe the "summation method", which was developed in Japan in the 1960s at the International Biological Program (IBP) to facilitate standardization in the absence of complex instruments under field conditions. Global climate change prompted to development of this "summation method" as an improved "biometric method" in the 1990s. Biometric-based estimates of NPP are conceptually defined as the total amount of new organic matter produced during an interval per unit area at the ecosystem scale, and are expressed as the sum of stand increments of living biomass (*SI*), newly produced aboveground litter (L_{an}), and fine root production (P_{fr}). The *SI* of above- and belowground (coarse roots) biomass can be estimated by tracking the survival and diameter of individual tree stems in a permanent plot. Aboveground litter of short-lived organs (L_{an}), such as deciduous leaves, flowers, and fruits, can be determined using litter traps that are set on the forest floor. Although methods for determining P_{fr} remain unstandardized, 1-year turnover of fine roots is often considered an estimate of fine root dynamics ($P_{fr} \approx$ mean fine root biomass). In a study of the Takayama Experimental Forest, we demonstrated correlations of biometric-based NPP estimates with various methods, such as simulated canopy photosynthesis by scaling up leaf photosynthesis and incorporating values obtained using eddy covariance. The resulting biometric method has sufficient sensitivity to demonstrate climate-induced year-to-year variations of tree growth and allocation of carbon inputs by NPP in forest ecosystems.

Abbreviations: B – Forest biomass; B_{t1} – Forest biomass at time t_1; B_{t2} – Forest biomass after an interval at time t_2; B_{2n} – The amount of new organic matter retained by live plants after an interval at time t_2; BI_s – Biomass increments of surviving trees during an interval; BI_i – Biomass increments of ingrowth trees during an interval; *D,* DBH – Diameter at breast height; GPP – Gross primary production; IPCC – Intergovernmental Panel of Climate Change; IBP – International Biological Program; LAI – Leaf area index; L – The amount of loss of organic matter from plant biomass during an interval; L_{an} – The amount of aboveground plant litter produced and shed during an interval; L_n – The amount of organic matter both produced and lost by plants during an interval; L_o – The amount of loss of old plant biomass present at time t_1 during an interval; M – Necromass by tree mortality during an interval; NEP – Net ecosystem production; NPP – Net primary production; P_n – The amount of organic matter newly produced during an interval; P_{fr} – Fine root production; RA – Autotrophic respiration (plant respiration); RE – Ecosystem respiration; RH – Heterotrophic respiration; RH_{CWD} – Heterotrophic respiration that decomposed coarse woody debris; RH_{SOM} – Heterotrophic respiration that decomposed litter and soil organic matter; SI – Stand increment of forest biomass; V_{cmax} – Maximum velocity of carboxylation; W – Dry mass of tree; W_s – Dry mass of tree stem; ρ – Species-specific stem wood density

I. Introduction

Solar radiation provides energy for the entire terrestrial life and enters the biosphere as organic matter following photosynthetic assimilation by green plants (Hutchinson 1970). However, only a small portion of the solar radiation that reaches the biosphere is converted into organic matter, and the rate at which the production of organic matter varies spatially depends on the climatic conditions. Net primary production (NPP) refers to the net amount of carbon and energy fixed by photosynthesis in green plants, and is critical as an indicator of human food supply, which is almost solely dependent on plant productivity, as well as wood for construction and fuel (Imhoff et al. 2004).

Production ecology at the ecosystem scale has flourished since the 1960s within the International Biological Program (IBP), which considers the biological basis of productivity and human welfare. Recognizing the problem of a rapidly increasing human population, this program takes scientific knowledge as the foundation for rational resource management. IBP has instigated numerous ecological production studies in various biomes to map global NPP and to investigate controlling climatic conditions (Lieth and Whittaker 1975). However, structural complexities and volumes of biomass hamper estimates of NPP in forest ecosystems. Thus, in Japan, the "summation method" was developed to estimate forest NPP in various tropical–boreal forest ecosystems and to facilitate standardization in the absence of complex instruments under field conditions (Newbould 1970; Shidei and Kira 1977; Satoo 1982). NPP correlates most strongly with precipitation. When dry ecosystems are excluded, NPP also increase exponentially with increasing temperature. Regression models of global primary productivity (Lieth 1975) have been derived from empirical relationships between climate and NPP.

In the 1980s, scientists indicated that human activities are leading to increases in atmospheric CO_2 levels (Esser 1987). However, the understanding of the global carbon budget and the effects of climatic change remained approximate and were under continuing investigation. In particular, the first report of the Intergovernmental Panel on Climate Change (IPCC) revealed a "missing carbon sink" that comprised the difference between the net annual anthropogenic addition of carbon (C) to the atmosphere and the annual sum of the net increase in atmospheric C (IPCC 1990). Subsequently, this missing carbon sink was presumed to reflect net oceanic uptake over the past two decades, and suggested that forest ecosystems play a potentially important role as residual terrestrial C sinks, and measurements of spatiotemporal variations in productivity are essential for understanding and projecting the global carbon cycle (Schimel et al. 2001).

A micrometeorological method for measuring CO_2 exchange between forest canopy and the atmosphere under field conditions was developed in the 1990s using a flux tower (Baldocchi 2003; Saigusa et al. 2002) and is known as the "eddy covariance method" (cf. Chap. 10, Kumagai 2016). However, site-level component estimates must be cross-checked between eddy covariance and inventory data (Barford et al. 2001; Black et al. 2007; Gough et al. 2008). Thus, the requirement of inventory-based carbon dynamics led to the development of the summation method as an improved "biometric method" for use beneath flux towers (Curtis et al. 2002). Accordingly, precise biometric measurements are used to directly estimate assimilated carbon partitioning and sequestration into woody biomass or dead necromass pools in forest ecosystems (Ohtsuka et al. 2013). Pan et al. (2011) presented bottom-up estimates of C stocks and fluxes for the world's forests based on inventory data. In their study, the total forest sink from 1990 to 2007 was 2.4 ± 0.4 Pg C y^{-1} globally, which is equivalent to the terrestrial sink deduced from fossil fuel emissions, land-use changes, and oceanic and atmospheric sinks.

The biometric method evaluates spatial variability of NPP at different biomes and also temporal variability of NPP, such as that from climate-induced year-to-year changes of tree growth (Clark and Clark 1994; Clark et al. 2003; Ohtsuka et al. 2009), and variations during forest stand development (Shan et al. 2001; Meigs et al. 2009; Ohtsuka et al. 2010). Long-term inventory forest ecosystem data from standardized and highly accurate methods are gaining importance because life cycle analyses of climate and disturbance effects are increasingly necessary for predictions of forest C stocks under current and future climates. In this chapter, we describe how forest production rates can be estimated using the summation method and how this biometric method has been improved with field measurements in permanent plots. We also discuss how biometric-based estimates can be applied to evaluate tower-based measurements of forest C flux, as demonstrated in experiments at the Takayama Experimental Forest.

II. Production Processes at Ecosystem Scales

Gross primary production (GPP) refers to photosynthetic assimilation rates at the ecosystem scale. Carbon that enters ecosystems as GPP accumulates within ecosystems as organic matter and returns to the atmosphere via respiration. About half of GPP is respired by plants to support growth and maintenance (Waring et al. 1998). Hence, NPP refers to the total net photosynthetic production of an entire ecosystem and is the difference between GPP and total autotrophic (plant) respiration (RA).

Net ecosystem production (NEP) is defined as the rate of carbon accumulation in an ecosystem (Randerson et al. 2002). CO_2 exchange between the forest canopy and the atmosphere is often measured using the eddy covariance method, and NEP is calculated as the balance between autotrophic photosynthetic assimilation (GPP) and respiratory effluxes at the ecosystem scale (ecosystem respiration, RE). Alternatively, biometric-based NEP can be calculated from ecological inventories of various compartments and field-based flux measurements (Curtis et al. 2002; Ohtsuka et al. 2007, 2010). RE comprises respiratory effluxes from autotrophs (RA) and heterotrophs (RH), and biometric-based estimations of NEP beneath a flux tower can then be used to determine the balance between NPP and RH in an ecosystem as follows:

$$\begin{aligned} \mathrm{NEP} &= \mathrm{GPP} - \mathrm{RE} \\ &= (\mathrm{NPP} + \mathrm{RA}) - (\mathrm{RA} + \mathrm{RH}) \\ &= \mathrm{NPP} - \mathrm{RH} \end{aligned} \tag{12.1}$$

III. Inventory-Based Forest Net Primary Productivity (NPP) Estimates

A. Summation Method

It is impractical to perform inventory-based estimations of forest NPP in terms of the difference between GPP and RA. In the summation method, NPP is defined as the total new organic matter produced during an interval per unit area, and it can be expressed in units of dry organic matter (ton ha^{-1} $year^{-1}$). Figure 12.1 shows schematic changes in biomass in a forest ecosystem, where B_{t1} is forest biomass at time t_1 and B_{t2} is forest biomass after an interval (usually > 1 year) at time t_2. NPP comprises newly produced organic matter during the same interval (P_n). The fraction of P_n that accumulates during the growth of plant parts is lost during the same interval (L_n), and B_{2n} is the new organic matter retained in the biomass at time t_2. Old biomass present at t_1 is also lost during the same interval (L_o). Thus, B_{t2} is defined by the following equation:

$$B_{t2} = (B_{t1} - L_o) + (P_n - L_n)$$

Thus,

$$\begin{aligned} \mathrm{NPP}(P_n) &= (B_{t2} - B_{t1}) + (L_o + L_n) \\ &= \Delta B + L \end{aligned} \tag{12.2}$$

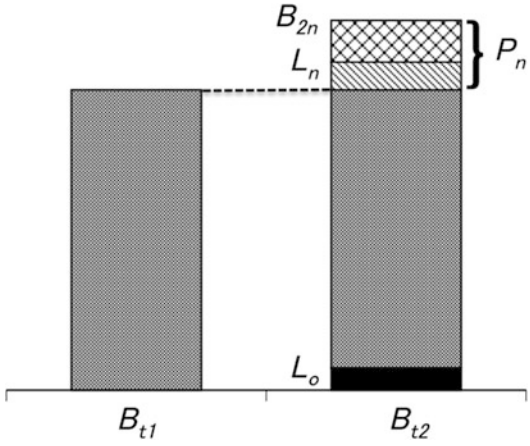

Fig. 12.1. Schematic diagram showing the change in forest biomass during an interval between times t_1 and t_2. B_{t1} and B_{t2} are forest biomass at times t_1 and t_2, respectively. NPP is defined as newly produced organic matter during the interval ($P_n = B_{2n} + L_n$). Fractions of P_n (L_n) and B_{t1} (L_o) are lost during the interval because of plant death, herbivory, etc. B_{2n} is new organic matter retained by biomass at time t_2

These equations form the basic principle of the summation method and can be used to estimate NPP as the sum of the biomass increment (ΔB) and the output terms (L) without measuring input (Ogawa 1977).

Values of ΔB are determined by conducting censuses at least twice at times t_1 and t_2, although this is often impractical, especially in forest communities. Alternatively, stem analyses are commonly performed by measuring increments of stem volumes in sample trees over several years. Stem volume is calculated as the change in the volume of each cylinder, as delineated by the annual rings of each disk, and the cross-sectional area of each cylinder is taken as the mean area of the rings at each end of the cylinder (Fig. 12.2a). Stem volume increments are then converted into dry mass growth using volume-to-mass ratios for each disk. The total stem growth in the stand (ΔB) is calculated from all present tree stems

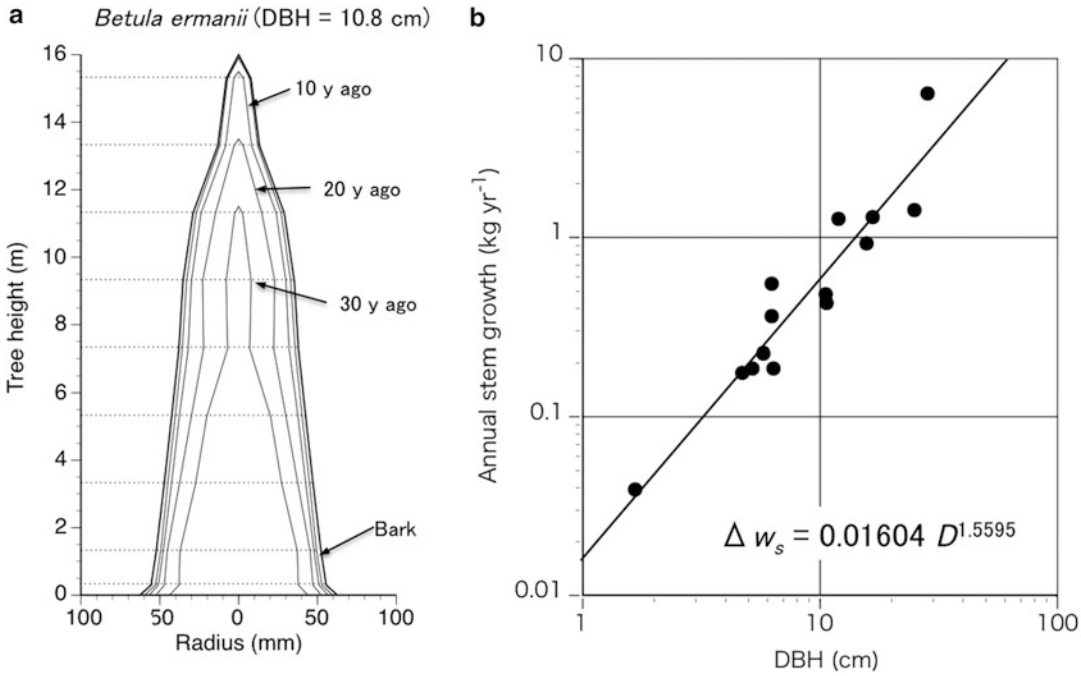

Fig. 12.2. Example of stem analysis of *Betula ermanii*. (**a**) Stem volume increment of the sample tree was measured from diameter growth of annual rings of 10 disks at different tree heights, as shown by broken lines and the disk at 0 m. (**b**) Allometric relationship between annual stem growth of sample trees (Δw_s) and their DBH (D) using the stem analysis

Fig. 12.3. A litter trap set on the forest floor. The trap was made from small mesh net and had an area of 1 m^2

using the logarithmic relationship between annual increases in stem mass (Δw_s) and diameters at breast height (DBH) in sample trees (Fig. 12.2b) as follows:

$$\Delta w_s = a\ D^k \tag{12.3}$$

where a and k are constants and D is the DBH of sample trees.

Loss due to shedding of leaves or death of plants (litter) in forest ecosystems can be estimated using litter traps, and losses other than litter fall, such as herbivore loss, are frequently considered negligible. These litter traps are baskets with small mesh nets; they usually cover an area of 1 m^2 (Fig. 12.3) and are set on the forest floor to trap aboveground litter, such as leaves, twigs, and fruits. Litter fall is collected every month and is oven-dried to a constant mass. The summation method using Eq. 12.2 is easy to use under field conditions because it is not necessary to separate the loss of organic matter into old parts (L_o, barks and branches produced outside the measuring period) and new parts (L_n, leaves produced by deciduous trees during the current year).

The summation method was first proposed in the 1960s and still provides reliable standardized NPP estimates in the absence of complex instruments under field conditions. However, temporal resolutions of eddy covariance and summation methods differ greatly; although the former measures carbon accumulation rates on an hourly to daily time scale, the latter measures these on a yearly scale and is based on longer average data. Ogawa (1977) noted that the estimation of biomass increments using the logarithmic relationship between annual increases in stem mass and DBH (Eq. 12.3) is not actually identical with ΔB because the growth of large trees that die during the interval is ignored in stem analyses. Hence, field-measurement-based parameters are not clearly defined in the summation method, restricting ΔB to a long-term average of aboveground biomass increments, L to aboveground litter fall, and NPP to the sum of ΔB and L.

Table 12.1. The components of forest NPP including the organic matters to be quantified in field conditions

The components of forest NPP		Quantified method
Increments of new organic matter that retained by biomass at the end of an interval (B_{2n} in Fig. 12.1)		
Aboveground	Stand Increment of biomass *(SI)*	Allometry
Belowground	Stand Increment of coarse roots *(SI)*	Allometry
	Net fine root increment	Minirhizotoron or assumption of no increase
	Stores of non–structural carbohydrate	Not quantified
Losses of new organic matter that produced during an interval (L_n in Fig. 12.1)		
Aboveground	Fine litter fall (L_{an})	Litter traps
	Losses to herbivores	Litter traps with metabolism experiment
	Volatile and leached organics	Not quantified
Belowground	Dead fine roots ($\approx P_{fr}$)	Minirhizotoron or repeated sampling of fine root biomass
	Root losses to herbivores	Not quantified
	Root exudates	Not quantified
	Carbohydrate export to symbionts	Not quantified

B. Biometric Estimates of NEP and NPP Beneath a Flux Tower

Biometric NEP beneath a flux tower is a measure of the balance between NPP and RH in an ecosystem (Eq. 12.1). Almost all RH arise from the soil layer in forest ecosystems, which are more or less detritus-based trophic systems. Therefore, soil respiration is an important parameter in biometric-based estimations of NEP. Soil respiration is divided into heterotrophic respiration that decomposes litter and soil organic matter (RH_{som}) and plant root respiration that decomposes plant assimilated organic matter (Hanson 2000; Kuzyakov 2006). Moreover, dead wood on forest floors (coarse woody debris) is an important component that is decomposed by heterotrophs (RH_{cwd}); however, it is not usually included in the estimates of soil respiration (Gough et al. 2007; Ohtsuka et al. 2014). Therefore, biometric-based NEP is described as follows:

$$\mathrm{NEP} = \mathrm{NPP} - (\mathrm{RH_{som}} + \mathrm{RH_{cwd}}) \qquad (12.4)$$

Comparisons of biometric- and eddy covariance-based NEP estimates in forest ecosystems indicate the need for improvement of the summation method with adjustments of time scales and inclusion of other components, especially those from below the ground. Accordingly, the biometric-based estimates of NPP included estimates of new organic matter retained by live plants at the end of an interval and organic matter produced and lost by the plants during the same interval (Table 12.1). Increments of new organic matter are conceptually equivalent to B_{2n}, and losses of new organic matter are conceptually equivalent to L_n in Fig. 12.1. Hence, biometric-based estimates of NPP do not differ from those of the summation method, and is described as follows:

$$\mathrm{NPP}(P_n) = B_{2n} + L_n \qquad (12.5)$$

Note that B_{2n} differs from ΔB in Eq. 12.2, and L_n is only the fraction of losses that were produced during the interval ($L_n \neq L$).

Reliable assessments of forest NPP using the biometric method will require quantification of all materials that contribute to total NPP (Table 12.1). Although the components of all organic matter that are fixed during an interval are readily conceptualized (Table 12.1), it is difficult to measure these parameters (B_{2n} and L_n) directly in the field because of transformations that occur during measurement intervals. Instead, NPP must be estimated on a suite of measurement types, invoking numerous underlying assumptions of field- measurement-based operational estimates (Clark et al. 2001). Thus, field-measurement- based parameters must be clearly defined (Table 12.1). B_{2n} mainly

comprises *SI* of aboveground and coarse root biomass in forest ecosystems. L_{an}, as a principal part of L_n, is defined as aboveground litter to accommodate the loss of new organic matter produced by plants during an interval.

IV. Field NPP Measurements

Since the 1980s, the dynamics of plant communities in forest ecology have predominantly been assessed with long-term monitoring of annual tree survival and growth in large permanent plots (Clark et al. 2003). This technique could be adapted for the study of forest production in the Takayama Experimental Forest (Ohtsuka 2012), and biometric-based estimations of NPP can be used to standardize the methods for field measurements.

Takayama Experimental Forest is located on the mid-slope of Mt. Norikura at the Takayama Field Station (36°08′N, 137°25′E, 1420 m above sea level), River Basin Research Center, Gifu University, central Japan. A tower for measuring CO_2 flux using the eddy covariance method is located in a hilly area (Yamamoto et al. 1999), and a permanent plot of 1 ha (100 × 100 m) was established on a west-facing slope to study biometric estimations of NEP in 1998. The flux tower is included in the permanent plot, and temporal variations in canopy leaf area index (LAI) and leaf photosynthetic capacity (V_{cmax}) were monitored to assess seasonal and interannual variations in forest canopy photosynthesis (Muraoka et al. 2010). Further details of the site are described in previous studies by Saigusa et al. (2002), Murayama et al. (2003) and Ohtsuka et al. (2005). The vegetation in the permanent plot is that of a cool-temperate deciduous broad-leaved forest and the dominant tree species are *Quercus crispula*, *Betula ermanii*, and *B. platyphylla* var. *japonica*.

A. Increments of Organic Matter

1. Aboveground Biomass

SI of aboveground biomass can be estimated by tracking the survival and DBH of individual tree stems of trees with a minimum DBH in a permanent plot as follows:

$$SI = \sum BI_s + \sum BI_i \qquad (12.6)$$

where BI_s represents aboveground biomass increments of surviving trees in the plot and BI_i represents aboveground biomass increments of ingrowth trees that reach the minimum DBH during the study period. Increments of biomass for each tree were computed as the difference between estimated biomass at the beginning and end of study periods using allometric equations. Tree biomass allometric equations were derived by harvesting trees and determining dry biomass (W) relative to DBH (D) as follows:

$$W = b\ D^c \qquad (12.7)$$

where b and c are constants. We did not measure DBH of ingrowth trees in the previous year and assumed biomass at the beginning as the tree biomass of minimum DBH. If the measurement interval was 1 year, increases in woody masses of trees that died during the interval were ignored. To eliminate duplicate measurements of the same foliage in NPP estimates, aboveground biomass increments are estimated using biomass allometric equations that exclude foliage mass in deciduous forests.

A metallic, narrow width tape measure (e.g., Diameter Tape; Nihon Doki Co., Ltd.) was used for field DBH measurements, which were taken at the same painted position to reduce human error, although some diameter growth data may indicate negative increments. Some investigators record negative diameter growth as a biomass increment

Fig. 12.4. Example of a dendrometer used to measure annual tree growth under field conditions. This dendrometer consists of an aluminum band with a stainless spring

of 0. However, some weakened tree stems show decreased diameters. Moreover, as suggested by Clark et al. (2001), among trees that do not grow during a census interval, approximately half of their increments will be measured as negative and half as positive. Thus, discarding false negatives and retaining false positives causes artificial gains of stand biomass, necessitating inclusion of negative biomass increments in Eq. 12.6.

Annual diameter growth can be measured using a dendrometer to reduce human error (Fig. 12.4). However, dendrometer measurements are not practical for all trees in large permanent plots and are best used in practice for trees with large diameters that contribute a large proportion of *SI*. Moreover, dendrometers require maintenance over long periods of time because the springs and bands rust, and they can be destroyed by deep snow above breast height during winter in cool-temperate regions.

In the Takayama Forest, we generated allometric equations for aboveground stem biomass (W_s) from 24 sample trees with DBHs of 5–37 cm (Ohtsuka et al. 2005) as follows:

$$W_s = 0.1133\ \mathrm{DBH}^{2.334} \tag{12.8}$$

We also measured annual increases in DBH of all tree stems in the permanent plot during late autumn (November to December) at the same painting position on all living stems of trees with DBH >5 cm. Moreover, to accommodate deciduous species, annual woody mortality and recruitment was estimated from annual tree censuses that were conducted in the plot during each summer. Thus, *SI* (aboveground and coarse roots) and necromass from annual tree mortality (M) were monitored annually in the permanent plot (Fig. 12.5a), and changes in forest biomass ($\Delta B = SI - M$) were measured (Fig. 12.5b). Despite high *SI*, many trees died at the Takayama Experimental Forest during 2001–2002 and biomass decreased ($\Delta B < 0$) during the interval (Fig. 12.5b).

Biomass accounting using allometric equations is a potential source of error in the estimations of *SI*. Thus, the importance of site-specific allometric equations for accurate estimates of tree biomass is widely recognized, and these reflect intersite variations in factors such as tree architecture and wood density. Moreover, interpolation

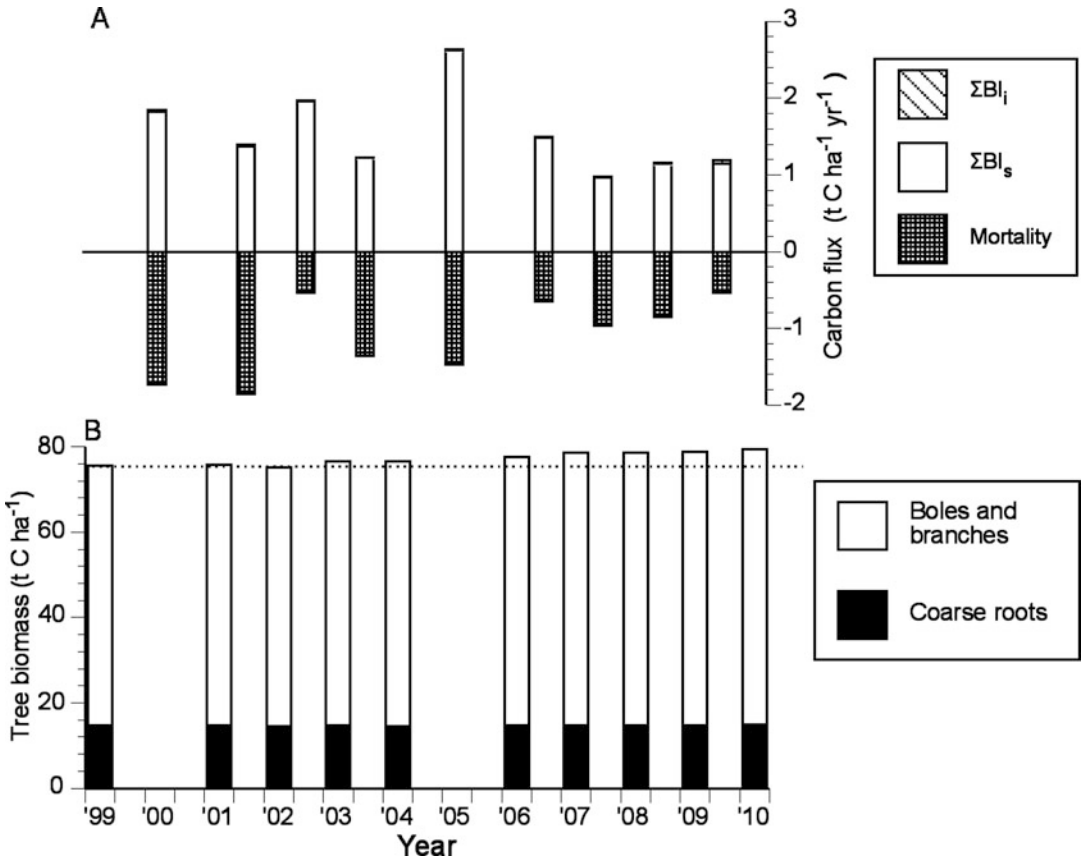

Fig. 12.5. Monitoring of forest stand dynamics and annual biomass change during 1999–2010 in the Takayama Forest. (**a**) Annual stand increment (*SI*) is the sum of biomass increments of individual surviving trees (ΣBI_s) and biomass increment(s) of ingrowth (ΣBI_i). Carbon fluxes (A) during 1999–2001 and 2004–2006 show the total for 2 years, and thus, the unit is t C ha^{-1} 2 $year^{-1}$ only for these two periods. (**b**) Forest biomass change with *SI* and necromass of mortality (*M*) as $\Delta B = SI - M$

using allometric equations with insufficient samples sizes leads to large errors because tree biomass increases exponentially with DBH. Komiyama et al. (2011) recently described generalized allometric equations for Japanese cool-temperate regions, including conventional allometric equations and equations that include species-specific stem wood density (ρ, kg m^{-3}). These equations were derived from 100 sample trees with DBHs of 5–67 cm, and included 20 tree species of deciduous and evergreen coniferous trees. In the present study, these generalized equations produced almost the same value as Eq. 12.8 when DBH was <10 cm (Fig. 12.6). However, generalized conventional allometric equations indicated 33 % larger biomass at 50-cm DBH and 38 % larger biomass at 70-cm DBH (almost the largest living tree in the Takayama Forest) compared with values from Eq. 12.8. Moreover, when tree density was added as a parameter, the difference was greater for *Q. crispula*. Hence, accurate biomass estimates are critical for the few large trees, and large sample sizes are essential for the derivation of allometric equations that enable interpolation of tree biomass (Chave et al. 2005; Ketterings et al. 2001).

Estimates of biomass are also confounded by seasonal timings of diameter measurements, because annual diameter growth is always <1 cm and is mostly <0.5 cm $year^{-1}$ in the Takayama Forest. Thus, inappropriate tree measurement methods strongly affect *SI* estimates. In cool-temperate deciduous

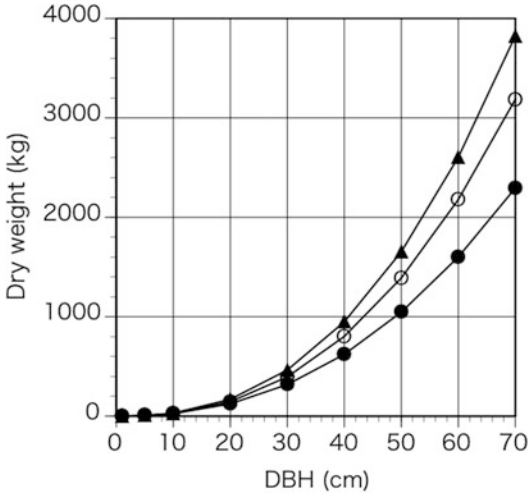

Fig. 12.6. Estimation of individual tree aboveground woody mass (W kg, except for foliage) using three allometric equations relating biomass to DBH (D cm). ●, Allometry in the Takayama Forest (Ohtsuka et al. 2005, $W = 0.1133\ D^{2.334}$); ○, generalized conventional allometry for the Japanese cool-temperate region (Komiyama et al. 2011, $W = 0.08977\ D^{2.466}$); and ▲, generalized allometry using species-specific stem-wood density ($W = 0.1853\ \rho D^{2.491}$). We used the stem wood density of *Quercus crispula* ($\rho = 0.5228$ kg m^{-3}), which is the dominant species in the Takayama Forest, as an example

forests, diameter growth precedes leaf budbreak in spring in ring-porous species such as *Quercus* spp., and diameter growth begins after leaf budbreak in diffuse-porous species such as *Acer* spp. (Komiyama 1991). Hence, estimates of annual tree growth require measurements of DBH in autumn after the cessation of diameter growth in both ring- and diffuse-porous species and not in early spring before leaf flush.

2. Belowground Biomass

An allometric equation incorporating belowground coarse roots and DBH was derived from tree harvests (Ohtsuka et al. 2005; Komiyama et al. 2011) using the same approach as for aboveground parts. The annual *SI* of belowground coarse roots was estimated, and the potential sources of error were identical to those for aboveground *SI*. However, definitions of coarse and fine roots are critical to the application of this method. The smallest roots that are commonly classified as "coarse roots" (often 2–10 mm in diameter) are unlikely to be well characterized in biomass allometric approaches because of breakage and incomplete sampling during the excavation of root systems (Clark et al. 2001). Moreover, net fine root increments are difficult to measure because they are short lived and their appearance is spatially and horizontally variable. Methods for assessing the production of fine roots are discussed in the last part of this article.

Temporary stores of assimilated carbon form another incremental pool of organic matter. However, it remains impossible to estimate the annual accumulation of non-structural carbohydrates in forest ecosystems using allometric equations. Nonetheless, several studies suggest the importance of starch accumulation in forest ecosystems, and this may account for discrepancies between interannual variations in eddy-covariance-based and biometric-based estimates. For example, interannual changes in tower-based GPP estimates did not correlate with changes in tree rings in a Scots pine forest growing in central Siberia (Shibistova et al. 2002). These data suggested that interannual changes in the demand of carbohydrates for new stem production might be compensated by changes in growth rates of other parts of the tree or by increased starch accumulation.

B. Loss of Organic Matter

1. Aboveground Losses

The above-ground plant litter of short-lived organs (L_{an}) was collected every month from litter traps set on the forest floor (Fig. 12.3). The litter was separated into foliage, other newly produced organs (such as flowers, fruits, and stipules), woody materials, and other litter (such as insect feces), and parts were oven-dried to a constant mass and were weighed. In cool-temperate regions,

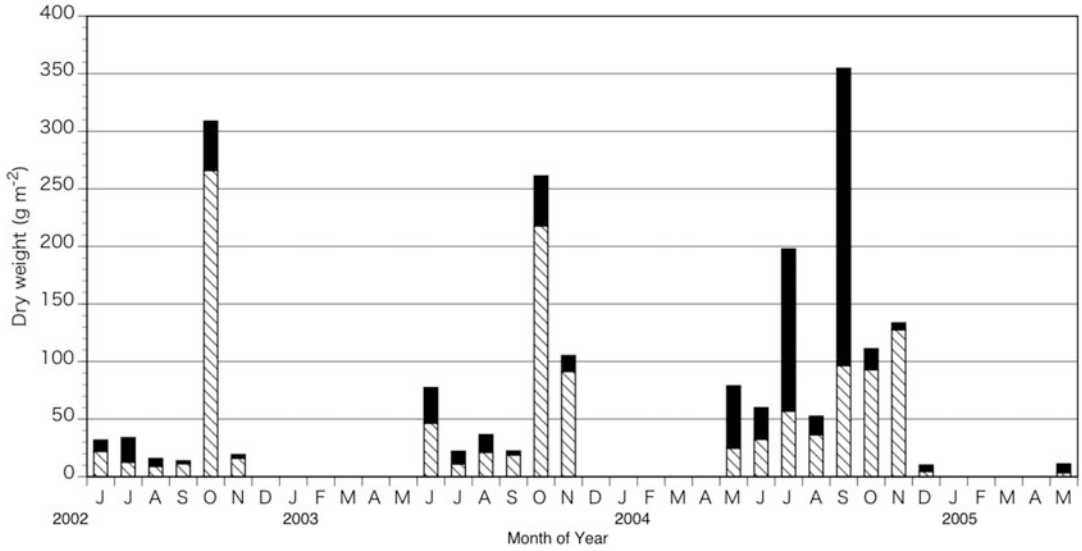

Fig. 12.7. Seasonal changes in litter mass using 14 litter traps in the Takayama Forest. ▧, Foliage mass; ■, other woody materials. It is difficult to collect material in winter (usually from December to the following April) in the Takayama Forest because of heavy snowfall. However, we set litter traps in winter, and winter litter was collected in early spring before leaf flush (usually in early May after snow melt) and added to the annual production of the preceding year

accumulated snow fall hampers the collection of litter from litter traps during winter. However, some dead leaves remain on the branches after leaf senescence, and fall as a result of snow events. Thus, litter traps were set in winter and litter that was collected early in spring before leaf flush was added to the annual production of the preceding year.

NPP studies are notoriously unstandardized for woody fine litter fall. Because large fallen branches are mostly woody materials produced in previous years, they were excluded from the calculation of L_{an}. However, large amounts of woody material may be shed during measurement intervals, and sample trees that are used to derive allometric equations may include those shedding woody material. Thus, woody material was included in the calculation of NPP. Accordingly, inter-trap variance in woody litter mass was higher than that in fine litter because of the presence of unusually large items, such as large dead branches trapped under field conditions. Year-to-year variance in woody litter mass was also higher than that in foliage litter, and a large amount of woody material was shed in winter and early spring following snowfall. Thus, long-term measurements require estimates of annual woody litter mass from the winter season in forest ecosystems.

Forests that are entirely composed of evergreen trees, whose leaves remain for >1 year, require special consideration because annual leaf litter fall from these species includes production from both current and previous years. Accordingly, foliage mass initially increases with forest age and subsequently reaches an equilibrium in the middle stages of stand development. The current year and all previous years should therefore be included in the estimates of annual NPP to accommodate mass balance considerations in mature evergreen forests.

In the present study, 14 litter traps were set at varying topographical positions in the Takayama Forest, and plant litter was collected every month in the snow-free season (usually May–November; Fig. 12.7). Foliage

Table 12.2. Annual total litter mass (dry weight) and coefficient of variation (CV) among 14 litter traps in the Takayama Forest during 2001–2009

Year	2001	2002	2003	2004	2005	2006	2007	2008	2009
Foliage litter (g m^{-2} $year^{-1}$)	387.3	382.8	384.4	450.0	362.9	347.1	362.8	340.8	357.2
CV (n = 14)	13.3	11.4	14.8	9.1	12.2	12.4	13.5	11.4	14.4
Required trap number	8	6	10	4	7	7	9	6	10
Other woody litter (g m^{-2} $year^{-1}$)	137.1	117.9	142.0	481.0	73.6	222.4	114.3	461.9	168.3
CV (n = 14)	72.1	40.5	64.7	89.8	45.7	141.8	34.5	206.8	47.9
Required trap number	243	77	195	376	98	938	56	1994	107

We calculated required litter trap numbers using an equation described in Adachi et al. (2005) within a specified confidence interval: $n = t_a^2 s^2 / D^2$, where n is the required sample size, t_a is the Student's t statistic with degrees of freedom at the a confidence level, s is the standard deviation of litter mass, and D is the specified error limit .In the present study, we estimated the required number of litter traps at the 95 % confidence level and specified error limits equal to 10 % of the sample means.

litter volumes differed little between litter traps and survey years (Table 12.2) in the Takayama Forest. Coefficients of variation (CV) of foliage litter among traps for each year ranged from 9.1 to 14.8 between 2001 and 2009, and the required sample size (number of traps) to estimate with a ±10 % error of mean foliage litter mass was only 4–10. Hence, field studies based on presampling quantifications of inter-trap variances in collected material are required, and 10 litter traps might be sufficient under a closed canopy in cool-temperate deciduous forests. The required sample size (trap numbers) for estimating woody litter fall was 56–1994 (Table 12.2), requiring at least 10 % of the forest area for the accurate estimation of woody litter. Thus, woody litter was excluded from the calculation of L_{an} in the Takayama Forest.

2. Fine Root Dynamics

Owing to methodological challenges and incomplete measurements, belowground production in forests remains poorly understood, especially in terms of fine roots. Fine roots are considered to be the most biologically active and show rapid turnover (Eissenstat and Yanai 1997). However, these roots usually contribute little to total root biomass, with fine root production (P_{fr}) contributing >30 % of tree NPP, and fine root biomass contributing <2 % of tree biomass in the Takayama Forest (Ohtsuka et al. 2005). However, estimates of both fine root production and fine root biomass remain uncertain owing to temporal and spatial variability (Vogt et al. 1998; Brunner et al. 2013).

The minirhizotron approach is based on sequential video images that are recorded by a camera within a buried transparent tube (Fig. 12.8a, b) and that enable direct observations of growth and mortality of fine roots (Aerts et al. 1989; Steele et al. 1997). However, the instrument is expensive. Moreover, it is difficult to distinguish between live and dead roots using scanned data (Fig. 12.8c, d), and no methods for the precise estimations of fine root growth and dead fine root length have been reported. Therefore, it remains impossible to standardize estimates of fine root production for the biometric determinations of NPP in forest ecosystems.

Previous studies have estimated belowground carbon dynamics based on the assumption that fine roots turn over annually (Trumbore et al. 1995). In the absence of increases in fine root biomass, annual new production of fine roots is almost equal to the production of dead fine roots, irrespective of current and previous fine roots. In the Takayama Forest, annual fine root production (P_{fr}) was estimated at 1.8 t C ha^{-1} $year^{-1}$ using a minirhizotron approach (Satomura et al. 2006), and it was similar to the mean fine root biomass (1.6 t C ha^{-1}), indicating a fine root turnover time of 0.89 $year^{-1}$. Brunner et al. (2013) recently reviewed root turnover in common European forests,

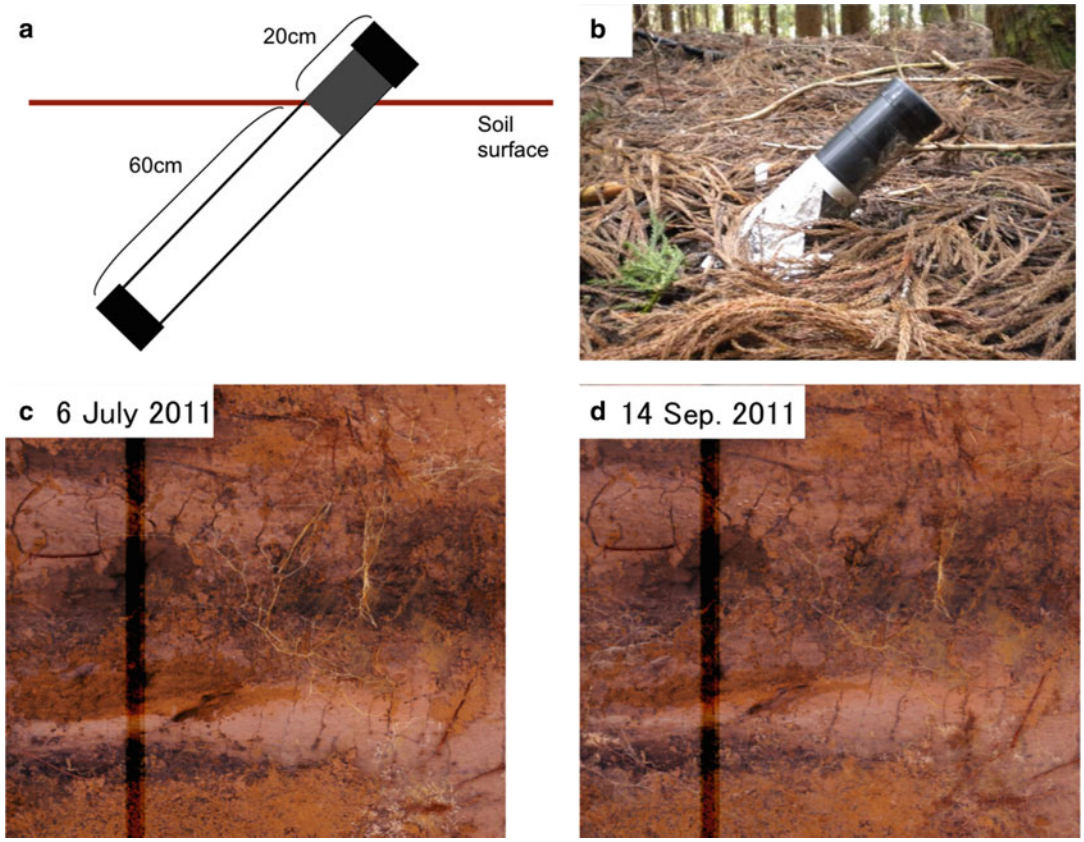

Fig. 12.8. (**a, b**) A transparent tube with a minirhizotron is used to measure fine root growth and death rates on the basis of sequential video images. (**c, d**) Examples of successive root scan data for July 6 and September 14 in a cool-temperate forest

and suggested that the turnover time of fine roots for end users ranged from 0.88 to 1.11 year^{-1}. Therefore, the assumption of a 1-year turnover of fine roots (P_{fr} ≈ mean annual fine root biomass ≈ annual dead fine root nercromass) is practical for estimating fine root dynamics in the field, and repeated destructive sampling is recommended for assessments of standing stocks of fine roots for biometric-based estimations of NPP.

3. Other Losses

Few studies of aboveground losses to herbivores have been performed using biometric-based estimations of NPP, and herbivore loss is often considered negligible in healthy stands (Kimura et al. 1982; Schowalter et al. 1986). Clark et al. (2001) estimated the potential impact of leaf herbivory in field measurements of NPP components and assumed that 15 % of the mass of new foliage is lost to herbivores and NPP may be underestimated by a maximum of 7 % in tropical forests. However, the importance of herbivore losses depends on forest community types. For example, cycling outbreaks of several forest-defoliating insects are well known in Japan (Kamata 2002) and contribute considerable interannual variations in biometric-based NPP estimates. Caterpillars that eat live leaves can be trapped using litter traps as they drop, allowing the estimation of herbivore loss for caterpillars using metabolic experiments. However, estimating herbivore losses using litter traps requires the use of a

net with a fine mesh and more frequent collection of litter from the field. This might be important in monodominated forests, such as cool-temperate beech forests (Liebhold et al. 1996), although no large defoliations due to caterpillar outbreaks were observed during 1998–2010 in the Takayama Forest.

Bekku et al. (1997) found that root exudates accounted for 3–13 % of NPP in temperate weed communities. However, no studies have included estimates of root exudates, root herbivory, or volatile or leached organic carbon as losses of organic matter in biometric estimations of NPP in forest ecosystems. Thus, the potential impact of other losses on NPP remains unclear, especially from belowground parts.

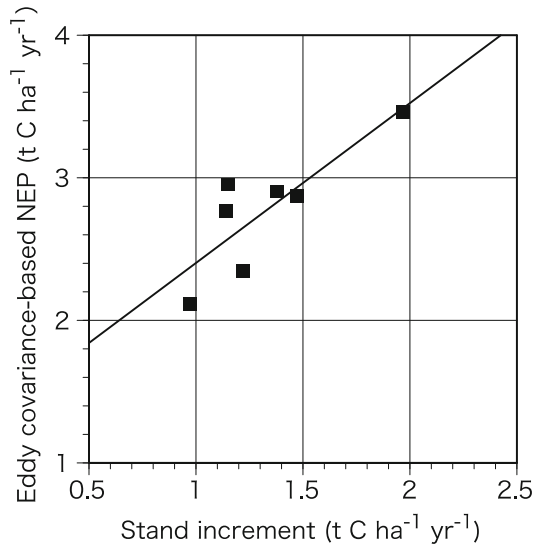

Fig. 12.9. Relationship between annual stand increment of biomass (*SI* in Fig. 12.5) and eddy covariance-based NEP estimates over the 10-year study period in the Takayama Forest. *SI* was positively correlated with NEP estimated using the eddy covariance-based method, while the value was smaller than the NEP value

V. Comparisons of NPP Estimates in the Takayama Experimental Forest

Annual measurements of DBH growth and mortality were taken in the Takayama Experimental Forest from 1998, and *SI* and L_{an} (foliage litter mass) were calculated (Fig. 12.5, Table 12.2). Fine root production (P_{fr}) was estimated as 1.8 t C ha^{-1} year^{-1} using a minirhizotron camera and was assumed to be annually constant. Thus, we presented annual biometric-based NPP estimates for trees as $SI + L_{an} + P_{fr}$ during the study period. Year-to-year variance in biometric-based NPP estimates allowed comparison with the interannual variability of eddy-covariance-based NEP estimates, and with the exception of 2-year values (Fig. 12.5a), *SI* varied between 0.97 t C ha^{-1} year^{-1} in 2007 and 1.96 t C ha^{-1} year^{-1} in 2002. In contrast, L_{an} was almost constant, irrespective of the climatic variation in the Takayama Forest (Table 12.2). Trends in interannual variation in eddy-covariance-based NEP estimates were positively correlated with those of *SI* (Fig. 12.9), suggesting that interannual variability in ecosystem C exchange was directly responsible for much of the interannual variation in tree production (Ohtsuka et al. 2009). Early in the growing season, temperature and early leaf flush were shown to be prime determinants of tree production in the Takayama Forest, in both eddy covariance (Saigusa et al. 2005) and GPP simulation analyses (Muraoka et al. 2010).

These parallel changes in biometric and eddy covariance NEP estimates confirm the reliability of both annual estimates. Moreover, although *SI* represents actual annual C sequestration as forest woody mass, it is smaller than annual eddy-covariance-based NEP estimates (Fig. 12.9), which indicates C sequestration in tree biomass and in other C pools. These "missing sinks" at the Takayama Forest suggest constant net accumulation in nonliving pools (such as dead trees and humus in the soil) or indicate large contributions of other NPP fractions.

Muraoka et al. (2010) simulated year-to-year variations in GPP estimates using a land surface model with adjustments of model parameters such as V_{cmax} and LAI. Leaf-photosynthesis-based GPP estimates in the

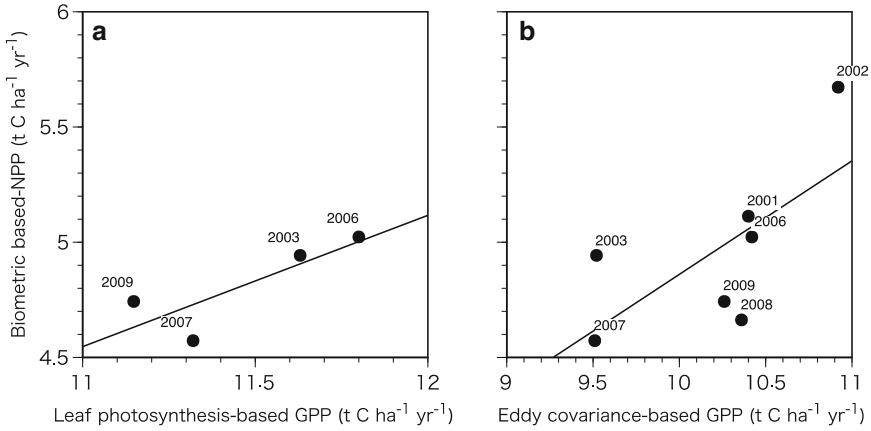

Fig. 12.10. Relationship between leaf photosynthesis-based GPP estimates (**a**), eddy covariance-based GPP estimates (**b**), and biometric-based NPP estimates in various years in the Takayama Forest. Survey year is shown in the figure

Takayama Forest revealed that temporal variations in LAI and V_{cmax} had marked effects on GPP, especially during the leaf expansion period. Subsequently, simulated annual GPP estimates were correlated with biometric-based NPP estimates, although matching data were only available for 4 years (Fig. 12.10a), and eddy-covariance-based GPP estimates were also correlated with biometric-based NPP estimates (Fig. 12.10b). Biometric-based NPP estimates were 40–42 % of simulated annual GPP estimates and were 45–52 % of eddy-covariance-based GPP estimates; these estimates corresponded with those in forest ecosystems that were similarly partitioned between plant respiration and NPP (Waring et al. 1998). However, overestimates of simulated GPP may follow over simplifications of canopy structure, averaging of leaf-level parameters for dominant tree species, and definitions of canopy structures as monolayers, even after consideration of leaf phenology and ecophysiology.

VI. Conclusions

Global climate change prompted to development of the "summation method" as an improved "biometric method" in the 1990s. The biometric method clearly defines field-measurement- based parameters and is expressed as the sum of SI, L_{an}, and P_{fr} of living biomass over a year. However, biometric estimates of annual NPP ($SI + L_{an} + P_{fr}$) that are produced by tracking the survival and diameter of individual tree stems in a permanent plot are underestimates of actual NPP values ($B_{2n} + L_n$), because other losses, including herbivores and root exudates, are excluded. However, precise field measurements for biometric estimates of NPP in the long-term permanent plot in the Takayama Experimental Forest were well correlated with the estimates of NPP from other methods, including those from simulations of canopy photosynthesis and from eddy covariance. Thus, biometric measurements of NPP can be used to evaluate climate-induced year-to-year variations in tree growth and in assimilated carbon partitioning into woody biomass, coarse woody debris, and soil organic carbon in forest ecosystems. Thus, long-term monitoring of forest ecosystems for biometric and eddy covariance analyses will provide an integrated, multidisciplinary database for the future, and may allow life cycle analyses of the effects of climate change and disturbances on forest C allocation and stocks.

Acknowledgements

We thank K. Kurumado and Y. Miyamoto of the Takayama Field Station of Gifu University for their support of field. Thanks are also due to Drs. H. Kondo of AIST, W. Mo-Kishimoto of NIAES and M. Adachi of NIES. This study was supported by KAKENHI (JSPS, no. 21310009) to TO, JSPS-NRF-NSFC A3 Foresight Program and Research and Education Funding for JALPS (Japanese Alps Inter-University Cooperative Project), MEXT, Japan.

References

Adachi M, Bekku YS, Konuma A, Kadir WR, Okuda T, Koizumi H (2005) Required sample size for estimating soil respiration rates in large areas of two tropical forests and of two types of plantation in Malaysia. For Ecol Manage 210:455–459

Aerts R, Berendse F, Klerk NM, Bakker C (1989) Root production and root turnover in two dominant species of wet heathlands. Oecologia 81:374–378

Baldocchi DD (2003) Assessing the eddy covariance technique for evaluating carbon dioxide exchange rates of ecosystems: past, present and future. Glob Change Biol 9:479–492

Barford CC, Wofsy SC, Goulden ML, Munger JW, Pyle EH, Urbanski SP, Hutyra L, . . ., Moore K (2001) Factors controlling long- and short-term sequestration of atmospheric CO_2 in a mid-latitude forest. Science 294:1688–1691

Bekku Y, Kimura M, Ikeda H, Koizumi H (1997) Carbon input from plant to soil through root exudation in *Digitaria adscendens* and *Ambrosia artemisiifolia*. Ecol Res 12:305–312

Black K, Bolger T, Davis P, Nieuwenhuis M, Reidy B, Saiz G, Tobin B, . . ., Osborne B (2007) Inventory and eddy covariance-based estimates of annual carbon sequestration in a Sitka spruce (*Picea sitchensis* (Bong.) *Carr.*) forest ecosystem. Eur J For Res 126:167–178

Brunner I, Bakker MR, Björk RG, Hirano Y, Lukac M, Aranda X, Børja I, . . ., Ostonen I (2013) Fine-root turnover rates of European forests revisited: an analysis of data from sequential coring and ingrowth cores. Plant Soil 362:357–372

Chave J, Andalo C, Brown S, Cairns MA, Chambers JQ, Eamus D, Fölster H, . . ., Yamakura T (2005) Tree allometry and improved estimation of carbon stocks and balance in tropical forests. Oecologia 145:87–99

Clark DA, Clark DB (1994) Climate-induced annual variation in canopy tree growth in a Costa Rican tropical rain forest. J Ecol 82:865–872

Clark DA, Brown S, Kicklighter W, Chambers JQ, Thomlinson JR, Ni J (2001) Measuring net primary production in forests: concepts and field methods. Ecol Appl 11:356–370

Clark DA, Piper SC, Keeling CD, Clark DB (2003) Tropical rain forest tree growth and atmospheric carbon dynamics linked to interannual temperature variation during 1984–2000. Proc Natl Acad Sci U S A 100:5852–5857

Curtis PS, Hanson PJ, Bolstad P, Barford C, Randolph JC, Schmid HP, Wilson KB (2002) Biometric and eddy-covariance based estimates of annual carbon storage in five eastern North American deciduous forests. Agric For Meteorol 113:3–19

Eissenstat DM, Yanai RD (1997) The ecology of root lifespan. Adv Ecol Res 27:1–60

Esser G (1987) Sensitivity of global carbon pools and fluxes to human and potential climatic impacts. Tellus B 398:245–260

Gough CM, Vogel CS, Kazanski C, Nagel L, Flower CE, Curtis PS (2007) Coarse woody debris and the carbon balance of a north temperate forest. For Ecol Manage 244:60–67

Gough CM, Vogel CS, Schmid HP, Su H-B, Curtis PS (2008) Multi-year convergence of biometric and meteorological estimates of forest carbon storage. Agric For Meteorol 148:158–170

Hanson PJ (2000) Separating root and soil microbial contributions to soil respiration: a review of methods and observations. Biogeochemistry 48:115–146

Hutchinson GE (1970) The biosphere. Sci Am 223:45–53

Imhoff ML, Bounoua L, Ricketts T, Loucks C, Harriss R, Lawrence W (2004) Global patterns in human consumption of net primary production. Nature 429:870–873

IPCC (1990) Climate Change: The IPCC Scientific Assessment, The first assessment report of the IPCC. Cambridge University Press, Cambridge

Kamata N (2002) Outbreaks of forest defoliating insects in Japan, 1950–2000. Bull Entomol Res 92:109–117

Ketterings Q, Coe R, van Noordwijk M, Ambagau Y, Palm CA (2001) Reducing uncertainty in the use of allometric biomass equations for predicting above-ground tree biomass in mixed secondary forests. For Ecol Manage 146:199–209

Kimura M, Funakoshi M, Sudo S, Masuzawa T, Nakamura T, Matsuda K (1982) Productivity and

mineral cycling in an oak coppice forest. 2. Annual net production of the forest. Bot Mag Tokyo 95:359–373

Komiyama A (1991) Relationships between stem-diameter growth periods and leaf growth periods of deciduous broadleaved tree species with reference to environmental factors. J Jpn For Soc 73:409–418, In Japanese with English summary

Komiyama A, Nakagawa M, Kato S (2011) Common allometric relationships for estimating tree biomasses in cool temperate forests of Japan. J Jpn For Soc 93:213–219, In Japanese with English summary

Kumagai T (2016) Observation and modeling of net ecosystem carbon exchange over canopy. In: Hikosaka K, Niinemets Ü, Anten N (eds) Canopy Photosynthesis: From Basics to Applications. Springer, Berlin, pp 269–287

Kuzyakov Y (2006) Sources of CO_2 efflux from soil and review of partitioning methods. Soil Biol Biochem 38:425–448

Liebhold A, Kamata N, Jacob T (1996) Cyclicity and synchrony of historical outbreaks of the beech caterpillar, *Quadricalcarifera punctatella* (Motschulsky) in Japan. Res Popul Ecol 38:87–94

Lieth H (1975) Modeling the primary productivity of the world. In: Lieth H, Whittaker RH (eds) Primary Productivity of the Biosphere. Springer, New York, pp 237–263

Lieth H, Whittaker RH (1975) Primary Productivity of the Biosphere. Springer, New York

Meigs GW, Donato DC, Campbell JL, Martin JG, Law BE (2009) Forest fire impacts on carbon uptake, storage, and emission: the role of burn severity in the eastern Cascades, Oregon. Ecosystems 12:1246–1267

Muraoka H, Saigusa N, Nasahara KN, Noda H, Yoshino J, Saitoh TM, Nagai S, . . ., Koizumi H (2010) Effects of seasonal and interannual variations in leaf photosynthesis and canopy leaf area index on gross primary production of a cool-temperate deciduous broadleaf forest in Takayama, Japan. J Plant Res 123:563–576

Murayama S, Saigusa N, Chan D, Yamamoto S, Kondo H, Eguchi Y (2003) Temporal variations of atmospheric CO_2 concentration in a temperate deciduous forest in central Japan. Tellus B 55:232–243

Newbould PJ (1970) Method for Estimating the Primary Production of Forests. Second Printing, IBP Handbook No.2, Blackwell Scientific Publications, Oxford

Ogawa (1977) Principles and methods of estimating primary production in forests. In: Shidei T, Kira T (eds) Primary Productivity of Japanese Forests- Productivity of Terrestrial Communities, vol 16, JIBP Synthesis. University of Tokyo Press, Tokyo, pp 29–35

Ohtsuka T (2012) Carbon cycling at Takayama forest: results from intensive studies in the last decade, and further studies for a next decade. Jpn J Ecol 62:31–44, In Japanese with English summary

Ohtsuka T, Akiyama T, Hashimoto Y, Inatomi M, Sakai T, Jia S, Mo W, . . ., Koizumi H (2005) Biometric based estimates of net primary production (NPP) in a cool-temperate deciduous forest stand beneath a flux tower. Agric For Meteorol 134:27–38

Ohtsuka T, Mo W, Satomura T, Inatomi M, Koizumi H (2007) Biometric based carbon flux measurements and net ecosystem production (NEP) in a temperate deciduous broad-leaved forest beneath a flux tower. Ecosystems 10:324–334

Ohtsuka T, Negishi M, Sugita K, Iimura Y, Hirota M (2013) Carbon cycling and sequestration in a Japanese red pine (*Pinus densiflora*) forest on lava flow of Mt Fuji. Ecol Res 28:855–867

Ohtsuka T, Saigusa N, Koizumi H (2009) On linking multiyear biometric measurements of tree growth with eddy covariance-based net ecosystem production. Glob Change Biol 15:1015–1024

Ohtsuka T, Shizu Y, Nishiwaki A, Yashiro Y, Koizumi H (2010) Carbon cycling and net ecosystem production at an early stage of secondary succession in an abandoned coppice forest. J Plant Res 123:393–401

Ohtsuka T, Shizu Y, Hirota M, Yashiro Y, Jia S, Iimura Y, Koizumi H (2014) Role of coarse woody debris in the carbon cycle of Takayama forest, central Japan. Ecol Res 29:91–101

Pan Y, Birdsey RA, Fang J, Houghton R, Kauppi PE, Kurz WA, Phillips OL, . . ., Hayes D (2011) A large and persistent carbon sink in the world's forests. Science 333:988–993

Randerson JT, Chapin FS III, Harden JW, Neff JC, Harmon ME (2002) Net ecosystem production: a comprehensive measure of net carbon accumulation by ecosystems. Ecol Appl 12:937–947

Saigusa N, Yamamoto S, Murayama S, Kondo H (2005) Inter-annual variability of carbon budget components in an AsiaFlux forest site estimated by long-term flux measurements. Agric For Meteorol 134:4–16

Saigusa N, Yamamoto S, Murayama S, Kondo H, Nishimura N (2002) Gross primary production and net ecosystem production of a cool-temperate deciduous forest estimated by the eddy covariance method. Agric For Meteorol 112:203–215

Satomura T, Hashimoto Y, Koizumi H, Nakane K, Horikoshi T (2006) Seasonal patterns of fine root

demography in a cool-temperate deciduous forest in central Japan. Ecol Res 21:741–753
Satoo T (1982) Forest Biomass. Edited and revised by Madgwick HAI, Martinus Nijhoff/Dr W. Junk Publishers, The Hague
Schimel DS, House JI, Hibbard KA, Bousquet P, Ciais P, Peylin P, Braswell BH, . . ., Wirth C (2001) Recent patterns and mechanisms of carbon exchange by terrestrial ecosystems. Nature 414:169–172
Schowalter TD, Hargrove WW, Crossley DA (1986) Herbivory in forested ecosystems. Annu Rev Entomol 31:177–196
Shan J, Morris LA, Hendrick RL (2001) The effects of management on soil and plant carbon sequestration in slash pine plantations. J Appl Ecol 38:932–941
Shibistova O, Lloyd J, Zrazhevskaya G, Arneth A, Kolle O, Knoglobhl A, Astrakhantceva N, . . ., Schmerler J (2002) Annual ecosystem respiration budged for a *Pinus sylvestris* stand in central Siberia. Tellus 54B:568–589
Shidei T, Kira T (1977) Primary productivity of Japanese Forests- Productivity of Terrestrial Communities, vol 16, JIBP Synthesis. University of Tokyo Press, Tokyo
Steele SJ, Gower ST, Vogel JG, Norman JM (1997) Root mass, net primary production and turnover in aspen, jack pine and black spruce forests in Saskatchewan and Manitoba, Canada. Tree Physiol 17:577–587
Trumbore SE, Davidson EA, Barbosa de Camargo P, Nepstad DC, Martinelli LA (1995) Belowground cycling of carbon in forests and pastures of Eastern Amazonia. Global Biogeochem Cycles 9:515–528
Vogt KA, Vogt DJ, Bloomfield J (1998) Analysis of some direct and indirect methods for estimating root biomass and production of forests at an ecosystem level. Plant Soil 200:71–89
Waring RH, Landsberg JJ, Williams M (1998) Net primary production of forests: a constant fraction of gross primary production? Tree Physiol 18:129–134
Yamamoto S, Murayama S, Saigusa N, Kondo H (1999) Seasonal and inter-annual variation of CO_2 flux between a temperate forest and the atmosphere in Japan. Tellus B 51:402–413

Part V

Application to Ecological and Evolutionary Processes

Chapter 13

Optimization and Game Theory in Canopy Models

Niels P.R. Anten*
Crop and Weed Ecology, Centre for Crop Systems Analysis, Wageningen University, Wageningen, The Netherlands

Summary

Ecological optimization theory in combination with canopy modeling is increasingly being accepted as a powerful tool in various scientific fields including ecology, crop science and global change biology. However, the success of this approach critically depends on the adequate choice of optimization criteria and on the structure and assumptions of the canopy models to which it is linked. This chapter starts with the conventional optimization criterion, that of static plant simple optimization, whereby traits are assumed optimal when whole-canopy carbon gain is maximized. It shows how this approach has been widely and often successfully used but also how it often fails to capture key features of vegetation stands. It then lays out a number innovative steps by which optimization could be made more amenable to our understanding of real plant

*Author for correspondence, e-mail: niels.anten@wur.nl

K. Hikosaka, Ü. Niinemets, and N.P.R. Anten (eds.), *Canopy Photosynthesis: From Basics to Applications*, DOI 10.1007/978-94-017-7291-4_13

systems. These include: the introduction of evolutionary game theory that takes plant competition into account, the shift from static photosynthesis to dynamic growth models and expanding from simple fitness proxies such as photosynthesis to local population growth. Overall it is argued that future optimization models should employ combinations of these elements.

Keywords Climate change • Crop models • Growth dynamics • Evolutionary game theory • Optimality • Traits

I. Introduction

A long standing challenge in ecological research is the development of a theoretical framework that explains how emerging properties at the level of plant communities or ecosystems, i.e., vegetation structure, productivity and other ecosystem functions arise from basic physiological processes and plant functional traits. Firstly, physiological and structural traits generally define the functioning of plant parts (e.g., leaves, stems, roots, etc.) but their fitness consequences are expressed at the individual and population level. Second, novel molecular techniques in crop breeding are enabling us to manipulate individual physiological processes in plants. But the consequences for yields must be assessed at the level of crop stands (Yin and Struik 2010). Canopy models are a key element of such a theoretical framework as they enable us to scale from basic physiological and morphological leaf traits to the structure (e.g. leaf area and height) and functioning (net carbon uptake through photosynthesis and transpiration) at the level of vegetation stands (e.g. de Pury and Farquhar 1997).

Based on our current physiological and biophysical knowledge of leaf photosynthesis and plant structure, complicated models are available that can simulate canopy photosynthesis if leaf properties of all plants in the canopy are known (Chap. 9, Hikosaka et al. 2016). Such models have been widely used in e.g. agricultural research (see van Ittersum et al. 2003). There are, however, important drawbacks associated with this model approach (Dewar et al. 2009). First, they usually rely on a large amount of empirical data. These data are often hard to obtain, especially in the case of complex natural vegetation or when the simulation objective is the future, as in the case of studies that attempt to predict the impacts of climate change on vegetation processes. Second, due to their reliance on empirical data, these models often fail to capture many of the key biological mechanisms underlying canopy photosynthesis. Relationships between traits are often based on correlations rather than physiological relationships.

Abbreviations: A_D – Daily leaf photosynthesis (mol CO_2 d^{-1} m^{-2}); A_{max} – Light saturated leaf photosynthesis (μmol CO_2 s^{-1} m^{-2}); A_0 – Light saturated leaf photosynthesis of the top most leaf in the canopy (μmol CO_2 s^{-1} m^{-2}); β – Degree to which canopies of neighboring plants are mixed.; *Cb* – Crown base of a plant (when r or m are added it refers to a resident or mutant).; f – Cumulated amount of LAI above a given point (m^2 m^{-2}); *fr* – Frequency of a strategy in a population (dimensionless); f_{st} – Fraction of NPP allocated to stem growth (dimensionless); F – General indicator of fitness (no units); H_{max} – Maximum tree height; $I(f)$ – Light intensity (photon flux density) at depth f in the canopy (μmol s^{-1} m^{-2}); I_0 – Light intensity (photon flux density) above the canopy (μmol s^{-1} m^{-2}); k – Extinction coefficient for light; λ – A Lagrangian multiplier; LAI – Leaf area index (m^2 m^{-2}); LMA – Leaf mass per unit area (g m^{-2}); M_s – Stem mass per unit length (g m^{-1}); NPP – Net primary productivity (e.g. g $plant^{-1}$ day^{-1} but definition per unit land area also possible); N_{area} – Leaf nitrogen content per unit area (mmol m^{-2}); N_o – N_{area} of the top most leaf in the canopy (mmol m^{-2}); p – The fraction of the shading that plant experiences being caused by its own leaves; P – General indicator of plant performance (no units) often used as fitness proxy (e.g. photosynthesis growth etc); R – General indicator for resources (no units); r_{eff} – Fraction of nitrogen that plants resorb from senescing leaves; S_d – Solar beam

Optimality theory provides a simple but potentially more powerful alternative (Farquhar 1989; Parker and Maynard Smith 1990; Dewar et al. 2009). Optimality theory is based on the concept that some performance measure is maximized with respect to one or more plant traits and considering one or more limiting factors. As such, optimality models limit the degree of uncertainty by imposing a restriction that plants select for trait values that provide the highest performance (Franklin et al. 2012). Performance measures are generally ecologically or evolutionarily inspired and can in some way be related to fitness (i.e., fitness proxies). Optimal values of traits such as leaf nitrogen content, leaf area index (LAI, the amount of leaf area per unit soil area), stomatal conductance or leaf photosynthetic capacity are emergent outcomes rather than input parameters or subroutines (McMurtrie et al. 2008).

Optimality models, however, come with their own set of problems. Important in this respect is the question of the optimization criterion: what, if anything, do plants maximize and over what time span (Kull 2002). This question is not just a modeling issue but is a key question in plant ecological research. Naturally, assumptions need to be made in this respect for the simple reason that we still do not know how, and in what way, plant traits are selected for. Yet, a critical review of the optimization approaches that have been used to date is important in driving this debate further.

Most optimization models in plant canopy research use what I denote here as simple optimization, which assumes that plant traits are optimal when they result in maximum whole-stand photosynthesis (or some other performance measure such as net primary production, NPP). This assumes that traits that maximize individual fitness are manifest as optimal characteristics at the stand level (Hikosaka and Hirose 1997; Anten 2005), and, that the payoff associated with the trait values of one individual are independent of its neighbors. This assumption evidently does not hold true for vegetation stands that usually consist of very different individual plants and where plants strongly influence each other's light climate and nutrient availability.

Another characteristic of many current optimization models is that they treat plant canopies as static. This ignores that plant canopies develop through a dynamic growth process where new structures (leaves, stems and branches) are produced, resources are reallocated and senescent structures die (Franklin and Agren 2002; Hikosaka 2005). A final important assumption lies with the performance measures used. Most models use canopy photosynthesis or growth (NPP) as a fitness proxy. Evidently some measure along the lines of lifetime reproduction, that includes characteristics such as fecundity and mortality risk, would be better (Geritz et al. 1998; McGill and Brown 2007).

This chapter aims to provide a critical appraisal of the application of optimization theory in canopy models. It starts out with discussing static-plant simple optimization (SSO) models, showing how this approach has been widely and often successfully used, but also, how it often fails to capture key features of vegetation stands. It then discusses the inclusion of evolutionary game theory and dynamic growth processes (especially leaf turnover) into optimization models. Particular emphasis is placed on the potential for combining these elements. The final section discusses the possibilities of linking canopy models to demographic processes such that the impact of variation in canopy traits on population dynamics can be assessed.

II. Static-plant Simple Optimization

Static-plant simple optimization (SSO) is currently the most widely used optimization approach in canopy models. It is essentially based on the following relationship;

$$\frac{\partial P(x_1, x_2, x_n)}{\partial x_i} = 0 \qquad (13.1a)$$

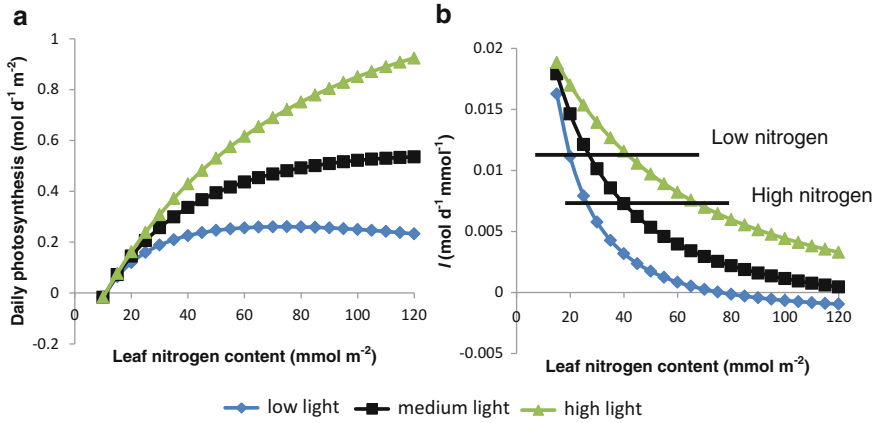

Fig. 13.1. (**a**) A simulation of daily leaf photosynthesis (A_D) as a function of leaf nitrogen content per unit area (N_{area}) and (**b**) the marginal change in A_D (λ) of a small change in N_{area} ($\lambda = \Delta A_D/\Delta N_{area}$ i.e., Eq. 13.2 but taking discrete N_{area} steps of 5 mmol m^{-2}). *Horizontal lines* in (b) indicate constant λ values and thus optimal nitrogen distributions for a given total nitrogen shared by the three leaves. Lower values of λ are associated with high amounts of nitrogen. For simplicity only 3 leaves are shown but the analysis can evidently extended to a whole canopy

under the condition that:

$$R = \gamma \tag{13.1b}$$

where P denotes a performance measure (e.g. canopy photosynthesis, NPP etc) and x are traits (like leaf area, leaf angle, leaf nitrogen content or photosynthetic and respiratory traits), R is a given resource (e.g. nitrogen or water) and γ a constant. All parameters are treated as static, that is, no time dependent changes in their values are taken into account. Below I give a number of examples of how this approach has been applied.

A. Optimal Leaf Nitrogen Distribution

A large number of studies (e.g. Field 1983; Hirose and Werger 1987; Anten et al. 1995a; Posada et al. 2009; Hikosaka 2014) have analyzed distribution patterns of leaf nitrogen contents per unit area (N_{area}) in the canopy (see reviews Kull 2002; Niinemets 2007). A large part of leaf nitrogen is associated with rate limiting elements of the photosynthetic process, resulting in a strong positive correlation between photosynthesis at saturating light (A_{max}) and N_{area} (Field and Mooney 1986). Conversely, the correlation between net photosynthesis at low light and N_{area} is much weaker or even negative (Hirose and Werger 1987). Thus, for plants in dense vegetation, a non-uniform leaf nitrogen distribution whereby N_{area} declines with light availability from the top towards the bottom of the canopy results in a larger canopy photosynthesis than a uniform N_{area} distribution, in which N_{area} of all leaves equals the mean.

Whole canopy photosynthesis is maximized with respect to nitrogen use, when nitrogen is distributed among the leaves in the canopy such that any further reallocation of nitrogen between the leaves cannot increase canopy carbon gain. This optimality criterion is given as (Field 1983):

$$\frac{\partial A_D}{\partial N_{area}} = \lambda \tag{13.2}$$

where A_D is daily leaf photosynthesis (mol CO_2 d^{-1} m^{-2}), λ (mol CO_2 d^{-1} mmol N^{-1}) is a Lagrangian multiplier, which depends on total canopy nitrogen (Field 1983). Since $\partial A_D/\partial N_{area}$ is a positive function of light and negative function of N_{area} (see Fig. 13.1), Eq. 13.2 predicts that N_{area} should decline from the top towards the bottom of the canopy. A similar analysis can be conducted on a

mass basis, i.e. assuming that leaf mass per area (LMA) rather than N_{area} determines leaf photosynthesis. In that case, N_{area} in Eq. 13.2 would be replaced by LMA. However, while Eq. 13.2 provides the condition for the optimal distribution, it does not define its shape.

It was theoretically derived that if A_{max} is proportionately related to N_{area} and if other characteristics of the light response of leaf photosynthesis do not differ between leaves, canopy photosynthesis is maximized if plants allocate more nitrogen towards higher, more illuminated leaves and less to lower, more shaded ones in such a way that the N_{area} distribution parallels the light distribution in the canopy (Farquhar 1989; Anten et al. 1995a). Mathematically this can be described as:

$$N_{area}(f) = N_0 I(f)/I_0 \tag{13.3a}$$

so that

$$A_{max}(f) = A_0 I(f)/I_0 \tag{13.3b}$$

where N_o and A_o are the N_{area} and A_{max} of an un-shaded leaf at the top of the canopy, I_o and $I(f)$ the light intensity incident on leaves at the top or at depth f (measured in LAI units) in the canopy, respectively. Consistent with this prediction non-uniform patterns of N_{area} distribution have been found in canopies of a wide variety of plants (see review by Hirose 2005). In all cases, optimal within-canopy variation in nitrogen resulted in considerable increases in estimated carbon gain as compared to the uniform nitrogen distribution (see Hirose 2005). However actual N_{area} distributions were also consistently more uniform than the predicted optimal distribution with actual rates of canopy photosynthesis 4–15 % lower than the maximum values predicted in these canopies (Kull 2002, but see Koyama and Kikuzawa 2010).

B. Optimal Leaf Area Index

LAI serves as the dominant control of vegetation productivity such as gross and net primary production (e.g., Kira 1991; Lindroth et al. 2008) because it is a major determinant of canopy light interception and hence photosynthesis. It also plays a key role in regulating vegetation climate feedbacks as it strongly influences evapotranspiration and surface albedo (van den Hurk et al. 2003). There is thus considerable need for models that are capable of predicting LAIs.

If photosynthesis were only limited by light availability, canopy carbon gain could be increased by adding new leaves until the daily light compensation point of the lowermost leaves has been achieved (Monsi and Saeki 1953). Beyond this optimum, a further increase of LAI reduces canopy carbon gain as the carbon balance of additional leaves in lower canopy becomes negative. From this perspective a number of predictions can be made. LAI should increase with the amount of incident radiation, while plants with vertically inclined leaves that allow more light to penetrate vegetation should have higher LAIs. Initial models only considered leaf respiration to calculate the light-compensation point (Monsi and Saeki 1953; Saeki 1960) but later studies expanded this to include the additional costs associated with producing and maintaining structures (roots, stems and branches) that support a leaf (Givnish 1988; Reich et al. 2009). With this expanded model Reich et al. (2009) estimated for a suite of shrub species that plants indeed dropped their leaves when the net carbon balance of these leaves including support costs was zero. Other studies (Oikawa et al. 2005; 2006) however, documented that leaves are often dropped well before their carbon balance reaches zero especially at low nitrogen availability from the soil.

There is a general increase of LAI with increasing soil nitrogen availability (e.g. Albaugh et al. 1998), indicating that in natural conditions, leaf area growth is usually strongly limited by the availability of nutrients, especially nitrogen. If the total amount of nitrogen in the leaves is fixed, an increase in LAI will not only result in increased light capture but also in a reduction of N_{area} and thus A_{max}. Considering this constraint, an optimal LAI can be defined beyond which an increase in light capture no longer compensates for the reduction in leaf A_{max}

values (Anten et al. 1995b). Based on this concept it can further be predicted that for a given amount of canopy N, leaf area production should increase and N_{area} decrease with increasing leaf photosynthetic nitrogen-use efficiency, A_{max}/N_{area}, and that leaf production should be lower and N_{area} higher with an increase in quantum yield of photosynthesis increases (Anten et al. 1995b). Interestingly atmospheric CO_2 increases both A_{max}/N_{area} and the quantum yield such that its effects on LAI under limited nitrogen availability are predicted to be small (Anten et al. 2004).

Similar to the case of nitrogen limitation, an optimal LAI can also be defined with respect to water availability, as this may constrain the transpiration of plants and thus their stomatal conductance. Thus, assuming plants can transpire a given total amount of water, an optimal LAI can be defined at which the benefits of increased light capture no longer compensate for the negative effect of a lower stomatal conductance (McMurtrie et al. 2008). McMurtrie et al. (2008) developed an SSO model that determines the optimal LAI relative to both water and nitrogen availability, and predicted that under water limitations, LAIs will increase and mean stomatal conductance will decline with CO_2 elevation (see also van Loon et al. 2014). Both predicted effects may have important feedbacks on climate (Villa et al. 2012).

Comparisons of these model predictions to real data indicates that these models for optimal LAI provide good qualitative predictions of real LAI values. For example, the observation that C_4 plants typical have higher A_{max}/N_{area} and produce more leaves with lower N_{area} (Sage and Pearcy 1987) is consistent with predictions. Vegetation responses to elevated CO_2 were also well predicted (Hirose et al. 1997; Anten et al. 2004; McMurtrie et al. 2008). Anten et al. (1998) compared optimal LAIs to real values from stands of a suite of species including both agricultural and wild plants (Fig. 13.2). There was a strong positive correlation between predicted and actual LAIs with $r^2 > 0.7$. Apparently, the model for optimal LAI could explain more than 70 % of the variation in LAI across species, indicating that

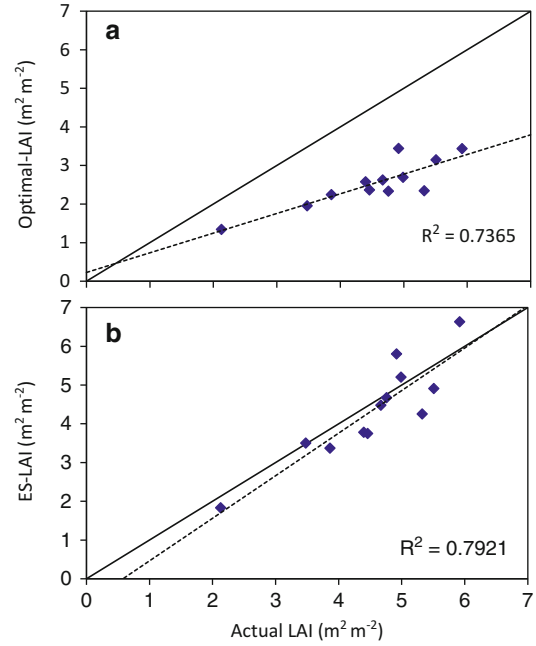

Fig. 13.2. (**a**) Optimal (optimal LAI) and (**b**) evolutionarily stable leaf area indices (ES-LAI) plotted against the actually measured LAI. Solid lines indicate 1:1 correspondence and dashed lines linear regressions. Numbers indicate 1,2 *Sorghum bicolor* high and low nitrogen availability, 3,4 *Oryza sativa* high and low nitrogen availability, 5,6 *Amaranthus cruentus* high and low nitrogen availability, 7 *Glycine max* (Raw data for 1–7 taken from Anten et al. 1995b) 8 *Leersia hexandra*, 9 *Hymenachne amplexicaulis*, 10 *Paspalum fasciculatum* and 11,12 *Hyparrhenia rufa* dense and open stand (8–12 raw data taken from Anten et al. 1998) (Redrawn from Anten 2002)

the assumed causal relationship between interspecific variation in structural and physiological traits and stand structure and functioning are at least qualitatively well predicted. Quantitatively however LAIs were poorly predicted with real LAIs being consistently larger than predicted values (Fig. 13.2).

C. Differences Between Predicted and Actual Values

As noted, there are important and consistent differences between the observed canopy traits and values predicted from simple optimization models. Particularly, observed nitrogen distributions tend to be more

uniform while LAIs are larger than predicted. There are basically two explanations for this discrepancy: (i) the simplifications in the canopy models used render inaccurate predictions or (ii) the optimization goal function has not been adequately set, that is, the optimization criterion has not been correctly defined. In this Sect. I shortly deal with the first explanation while the second will be dealt with in the remainder of the chapter.

Studies that apply optimization theory in canopy models typically make a number of assumptions that may not be realistic. Regarding the costs of leaf production or nitrogen reallocation, only leaf maintenance respiration is usually considered. This ignores the costs associated with nitrogen reallocation in the canopy (Field 1983) as well additional costs of leaf production (Givnish 1988). The latter includes construction costs of leaves and the additional costs of structures (stems and roots) needed to support leaves. One model that included these costs (Reich et al. 2009) obtained accurate predictions of leaf death.

Most optimization models consider only a limited set of stress factors; generally only light and/or nitrogen limitation while some models also consider water limitations (e.g. McMurtrie et al. 2008; Niinemets 2012). Under natural conditions plants are evidently exposed to many additional stressors. Several herbivores for instance favor leaves with high nitrogen content, and plants may thus maintain lower than optimal nitrogen contents to avoid herbivory (Stockhoff 1994). Plants in the top of the vegetation are also prone to wind, and nitrogen losses due to wind damage increase with increasing nitrogen content of leaves (Yasumura et al. 2006). Finally, resources other than light, nitrogen and water may limit plant photosynthesis and growth. Phosphorus for example is an important limiting factor in many (especially tropical) growth environments (Lambers et al. 1998). Inclusion of these aspects could improve the predictions made from optimization models, and should be considered more carefully in future models.

III. Application of Evolutionary Game Theory in Canopy Models

As noted, a possible explanation for the discrepancy between predictions from simple optimization models and real values may lie with the chosen optimization criterion. Simple optimization defines traits as optimal when they result in maximum performance at the vegetation-level, i.e., that of the plant community. Stands of vegetation consist of individual plants and this definition therefore implicitly assumes that characteristics that maximise fitness of individuals within a stand are manifest as optimal characteristics at the stand level. This in turn is subject to the condition that the optimum for one individual is independent of the characteristics of its neighbours (Parker and Maynard Smith 1990). This certainly does not hold true for dense stands of vegetation, where plants grow closely together and strongly influence the amounts of light, water and nutrients that come available to their neighbours. In such cases evolutionary game theory (EGT) in which the performance of individual plants is considered relative to the characteristics of their neighbours (Riechert and Hammerstein 1983), is a more relevant approach. This section first gives a short overview of some concepts used in EGT models, and will subsequently discuss a number of vegetation characteristics that have been analyzed game theoretically.

A. The Competitive Optimum and the Definition of an Evolutionary Stable Strategy

1. Continuous Single Traits

The theory of evolutionarily stable strategies (ESS) assumes that no change in a characteristic can increase an individual's fitness over that of other individuals with the same strategy (Maynard Smith 1974; Givnish 1982; Sakai 1991). Mathematically this can defined as follows:

$$F\left(x_i, x_i^*\right) < F\left(x_i^*, x_i^*\right), x_i \neq x_i^* \qquad (13.4a)$$

with F fitness, x a strategy value. x_i^* is therefore the evolutionarily stable strategy. In most canopy studies whole-plant photosynthesis or growth are considered as fitness proxies (which as discussed in Sect. VI is evidently subject to debate). For instance in the case of an ESS for leaf area production with photosynthesis as fitness proxy, Eq. 13.4a can be rewritten as:

$$P\left(L_i, L_i^*\right) < P\left(L_i^*, L_i^*\right), L_i \neq L_i^* \qquad (13.4b)$$

with P indicating a fitness proxy and L stands for the LAI of an individual plant. This is equivalent to the condition that the partial derivative of P_i to its leaf area index (L_i) equals zero:

$$\partial P_i\left(L_i, L_i^*\right)/\partial L_i\big|_{L_i=L_i^*} = 0 \qquad (13.5)$$

where L_i^* is the evolutionary stable leaf area. This can then be scaled to an ES-LAI of the vegetation stand by multiplying L_i^* by the density of plants.

2. Pay off Matrices of Discreet Strategies

The analysis provided above assumes the situation whereby there is a homogenous resident population playing a single strategy and addresses the question whether this population can be invaded by a mutant that plays a slightly different strategy. This analysis can be extended by considering population constituting of individuals with different discrete strategies, using a so-called payoff matrix. I explain this approach based on the example from Pronk et al. (2007). They considered a population in which there are plants with ten different height investment strategies. Plants either allocate a small fraction of their resources to height growth (in terms of additional stem mass) and a large fraction to the production of leaves or vice versa (strategies 1–10 represented increasing height investment). As described below, the benefits of large investment in height is the ability to shade neighbors but the cost is that there is less resource to invest in leaf area growth and associated photosynthesis and future growth. Pronk et al. assumed a competitive arena divided into sub-sections in which plants competed in a one-on-one setting. All strategies were assumed to be equally present and randomly mixed. Thus plants can interact with all other strategies, including their own, resulting in the following matrix.

$$\begin{bmatrix} P_{i,j} & .. & P_{n,j} \\ .. & \square & .. \\ P_{i,n} & .. & P_{in,n,j} \end{bmatrix} \qquad (13.6)$$

Here, $P_{i,j}$ represents the pay-off of an i strategist interacting with a j strategist, over one simulation cycle. Thus it holds that if $P_{i,j} > P_{j,i}$, then strategist i outperforms strategist j. The payoff matrix obtained by Pronk et al. is shown in Fig. 13.3.

The total payoff of strategy i in the whole competitive arena (P_i) depends on both its payoffs against each of the other strategies and the chance that it encounters each of them. The latter depends on the frequency at which it occurs and the frequency at which all other strategies occur. P_i can thus be quantified as:

$$P_i = fr_i \sum P_{ij} fr_j \qquad (13.7)$$

with fr_i and fr_j the relative frequencies at which strategies i and j occur.

Pronk et al. developed their approach for annual plants, where the life time performance of an individual is equal to its seasonal seed production, and where at any point in time there is only a single generation of plants. Thus, they could assume that the frequency at which a strategy occurs in a subsequent generation is equal to its share in the performance in the current generation:

$$fr_{i(t+1)} = \frac{P_{it}}{\sum P_{jt}} \qquad (13.8)$$

A strategy can be considered to become extinct if its frequency drops below a given threshold level. The caption of Fig. 13.3 describes how the ESS (in this case 17 % of NPP being invested in height growth) can be derived from the payoff matrix.

	Target individual (potential mutant)									
	Type 1	Type 2	Type 3	Type 4	Type 5	Type 6	Type 7	Type 8	Type 9	Type 10
% NPP	2	7	12	17	22	27	32	37	42	47
Resident										
Type 1	1.67	3.52	3.49	3.45	3.4	3.34	3.26	3.17	3.06	2.9
Type 2	0.7	1.72	3.49	3.45	3.4	3.34	3.26	0.38	0.27	0.2
Type 3	0.78	0.92	1.72	3.45	3.4	0.66	0.45	0.33	0.25	0.2
Type 4	0.92	1.02	1.23	1.7	1	0.68	0.48	0.36	0.27	0.21
Type 5	1.09	1.22	1.62	3.45	1.68	0.84	0.58	0.42	0.31	0.23
Type 6	1.29	1.53	3.49	3.45	3.4	1.65	0.77	0.52	0.37	0.27
Type 7	1.52	2.13	3.49	3.45	3.4	3.34	1.61	0.72	0.47	0.33
Type 8	1.78	3.52	3.49	3.45	3.4	3.34	3.26	1.57	0.67	0.43
Type 9	2.08	3.52	3.49	3.45	3.4	3.34	3.26	3.17	1.52	0.61
Type 10	2.41	3.52	3.49	3.45	3.4	3.34	3.26	3.17	3.06	1.44

Fig. 13.3. An example of a payoff matrix to determine the evolutionary stable biomass investment in height growth. The matrix represents the seed production (in grams per individual plant) in pair-wise competition between two plant types with different height investment expressed as a percentage of NPP (i.e. the numbers 2, 12, 17 etc depicted in the *first row* and *column*). Seed productions were calculated with a dynamic plant growth model (for details see Pronk et al. 2007) assuming 200 plants/m^2 and a season length of 250 days. *Columns* indicate target plants that can mutate and rows residents. The ESS is 17 % of NPP invested in height. This can be understood as follows. When type 4 (17 % investment) is the resident, all no strategy can result in a higher seed production than that of type 4 itself (the value 1.7 is the value in the *row* of type 4), and Eq. 13.3 holds. That same value 1.7 is also the lowest in the *column* which in combination with previous entails that as a mutant Type 4 can invade when any of the other strategies are the resident (Redrawn from Pronk et al. 2007)

B. Evolutionary Game Theory in Canopy Studies

Evolutionary game theory has been applied in canopy studies to analyze the adaptive significance of a number of traits. Below I discuss a few examples.

1. Plant Height

The most studied trait is plant height, one of the most obviously density-dependent characteristics of plants. Height growth involves costs. This is firstly because taller structures require stronger support structures (McMahon 1973) and taller plants thus have a higher fractional allocation of resources to stems and branches and a smaller allocation to leaves (Stutzel et al. 1988). Secondly in trees there are hydraulic limitations to height caused by: increased resistance in longer transport vessels and increased gravitational potential opposing the ascent of water (Ryan et al. 2006). Consequently leaf stomatal conductance and photosynthesis become constrained in tall trees (Ryan et al. 2006). Thus, net carbon gain of plants would be maximized if plants were relatively short. However, such vegetation would not be evolutionarily stable as it could be invaded by mutant plants that are taller and thus shade their neighbors. Givnish (1982) derived that this process of mutant invasions will repeat itself until the added benefits of increased height no longer compensate for the added costs. At this stage a stable equilibrium canopy height, i.e., an ESS, is achieved at which no individual plant can increase its carbon gain by changing its height. A stable condition could be derived because he assumed the marginal benefit of overtopping neighbor plants to be constant, while the costs of height growth (i.e. investment in support at the expense of leaf growth) to increase disproportionately with height. Based on the above-mentioned mechanical and hydrological constraints, the latter seems reasonable.

Using this concept it was predicted that plant height should increase with increasing density, that is, an increasing degree to which

plants influence each other's light climate (Givnish 1982; Iwasa et al. 1984; Falster and Westoby 2003; Pronk et al. 2007). Such conditions may arise in situations where plants grow closely together or in situations where individual plants can produce large leaf areas, which will happen under benign growth environments with favorable nutrient and water availability. Conversely, shorter stature would be favoured in more open stands and dry and/or low nutrient conditions. Short stature would also be favoured if costs of height growth are high which may occur e.g. in windy environments where plants are exposed to mechanical stress (Ennos 1997).

These predictions are all clearly in line with observations. Particularly the density-dependent increase in height growth in response neighbour plant proximity has been clearly documented (Smith 1982; Schmitt et al. 1999). The physiological regulation of this response is also becoming increasingly well understood (see Chap. 6, de Wit and Pierik 2016). The prediction that taller individuals should have higher fitness in crowded stands while shorter individuals should do better in sparser vegetation (Givnish 1982; Iwasa et al. 1984) has also been verified experimentally (e.g. Dudley and Schmitt 1996).

Another prediction from EGT models is that while plants in dense vegetation should grow tall to keep up with their neighbours, they should not overtop them. Nagashima and Hikosaka (2011) tested this prediction in an experiment where they elevated some plants but not others. Indeed plants exhibited so called height convergence whereby elevated plants grew slower in height than non-elevated ones. Another experiment (Vermeulen et al. 2008), raised cylinders packed with green foil that transmits the same spectral composition of light as leaves around *Potentilla reptans* plants at different rates, thus simulating neighboring vegetation growing at different rates. Intriguingly height growth in plants kept exact pace with the cylinders (i.e., they grew fast only when cylinders were raised fast), again indicating a pattern whereby plants keep their leaves at exactly the top of the vegetation. Plants possibly detect this through changes in light quantity and quality and possibly by increased exposure to wind and associated swaying (Nagashima and Hikosaka 2012).

2. Leaf Angle

Leaf angle is commonly defined as the mean inclination angle (i.e. angle between the leaf plane and the horizontal), though declination angle (leaf angle measure relative to the vertical) is sometimes also used. As explained in Chap. 1 (Goudriaan 2016), the leaf angle distribution of plants plays an important role in determining light interception. With the vertical components of light predominating, horizontally projected leaves capture light more efficiently than vertical ones; canopies with horizontal leaves have a higher extinction coefficient for light (k, Monsi and Saeki 1953). Monsi and Saeki (1953) thus derived that there is an optimal leaf angle distribution and that this optimum depends on the LAI of the stand. If LAI were low, horizontal leaves, resulting in a high light extinction coefficient, would be optimal because they facilitate maximum light capture. If LAI were large, canopy photosynthesis would be maximized if leaves were vertically inclined. A high k implies that the leaves at the top of the canopy receive very high light intensities while those at the bottom get very little light. Because of the curvilinear relationship between light and photosynthesis, leaves cannot efficiently photosynthesise at very high light levels, while leaves at very low light might have negative carbon gain. A low k facilitates a more even distribution of light among leaves. This prediction regarding optimal leaf angles verified in experiments where leaf angles were manipulated (Monsi et al. 1973). It is also in line with the fact that modern high-yielding cereal crop varieties tend to have more vertically inclined leaves than older varieties.

Yet, contrary to the predictions from optimal leaf angle models, most wild plants in

dense vegetation tend to have horizontally projected leaves (Hikosaka and Hirose 1997). Why is this? A similar argument applies as in the case of plant height. A vegetation stand composed of plants with vertically inclined leaves, can be invaded by a mutant individual that projects its leaves horizontally, as such a plant would be able to capture a larger fraction of the available light, and thus photosynthesize, grow and reproduce at a higher rate than the resident population.

Hikosaka and Hirose (1997) developed a model with which they analysed the effect of leaf angle distribution on competition between plants. They explicitly considered the degree of interaction between individuals in the stand by introducing the parameter p, which denotes the degree to which the light environment experienced by a plant is determined either by its own leaves or that of its neighbors. A p value of 1 (p ranges between 0 and 1) means that plants only influence their own light climate, while a very low p means that the light climate of plants is mostly determined by their neighbors. Hikosaka and Hirose (1997) showed that in most vegetation stands, horizontal leaves would be evolutionarily stable. The only exception would be formed by stands with minimal interaction between plant canopies ($p >= 0.9$) or a very high LAI. Leaf angle, like plant height, can thus be viewed as a density-dependent trait, i.e., horizontal leaves being favored where there is strong inter-plant interaction and vertical leaves favored when this is not the case.

Tremmel and Bazzaz (1993) conducted an experiment where they let target and neighbour plants of different species compete against each other. They found that target plants performed better than their neighbors if they had more horizontal leaves than the neighbors, which supports the prediction from Hikosaka and Hirose (1997).

3. Leaf Area

As noted above plant stands consistently have larger leaf area indices than the optimal values that would maximize whole-stand carbon gain (Anten et al. 1998). This discrepancy can be explained in the same way as in the case of plant height and leaf angle. Say that in a stand with optimal LAI there would be a mutant that produces more leaf area than its neighbors. This individual would be able to capture a larger fraction of the available light and thus increase its photosynthesis.

Recent studies (Schieving 1998; Schieving and Poorter 1999; Anten and Hirose 2001; Anten 2002; Lloyd et al. 2010) have analyzed leaf area growth of plants from a game theoretical perspective. It was derived theoretically that the ES-LAI of a stand should always be greater than the optimal one (Schieving 1998; Anten 2002). Figure 13.4 visualizes this difference between simple optimization of LAI and competitive optimization through application of EGT (van Loon et al. 2014).

As with leaf angle, the ES-LAI value was strongly dependent on the assumed degree of interaction between individuals (Anten 2002) where the latter was indicated by a parameter β being the degree to which canopies of neighboring plants are mixed (i.e., $\beta = 1$ is no mixing and β approaching 0 indicates full mixture). Note that parameter is slightly different from the parameter p described above. While p refers to the partitioning of light among neighboring plants, β refers the fraction of leaf area that each has within a given space. It was shown that ES-LAI strongly increases with increasing degrees of non-self- interaction, i.e., decreasing values of β from 1 (indicating only self-interaction) to 0 (indicating only non-self-interaction). This makes sense as the payoff of increasing LAI increases when it is associated with shading neighbor plants rather than self-shading. Anten (2002) showed when β was assumed to be 0.5 the predicted ES-LAIs closely corresponded with observed values for a wide variety of vegetation stands. Van Loon et al. (2014) used a very similar model (also assuming $\beta = 0.5$) and was able to predict the effect of elevated CO_2 on LAI, leaf photosynthesis

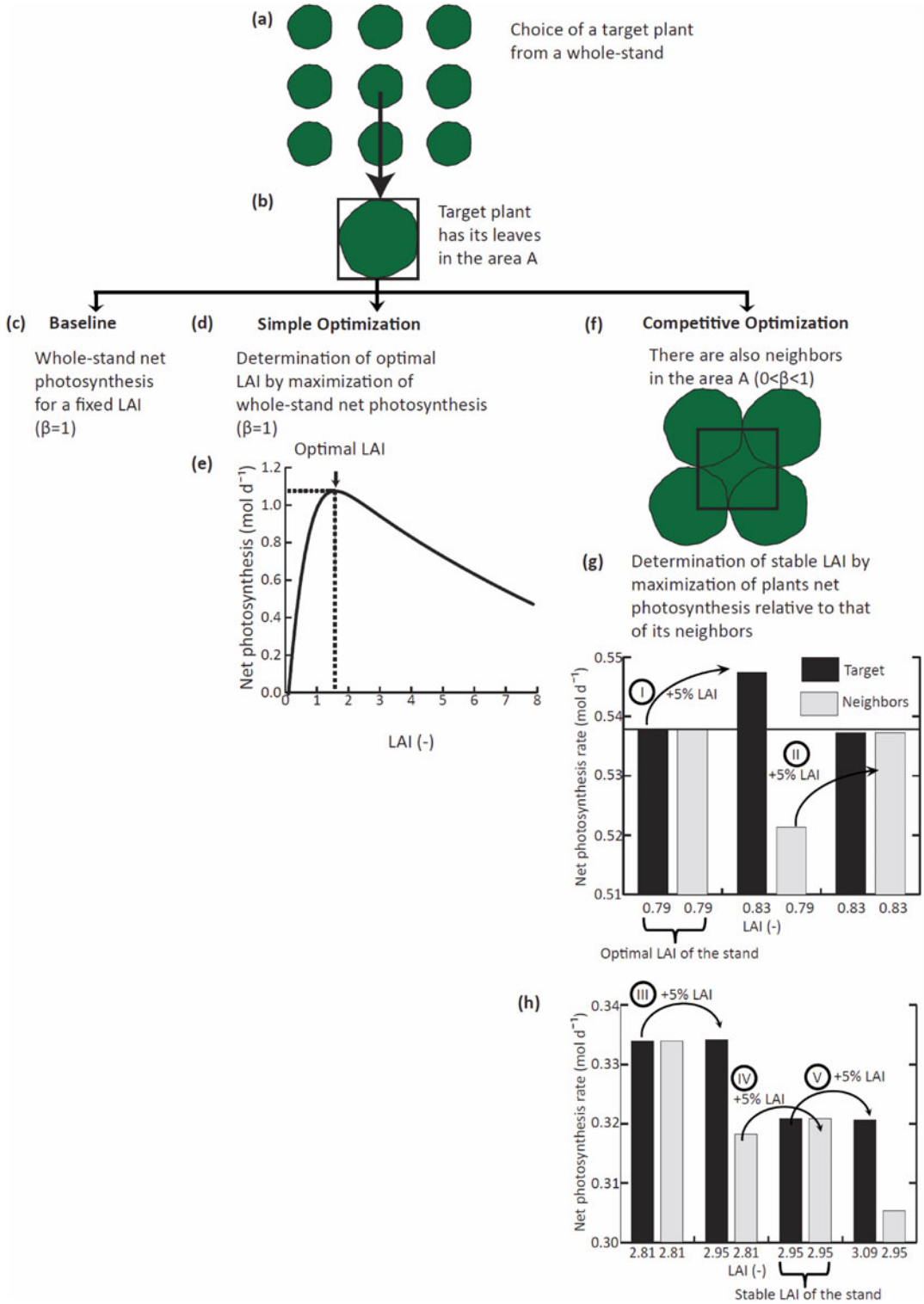

Fig. 13.4. Overview of determination of optimal LAI and evolutionarily stable LAI. (**a**) From a whole-stand a target plant is defined (*top down view*). (**b**) The target plant has its leaves in a specified area (area A; $A = 1\ \mathrm{m}^2$).

and stomatal conductance as found in more than 100 field-applied elevated CO_2 experiments. However, these seemingly encouraging results, in fact do not verify the model as the real degrees of inter-plant interaction were not measured.

C. Plant Growth Forms and the Degree of Interplant Interactions

As noted above the evolutionary stable value for increasing investment in resource harvesting (i.e., tall stature, large LAIs composed of horizontally oriented leaves) increases with the degree to which plants influence each other's light climate. Note that parallel analysis can be done for below-ground interactions. The degree of interaction may vary between species depending on their growth and shoot architecture. Unfortunately this interaction has rarely been quantified, the only one known to me being Hikosaka et al. (2001) who estimated that in dense stands of the herbaceous annual *Xanthium canadense*, only 30 % of the light gradient that plants experienced was caused by self-shading ($p \approx 0.3$). Interestingly, *X. canadense* tends to have horizontally projected leaves and forms stands with high K values (Anten and Hirose 1998, 2001) as predicted by Hikosaka and Hirose (1997).

Trees tend to have broader canopies than herbaceous plants and may thus have relatively more self-shading. Interestingly results from simple optimization models for tree canopy characteristics seem to reasonably well predict real values (e.g. Franklin 2007, 2012), which would confirm this idea. Climbing plants, on the other hand, will be shaded mostly by leaves of other plants as they tend to spread their leaves through canopies of other plants.

Clonal plants (plants that can reproduce through production of vegetative offspring) are an especially interesting group of plants when considering group vs individual level optimization. Many clonal species produce short runners whereby vegetation offspring is placed closely around the mother plant, thus creating mono-clonal patches (i.e., the so-called phalanx growth strategy, Lovett-Doust 1981). Such plants should be expected to exhibit traits that are closer to simple optima than many non-clonal species or clonal species with longer spacers and a larger degree of inter-genotypic mixing (i.e., with a guerilla-type growth form Lovett-Doust 1981). This prediction to my knowledge has not been systematically tested.

Another interesting factor that may drive variation in self vs non-self interaction in plant canopies is solar inclination angle, being negatively correlated with latitude. The path length of a solar beam through vegetation increases with solar inclination angle; in other words, before reaching the leaves of a given plant, light has to pass through more leaf area of neighbors. Vermeulen (2014) analyzed evolutionary stable canopy depth of trees in relation to changing solar angles using an EGT model.

Fig. 13.4. (continued) (**c**) If there are no neighbors in the area *A*, then the simple optimization is performed ($\beta = 1$, β is the ratio of targets leaf area to the total leaf area in the area A), (**d**) by maximization of whole-stand net photosynthesis to determine the optimal LAI. (**e**) If there are next to the target plant neighbors in the area *A* ($0 < \beta < 1$), then competitive optimization is performed. (**f**) The evolutionarily stable LAI is defined by maximization of the plants net photosynthesis rate relative to that of its neighbors. To determine this several steps should be taken. (Step I) Increase the LAI of the target plant to 5 % more than the optimal LAI (which maximizes net photosynthesis for the whole-stand, indicated by a black line). By unilaterally increasing its leaf area, the target plant captures a larger fraction of the available light, resulting in an increase in net photosynthesis rate of the target plant. (Step II) The neighbor increases its LAI also by 5 %, and as such the LAI of the whole stand was also increased by 5 %. Increasing the LAI of the stand above its optimal LAI will reduce the net photosynthesis of the whole stand. (**g**) This process was repeated (Step III and IV), until a value of the LAI of the stand was found at which a further change in the LAI of the target plant did not increase the net photosynthesis rate of the target plant (Step V), which then is the stable LAI (Figure redrawn from van Loon et al. 2014)

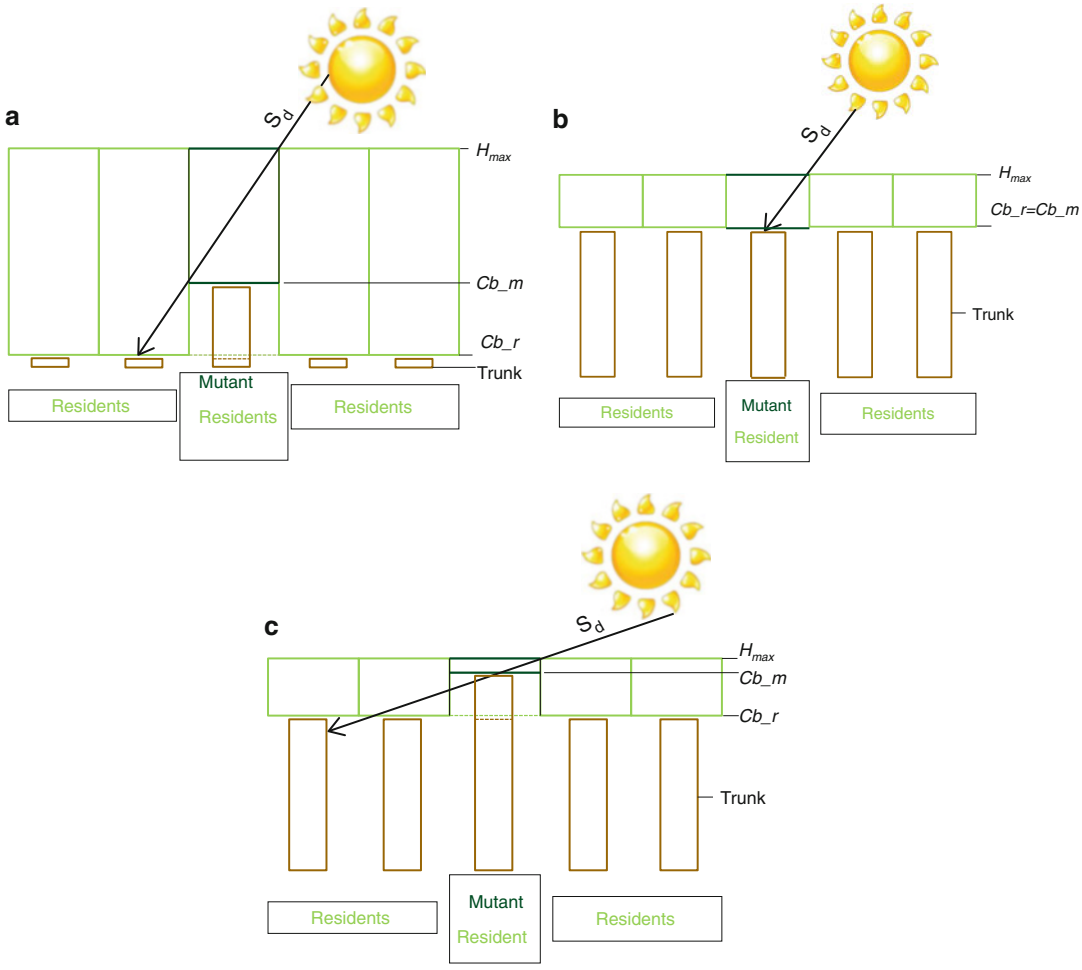

Fig 13.5. Fraction of the leaves within a crown that is at least partly shaded by the crown of neighbouring trees, as a function of crown base height and solar inclination angle. If the solar inclination angle is not equal to 90°, and under the assumption that the maximum height of the tree (H_{max}) does not change, the leaves within the tree can be divided between leaves that are at least partly shaded by neighboring trees (below the line indicated by S_d), and leaves that are only shaded by leaves of the same tree (above this line). When the crown base (*Cb*) is low, the ratio of leaves that is at least partly shaded by neighbors is high (large part of the crown below the line S_d; see figure **a**), and thus non-self interaction is high. This can lead to selection for higher crown base, as this increases the average leaf height and thus higher light capture for the tree (see shift from crown base height of the residents (*Cb_r*) to that of a mutant with a higher value (*Cb_m*). At high crown base, however, the non-self interaction is low, as most of the leaves are no longer shaded by neighboring trees (see figure **b**). When the Sun is on average lower in the sky (i.e. a low solar inclination angle), the fraction of non-self interaction increases, as more leaves are shaded by neighboring trees. Hence, with decreasing solar inclination angle, selection towards thinner crowns is predicted to be stronger. More detailed analysis shows that the same increase of non-self interaction with decreasing solar inclination angle also occurs for the leaves that are at least partly shaded by neighboring tree (i.e. for leaves under de S_d line, fig c; see for more detail Vermeulen 2014)

He found that trees should have higher canopy bases and thus shallower canopies with decreasing solar angle and thus with increasing latitude. Raising the canopy base is a competitive strategy as leaves on average will be higher in the vegetation improving the competitive status of a plant. The payoff of this strategy was greater when non-self interaction increased under lower solar inclination (see details in Fig. 13.5). Intriguingly

this finding was contrary to the often held belief that trees at higher latitudes should have deeper crowns as this enables them to more efficiently capture the light that comes in at low elevation angles (e.g. Terborgh 1985; King and Clark 2011).

An important further assumption of most EGT canopy models is that they assume a completely homogenous resident population in which all individuals are identical. By consequence, a given change in strategy will have the same effect irrespective of the plant that exhibits this change. In real life of course most vegetation is made up of genetically different plants; as noted above even in mono-species vegetation of clonal plants, different genotypes with a set of different characteristics often grow together. The effect of e.g. an increase in leaf area will depend on other traits (e.g. photosynthetic and respiratory traits, leaf area, nitrogen uptake etc) and thus this effect will differ between genotypes. Vermeulen et al. (2013) analyzed experimental stands of *Potentilla reptans* in which 10 genotypes grew together. They found the leaf area of the dominant genotype to be an ESS in the sense that this genotype was stable against changes in leaf area of itself, but that the other genotypes were not at an ESS. This creates a potential instability even for the dominant genotype, because invasions by mutants in the other genotypes would change the vegetation structure whereby the dominant genotype is no longer at an ESS. Clearly, this situation is even more complicated in multi-species stands and thus further development of multi-player game models for plant canopies is urgently needed.

IV. Dynamic Plant Simple Optimization Models

One important characteristic common to the models discussed above is that they do not account for canopy dynamics (but see e.g. Fournier and Andrieu 1998). Canopy development is a dynamic process that includes internode elongation, branching, changes in leaf inclination angle, redistribution of resources from older to younger leaves and the subsequent birth and death of leaves. To adequately model canopy structure and to link it to underlying physiological mechanisms, these processes should be accounted for.

A. Dynamic Models of Leaf Area Growth and Nitrogen Dynamics

The above-mentioned studies on optimal nitrogen distribution and LAI considered these traits to be static. As plants grow new leaves are produced while old ones senesce and when leaves are shed some of the resources are reallocated to support new leaf growth while some are lost. Franklin and Ågren (2002) developed a dynamic model to analyze photosynthetic nitrogen-use efficiency in plant canopies including leaf turnover and nitrogen resorption. They proposed that it is beneficial for a plant to drop a leaf if the increase in plant photosynthesis that can be achieved elsewhere in the plant with the nitrogen that is resorbed from that leaf exceeds its own photosynthesis. This approach was later expanded by (Hikosaka 2003, 2005). These dynamic models make a number of interesting predictions: LAI decreases with an increasing resorption efficiency r_{eff} (the fraction of nitrogen that plants resorb from senescing leaves) and is very sensitive to variation in the rate of nitrogen uptake and the nitrogen content of dead leaves.

Notably however, for any $r_{eff} < 1$ (i.e., at least some nitrogen being lost when leaves are dropped) the model predicted larger optimal LAI values than the static-plant optimization (SSO) model of Anten et al. (1995b) and these values were reasonably close to the measured values (Franklin and Ågren 2002). This raises the question as to why a dynamic model predicts larger optimal LAIs than a static model? The explanation is that if LAI of a vegetation stand exceeds the optimal as defined by Anten et al. (1995b), LAI can only be reduced by dropping leaves, but

for $r_{eff} < 1$ this entails nitrogen losses thus indirectly losses in photosynthetic capacity of the plant.

The above-mentioned models (Franklin and Ågren 2002; Hikosaka 2003) used canopy photosynthesis as a performance measure. Several dynamic models have since then been published that expand this approach to simulate growth including respiration and turnover of non-photosynthetic tissue. Franklin (2007) simulated the dynamics of tree growth in forests, including respiration and turnover of non-photosynthetic tissue and, in a later version (Franklin et al. 2009), costs of nitrogen uptake. He considered maximization of net mass increment – the difference between photosynthetic carbon gain and carbon losses through respiration and turn over – as an optimization criterion. The rationale behind this was that plant size, which is the accumulation of net mass increment, is closely related to reproductive success. The model gave reasonably good predictions of biomass increment as well as the relative effects of CO_2 elevation on LAI, canopy photosynthesis and NPP, obtained from field applied elevated CO_2 (FACE) experiments conducted for several tree species. Mäkelä et al. (2008) considered optimization of three traits, canopy-average leaf nitrogen content per unit mass, canopy leaf mass and the amount of fine-root biomass at which NPP was maximized. They further assumed steady state conditions with respect to both C (growth equals litter production) and nitrogen (nitrogen uptake equals nitrogen loss) and successfully predicted leaf and fine root biomass in stands of *Pinus silvestris* and *Picea abies.*

In short, dynamic-plant simple optimization (DSO) models have taken important innovative steps by introducing leaf turnover and nitrogen resorption rates and nitrogen uptake from the soil to optimality models. When linked to the broad empirical literature on the ecological aspects of leaf dynamics (see Aerts and Chapin 2000; Wright et al. 2004), this provides an important new tool to analyze the adaptive significance of these traits.

B. Functional Structural Models

While the above-mentioned dynamic models entail an important step forward, their dynamics is still limited to leaf turnover, with growth in other organs (stems, branches an petioles) not being considered. Furthermore the structural consequences of growth – e.g. the location and thus the specific shading effect of a newly produced leaf -- were also not taken into account. This gap can be overcome by the application of so-called plant functional structural modeling (FSP modeling) (Evers et al. 2007, 2010; Vos et al. 2010). This methodology explicitly considers the structure of plants and the physiological functions that govern plant development. It can for example be used to model the complicated interplay between light signaling in plant canopies and associated plastic responses in e.g. internode elongation and leaf angle (e.g. de Wit et al. 2012). Details of this modeling approach are discussed in Chap. 8 (Evers 2016). Important challenges lie in linking these responses with optimization techniques. For example, by combining FSP modeling with dynamic optimization one can analyze how architectural growth traits and their physiological regulation scale to vegetation structure and functioning. Specifically it can be analyzed how these dynamic processes determine crop yields, which is currently an important knowledge gap in crop science.

V. Dynamic Game Theoretical Models

As discussed above, the last decade has seen two important advances in canopy optimality models: the application of evolutionary game theory that considers optimal traits of individual plants relative to their neighbors and dynamic plant optimization that takes dynamic growth processes into account. The challenge lies in combining these two approaches (Anten and During 2011). Such a combined approach would enable us to analyze how selection may have acted on

dynamic growth processes in plant canopies (e.g., leaf dynamics or the elongation and dynamics of support structures).

One of the first models that attempted to combine EGT with dynamic plant modeling was Pronk (2004) and Pronk et al. (2007). They game theoretically analyzed height growth taking into account that height growth itself is dynamic and secondly that height growth is associated with production of new leaves at the top of the canopy and possibly loss of leaves at the bottom. Height growth was defined as the quotient of the amount of assimilates allocated to stem growth and the amount of mass per unit height (M_s) multiplied by the construction costs of stem tissue (cs).

$$\mathrm{d}(h)/dt = f_{st} * \mathrm{NPP}/(M_s * cs) \qquad (13.7)$$

with h height, f_{st} the fraction of NPP allocated to stem growth (see Pronk 2004 for more details). The second more complicated step involved the changes in leaf area distribution as plants grow taller. Pronk et al solved this by a priori defining a general form of vertical leaf area distribution (Caton et al. 1999).

$$\lambda(h) = p_o \cdot \frac{L_t}{h_{pt}} \left(\frac{h}{h_{pt}}\right)^{p1} \cdot \left(1 - \frac{h}{h_{pt}}\right)^{p2} \qquad (13.8)$$

with $\lambda(h)$ the leaf area density (amount of leaf area per air volume), L_t the leaf area index of the plant, h_{pt} the total plant height (distance between soil and top leaf) and h the height at which λ is calculated. $p0, p1$ and $p2$ are parameters that define the form of the distribution. The shape of the distribution is essentially defined by $p1$ and $p2$: $p1 > p2$ implies canopies with leaves concentrated towards the top (as in many erect dicot species) and $p1 < p2$ leaves being concentrated more in the lower layers (e.g. many grasses tend to grow from basal meristems) (see Fig. 14.2 in Chap. 14, Anten and Bastiaan 2016). Key to this approach is that Eq. 13.8 defines the vertical pattern of leaf production and loss as visualized in Fig. 14.2 in Chap. 14 (Anten and Bastiaan 2016).

Regarding game theoretical modeling of leaf turnover, Hikosaka and Anten (2012) developed a model that essentially extended the approach of Hikosaka (2003). The canopy was divided into 100 horizontal canopy layers with equal leaf area. Leaf area growth was calculated by allocating a certain percentage of NPP to leaf growth correcting for leaf mass per area as well as leaf construction costs. For leaf senescence three vertical patterns were considered: Case 1 leaves are equally dropped from all layers; Case 2 leaves are strictly dropped from the lowest layers; and the intermediate Case 3 leaves are dropped from all layers but preferentially from lower layers. The timing of leaf senescence was analyzed game theoretically as a density dependent trait. The ESS temporal pattern in leaf senescence was defined as the one at which no change in this pattern could give an individual a benefit in terms of canopy photosynthesis. The LAI and associated canopy photosynthesis were thus emergent traits determined by the leaf area growth and the density-dependent timing of leaf senescence.

Hikosaka and Anten (2012) showed that stable LAI values depended not only on the assumed degree to which plants influence each other's light climate, as had been shown in static-plant EGT models, but also on the pattern of leaf senescence. ES-LAI values increased with the degree leaves are dropped from higher rather than lower canopy layers. This is understandable as leaves from high layers play a more important role in light competition and dropping them thus entails a larger loss in competitive ability. The ability of this model to predict real measured LAI values also depended on the assumed degrees of interaction as well the pattern of leaf senescence. Case 3, the assumption that leaves are preferentially but not exclusively from lower canopy layers, however, provided the best predictions (Fig. 13.6).

Clearly the models discussed above entail the first steps in combining EGT with dynamic plant modeling. Yet they are still incomplete. For example, Pronk et al.

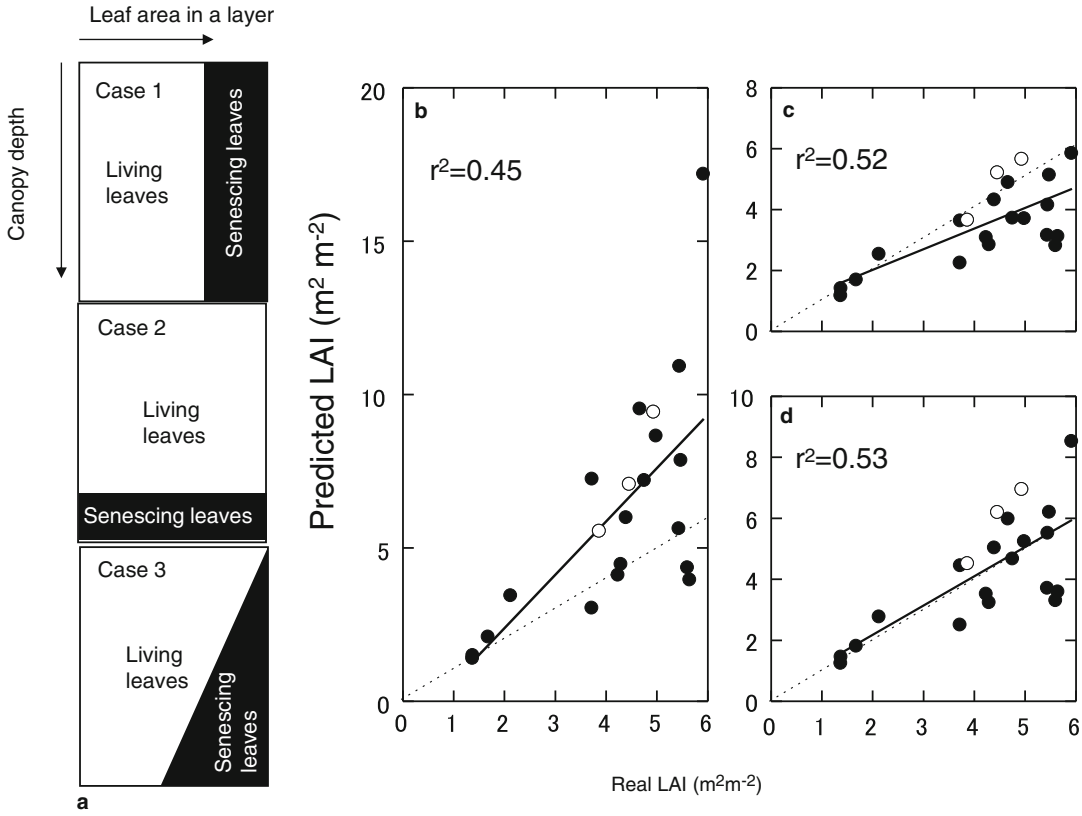

Fig. 13.6. Summary results for predicted LAI values with a dynamic-plant game theoretical model. (**a**) The assumed leaf senescence patterns: Case 1 leaves are dropped from all canopy layers equally, Case 2 leaves are only dropped from the bottom of the canopy and the intermediate Case 3 where leaves are dropped from all layers but preferentially from the bottom. (**b**–**d**) Predicted and real leaf area index (LAI) using data obtained from 21 stands of 10 species (see Table S1 in Hikosaka and Anten (2012) for species list), b, c, and d shows Case 1, 2 and 3 respectively (Figure redrawn with permission from Hikosaka and Anten 2012)

(2007) consider the vertical dynamics in leaf area but do not consider the nitrogen dynamics associated with the uptake from the soil, reallocation from senescent leaves and losses. Hikosaka and Anten (2012) on the other hand, did not consider height growth and associated placement of leaves at the top of the canopy. Thus there remains a challenge in developing game theoretical models that include all key features of canopy dynamics: i.e., stem and branch production and elongation, uptake of resources, leaf turn over and associated redistribution of nitrogen.

To my opinion some of these issues can be addressed by employing functional structural modeling (FSPM). As described in Sect. IV and in Chap. 8 (Evers 2016), FSP models explicitly address the production and growth of structural plant elements (e.g. leaves, petioles, branches and stems) in a realistic 3D setting. FSPM could be linked to physiological models that grasp leaf turn over and associated nitrogen dynamics (e.g. Hikosaka 2003) and then used in EGT analyses. As such an integrated dynamic analysis of the adaptive significance of variation in plant structural traits is possible.

VI. Choice of Fitness Proxy

As noted, the key element in ecological optimization modeling, at least when applied to wild plants, is the underlying assumption

that trait values that are selected for are those that maximize fitness. An important advantage of this approach is that the plant trait values in a model are derived from ecological principles largely reducing the difficulty of parameterization. Ideally a measure such as lifetime reproduction should thus be used as a goal function. Most, current optimization models, however, use either canopy photosynthesis (e.g. Anten 2002; Hikosaka 2003) or net growth (photosynthesis – respiration – turnover) (e.g. Franklin et al. 2009; Sterck et al. 2011). The underlying argument is that rapid assimilation provides the resources for growth, enabling plants to successfully compete for additional resources and reproduction.

Evidently, lifetime reproduction is determined by more factors than just growth (i.e., adult survival, fecundity and successful establishment of new recruits), and tradeoffs may exist between these demographic rates. For example under adverse conditions such as in tropical forest understory, variation in growth across species tends to be negatively correlated with survival; pioneer species exhibiting more rapid growth but high rates of mortality than shade-tolerant species (e.g. Poorter 2005). This suggests that under these conditions there is selection for traits that facilitate survival rather than for growth related traits. Population models confirm this notion, with variation in population growth of long-lived understory species being more sensitive to variation in survival than to variation in growth or annual reproduction (e.g. Zuidema et al. 2007).

Recently Dybzinski et al. (2011) developed a forest canopy model based on the concept of adaptive dynamics (Brown and McGill 2007), which intended to use lifetime reproduction as a performance measure, i.e., substituting P in Eq. 13.4 by W which they indicated as lifetime reproduction. In essence their model considers forests to be composed of two layers: canopy and understory, with the former being composed of reproductively active adults and the latter of juveniles. Competition was assumed to be for nitrogen only; the relative uptake of nitrogen out of the soil nitrogen being directly proportional to fine root mass. Thus, an individual with a greater allocation to fine roots than its neighbors can acquire a larger share of the available nitrogen albeit at the cost of producing extra roots. As in previous EGT models a series of invasions of a resident by mutant individuals was simulated until a stable strategy defined by Eq. 13.3 was met: no change in allocation could give an individual an increase in life time reproduction.

This model was applied to the publicly available FLUXNET data base and patterns of leaf, stem and fine root allocation were well predicted. Particularly the model predicted an apparent tradeoff between stem and fine root allocation. But some other trends were not well predicted, particularly the observed increase in root growth at greater nitrogen availability. While this model approach definitely needs further improvement, it represents an important new direction: linking EGT canopy modeling to mechanistic models of plant demography. To my opinion this is an important new direction in canopy modeling.

VII. Conclusions

Application of optimization theory in canopy modelling is useful in at least two regards. Firstly it provides a simple but plausible framework to scale from individual organ-level processes, such as leaf photosynthesis, to the structure and functioning of vegetation stands. As such it is now increasingly being used as a tool in predictive modelling of e.g. climate change effects on vegetation. Similarly in this regard it can be used in model-guided crop breeding, that is, model design of optimal traits for maximal crop functioning. Secondly, optimization provides a modelling tool to analyse natural selection in plant communities and its effect on community functioning. Here, I have shown that the assumption of simple optimization (traits being optimal when community functioning is maximized), that

predominates most current optimization models, might be flawed as it fails to capture that natural selection acts at the level of individual plants and not at the community level and is strongly mediated by plant-plant interactions. Game theoretical models do capture these aspects but most are overly simplified with respect to plant architecture and growth dynamics and the fitness proxy that is used as a goal function (i.e. often canopy photosynthesis or growth). Important steps can be made by combining game theory with more advanced modelling currently available such as functional-structural modelling and by including the dynamic interactions between plants and their (a) biotic environment.

Acknowledgments

I thank, Kouki Hikosaka, Marloes van Loon, Peter Vermeulen and an anonymous reviewer for valuable comments on the manuscript.

References

Aerts R, Chapin FS III (2000) The mineral nutrition of wild plants revisited: a re-evaluation of processes and patterns. Adv Ecol Res 30:1–67

Albaugh T, Allen H, Dougherty P, Kress L, King J (1998) Leaf area and above and belowground growth responses of loblolly pine to nutrient and water additions. For Sci 44:317–328

Anten NPR (2002) Evolutionarily stable leaf area production in plant populations. J Theor Biol 217:15–32

Anten NPR (2005) Optimal photosynthetic characteristics of individual plants in vegetation stands and implications for species coexistence. Ann Bot 95:495–506

Anten NPR, Bastiaans L (2016) The use of canopy models to analyze light competition among plants. In: Hikosaka K, Niinemets Ü, Anten N (eds) Canopy Photosynthesis: From Basics to Applications. Springer, Berlin, pp 379–398

Anten NPR, During HJ (2011) Is analyzing nitrogen-use efficiency at the plant canopy level a matter of choosing the right optimization criterion. Oecologia 167:293–303

Anten NPR, Hirose T (1998) Biomass allocation and light partitioning among dominant and subordinate individuals in *Xanthium canadense* stands. Ann Bot 82:665–673

Anten NPR, Hirose T (2001) Limitations on photosynthesis of competing individuals in stands and the consequences for canopy structure. Oecologia 129:186–196

Anten NPR, Schieving F, Medina E, Werger MJA, Schuffelen P (1995a) Optimal leaf area indices in C_3 and C_4 mono- and dicotyledonous species at low and high nitrogen availability. Physiol Plant 95:541–550

Anten NPR, Schieving F, Werger MJA (1995b) Patterns of light and nitrogen distribution in relation to whole canopy carbon gain in C_3 and C_4 mono- and dicotyledonous species. Oecologia 101:504–513

Anten NPR, Werger MJA, Medina E (1998) Nitrogen distribution and leaf area indices in relation to photosynthetic nitrogen use efficiency in savanna grasses. Plant Ecol 138:63–75

Anten NPR, Hirose T, Onoda Y, Kinugasa T, Kim HY, Okada M, Kobayashi K (2004) Elevated CO_2 and nitrogen availability have interactive effects on canopy carbon gain in rice. New Phytol 161:459–471

Caton BP, Foin TC, Hill JE (1999) A plant growth model for integrated weed management in direct-seeded rice. III. Interspecific competition for light. Field Crop Res 63:47–61

de Pury D, Farquhar GD (1997) Simple scaling of photosynthesis from leaves to canopies without the errors of big-leaf models. Plant Cell Environ 20:537–557

de Wit M, Pierik R (2016) Photomorphogenesis and photoreceptors. In: Hikosaka K, Niinemets Ü, Anten N (eds) Canopy Photosynthesis: From Basics to Applications. Springer, Berlin, pp 171–186

de Wit M, Kegge W, Evers JB, Vergeer-van Eijk MH, Gankema P, Voesenek LACJ, Pierik R (2012) Plant neighbor detection through touching leaf tips precedes phytochrome signals. Proc Natl Acad Sci U S A 109:14705–14710

Dewar RC, Franklin O, Mäkelä A, McMurtrie RE, Valentine HT (2009) Optimal function explains forest responses to global change. Bioscience 59:127–139

Dudley SA, Schmitt J (1996) Testing the adaptive plasticity hypothesis: density dependent selection on manipulated stem length in *Impatiens capensis*. Am Nat 147:445–465

Dybzinski R, Farrior C, Wolf A, Reich PB, Pacala SW (2011) Evolutionary stable strategy carbon allocation to foliage wood and fine roots in trees

competing for light and nitrogen: an analytically tractable individual-based model and quantitative comparisons to data. Am Nat 177:153–166

Ennos AR (1997) Wind as an ecological factor. Trends Ecol Evol 12:108–111

Evans JR (1989) Photosynthesis and nitrogen relationships in leaves of C_3 plants. Oecologia 78:9–19

Evers JB (2016) Simulating crop growth and development using functional-structural plant modeling. In: Hikosaka K, Niinemets Ü, Anten N (eds) Canopy Photosynthesis: From Basics to Applications. Springer, Berlin, pp 219–236

Evers JB, Vos J, Chelle M, Andrieu B, Fournier C, Struik PC (2007) Simulating the effects of localized red:far-red ratio on tillering in spring wheat (*Triticum aestivum*) using a three-dimensional virtual plant model. New Phytol 176:325–336

Evers JB, Vos J, Yin X, Romero P, van der Putten PEL, Struik PC (2010) Simulation of wheat growth and development based on organ-level photosynthesis and assimilate allocation. J Exp Bot 61:2203–2216

Falster DS, Westoby M (2003) Plant height and evolutionary games. Trends Ecol Evol 18:337–343

Farquhar GD (1989) Models of integrated photosynthesis of cells and leaves. Philos Trans R Soc B 323:357–367

Field C (1983) Allocating leaf nitrogen for the maximization of carbon gain: leaf age as a control on the allocation program. Oecologia 56:341–347

Field C, Mooney HA (1986) The photosynthesis-nitrogen relationship in wild plants. In: Givnish TJ (ed) On the economy of plant form and function. Cambridge University Press, Cambridge, pp 25–55

Fournier C, Andrieu B (1998) A 3D architectural and process-based model of maize development. Ann Bot 81:233–250

Franklin O (2007) Optimal nitrogen allocation controls tree responses to elevated CO_2. New Phytol 174:811–822

Franklin O, McMurtrie RE, Iversen CM, Crous KY, Finzi AC, Tissue DT, Ellsworth DS, Oren R, Norby RJ (2009) Forest fine-root production and nitrogen use under elevated CO2: contrasting responses in evergreen and deciduous trees explained by a common principle. Glob Chang Biol 15:132–144

Franklin O, Ågren GI (2002) Leaf senescence and resorption as mechanisms of maximizing photosynthetic production during canopy development at N limitation. Func Ecol 16:727–733

Franklin O, McMurtrie RE, Iversen CM, Crous KY, Finzi AC, Tissue DT, Ellsworth DS, . . ., Norby RJ (2009) Forest fine-root production and nitrogen use under elevated CO_2: Contrasting responses in evergreen and deciduous trees explained by a common principle. Global Change Biol 15:132–144

Franklin O, Johanson J, Dewar RC, Dieckman U, McMurtrie RE, Branstrom A, Dybzinski R (2012) Modelling carbon allocation in trees: a search for principles. Tree Physiol 32:648–666

Geritz SAH, Kisdi E, Meszena G, Metz JAJ (1998) Evolutionarily singular strategies and the adaptive growth and branching of the evolutionary tree. Evol Ecol 12:35–57

Givnish TJ (1982) On the adaptive significance of leaf height in forest herbs. Am Nat 120:353–381

Givnish TJ (1988) Adaptation to sun and shade: a whole-plant perspective. Aus J Plant Physiol 15:63–92

Goudriaan J (2016) Light distribution. In: Hikosaka K, Niinemets Ü, Anten N (eds) Canopy Photosynthesis: From Basics to Applications. Springer, Berlin, pp 3–22

Hikosaka K (2003) A model of dynamics of leaves and nitrogen in a canopy: an integration of canopy photosynthesis, leaf life-span and nitrogen-use efficiency. Am Nat 162:149–164

Hikosaka K (2005) Leaf canopy as a dynamic system: ecophysiology and optimality in leaf turnover. Ann Bot 95:521–533

Hikosaka K (2014) Optimal nitrogen distribution within a leaf canopy under direct and diffuse light. Plant Cell Environ 9:2077–2085

Hikosaka K, Anten NPR (2012) An evolutionary game of leaf dynamics and its consequences for canopy structure. Func Ecol 26:1024–1032

Hikosaka K, Hirose T (1997) Leaf angle as a strategy for light competition: optimal and evolutionary stable light-extinction coefficient within a leaf canopy. Ecoscience 4:501–507

Hikosaka K, Nagashima H, Harada Y, Hirose T (2001) A simple formulation of interaction between individuals competing for light in a monospecific stand. Func Ecol 15:642–646

Hikosaka K, Kumagai T, Ito A (2016) Modeling canopy photosynthesis. In: Hikosaka K, Niinemets Ü, Anten N (eds) Canopy Photosynthesis: From Basics to Applications. Springer, Berlin, pp 239–268

Hirose T (2005) Development of the Monsi–Saeki theory: an introduction to the study of canopy structure and function. Ann Bot 95:483–494

Hirose T, Werger MJA (1987) Nitrogen use efficiency in instantaneous and daily photosynthesis of leaves in the canopy of *Solidago altissima* stand. Physiol Plant 70:215–222

Hirose T, Ackerly DD, Traw MB, Ramseier D, Bazzaz FA (1997) CO2 elevation, canopy photosynthesis and optimal leaf area index in annual plant stands. Ecology 78:2338–2350

Iwasa Y, Cohen D, Leon DA (1984) Tree height and crown shape as a result of competitive games. J Theor Biol 112:279–298

King DA, Clark DA (2011) Allometry of emergent tree species from saplings to above-canopy adults in a Costa Rican rain forest. J Trop Ecol 27:573–579

Kira T (1991) Forest ecosystems of East and Southeast Asia in a global perspective. Ecol Res 6:185–200

Koyama K, Kikuzawa K (2010) Geometrical similarity analysis of photosynthetic light response curves, light saturation and light-use efficiency. Oecologia 164:53–63

Kull O (2002) Acclimation of photosynthesis in canopies: models and limitations. Oecologia 133:267–279

Lambers H, Cambridge ML, Pons TL (1998) Physiological Ecology. Springer Verlag, New York

Lindroth A, Lagergren F, Aurela M et al (2008) Leaf area index is the principal scaling parameter for both gross photosynthesis and ecosystem respiration of northern deciduous and coniferous forests. Tellus B 60:129–142

Lloyd J, Patiño S, Paiva RQ, Nardoto GB, Quesada CA, Santos AJB, Baker TR, . . ., Mercado LM (2010) Optimization of photosynthetic carbon gain and within-canopy gradients of associated foliar traits for Amazon forest trees. Biogeosciences 7:1833–1859

Lovett-Doust L (1981) Population dynamics and local specialization in a clonal perennial (*Ranunculus repens*). J Ecol 69:743–755

Mäkelä A, Valentine HT, Helmisaari H-S (2008) Optimal co-allocation of carbon and nitrogen in a forest stand at steady state. New Phytol 180:114–123

Maynard-Smith J (1974) The theory of games and the evolution of animal conflicts. J Theor Biol 47:209–221

McGill B, Brown J (2007) Evolutionary game theory and adaptive dynamics of continuous traits. Annu Rev Ecol Evol Syst 38:403–435

McMahon T (1973) Size and shape in biology. Science 179:1201–1204

McMurtrie RE, Norby RJ, Medlyn BE, Dewar RC, Pepper DA, Reich PB, Barton CVM (2008) Why is plant growth response to elevated CO_2 amplified when water is limiting but reduced when nitrogen is limiting? Func Plant Biol 35:521–534

Monsi M, Saeki T (1953) Über den Lichtfaktor in den Pflanzengesellschaften und seine Bedeutung für die Stoffproduktion. Jpn J Bot 14:22–52. *Translated as*: Monsi M, Saeki T (2005) On the factor light in plant communities and its importance for matter production. Ann Bot 95:549–567

Monsi M, Uchijima Z, Oikawa T (1973) Structure of foliage canopies and photosynthesis. Annu Rev Ecol Syst 4:301–327

Nagashima H, Hikosaka K (2011) Plants in a crowded stand regulate their height growth so as to maintain similar heights to neighbours even when they have potential advantages in height growth. Ann Bot 108:207–214

Nagashima H, Hikosaka K (2012) Not only light quality but also mechanical stimuli are involved in height convergence in crowded *Chenopodium album* stands. New Phytol 195:803–811

Niinemets Ü (2007) Photosynthesis and resource distribution through plant canopies. Plant Cell Environ 30:1052–1071

Niinemets Ü (2012) Optimization of foliage photosynthetic capacity in tree canopies: towards identifying missing constraints. Tree Physiol 32:505–509

Oikawa S, Hikosaka K, Hirose T (2005) Dynamics of leaf area and nitrogen in the canopy of an annual herb, Xanthium canadense. Oecologia 143:517–526

Oikawa S, Hikosaka K, Hirose T (2006) Leaf lifespan and lifetime carbon balance of individual leaves in a stand of an annual her, Xanthium canadense. New Phytol 172:104–116

Parker GAJ, Maynard-Smith J (1990) Optimality theory in evolutionary biology. Nature 348:27–33

Poorter L (2005) Resource capture and use by tropical forest tree seedlings and their consequences for competition. In: Burslem DF, Pinard MA, Hartley SE (eds) Biotic Implication in the Tropics: Their Role in Maintenance of Species Diversity. Cambridge University Press, Cambridge, pp 35–64

Posada JM, Lechowicz MJ, Kitajima K (2009) Optimal photosynthetic use of light by tropical tree crowns achieved by adjusting of individual leaf angles and nitrogen contents. Ann Bot 103:795–805

Pronk TE (2004) The role of plant traits in the regulation of diversity. PhD thesis, Utrecht University, Utrecht, The Netherlands

Pronk TE, Schieving F, Anten NPR, Werger MJA (2007) Plants that differ in height investment can coexist if they are distributed non-uniformly within an area. Ecol Complex 4:182–191

Reich PB, Falster DS, Ellsworth DS, Wright IJ, Westoby M, Oleksyn J, Lee TD (2009) Controls on declining carbon balance with leaf age among 10 woody species in Australian woodland: do leaves have zero daily net carbon balances when they die? New Phytol 183:153–166

Riechert SE, Hammerstein P (1983) Game theory in the ecological context. Annu Rev Ecol Syst 14:377–409

Ryan MG, Phillips N, Bond BJ (2006) The hydraulic limitation hypothesis revisited. Plant Cell Environ 29:367–381

Sage RF, Pearcy RW (1987) The nitrogen use efficiency of C3 and C4 plants. II. Leaf nitrogen effects on the gas exchange characteristics of *Chenopodium album* (L.) and *Amaranthus retroflexus (L.)*. Plant Physiol 84:959–963

Saeki T (1960) Interrelationships between leaf amount, light distribution and total photosynthesis in a plant community. Bot Mag Tokyo 73:55–63

Sakai S (1991) A model analysis for the adaptive architecture of herbaceous plants. J Theor Biol 148:535–544

Schieving F (1998) Plato's plant. Ph.D. thesis, Utrecht University, Backhuys Publ., Leiden

Schieving F, Poorter H (1999) Carbon gain in a multispecies canopy: the role of specific leaf area and photosynthetic nitrogen-use efficiency in the tragedy of the commons. New Phytol 143:201–211

Schmitt J, Dudley SA, Pigliucci M (1999) Manipulative approaches to testing adaptive plasticity: phytochrome-mediated shade-avoidance responses in plants. Am Nat 154:S43–S54

Smith H (1982) Light quality, photoreception and plant strategy. Annu Rev Plant Physiol 33:481–518

Sterck F, Markesteijn L, Schieving F, Poorter L (2011) Functional traits determine trade-offs and niches in a tropical forest community. Proc Nat Ac Sci USA 108:20627–20632

Stockhoff BA (1994) Maximisation of daily canopy photosynthesis: effects of herbivory on optimal nitrogen distribution. J Theor Biol 169:209–220

Stutzel H, Charles-Edwards DA, Beech DF (1988) A model of the partitioning of new aboveground dry matter. Ann Bot 50:370–376

Terborgh J (1985) The vertical component of plant species diversity in temperate and tropical forests. Am Nat 126:760–776

Tremmel DC, Bazzaz FA (1993) How neighbor canopy architecture affects target plant performance. Ecology 7:2114–2124

van den Hurk BJJM, Viterbo P, Los SO (2003) Impact of Leaf Area Index seasonality on the annual land surface evaporation in a global circulation model. J Geophys Res 108:4191–4199

van Ittersum MK, Leffelaar PA, van Keulen H, Kropff MJ, Bastiaans L, Goudriaan J (2003) On approaches and applications of the Wageningen crop models. Eur J Agron 18:204–231

van Loon M, Schieving F, Rietkerk M, Dekker SC, Sterck F, Anten NPR (2014) How light competition between plants affects their response to climate change. New Phytol 203:1253–1265

Vermeulen PJ (2014) Crown depth as a result of evolutionary games: decreasing solar elevation should lead to shallower not deeper crowns. New Phytol 202:1249–1256

Vermeulen PJ, Anten NPR, Schieving F, Werger MJA, During HJ (2008) Height convergence in response to neighbor growth in the stoloniferous plant *Potentilla reptans*. New Phytol 177:688–697

Vermeulen PJ, Anten NPR, Stuefer JF, During HJ (2013) Whole-canopy carbon gain as a result of selection on individual performance of ten genotypes of a clonal plant. Oecologia 172: 327–337

Vila-Guerau de Arellano J, van Heerwaarden CC, Lelieveld J (2012) Modelled suppression of boundary-layer clouds by plants in a CO_2-rich atmosphere. Nat Geosci 5:701–704

Vos J, Evers JB, Buck-Sorlin GH, Andrieu B, Chelle M, de Visser PHB (2010) Functional-structural plant modelling: a new versatile tool in crop science. J Exp Bot 61:2102–2115

Wright IJ, Reich PB, Westoby M, Ackerly DD, Baruch Z, Bongers F, Cavendar-Bares J, . . ., Villar R (2004) The worldwide leaf economics spectrum. Nature 428:821–827

Yasumura Y, Hikosaka K, Hirose T (2006) Resource allocation to vegetative and reproductive growth in relation to mast seeding in *Fagus crenata*. For Ecol Manag 229:228–233

Yin X, Struik PC (2010) Modeling the crop: from system dynamics to systems biology. J Exp Bot 61:2171–2183

Zuidema PA, DeKroon H, Werger MJA (2007) Testing sustainability by prospective and retrospective demographic analyses: evaluation for palm leaf harvesting. Ecol Appl 17:118–128

Chapter 14

The Use of Canopy Models to Analyze Light Competition Among Plants

Niels P.R. Anten*
Crop and Weed Ecology, Centre for Crop Systems Analysis, Wageningen University, Wageningen, The Netherlands

and

Lammert Bastiaans
Crop and Weed Ecology, Centre for Crop Systems Analysis, Wageningen University, P.O. Box 430, 6700 AK Wageningen, The Netherlands

Summary

Competition for light among plants is an important factor determining plant trait evolution and community dynamics. It may also strongly modulate crop production. Canopy models provide a useful means of analyzing light competition. This use however entails that these models take account of the interactions between individual plants in vegetation stands, which is challenging. Here we first discuss how light acquisition and photosynthesis by individual plants in vegetation stands can be modeled focusing on relatively simple approaches to this problem. We then give examples of how such canopy models have been used to analyze plant light competition in natural vegetation and in crops. We first analyze the extent to which competition for light is size asymmetric. We demonstrate that, contrary to common belief, this is not always the case. Notably competition between plants of different species tends to be more symmetric

*Author for correspondence, e-mail: niels.anten@wur.nl

e-mail: lammert.bastiaans@wur.nl

K. Hikosaka, Ü. Niinemets, and N.P.R. Anten (eds.), *Canopy Photosynthesis: From Basics to Applications*, DOI 10.1007/978-94-017-7291-4_14

than competition among plants of the same species. We then focus on crop-weed interactions, and show how canopy models have enabled us to identify the traits that make crops most effective in competing with weeds. Together these examples illustrate how canopy models can strongly contribute to our mechanistic understanding of plant competition for light.

Keywords Competition • Crop ecology • Grasslands • Natural selection • Weed research

I. Introduction

Light is the energy source for photosynthesis and thus one of the primary limiting resources for plant growth and reproduction. In many growth environments fitness of plants is strongly influenced by their ability to capture light. In dense vegetation light often becomes a contested resource; since plants shade one another, the light acquisition and use by one individual influence the light availability for others. If concomitantly total availability is below the combined needs of the plants in the vegetation stand, competition ensues (Clements et al. 1929).

Competition for light is believed to be an important factor determining the evolution of aboveground plant traits (Weiner 1990). For example trees probably evolved to become as tall as they are to a large extent as a result of light competition (Givnish 1982; Falster and Westoby 2003; see Chap. 13, Anten 2016). Similarly the shade avoidance syndrome, the tendency of many plant species to increase stem elongation and reduce branching and stem radial growth, in response to neighbor proximity, is adaptive as it enables plants to compete for light when this is needed (see Chap. 6, de Wit and Pierik 2016). Thus quantifying the relationship between plant traits and their ability to successfully compete for light is an important issue in plant ecological and evolutionary research.

Understanding the mechanisms determining light competition is important in agricultural science as well. Traits that favor light competition – tall stature, large leaf areas and rapid leaf turnover -tend to go at the expense of seed production (see Chap. 13, Anten 2016). That is because the energy plants invest in light harvesting structures cannot simultaneously be invested in other functions. Not surprisingly, plant breeders have spent much effort developing cultivars that remain relatively short and strong when grown in dense stands and this has contributed to the large increases in crop yields that have been achieved during the last decades (Barneix 1990). However, the recent development of herbicide resistance

Abbreviations: f_{SL} – Fraction of sunlit leaf area; G – Whole-plant growth; h – Height in the canopy; h_{pt} – Plant height; i – Counter in subscripts indicating canopy layers; I_{bsa} – Scattered component of direct radiation; I_{da} – Diffuse sky photon flux density; I_L – Absorbed photon flux per unit leaf area; I_o – General indicator for amounts of light above the canopy; I_{ob} – Direct beam photon flux density above a canopy layer; I_{od} – Diffuse sky photon flux density above a canopy layer; j – Counter in subscripts indicating individual plant within species; k – Counter in subscripts indicating species; K_b – Extinction coefficient for direct beam radiation; K_d – Extinction coefficient for diffuse light; L – Cumulative leaf area index measured from the top of the canopy; l – Counter in subscripts indicating elevation zones on the sky dome; LAI – Amount of leaf area per unit soil area; LAR – Leaf area per unit plant mass; LMR – Leaf mass per unit plant mass; LUE – Whole-plant photosynthesis per unit of absorbed light; M – Whole-plant mass; O – Projection of a leaf into the direction of the sun; P – Indicator of photosynthesis; P_L – Photosynthesis per unit leaf area; p_{max} – Light saturated photosynthesis per unit leaf area; p_0 p_1 p_2 – Parameters indicating the shape of the leaf area distribution; r_d – Dark respiration per unit leaf area; RGR – Growth per unit plant mass; RUE – Growth per unit of absorbed light; SH – Subscript referring to leaves being shaded; SL – Subscript referring to leaves being sunlit; SLA – Leaf area per unit leaf mass; Z_l – Fraction of diffuse sky radiation coming from elevation zone l on the sky dome; α – Leaf absorption coefficient; β – Solar inclination angle; γ – Canopy reflectance; ϕ – Initial slope of the light response curve; Φ – General indicator of light capture; Φ_{area} – Whole-plant light capture per unit leaf area; Φ_{mass} – Whole-plant light capture per unit plant mass; λ – Amount of leaf area per unit air volume; θ – Curvature of the light response curve; ζ – Cumulative leaf area index counted from the top of a canopy layer

in weeds, the environmental implications of herbicide use and the large costs of weeding are creating a demand for crop varieties with a greater capacity to compete with weeds (Bastiaans et al. 1997; Moss 2003).

The relationship between structure of individual plants in a vegetation stand and the intensity and directional distribution of light in the canopy is quite complex and cannot be quantified with measurements alone. A canopy modeling approach thus becomes imperative. Most canopy models, including most that are discussed in this book, treat vegetation stands as a unit. This is usually appropriate if the objective is to quantify processes such as gas exchange, growth or yields at the whole-stand level, which is the case in many agricultural, ecological, biogeochemical studies (but see Chap. 8, Evers 2016). However, in the case of modeling competition, more detailed approaches are needed that consider the individual plants within the vegetation stand and differences in traits between them.

In this chapter we discuss how canopy models can be used to analyze light competition between individual plants. We start by discussing the technical aspects of modeling light acquisition and photosynthesis of individual plants or individual species in vegetation stands, and present a detailed example of one of the simpler approaches (layered models) that can be used to this end. We then discuss how canopy models have been used in fundamental ecological research to determine the basic mechanisms underlying competition. We focus on the extent to which competition for light among plants can be considered to be asymmetric and whether this would be different depending on whether one considers competition between or within species. The final part of this chapter will deal with the application of canopy models to analyze crop-weed interactions. Whereas these models were initially developed to better predict the necessity for applying curative weed control measures, such as the above-mentioned use of herbicides, they gradually evolved into tools for helping identify the main modes for turning the crop-weed competitive balance to the benefit of the crop.

II. Modeling Light Acquisition and Photosynthesis

Light competition between plants is in the first place determined by differences in their ability to capture light, and subsequently by their efficiency in utilizing this light for growth, which in turn enables them to compete further. These processes in turn are related to a suite of plant traits – i.e., plant height, leaf area distribution, leaf angle and leaf optical characteristics, as well as photosynthetic and respiratory traits – all of which can differ substantially both within and among species. In addition, in mixed species stands different species may be clustered. For example, in mixed cropping systems, different species are often planted in separate rows. The essence of using models to analyze competition is that this variation among individuals needs to be somehow captured. This variation can be quantified in various ways. The most accurate and realistic way is to model the 3D structure of every plant in a vegetation stand; functional-structural models approach this ideal and have been used to model light competition (Evers et al. 2007; DeJong et al. 2011; Bongers et al. 2014; Chap. 13, Evers 2016). Such approaches may help understanding particularly how plant architectural traits and their physiological regulation contribute to their ability to compete for light (e.g. Vos et al. 2010), but also involve detailed parameterization. In many cases however simpler approaches may suffice.

Another element that needs to be considered is that direct beam irradiance and light, diffuse sky irradiance and light that is scattered in the canopy are considered separately and not averaged. First, at a given layer within the canopy light intensity can be heterogeneous; e.g. some leaves will be exposed to direct beam irradiance while others are in the shade. Because of the saturating nature of the light response curve averaging will lead to overestimation of photosynthesis. Typically this can be in the order of 20–30 % (de Pury and Farquhar 1997). Second, the directional distribution of these radiation components differs and thus e.g. consequences of interspecific variation in leaf angle distribution can only be assessed if these radiation components are properly accounted for.

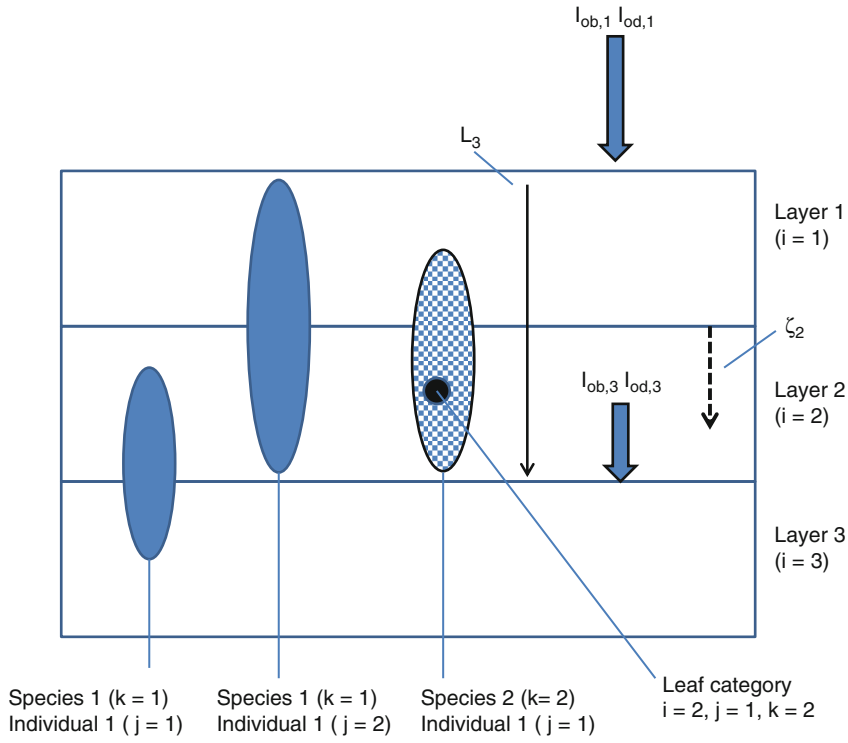

Fig. 14.1. A conceptual visualization of the layered multi-species model as described by Eqs. 14.1, 14.2, 14.3, 14.4, 14.5, 14.6a, 14.6b, 14.7, 14.8a, 14.8b, and 14.9. The vegetation is divided in layers *i*. There are species (here indicated by the *filled* and *checker board* canopies) for which the counter *k* is used (for clarity individual plants were drawn as discrete elements but the model assumes them to be homogeneously mixed within each horizontal layer). Individuals within species are indicated with a counter j. Each individual can have its leaves in more than one layer. Thus leaves of individuals are indicated by an *i*, *j* and *k* value. The model calculates the light intensity above each layer ($I_{ob,i}$ and $I_{od,i}$ for the solar beam and diffuse radiation, respectively, as indicated by the thick arrow) as a function of the total cumulated leaf area index above the layer indicated with L_i (indicated by the thin black arrow). Light intensity absorbed by leaves within the layer is then calculated as a function of $I_{ob,i}$ and $I_{od,i}$, and the cumulated LAI from the top of the layer (i.e., starting at 0 at the top of the layer indicated by the dashed arrow) to the point where the leaves are (ζ_i). Note that the explanation in this caption is simplified and the true calculation procedure is explained in the main text

Here we discuss two examples of simple models that account for both variation in between species and the distribution of different components of radiation in the vegetation: layered models (in detail) and continuous models (briefly).

A. Layered Models

1. Light Partitioning

One approach to deal with differences in height and vertical leaf area distribution between individuals is to divide the vegetation into horizontal layers, and assume that within a layer, leaf area of different individuals is homogeneously distributed (see Fig. 14.1 for a conceptual representation of this approach). Several studies have used this approach for natural vegetation (e.g. Ryel et al. 1990; Hirose and Werger 1995; Anten and Hirose 1999, 2003; Selaya et al. 2007; see Sect. III) and crop stands (Kropff 1988; Baumann et al. 2002; see Sect. IV). Here, we outline a somewhat simplified version of this approach. Let *i* be the counter for canopy layers and *j* indicate different individuals, and, in the case of mixed species stands, *k* indicates the species (Fig. 14.1). Then total light acquisition by an

individual in the stand ($\Phi_{j,k}$) is given as the summation of its light acquisition (Φ_{ijk}) in each of the layers in which it has leaves.

$$\Phi_{j,k} = \sum\nolimits_i \Phi_{i,j,k} \tag{14.1}$$

Light models typically calculate the light intensity at a given point in the canopy (I) as a function of the light intensity above the canopy (I_o) and cumulative LAI above a given point in the canopy (L): $I = I_o e^{(-KL)}$. As mentioned, the model presented here is layered. It thus assumes the vegetation to be built up of a number of stacked canopy layers, whereby light transmitted through layer i is the light that is incident at the top of layer $i + 1$(i.e. the $I_{o,i+1}$ value). There is a cumulative leaf area index (L_i calculated from the top of the stand) above each layer i. Within each layer, one has to account for the cumulative LAI from the top of the layer to a given point within the layer denoted as ζ, with $\zeta = 0$ at the top of the layer and $\zeta = (L_{i+1} - L_i)$ at the bottom (see also Fig. 14.1).

As noted it is crucial to distinguish between direct and diffuse components of radiation. In this respect, most models are based on the so-called two leaf class approach (e.g. Spitters 1986; de Pury and Farquhar 1997), which assumes that at a given layer in the canopy, leaves are either in the shade (shaded leaves) or are directly exposed to a direct sun beam (sunlit leaves). The latter are assumed to receive full, unobstructed light, which ignores the role of penumbral effects. Thus Φ_{ijk} can be written as the sum of the irradiance intercepted in layer i by the sunlit leaf area ($\Phi_{SL,ijk}$) and that intercepted by shaded leaf area ($\Phi_{SH,ij}$), which in turn are the integrals of the light absorbed in layers ($I_{SL,ijk}$ and $I_{SH,ijk}$, respectively) over the leaf area index of that layer. Similarly photosynthesis at a given layer will have to be calculated as the sum of the photosynthesis by sunlit leaves and that of shaded leaves corrected by the fraction of leaves that are sunlit (see below).

Light (i.e., the photon flux) absorbed by shaded foliage of individual j of species k in canopy layer i is given as:

$$I_{SH,ijk} = I_{da,ijk} + I_{bsa,ijk} \tag{14.2}$$

where $I_{da,ijk}$ and $I_{bsa,ijk}$ indicate the diffuse light (derived diffuse sky irradiance) and the scattered component of direct beam irradiance. The latter accounts for the fact that the direct beam irradiance is partly reflected and transmitted by leaves in many directions, and can thus also be intercepted by shaded leaves.

Sunlit leaves also receive diffuse and scattered radiation, and in addition they receive unobstructed beam radiation. The photon flux absorbed by a single sunlit leaf of plants of species k, height class j at given height in canopy layer i (I_{SLijk}) is given as:

$$I_{SLijk} = O_{ijk} I_{ob} \alpha_k / \sin\beta + I_{SHijk} \tag{14.3}$$

where O_{ijk} is the projection of a single leaf into the direction of the sun, and β the solar elevation angle. O_{ijk} depends on the solar elevation angle, and the leaf inclination and azimuth angles, and can be calculated following standard geometric approaches (see e.g. Goudriaan 1988).

The next step entails the calculation of the distribution of diffuse sky and scattered and direct beam radiance in the canopy. As we deal with a layered model this involves the calculation of radiation both above each layer and the light distribution within each layer. The average beam irradiance above layer i in the canopy ($I_{ob,i}$) is found as:

$$I_{ob,i} = (1-\gamma) I_{0b} \exp\left(\sum_i \sum_j \sum_k -K_{B,k} \alpha_k^{0.5} L_{ijk} \right) \tag{14.4}$$

Here $K_{B,k}$ indicates the extinction coefficient of species k for direct beam radiation assuming black non-scattering leaves, α_k the leaf

absorbance of this species (the extinction and absorption coefficients are thus assumed to be constant both within and between plants of the same species), γ is the canopy reflectance and L_{ijk} the amount leaf area of individual j of species k in layer i. Since species can differ widely in their leaf angle distribution, which in turn strongly determines the extinction coefficient (Monsi and Saeki 1953), as well as in their leaf optical traits, $K_{B,k}$ and α_k need to be calculated for each species separately. $K_{B,k}$ can be calculated from the leaf angle distribution (e.g. Goudriaan 1988; see Chap. 1, Goudriaan 2016). α_k can be measured or calculated from the leaf chlorophyll content, which in turn can be estimated with a chlorophyll meter (e.g. Anten and Hirose 1999). The calculation of γ is given in Chap. 1 (Goudriaan 2016) but a reasonable value for many canopies is 0.05.

While direct beam irradiance has an angle of incidence equal to the elevation angle of the sun, diffuse radiation originates from different parts of the sky dome and is thus incident under various angles (see Chap. 1, Goudriaan 2016). But this calculation can be simplified by assuming that diffuse radiation can be represented by a summation of radiation components each of which originates from a different ring zone of the sky, and has an angle of incidence equal to the center angle of each zone (Goudriaan 1977). We distinguish three 30° sky zones (0°–30°, 30°–60°, 60°–90° with elevation angles 15°, 45° and 75°, respectively). Thus the diffuse PFD on a horizontal plane originating from sky elevation zone l above layer i ($I_{od,il}$) is found as:

$$I_{od,il} = Z_l(1-\gamma)I_{0d}\exp\left(\sum_i \sum_j \sum_k \sum_l -K_{d,kl}\alpha_{jk}^{0.5}L_{ijk}\right) \tag{14.5}$$

with $K_{d,kl}$ the extinction coefficient of non-scattering leaves of species k for radiation component l (as with $K_{b,k}$ it can be calculated from the leaf angle distribution) and I_{od} the diffuse sky irradiance above the canopy. Z_l is the fraction of diffuse radiation originating from sky zone l, and its value depends on the assumptions regarding the irradiance distribution across the sky dome. The easiest assumption in this respect is that of the uniform overcast sky, which assumes that every element on the sky dome has the same irradiance. A more common and realistic assumption is that of a standard overcast sky, that corrects for the fact that the sky brightness increases towards the zenith (see Goudriaan 1977).

Now that the amount of radiation at the top of each layer is known, the distribution of light absorption within each layer should be calculated particularly that of diffuse and scattered beam radiation. The absorbed diffuse irradiance ($I_{da,ijk}$) within a given canopy layer can now be calculated as:

$$I_{da,ijkl} = I_{od,il}K_{d,kl}\alpha_k^{0.5}\exp\left(\sum_j \sum_k -K_{d,kl}\alpha_k^{0.5}\zeta_{ijk}\right) \tag{14.6a}$$

$$I_{da,ijk} = \sum_l I_{da,ijkl} \tag{14.6b}$$

with $I_{da,ijkl}$ the absorbed diffuse irradiance originating from elevation l. The absorbed scattered beam irradiance ($I_{bsa,ijk}$) is then:

$$I_{bsa,ijk} = I_{ob,i}K_{b,k}\left[\alpha_k^{0.5}\exp\left(\sum_j \sum_k -K_{b,k}\alpha_k\zeta_{ijk}\right) - \frac{\alpha_k}{(1-\gamma)},\exp\left(\sum_j \sum_k -K_{b,k}\zeta_{ijk}\right)\right] \tag{14.7}$$

ζ_{ijk} is the cumulative amount of leaf area of foliage class jk within height class i (de Pury and Farquhar 1997; see above). Roughly, the first expression on the right hand side of the equation depicts the total of direct radiation at depth ζ in the canopy and the second expression the part of this radiation that is scattered.

2. Linking Light Absorption to Photosynthesis

In order to calculate photosynthesis of a given plant of a given species, one needs to know first how much light is absorbed by the sunlit and shaded leaves (as calculated in the previous section) of this plant and subsequently the photosynthetic characteristics of these leaves. As noted above, distinction is made between sunlit and shaded leaf area, thus photosynthesis needs to be calculated for these classes separately. This can be done as follows:

$$P_{ijk} = \frac{L_{ijk}}{\sum_j \sum_k L_{ijk}} \int_0^{L_i} \left[f_{SL,i} P_{SL,ijk} + (1 - f_{SL,i}) P_{SH,ijk} \right] \tag{14.8a}$$

$$P_{jk} = \sum_i P_{ijk} \tag{14.8b}$$

where P_{jk} is the total photosynthesis of individual j of species k, P_{ijk} and L_{ijk} the photosynthesis and area of all the leaves of this plant in layer i, $P_{SL,ijk}$ and $P_{SH,ijk}$ the photosynthesis of sunlit and shaded leaf area, respectively and $f_{SL,i}$ the fraction sunlit leaf area in layer i. $f_{SL,i}$ in turn is given as:

$$f_{SL,i} = \exp\left(\sum_i \sum_j \sum_k -K_{b,k} L_{ijk} \right) \exp\left(\sum_j \sum_k -K_{b,k} \zeta_{ijk} \right) \tag{14.9}$$

Note that the two exponential expressions are used to accommodate for the layered structure of the model: the left expression indicating the fraction of sunlit leaf area at the top of layer i and the right expression the fraction thereof that is sunlit at depth ζ_i within the layer.

$P_{SL,ijk}$ and $P_{SH,ijk}$ can be calculated by substituting Eqs. 14.2 and 14.3 into a suitable expression for the light response of photosynthesis. Different equations are used to describe the light response of leaf photosynthesis. The simplest approach is to describe it using an empirically fitted equation, of which the non-rectangular hyperbola is a good example:

$$P_L = \frac{(p_{\max} + \phi I_L) - \left[(p_{\max} + \phi I_L)^2 - 4\phi\theta p_{\max} I_L \right]^{0.5}}{(2\theta)} - r_d \tag{14.10}$$

where I_L is the absorbed photon flux, p_{max} (μmol m^{-2} s^{-1}) the light saturated rate of gross photosynthesis, r_d the dark respiration (μmol m^{-2} s^{-1}) and ϕ and θ the quantum yield (mol mol^{-1}) and curvature factor, respectively (Marshall and Biscoe 1980). Thus, $I_{SH,i,j,k}$ can be used to calculate $P_{SH,ijk}$ and $I_{SL,i,j,k}$ to calculate $P_{SL,ijk}$. All these characteristics may vary inter- and intra-specifically. A more biochemical model that describes photosynthesis in terms of Rubisco-limited and RuBP-regeneration limited carboxylation as a function of CO_2 (and thus stomatal conductance), temperature and light (Farquhar et al. 1980) is more commonly used. But in this chapter, we focus on the details of plant interactions in terms of light capture, and thus for simplicity present the more empirical photosynthesis model. The parameters of these photosynthesis equations can all be measured with an infra-red gas analyzer linked to a gas exchange system (e.g. Hirose and Werger 1987; Hikosaka et al. 1999; Yin and Struik 2010). Section III of this chapters discusses several examples of work that has been done using models that are very similar to the one just described.

B. Continuous Models

The use of layered models has advantages in that it is compatible with the stratified clipping method that is most commonly used to describe the vertical distribution of leaf area in the canopy (Monsi and Saeki 1953).

A disadvantage of this method is that it uses discrete values of the leaf area per species per layer. As a result, the description of the leaf area distribution is rather complicated and not very suitable for mathematical analyses. An alternative approach is to use a continuous function for the vertical leaf area distribution. However, such a function needs to be flexible enough to accommodate the variation in leaf area distribution commonly found in plants; some plants (e.g. rosette type plants) tend to concentrate their leaves towards the bottom whereas many annual herbs as well as trees concentrate their leaves more towards the top. Caton et al (1999) introduced the following distribution function, which more or less accounts for this variation.

$$\lambda(h) = p_0 \frac{L_t}{h_{pt}} \left(\frac{h}{h_{pt}}\right)^{p_1} \left(1 - \frac{h}{h_{pt}}\right)^{p_2} \qquad (14.11)$$

where λ denotes the leaf area density (m^2 leaf per m^3 air) that is calculated as a function of height h in the canopy, L_t is the leaf area index of the plant, h_{pt} is the plant height and p_0, p_1 and p_2 are shape parameters. By setting high p_1/p_2 ratios leaf area distributions that are concentrated at the top of the vegetation can be simulated and the opposite can be achieved by setting low p_1/p_2 ratios (Fig. 14.2a). Height and leaf area growth can also be simulated assuming plants to maintain a given leaf area distribution relative to their height (keeping p_1/p_2 constant), and more or less realistically simulating the pattern whereby leaves are produced at the top of the canopy and dropped at the bottom (Fig. 14.2b).

III. Applications in Fundamental Ecology: The Case of Asymmetry in Competition

Resource competition is in the first place related to size; larger individuals are generally able to acquire larger amounts of resources than smaller individuals. One of the key questions in plant ecology however is whether or not this resource acquisition is proportional to size. This has been framed in the terms 'size-symmetric' and 'size-asymmetric' (Weiner 1990; Schwinning and Weiner 1998). Competition is size-symmetric when larger individuals in a population acquire resources in proportion to their size share, and it is size-asymmetric if they acquire a larger than proportional amount. Theoretical studies have shown that the degree of asymmetry of resource competition can have enormous implications for population dynamics (e.g., Łomnicki 1980) and evolution (Wall and Begon 1985). Under asymmetric competition, size frequency distribution will tend to become more skewed while size frequency distributions will remain constant under symmetric competition. For mixed species communities it has been argued that asymmetric competition is an important driving force that determines community structure while symmetric competition has been associated with species diversity (Kohyama 1992; Hara 1993).

Most studies intuitively assume that competition for light is size-asymmetric while competition for soil resources (water and nutrients) is size-symmetric. This assumption is based on the fact that light is predominantly supplied in a vertical direction and that consequently bigger, taller plants can shade smaller ones but not *vice versa* (Weiner 1986). By contrast, soil resources are not supplied directionally and can therefore not be similarly pre-empted. Yet, there seems to be very little quantitative support for this assumption; surprisingly few studies have actually attempted to quantify the asymmetry of competition for nutrients (Schwinning and Weiner 1998; Berntson and Wayne 2000; Hikosaka and Hirose 2001).

Asymmetry of competition specifically refers to size, but does not define what size measure should be used. Several measures of plant size exist including: height, crown volume, standing leaf area, and the plant fresh- and dry mass. Several studies have used

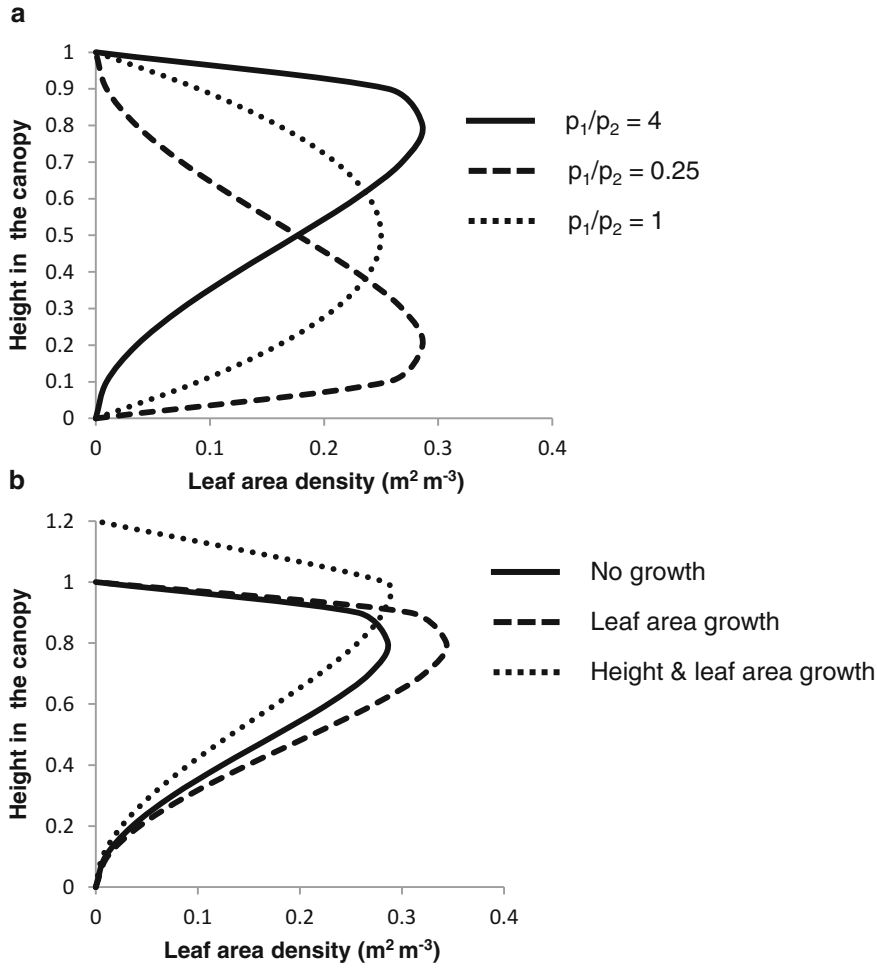

Fig. 14.2. The vertical distribution leaf area in a vegetation stand as calculated with Eq. 14.11 (Caton et al. 1999; Pronk et al. 2007). (**a**) Shows that this approach can elegantly model different leaf area distribution patterns as they may occur depending on the canopy architecture of different species, by simply changing the p_1/p_2 ratio. Plant height h_{pt}, plant leaf area index (L_t) and p_0 were all set to 1 (m, m^2/m^2 and dimensionless respectively), and p_1 to 2, 1 and 0.5 and p_2 to the same values but in reverse order. (**b**) Shows that plant leaf area and height growth can be modeled more or less simulating the effect of leaves being produced at the top and dropped at the bottom of the canopy. The same values were used as in (**a**) but height and leaf area growth entailed 20 % increases in these traits and p_1 and p_2 were set al 2 and 0.5, respectively

different measures to infer size-asymmetry of light competition: height (Givnish 1982), leaf area (Schwinning and Weiner 1998) and mass (e.g. Hikosaka et al. 1999). The use of different size measures can lead to different conclusions; e.g., light capture is often found to increase disproportionally against leaf area and plant height but not against plant mass (Hirose and Werger 1995; Berntson and Wayne 2000). All size measures have their merit, for example a study that focuses on the adaptive significance of height growth may use height as a measure, and similarly leaf area would be useful if leaf investment is the trait under investigation. In this chapter, however, we call for a wider use of plant dry mass as a size measure for the following reasons.

1. Plant mass most closely reflects past assimilation by the plant and thus past resource acquisition. Thus, light acquisition per unit mass

reflects the efficiency with which this past acquisition is being employed to acquire more resources (Hirose and Werger 1995).

2. Plants are highly integrated organisms. The organs of a plant cannot function independently from the other organs. For example, in order to capture large amounts of light in a crowded stand, leaves have to be placed high in the canopy. However, these leaves have to be supported by stems and branches or else they will fall to the ground. Thus, stems and branches are crucial in facilitating light acquisition and are therefore involved in its acquisition. Similarly, the production and functioning of leaves depends on water and nutrients supplied by roots while the roots would not be able to acquire belowground resources without the carbon supplied by the leaves. Thus, in a sense, all parts of the plant are in some way involved in the acquisition of every resource.

A. Light Acquisition Relative to Plant Mass

Several studies have used canopy models similar to the one described in Sect. II.A.1 to quantify light acquisition relative to plant mass. Assuming that the relationship between light acquisition by a plant (Φ) and plant mass (M) goes through the origin, which is reasonable since no leaf area means no light capture and viable plants need at least some leaf area, this relationship can be plotted as follows:

$$\Phi = aM^b \tag{14.12}$$

where a is a constant and b the scaling parameter that determines the shape of the relationship (see Fig. 14.3). If $b = 1$ the relationship is linear, and as it runs through the origin, light acquisition is exactly proportional to mass, that is, light capture per unit mass (Φ_{mass}) is not significantly related with mass itself. It can thus be regarded as size-symmetric. Conversely if $b > 1$, then light capture is size-asymmetric, large plants acquiring disproportionately more light than smaller ones, and Φ_{mass} increases with M.

Hirose and Werger (1995) applied this approach to compare light acquisition between species in a grassland. They used a layered canopy model (albeit one that did not distinguish between direct and diffuse light components) to calculate Φ at the species level and then plotted this against mass of each species in the stand, using Eq. 14.12. They thus obtained $b = 0.941$ which was not significantly different from 1. Indeed, species of different sizes had very comparable Φ_{mass} values. Apparently contrary to the commonly held view of asymmetric light competition (see above), this showed that light acquisition in dense vegetation among species can be size-symmetric. Similar results have subsequently been obtained in other studies both in grasslands (Anten and Hirose 1999; Werger et al. 2002; Aan et al. 2006), semi woody wetland vegetation (Kamiyama et al. 2010) and in secondary tropical forest (Selaya et al. 2007, 2008). Notable exceptions are results for a mature warm temperate rain forest stand (Onoda et al. 2014). Apparently size-symmetric light acquisition between species is rather common for vegetation whose LAI is up to 3 (Fig. 14.4). At higher LAI levels however light b values become larger than 1 indicating size-asymmetric light acquisition (see Fig. 14.4).

How does this apparent discrepancy arise, that is, how can light acquisition be size-symmetric even if light is mostly a pre-emptible resource? To better understand how different plant traits contribute to size-dependent light acquisition, Φ_{mass} can be factorized as:

$$\Phi_{mass} = \Phi_{area} * LAR \tag{14.13}$$

with Φ_{area} light acquisition divided by the amount of leaf area, thus representing the mean light absorption per unit leaf area of a plant, and LAR the leaf area per unit mass

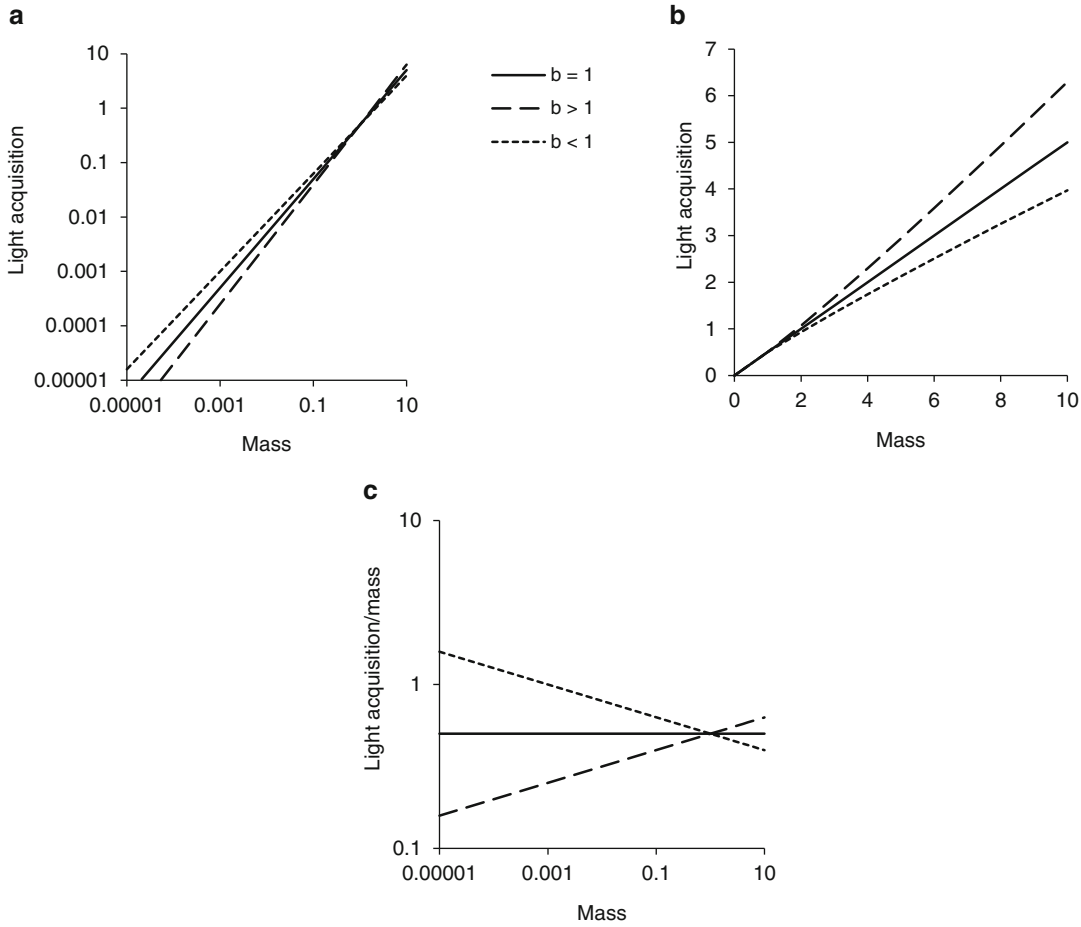

Fig. 14.3. Hypothetical relationships between light acquisition (Φ) and plant mass (M), plotted on either (**a**) logarithmic or (**b**) linear scales, and (**c**) the associated relationships between resource acquisition per unit mass (Φ_{mass}) as calculated with a power function $\Phi = aM^b$ (Eq. 14.12). Three cases are considered: $b = 1$ indicating perfect size-symmetry, $b > 1$ indicating partial size-asymmetry and $b < 1$ indicating partial size-symmetry (see text)

(Hirose and Werger 1995). LAR itself can then be factorized as:

$$LAR = SLA * LMR \qquad (14.14)$$

with SLA the leaf area per unit leaf mass and LMR the fraction of shoot mass invested in leaves. Thus efficiency of light acquisition is broken down into three types of traits: those associated with the positioning of leaves relative to the light gradient in the canopy (Φ_{area}), biomass allocation (LMR) and leaf structure (SLA).

It was thus shown that tall species have higher Φ_{area} than shorter ones, which is logical as light availability declines from the top towards the bottom of the canopy (e.g. Hirose and Werger 1995; Anten and Hirose 1999; Aan et al. 2006; Kamiyama et al. 2010). The similarity in Φ_{mass} between plants of different sizes thus arises from the fact that taller species had both lower LMR and lower SLA resulting in considerably lower LAR values than short species. Negative correlations between LMR are probably associated with biomechanical constraints, taller plants having to invest disproportionate amounts of mass in support structures and less in leaves in order to remain mechanically stable (Niklas 1992). Lower SLA in

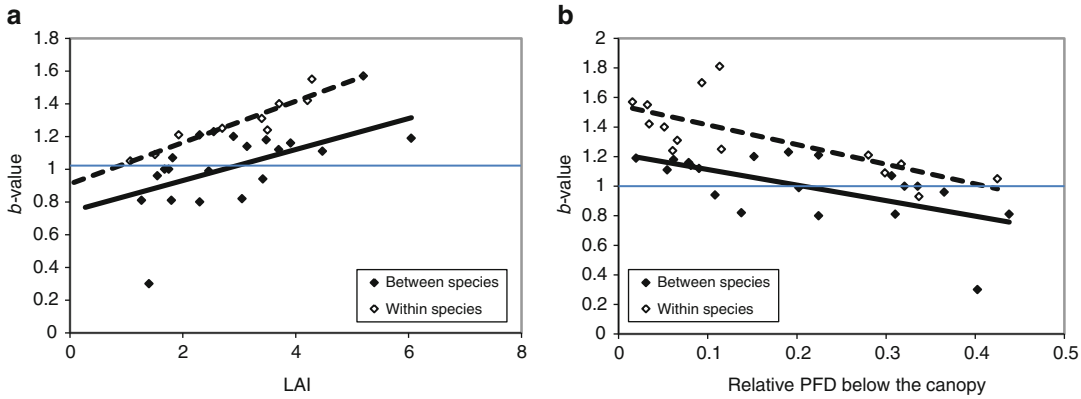

Fig. 14.4. Exponents (i.e., *b* values) in the power relation between whole-plant light acquisition (Φ) and plant aboveground mass (*M*, i.e., $\Phi = aM^b$, Eq. 14.12) plotted against two measure of stand density: the leaf area index (**a**) and the relative light intensity below the vegetation (**b**). *Open symbols* indicate relationships across individuals of the same species and *closed symbols* for relationships between species. The *horizontal line* $b = 1$, perfect size symmetry. Values above this line indicate size-asymmetric competition for light (see text). Data were obtained from Aan et al. (2006), Anten and Hirose (1998, 1999), Hikosaka et al. (2003), Hirose and Werger (1995), Selaya et al. (2008), Vermeulen et al. (2008)

taller species could be associated with acclimation or adaptation to higher light availability or (e.g. in tall trees) greater hydraulic stress (Lambers et al. 1998). Apparently, species of different stature can be equally efficient in acquiring light and it was argued that this may in part explain why these species co-exist (Hirose and Werger 1995).

Similar analyses (Eqs. 14.12, 14.13 and 14.14) were done to analyze light competition among plants of the same species. Interestingly, for stands of the annual species *Xanthium canadense* it was found that taller individuals captured disproportionately more light ($b > 1$) and thus had higher Φ_{mass} values than their shorter con-specifics (Anten and Hirose 1998). This result was consistent across various vegetation stands (Anten and Hirose 1998; Hikosaka et al. 2003; see Fig 14.4). Apparently, within species light acquisition is clearly and consistently size-asymmetric even in very open stands (i.e., LAI of around 1).

Why is there this difference between inter- and intra-specific light competition? Equations 14.13 and 14.14 can be helpful in this respect. That is, either the size-dependent increase in Φ_{area} should be larger within species than among species or the size dependent decline in LAR should be smaller. To visualize how this problem can be addressed we compared the results from two different stands with similar LAI (~2.5) to correct for overall stand density, one being a mono-species stand of *Xanthium canadense* (Anten and Hirose 1998) and the other being mixed species tall-grass meadow dominated by *Miscanthus sinensis* (Anten and Hirose 1999). In the former the *b* value was estimated to be 1.25 and in the latter 0.99. In the mono-stand, LAR values ranged from 0.012 $m^2\ g^{-1}$ in the smallest individuals to 0.03 $m^2\ g^{-1}$ in the largest (a 2.5 fold variation) while in the mixed stand this range was 0.01–0.04 $m^2\ g^{-1}$, a four-fold range. Φ_{area} differed by a factor 7 (highest and lowest values were about 28 and 4 mol m^{-2} day) in the mono-stand and by a factor 3.6 (8–29 mol $m^{-2}\ day^{-1}$) in the mixed stand. Apparently both factors, a larger variation in LAR and a smaller variation in Φ_{area} can play a role in making light competition among species relatively more symmetric. The former could be attributed to the fact that plasticity (i.e. within-species variation) in the traits that underlie SLA and LMR could have been smaller than

genetic variation across species. Indeed particularly variation in LMR was larger across species in the tall-grass meadow than within species in the Xanthium stand. This pattern could be due to the inherent differences in architecture between species; the smaller species that had very large LMR values in the tall-grass meadow tended to be rosette and stoloniferous plants, their vertical structures all being leaves. Taller species, on the other hand, produced vertical stems. The relatively small variation in Φ_{area} across species could be related to inherent differences in canopy structure. In the case of the tall-grass meadow, the dominant grass had relatively vertically inclined leaves while the forbs in the lower layers of the canopy had more horizontal leaves and shallow crowns. The latter traits are particularly beneficial for light acquisition in lower canopy layers where vertical light components predominate. Evidently, it should be noted that this comparison is based on a rather limited data set, and more research is needed to better understand the factors that make light competition among species more symmetric than competition within species.

B. Growth and Radiation-Use Efficiency

Differences in growth between individuals are not only determined by their resource acquisition but also by their ability to use these resources for growth. In the case of light, this relationship can be formulated as follows:

$$G = \Phi^* \text{ RUE} \qquad (14.15a)$$

$$\text{RGR} = \Phi_{mass}^* \text{ RUE} \qquad (14.15b)$$

with G and RGR absolute growth and growth rate per unit mass, respectively and RUE the growth rate per unit of absorbed light (Hikosaka et al. 1999). This approach is commonly used in crop modelling (see van Ittersum et al. 2003) but is less commonly used to analyse light competition among individual plants. When considering asymmetry in light competition, it is also important to take this factorization into account. In theory competition in terms of light acquisition can be size asymmetric, Φ_{mass} increasing with plant mass, while overall competition can be size symmetric; carbon gain or growth scaling linearly with size (RGR being size-independent) and vice versa (Onoda et al. 2014). Ultimately this depends on the way RUE scales with size.

There are several reasons to assume that larger plants may have smaller RUE values than smaller plants (see also Onoda et al. 2014). First, as noted above, larger plants have relatively more non-photosynthetic tissue possibly resulting in more respiration per unit of photosynthetic tissue (Givnish 1982). Second, due to the concave shape of the light response of leaf photosynthesis, photosynthetic light-use efficiency (often abbreviated as LUE and thus RUE) tends to be lower at high light intensities. As noted above, in dense vegetation, larger and taller plants tend to have their leaves more exposed to the light. Thus, if every plant in a stand were to have the same photosynthetic and respiratory characteristics – e.g., the same parameter values of light response of leaf photosynthesis (see Eq. 14.10) and mass-based respiration rates- then in dense vegetation RUE should decline with plant size, unless the light levels at which smaller plants are growing are very close to their light saturation point. In forest vegetation photosynthesis of the taller plants can be further inhibited by hydraulic limitations (e.g. Ryan and Yoder 1997), photo-inhibition (e.g. Werner et al. 2001) and greater wind loading (e.g. Yasumura et al. 2002). On the other hand, in most vegetation taller species tend to be light-demanding and shorter ones shade tolerant, and leaf photosynthetic capacities tend to be higher for the former than for the latter. In terms of RUE this could partly compensate for the above-mentioned factors, indicating that RUE of taller species may not necessarily be lower than that of shorter species in vegetation.

Hikosaka et al. (1999) applied a canopy model to compare light capture, whole-plant photosynthesis and photosynthesis/light

(LUE) between plants of different size in a mono-species stand of the annual plant *Xanthium canadense*. As noted above, larger individuals in this stand, exhibited higher light capture per unit mass (Φ_{mass}) than smaller ones. LUE on the other hand, tended to be highest for plants of intermediate size occupying the middle layers of the canopy, and lower for plants that were either very small or very large. This pattern can be explained by two phenomena. First very small plants were growing at light levels that were close to their light compensation point, the minimal amount of needed for photosynthesis plants to exceed respiration. This resulted in low LUEs. Second, while plants plastically adjusted their photosynthetic capacity to the light level at which they were growing, this adjustment was insufficient for the tallest plants to maintain LUE at similar levels as plants of intermediate size.

Photosynthesis per unit mass being the product of Φ_{mass} and LUE, increased with plant size for smaller plants but then leveled off, intermediate and large-sized plants tending to have similar net-photosynthesis per unit mass. Thus differences in photosynthesis among the smaller plants was asymmetric, both light acquisition relative to size and light use increasing with plant size. Conversely among larger plants these differences were size-symmetric: size-asymmetric light acquisition being mitigated by a size-dependent decline in light-use.

Studies on interspecific interactions in multi-species stands obtained a different result. As noted above, Φ_{mass} was rather constant across species at least in vegetation stands with an LAI up to about 3 m^2 m^{-2} (Fig. 14.4). LUE however tended to be higher in taller species than in smaller ones, both in a tall-grass meadow (Anten and Hirose 2003) and in a very young secondary tropical forest (van Kuijk et al. 2008; Selaya and Anten 2010). As a result net whole-plant photosynthesis scaled disproportionally with size and thus while light acquisition was size-symmetric overall competition was size-asymmetric. The discrepancy in the results for the mono- and mixed stands again are likely associated with the fact that inherent differences in leaf photosynthetic traits across species are larger than differences within species. For example, in the tall-grass meadow the tall dominant species, *Miscanthus sinensis*, exhibited the C_4 photosynthetic pathway, which is physiologically and anatomically clearly different from the C_3 photosynthetic pathway of the smaller species. More subtle inherent differences in leaf photosynthetic exist between C_3 species. In early secondary tropical forest, for example, early pioneer species typically have higher photosynthetic capacities than their later successional counterparts (Selaya and Anten 2010).

A very different pattern than the one described above was observed in a mature evergreen forest stand (Onoda et al. 2014). Through a combination of light and growth measurements it was shown that taller species captured more light per unit mass (higher Φ_{mass}) and had lower growth per unit light (RUE) than shorter species; being the opposite trend as the one observed in herbaceous and secondary forest stands. A combination of factors may explain this difference. First, mature evergreen forests typically exhibit very high LAIs such that smaller species cannot compensate their lower Φ_{area} by having a higher LAR, thus shorter species had a lower Φ_{mass}. Second, in mature forest net growth of taller trees might be restricted by very large amounts non-photosynthetic respiring tissue and/or hydraulic limitations on photosynthesis (Ryan and Yoder 1997).

Together the results discussed in this section illustrate how canopy models can be used to mechanistically analyse modes of light competition in vegetation stands. It illustrates some general trends, particularly light competition within species being more likely to be size-asymmetric than light competition among species, and that models can be used to understand how such trends arise.

IV. Applications in Crop Science: The Case of Crop-Weed Interaction

Weeds are one of the most serious biotic production constraints in agriculture (Oerke 2006). Acting at the same trophic level, they compete for resources like light, water and nutrients with the crop. For a long time weed control has been one of the most labor demanding activities in crop production and for that reason the introduction of herbicides was an important trigger of the intensification of crop production systems, causing a major boost in labor-productivity. A couple of decades after the successful introduction of herbicides in the 1940s it became apparent that a too abundant use might seriously hamper the sustainability of this weed control option. Apart from environmental concerns, a major worry related to the use of chemical weed control was the increased risk of the development of herbicide resistance (e.g. Moss 2003). For that reason, routine application of herbicides at the start of a growing season was replaced by an economic threshold approach (Stern et al. 1959). A consequence of this approach is that the number of applications is reduced, as a weed control measure is restricted to situations where the financial gain exceeds the cost of control (Coble and Mortensen 1992). Basic requirement for its implementation is sound knowledge of the extent to which a given weed infestation is likely to reduce crop yield if left uncontrolled. It was in this context that Cousens (1985) compared a range of statistical models for their suitability to relate early-season weed infestation level to crop yield loss. More than twenty data sets, each containing marketable yields for at least eight weed densities, were used for this analysis. Eventually, a rectangular hyperbola was identified as the model providing the best description:

$$Y_L = \frac{iN_w}{\left(1 + \frac{iN_w}{m}\right)} \qquad (14.16)$$

In this equation Y_L is the percentage of yield lost because of weed competition and N_w is weed density. The elegance of this model is that it has two parameters that are both easily interpreted in agronomic terms. Parameter i expresses the percentage yield loss per unit weed density as weed density approaches zero, and parameter m expresses the percentage yield loss at very high weed densities, or the maximum percentage yield loss. The asymptotic shape of the curve suggests that the yield loss caused by the first weed added to a weed-free crop has the strongest effect on crop production. The further yield loss caused by additional weeds gradually diminishes with weed plant density, owing to an increased intra-specific competition among weed plants. Typically, resource capture of an additional weed is not just at the cost of the crop, but also reduces the growth of the other weed plants. In situations with a very competitive weed, crop yield at higher weed densities will be completely lost and parameter m will become 100 %, turning the model in a simple one-parameter model.

Though the descriptive capacity of this model is undisputed, its predictive ability is debatable. In a study on the damage of *Echinichloa crus-galli* in a maize crop it was observed that in two consecutive years parameter i varied from about 0.1 % in the first year to about 4.4 % yield loss per unit weed density in the second year of experimentation (Kropff et al. 1984). Obviously parameter i is not a constant for a given crop-weed combination, but is strongly influenced by for instance environmental factors. To obtain a better insight in the factors that do have a strong influence on the competitive relations between crop and weed plants, a mechanistic model for interplant competition was developed (e.g. Spitters and Aerts 1983; Kropff 1988). This eco-physiological model simulates the supply, demand, capture and utilization of resources by the competing species to provide insight in the outcome and the dynamics of competition. In the model, most emphasis is on the distribution of light over the competing species, as under the Dutch conditions for which the model was originally developed water availability is hardly ever a

serious problem and fertilization generally results in an ample supply of nutrients. Light interception by the canopy is determined by the leaf area index and the light absorption characteristics of the competing species. The distribution of intercepted light over the species is further related to plant height and vertical leaf area distribution. The model that was used to calculate light capture and photosynthesis of the species in the crop stand was largely similar to the layered multi-species canopy model described earlier in this chapter (Eqs. 14.1, 14.2, 14.3, 14.4, 14.5, 14.6, 14.7 and 14.8). The only exception is that individuals within species were not discerned, i.e., only species were distinguished.

Model analyses revealed that the relative time of emergence is a key-factor determining the crop-weed competitive relations. Weeds emerging a few days before crop establishment have a much stronger influence than weeds emerging simultaneously with the crop. In retrospect this also explained the previously reported difference in parameter *i* characterizing the maize-*E. crus-galli* relationship for the two consecutive years of experimentation. Model analysis further showed that a close relationship existed between relative leaf area shortly after crop emergence and final crop yield. The observation suggests that, rather than using weed density as such, it is better to consider the size of the weed plants at the moment of observation as well. In this way the stronger competitiveness of earlier emerged weed plants is accounted for. As a result an alternative model was developed in which yield loss is related to relative leaf area of the weeds (defined as the share of the weed species in the total leaf area) shortly after crop emergence (Kropff and Spitters 1991). Indeed relative weed leaf area was found to be superior over weed density as an explanatory variable, particularly if results from more than one site and year were simultaneously considered.

More recently, a greater interest in preventative weed management has developed (e.g. Mortensen et al. 2000; Liebman 2001). Cultural weed control, also referred to as ecological weed management, can be defined as any adjustment or modification to the general management of the crop that contributes to the regulation of weed populations and reduces the negative impact of weeds on crop production. One of the possibilities to reduce the dependence on curative control measures (such as the use of chemical herbicides) is to increase the competitive ability of the crop relative to that of the weeds. Such an increased competitive ability can be realized through increasing the competitiveness at either the individual plant level or at the plant population level (Bastiaans et al. 2008). An increased seeding rate, or a more homogeneous crop spatial arrangement are examples of this last option. At the individual plant level, the focus could be on creating an initial size advantage. Selection for larger seeds, seed priming or the use of transplants, are means of providing crop plants with a favorable starting position. Breeding for more competitive cultivars is another option.

Obviously mechanistic models for crop-weed interaction can be of great help to quantify the relevance of the different options in helping minimize the negative effect of weeds on crop production (e.g. Bastiaans et al. 2000). Analyzing the results of a field experiment by means of a simulation model was used to identify the rice traits responsible for competitiveness (Bastiaans et al. 1997). A sensitivity analysis with the model showed that early growth characteristics and maximum plant height gave considerable reductions in simulated weed biomass, indicating their importance for weed-suppressive ability. Increases in light extinction coefficient, specific leaf area and crop growth rate only resulted in marginal reductions in weed biomass, indicating that these traits are not major determinants of weed-suppressive ability. In addition the model revealed that, unlike for instance light extinction coefficient, early growth characteristics did not bear any trade-offs towards yielding ability. These results exemplify the role of mechanistic

simulation models in guiding the plant breeding process: the models enable a quantitative estimation of the potential contribution of various traits to an increased competitive ability. Later experiments with a wide range of rice genotypes confirmed the dominant role of early crop vigor in weed suppressive ability (Zhao et al. 2006). The experiments also confirmed that, in rice, weed suppressive ability and yielding ability are compatible.

V. Concluding Remarks

Light is the principle source of energy supporting plant life, and, in growth environments that facilitate dense vegetation, competition for this resource is believed to be an important factor determining the evolution of aboveground plant traits. In crop stands competition for light between crops and weeds and between different crops (e.g. in multispecies cropping systems) can strongly impact yields. Early studies (see Keddy 1989) analyzed competition in a phenomenological way, often describing competition in terms of simple parameters that represent the effects of species on themselves and on other species. Such studies have provided insights in for example the conditions under which species co-existence may occur, but do not provide mechanistic insights into the way plants interact with each other. In this chapter we have shown how for light competition, individual plant based canopy models can fill this knowledge gap. We documented the way in which canopy models have been used to identify how trait differences between plants shape competitive interactions. This may help link species trait variation to community dynamics in natural vegetation and provide key insights into crop-crop or crop-weed interactions. Nevertheless the models described in this chapter are still rather simplistic. They are one-dimensional treating vegetation as being horizontally homogenous. As such they are not suitable to describe distinctly heterogeneous vegetation: e.g. row crops (including mixed-species crops in rows) or natural vegetation with clustered elements. Similarly they cannot include plant architectural traits such as leaf size and shape, branching patterns. Several model approaches described elsewhere in this book have been developed that may accommodate these issues; such as models that describe row crops (see Chap. 1, Goudriaan 2016), and functional structural plant modeling (FSPM, Vos et al. 2010; Chap. 8, Evers 2016) that simulates the 3D realistic architecture of plants. Such models in turn can be linked to the rapid progress on our knowledge of the physiological pathways that regulate plant neighbor detection and associated responses (e.g. shade avoidance, discussed in Chap. 6, de Wit and Pierik 2016) to obtain understanding of the functional significance of the these pathways. Application of game theory (as discussed in Chap. 13, Anten 2016) in this context can aid in analyzing how natural selection may have acted on genetic variation in neighbor-induced responses and thus further our understanding on how light competition acts as a factor in driving the evolution of aboveground plant traits. Finally links need to be made to root models to understand the interplay between above- and belowground interactions.

Acknowledgements

Part of this work was supported by a Japan Society for Promotion of Science Research Fellowship to NPRA.

References

Aan A, Hallik LEA, Kull O (2006) Photon flux partitioning among species along a productivity gradient of an herbaceous plant community. J Ecol 94:1143–1155

Anten NPR (2016) Optimization and game theory in canopy models. In: Hikosaka K, Niinemets Ü, Anten N (eds) Canopy Photosynthesis: From Basics to Applications. Springer, Berlin, pp 355–377

Anten NPR, Hirose T (1998) Biomass allocation and light partitioning among dominant and subordinant individuals in *Xanthium canadense* stands. Ann Bot 82:665–673

Anten NPR, Hirose T (1999) Interspecific differences in above-ground growth patterns result in spatial and temporal partitioning of light among species in a tall-grass meadow. J Ecol 87:583–597

Anten NPR, Hirose T (2003) Shoot structure, leaf physiology and daily carbon gain of plant species in a tallgrass meadow. Ecology 84:955–968

Barneix AJ (1990) Yield variation in wheat: nitrogen accumulation, light interception and harvest index. In: Lambers H, Cambridge ML, Konings H, Pons TL (eds) Causes and Consequences of Variation in Growth Rate and Productivity of Higher Plants. SPB Academic Publishing, The Hague, pp 87–100

Bastiaans L, Kropff MJ, Kempuchetty N, Rajan A, Migo TR (1997) Can simulation models help design rice cultivars that are more competitive against weeds? Field Crop Res 51:101–111

Bastiaans L, Kropff MJ, Goudriaan J, Van Laar HH (2000) Design of weed management systems with a reduced reliance on herbicides poses new challenges and prerequisites for modeling crop-weed interactions. Field Crop Res 67:161–179

Bastiaans L, Paolini R, Baumann DT (2008) Focus on ecological weed management: what is hindering adoption? Weed Res 48:481–491

Baumann DT, Bastiaans L, Goudriaan J, Van Laar HH, Kropff MJ (2002) Analysing crop yield and plant quality in an intercropping system using an eco-physiological model for interplant competition. Agric Syst 73:173–203

Berntson GM, Wayne PM (2000) Characterizing the size dependence of resource acquisition within crowded plant populations. Ecology 81:1072–1085

Bongers FJ, Evers JB, Anten NPR, Pierik R (2014) From shade avoidance responses to plant performance at vegetation level: using virtual plant modelling as a tool. New Phytol 204:268–272

Caton BP, Foin TC, Hill JE (1999) A plant growth model for integrated weed management in direct-seeded rice. III. Interspecific competition for light. Field Crop Res 63:47–61

Clements FE, Weaver JE, Hanson HC (1929) Plant Competition: An Analysis of Community Functions. Carnegie Institution, Washington, DC

Coble HD, Mortensen DA (1992) The threshold concept and its application in weed science. Weed Technol 6:191–195

Cousens R (1985) An empirical model relating crop yield to weed and crop density and a statistical comparison with other models. J Agric Sci 105:513–521

De Pury DGG, Farquhar GD (1997) Simple scaling of photosynthesis from leaves to canopies without the errors of big-leaf models. Plant Cell Environ 20:537–557

de Wit M, Pierik R (2016) Photomorphogenesis and photoreceptors. In: Hikosaka K, Niinemets Ü, Anten N (eds) Canopy Photosynthesis: From Basics to Applications. Springer, Berlin, pp 171–186

DeJong TM, Da Silva D, Vos J, Escobar-Gutiérrez AJ (2011) Using functional–structural plant models to study, understand and integrate plant development and ecophysiology. Ann Bot 108:987–989

Evers JB (2016) Simulating crop growth and development using functional-structural plant modeling. In: Hikosaka K, Niinemets Ü, Anten N (eds) Canopy Photosynthesis: From Basics to Applications. Springer, Berlin, pp 219–236

Evers JB, Vos J, Chelle M, Andrieu B, Fournier C, Struik PC (2007) Simulating the effects of localized red:far-red ratio on tillering in spring wheat (*Triticum aestivum*) using a three-dimensional virtual plant model. New Phytol 176:325–336

Falster DS, Westoby M (2003) Plant height and evolutionary games. Trends Ecol Evol, 18: 337–343

Farquhar GD, von Caemmerer S, Berry JA (1980) A biochemical model for photosynthetic CO_2 assimilation in leaves of C_3 species. Planta 149:78–90

Givnish TJ (1982) On the adaptive significance of leaf height in forest herbs. Am Nat 120:353–381

Goudriaan J (1977) Crop Micrometeorology: A Simulation Study, Simulation monographs. Pudoc, Wageningen

Goudriaan J (1988) The bare bones of leaf angle distribution in radiation models for canopy photosynthesis and energy exchange. Agric For Meteorol 43:155–169

Goudriaan J (2016) Light distribution. In: Hikosaka K, Niinemets Ü, Anten N (eds) Canopy Photosynthesis: From Basics to Applications. Springer, Berlin, pp 3–22

Hara T (1993) Mode of competition and size-structure dynamics in plant communities. Plant Species Biol 8:75–84

Hikosaka K, Hirose T (2001) Nitrogen uptake and use by competing individuals in *Xanthium canadense* stand. Oecologia 126:174–181

Hikosaka K, Sudoh S, Hirose T (1999) Light acquisition and use of individuals competing in dense stand of an annual herb *Xanthium canadense*. Oecologia 118:388–396

Hikosaka K, Yamano T, Nagashima H, Hirose T (2003) Light acquisition and use of individuals as influenced by elevated CO_2 in even-aged monospecific stands of *Chenopodium album*. Funct Ecol 17:786–795

Hirose T, Werger MJA (1987) Nitrogen use efficiency in instantaneous and daily photosynthesis of leaves in the canopy of a *Solidago altissima* stand. Physiol Plant 70:215–222

Hirose T, Werger MJA (1995) Canopy structure and photon flux partitioning among species in a herbaceous plant community. Ecology 76:466–474

Kamiyama C, Oikawa S, Kubo T, Hikosaka K (2010) Light interception in species with different functional groups coexisting in moorland plant communities. Oecologia 164:591–599

Keddy PA (1989) Competition. Chapman and Hall, London

Kohyama T (1992) Size-structured multi-species of rain forest trees. Func Ecology 6:206–212

Kropff MJ (1988) Modelling the effects of weeds on crop production. Weed Res 28:465–471

Kropff MJ, Spitters CJT (1991) A simple model of crop loss by weed competition from early observations on relative leaf area of the weeds. Weed Res 31:97–105

Kropff MJ, Vossen FJH, Spitters CJT, de Groot W (1984) Competition between a maize crop and a natural population of *Echinochloa crus-galli* (L.). Neth J Agric Sci 35:525–528

Lambers H, Chapin FS III, Pons TL (1998) Plant Physiological Ecology. Blackwell, Malden

Liebman M (2001) Weed management: a need for ecological approaches. In: Liebman M, Mohler CL, Staver CP (eds) Ecological Management of Agricultural Weeds. Cambridge University Press, Cambridge, pp 1–39

Łomnicki A (1980) Regulation of population density due to individual differences and patchy environment. Oikos 35:185–193

Marshall B, Biscoe PV (1980) A model for C3 leaves describing the dependence of net photosynthesis on irradiance. J Exp Bot 31:29–39

Monsi M, Saeki T (1953) Über den Lichtfaktor in den Pflanzengesellschaften und seine Bedeutung für die Stoffproduktion. Jpn J Bot 14:22–52. *Translated as*: Monsi M, Saeki T (2005) On the factor light in plant communities and its importance for matter production. Ann Bot 95:549–567

Mortensen DA, Bastiaans L, Sattin M (2000) The role of ecology in the development of weed management systems: an outlook. Weed Res 40:49–62

Moss SR (2003) Herbicide resistance in weeds: current status in Europe and guidelines for management. Pestic Outlook 14:164–167

Niklas KJ (1992) Plant Biomechanics: An Engineering Approach to Plant Form and Function. University of Chicago Press, Chicago

Oerke EC (2006) Crop losses to pests. J Agric Sci 144:31–43

Onoda Y, Salunga E, Anten NPR, Yahara T (2014) Tradeoff between light interception efficiency and light use efficiency – implication for species coexisting in one-sided light competition. J Ecol 102:167–175

Pronk TE, Schieving F, Anten NPR, Werger MJA (2007) Plants that differ in height investment can coexist if they are distributed non-uniformly within an area. Ecol Complex 4:182–191

Ryan M, Yoder B (1997) Hydraulic limits to tree height and tree growth. Bioscience 47:235–241

Ryel RJP, Barnes W, Beyschlag W, Caldwell MM, Flint SD (1990) Plant competition for light analyzed with a multispecies canopy model. I. Model development and influence of enhanced UV-B conditions on photosynthesis in mixed wheat and wild oat canopies. Oecologia 82:304–310

Schwinning S, Weiner J (1998) Mechanisms determining the degree of size asymmetry in competition among plants. Oecologia 113:447–455

Selaya NG, Anten NPR (2010) Leaves of pioneer and late successional species have similar life time carbon gain in tropical secondary forest. Ecology 91:1102–1113

Selaya NG, Anten NPR, Mathies M, Oomen RJ, Werger MJA (2007) Aboveground biomass investments and light interception of tropical forest trees and lianas early in succession. Ann Bot 99:141–151

Selaya NG, Oomen RJ, Netten J, Werger MJA, Anten NPR (2008) Biomass allocation and leaf life span in relation to light interception by tropical forest plants during the first years of secondary succession. J Ecol 96:1211–1221

Spitters CJT (1986) Separating the diffuse and direct component of global radiation and its implications for modelling canopy photosynthesis. II. Calculation of canopy photosynthesis. Agric For Meteorol 38:239–250

Spitters CJT, Aerts R (1983) Simulation of competition for light and water in crop weed associations. Asp Appl Biol 4:467–484

Stern VM, Smith RF, van den Bosch R, Hagen KS (1959) The integrated control concept. Hilgardia 29:81–101

van Ittersum MK, Leffelaar PA, van Keulen H, Kropff MJ, Bastiaans L, Goudriaan J (2003) On approaches and applications of the Wageningen crop models. Eur J Agron 18:204–231

van Kuijk M, Anten NPR, Oomen RJ, Werger MJA (2008) The limited importance of size-asymmetric light competition and growth of pioneer species in early secondary forest succession. Oecologia 157:1–12

Vermeulen PJ, Stuefer JF, During HJ, Anten NPR (2008) Leaf investment and light partitioning among leaves

of different genotypes of the clonal plant *Potentilla reptans* in dense stands after five years of competition. Ann Bot 102:935–943

Vos J, Evers JB, Buck-Sorlin GH, Andrieu B, Chelle M, de Visser PHB (2010) Functional-structural plant modelling: a new versatile tool in crop science. J Exp Bot 61:2102–2115

Wall R, Begon M (1985) Competition and fitness. Oikos 44:356–360

Weiner J (1986) How competition for light and nutrients affects size variability in *Ipomoea tricolor* populations. Ecology 67:1425–1427

Weiner J (1990) Asymmetric competition in plant populations. Trends Ecol Evol 5:360–364

Werger MJA, Hirose T, During HJ, Heil GW, Hikosaka K, Ito T, Nachinshonhor UG, . . ., Anten NPR (2002) Light partitioning among species and species replacement in early successional grassland. J Veg Sci 13:615–626

Werner C, Ryel RJ, Correia O, Beyschlag W (2001) Effects of photoinhibition on whole-plant carbon gain assessed with a photosynthesis model. Plant Cell Environ 24:27–40

Wright IJ, Reich PB, Westoby M, Ackerly DD, Baruch Z, Bongers F, Cavendar-Bares J, . . ., Villar R (2004) The worldwide leaf economics spectrum. Nature 428:821–827

Yasumura Y, Hikosaka K, Matsui K, Hirose T (2002) Leaf-level nitrogen use efficiency of canopy and understorey species in a beech forest. Funct Ecol 16:826–834

Yin X, Struik PC (2010) Modelling the crop: from systems dynamics to systems biology. J Exp Bot 61:2171–2183

Zhao DL, Atlin GN, Bastiaans L, Spiertz JHJ (2006) Cultivar weed-competitiveness in aerobic rice: heritability, correlated traits, and the potential for indirect selection in weed-free environments. Crop Sci 46:372–380

Chapter 15

Axiomatic Plant Ecology: Reflections Toward a Unified Theory for Plant Productivity

Kihachiro Kikuzawa*
Ishikawa Prefectural University, Nonoichi, Japan
Onoecho 14-16, Zushioku, Yamashina, Kyoto 607-8453, Japan
and
Martin J. Lechowicz
Department of Biology, McGill University,
1205 Avenue Dr. Penfield, Montréal, QC H3A 1B1, Canada

*Author for correspondence, e-mail: kkikuzawa@kyoto.zaq.jp

e-mail: martin.lechowicz@mcgill.ca

K. Hikosaka, Ü. Niinemets, and N.P.R. Anten (eds.), *Canopy Photosynthesis: From Basics to Applications*, DOI 10.1007/978-94-017-7291-4_15

Summary

Starting from an axiom that sunlight is the fundamental energy source for green plants, we derived some theorems in plant ecology. We began by reviewing the Monsi-Saeki model, which was the first to relate the structure of canopy and productivity. Optimum leaf area (and thus leaf biomass) were predicted from the Monsi-Saeki model, which also introduced the concept of constant final yield per unit land area. A relationship between total biomass (y) and plant number (n) per unit land area was derived by combining the principles of constant final yield and logistic plant growth, which is based upon the diminishing return of total individual photosynthesis due to self-shading, An analogous equation was obtained in the analysis of cumulative plant biomass (Y) against cumulative plant number (N) within a stand. Mass-number relationships among stands (y-n) and within a stand (Y-N) were revealed to be the same under one-sided competition for light. The self-thinning line is the point where individual plant's growth becomes zero on the translocation of a Y-N relationship through time. Self-thinning is expected to occur due to the death of the smallest plants

Abbreviations: A – Specific parameter of the Y to N relationship that represents the reciprocal of maximum total biomass in a stand; α – Stand compactness; $a_1 \sim a_5$ – Regression coefficients; B – Specific parameter of the Y to N relationship that represents the reciprocal of maximum plant mass in a stand; $b_1 \sim b_3$ – Regression coefficients; $\beta_1 \tilde{} \beta_3$ – Degree of one- (and two) sided competition; B_L – Leaf biomass of a stand per unit land area; C – Construction cost of unit leaf area; χ – Number of leaves that the solar flux encounters before reaching certain depth of a canopy; CV – Coefficient of variation; δ – Power exponent of allometry between H_{max} and w_{max}; d – Dry matter density of a stand; F – Cumulative leaf area from the top per unit land area; f – Favorable period for photosynthesis; F_{opt} – Optimum leaf area of a stand which gives the maximum surplus production; G – Cumulative gain by a single leaf per unit leaf area; g – Marginal gain or G per time; GPP – Gross primary production; H_{max} – Height of the hypothetical largest plant in a stand; I_o – Irradiance at the top of a canopy; I – Irradiance at a certain depth of a canopy; K – light extinction coefficient; $K_1 \sim K_6$ – Regression coefficient; L – Leaf longevity; L_f – Functional leaf longevity; LAI – Leaf area index; λ – Intrinsic growth rate of average plant mass; LMA – Leaf mass per leaf area; m – Mean labor time in a day for photosynthesis; N – Number of plants in a unit land area from the largest to a certain sized one.; N_0 – Number of plants in a unit land area in the course of self-thinning; n – Number of plants per unit land area; N_B – N axis of base point of Y-N curve; P – Instantaneous gross photosynthetic rate of a canopy per unit land area; p – Instantaneous gross photosynthetic rate of a leaf per unit leaf area; p' – Net photosynthetic rate of a leaf per unit leaf area; p_{day} – Daily photosynthetic rate per unit leaf area; p_{max} – Mean maximum photosynthetic rate of a leaf; PPFD – Photosynthetic photon flux density; P_s – Instantaneous surplus production of a stand per unit land area; P_{year} – Annual photosynthetic rate of a stand per unit land area; r – Instantaneous respiration rate of a leaf per unit leaf area; RGR – Relative growth rate; S – Land area which the plant canopy occupies; s – Leaf area of a single leaf which comprises the canopy; t – Time; t_{opt} – Optimal leaf longevity; t_{pot} – Time at which daily photosynthetic rate is zero; w – Individual plant mass; $\overline{w}$ – Average plant mass; w_L – Leaf biomass of an individual plant; $\overline{w}_o$ – Initial average plant mass; $\overline{w}_{max}$ – Maximum asymptotic average plant mass which average plant reaches with time; w_{max} – Hypothetical maximum plant mass in a stand when number of plant (N) reaches zero which can be obtained as the reciprocal of parameter B of Y to N relationship; WBE – West Brown and Enquist's scaling theory; Y – Biomass of plants from the largest to a certain sized one in a unit land area; Y_B – Y axis of base point of Y-N curve; y_{final} – Total biomass of plants per unit land area after canopy closure when the effect of planting density on total biomass is diminished; Y_∞ – Asymptotic total biomass of plants per unit land area when maximum number of plants are packed into the space which is obtained as the reciprocal of parameter A of Y to N relationship; y – Total biomass of plants per unit land area; Y_0 – Total biomass of plants per unit land area in the course of self-thinning

shaded by larger plants. The Monsi-Saeki modeling framework was reoriented considering leaf longevity, which is the optimal timing to replace individual leaves to maximize carbon gain of the plant. Under canopy ergodic hypothesis, which supposes space-time equivalence in the performance of leaves, leaf longevity can be used to circumvent the difficulties in the scaling from leaf to canopy. Gross primary production then can be estimated using functional leaf longevity together with the mean labor time of a leaf, two measures of the time during the leaf span when it can be photosynthetically active. Finally, if leaf longevity is used in a species-specific normalization constant, plant productivity can be described as an allometric function of plant mass. In that case, the relative growth rate of plants can be shown to have an inverse relationship to leaf longevity.

Keywords Leaf longevity • Self thinning • Primary production • Logistic growth

I. Introduction

Plant ecologists have identified empirically many quantitative trends, laws and rules related to the basis for variation in plant productivity including the law of constant final yield in plant communities (Kira et al. 1953), the self-thinning rule (Yoda et al. 1963), the leaf size-twig size spectrum (Wright and Westoby 2002), the leaf economic spectrum (Wright et al. 2004), the leaf size-number tradeoff (Kleiman and Aarssen 2007), and the rules for scaling biomass allocation on plant size (Enquist and Niklas 2001) among others. Ideally such inductive generalizations could be derived from first principles in a unified mechanistic theory for plant productivity from the scale of single leaves on individual plants to multispecies aggregations of plants in communities and ecosystems.

In this chapter, as a stimulus to future work toward a unified, cross-scale theory of plant productivity, we sketch an outline of important generalizations and key elements in existing theory, beginning with pioneering work at the level of plant communities and then extending into work at the level of leaves and whole plants. We emphasize theory developed by mathematical analysis from first principles, but also comment on studies using simulation models to elucidate fundamental mechanisms underlying observed but still poorly understood aspects of the production process. We start from a premise that in general the single most critical resource governing the ecology and evolution of variation in the processes involved in plant productivity is the availability of photosynthetically active radiation. We take this premise as an axiom, and review the mathematical derivation of a series of relationships organizing plant productivity at the community level before turning to the different streams of inquiry that have sought to develop theory at the leaf and whole-plant levels linked to these relationships at the community level. We complement this deductive approach with selected inductive generalizations that invite development or extension of existing theory. Our aims are (1) to show the inherent coherence of the relationships organizing variation in plant productivity among species and plant communities at scales from leaves on an individual plant up to entire communities and (2) to reflect on the avenues for future work toward a truly unified, cross-scale theory for plant productivity that is firmly grounded in the processes governing productivity at the level of individual plants.

II. Productivity Relationships in Populations and Communities

A. Monsi-Saeki Model

We begin with the pioneering work by Monsi and Saeki (1953) who were the first to develop general theory for the relationship

between the structure and productivity of vegetation built on the premise that the capture of light energy was a critical determinant of variation in productivity. They partitioned the above-ground biomass in a plant community into its productive (leaves) and non-productive (branch and stem) parts as a function of height above the ground, showing that allocation to leaves peaks at an intermediate depth in a plant canopy and that non-productive components steadily increase with depth. The subsequent development of theory for plant productivity in plant canopies was strongly influenced by this pioneering work, which itself built on seminal physiological work in the 1930s on the conversion of CO_2 taken up in photosynthesis to dry matter (Boysen-Jensen 1932 as cited in Hirose 2005).

To link this bipartite partitioning of vegetation structure to function, Monsi and Saeki (1953) turned first to developing theory for the productive parts. They considered the photosynthetic interception of photons by a leaf of area s in a space of area S. The photon flux not intercepted by the target leaf is $I_o(1 - s/S)$. If the solar flux at the canopy surface encounters χ leaves before reaching the certain level of the canopy, then the irradiance at that level (I) is given by $I_o(1 - s/S)^{\chi}$, which is equivalent to $I = I_o e^{\chi log(1-s/S)}$. Monsi and Saeki generalized this analysis, expressing the vertical distributions of productive parts in terms of leaf area per unit land area per unit canopy depth (F). When we quantify F as $\chi s/S$ and define k as $-(S/s)log(1 - s/S)$, we obtain $I = I_o e^{-kF}$ where k is an extinction coefficient and I_o is irradiance at the top of the canopy. This is essentially an ecological expression of Beer's law (cf. Chap. 1, Goudriaan 2016) for light extinction in closed plant canopies showing that *irradiance diminishes exponentially with depth in the plant canopy* (**THEOREM 1**).

Monsi and Saeki (1953) further derived a function for gross photosynthesis against F at the canopy level by combining the relationship $I = I_o e^{-kF}$ (i.e. Theorem 1) with a simple expression for a saturating response of instantaneous gross photosynthesis (p) to irradiance at the leaf-level:

$$p = \frac{b_1 I}{1 + a_1 I} \tag{15.1}$$

where a_1 and b_1 are parameters specific to the particular plant or vegetation canopy under consideration. They expressed the amount of light absorbed by a thin layer of leaf ($\triangle F$) as $-dI/dF$. From Theorem 1 this is $kI_o e^{-kF}$, which when substituted into Eq. 15.1 and integrated from zero to F yields an asymptotic equation

$$P = \frac{b_1}{a_1 k} \ln\left(\frac{1 + a_1 k I_0}{1 + a_1 k I_0 e^{-kF}}\right) \tag{15.2a}$$

Where P is the instantaneous canopy gross photosynthesis (gross production) per unit land area. This relationship at the canopy level in fact saturates with any monotonically increasing function for gross photosynthesis, even a simple linear increase such as $p = a_2 I$, which on integration yields

$$P = a_2 I_o\left(1 - e^{-kF}\right). \tag{15.2b}$$

Where a_2 is a regression constant. Hence the critical determinant of the saturation curve at the canopy level is the influence of the vertical structure of the canopy on the decay of irradiance with canopy depth, a point that will figure centrally in the subsequent development of theory.

By accounting for leaf respiration effects on gross photosynthesis Monsi and Saeki (1953) and Monsi (1960) further showed that *a plant canopy has maximum net productivity gain at an intermediate value of leaf area index (F)* **(THEOREM 2)**. Corresponding to Eqs. 15.2a and 15.2b, the equations for net photosynthesis are given as

$$p' = \frac{b_1 I}{1 + a_1 I} - r \tag{15.3a}$$

and

$$p' = a_2 I - r \tag{15.3b}$$

Where p' is instantaneous net photosynthesis of a leaf per unit leaf area and r is instantaneous respiration of a leaf per unit leaf area. The comparable equations for surplus production at the canopy level are given by combining these equations with Theorem 1:

$$P_s = \frac{b_1}{a_1 k} \ln\left(\frac{1 + a_1 k I_0}{1 + a_1 k I_0 e^{-kF}}\right) - rF \tag{15.4a}$$

and

$$P_s = a_2 I_o \left(1 - e^{-kF}\right) - rF \tag{15.4b}$$

Where P_s is instantaneous surplus production of a stand per unit land area (Monsi 1960). The leaf area index that maximizes net production in a fully-developed, closed vegetation canopy is then:

$$F_{opt} = \frac{1}{k} \ln\left(\frac{k I_0 (b_1 - a_1 r)}{r}\right) \tag{15.5a}$$

and

$$F_{opt} = \left(\frac{1}{k}\right) \ln\left(\frac{a_2 k I_0}{r}\right) \tag{15.5b}$$

The value of F_{opt} in a particular situation will vary as a function of both ecological and evolutionary influences on the parameters in Eqs. 15.5a and 15.5b. The values of leaf area index (F) actually observed in almost a thousand natural and managed vegetation canopies had a median value of 4.4 (lower quartile 2.6, upper quartile 6.5; Scurlock et al. 2001). One source of this variation in mono-specific plant canopies is simply the evolutionary diversification of plant respiration rate, photosynthetic light response, and canopy architecture affecting the light extinction rate. A second source of variation is the ecological response of individual plants to their neighbors in mixed-species vegetation, which can lead to values of F at the scale of the vegetation canopy that differ from F_{opt} predicted for a single target species (Anten 2002 and 2005; Chap. 13, Anten 2016). Since F_{opt} for a given situation is taken to be constant (cf. Eqs 15.5a and 15.5b) any changes in F due to interactions among neighboring plants, however, should be proportional to F_{opt} (Anten 2002).

B. Logistic Growth of Plant Mass

The preceding theoretical analyses focused on spatial deployment of leaf area, the critical parameter on the supply-side of productivity, but equally important are questions of investments of photosynthetic products – biomass – that influence the potential for future photosynthetic gains. At the level of leaves the relationship between the area available for the harvest of light energy and the investment of biomass in light harvesting is expressed by the leaf mass per unit area (LMA). Multiplying LAI with LMA converts leaf area to leaf biomass. Since (a) an F_{opt} exists in a given situation (Theorem 2), (b) LMA is a reasonably stable characteristic of individual species under similar light conditions, and (c) species occur in a restricted set of environmental conditions, we therefore can expect that the foliar biomass per unit land area might be roughly constant in fully mature mono-specific stands of a given species. For example, Tadaki (1986) found relatively low standard deviations of mean foliar biomass across a wide sample of stands varying in site quality, density, age, and tree height. He reported foliar biomass for 58 Japanese *Fagus* stands as 380 ± 160 g m^{-2} (42 % coefficient of variation; CV), for 39 *Betula* stands as 220 ± 110 g m^{-2} (50 % CV), for 20 evergreen *Quercus* stands as 840 ± 200 g m^{-2} (24 % CV), for 120 stands of *Pinus densiflora* as 640 ± 130 g m^{-2} (20 % CV), for 126 stands of *Cryptomeria japonica* as 1960 ± 440 g m^{-2} (22 % CV), and for 47 stands of *Abies* species 1680 ± 490 g m^{-2} (29 % CV). Since foliar biomass in young, unclosed stands increases with stand age until canopy closure, this degree of constancy can be expected only in fully mature,

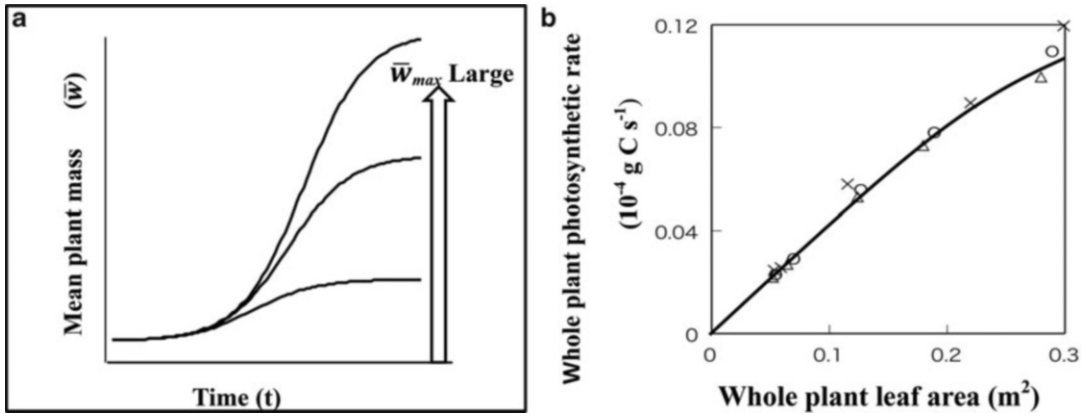

Fig. 15.1. (**a**) Schematic diagram of logistic growth (Eq. 15.8) with different asymptotic values ($\overline{w}_{max}$). (**b**) Whole plant photosynthetic rate (P) against whole plant leaf area (F) which are surrogates of daily growth (dw/dt) and plant mass (w) of logistic equation (Eq. 15.7), respectively. The relationship was regressed by a quadratic equation as is required by the logistic equation (Eq. 15.7) (Koyama and Kikuzawa 2009). $P = -4.02*10^{-5}\ F^2 + 4.95*10^{-5}\ F + 7.39*10^{-9.}$ Different *symbols* indicate different individuals

closed canopies (Kira and Shidei 1967; Tadaki 1986).

This tendency to converge to a stand level F_{opt} arises at least in part through density-dependent interactions between the mass of individual plants and their combined mass at the stand or community level that were recognized in early studies of controls on agricultural yield (cf. Chap. 14, Anten and Bastiaans 2016; Weiner and Freckleton 2010). For example, Kira et al. (1953) planted soy-beans in a field at different planting densities per unit land area (Fig. 15.2b). Initial plant size ($\overline{w}_o$, mean seed mass) was equal across stands, but differences in the mean plant mass in each stand became evident soon after seedling emergence. In sparser stands, mean plant mass became greater than in the denser stands. On the other hand, the total plant mass per unit land area (final yield) increased with planting density, but this increase was asymptotic. As a result after enough time had elapsed and canopy closure had occurred, the biomass of each stand was equivalent and was independent of planting density. Shinozaki and Kira (1956) designated this outcome "the law of constant final yield", which is expressed as

$$\frac{\partial y}{\partial n} = 0 \tag{15.6}$$

where y is biomass per unit land area and n is planting density (i.e. number of plants per unit land area). This relationship can be shown to be consistent with self-shading effects (Koyama and Kikuzawa 2009), with the existence of an optimum leaf area in Monsi-Saeki theory, and with the roughly equivalent leaf biomass per unit land area observed in comparisons among diverse forests (Tadaki 1986).

Koyama and Kikuzawa (2009) (Fig. 15.1b) showed from first principles that *the logistic growth of individual plants arises in shading effects.* **THEOREM 3.** Logistic growth can be expressed as:

$$\frac{d\overline{w}}{dt} = \lambda \overline{w}\left(1 - \frac{\overline{w}}{\overline{w}_{max}}\right) \tag{15.7}$$

where $\overline{w}_{max}$ is the asymptote of mean individual mass $\overline{w}$ with time and λ is the intrinsic growth rate of mean plant mass. Integration of Eq. 15.7 gives:

$$\overline{w} = \frac{\overline{w}_{max}}{1 + a_3 e^{-\lambda t}} \tag{15.8}$$

Where a_3 is an integration constant. This equation gives sigmoidal curves with different asymptotes depending on $\overline{w}_{max}$ values (Fig. 15.1a). Given the inherently logistic growth of individual plants that arises in self-shading, we can consider the density dependence of mean plant mass ($\overline{w}$) at a given time (τ) after seedling emergence. If we fix $t = \tau$, then $e^{-\lambda\tau}$ in Eq. 15.8 can be considered constant and since $\overline{w}_{max}$ in Eq. 15.8 is the asymptotic value of mean plant mass after canopy closure (Fig. 15.1a), then the asymptotic value of mean individual plant mass is inversely proportional to planting density:

$$n\ \overline{w}_{max} = y_{final} \tag{15.9}$$

where y_{final} is the final yield, or asymptotic total biomass of plants after canopy closure. By the law of constant final yield (Eq. 15.6), y_{final} in Eq. 15.9 is independent of n. Seed mass at time $t = 0$ is independent of density and is obtained from Eq. 15.8 as:

$$\overline{w}_0 = \frac{\overline{w}_{max}}{1 + a_3} \tag{15.10}$$

Substitution of $\overline{w}_{max}$ (Eq. 15.9), a_3 (Eq. 15.10) and $e^{-\lambda\tau}$ into (Eq. 15.8) yields:

$$\overline{w} = \frac{1}{a_4 n + b_2} \tag{15.11}$$

where $a_4 = \left(1 - e^{\lambda\tau}\right)/y_{final}$ and $b_2 = e^{-\lambda\tau}/\overline{w}_o$. Since a_4 and b_2 are independent of n, Eq. 15.11 expresses the effect of planting density (n) on mean individual plant mass ($\overline{w}$), with a_4 and b_2 being parameters that are constant at a given time but change with time (Fig. 15.2a, b). This equation, first obtained by Shinozaki and Kira (1956) (Fig. 15.2b), has been applied to many stands of both herbaceous and woody plants and is supported by considerable experimental evidence (Weiner and Freckleton 2010). By multiplying both sides of Eq. 15.11 by planting density (n) we obtain the relationship between planting density and stand biomass (y) (Fig. 15.2c):

$$y = \frac{n}{a_4 n + b_2} \tag{15.12}$$

Equations 15.11 and 15.12 are equivalent descriptions of the asymptotic relationship between initial plant density and the mean mass of an individual plant (Eq. 15.11) or the total plant biomass in the stand (Eq. 15.12).

C. Size Inequality Among Plants

Having established the consistent relationships between initial stem density and both the *mean* and the *total* plant mass that prevail in comparisons among a set of plant stands, we can turn our attention to the size inequalities among individual plants in a given stand. It is well known that the size frequency distribution of individual plant mass, which at the time of planting is initially a normal distribution of propagule mass with fairly small standard deviation, becomes an inverse J-shaped frequency distribution increasingly skewed to smaller individuals over time (Koyama and Kira 1956). Hozumi et al. (1968) expressed this size hierarchy within a single stand by ordering plants from the largest to smallest individual and assessing their cumulative number (N)

$$N = \sum_{w}^{w_{max}} n_i = \int_{w}^{w_{max}} \phi(w)dw \tag{15.13a}$$

and cumulative mass (Y):

$$Y = \sum_{w}^{w_{max}} w_i n_i = \int_{w}^{w_{max}} w\phi(w)dw \tag{15.13b}$$

where n_i is the number of individual plants in size class w_i, and $\emptyset(w)$ is the distribution density function of w. Hozumi et al. (1968) found in many forest stands, that the relationship between the cumulative number and mass of individuals within a stand could be described as:

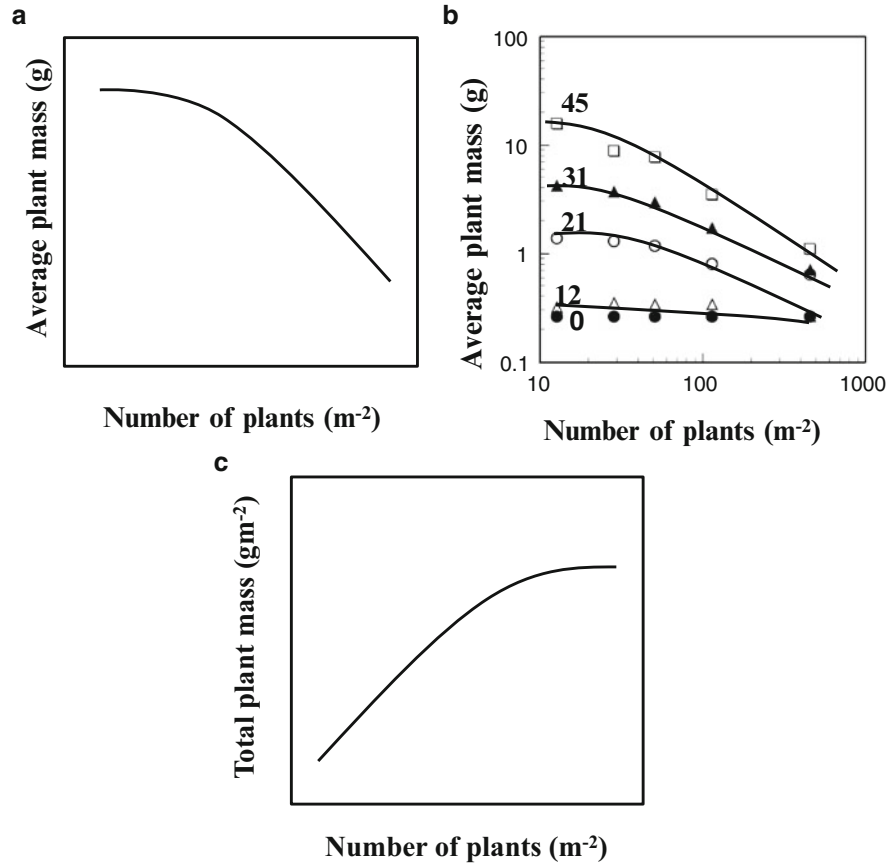

Fig. 15.2. Schematic representations of Eqs. 15.11 and 15.12 and the application of Eq. 15.11 to actual data of plant populations
(**a**) Eq. 15.11, or the relationship between average plant mass ($\overline{w}$) and plant number per unit land area $(n)\overline{w} = \frac{1}{a_4 n + b_2}$, represents the decreasing curve, when n is large $\overline{w}$ reaches zero and n is small, $\overline{w}$ reaches a constant value
(**b**) Application of Eq. 15.11 to experimental data. Soybeans were sown different numbers per square meter at time zero. Plants emerged from the seeds were weighed at different times (days) which were affixed to each symbol. Each time, average plant masses (Y axis) were shown in relation to plant number (X axis) on the double log scale, and regressed by Eq. 15.11, which well described the relationship with different parameters (Redrawn using data by Kira et al. 1953)
(**c**) Eq. 15.12 or relationship between biomass per unit land area $(y = \overline{w}n)$ and plant number per unit land area $(n)y = \frac{n}{a_4 n + b_2}$ represents increasing function with an asymptote

$$Y = \frac{N}{AN + B} \tag{15.14}$$

where Y is the cumulative biomass of N individuals within a single stand ranked from the largest to the smallest and A and B are fitting parameters. Though empirically fitted, parameters have the following meanings,

$$A = \frac{1}{Y_\infty} \tag{15.15a}$$

$$B = \frac{1}{w_{max}} \tag{15.15b}$$

where Y_∞ is the hypothetical maximum biomass of a fully packed stand when N reaches infinity in Eq. 15.14 and w_{max} is the

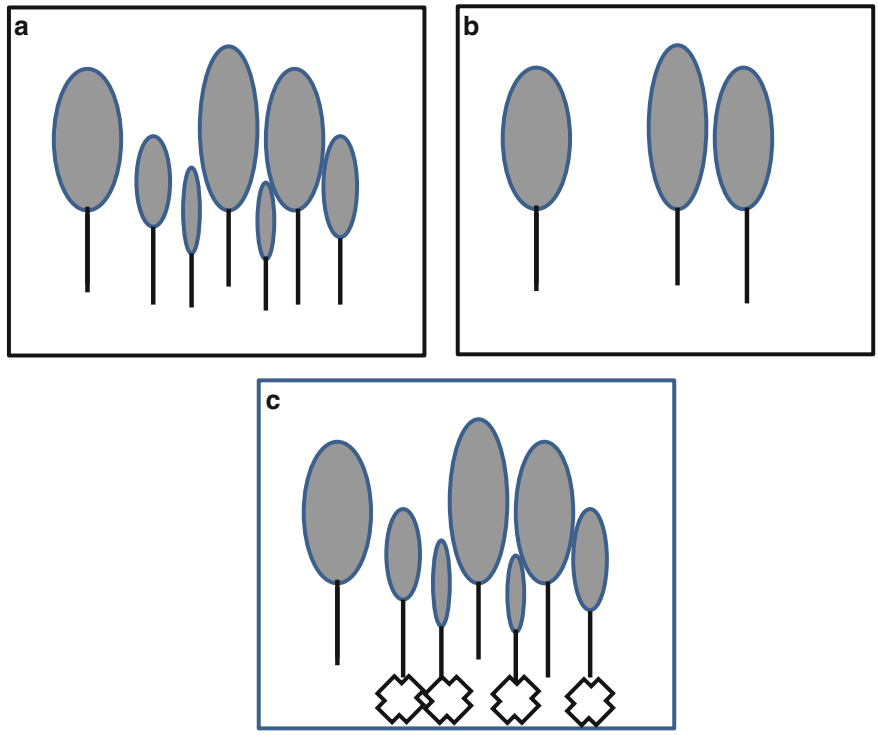

Fig. 15.3. Exploring the basis of density-yield relationships among (panels a, b) versus within (panel c) stands or plant populations.
(**a**) Dense stand with n_1 (7) plants.
(**b**) Sparse stand with n_2 (3) plants. The relationship between stand a and b is expressed by Eq. 15.12.
(**c**) A replica of panel a but the smallest 4 plants are marked with crosses. The remainder n_2 (3) plants are the same that in stand b because the smallest plants do not affect the largest plants within the stand. Therefore, the relationship between total n_1 (7) plants and the largest n_2 (3) plants is expressed by Eq. 15.12. Thus we can conclude Eq. 15.14 is identical with Eq. 15.12

hypothetical maximum plant mass when N reaches zero in Eq. 15.14.

Comparison of Eqs. 15.12 and 15.14 indicates that *the size hierarchy among individual plants within a stand is the same as that of mean plant mass among stands* (Kikuzawa 1999*)*. **THEOREM 4.**

Kikuzawa (1978, 1982) found this relationship held for data from many forest stands in Hokkaido, which prompted him to investigate the possibility that the remarkably similar form of the yield density relationship within (Eq. 15.14) versus among (Eq. 15.12) stands might arise in one-sided competition for light among neighboring individuals. Under the assumption of one-sided competition for light (i.e. a "dark leaf" hypothesis; Duursma et al. 2011), consider two plant populations of the same age but different initial densities (Fig. 15.3). The number of plants per unit land area in a dense stand (Fig. 15.3a) is n_1 ($n_1 = 7$) and in a sparse stand (b) is n_2 ($n_2 = 3$). Since the four (n_1-$n_2 = 4$) smallest plants in the dense stand do not affect the growth of the largest n_2 (3) plants in the same stand and the relationship between the plant biomass per unit land area and population density of the two stands is described by Eq. 15.12, we can expect the larger n_2 individuals in the dense stand (panel a) to be identical in size to n_2 individuals in the sparse stand (panel b) where n_2 plants were initially planted. Within the dense stand (cf. panel c in

Fig. 15.3) the largest n_2 plants and the total n_1 must also be related by Eq. 15.12 since the largest n_2 plants in the dense stand (panel a) are identical to the total n_2 plants in the sparse stand (panel b). This argument can be made for any $n_1 \sim n_2$ combinations, so we can conclude logically that under entirely one-sided competition the relationship in Eq. 15.12 also must hold between cumulative plant size (Y) and cumulative plant number (N) from the largest individual within a single stand (Eq. 15.14). In other words, under entirely one-sided competition, the among-stand parameters a_4 and b_2 in Eq. 15.12 and the among-individual parameters A and B in Eq. 15.14 are respectively identical (Kikuzawa 1999).

D. One Sided Competition

The relationships between plant numbers and total biomass within versus among stands also can be derived more generally without imposing the assumption of wholly one-sided competition. Consider a general growth equation for an individual focal plant that allows for the effects of stem density and interactions among individual plants (Yokozawa and Hara 1992):

$$\frac{dw}{dt} = w\left[\beta_1 - \beta_2 \int_{w_{min}}^{w_{max}} w\phi(w)dw - \beta_3 \int_{w}^{w_{max}} w\phi(w)dw\right] \tag{15.16}$$

Without constraints, a plant will grow exponentially as a function of the proportionality constant β_1. The second term in the bracket represents the effect of total plant biomass in the stand from the smallest plant (w_{min}) to the largest (w_{max}) on the growth of individual plants, essentially the constraints on individual growth arising in two-sided competition. The third term in the bracket represents the effect of larger neighbors on the focal plant, an expression of one-sided competition. If $\beta_2 = 0$ and $\beta_3 > 0$, then competition is wholly one-sided and Eqs. 15.12 and 15.14 are identical (Kobayashi and Kikuzawa 2000). If $\beta_2 > 0$ and $\beta_3 = 0$, then competition is wholly two-sided, and if $\beta_2 > 0$ and $\beta_3 > 0$, then the competition is asymmetric to some degree (Yokozawa and Hara 1992).

This generalization of the relationship between stem density and the biomass of plants singly or in aggregate within and among stands better reflects the range of possibilities in nature. Because of variation in canopy architecture within and among neighboring plants within a single species stand, competition for incoming solar radiation tends to be asymmetric but is only rarely wholly one-sided (cf. Chap. 14, Anten and Bastiaans 2016). The shallower the individual canopy and the greater the hierarchy among individual heights, the more asymmetric are competitive interactions. For example, in the canopy of a *Betula ermanii* stand larger individuals were not heavily shaded even in the lowest part of their crowns and smaller individuals were heavily shaded by their larger neighbors, while in *Picea abies* stands even larger individuals were shaded in the lowest part of their crowns (Kikuzawa and Umeki 1996).

E. Position of Y-N Curve

The two Eqs. 15.15a and b fix the asymptotic lines along a curve relating the total biomass of plants comprising a stand to the number of plants in the stand. One extreme is when the total biomass is distributed among an infinite number of individual plants (Eq. 15.15a) and the other when the biomass of a single individual plant comprises the total biomass of the stand (Eq. 15.15b). Neither extreme is of particular interest in reality, but these extremes help place the possible relationships between the total biomass in a given stand and the number of plants in the stand in an informative graphical context: a *Y-N* curve. Eq. 15.14 basically represents the relationship between cumulative number and cumulative mass in a stand at a time, which follows an asymptotic curve in this yield-density space. The position of any stand in a *Y-N* curve at a point in time is given by

its base point, $[Y_B,N_B]$ (Shinozaki and Kira 1961):

$$Y_B = \frac{1}{2A} \tag{15.17a}$$

and

$$N_B = \frac{B}{A} \tag{15.17b}$$

Note that parameter B is equal to the reciprocal of w_{max}, or the hypothetical maximum tree weight at a time, which in turn must be related its height as

$$w_{max} = K_1 H_{max}{}^{\delta} \tag{15.18a}$$

where H_{max} is the hypothetical maximum height for a tree with mass w_{max} and K_1 is the normalization constant of the allometry (Enquist and Bentley 2012). The power δ usually takes a value around 3. From Eq. 15.15b, we then obtain

$$B = K_1{}^{-1} H_{max}{}^{-\delta} \tag{15.18b}$$

In summary, there are predictably consistent relationships between the height of growing vegetation over time and the mass of plants individually and in aggregate.

F. Dry Matter Density

Kira and Shidei (1967) proposed the *concept of dry matter density.* With a focus on forest communities, they considered the above-ground biomass (both productive and non-productive) in a forest stand at a point in time and defined dry matter density (d) as the total above-ground biomass per unit stand volume. The latter is defined by the product of maximum stand height (H_{max}) and land area occupied by the stand. We can postulate that the dry matter density of mature forest communities with a closed canopy is constant across variation in canopy height. The rationale for this constancy in dry matter density is based on the constancy of foliage biomass in mature canopies (Theorem 2). We have some evidence that in pine stands (Tadaki et al. 1979) the dry matter density increased with time to a stable value after canopy closure (Fig. 15.4). Since by definition dry matter density (d) is Y/H_{max}, d can be expressed by parameters A and B in the *Y-N* relations using Eqs. 18.15a and 15.18a, b as

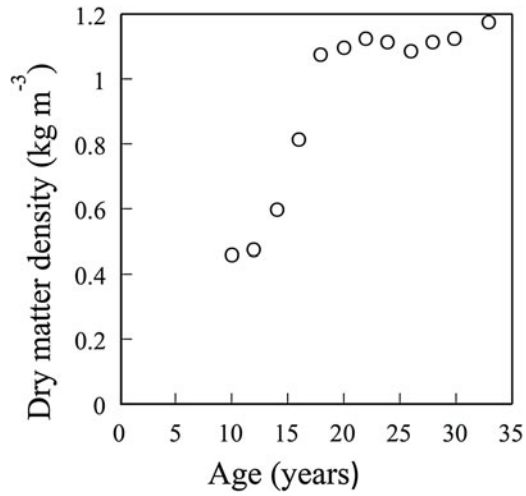

Fig. 15.4. Dry matter density (d) in a typical forest stand (*Pinus densiflora*) plotted against time since stand establishment (Drawn after Tadaki et al. 1979)

$$d = K_1^{\frac{1}{\delta}} A^{-1} B^{\frac{1}{\delta}} \tag{15.19a}$$

If d is constant through time after canopy closure as expected, then it follows that

$$A(t) = K_2 B(t)^{\frac{1}{\delta}} \tag{15.19b}$$

where $K_2 = d^{-1} K_1{}^{\frac{1}{\delta}}$

G. Tracking Stand Development in Yield-Density (Y-N) Space

Over the course of stand development, the base point of a *Y-N* curve will shift toward the upper-left because of the asymmetric growth of trees within a stand. Larger trees gain a disproportionately greater increment, smaller trees a lesser increment; suppressed

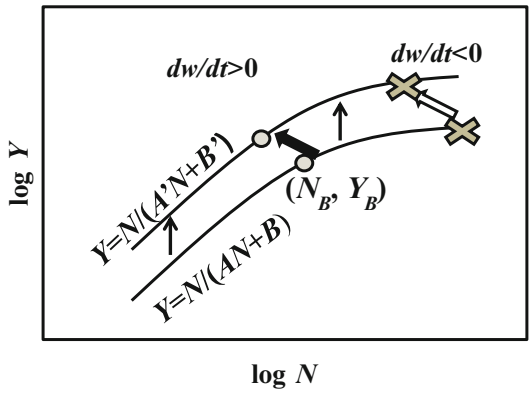

Fig. 15.5. Translocation of a *Y-N* curve with the growth of individual trees in a stand over time. The thin upper arrows illustrate the cumulative biomass increment (Y) at selected positions along the gradient of trees ranked from largest to smallest (N). At the rightmost positions at a given time (shown by *crosses*), the growth increment of the smallest trees can drop to zero ($dw/dt = <0$) and as these trees die the *Y-N* curve will be shortened (i.e. its end point shifted leftward as shown by the *open oblique arrow*). Because larger trees grow disproportionately more than smaller trees in competitive interactions, the position of the *Y-N* curve itself also shifts upper-left. The trajectory of the base-point of the *Y-N* curve ($N_B = B/A$, $Y_B = 1/(2A)$ shown by *circles*) tracks this shift over time (shown by *closed oblique arrow*). The upper-left movement of the *Y-N* curve as a whole will be expressed by $Y_B = K_3 N_B{}^{-1/(\delta-1)}$. Hence the initial *Y-N* curve expressed by $Y = N/(AN + B)$ through time will shift to $Y = N/(A'N + B')$

trees have zero gain and die out through self-thinning of the stand (Fig. 15.5). Kikuzawa (1993) gives an example of how the upper-leftward movement of the *Y-N* curve in a *Betula* stand can be tracked through the corresponding movement of the base point of the curve (Y_B, N_B). This can be obtained by substitution of Eq. 15.19b into Eqs. 15.17a and 15.17b and diminishing B.

$$Y_B = K_3 N_B{}^{\frac{-1}{\delta-1}} \tag{15.20}$$

Where $K_3 = 2^{-1} K_2{}^{-\delta/(\delta-1)}$.

Hence, if the dry matter density (d) is maintained constant, the *Y-N* curve moves obliquely from lower right to upper left along the line shown in Eq. 15.20 as illustrated in Fig. 15.5 (Kikuzawa 1999).

H. Growth and Death of Plants

Consider the growth and death of individual plants under the conditions of equation (18.14) and one-sided competition. Differentiation of Eq. 15.14 gives $dY/dN = B/(AN + B)^2$. Since $dY/dw = -w\phi(w)$ and $dN/dw = -\phi(w)$ from Eqs. 15.13a and 15.13b, the change in individual plant mass ($dY/dN = w$) is then given by

$$w = \frac{B}{(AN + B)^2} \tag{15.21}$$

Under one-sided competition the order of individual plants surviving within a stand is unchanging – N is essentially independent of time (e.g. Kikuzawa 1993, 1999). Hence substitution of Eq. 15.19b into Eq. 15.21 gives

$$w = \frac{K_2{}^{-\delta} A(t)^{\delta}}{\left[A(t)N + K_2{}^{-\delta} A(t)^{\delta}\right]^2} \tag{15.22}$$

This is a growth equation for individual plant mass as a function of $A(t)$, or the reciprocal of ideal stand biomass.

I. The Dynamics of Tree Death–Self-Thinning

There is a limit to the number of plants that can occupy a given area and this limit shifts over the course of stand development following the equation

$$\overline{w} = a_5 n^{-b_3}. \tag{15.23}$$

where $\overline{w}$ is mean plant mass, n is the number of plants in the stand, and a_5 and b_3 are constants (Fig. 15.6). The exponent b_3 is usually around 1.5, so Eq. 15.23 is referred to as the *−3/2th power law of self-thinning* (Yoda et al. 1963), which can be applied to stands in which plants eventually will die due to competition for light but are still growing. Rewritten in terms of stand biomass (y) this is:

$$y = a_5 n^{-b_3+1} \tag{15.24}$$

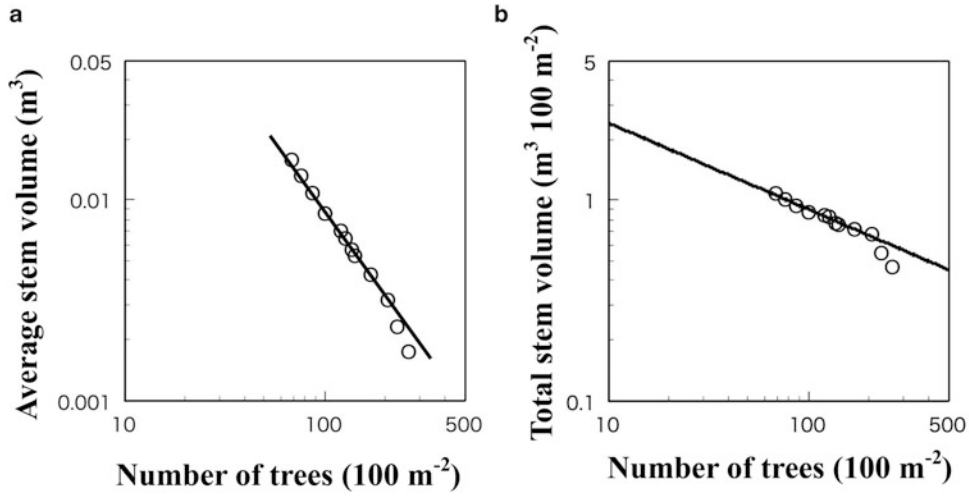

Fig. 15.6. An example of self-thinning in a birch stand.
(**a**) Increase in average stem volume (which is the surrogate of tree mass) with decrease in tree number on a unit land area. Self-thinning considers the situation where plants vigorously grow but some of them died due to crowding. The slope of the line on a double log scale was −1.43 (Redrawn from Kikuzawa 1999)
(**b**) Increase in stand stem volume with decrease in tree number. The same data of panel a is redrawn for the stand level. The slope was −0.43

In Eq. 15.24 the exponent $-b_3 + 1$ is $-1/2$ if the value of b_3 is 3/2. The exponent 3/2 arises in the general relationship between volume and area when plants fully occupy an available space of unit dimension, so plant mass should be proportional to the 3rd power of the unit dimension and the area covered to the 2nd power, hence $b_3 = 3/2$. Based on differing assumptions about the basis of self-thininng, the theory of metabolic scaling predicts $b_3 = 4/3$ (Enquist et al. 1998; Enquist and Bentley 2012). Many studies of thinning in plant stands report exponents around these values.

If we can theoretically obtain the condition that $dw/dt = 0$, then we will establish that *self-thinning is a process in which smaller plants die due to suppression by larger neighboring plants as a stand develops*. **THEOREM 5.** Building on earlier analyses and making some simplifying assumptions, we can derive such an equation describing the progress of self-thinning over time in a given stand by differentiating Eq. 15.22 with time; $\frac{dw}{dt} = \frac{dw}{dA}\frac{dA}{dt}$. We know from Eq. 15.16 that dA/dt is ever decreasing, so the value of dw/dt mostly depends on dw/dA. Designate the value of N that gives $dw/dA = 0$ as N_o, which is given as $N_o \propto A^{\delta-1}$. Substitution of this equation into Eq. 15.14 gives

$$Y_o = K_4 N_o^{-1/(\delta-1)}. \tag{15.25}$$

where Y_o is total plant biomass per unit land area in the course of self-thinning and

$$K_4 = \left[\left(\frac{\delta-2}{\delta}\right)^{1/(\delta-1)}\left\{1+\left(\frac{\delta-2}{\delta}\right)^{\delta}\right\}\right]^{-1} K_2^{-\delta/(\delta-1)}.$$

This equation is essentially the same as Eq. 18.24 and is nothing but the self-thinning line. From Eq. 18.18a, δ is expected to take a value around 3. If δ is exactly 3, then the power of Eq. 18.25 becomes $-1/2$, suggesting the $-3/2$th power law and if δ is 4 the power becomes $-1/3$, suggesting the $-4/3$th scaling law (Enquist et al 1998; West et al. 1997, 2009). In fact the power (the slope of the self-thinning line) can take many values depending on the value of δ, which usually falls between 2 ~ 4.

J. Stand Compactness

Interestingly, the exponent in Eq. 15.25, $-1/(\delta - 1)$, is the same as that in Eq. 15.20 defining the trajectory of the *Y-N* curve under the condition that dry matter density is constant. The self-thinning line is parallel to the trajectory of the base point of the *Y-N* curve on a double logarithmic scale (cf. Kikuzawa 1993). In other words, the base point in a self-thinned stand that is fully stocked is parallel to the self-thinning line. Conversely, we can assume that if the base point of any stand is near the base point line shown by Eq. 15.20, the stand must be fully stocked, and if the base point of any stand is less than the base point line, then the stand can be considered understocked. Note that the terms N_B and Y_B in Eq. 15.20 can be modified by a factor alpha $(0 < \alpha \leq 1)$ expressing the degree of stocking in a stand, or its compactness: $N_B{}' = \alpha N_B$ and $Y_B{}' = \alpha Y_B$. The greater alpha, the more fully stocked or compact is the stand (Kikuzawa 1983). Substitution of αN_B, αY_B into Eq. 15.17a,b and Eq. 15.20 gives the compactness as

$$\alpha = (2K_3)^{-(\delta-1)/\delta} A^{-1} B^{1/\delta}. \qquad (15.26)$$

This equation is essentially the same as Eq. 15.19a, indicating that compactness is essentially equivalent to a measure of dry matter density.

K. Summary: Roots of Current Theory for Canopy-Level Productivity

To this point we have traced the development of key elements in theory built on the work of Monsi and Saeki (1953) for the production ecology of plant populations and communities. We began with their analysis of vertical stratification in the photosynthetic and non-photosynthetic components in a plant canopy, and laid out a series of results that organize our understanding of plant production at the population and community levels. These include the following theorems derived on an axiomatic assumption that irradiance is the primary resource limiting plant production:

1. Irradiance diminishes exponentially with depth in the plant canopy.
2. A plant canopy has maximum surplus productivity gain at an intermediate value of the leaf area index due to the balance between self-shading and maintenance.
3. The logistic growth of individual plants in populations arises in shading effects, which finally derives mean plant mass-density relationships..
4. The size hierarchy among individual plants within a stand is the same as that of mean plant weight among stands.
5. Self-thinning is a process in which smaller plants die due to suppression by larger neighboring plants as a stand develops.

The subsequent development of theory for plant productivity has built on these foundations as well as adopting more novel approaches. In the following sections we summarize refinements to the basic conceptual framework pioneered by Monsi and Saeki (1953), introduce other approaches to a unified theory for plant productivity, touch on some poorly addressed aspects of productivity in natural vegetation, and close by reflecting on how a unified theory for plant productivity might emerge.

III. Toward a Unified Theory of Plant Productivity

A. Building on the Foundation Initiated by Monsi-Saeki (1953)

Generally speaking refinement of the Monsi-Saeki perspective on productivity (Monsi and Saeki 1953; Monsi et al. 1973) has taken a decidedly mechanistic and reductionist approach. Improving theory for the productivity of vegetation has been characterized as a problem of scaling up biochemical processes at the leaf level – "scaling from leaf to canopy" (Amthor 1994).

Indeed Monsi and Saeki (1953) themselves considered that processes operating at the level of single leaves would be analogous to those in the vegetation canopy, essentially treating the plant canopy as a "big-leaf". Their simple function for photosynthesis (cf. Eq. 15.1) eventually was replaced by a more biochemically sophisticated one (Farquhar et al. 1980; see Chap. 3, Hikosaka et al. 2016) that allowed photosynthetic rate to be limited by either the uptake of CO_2 (Rubisco-limitation) or irradiance (electron transport limitation) and linked to a model for the optimal investment of nitrogen as a function of insolation gradients within the canopy (Field 1983). Many models of canopy photosynthesis have been built on the premise of maximizing photosynthetic gain within the constraints of nitrogen limitation (cf. Chap. 13, Anten 2016), which is consistent with the observed role of LAI and foliar nitrogen concentration in predicting net primary production across a wide range of ecosystems (Reich 2012). Hikosaka (2003, 2005) provides a good example of a model for canopy photosynthesis that adopts the traditional Monsi-Saeki emphasis on LAI but builds on the premise of a nitrogen constraint on optimization of carbon gain to predict the dependence of canopy photosynthesis on leaf turnover in time. Despite the apparent rigor of such contemporary analyses in the Monsi-Saeki tradition, discrepancies between theoretical expectations and observations (Hirose 2005; Posada et al. 2009) call into question the generality of both the premise of nitrogen limitation and the simple "big-leaf" perspective (Friend 2001; Sprintsin et al. 2012).

Within the crown of a single plant or in a vegetation canopy, two aspects of spatiotemporal variation are not in accord with a "big-leaf" perspective on theory for productivity. Both have to do with difficulties integrating the contribution of the many individual leaves to LAI as a canopy-level trait. First, the insolation regime for leaves at different positions within the crown of a single plant or in the canopy of vegetation is not well-described by Beer's Law (cf. Theorem 1). Sunflecks readily penetrate openings in a crown or canopy (Pearcy 1990), briefly exposing interior leaves to the high PPFD levels more typical of outermost leaves. Second, outermost leaves are generally younger than interior leaves, with consequent age-dependent differences in production processes. A single equation (cf. Eqs. 15.2a and 15.2b) characterizing all leaves in the crown of an individual plant clearly is not realistic, even setting aside the greater differences that can arise in the canopy of a plant community composed of functionally diverse species. Adjusting nitrogen investment and photosynthetic function to insolation gradients within the canopy (Field 1983) unfortunately does not entirely solve this problem (Anten and During 2011; Sprintsin et al. 2012). Treating the canopy as though it had two layers differing in insolation regime, one shaded and the other sunlit (de Pury and Farquhar 1997), improves predictions of canopy-level gross primary productivity but still does not adequately allow for the inherent complexity of canopy structure (Sprintsin et al. 2012).

It is therefore fair to question whether theory rooted at the level of photosynthetic biochemistry is the only, or even necessarily the best, foundation for predicting productivity at the level of plant communities and ecosystems. Any reductionist and mechanistic approach to theory has to define some lower bound, a level of process that generates and to some degree regulates related process higher in a hierarchy of biological organization. Theory for productivity at the community and ecosystem level originating in the work of Monsi and Saeki (1953) has built on an increasingly deep understanding of the resource dependencies of the fundamental photosynthetic process at the biochemical level within leaves, but with relatively little concern for variation in resource availability or functional variation at the whole-plant level. Two alternative streams of theory for plant productivity have emerged that consider the effects of mechanism affecting

productivity at scales intermediate to sites of photosynthesis within leaves and the productivity of entire plant communities. We now consider each of these in turn.

B. Reorienting the Focal Scale for a Theory of Productivity: Leaves

The "big-leaf" perspective on scaling from "leaf to canopy" in fact is not about the leaf *per se*, but rather the photosynthetic and respiratory processes occurring at cellular and tissue levels within a leaf. This biochemical focus follows early work on the physiological basis of biomass production (Boysen-Jensen 1932; cited in Hirose 2005), but ignores an earlier tradition (Blackman 1919) that uses a leaf area ratio (LAR) and net assimilation rate (NAR) to calculate a relative growth rate (RGR) for biomass directly (cf. Hunt 1978; Lambers et al. 2008). Since there is no logical necessity to root a theory of plant productivity at the biochemical level as opposed to the level of the leaf as the photosynthetic organ driving growth in biomass, a first alternative to the Monsi-Saeki approach therefore could be to reframe theory for productivity at the level of the leaf itself. The leaf is after all a key functional unit in the production process, the sole plant organ dedicated to photosynthesis and the source of the photosynthate essential for plant growth as well as reproduction. Photosynthetic responses to irradiance and other environmental factors are primarily studied at the level of intact leaves, thus providing a coherent and functionally meaningful aggregate of the activities involved in plant production at tissue and subcellular levels. There also is a high degree of functional integration between photosynthetic rates at the leaf level and other foliar characteristics, including foliar nitrogen concentration (Wright et al. 2004). Leaves also occupy terminal positions in the vascular architecture of plants, controlling flows of water and mineral resources through their stomatal activity. Finally, leaf longevity can provide a biologically meaningful unit of time, potentially simplifying theory predicting temporal variation in productivity. Hence the leaf is a logical foundation on which to build alternative theory for plant productivity, and two bodies of theory have developed in which the leaf *per se* figures as the key element.

C. Reorienting the Framework in a Theory of Productivity: Leaf Longevity

In his theory for leaf longevity Kikuzawa (1991) laid a foundation for an alternative theory of plant productivity rooted at the leaf-level. Leaf longevity is part of a highly integrated suite of foliar traits (Wright et al. 2004; Shipley et al. 2006) directly linked to both the ecophysiological basis of productivity and the dynamics of LAI at the canopy-level (Hikosaka 2003). Under the axiomatic assumption that irradiance is the primary resource limiting plant production, Kikuzawa (1991) showed that to maximize carbon gain (G) at the level of an individual plant, the marginal gain (g) of leaves must be maximized:

$$g = \frac{1}{t}\{G\} = \frac{1}{t}\left\{\int_0^t p_{day}(t)dt - C\right\}$$
$$= \frac{1}{t}\left\{\int_0^t p_{day}(0)\left(1 - \frac{t}{t_{pot}}\right)dt - C\right\} \quad (15.27)$$

where t is time (days), $p_{day}(t)$ is daily net production expressed by parameters $p_{day}(0)$ (initial daily photosynthetic gain) and $1/t_{pot}$ (rate of decline in photosynthetic capacity over time; t_{pot} is a day when net production becomes zero or potential leaf longevity) and C is construction cost of a leaf (Fig. 15.7b). Cost (C) is considered the product of energy required to convert a unit of glucose to unit of leaf tissue and the leaf mass per unit leaf area (LMA). Analytical solution of Eq. 15.27 gives:

$$t_{opt} = \left(\frac{2t_{pot}C}{p_{day}(0)}\right)^{\frac{1}{2}} \quad (15.28)$$

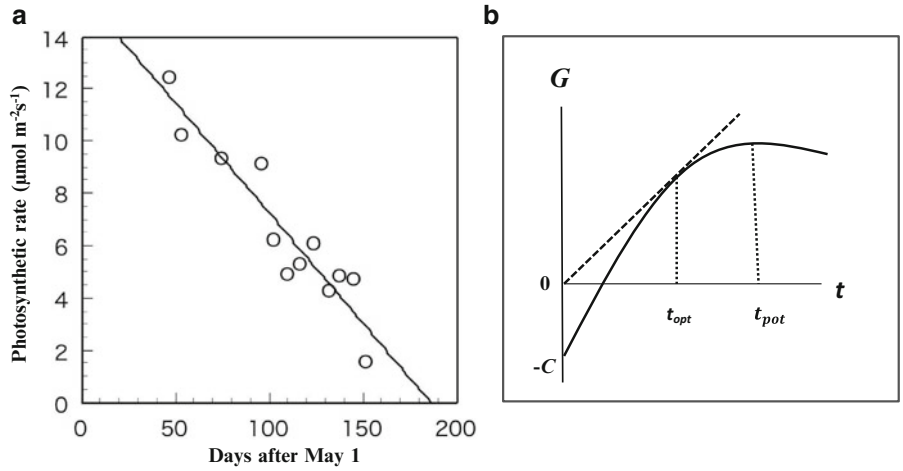

Fig. 15.7. Photosynthetic gain by a single leaf.
(**a**) Time trend of instantaneous photosynthetic rate of a beech (*Fagus crenata*) leaf with time. A same leaf was repeatedly measured within a season. The light saturated net photosynthetic rate declined with time because of leaf's ageing. (Koyama and Kikuzawa 2010). The decline of the photosynthetic rate is expressed by a line, $p = p(0)(1 - t/t_{pot})$, where $p(0)$ is instantaneous photosynthetic rate at time zero and t_{pot} is the potential leaf longevity when the photosynthetic rate is zero.
(**b**) Schematic representation of the relationship between the cumulative net photosynthetic gain by a single leaf (G) and time after leaf emergence (t). The gain curve increases from minus C, or the cost for leaf (materials and constructive cost). The gain increases with time but with diminishing return. The cumulative gain no more increases beyond time t_{pot} at which the instantaneous gain becomes zero because of balancing of decreased photosynthetic gain due to leaf's ageing and maintenance cost (respiration loss). This timing is optimal to maximize gain by the leaf, but is not optimal for the plant. The timing (t_{opt}) at which a line started from the origin touches the gain curve is the optimal to maximize gain of the plant. At t_{opt}, the gain per unit time, or the marginal gain ($g = G/t$) is maximal

In other words, *leaf longevity is a function of the maximum photosynthetic capacity of a newly formed leaf, the rate of decline in photosynthetic capacity with leaf age, and the initial construction cost of the leaf.* (**THEOREM 6)**. From Eq. 15.28, we can expect that leaf longevity will be positively correlated with LMA, and negatively correlated with both photosynthetic capacity and the rate of decline in photosynthetic capacity. These expectations are consistent with empirical observations and experiments (Kikuzawa and Lechowicz 2011).

There is, however, another view that accounts for differences in leaf longevity not as the outcome of maximizing marginal gain but rather by time discounting of investments in carbon, nitrogen and phosphorus (Falster et al. 2011); this perspective is consistent with a recent model following a "big-leaf" approach that maximizes canopy carbon export over the lifespan of leaves (McMurtrie and Dewar. 2011). Both these views on the role of leaf longevity on plant productivity are set in the same fundamental ecophysiological framework, but treat the integration of time effects at different scales. Kikuzawa (1991) integrates carbon gain over the lifetime of single leaf whereas given a value for leaf longevity Falster et al. (2011) integrate carbon gain over the lifetime of the whole-plant. Both views are legitimate in their own right, but which provides the basis for a simpler general theory of plant productivity?

Since we routinely measure photosynthesis and productivity per unit time, the Falster et al. (2011) view would appear to be in better accord with the Monsi-Saeki tradition as well as more consistent with evolutionary assessments of fitness variation among individual plants. There are, however,

conceptual as well as computational difficulties integrating the processes of productivity over time because the factors affecting the processes are not constant in time. For example, photosynthesis cannot occur at night, which means that away from the equator the time available for leaf function will vary predictably with latitude as well as less predictably with variable seasonal and diurnal variations in temperature and moisture that affect photosynthetic activity. Since photosynthetic function is inherently environmentally dependent and the environment inherently variable in time, theory built on a premise of pay back on investments over time should integrate a measure of time weighted by potential for photosynthetic activity – *mean labor time* (Kikuzawa et al. 2004). Mean labor time is the average time period within a day when a leaf can actually carry out photosynthesis in a given environment. Similarly, in assessing annual productivity one ideally should discount days in the year when seasonal conditions are wholly unfavorable for photosynthesis – in other words measure *functional leaf longevity* (Kikuzawa and Lechowicz 2006). The return on investment in leaf construction that determines longevity can only occur during diurnal and seasonal periods favoring photosynthetic activity. Together the concepts of mean labor time and leaf longevity therefore define the actual duration of photosynthetic activity required functional to maximize the marginal gain on investments in a leaf. A general theory scaling productivity from single leaves to the canopies of mature plant communities may in fact be simpler and more robust based on this effective payback time rather than the progress of time unweighted by potential for photosynthetic activity.

D. Canopy Ergodic Hypothesis

The value of scaling time weighted by the potential for photosynthetic function is strengthened by the possibility that the photosynthetic production of a single leaf through its lifetime is equivalent to the summed production of leaves from the top to the bottom of a canopy at a point in time – the canopy ergodic hypothesis of Kikuzawa et al. (2009). In a plant canopy, the microenvironmental condition around a given leaf will change with time. A single leaf initiated along a shoot in the outer canopy generally will be shaded gradually by other leaves as growth continues through a season – the relative position of the leaf will sink deeper into the expanding canopy. Put in another way, a single leaf over time functions in a gradient of microenvironmental conditions similar to the microenvironmental gradient from the top to the bottom of the canopy at a point in time. The canopy ergodic hypothesis holds that as a consequence there is space-time equivalence in the performance of leaves in a canopy (Kikuzawa et al. 2009). This supposition, which has some empirical support (Kikuzawa et al. 2009; Koyama and Kikuzawa 2009), circumvents the needs to estimate the number of leaves in the canopy to extend the theory for leaf longevity to the canopy (cf. Hikosaka 2005) and provides a scaling strategy that collapses the spatiotemporal complexity of the plant canopy in ways that can simplify a general theory for plant productivity.

We might question whether the degree to which canopy ergodicity holds will depend on patterns of leaf turnover and canopy growth. We generally expect that in a rapidly growing canopy with indeterminate shoot growth (successive leafing), leaves will have high but quickly declining photosynthetic rate, low LMA and short longevity to most effectively utilize the short period of high irradiance before shoot growth leads to their being shaded (Kikuzawa et al. 1996). The same logic applies to evergreen species but integrated over a longer time period defined by leaf longevity. Conversely, if all leaves appear simultaneously (flushing), the insolation regime of individual leaves will be fixed by their position in the plant crown and will not change through their life-time (Kikuzawa 1995, 2003; Umeki et al. 2010). Ergodicity therefore would not hold for

leaves in a given flush because there will be no change in the insolation regime of a leaf over its life-time. In principle, however, ergodicity may still hold for the succession of individual leaves at a given crown position over time; it should only be the rate of crown expansion and the crown architecture that set the time interval over which ergodicity applies.

The canopy ergodic hypothesis is consistent with the idea that the product of a leaf's lifetime photosynthetic gain and the annual leaf production rates in a stand should give an estimate of the annual primary production (P_{year}) of the stand. (Kikuzawa and Lechowicz 2006):

$$P_{year} = \left(m p_{max} L_f\right)\left(f\frac{B_L}{L_f}\right) \qquad (15.29)$$

where the term in the first parenthesis estimates the lifetime photosynthetic gain of a single leaf (G) and the term in the second parenthesis estimates the leaf production rate during the time of the year when photosynthetic activity is possible. The first term is the product of mean labor time (m), mean maximum instantaneous net photosynthetic rate (p_{max}) and functional leaf longevity (L_f). The second term (annual leaf production) is the leaf biomass per unit ground area (B_L) multiplied by favorable days (f) within a year, divided by the number of days over the leaf lifespan that are favorable for photosynthetic activity (L_f); note that this leaf production rate is not estimated using simply the leaf longevity unadjusted for unfavorable conditions for photosynthesis – the subscript f indicates days favorable for photosynthesis over the leaf lifespan. The apparent differences in leaf production rates between aseasonal and seasonal forests disappear when leaf biomass is scaled against functional leaf longevity, L_f. As a first approximation, leaf production rates per days suitable for photosynthetic activity appear to be invariant among forests (Kikuzawa and Lechowicz 2006). In turn gross primary production (GPP) then can be estimated as a simple fraction (k) of P_{year} (Eq. 15.29; Koyama and Kikuzawa 2010).

In summary, a theory of plant productivity rooted at the level of the leaf as a photosynthetic organ provides an alternative approach to "scaling from leaf to canopy" (Amthor 1994). Taking theory for leaf longevity (Kikuzawa 1991) as a starting point for a more general, cross-scale theory of plant productivity subsumes the biochemical intricacies of photosynthetic process (Farquhar et al. 1980), the alternative tradeoffs among foliar traits (Wright et al. 2004) and resource constraints on productivity (Field 1983) into a single key variable that lends itself to a tractable general analysis. Leaf longevity also provides a biologically based approach to rescaling time that can account for transient environmental conditions complicating the integration of productivity processes that operate on time scales ranging from seconds to decades. In approaching theory for plant productivity from this starting point, there is an implicit assumption that leaf longevity provides an effective index of myriad alternative tradeoffs at the whole plant level that yield comparable fitness in a given environment (Marks and Lechowicz 2006). The canopy ergodicity hypothesis, an expression of this assumption at the whole-plant level, has been supported by studies of individual plants (Kikuzawa et al. 2009; Koyama and Kikuzawa 2009). The degree to which this assumption holds for the canopy in mixed-species vegetation remains an open question, but the observed invariance in leaf production rates per days suitable for photosynthetic activity independent of species composition supports this supposition (Kikuzawa and Lechowicz 2006). Finally, the fact that both the number of leaves and the metabolic rates of plants scale as the ¾ power of plant mass (Enquist et al. 1999; Savage et al. 2010) also suggest the existence a fundamental integration of function centered on the leaf as a photosynthetic organ that operates across species.

E. Reorienting the Framework in a Theory of Productivity: Plant Size

The Monsi-Saeki perspective led to considerable understanding of the role of size hierarchies in the productivity of plant communities, especially in mono-specific crops (Weiner and Freckleton 2010). Size-dependence also has long figured in models of self-thinning in multi-species forest communities (Zeide 2010), including sophisticated models of forest dynamics based on competitive interactions among neighboring individuals that have profound implications for understanding productivity at the ecosystem level (Purves and Pacala 2008). Plant size is really no more than a measure of the net cumulative production of an individual plant over its lifetime, a measure directly dependent on down-scale productivity process and certainly potentially relevant to up-scaling productivity to the community and ecosystem level. It therefore is reasonable to consider plant size *per se* as the focus of a general theory for plant growth and productivity, and indeed West et al. (1997, 1999, 2001) laid the groundwork for just such a model. Their WBE network model seeks to explain allometric scaling laws in plant biology (Enquist and Niklas 2001) as the outcome of the way that the architecture of vascular systems controls the scaling of surface areas where resources are exchanged between the plant and environment. In the case of plants xylem and phloem comprise an integrated vascular system at the whole-plant level with root surfaces as sites of uptake for water and minerals and leaves as sites of uptake for carbon dioxide and solar energy. The WBE theory treats leaves as the "terminal metabolic units" in this branching vascular system that affect the normalization of general scaling relationships across taxa and environments (Enquist and Bentley 2012). Enquist (2002) summarizes the early development of this WBE model at the whole-plant level and has since refined the treatment of vascular structure that forms the fundamental basis of the model (Savage et al. 2010; Enquist and Bentley 2012) as well as extended the theory to plant productivity at the community and ecosystem level (Enquist et al. 2009; West et al. 2009). This approach through plant size-dependence, which is part of a larger body of theory in metabolic ecology (Sibly et al. 2012), essentially shifts the focus around which broader theory for plant productivity is framed by scaling from the organismal level (Enquist et al. 2003) rather than the traditional leaf level (Amthor 1994). This is not to say that this organism-centered approach ignores processes at the organ, tissue and cellular levels, only that lower level processes are predicted as intrinsically size-dependent outcomes at the whole-plant level that are organized by the behavior of leaves as the terminal units in the integrated vascular system. Here we touch on elements of this size-based theory that link to aspects of alternative theory for plant productivity and that suggest the possible emergence of a single coherent, cross-scale theory for plant productivity.

The WBE approach provides a mechanistic rationale in vascular architecture for the fact that any plant attribute (V) can be specified as a size-dependent function:

$$V = V_0 w_j^{\delta_a} \tag{15.30}$$

Where V_0 is a normalization constant for a particular attribute V, w_j is some measure of plant size including plant mass w, and δ_a is an exponent defining how V changes with w_j. If $\delta_a = 1$ the size-dependency is scaled linearly on size or isometrically, that is doubling w_j also doubles V. Any other value of δ_a indicates a nonlinear or allometric scaling; for example, doubling w_j might quadruple v ($\delta_a = 2$). This sort of size-dependent scaling, which has long been recognized in biology, can be understood on a mechanistic basis as the outcome of constraints on efficiently moving resources between sites of acquisition (leaves for energy and carbon uptake, roots for water and mineral nutrient uptake) and the various tissues in which

these resources are metabolized (West et al. 1997, 1999, 2001).

A focus on plant size naturally leads initially to questions of the change in the size of individual plants over time – in other words definition of a size-dependent rate of plant growth, dw/dt. The WBE approach leads to the general prediction that the growth rate of individual plants should scale as the ¾ power of biomass (Enquist 2002). Enquist and Bentley (2012) further express the growth rate of individual plants as:

$$dw/dt = K_5 w_L \qquad (15.31)$$

where K_5 is a normalization constant and w_L is the plant biomass invested in leaves, which is a more directly connected to the role of the leaf as a photosynthetic organ. (But it leads to non-realistic exponential growth, it only is true in the case of small plants.) They show how $K_5 = NAR \times SLA$ where NAR is the net carbon gain per unit leaf area and SLA is the leaf area per unit mass – key elements in the tradition of plant growth analysis (Hunt 1978) that traces back to Blackman (1919). Leaf weight ratio (LWR), the inverse of LAR in traditional plant growth analysis, in turn is equivalent to w_L, thus providing a link between the allometric scaling of growth and plant traits traditionally used to quantify productivity at the whole-plant level (Hunt 1978). There is an attractive simplicity in this size-dependent perspective on growth and productivity at the whole-plant level compared to the biochemical focus used in theory built on the early work of Monsi and Saeki (1953).

Moreover, West et al. (2009) show that the size-dependent relationships at the level of a single plant scale up to the level of the plant community, at least for forest tree communities (Enquist et al. 2009). They derive predictions for a wide variety of community level characteristics using established allometric relationships based on either trunk radius or mass: (a) the size distribution of individual trees in a mature forest, (b) the spacing of individuals, (c) the overlap of individual tree crowns, (d) the mortality rate for individual trees and (e) the fluxes of energy and materials in the forest. They make the intriguing argument that a forest community assembles in such a way that "...the network of interacting trees in the forest is essentially identical to the network of branches of an individual tree" (West et al. 2009). In other words they essentially posit a "big-tree" approach to scaling the productivity of forests.

F. Toward a Unified Theory for Plant Productivity

We have identified three approaches to theory for plant productivity from the level of leaves to ecosystems, one more mature and two others only relatively recently developed. The earliest and most developed approach builds on the pioneering work on Monsi and Saeki (1953) on the production ecology of the canopy in plant communities; the focal scale in this theory is the canopy itself, generally treated as though it were a "big-leaf" in terms of photosynthetic and respiratory metabolism. Kikuzawa (1991) alternatively took the leaf as the focal scale for a theory for canopy productivity, arguing that the productivity of a single leaf over its life-span scales up to the productivity of the plant on which it is borne, his canopy ergodicity hypothesis (Kikuzawa et al. 2009). Finally, Enquist and colleagues (West et al. 1997, 1999, 2001; Enquist 2002; Savage et al. 2010; Enquist and Bentley 2012) developed theory using size-dependencies originating in the vascular network at the focal scale of the whole-plant and showed that the structure and function of the network of trees comprising the forest was self-similar to that in a single tree (Enquist et al. 2009; West et al. 2009).

There are strengths in all three approaches, but they share one significant weakness: all of them are derived and tested in the context of single plants or communities consisting of a single plant species. Theory for the productivity of mono-specific plant communities is of course highly useful

for agricultural crops and forest plantations, but not as useful for natural plant communities. Community-wide predictions of productivity for natural communities based on the Monsi-Saeki approach typically are based on the dominant species in the community or a species representing a certain functional type, which is neither a very general nor entirely reliable simplification. Theory built on leaf longevity and the ergodicity hypothesis also is oriented to the scale of the canopy of individual plants, not the entire plant community, although there is some indication that it can be used to estimate GPP at the community level (Kikuzawa and Lechowicz 2006). Finally, although the size-dependencies that underpin metabolic theory are general in form, they are subject to species-specific normalization and hence would also require some sort of community aggregated estimate for predicting the productivity of mixed-species communities. Given the parallel uncertainties and difficulty of predicting community assembly (Weiher et al. 2011), a general, cross-scale theory for productivity in mixed-species communities may appear to be an impossible objective.

We suggest, however, that combining elements of theory based on leaf longevity and size-dependence may yield robust predictions for the productivity of specific plant communities. This possibility builds first on the observation that a forest taken as a whole is structured and functions in ways mathematically analogous to an individual tree (Enquist et al. 2009; West et al. 2009). Secondly, there is evidence (Messier et al. 2010) that at the scale of neighboring trees there is no variance component associated with key foliar traits such as LMA regardless of variation in the identity of neighboring species – some trait-based process of community assembly appears to structure the functional character of forests at local scale. Thirdly, foliar traits are both implicated in this trait-based assembly process and individual leaves are the metabolic drivers that organize the flow of resources in the vascular networks of individual trees and the forest (Enquist and Bentley 2012). It therefore is possible that the community aggregated value or community-wide mass ratio (cf. Grime 1998; Shipley 2010) of leaf longevity – the mean leaf longevity weighted by the relative abundance of the species in the community – could function as the normalization factor adjusting the general size-dependent relationships to a particular locality. In other words, leaf longevity may be the key driver normalizing the allometric relationships (cf. Eq. 15.30) for individual species and also at the community level. This possibility is supported by the negative correlation between the leaf longevity and relative growth rate of individual plants (Seiwa and Kikuzawa 2011), which suggests that the inverse of leaf longevity is essentially equivalent to K_5 in Eq. 15.31. Kikuzawa et al. (2013) tackled this problem to find a new allometric equation having inverse of leaf longevity (L) as a normalization constant. They derived the following equation to express the relative growth rate of individual plant.

$$RGR = \frac{3fCK_6}{L} w^{\delta_b - 1} \tag{15.32}$$

Where K_6 is a normalization constant of leaf mass-plant mass allometry. As mentioned above, δ_b takes value around 3/4 but takes near unity in case of tree seedlings (Eq. 15.31). In that case, RGR is inversely proportional to leaf longevity.

$$RGR = \frac{3fCK_6}{L} \tag{15.33}$$

Taken together these observations support the idea that both community assembly and forest productivity may depend not so much on the species-specific details of interactions among neighboring plants as on the filling in of a template for a transport network that maximizes entropy production in the free flow of resources driving plant productivity (Dewar 2010; Shipley 2010). This is a promising avenue toward a general, cross-scale theory for plant productivity.

Acknowledgements

We thank Martijn Slot, Kouki Hikosaka and Yasuo Konno for their review and comments on the manuscript. This analysis was initiated when MJL held an appointment as a visiting professor at Ishikawa Prefectural University funded by the Foundation of Science-Technology Center in Central Japan (Nagoya Fund). The work was also supported by MESSC of Japan #20370014 for KK.

References

Amthor JS (1994) Scaling CO_2-photosynthesis relationships from the leaf to the canopy. Photosynth Res 39:321–350

Anten NPR (2002) Evolutionary stable leaf area production in plant populations. J Theor Biol 217:15–32

Anten NPR (2005) Optimal photosynthetic characteristics of individual plants in vegetation stands and implications for species coexistence. Ann Bot 95:495–506

Anten NPR (2016) Optimization and game theory in canopy models. In: Hikosaka K, Niinemets Ü, Anten N (eds) Canopy Photosynthesis: From Basics to Applications. Springer, Berlin, pp 355–377

Anten NPR, Bastiaans L (2016) The use of canopy models to analyze light competition among plants. In: Hikosaka K, Niinemets Ü, Anten N (eds) Canopy Photosynthesis: From Basics to Applications. Springer, Berlin, pp 379–398

Anten NPR, During HJ (2011) Is analyzing the nitrogen use at the plant canopy level a matter of choosing the right optimization criterion? Oecologia 167:293–303

Blackman VH (1919) The compound interest law and plant growth. Ann Bot 33:353–360

Boysen-Jensen P (1932) Die Stoffproduktion der Pflanzen. Jena

de Pury DGG, Farquhar GD (1997) Simple scaling of photosynthesis from leaves to canopies without the errors of big-leaf models. Plant Cell Environ 20:537–557

Dewar RC (2010) Maximum entropy production and plant optimization theories. Philos trans Roy Soc B 365:1429–1435

Duursma RA, Falster DS, Valladares F, Sterck FJ, Pearcy RW, Lusk CH, Sendall KM, …, Ellsworth DS (2011) Light interception efficiency explained by two simple variables: a test using a diversity of small- to medium-sized woody plants. New Phytol 193:397–408

Enquist BJ (2002) Universal scaling in tree and vascular plant allometry: toward a general quantitative theory linking plant form and function from cells to ecosystems. Tree Physiol 22:1045–1064

Enquist BJ, Bentley LP (2012) Land plants: new theoretical directions and empirical prospects. In: Sibly RM, Brown JH, Kodric-Brown A (eds) Metabolic Ecology: A Scaling Approach. Wiley, New York, pp 164–187

Enquist BJ, Niklas KJ (2001) Invariant scaling relations across tree-dominated communities. *Nature* 410:655–660

Enquist BJ, Brown JH, West GB (1998) Allometric scaling of plant energetics and population density. Nature 395:163–165

Enquist BJ, West GB, Charnov EL, Brown JH (1999) Allometric scaling of production and life-history variation in vascular plants. Nature 401:907–911

Enquist BJ, Economo EP, Huxman TE, Allen AP, Ignace DD, Gillooly JF (2003) Scaling metabolism from organisms to ecosystems. Nature 423:639–642

Enquist BJ, West GB, Brown JH (2009) Extensions and evaluations of a general quantitative theory of forest structure and dynamics. Proc Natl Acad Sci U S A 106:7046–7051

Falster DS, Reich PB, Ellsworth DS, Wright IJ, Westoby M, Oleksyn J, Lee TD (2011) Lifetime return on investment increases with leaf lifespan among 10 Australian woodland species. New Phytol 193:409–419

Farquhar GD, Caemmerer S, Berry JA (1980) A biochemical model of photosynthetic CO2 assimilation in leaves of C3 species. Planta 149:78–90

Field CB (1983) Allocating leaf nitrogen for the maximization of carbon gain: leaf age as a control on the allocation program. Oecologia 56:341–347

Friend AD (2001) Modelling canopy CO_2 fluxes: are "big-leaf" simplifications justified? Glob Ecol Biogeogr 10:604–619

Goudriaan J (2016) Light distribution. In: Hikosaka K, Niinemets Ü, Anten N (eds) Canopy Photosynthesis: From Basics to Applications. Springer, Berlin, pp 3–22

Grime J (1998) Benefits of plant diversity to ecosystems: immediate, filter and founder effects. J Ecol 86:902–910

Hikosaka K (2003) A model of dynamics of leaves and nitrogen in a canopy: an integration of canopy photosynthesis, leaf life-span, and nitrogen use efficiency. Am Nat 162:149–164

Hikosaka K (2005) Leaf canopy as a dynamic system: ecophysiology and optimality in leaf turnover. Ann Bot 95:521–533

Hikosaka K, Noguchi K, Terashima I (2016) Modeling leaf gas exchange. In: Hikosaka K, Niinemets Ü, Anten N (eds) Canopy Photosynthesis: From Basics to Applications. Springer, Berlin, pp 61–100

Hirose T (2005) Development of the Monsi-Saeki Theory on canopy structure and function. Ann Bot 95:483–494

Hozumi K, Shinozaki K, Tadaki Y (1968) Studies on the frequency distribution I. A new approach toward the analysis of the distribution function and the −3/2th power distribution. Jpn J Ecol 18:10–20

Hunt R (1978) Plant Growth Analysis. Edward Arnold, London

Kikuzawa K (1978) Yield-density diagram of natural deciduous hardwood forest stands in Hokkaido. J Jpn For Soc 60:56–63

Kikuzawa K (1982) Yield-density diagram for natural deciduous broad-leaved forest stands. For Ecol Manag 4:341–358

Kikuzawa K (1983) Yield-density diagram: compactness index for stands and stand components. For Ecol Manag 7:1–10

Kikuzawa K (1991) A cost-benefit analysis of leaf habit and leaf longevity of trees and their geographical pattern. Am Nat 138:1250–1263

Kikuzawa K (1993) Self-thinning line and B-point line of the yield-density diagram in a young birch stand. For Ecol Manag 58:287–298

Kikuzawa K (1995) Leaf phenology as an optimal strategy for carbon gain in plants. Can J Bot 73:158–163

Kikuzawa K (1999) Theoretical relationships between mean plant size, size distribution and self thinning under one-sided competition. Ann Bot 83:11–18

Kikuzawa K (2003) Phenological and morphological adaptations to the light environment in two woody and two herbaceous plant species. Funct Ecol 17:29–38

Kikuzawa K, Lechowicz MJ (2006) Toward synthesis of relationships among leaf longevity, instantaneous photosynthetic rate, lifetime leaf carbon gain and the gross primary production of forests. Am Nat 168:373–383

Kikuzawa K, Lechowicz MJ (2011) Ecology of Leaf Longevity. Springer, New York

Kikuzawa K, Umeki K (1996) Effect of canopy structure on degree of asymmetry of competition in two forest stands in northern Japan. Ann Bot 77:565–571

Kikuzawa K, Koyama H, Umeki K, Lechowicz MJ (1996) Some evidence for an adaptive linkage between leaf phenology and shoot architecture in sapling trees. Funct Ecol 10:252–257

Kikuzawa K, Shirakawa H, Suzuki M, Umeki K (2004) Mean labor time of a leaf. Ecol Res 19:365–374

Kikuzawa K, Yagi M, Ohto Y, Umeki K, Lechowicz MJ (2009) Canopy ergodicity: can a single leaf represent an entire plant canopy? Plant Ecol 202:309–323

Kikuzawa K, Seiwa K, Lechowicz MJ (2013) Leaf longevity as a normalization constant in allometric predictions of plant production. PLoS ONE 8: e81873

Kira T, Shidei T (1967) Primary production and turnover of organic matter in different forest ecosystems of the western Pacific. Jpn J Ecol 17:70–87

Kira T, Ogawa H, Sakazaki N (1953) Intraspecific competition among higher plants I. Competition-yield-density interrelationship in regularly dispersed populations. J Inst Polytech Osaka City Univ 4:1–16

Kleiman D, Aarssen LW (2007) The leaf size/number trade-off in trees. J Ecol 95:376–382

Kobayashi Y, Kikuzawa K (2000) A single theory explains two empirical laws applicable to plant populations. J Theor Biol 205:253–260

Koyama K, Kikuzawa K (2009) Is whole-plant photosynthetic rate proportional to leaf area? A test of scalings and logistic equation by leaf demography census. Am Nat 173:640–649

Koyama K, Kikuzawa K (2010) Can we estimate forest gross primary production from leaf lifespan? A test in a young *Fagus crenata* forest. J Ecol Field Biol 33:253–260

Koyama H, Kira T (1956) Intraspecific competition among higher plants. VIII. Frequency distribution of individual plant weight as affected by the interaction between plants. J Inst Polytech Osaka City Univ D7:73–94

Lambers HF, Chapin FS, Pons TL (2008) Plant Physiological Ecology. Springer, New York

Marks CO, Lechowicz MJ (2006) Alternative designs and the evolution of functional diversity. Am Nat 167:55–67

McMurtrie RE, Dewar RC (2011) Leaf-trait variation explained by the hypothesis that plants maximize their canopy carbon export over the lifespan of leaves. Tree Physiol 31:1007–1023

Messier J, McGill B, Lechowicz MJ (2010) How do traits vary across ecological scales? Ecol Let 13:838–848

Monsi M (1960) Dry-matter reproduction in plants 1. Schemata of dry-matter reproduction. Bot Mag Tokyo 73:81–90

Monsi M, Saeki T (1953) Über den Lichtfackor in den Pflanzengesellschaften und seine Bedeutung für die Stoffproduktion. Jpn J Bot 14:22–52. *Translated as:* Monsi M, Saeki T (2005) On the factor light in plant

communities and its importance for matter production. Ann Bot 95:549–567
Monsi M, Uchijima Z, Oikawa T (1973) Structure of foliage canopies and photosynthesis. Annu Rev Ecol Syst 4:301–327
Pearcy RW (1990) Sunflecks and photosynthesis in plant canopies. Annu Rev Plant Physiol Plant Mol Biol 41:421–453
Posada JM, Lechowicz MJ, Kitajima K (2009) Optimal photosynthetic use of light by tropical tree crowns achieved by adjustment of individual leaf angles and nitrogen contents. Ann Bot 103:795–805
Purves D, Pacala S (2008) Predictive models of forest dynamics. Science 320:1452–1453
Reich PB (2012) Key canopy traits drive forest productivity. Proc R Soc B 279:2128–2134
Savage VM, Bentley LP, Enquist BJ, Sperry JS, Smith DD, Recih PB, von Allmen EI (2010) Hydraulic trade-offs and space filling enable better predictions of vascular structure and function. Proc Natl Acad Sci U S A 107:22722–22727
Scurlock JMO, Asner GP, Gower ST (2001) Global Leaf Area Index from Field Measurements, 1932–2000. Data set. Available at [http://www.daac.ornl.gov Oak Ridge National Laboratory Distributed Active Archive Center, Oak Ridge, TN. doi:10.3334/ORNLDAAC/584
Seiwa K, Kikuzawa K (2011) Close relationship between leaf life span and seedling relative growth rate in temperate hardwood species. Ecol Res 26:173–180
Shinozaki K, Kira T (1956) Intraspecific competition among higher plants. VII Logistic theory of the C-D effect. J Inst Polytech Osaka City Univ D7:35–72
Shinozaki K, Kira T (1961) The C-D rule, its theory and practical uses. J Biol Osaka City Univ 12:69–82
Shipley B (2010) From Plant Traits to Vegetation Structure: Chance and Selection in the Assembly of Ecological Communities. Cambridge University Press, Cambridge
Shipley B, Lechowicz MJ, Wright I, Reich PB (2006) Fundamental tradeoffs generating the worldwide leaf economics spectrum. Ecology 87:535–541
Sibly RM, Brown JH, Kodric-Brown A (eds) (2012) Metabolic Ecology: A Scaling Approach. Wiley, New York
Sprintsin M, Chen JM, Desai A, Gough CM (2012) Evaluation of leaf-to-canopy upscaling methodologies against carbon flux data in North America. J Geophys Res 117:G01023
Tadaki Y (1986) Productivity of forests in Japan. In: Fujimori T, Whitehead D (eds) Crown and Canopy Structure in Relation to Productivity. Forestry and Forest Products Research Institute, Ushiku, pp 7–25
Tadaki Y, Takeuchi I, Kawahara T, Sato A, Hatiya K (1979) Growth analysis on the natural stands of Japanese red pine (*Pinus densiflora* Sieb et Zucc) 3 Results of experiment (Research note). Bull For For Prod Res Inst 305:125–144
Umeki K, Kikuzawa K, Sterck FJ (2010) Influence of foliar phenology and shoot inclination on annual photosynthetic gain in individual beech saplings: a functional-structural modeling approach. For Ecol Manag 259:2141–2150
Weiher E, Freund D, Bunton T, Stefanski A, Lee T, Bentivenga S (2011) Advances, challenges and a developing synthesis of ecological community assembly theory. Philos Trans Roy Soc B 366:2403–2413
Weiner J, Freckleton RP (2010) Constant final yield. Annu Rev Ecol Evol Syst 41:173–192
West GB, Brown JH, Enquist BJ (1997) A general model for the origin of allometric scaling laws in biology. Science 276:122–126
West GB, Brown JH, Enquist BJ (1999) A general model for the structure and allometry of plant vascular systems. Nature 400:664–667
West GB, Brown JH, Enquist BJ (2001) A general model for ontogenetic growth. Nature 413:628–631
West GB, Enquist BJ, Brown JH (2009) A general quantitative theory of forest structure and dynamics. Proc Natl Acad Sci U S A 106:740–745
Wright IJ, Westoby M (2002) Leaves at low versus high rainfall: coordination of structure, lifespan and physiology. New Phytol 155:403–416
Wright IJ, Reich PB, Westoby M, Ackerly DD, Baruch Z, Bongeers F, Cavender-Bares J, . . ., Villar R (2004) The worldwide leaf economics spectrum. Nature 428:821–827
Yoda K, Kira T, Ogawa H, Hozumi K (1963) Self-thinning in overcrowded pure stands under cultivated and natural conditions. J Biol Osaka City Univ 14:107–129
Yokozawa M, Hara T (1992) A canopy photosynthesis model for the dynamics of size structure and self-thinning in plant populations. Ann Bot 70:305–316
Zeide B (2010) Comparison of self-thinning models: an exercise in reasoning. Trees 24:1117–1126

Subject Index

K. Hikosaka, Ü. Niinemets, and N.P.R. Anten (eds.), *Canopy Photosynthesis: From Basics to Applications*, DOI 10.1007/978-94-017-7291-4